Advanced receivers and waveforms for UAV/Aircraft aeronautical communications

Bilel Raddadi

THÈSE

En vue de l'obtention du

DOCTORAT DE L'UNIVERSITÉ DE TOULOUSE

Délivré par :

Institut National Polytechnique de Toulouse (Toulouse INP)

Discipline ou spécialité :

Réseaux, Télécommunications, Systèmes et Architecture

Présentée et soutenue par :

M. BILEL RADDADI

le mardi 3 juillet 2018

Titre :

Récepteurs avancés et nouvelles formes d'ondes pour les communications aéronautiques

---

Ecole doctorale :

Mathématiques, Informatique, Télécommunications de Toulouse (MITT)

Unité de recherche :

Institut de Recherche en Informatique de Toulouse (I.R.I.T.)

Directeur(s) de Thèse :

M. CHARLY POULLIAT

MME MARIE LAURE BOUCHERET

Rapporteurs :

M. EMMANUEL BOUTILLON, UNIVERSITE DE BRETAGNE SUD

M. JEAN-PIERRE CANCES, UNIVERSITE DE LIMOGES

Membre(s) du jury :

Mme INBAR FIJALKOW, ENSEA, Président

M. CHARLY POULLIAT, INP TOULOUSE, Membre

M. MARCO DI RENZO, CNRS PARIS, Membre

Mme MARIE LAURE BOUCHERET, INP TOULOUSE, Membre

Mme NATHALIE THOMAS, INP TOULOUSE, Membre

Remerciements

Je souhaite tout d'abord remercier celle sans qui cette thèse n'aurait pas pu se réaliser, car, à vrai dire, c'est la première personne qui m'a accueilli au sein du laboratoire et m'a présenté au reste de l'équipe. Il s'agit de Nathalie Thomas, ma co-directrice de thèse, qui m'a donné le premier coup de pouce et m'a surveillé de près et de loin le long de ma thèse. Encore, je dis merci à Nathalie Thomas pour ses nombreuses relectures et pour sa gentillesse.

Ensuite, je tiens à remercier mes directeurs de thèse pour m'avoir fait confiance, et soutenu durant ma thèse. Plus spécialement, je remercie Charly Poulliat, mon *sacré* directeur de thèse, qui a su me faire confiance et me laisser toute la liberté de mener mon travail dans la direction que je souhaitais tout en m'accompagnant de ses conseils toujours avisés. Il m'a donné une grande autonomie et a fait preuve d'une disponibilité hors du commun. Du fond de mon cœur, je dis un très grand MERCI à Charly Poulliat.

Sans oublier, bien sûr, Marie-Laure Boucheret, ma directrice de thèse qui m'a encouragé beaucoup. Avec beaucoup de sincérité, je tiens à exprimer mes remerciements à Marie-Laure Boucheret pour ses éclairages salutaires et pour tous ses conseils précieux. Je te suis profondément reconnaissant pour ce que tu as fait pour moi. Une chose est sure : je n'oublierais jamais.

Durant ma première année de thèse, j'ai aussi eu des échanges avec Benjamin Gadat ingénieur de recherche à Airbus D&S. Je souhaiterai le remercier pour sa précieuse collaboration. Je remercie aussi Nicolas Van Wambeke, ingénieur de recherche à Thalès Alinea Space, pour sa disponibilité et sa collaboration durant les deux dernières années de ma thèse.

J'adresse mes sincères remerciements à Jean Pierre Cances Professeur à l'université de Limoges ainsi que Emmanuel Boutillon professeur à l'Université Bretagne Sud, Lorient pour leur lecture minutieuse de mon manuscrit et pour avoir accepté de rapporter cette thèse. Que soient aussi remerciés Marco Di Renzo chargé de recherche à SUPÉLEC Paris et Inbar Fijalkow professeure à l'université de Cergy-Pontoise m'ont fait l'honneur d'examiner ma thèse.

Je souhaite également remercier tout le personnel de TéSA et de l'équipe SC de l'IRIT, Corinne Mailhes, Marie Chabert, Cédric Févotte, Nicolas Dobigeon ... pour leur accueil. Il y a aussi, Sylvie Eichen, Sylvie Armengaud , Annabelle Sansus et Isabelle Vasseur que je remercie et qui nous rendent la vie bien plus facile. J'adresse ma gratitude à tous ceux qui sont au cœur de la vie de doctorant, les autres doctorants et tous les jeunes que j'ai côtoyé Alberto, Olivier, Romain, Charles-Ugo, Serdar, Tarik, Mouna, Bouchra, Farouk, Abdelaziz et bien d'autres. Je garderai en mémoire les moments magnifiques que nous avons partagés ensemble et je vous

souhaite à tous tout le bonheur et la réussite que l'on peut espérer.

Enfin, et le meilleur pour la fin, je remercie tout particulièrement ma famille qui m'a toujours soutenu, surtout ma mère Saida qui depuis mon enfance n'a cessé de me soutenir, de m'encourager, de m'accompagner dans tous les moments, pour me donner goût à la vie et pour que je puisse devenir la personne que je suis à présent.

Bilel

Résumé

De nos jours, L'utilisation des drones ne cesse d'augmenter et de nombreuses études sont réalisées afin de mettre en place des systèmes de communication dronique destinés à des applications non seulement militaires mais aussi civiles. Pour le moment, les règles d'intégration des drones commerciaux dans l'espace aérien doivent encore être définies et le principal enjeu occupation est d'assurer une communication fiable et sécurisée. Cette thèse s'inscrit dans ce contexte de communication.

Motivée par la croissance rapide du nombre des drones et par les nouvelles générations des drones commandés par satellite, la thèse vise à étudier les différents liens possibles qui relient le drone aux autres composants du système de communication. Trois principaux liens sont à mettre en place : le lien de contrôle, le lien de retour et le lien de mission. En raison de la rareté des ressources fréquentielles déjà allouées pour les futurs systèmes droniques, l'efficacité spectrale devient un paramètre crucial pour leur déploiement à grande échelle. Afin de mettre en place un système de communication par drones spectralement efficace, une bonne compréhension des canaux de transmission pour chacune des trois liaisons est indispensable, ainsi qu'un choix judicieux de la forme d'onde.

Cette thèse commence par étudier les canaux de propagation pour chaque liaison : canaux de type mutitrajets avec ligne de vue directe, dans un contexte d'utilisation de drones à moyenne altitude et longue endurance (drones MALE). L'objectif de cette thèse est de proposer de nouveaux algorithmes de réception permettant d'estimer et égaliser ces canaux de propagation muti-trajets. Les méthodes proposées dépendent du choix de la forme d'onde. Du fait de la présence d'un lien satellite, les formes d'onde considérées sont de type mono-porteuse (avec un faible facteur de crête) : SC et EW-SC-OFDM. L'égalisation est réalisée dans le domaine temporel (SC) ou fréquentiel (EW-SC-OFDM).

L'architecture UAV prévoit l'implantation de deux antennes placées aux ailes. Ces deux antennes peuvent être utilisées pour augmenter le gain de diversité (gain de matrice de canal). Afin de réduire la complexité de l'égalisation des canaux, la forme d'onde EW-SC-OFDM est proposée et étudiée dans un contexte muti-antennes, dans le but d'améliorer l'endurance de l'UAV et d'accroître l'efficacité spectrale, une nouvelle technique de modulation est considérée: Modulation spatiale (SM). Dans SM, les antennes de transmission sont activées en alternance. L'utilisation de la forme d'onde EW-SC-OFDM combinée à la technique SM nous permet de proposer de nouvelles structures modifiées qui exploitent l'étalement spectrale pour mieux protéger des bits de sélection des antennes émettrices et ainsi améliorer les performances du système.

Abstract

Nowadays, several studies are launched for the design of reliable and safe communications systems that introduce Unmanned Aerial Vehicle (UAV), this paves the way for UAV communication systems to play an important role in a lot of applications for non-segregated military and civil airspace. Until today, rules for integrating commercial UAVs in airspace still need to be defined, the design of secure, highly reliable and cost effective communications systems still a challenging task. This thesis is part of this communication context.

Motivated by the rapid growth of UAV quantities and by the new generations of UAVs controlled by satellite, the thesis aims to study the various possible UAV links which connect UAV/aircraft to other communication system components (satellite, terrestrial networks, etc.). Three main links are considered : the Forward link, the Return link and the Mission link. Due to spectrum scarcity and higher concentration in aircraft density, spectral efficiency becomes a crucial parameter for large-scale deployment of UAVs. In order to set up a spectrally efficient UAV communication system, a good understanding of transmission channel for each link is indispensable, as well as a judicious choice of the waveform.

This thesis starts to study propagation channels for each link : a mutipath channels through radio Line-of-Sight (LOS) links, in a context of using Medium Altitude Long drones Endurance (MALE) UAVs. The objective of this thesis is to maximize the solutions and the algorithms used for signal reception such as channel estimation and channel equalization. These algorithms will be used to estimate and to equalize the existing muti-path propagation channels. Furthermore, the proposed methods depend on the chosen waveform. Because of the presence of satellite link, in this thesis, we consider two low-papr linear waveforms : classical Single-Carrier (SC) waveform and Extended Weighted Single-Carrier Orthogonal Frequency-Division Multiplexing (EWSC- OFDM) waveform. channel estimation and channel equalization are performed in the time-domain (SC) or in the frequency domain (EW-SC-OFDM).

UAV architecture envisages the implantation of two antennas placed at wings. These two antennas can be used to increase diversity gain (channel matrix gain). In order to reduce channel equalization complexity, the EW-SC-OFDM waveform is proposed and studied in a muti-antennas context, also for the purpose of enhancing UAV endurance and also increasing spectral efficiency, a new modulation technique is considered : Spatial Modulation (SM). In SM, transmit antennas are activated in an alternating manner. The use of EW-SC-OFDM waveform combined to SM technique allows us to propose new modified structures which exploit excess bandwidth to improve antenna bit protection and thus enhancing system performances.

Table of Acronyms

UAV	*Unmanned Air Vehicle*
UAS	*Unmanned Aircraft System*
RPA	*Remotely Piloted Aircraft*
RPS	*Remote Pilot Station*
GES	*Ground Earth Station*
GCS	*Ground Control Station*
LOS	*Line of Sight*
NLOS	*non Line of Sight*
RLOS	*Radio Line of Sight*
BRLOS	*Beyond Radio Line of Sight*
C3	*Command, Control and Communications*
C2	*Command & Control*
ATC	*Air Traffic Control*
ICAO	*International Civil Aviation Organization*
SARPS	*Standards and Recommended Practices*
FWD	*Forward link*
RTN	*Return link*
TRL	*Terrestrial link*
S2A	*Satellite-to-Aircraft channel*
A2S	*Aircraft-to-Satellite channel*

A2G	*Aircraft-to-Ground channel*
DVB	*Digital Video Broadcasting*
DVB-S	*Digital Video Broadcasting Satellite*
ETSI	*European Telecommunications Standards Institute*
LTE	*Long Term Evolution*
RF	*Radio Frequency*
DFT	*Discrete Fourier Transform*
OFDM	*Orthogonal Frequency Division Multiplexing*
CP	*Cyclic Prefix*
HPA	*High Power Amplifier*
PAPR	*Peak to Average Power Ratio*
SC	*Single Carrier*
EW SC-OFDM	*Extended Weighted Single Carrier Orthogonal Frequency-Division Multiplexing*
SIMO	*Single-Input Multiple-Output*
MIMO	*Multiple-Input Multiple-Output*
SM	*Spatial Modulation*
MMSE	*Minimum Mean Square Error*
ML	*Maximum Likelihood*
MAP	*Maximum A Posteriori*
BCJR	*Bahl Cocke, Jelinek, and J. Raviv (algorithm)*
SNR	*Signal-to-Noise Ratio*
RRC	*Root-Raised Cosine*
FTN	*Faster-Than-Nyquist*
SISO	*Soft Input Soft Output*
EXIT	*EXtrinsic Information Transfer*
ISI	*Inter-symbol Interference*

LDPC	*Low Density Parity Check*
CC	*Convolutional code*
BPSK	*Binary Phase Shift Keying*
QAM	*Quadrature and Amplitude modulations*
QPSK	*Quadrature Phase Shift Keying*
BER	*Bit Error Rate*
BICM	*Bit Interleaved Coded Modulation*
AWGN	*Additive White Gaussian Noise*
FFT	*Fast Fourier Transform*
IFFT	*Inverse Fast Fourier Transform*
FDE	*Frequency Domain Equalization*

Contents

Introduction

0.1 MOTIVATIONS

Unmanned Aerial Vehicle (UAV) systems are being increasingly studied in a broad spectrum of applications and contexts. Examples include disaster relief, public safety, and first responders, precision agriculture, environmental monitoring, infrastructure surveillance and monitoring, and fault detection. However, the contrasts between the complexity of the operational environment, the diverse UAV tasks, and the intrinsic limitations of the UAV platform are apparent and pose multiple technical challenges that need to be overcome.

Nowadays, UAV[1] (Unmanned Air Vehicle) fly almost exclusively in reserved airspace. However, in the near future, several civil and military applications will require remote controlled aircrafts to monitor a very large civilian land area. Indeed, thanks to UAVs, many complex mission will be feasible, such as the collection of information in areas humans cannot reach, either because of safety issues (like working within a radioactive cloud), or other issues related to human beings (like working over enemy places) [18] [41].

Soon, all civil and military UAS applications will require access to non-segregated airspace at some point in the flight pattern, even if that access is only required for transit to mission area. The aim is thus to achieve seamless integration into air traffic system with an equivalent level of safety as a manned aircraft. Insertion problems are to be solved progressively by 2020 [22] or earlier.

UAV technology is already fairly well-developed and development as well as maintenance costs are significantly lower than that of traditional manned aircraft systems [6]. For that reason, several studies are launched for the design of highly reliable and cost-effective communications systems that introduce UAV, this paves the way for UAV networks to play an important role in a lot of applications. Not only are UAVs cost-effective, the applications for government and commercial purposes are varied: transportation, communications infrastructure, humanitarian and public safety deployments, among others [59]. For instance, as part of Google Project Loon, high altitude and large-scale UAV LTE eNodeBs were proposed as alternatives for terrestrial eNodeBs [21].

A key driver is the ability to ensure safe and secure communications between the Remote Pilot Station (RPS) and the UAV. These safety of life flows are often referred to as C3 (Command, Control and Communications). With the introduction of long range and endurance UAV, there is a growing requirement for BRLOS (Beyond Radio Line of Sight) capabilities.

[1] an UAV is an aircraft without a human pilot aboard.

When beyond the radio line-of-sight, today's UAV mainly use Ku-band FSS (Fixed Satellite Service) satellite communications, often through commercial satellites, which are utilized thanks to transponder lease schemes. When under radio line-of-sight conditions, they rely on a wide range of solutions, mainly in C, Ku, S and UHF bands. However, in order to fly within non-segregated airspace, ICAO (International Civil Aviation Organization) demands, as per its position expressed towards ITU, the use of frequency bands allocated to civil aviation services for C3 when flying in non-segregated airspace. This position is likely to be turned into a mandate through the definition of ICAO C3 SARPS (Standards and Recommended Practices). A paradigm shift in UAV communications is thus required.

The International Civil Aviation Organization (ICAO) decided that UAV control and non-payload communication (CNPC) links must operate over protected spectrum [67]. Such spectrum will be allocated through the International Telecommunications Union Radio communication Sector (ITU-R). ITU-R has computed bandwidth requirements of 34 MHz for LoS CNPC links and 56 MHz for BLoS satellite CNPC links to allow for future UAS CNPC spectrum allocation [59]. Internationally discussed frequencies for LoS CNPC on the World Radio communication Conference (WRC) in 2015 are, amongst others, 960-977 MHz and 5030-5091 MHz [67]. UAV spectrum in the 1755 MHz band is considered for relocation in the US. We can infer from the bandwidth requirement and the potential frequency ranges that future UAS operations are likely to occur on multiple, at least two, non-contiguous bands. Usually guard bands are required on both sides of each allocated band to reduce the effect of out-of-band interference making such solution less spectrally-efficient than a single, large bandwidth solution. Furthermore, propagation behavior for 960 MHz and 5030 MHz distinctly differs. The exchange of rich content data or streaming high-definition video, for example, requires a significant amount of spectrum, proportional to the desired throughput and quality. When the air becomes more congested, more bandwidth will be needed to accommodate the desired communication needs.

The aforementioned bandwidth calculations by the ITU-R are rather pessimistic because they only account for time-sparse video data exchange for sense and avoid (S&A) applications in environments with relatively low UAV densities. It is likely that future UAV links will be throughput-intensive and the above discussed dedicated CNPC spectrum will not be sufficiently available to carry payload data. New ways of spectrum management-apart from simply allocating more bandwidth-need to be considered. On the one hand spectrum sharing is an efficient concept to satisfy bandwidth demand in an opportunistic way, when and where needed. On the other hand, the search for a robust spectrally-efficient waveform is also necessary to utilize spectrum more efficiently.

0.2 Context of study

Unmanned Aerial Vehicle (UAV) systems are being increasingly studied in a broad spectrum of applications and contexts. Examples include disaster relief, public safety, and first responders, precision agriculture, environmental monitoring, infrastructure surveillance and monitoring, and fault detection. However, the contrasts between the complexity of the operational environment, the diverse UAV tasks, and the intrinsic limitations of

the UAV platform are apparent and pose multiple technical challenges that need to be overcome. In particular, autonomous operation of the UAVs requires making sense of the surrounding environment, complex decision making, and coordination with other UAVs and ground resources. Urban scenarios create additional challenges in terms of complexity, spectrum availability, and safety.

In fact, increasing UAV densities will bring along challenges in S&A, radio spectrum allocation [109] as well as UAV type-specific NAS integration [115]. The successful integration of unmanned aircraft in non-segregated airspace relies heavily on robust command and control communication links. Whereas UAV flight operation control signaling requires low throughput, and spectrum will likely be allocated for this purpose, the data rates for transmitting the information content that the UAV sensors gather can be significant and will grow with technology advancements. Recent predictions reveal that UAV quantities for the commercial and public sector will outnumber deployed UAVs for DoD. Today's and future missions of these aircraft increasingly rely on the information exchange of real time payload data leading to a spectrum management problem. To alleviate this problem, one solution to the problem is the increase in spectral efficiency. Another solution is using higher frequencies (where there is more spectrum) or better spectrum management, in general.

Future designers of UAVs, in particular civil and public UAVs, need to be aware of intensified safety requirements and spectrum scarcity due to higher concentration in aircraft density. Hence, One of the challenging task is the design of efficient UAV systems with efficient waveform and spectrum management implementation. In this thesis, the spectral scarcity problem is addressed and new efficient waveforms are proposed.

Motivated by recent prediction of UAV quantities, revealing the importance of MALE [2] and HALE[3] UAVs, the thesis determines the performance of communication system in terms of spectral efficiency and Bit Error Rate for the the three existing links: the forward link, the return link and the mission link.

With a system that envisages the installation of several thousand satellite-controlled drones, it is essential to study the various possible links by modeling each propagation environment. On the basis of the channel models already proposed for each communication link, the objective is to find appropriate solutions to combat the aeronautical channel effect and ensure a « non-erroneous » communication between the transmitter and the receiver.

In this context, the study of new waveforms appears to be required. From the point of view of the terminal, it is possible to achieve an efficient TX power and therefore to improve the link budget. In this thesis, we study the classical linear modulations such as QPSK, 8-PSK etc. Additionally, we are interested in a specific low PAPR linear waveforms such as Single Carrier (SC) and Extended Weighted Single Carrier Orthogonal Frequency-Division Multiplexing (EW SC-OFDM). SC is a classical linear waveform suitable in satellite context. Whereas, EW SC-OFDM is a new single-carrier waveform which offers a good spectral occupation and also can allow us to use a simple frequency domain equalization at the receiver.

Despite the fact that the performances of some schemes using AWGN channels in Nyquist signaling are known and well controlled, those on aeronautical channels are not well known. On this basis, researches are being carried out to study the model of the aeronautical channel for the various possible links such as the

[2] A medium-altitude long-endurance UAV.
[3] A high-altitude long-endurance UAV.

control link (the forward link and the return link) and the mission link. In the beginning of this thesis, the forward link is studied for both the single-carrier (SC) and the SC-OFDM waveform. This study is based on a given Two-ray model. Thanks to this simple channel modeling, it is easy to prove That the equivalent baseband communication channel is a sparse channel. The sparse form allows us to propose a new reduced complexity channel equalization structure and new efficient channel estimation method. Then, for the return link, the propagation channel is assumed Additive White Gaussian Noise (AWGN) and two scenarios are distinguished: the first one is when we consider Nyquist signaling at the transmitter. Whereas, the second scenario is when we consider Fast-Than-Nyquist (FTN) signaling at the transmitter. For Nyquist signaling, the performances are well known. However, for FTN signaling is not necessary the case and the objective is to design a corresponding receiver that achieves a good trade-off between the resulting computational complexity and the obtained Bit error rate performance.

For the mission link, exchanging rich content data or broadcasting high-definition video, for example, requires reliable communication. However, for some hostile environments, communication becomes difficult. Since the UAV presents two transmit/receive antennas placed at the extremity of these two wings, one of the possible solutions is to switch to conventional MIMO communication. But, this solution can be offered at the expense of the UAV endurance. To avoid this problem, a new modulation technique has been proposed: Spatial modulation (SM). SM is based on transmit antennas selection and it can offer an efficient consumption of energy at the transmitter. The main advantage of SM technique is to exploit the diversity gain and to improve spectral efficiency. In the last chapter of this thesis, new SM schemes are introduced for the mission link and system performance analysis is discussed for different possible environments. Finally, the thesis establishes some concepts of what future UAV waveforms may look like.

0.3 Structure of the manuscript

- *Chapter 1 :* The aim of this chapter is to determine the different parameters of the aeronautical channel such as the time profile, the coherence time, the coherence bandwidth, etc. for both control link (the forward channel and the return channel) and the mission link (the mission channel).

- *Chapter 2 :* Since the classical single-carrier (SC) and the Extended Weighted Single Carrier Orthogonal Frequency-Division Multiplexing (EW SC-OFDM) are two low PAPR linear waveforms which are suitable to satellite context, a study of system performance using SC and EW SC-OFDM waveforms is introduced in Chapter 2. This chapter addresses both channel estimation methods and channel equalization at reception. Moreover, Nyquist signaling and Fast Than Nyquist (FTN) are considered at the transmitter.

- *Chapter 3 :* Knowing the explicit expression of the satellite-to-aircraft (S2A) propagation channel, this chapter aims to study the viability of these two waveforms SC and EW SC-OFDM waveforms for the forward link. Moreover, thanks to the particular form of S2A channel, it is possible to propose new adequate solutions for both channel estimation and channel equalization tasks. At the ground earth station (GES) transmitter, Nyquist and FTN signaling are considered. For SC waveform, by exploiting the

particular form of the S2A channel, new channel estimation methods and new sub-optimal but efficient channel equalization structures are proposed for the UAV/aircraft receiver for both Nyquist/FTN signaling. Whereas, for EW SC-OFDM waveform, a reduced complexity channel equalization is considered for the receiver. Additionally, a simple channel estimation method suitable for FTN/Nyquist signaling is presented.

- *Chapter 4 :* For the return link, an AWGN aircraft-to-satellite (A2S) channel is considered. For the UAV/aircraft transmitter, two linear waveforms are considered: SC and EW SC-OFDM. By considering AWGN channel, system performances are compared for both SC and EW SC-OFDM waveforms in Nyquist/FTN signaling. For the return link, channel estimation is not required. In Nyquist signaling, no channel equalization is required and the two waveforms SC and EW SC-OFDM waveforms give the same performances in terms of Bit Error Rate (BER). However, in FTN signaling it is not the case. However, in FTN signaling, there are an additional inter-symbol-interference (ISI) and thus it is necessary to consider channel equalization step in order to mitigate ISI. For EW SC-OFDM waveform, a simple frequency domain equalization with *a priori* is considered. Whereas, for SC waveform, we apply same reduced complexity equalization structure proposed for the forward link. As a result, system performances in terms of BER are no longer identical as for the Nyquist case.

- *Chapters 5-6:* Chapter 5-6 concern the mission link: the link between the UAV/aircraft transmitter and the ground control station (GCS) receiver. The mission is considered to be the link for a very large amount of data (live video, images etc.), this link requires a high bit rate. That's why a straightforward solution is to benefit from the diversity gain (matrix gain) which can provide multiple antennas communication to increase the throughput. This solution seems feasible since UAV/aircraft architecture envisages the implantation of two transmit/receive antennas placed at wings. However, the simultaneous use of these two antennas can affect UAV/aircraft endurance. In fact, doubling the number of active antennas means reducing half of endurance time. In order to overcome this problem and reduce energy consumption, one can think to use these two transmit antennas in an alternative manner. This is the main idea of Spatial Modulation (SM) technique. SM a is a new interesting technique initially introduced in [23] in 2001 , and later studied in details by Mesleh at al in [86][85]. In terms of energy consumption, SM configuration is equivalent to Single-Input Multiple-Output (SIMO). However, using SM technique can increase the overall spectral efficiency by the base-two logarithm of the number of transmit antennas compared the SIMO technique.
  Considering a possible line-of-sight (LOS) multipath aircraft-to-ground (A2G) channel between the UAV/aircraft transmitter and the GCS receiver, Chapter 5 study the existing solutions using SM technique over a Ricean MIMO channel. Essentially, two existing SM structures are considered at the transmitter: CP-aided OFDM-SM and CP-aided SC-SM. At reception, various receivers are studied and compared in terms of uncoded BER performances. On other hand, the SIMO system is introduced and its BER performances are compared to SM system. Simulation results are presented for different

values of Rice factor. The aims of this Chapter is to determinate what is the best existing combination (SM/SIMO configuration, ML/MRC/MMSE receiver) for both SC and OFDM systems that can offer the better BER performance for all possible values of Rice factor.

In Chapter 6, two modified SM structures are proposed: a modified CP-aided OFDM-SM structure and a modified CP-aided SC-SM structure. The first one aims to reduce the PAPR level compared to the classical OFDM-SM structure by adding a DFT-Precoding block for OFDM Signals. Whereas, the second one is designed to reduce the spectral occupancy of the SC-SM signals by adding a circular shaping filter just before transmit antenna selection. Furthermore, the two proposed modified SM structures operate with an oversampling factor. As a result, there are a bandwidth expansion. This bandwidth excess is exploited to improve antenna bit protection and thus enhancing BER performances. By following the same steps as in chapter 5, the two proposed SM structures are studied for different possible values of Rice factor in order to determine the best combination (SM/SIMO configuration, ML/MRC/MMSE receiver).

0.4 Contributions

- *SISO system*:

  1. *Contribution 1 :* an efficient time-domain channel estimation method [96], [101] is proposed: the main idea exploits the fact that certain aeronautical channel parameters can be perfectly known at the receiver by using a geometrical considerations (mainly the delays). By exploiting this geolocation *a priori*, a new channel estimation method using a parametric model is proposed. As a result, it is shown that we can considerably enhance the system performances in terms of mean square error (MSE). The average resulting MSE gain is about 11 dB compared to the classical unstructured LS estimator (without geolocation *a priori*).

  2. *Contribution 2 :* a sub-optimal, but efficient and reduced complexity time-domain channel equalization structure is proposed [100], [95]: there are two proposed channel equalization structures: the first one is dedicated to sparse channels and the second one is designed for non-sparse channels. The main objective of the two equalization structures is to reduce the computational complexity at the receiver without considerably degrading the system performances, i.e. to achieve a good trade-off between system performance and computational complexity. In the case of Nyquist signaling, it is shown that the equivalent baseband aeronautical channel has a sparse form. In order to reduce the complexity at the receiver, a trellis-based MAP equalization structure is proposed to equalize the received signal in the case of Nyquist signaling. Whereas, in the case of FTN signaling, the equivalent baseband channel is no longer sparse and the second structure appears suitable to equalize this type of channel.

     We note that the first equalizer structure uses an independent parallel trellis in order to reduce the memory length of the sparse channel. On the other hand the second equalization structure

takes into account only the central powerful taps for a mismatch forward equalization step. For the two equalization structures the interference term linked to the others neglected taps is iteratively removed after a finite number of «self-iterations».

- *MIMO system*:

  1. *Contribution 1 :* we propose a code-aided OFDM-SM structure with a reduced PAPR [99]: In order to maintain the advantage of the use OFDM technique for SM system and reduce the PAPR level at the transmitter, a modified CP-aided OFDM-SM structure is proposed. the PAPR reduction of this SM structure is based on DFT-Precoding for OFDM Signals. In [98, 117], DFT-precoded block is implemented in each transmitted antenna. The main idea of the proposed modified SM structure is to implement DFT-precoded block just before antenna selection. The main advantage of this choice is that it allows us a hardware complexity reduction (only one DFT-precoded block instead of many ones implemented for all transmitted antenna). Another advantage is that it is possible to consider an expanded bandwidth transmission and enhanced active antenna selection at the reception. Indeed, the SM transmitter can exploit bandwidth expansion to protect the transmit antenna bits.
  2. *Contribution 2 :* we propose a code-aided SC-SM structure with circular pulse shaping [97]: The proposed structure operates with only one Radio Frequency (RF) chain and uses a circular pulse shaping just before antenna selection. Furthermore, this structure operates with an oversampling factor and thus with a bandwidth expansion. The main idea behind the design of this structure is to exploit the excess bandwidth to protect antenna bits at the transmitter and thus to enhance BER performances at the receiver. Moreover, the use of pulse shaping at the transmitter allows us to have a better spectral occupancy and thus enhance the spectral efficiency. Additionally, since the proposed SC-SM is operating with one RF chain and is using a transmit pulse shaping, the considered SM structure is perfectly suitable to Faster-than-Nyquist (FTN) signaling and thus it is possible to increase more the spectral efficiency of the system.

0.5 List of publications

Journals

1. Bilel Raddadi, Charly Poulliat, Nathalie Thomas, Marie-Laure Boucheret and Benjamin Gadat, " Self-iterated trellis-based MAP equalizer for FTN Signaling using mismatch channel model approach." (To be submitted)

Patents

1. Bilel Raddadi, Benjamin Gadat, Charly Poulliat, Nathalie Thomas, Marie-Laure Boucheret, " Equalization method for parsimonious communication channel and device implementing the method.", Application Number:15/017226, Publication Date: 08/11/2016, URL : US 2016/0234044 A1.

International conferences

1. Bilel Raddadi, Nathalie Thomas, Charly Poulliat, Marie-Laure Boucheret and Benjamin Gadat, " On an efficient equalization structure for aeronautical communications via a satellite link. ", in *IEEE International Conference on Wireless and Mobile Computing,Networking and Communications (WiMob 2014)*, Larnaca, Cyprus, 08/10/2014-10/10/2014, IEEE, p. 396-401, october 2014.

2. Bilel Raddadi, Charly Poulliat, Nathalie Thomas, Marie-Laure Boucheret and Benjamin Gadat. , " Channel etimation with a priori position for aeronautical communications via a satellite link. ", in *IEEE International Conference on Personal, Indoor and Mobile Radio Communications (PIMRC 2015)*, Hong Kong, 30/08/2015-02/09/2015,IEEE, pp. 532-537, August 2015.

3. Bilel Raddadi, Nathalie Thomas, Charly Poulliat and Marie-Laure Boucheret, " On the use of spatial modulation in aeronautical communications. ", in *IEEE International Conference on Wireless and Mobile Computing,Networking and Communications (WiMob 2016)*, New york, USA, 17/10/2016-19/10/2016, IEEE, p. 396-401, october 2016.

4. Bilel Raddadi, Nathalie Thomas, Charly Poulliat, Marie-Laure Boucheret, "Code-aided Antenna Selection for Spectrally Shaped DFT-precoded OFDM Spatial Modulation (regular paper)." in *IEEE International Conference on Personal, Indoor and Mobile Radio Communications (PIMRC 2017)*, Montreal, Quebec, Canada, 08/10/2017-13/10/2017, IEEE, 2017.

National conferences

1. Bilel Raddadi, Nathalie Thomas, Charly Poulliat, Marie-Laure Boucheret and Benjamin Gadat, " Estimation de canal avec apriori de position pour les communications aeronautiques par satellite. ", in *Groupe*

de Recherche et d'Etudes du Traitement du Signal et des Images (GRETSI 2015), Lyon, 08/09/2015-11/09/2015, GRETSI CNRS, p. 1-4, septembre 2015.

2. Bilel Raddadi, Romain Tajan, Nathalie Thomas, Charly Poulliat and Marie-Laure Boucheret, " Nouvelle structure codée de modulation spatiale utilisant une signalisation plus rapide que Nyquist. ", in *Groupe de Recherche et d'Etudes du Traitement du Signal et des Images (GRETSI 2017)*, Juan-les-Pins, 05/09/2017-08/09/2017, GRETSI CNRS, septembre 2017.

Chapter 1

Aeronautical communications

Sommaire

1.1 Introduction

This chapter provides an overview of the existing communication types of UAVs. Mainly, there are three possible links that can be made by an UAV/aircraft (see Figure 1.1); two satellite data links which are an uplink (referred to as forward link) and a downlink (referred to as backward link). The third link is a terrestrial link designed for data gathering (mission link). The role and type of satellites are specified in Section 1.2.3. For each link of the three possible links, this chapter presents the physical layer specifications for the existing standards and give a special focus to the analytical model of the aeronautical channel. A summary is given at the end of this chapter. The reader can skip the details and can check directly the summary if he or she is familiar with the overall UAV context. The main contribution of this chapter is to combine relevant information in a complete form and state explicitly the digital communication models that will be used throughout this thesis.

1.2 Insertion of UAVs in civil airspace

1.2.1 Context

As of today, UAV (Unmanned Air Vehicle) fly almost exclusively in segregated airspace. However, in the near future, all civil and military UAS (Unmanned Aircraft System) applications will require access to non-segregated airspace at some point in the flight pattern, even if that access is only required for transit to mission area. The aim is thus to achieve seamless integration into air traffic system with an equivalent level of safety as a manned aircraft. Insertion problems are to be solved progressively by 2020 or earlier.

A key driver is the ability to ensure safe and secure communications between the Remote Pilot Station (RPS) and the UAV. These safety of life flows are often referred to as C3 (Command, Control and Communications). With the introduction of long range and endurance UAV, there is a growing requirement for BRLOS (Beyond Radio Line of Sight) capabilities.

When beyond the radio line-of-sight, today's UAV mainly use Ku-band FSS (Fixed Satellite Service) satellite communications, often through commercial satellites, which are utilized thanks to transponder lease schemes. When under radio line-of-sight conditions, they rely on a wide range of solutions, mainly in C, Ku, S and UHF bands. However, in order to fly within non-segregated airspace, ICAO demands, as per its position expressed towards ITU, the use of frequency bands allocated to civil aviation services for C3 when flying in non-segregated airspace. This position is likely to be turned into a mandate through the definition of ICAO C3 SARPS (Standards and Recommended Practices). A paradigm shift in UAV communications is thus required. ITU World Radio Conference (WRC) 2012 included an agenda item 1.3 covering UAV, the objective of which was to "consider spectrum requirements and possible regulatory actions, including allocations, in order to support the safe operation of UAS". As far as satellite communications are concerned, existing Aeronautical Mobile Satellite en-Route Service allocations (AMS(R)S) have been confirmed, in line with the ICAO position These allocations encompass the AMS(R)S L-band (1545-1555 MHz, 1646.5-1656.5 MHz) and the AMS(R)S 5GHz band (5000-5150 MHz). A subset of the latter (5030-5091 MHz) has been allocated to the Aeronautical Mobile

en-Route Service (AM(R)S) in order to accommodate UAS C3 Radio Line-Of-Sight (RLOS) communications.

1.2.2 UAV/aircraft links

For future civilian application, UAV/aircraft will present three links; a forward link, a return link and a mission link presented in Figure 1.1.

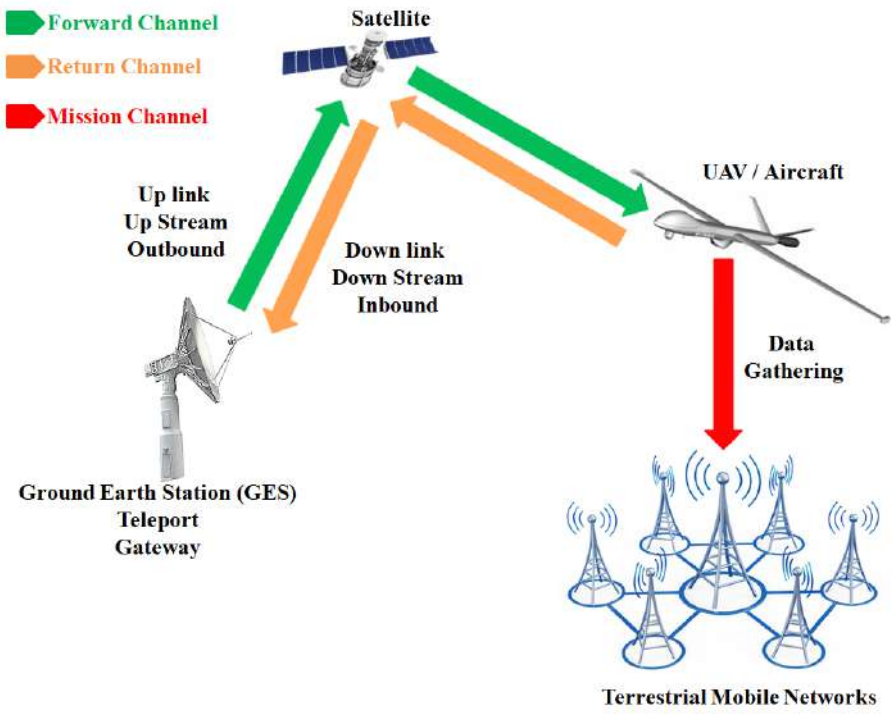

Figure 1.1: *UAV communication system*

1.2.3 Communications and Satellite role

The communication links between UAV (also known as RPA, i.e. Remotely Piloted Aircraft, according to the new ICAO denomination), UAV pilots and ATC (Air Traffic Control) are illustrated on Figure 1.2 Note that the UA (Unnamed Aircraft) is assumed to be within RLOS (Radio Line of Sight) of ATC (the ATC of the sector it's flying in) and that more than one RPS could be used for a single flight. It should be evident that if the UAV is BRLOS (Beyond Radio Line of Sight) of the UAV pilot, then all the information will have to be communicated through a satellite system.

In general, C3 transmissions will encompass the following types of data:

- UAV Command & Control data

    1. Initialization, configuration and mission upload messages sent infrequently during flight,

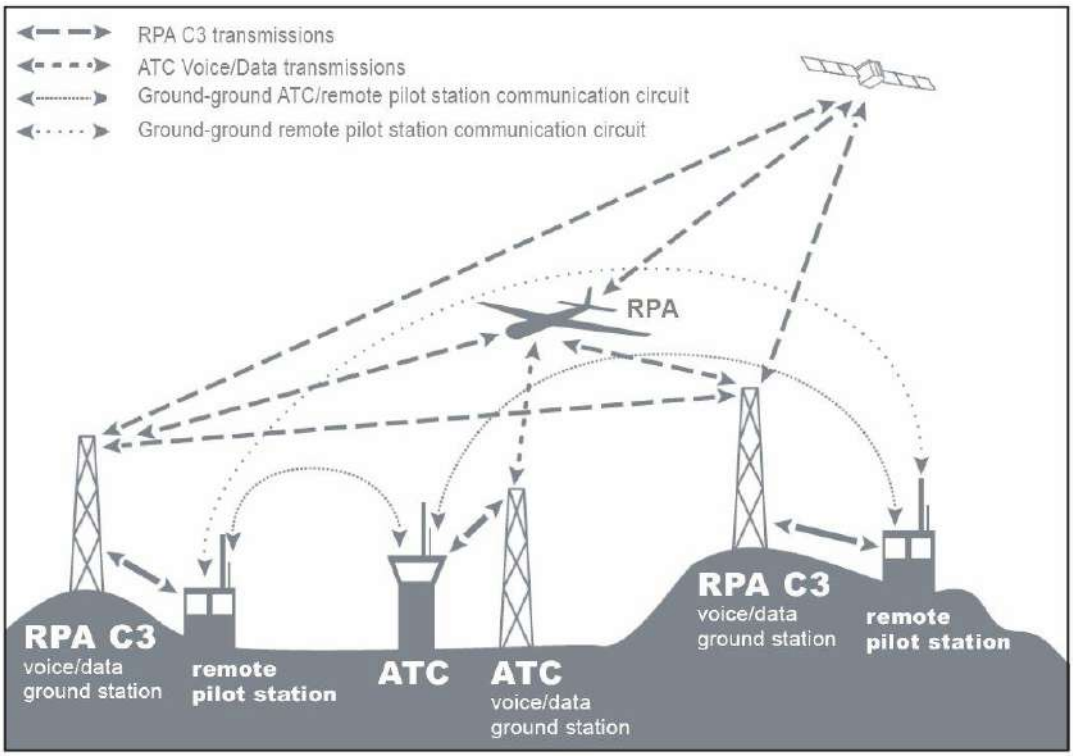

Figure 1.2: *UAS Communication links (adopted from ICAO Cir) [25].*

2. Messages sent to command the aircraft and its engines (the refresh rate depends on the level of autonomy of the UAV),
3. Flight status messages (speed, heading, position...) sent very frequently (up to 20 times per second for critical parameters) to control the aircraft,
4. Messages to set and control navigation receivers.

- Detect & Avoid (D&A) data: data associated to the Detect & Avoid function, which is equivalent to the piloting principle "see and avoid" used in all situations where permanent dangers exist due to the fact that external assistance (ATC) for the safety of the flight is not fully guaranteed.

1. "Detect" (or "surveillance") data (collected through existing surveillance systems such as radars or ADS-B or through new systems). Possibly, a video stream may be required for situational awareness purposes.
2. Configuration messages to adapt the operation of the D&A function depending on the flight conditions (area of flight, weather conditions...).
3. Status messages sent regularly so that the remote pilot can check the proper operation of the D&A function.

- ATC relay data: relay of voice and data ATC communications. As defined in [35], two concurrent architectures are considered as of today: ATC relay and non-ATC relay architectures. In case of non-ATC relay architecture, there is no ATC relay data to be conveyed by the UAS C3 satellite communication system (unless the direct link between the UACS and the ATCC is provided by this system and not by a terrestrial backbone).

1.3 Satellite Data Links: the forward link and the return link

1.3.1 Satellite Assumptions

The main assumptions regarding the satellite are that it is a transparent, geo-stationary satellite. It means that the perceived signal is only repeated by the satellite without any supplementary process. Moreover, for budget aspects, an hosted payload is considered for the satellite, which means that not all the power is dedicated to the C2 (Command & Control) mission.

1.3.2 The forward link: Satellite-to-Aircraft (S2A) Channel Model

Several studies ([53]-[77], among others) have looked at this model. The model we use and we present here is a compilation of these works. The propagation scenario is commonly represented by Figure 1.3.

For the forward link, The aeronautical satellite-to-aircraft (S2A) channel is characterized by three main

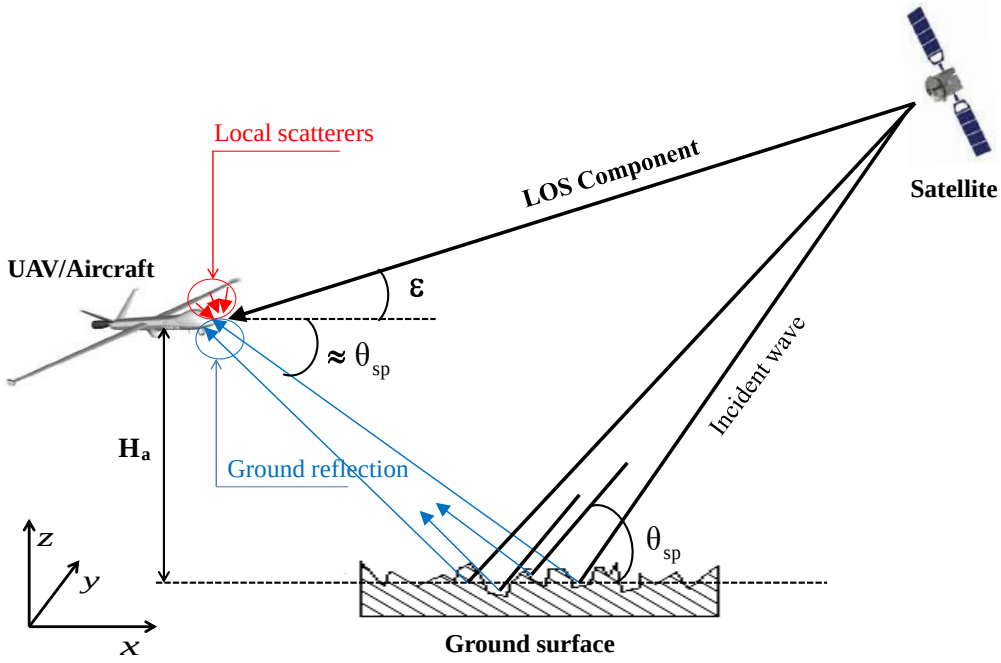

Figure 1.3: *Illustration of the geometry of the satellite-to-aircraft (S2A) communication channel. Local scatterers are illustrated with red, reflections from the ground with blue.*

paths. The first one arrives directly from the satellite and is a strong line of sight (LOS) component which is

present most of the time. Depending on the type of terrain and on the geometry, the second path (illustrated in blue in Figure 1.3) represents a multiple delayed reflections arriving from the ground at the aircraft with a certain attenuation compared to the LOS component. Also, a third path is considered (illustrated in red in Figure 1.3), representing local scatterers from the fuselage of the aircraft which might deteriorate the signal. Especially the big surface of the wings of the aircraft may be the source of non-negligible scattered components. Reflections from the ground and the fuselage will be referred to as multipath in the sequel.

1.3.2.1 Expression of S2A channel

: For the forward link, three main paths are considered. The First one arrives directly from the satellite to an UAV/aircraft receiver, this is the LOS path. The second and the third ones arrive respectively from wing surface and ground surface reflections. The expression of S2A channel is given as follows:

$$\begin{aligned} \mathrm{h}_a(t,\tau) = \sum_{n=0}^{\mathrm{N_m}-1} a_n(t)\ \delta(\tau-\tau_n) &= \frac{1}{\sqrt{\sum_{n=0}^{\mathrm{N_m}-1} \mathrm{P}_n}} \left\{ \sum_{n=0}^{\mathrm{N_m}-1} \alpha_n(t)\ \delta(\tau-\tau_n) \right\} \exp\left(2\pi j f_{\text{D-LOS}}\ t\right) \\ &= \underbrace{a_0(t)\ \delta(\tau-\tau_0)}_{\text{LOS Component}} + \underbrace{a_1(t)\ \delta(\tau-\tau_1)}_{\text{LS Component}} + \underbrace{a_2(t)\ \delta(\tau-\tau_2)}_{\text{GR Component}} \end{aligned} \tag{1.1}$$

with $\mathrm{N_m}$ denotes the number of considered paths. In the case of the S2A channel model, we have $\mathrm{N_m} = 3$. Indeed, the aeronautical channel presents three main paths: i. a LOS path with power P_0 and delay τ_0, ii. a LS path with power P_1 and delay τ_1 and iii. a GR path with power P_2 and delay τ_2 The three continuous coefficients $a_0(t)$, $a_1(t)$ and $a_2(t)$ denote the normalized continuous fading coefficients for the LOS, the LS and the GR paths, respectively. The coefficients $a_0(t)$, $a_1(t)$ and $a_2(t)$ are expressed as:

$$\begin{cases} a_0(t) &= \frac{1}{\sqrt{\mathrm{P}_0+\mathrm{P}_1+\mathrm{P}_2}}\ \alpha_0(t)\ \exp\left(2\pi j f_{\text{D-LOS}}\ t\right) \\ a_1(t) &= \frac{1}{\sqrt{\mathrm{P}_0+\mathrm{P}_1+\mathrm{P}_2}}\ \alpha_1(t)\ \exp\left(2\pi j f_{\text{D-LOS}}\ t\right) \\ a_2(t) &= \frac{1}{\sqrt{\mathrm{P}_0+\mathrm{P}_1+\mathrm{P}_2}}\ \alpha_2(t)\ \exp\left(2\pi j f_{\text{D-LOS}}\ t\right) \end{cases} \tag{1.2}$$

with $f_{\text{D-LOS}}$ denotes the frequency shift of the LOS component.

1.3.2.2 LOS Component

The LOS path undergoes several losses. The first one is the path loss effect due to free-space propagation. This path loss will be counted in the link-budget but it does not have a significant effect. The preponderant effect is the power of the LOS path compared to the other reflected paths. In the following we denote P_0 the power of the LOS path.

Another degradation impacting the LOS path is the propagation delay. Again, the delay of the LOS path τ_0 is not impacting, however the relative delay between the direct path and the other reflected path is impacting and will be detailed later. Note that the delay of each reflected paths denoted τ_l, is measured regarding to the first detectable signal at the receiver at $\tau_0 = 0$ [105]. Finally, the last effect degrading the quality of the LOS

signal is a so-called "Doppler-Shift". This Doppler can be classically calculated as follows:

$$f_{\text{D-LOS}} = \frac{v_x.\cos(\varepsilon) + v_z.\sin(\varepsilon)}{\lambda} \tag{1.3}$$

where λ denotes the wavelength, ε denotes the elevation angle of the UAV with respect to the GEO satellite (cf. Figure 1.3) and $\vec{v} = (v_x, v_y, v_z)$ the speed of the aircraft.
Finally, the continuous complex fading gain of the LOS component is denoted by $\alpha_0(t)$ and expressed as:

$$\alpha_0(t) = \sqrt{\text{P}_0}\ \exp\left(-2\pi j f_{\text{D-LOS}}\ t\right) \tag{1.4}$$

and thus by using (1.2), we can deduce that the normalized fading, $a_0(t)$, is time-invariant and having a constant value denoted by A_{LOS} and calculated as:

$$a_0(t) = \text{A}_{\text{LOS}} = \sqrt{\frac{\text{P}_0}{\text{P}_0 + \text{P}_1 + \text{P}_2}} \tag{1.5}$$

The corresponding delay, τ_0, is taken as a reference at the receiver:

$$\tau_0 = 0 \tag{1.6}$$

1.3.2.3 Local scatterers

Local scatterers (LS) are traditionally neglected [12], [89]. However, [120] characterized this reflection via a measurement campaign (the fuselage corresponding to an A340 airbus for several elevation angles and azimuths). This campaign yielded the following results:

- Local scatterers having a power P_1 which is a low power compared to that of LOS path (approximately a ratio of 14.2 dB):

$$\text{P}_1 = 10^{-1.42}.\text{P}_0 \tag{1.7}$$

- The Doppler Power Spectrum Density (D-PSD) of local scatterers varies according to a Gaussian distribution with a mean value $f_{\text{D-LS}}$ and a standard-deviation calculated as half the Doppler spread $\text{B}^{(1)}_{\text{rms}}$:

$$\text{D-PSD}\,(f) = \frac{\sqrt{2}}{\sqrt{\pi}.\text{B}^{(1)}_{\text{rms}}} \exp\left\{-2\left(\frac{f - f_{\text{D-LS}}}{\text{B}^{(1)}_{\text{rms}}}\right)^2\right\} \approx \frac{\sqrt{2}}{\sqrt{\pi}.\text{B}^{(1)}_{\text{rms}}} \exp\left\{-2\left(\frac{f - f_{\text{D-LOS}}}{\text{B}^{(1)}_{\text{rms}}}\right)^2\right\} \tag{1.8}$$

  where $\text{B}^{(1)}_{\text{rms}}$ is about 1 Hz and $f_{\text{D-LS}}$ is the Doppler shift and is assumed equal to $f_{\text{D-LOS}}$ (see equation Equation (1.3)). The continuous complex fading gain of the LS component is denoted by $\alpha_1(t)$ and verifies:

$$\mathbb{E}\left\{\alpha_1(t).\alpha_1^*(t+\Delta\tau)\right\} = \text{P}_1.\exp\left(-\pi^2.\text{B}^{(1)}_{\text{rms}}.|\Delta\tau|^2\right).e^{-2\pi j f_{\text{D-LOS}}.\Delta\tau} \tag{1.9}$$

  Since the weak the value of $\text{B}^{(1)}_{\text{rms}}$, LS component is assumed having a high time correlation.

- Local scatters having a low delay τ_1 (about 1 ns):

$$\tau_1 \approx 0 \tag{1.10}$$

  As a result, local scatterers are Ricean distributed with a high time correlation.

1.3.2.4 Ground reflection

In order to model the impact of the reflected path, it is necessary to measure its power denoted by P_2 with respect to the LOS path. This can be done using [61] and [62]. These documents give the same methodologies and formulas for calculating the impact of the reflected path with respect to the direct path:

$$10.\log_{10}\left(\frac{P_2}{P_0}\right) = C_\theta + D + 20.\log_{10}\left(|R_{circ}|\right) \qquad \text{with} \qquad R_{circ} = \frac{R_{TE}+R_{TM}}{2} \tag{1.11}$$

The power of specular component P_2 is calculated as a function of the Fresnel coefficients R_{TE} and R_{TM}. However, in low elevations, the curvature of the earth has to be taken into account in terms of the divergence coefficient D. Documents [61] and [62] define two correction factors: the divergence factor D and another correction factor C_θ. The divergence factor is expressed as:

$$D = 10.\log_{10}\left(1 + \frac{2.\sin\left(\gamma_{sp}\right)}{\cos\left(\theta_{sp}\right).\sin\left(\gamma_{sp}+\varepsilon\right)}\right) \tag{1.12}$$

with $\gamma_{sp} = 7,2.10^{-3}.H_a/\tan\left(\varepsilon\right)$ and θ_{sp} denoting the grazing angle to perpendicular incidence of the specular component:

$$\theta_{sp} = \varepsilon + 2.\gamma_{sp} \tag{1.13}$$

The correction factor is defined as:

$$C_\theta = \begin{cases} 0 & \theta_{sp} \geq 7° \\ \frac{7-\theta_{sp}}{2} & \theta_{sp} < 7° \end{cases} \tag{1.14}$$

The reflection coefficient is the ratio of the reflected electric field to the incident electric field. They are also dependent on the polarization of the incoming signal, i.e. the direction of the incident electric field and classified as transverse electric (TE) and transverse magnetic (TM) and are given by the expressions [111]:

$$R_{TE} = \frac{\sin(\theta_{sp}) - \sqrt{\eta - \cos^2(\theta_{sp})}}{\sin(\theta_{sp}) + \sqrt{\eta - \cos^2(\theta_{sp})}} \qquad R_{TM} = \frac{\eta\sin(\theta_{sp}) - \sqrt{\eta - \cos^2(\theta_{sp})}}{\eta\sin(\theta_{sp}) + \sqrt{\eta - \cos^2(\theta_{sp})}} \tag{1.15}$$

In the above expression, η denotes the complex relative permittivity. refer to [61] [62], η is defined by:

$$\eta = \varepsilon_r(f) + j\frac{\sigma_{eff}(f)}{\omega\varepsilon_0} = \varepsilon_r(f) + j\left[\frac{1}{2\pi\ c\ \varepsilon_0}\right]\ \lambda\ \sigma_{eff}(f) \approx \varepsilon_r(f) + j\ 60\ \lambda\ \sigma_{eff}(f) \tag{1.16}$$

with, $\varepsilon_0 = 8.85418710^{-12} F.m^{-1}$ is the vacuum permeability and $c = 3.10^8 m.s^{-1}$ is the of value to the speed of light in free space.

Suppose that incident electromagnetic wave propagates in free space, the quantities $\varepsilon_r(f)$ and $\sigma_{eff}(f)$ are the relative permittivity and the effective conductivity of the reflective surface. Typically, The values of $\varepsilon_r(f)$ and $\sigma_{eff}(f)$ depend on the nature of the reflective surface and also on the carrier frequency of the incident wave. Table 1.1 provides some typical electrical parameters of ground and water at $F_c = 1.54$ GHz [60].

Ground reflection, which is the most impacting phenomenon for the aeronautical channel, has been characterized by Bello in [12]. In his analysis Bello makes the assumption that ground-related reflections are that the

Surface	**Relative permittivity : ε_r**	**Effective conductivity : $\sigma_{\mathbf{eff}}$ $(S.m^{-1})$**
Salty sea water	81	3.5
Sea water	70	6
Fresh water	80	0.6
Ice water	3	0.01
Wet ground	30	0.5
Medium dry ground	15	0.125
Dry ground	3	0.0004
Very dry ground	3	0.00075

Table 1.1: *Typical Electrical Parameters at $F_c = 1.54$ GHz*

(x, y) coordinates of the point of impact of the LOS path on the ground are uniformly distributed. This leads to a Doppler Power Spectrum Density (D-PSD) which is Gaussian and which can be calculated as follows:

$$\text{D-PSD}\,(f) = \frac{\sqrt{2}}{\sqrt{\pi}.\mathrm{B}_{\mathrm{rms}}^{(2)}} \exp\left\{-2\left(\frac{f - f_{\text{D-GR}}}{\mathrm{B}_{\mathrm{rms}}^{(2)}}\right)^2\right\} \approx \frac{\sqrt{2}}{\sqrt{\pi}.\mathrm{B}_{\mathrm{rms}}^{(2)}} \exp\left\{-2\left(\frac{f - f_{\text{D-LOS}}}{\mathrm{B}_{\mathrm{rms}}^{(2)}}\right)^2\right\} \tag{1.17}$$

$f_{\text{D-GR}}$ and $\mathrm{B}_{\mathrm{rms}}^{(2)}$ are respectively the Doppler shift and the Doppler spread for the ground reflected path. Refer to Bello, the Doppler shift denoted $f_{\text{D-GR}}$, is defined as the mean of the distribution of Doppler frequencies and is assumed equal to $f_{\text{D-LOS}}$ (see Equation (1.3)). However, the Doppler spread denoted, $\mathrm{B}_{\mathrm{rms}}^{(2)}$, is defined by Bello as twice the standard-deviation of the distribution of Doppler frequencies. The expressions of $\mathrm{B}_{\mathrm{rms}}^{(2)}$ is given by the following expressions:

$$\mathrm{B}_{\mathrm{rms}}^{(2)} = \frac{4.[\sigma_{\mathrm{h}}.(\pi/180)]}{\lambda} \sqrt{\{v_x.\sin(\varepsilon) + v_z.\cos(\varepsilon)\}^2 + v_y^2.\sin^2(\varepsilon)} \tag{1.18}$$

In case of rough surfaces, the height variable h is assumed to be normally distributed, with zero-mean and standard deviation equal to σ_{h}. The larger gets, the rougher is the surface, the broader is the Doppler spectrum. Values around 4 m or less for σ_{h} are common maritime communications values.

The continuous complex fading gain of the ground reflection (GR) component is denoted by $\alpha_2(t)$ and verifies:

$$\mathbb{E}\{\alpha_2(t).\alpha_2^*(t + \Delta\tau)\} = \mathrm{P}_2.\exp\left(-\pi^2.\mathrm{B}_{\mathrm{rms}}^{(2)}.|\Delta\tau|^2\right).e^{-2\pi j f_{\text{D-LOS}}.\Delta\tau} \tag{1.19}$$

The correlation of complex fading $\alpha_2(t)$ is inversely proportional to $\mathrm{B}_{\mathrm{rms}}^{(2)}$ values. The most the ground surface is rough, the most the correlation is feeble.

On other hand, the delay of the specular reflected component can be determined based on geometrical considerations (see Figure 1.4). It is given by the path difference between the reflected and the LOS path divided by the speed of light. This leads to the following expression:

$$\tau_2 = \frac{b - a}{3.10^8} = \frac{\mathrm{H}_a}{3.10^8} \frac{1 - \cos(\varepsilon + \theta_{\text{sp}})}{\sin(\theta_{\text{sp}})} \approx \frac{\mathrm{H}_a}{3.10^8} \frac{1 - \cos(2.\varepsilon)}{\sin(\varepsilon)} = \frac{2.\mathrm{H}_a.\sin\varepsilon}{3.10^8} \tag{1.20}$$

with H_a denoting the height of the aircraft above the ground (see Figure 1.4).

It can be shown that all paths other than so-called specular reflection arrive in a sufficiently short time to justify a multipath model with only one «tap». This can be done by looking at the distribution of the delay

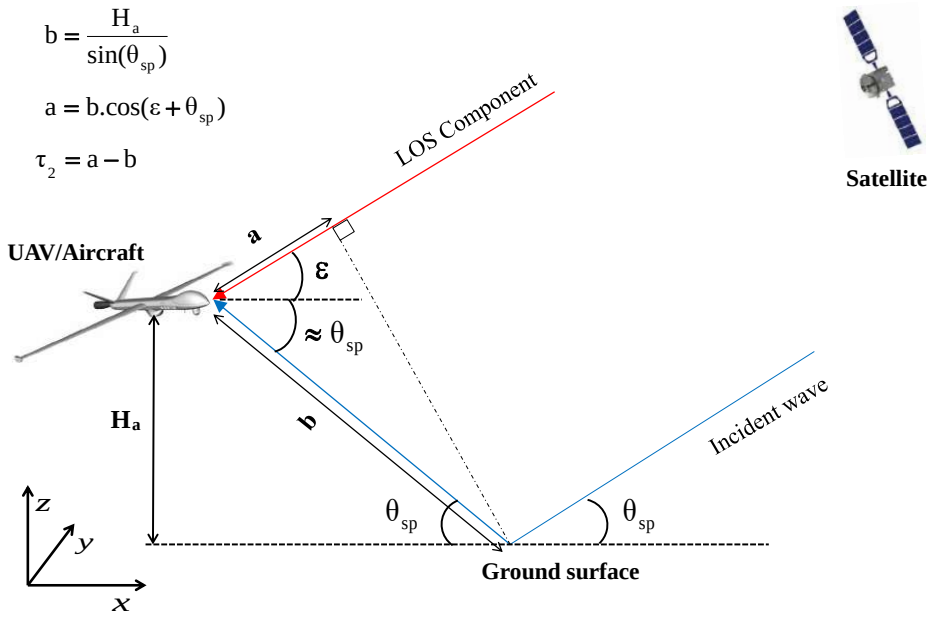

Figure 1.4: *Geometrical considerations on the delay of the specular component.*

ξ of the reflected components relative to the specular component. Taking again the Gaussian approximation (i.e. the coordinates (x, y) of the reflection points are assumed uniformly distributed) of [77], we obtain:

$$\mathrm{PDF}(\xi) = \frac{1}{\upsilon}\ \exp\left(-\frac{\xi.\left[\frac{1}{\sin(\varepsilon)}+\sin(\varepsilon)\right]}{2\ \upsilon}\right)\ I_0\left(\frac{\xi.\left[\frac{1}{\sin(\varepsilon)}+\sin(\varepsilon)\right]}{2\ \upsilon}\right) \tag{1.21}$$

with $\upsilon = [2.\sigma_{\mathrm{h}}.(\pi/180)]^2\ \frac{\mathrm{H}_a}{3.10^8}$ and I_0 is the modified Bessel function of order zero.
Refer to the determinated probability density function (PDF) of delays, some statistics can therefore be drawn on the relative delays of diffuse reflections with respect to the delay of specular reflection. For instance, for an UAV altitude of 10 km, tables 1.2 and 1.3 show some statistics on the relative delay ξ:

Relative delay ξ w.r.t specular reflection		**Elevation angle ε**	
		10°	80°
$\mathrm{PDF}(\xi)/\mathrm{PDF}(0)$	0.5	0.19 μ s	0.46 μ s
	0.1	1.63 μ s	1.51 μ s

Table 1.2: *Relative delay of multipath components w.r.t. specular reflection for an altitude of* 10 *km.*

These statistics make it possible to make an approximation of the model of multipaths with one «tap», which is in line with the various studies [53] [12] [89] [120].

Statistical parameters of ξ	**Elevation angle ε**	
	10°	80°
Mean value	1.69 μs	0.65 μs
Standard deviation	2.02 μs	0.66 μs
Variance	4.08 ps^2	0.43 ps^2

Table 1.3: *Mean, standard deviation, variance for ξ for different elevations at an altitude of 10 km.*

1.3.2.5 Final expression of S2A channel

Finally, given the fact that $\tau_1 \approx \tau_0 = 0$, the expression of the S2A is given by the following expression:

$$\mathrm{h}_a(t,\tau) = \sum_{n=0}^{\mathrm{N_m}-1} a_n(t)\ \delta(\tau-\tau_n) = (\mathrm{A_{LOS}} + \ a_1(t))\ \delta(\tau)\ +\ a_2(t)\ \delta(\tau-\tau_2) \tag{1.22}$$

Note that we consider a normalized aeronautical channel response:

$$|\mathrm{A_{LOS}}|^2 + \mathbb{E}\left\{|a_1(t)|^2\right\} + \mathbb{E}\left\{|a_2(t)|^2\right\} = 1 \tag{1.23}$$

1.3.2.6 C/M factor

To characterize multipath powers, the S2A channel is characterized by a carrier-to-multipath factor noted C/M and expressed as:

$$\begin{aligned}\mathrm{C/M\ [dB]} = 10.\log_{10}\left(\frac{\mathrm{P_0+P_1}}{\mathrm{P_2}}\right) &= 10.\log_{10}\left(\frac{\mathrm{P_0+P_1}}{\mathrm{P_0}}\right) - 10.\log_{10}\left(\frac{\mathrm{P_2}}{\mathrm{P_0}}\right) \\ &= 10.\log_{10}\left(1+10^{-1.42}\right) - [\mathrm{C}_\theta + \mathrm{D} + 20.\log_{10}(|\mathrm{R_{circ}}|)] \\ &\approx -\mathrm{C}_\theta - \mathrm{D} - 20.\log_{10}(|\mathrm{R_{circ}}|)\end{aligned} \tag{1.24}$$

Based on geometrical considerations, it is shown that C/M values depend on grazing angle values θ_{sp}. Since the value of θ_{sp} can be expressed as a function of the elevation angle ε as shown in Equation (1.13), therefore, we can deduct that C/M values are also depending on ε values. Moreover, we can show that C/M values are proportional to elevation angle values ε. By using geometric consideration, the value of the elevation angle can be calculated from geolocation data or GPS [1] coordinates such as the longitude, the latitude and the altitude. Let $(\Psi_a, \varphi_a, \mathrm{H}_a)$ and $(\Psi_s, \varphi_s, \mathrm{H}_s)$ are the latitude, the longitude and the altitude of an UAV/aircraft and a GEO satellite, respectively. The value of the elevation angle ε of the UAV/aircraft with respect of the GEO satellite can be determinated by using the following expressions:

$$\sin\varepsilon = \frac{\varpi - \frac{\mathrm{R_e+H}_a}{\mathrm{R_e+H}_s}}{\sqrt{(1-\varpi^2) + \left(\varpi - \frac{\mathrm{R_e+H}_a}{\mathrm{R_e+H}_s}\right)^2}} \qquad \cos\varepsilon = \frac{\sqrt{1-\varpi^2}}{\sqrt{(1-\varpi^2) + \left(\varpi - \frac{\mathrm{R_e+H}_a}{\mathrm{R_e+H}_s}\right)^2}} \tag{1.25}$$

with $\mathrm{R_e} = 6371\ km$ being the radius of the earth and,

$$0 \leq \varpi = \cos(\Psi_a)\cos(\Psi_s)\cos(\varphi_s - \varphi_a) + \sin(\Psi_a)\sin(\Psi_s) \leq 1 \tag{1.26}$$

[1] Global Positioning System.

Figure 1.5 shows some variation of the elevation angle ε as a function of the location of the UAV/aircraft in ECAC [2] area with an altitude of 10 km.

Measurement results of C/M factor in decibels are given as a function of the elevation angle ε in Figure 1.6.

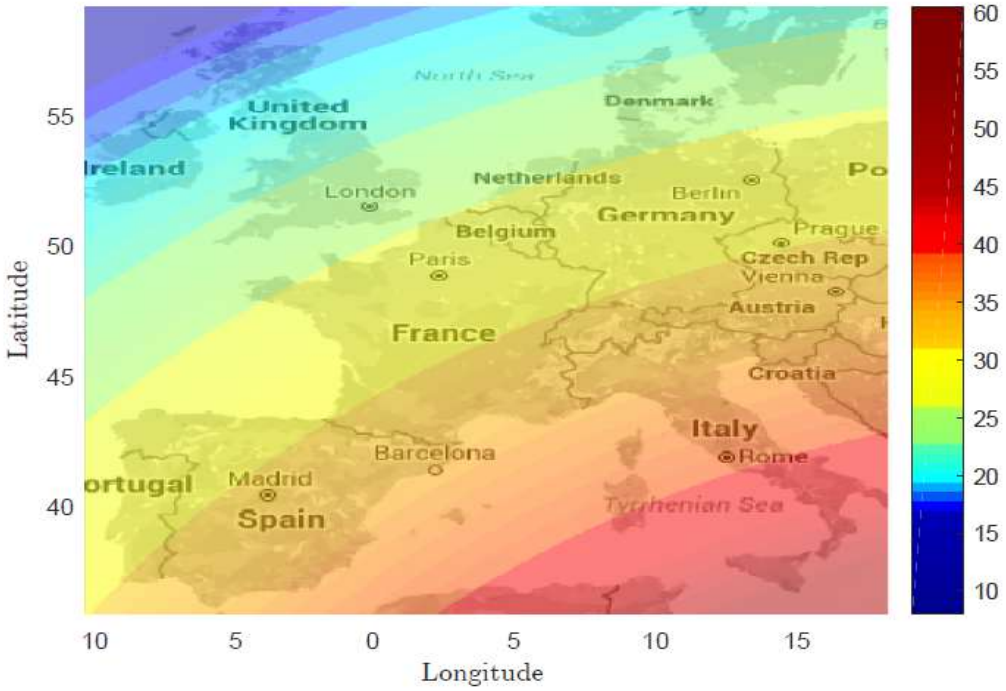

Figure 1.5: *Elevation angle between an aircraft of an altitude of $H_a = 10$ km and a GEO satellite 30° 12'E. For ECAC area, elevation angles are usually taken from 25 to 45 degrees.*

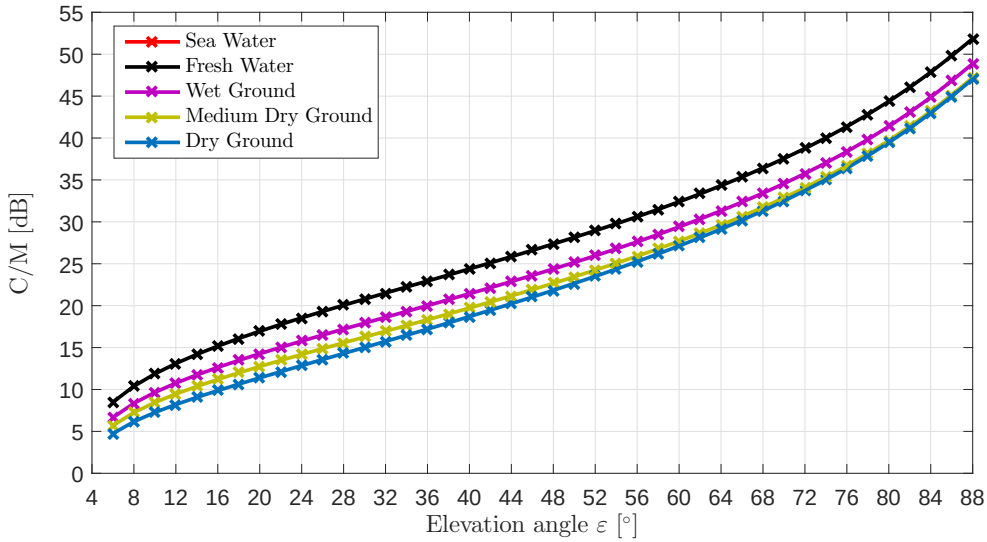

Figure 1.6: *C/M factor as function of the elevation angle for $H_a = 10$ km*

[2] Member states responsible for civil aviation.

1.3.3 Existing standards for forward link (FWD): Physical layer

Two satellite standards will be reviewed in this section. An aeronautical ESA standard [2] and the traditional DVB-S2(X) [38][123].

1.3.3.1 ANTARES CS standard

The ANTARES CS has been defined in the context of the ESA ARTES-10 (Iris) Programme for the purpose of satellite-based ATC/AOC communications. It has been proposed as a global standard to support long-term aircraft communication needs as required by future SESAR ATN/B3 applications («Full 4D»).
A MF-TDMA access scheme has been selected for the forward link. A Phase Shift Keying (PSK) modulation scheme is adopted which envisages several modulation levels, namely Q-PSK, 8-PSK and 16-APSK. The forward Error Correction (FEC) scheme is based on a Low Density Parity Check (LDPC) solution specifically designed for the aeronautical environment and adopting several code rates $R_c \in \{1/4; 1/3; 1/2; 2/3\}$. The selection of the MODCOD (combination of the modulation and FEC rate alternative) in ANTARES is based on an Adaptive Coding and Modulation (ACM) approach, which has been specifically designed to work adequately in mobile aeronautical environment, not only during nominal flight but also under aircraft manoeuvre conditions. Table 1.4 summarizes its main technical characteristics concerning physical layer.

Physical layer	
CS description	**Comments**
Access scheme	MF-TDMA (asynchronous random access)
Modulations	QPSK, 8-PSK, 16-APSK
Coding schemes	IRA LDPC (1/4,1/3,1/2, 2/3)
Pilot symbols	24 symbols
Roll-off factor/s	$\beta = 0.2$
Guard time	125 μs
Symbol rates (R_s)	$R_s = 160$ kbaud
Framing	86.35 ms
Channelization	200 kHz chunks
Diversity techniques supported	Time diversity (interleaving)
Fading mitigation techniques	ACM
Power control	Required
CRC (Error detection)	Yes (4-byte CRC at physical layer; optionally, additional 4-byte CRC to detect encapsulation errors)
Frequency band	Fixed link: Ku/Ka band Mobile link: L-band (AMS(R)S band)

Table 1.4: *Summary of ANTARES CS technical characteristics for FWD link*

The main strength of this candidate is that it has been specifically designed for an aeronautical satellite channel and for aircraft mobility and thus, especially from a physical layer point of view, it will have a good performance also for the RPAS use case. Another attractive aspect are the possible synergies with ATC/AOC communications, if the ATC/AOC system would be certified for both ATC/AOC and RPAS C2

communications. This may allow avoiding the installation of an additional antenna, decrease operational costs and reduce terminal costs (as certified equipment will have a broader market).

1.3.3.2 DVB-S2/S2x standard

DVB-S2 (Digital Video Broadcasting -Satellite 2) is the second-generation specification for satellite broadcasting. It offers a large capacity by using very high frequencies and can carry either unicast or broadcast traffic (like TV information programs). Compared to first-generation standard, DVB-S, the standard DVB-S2 has been proposed as a spectrally and power efficient transmission technology through using Amplitude and Phase Shift Keying (APSK) modulations and a class of capacity approaching block codes: Low Density Parity Check (LDPC) codes. The achieved system capacity gain over the First generation DVB-S can reach 30% [13]. Additionally, compared to the DVB-S standard, DVB-S2 offers the possibility of adapting the modulation and coding formats to the link quality with the so-called Adaptive Coding and Modulation (ACM) functionality.

Physical layer	
DVB-S2 description	**Comments**
Access scheme	commonly TDM, but may also be a MF-TDM.
Modulations	-Linear Modulation: QPSK, 8-PSK -Hierarchical modulation: 16-APSK & 32-APSK. (up to 256 APSK) were introduced in the recently adopted DVB-S2x [40].
Coding schemes	-Extended IRA LDPC (from 1/4 to 9/10). Two coded size (64800 bits and 16200 bits). Using a constant t=12 BCH as an outer code. -[40] specify new MODCODs (with an intermediate size of 32400 bits) and new code rate, in order to cover Very Low SNRs(VL-SNR).
Pilot symbols	a block of 36 unmodulated symbols is inserted every 16 slots of 90 symbols for synchronization
Roll-off factor/s	-DVB-S2: $\beta \in \{0.35, 0.25, 0.2\}$ -DVB-S2x: $\beta \in \{0.15, 0.1, 0.05\}$
Symbol rates (R_s)	No symbol rate is specified but it is commonly greater than 30 Mbauds.
Channelization	Not specified
Diversity techniques supported	Not specified. However, some MIMO techniques remain possible.
Fading mitigation techniques	ACM procedure that was mainly designed to counteract the rain effect in Ku/Ka propagation band.
Power control	An automatic gain control is proposed [39]
Frequency band	Fixed link: Ka/Q/V band

Table 1.5: *Summary of DVB-S2(X) technical characteristics for FWD link*

As an evolution of the standard DVB-S2, DVB-S2X relies on the same physical layer characteristics regarding the types of modulations and channel codes. However, there are some differences in the system parameters which can be summarized as follows:

- Small roll-offs (0.05 and 0.1) can be used leading to up to 15% gain in the system throughput.
- Finer modulations and coding rates.
- The modulation ring ratios can be jointly chosen with coding rates for given amplifier back-offs.

Table 1.5 summarizes its main technical characteristics concerning physical layer.

Concerning the physical layer, DVB-S2/S2x specifies a wide range of MODCODs, but especially for long length, with a minimal frame length of 16200 bits.

- In case of narrow band use (e.g. in case of C-Band usage or AMS(R)S band), this may be inappropriate for aeronautical scenarios. Indeed since in that case the channel model is rather a block fading channel than a fast fading channel, it may be better to perform inter-MODCODs interleaving in order to break fading correlations. Without specifying shorter frame length, the latency constraints may not be satisfied. As a consequence, efficient interleaving has to be defined. In addition, performances of DVB-S2/S2x on narrow carrier has to be validated, since it has rather been defined for large carriers.
- When no constraints are considered on the bandwidth (e.g. for K-band), the channel can be viewed as a fast fading channel, meaning that LDPC performances will be only a bit degraded when compared to AWGN channel. Since frame length is rather small, the specified MODCOD will be sufficient.

In case of ACM use, in order to perform an accurate channel estimation and Doppler compensation, it must be checked whether the pilot block that is inserted in DVB-S2/S2x frame is sufficient.

1.3.4 The return link: Satellite-to-Aircraft (S2A) Channel Model

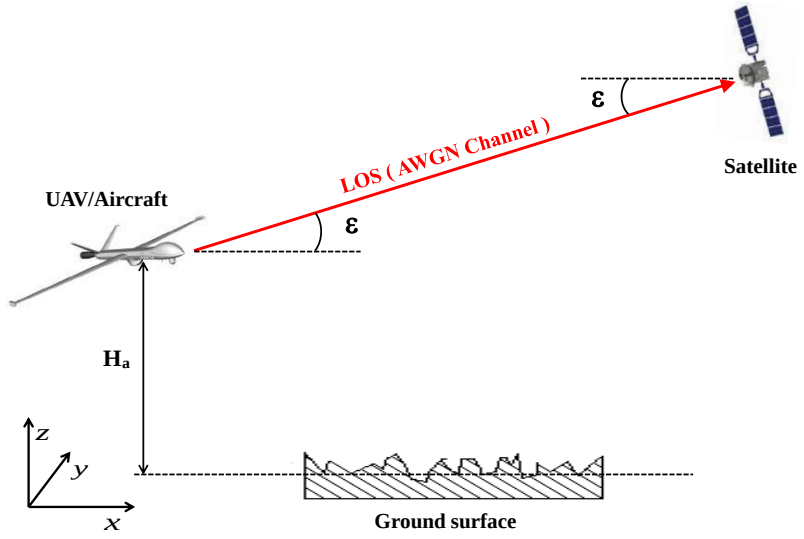

Figure 1.7: *Illustration of the geometry of the air-to-ground (A2S) communication channel. Only LOS path is considered.*

The aircraft-to-satellite (A2S) channel is assumed to be AWGN channel. Indeed, there are one line-of-sight (LOS) path. The LOS path (illustrated with red color in Figure 1.8) arrives directly from aircraft to GEO satellite. Its power is denoted by P_0. The delay of the LOS path is assumed equal to 0 i.e. $\tau_0 = 0$ [105]. Furthermore, the LOS path undergoes «Doppler-Shift» effect and this Doppler can be classically calculated as follows:

$$f_{\text{D-LOS}} = \frac{v_x.\cos(\varepsilon) + v_z.\sin(\varepsilon)}{\lambda} \tag{1.27}$$

where λ denotes the wavelength, ε denotes the elevation angle of the UAV with respect to the GEO satellite (cf. Figure 1.3) and $\vec{v} = (v_x, v_y, v_z)$ the speed of the aircraft. The expressed of the considered elevation angle ε is given in Equation (1.25).

Finally, the continuous complex fading gain of the LOS component is denoted by $\alpha_0(t)$ and expressed as:

$$\alpha_0(t) = \sqrt{\mathrm{P}_0}\ \exp(-2\pi j f_{\text{D-LOS}}\ t) \tag{1.28}$$

The corresponding delay is noted by τ_0 and is taken as a reference at the receiver:

$$\tau_0 = 0 \tag{1.29}$$

1.3.4.1 Expression of A2S channel:

The expression of the A2S channel is calculated as:

$$\mathrm{h}_a(t,\tau) = \sum_{n=0}^{\mathrm{N_m}-1} a_n(t)\ \delta(\tau-\tau_n) = \frac{1}{\sqrt{\mathrm{P}_0}}\ \alpha_0(t)\ \delta(\tau-\tau_0)\ \exp(2\pi j f_{\text{D-LOS}}\ t) = \delta(\tau) \tag{1.30}$$

Finally, we can deduct that the A2S channel is equivalent to AWGN channel:

$$\mathrm{h}_a(t,\tau) = \sum_{n=0}^{\mathrm{N_m}-1} a_n(t)\ \delta(\tau-\tau_n) = \delta(\tau) \tag{1.31}$$

1.3.5 Existing standards for return link (RTN): Physical layer

Two satellite standards will be reviewed in this section. An aeronautical ESA standard [2] and the traditional DVB-RCS(2) [38][37] [123].

1.3.5.1 ANTARES CS standard

The return link defined for the ANTARES communication standard is based on an asynchronous CDMA (A-CDMA) random access technique implementing a packet-based interference cancellation algorithm. A Dual-BPSK modulation scheme is selected, with user data transmitted on the I-channel and control data on the Q-channel. A Turbo Convolutional Code (TCC) with rate 1/3 is adopted as forward error correction (FEC) scheme.
Concerning physical layer, Table 1.6 summarizes its main technical characteristics. The return link access

Physical layer	
CS description	**Comments**
Access scheme	A-CDMA (E-SSA) (SF = 4 & SF = 16)
Modulations	Dual-BPSK
Coding schemes	Binary parallel TC (16 states) (1/3)
Pilot symbols	Not specified
Roll-off factor/s	$\beta = 0.2$
Guard time	Not specified
Symbol rates (R_s)	160 kchips
Framing	From 76.7 ms to 167.6 ms (depending on burst type)
Channelization	200 kHz chunks
Diversity techniques supported	Time diversity (interleaving)
Fading mitigation techniques	Spreading (SF = 4, SF = 16)
Power control	Not specified
CRC (Error detection)	Yes (4-byte CRC at physical layer; optionally, additional 4-byte CRC to detect encapsulation errors)
Frequency band	Fixed link: Ku / Ka band Mobile link: L-band (AMS(R)S band)

Table 1.6: *Summary of ANTARES CS technical characteristics for RTN link*

scheme of the ANTARES CS, based on random access, provides an optimal performance with a bursty traffic profile, but it may be less suited for the more sustained traffic profile to be expected in RPAS C2. This should be further investigated. Finally, video cannot be supported, due to the limited data rates, even if 400 kHz channels are used.

1.3.5.2 DVB-RCS(2) standard

DVB-RCS (Digital Video Broadcasting - Return Channel by Satellite) is designed by adding a return channel to the DVB-S2 and gives an interactive way for the services via satellite. DVB-RCS is a mature open source satellite communication standard with highly efficient bandwidth management. This make it a cost-efficient alternative solution for many users. It also provides an established foundation for further satellite communications research. The 5th revision of the DVB-RCS standard was completed in 2008. A major update included the very first broadband mobile standardization [37]. This extended version, formally referred to as "ETSI EN 301 790 v 1.5.1" [44] is also known as "DVB-RCS+M". The "+M" version added several new features, such as the ability to use "DVB-S2" bursts in the uplink channel back to the satellite. It incorporates signal fade mitigation techniques and other solutions to combat short term signal loss [1].
The core of DVB-RCS/RCS2 is a multi-frequency Time Division Multiple Access (MF-TDMA) transmission scheme for the return link, which provides high bandwidth efficiency for multiple users. In addition, DVB-RCS2 also includes CPM for use with amplifiers in saturated mode.

Concerning physical layer, Table 1.7 summarizes its main technical characteristics.

Physical layer	
DVB-RCS(2) description	**Comments**
Access scheme	MF-TDMA
Modulations	Linear Modulation: QPSK, 8-PSK and 16QAM Continuous Phase Modulation CPM: linear combination of RC and REC pulses shapes.
Coding schemes	-For linear modulation: a 16-states duo-binary turbo code (the original RCS adopted 8-states duo-binary turbo code). - For CPM: a convolutional code with constraint length equal to 3 or 4.
Pilot symbols	The repetition of, size of, content of the pilot block are configurable
Roll-off factor/s	For linear modulation: $\beta = 0.2$
Guard time	Not specified [37]
Symbol rates (R_s)	Not imposed. A maximum value is 2 Mbaud (with a spectral efficiency of 0.5 bit/s/Hz).
Channelization	Not specified
Diversity techniques supported	Not specified. A burst repetition may be applied and an interleave stage is specified
Power control	Not specified
Fading mitigation techniques	ACM procedure not specified
Frequency band	Fixed link: Ka/Ku band

Table 1.7: *Summary of DVB-RCS(2) technical characteristics for RTN link*

Concerning the physical layer, DVB-RCS2 has the advantage to propose a CPM scheme which relaxes the constraints on the UT HPA. However, the corresponding FEC scheme is a convolutional code which may be not sufficient with respect to the link budget. Maybe, a specific FEC scheme has to be developed in order to

increase physical layer performances.

Even if an aeronautical scenario has been taken into account, the antenna configuration that has been considered for simulations has to be consolidated. Indeed, the referenced paper concerning this scenario [37] has considered tracking and directive antenna, which has a direct impact on channel model and link budget.

1.4 Terrestrial Data Links: The mission link

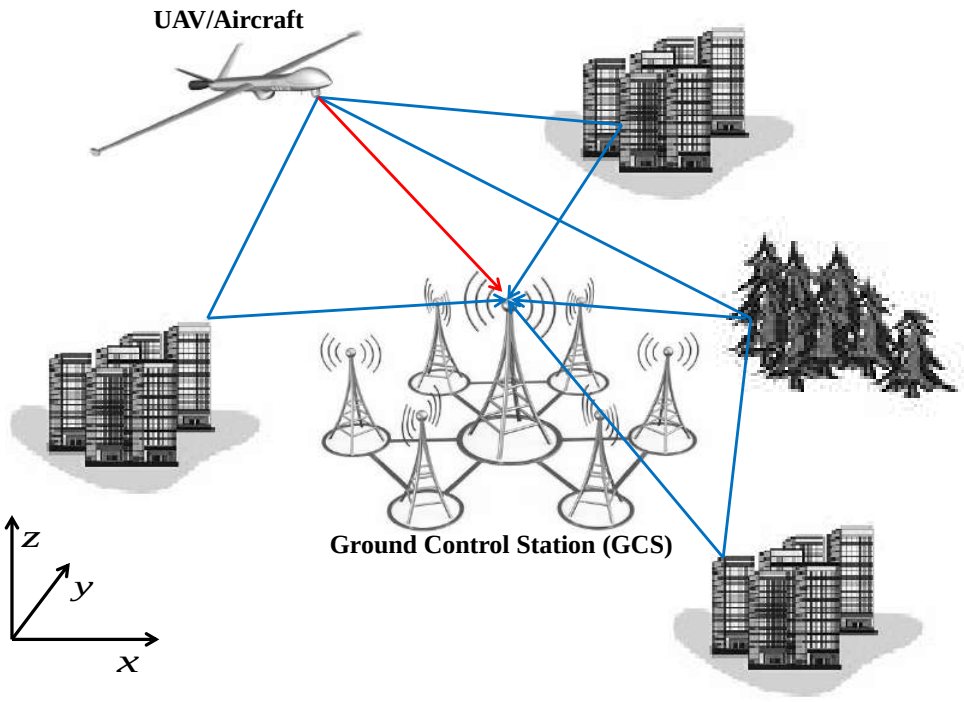

Figure 1.8: *Illustration of the geometry of the air-to-ground (A2G) communication channel. LOS path is illustrated with red, reflected paths with blue.*

1.4.1 Air-to-Ground (A2G) Channel Model

In this Section, we are interested in wideband-type A2G channels for the mission link. In the mission link, we have to deal with a multipath channel: the transmitted signal arrives at the receiver from various paths (see Figure 1.8) of different lengths and strengths. Assuming LOS communication, the aeronautical Aircraft-to-Ground (A2G) channel is characterized by two types of paths: a line-of-sight (LOS) path and other scattered components (reflected paths).

Environment	Low elongation low altitude	High elongation Median altitude	High elongation High altitude
Urban	NLOS	LOS	LOS
Flat desert	LOS	LOS	LOS
Mountainous	LOS	LOS	LOS
Coastal	LOS	LOS	LOS
Rural	LOS	LOS	LOS

Table 1.8: *Nature of aeronautical channels for different environments.*

1.4.2 General expression of the A2G channel

The air-to-ground (A2G) channel with time-variant baseband channel impulse response (CIR) $\mathrm{h}_a(t,\tau)$ in its most general form for a single-input single-output (SISO) antenna case is given by:

$$\begin{aligned}\mathrm{h}_a(t,\tau) = \sum_{n=0}^{\mathrm{N_m}-1} a_n(t)\ \delta(\tau-\tau_n) &= \frac{1}{\sqrt{\sum_{n=0}^{\mathrm{N_m}-1}\mathrm{P}_n}} \left\{\sum_{n=0}^{\mathrm{N_m}-1} \alpha_n(t)\ \delta(\tau-\tau_n)\right\} \exp\left(2\pi j f_{\text{D-LOS}}\ t\right) \\ &= \underbrace{a_0(t)\ \delta(\tau-\tau_0)}_{\text{LOS Component}} + \frac{1}{\sqrt{1+\mathrm{K_{LOS}}}} \underbrace{\sum_{n=1}^{\mathrm{N_m}-1} \widetilde{a}_n(t)\ \delta(\tau-\tau_n)}_{\text{ground reflected Components}}\end{aligned} \tag{1.32}$$

with $\mathrm{N_m}$ is the number of considered paths, P_0 is the power of the LOS path and for $n \geq 1$, P_n denotes the power of the n-th ground reflected path. The $\mathrm{K_{LOS}}$ factor is a ratio often taken in decibels that determines the power relationship between the LOS path and the other reflected paths. The ratio $\mathrm{K_{LOS}}$ is defined as:

$$\mathrm{K_{LOS}}\ [\mathrm{dB}] = 10\ \log_{10}\left(\frac{\mathrm{P}_0}{\sqrt{\sum_{n=1}^{\mathrm{N_m}-1}\mathrm{P}_n}}\right) \tag{1.33}$$

Note that in some environments, the LOS component is absent in most of time. For example, for an urban environment and in lower altitude, there is no visual line-of-sight (LOS) between the transmitting antenna and the receiving antenna ($\mathrm{P}_0 = 0$)[78]. In this context non-line-of-sight (NLOS) multipath channel is considered. Table.1.8 summarizes the nature of the aeronautical channel for different scenarios.

1.4.2.1 LOS path

The LOS path (illustrated with red color in Figure 1.8) arrives directly from aircraft to a Ground Control Station (GCS). The preponderant effect is the power of the LOS path compared to the other reflected paths. In the following we denote P_0 the power of LOS path. Another degradation impacting the LOS path is the propagation delay. Again, the delay of the LOS path τ_0 is not impacting, however the relative delay between the direct path and the other reflected path is impacting and will be detailed later. Note that the delay of

each reflected paths is denoted τ_l and measured relatively to the first detectable signal at the receiver at $\tau_0 = 0$ [105]. Finally, the last effect is the «Doppler-Shift». This Doppler can be classically calculated as follows:

$$f_{\text{D-LOS}} = \frac{\|\vec{v}\| . \cos(\varepsilon)}{\lambda} \tag{1.34}$$

where λ denotes the wavelength, ε denotes the elevation angle of the UAV/aircraft with respect to the GCS antenna and $\vec{v} = (v_x, v_y, v_z)$ the speed of the aircraft.

Assuming H_a is the altitude of the aircraft, H_{GCS} is the GCS height and D is the horizontal distance separating the aircraft and the GCS antenna. As shown in Figure 1.9, based on geometrical considerations, the elevation angle ε can determinated as follows:

$$\varepsilon = \arctan\left(\frac{\text{H}_a - \text{H}_{\text{GCS}}}{\text{D}}\right) \tag{1.35}$$

Assuming a typical UAV/aircraft altitude of 2100 m, a GCS antenna height of 10 m and an horizontal distance of 3000 m, one obtains $\varepsilon = 33.5^{\circ}$.

Finally, the continuous complex fading gain of the LOS component is denoted by $\alpha_0(t)$ and expressed as:

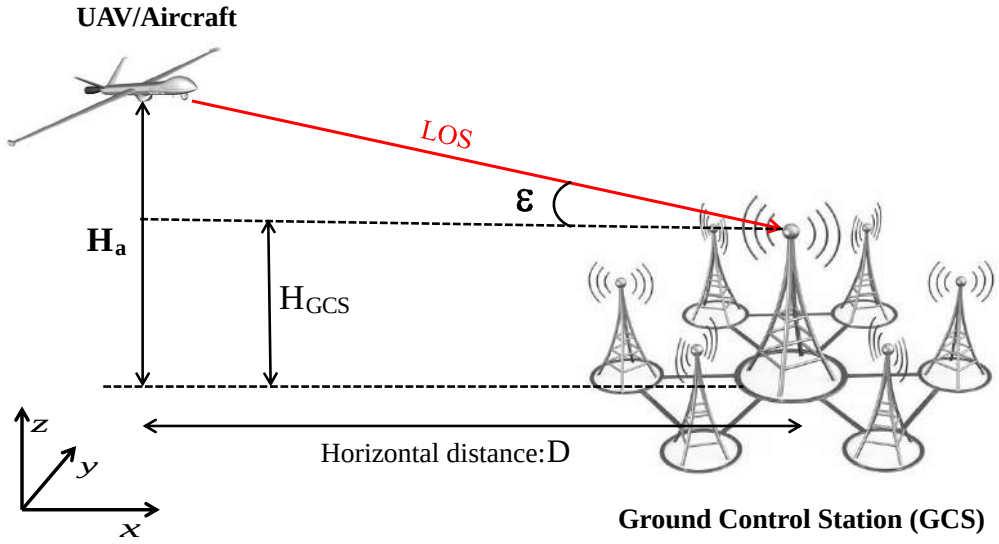

Figure 1.9: *Elevation angle based on geometrical considerations.*

$$\alpha_0(t) = \sqrt{\text{P}_0}\ \exp\left(-2\pi j f_{\text{D-LOS}}\ t\right) \tag{1.36}$$

and thus we can deduce that the normalized fading, $a_0(t)$, is time-invariant and having a constant value denoted by A_{LOS} and calculated as:

$$a_0(t) = \text{A}_{\text{LOS}} = \sqrt{\frac{\text{P}_0}{\sum_{n=0}^{\text{N}_\text{m}-1} \text{P}_n}} = \sqrt{\frac{\text{K}_{\text{LOS}}}{1+\text{K}_{\text{LOS}}}} \tag{1.37}$$

The corresponding delay is noted by τ_0 and is taken as a reference at the receiver:

$$\tau_0 = 0 \tag{1.38}$$

1.4.2.2 Reflected paths

The presence of reflected components makes the A2G channel model be a mutipath model. This phenomenon happens because the environment in which the aircraft flies is composed of several obstacles, both natural and artificial, which are located randomly on the ground. Rivers, mountains and buildings are examples of elements that can alter the signal physical characteristics, imposing different attenuations and phase changes. This random features of the environment makes it necessary to model the channel using a statistical approach. Over time a large number of distributions were proposed for various specifics cases. For simplification reasons, we assume that we have a number of $N_m - 1$ reflected paths. Each one has a continuous complex fading gain denoted by $\alpha_n(t)$ and a corresponding propagation delay denoted by $\tau_n > 0$ for $1 \leq n \leq N$. The time-correlation function of each complex variable $\alpha_n(t)$ depends on the so-called «Doppler-Spread» which is the most impacting. Additionally, the variable $\alpha_n(t)$ includes the «Doppler-Shift» phenomenon. the «Doppler-Shift» degradation is not very impacting. We denote P_n as the power of the n-th reflected path and it is given by:

$$P_n = \mathbb{E}\left\{|\alpha_n(t)|^2\right\} \tag{1.39}$$

The powers $\{P_n\}$ can be estimated by simulation. Indeed, the average number of signal components per delay interval can be considered as a good estimation of the power delay. By dividing by the total number of simulation we can obtain an histogram of received signal components and thus we can deduct the so-called «per delay bin probability». For a very large number of observations, the power per delay histogram is assumed to follow a Gaussian distribution with appropriate mean and standard deviation based on the geometry of the scene.

For instance, in [90], the table 1.9 is the result of simulation of 10000 PDPs. As typical values of delays and

Delay Range $[ns]$	**Average Number of Signal Components per Delay Bin**	**Delay Range** $[ns]$	**Average Number of Signal Components per Delay Bin**
$0-97$	2980/10000	$778-875$	167/10000
$97-195$	1530/10000	$875-973$	180/10000
$195-292$	1190/10000	$973-1070$	107/10000
$292-389$	620/10000	$1070-1167$	66.4/10000
$389-486$	404/10000	$1167-1264$	38.9/10000
$486-584$	253/10000	$1264-1362$	22.8/10000
$584-681$	163/10000	$1362-1459$	26.5/10000
$681-778$	167/10000	$1459-1556$	13.9/10000

Table 1.9: *Average Number of Signal Components per Delay Bin for an Elevation Angle of* $7.5°$ *[90] W. G. Newhall, R. Mostafa, C. Dietrich, C. R. Anderson, K. Dietze, G. Joshi, and J. H. Reed, « Wideband air-to-ground radio channel measurements using an antenna array at 2 GHz for low altitude operations,» Military Communications Conference, vol. 2, pp. 1422-1427, October 2003. Used under fair use, 2015.*

corresponding powers, literature [90] give a Power Delay Profile (PDP) with $N_m - 1 = 7$ which is defined by a

delay vector $\tau = [\tau_1, \tau_2, \ldots, \tau_7]$ and a corresponding power vector $\mathrm{P} = [\mathrm{P}_1, \mathrm{P}_2, \ldots, \mathrm{P}_7]$ given as:

$$\begin{cases} \tau & = [33, 70, 115, 175, 262, 405, 682] \quad (in\ nanoseconds) \\ 10.\log_{10}(\mathrm{P}) & = [-8.7, -9.6, -11.3, -13.4, -15.2, -17.0, -20.2] \quad (in\ decibels) \end{cases} \tag{1.40}$$

1.4.2.3 Doppler Effect

The scenario is characterized by fast fading: $\|\vec{v}\| = 25..40\ m/s$ [53]. During the arrival of the base station, the scattered components are typically not isotropically distributed, i.e. the beamwidth of the scattered components $\Delta_\varphi = |\varphi_{\mathrm{aH}} - \varphi_{\mathrm{aL}}|$ is less than 360° [53] and Δ_φ represents the beamwidth of arrival angles. In [36], a beamwidth less than 360° was considered and a corresponding Doppler Power Spectrum Density (D-PSD) was derived, assuming that the scatterers are uniformly distributed within the beamwidth. This non-isotropically distribution results in a Doppler probability density function P(f), that is only a part of the classical 2-D isotropic Doppler density function derived by Clarke distribution [26, 46]:

$$\text{D-PSD}(f) = \frac{1}{2.\pi.\frac{\Delta_\varphi}{360}\ f_{\max}\ \sqrt{1 - \left(\frac{f}{f_{\max}}\right)^2}} \tag{1.41}$$

$$f_{\max}\ \cos(\varphi_{\mathrm{aH}}) \leq f \leq f_{\max}\ \cos(\varphi_{\mathrm{aL}}) \qquad ; \qquad f_{\max} = \frac{\|\vec{v}\|}{\lambda}$$

1.4.2.4 Propagation delays

A simple geometrical analysis reveals that $\Delta d \approx \mathrm{H}_a$ [53] for air-ground links, if one dominant reflector is present, where H_a is the altitude of the aircraft. This geometrical analysis is based on the fact that during the flight, the aircraft distance to the base station is large compared to its altitude, so that the projected distance on the ground is about the same as the real distance. If now reflection, scattering, or diffraction occur on objects on the ground, the maximum detour distance can be estimated to be the aircraft altitude for air-ground communication:

$$\tau_{\max} = \frac{\Delta d}{3.10^8} \approx \frac{\mathrm{H}_a}{3.10^8} \tag{1.42}$$

Assuming a typical maximum altitude of 2100 m [16], one obtains $\tau_{\max} = 7000\ ns$.

1.4.2.5 Some existing Wideband A2G channels:

In literature, several wideband channels are studied. For example in 2003, the author of paper [90] gives some characteristics of wideband A2G channel considering LOS path. The considered elevation angle $\varepsilon \in \{7.5°; 15°; 22.5°; 30°\}$. In this case, an omni-directional antenna is implemented at the UAV/aircraft transmitter with a height from 450 to 950 Above Ground Level (AGL). In 2011, paper [69] shows some parameters of wideband A2G channel considering UAV/aircraft heights of 5000/8000/11000 Above mean sea level (AMSL), the UAV and the GCS antennas are both omni-directional. For this channel, the number of path is approximately equal to 1 i.e. mainly LOS path. This channel presents a minimum coherence bandwidth of 500 Hz ($\mathrm{B}_c^{\min} \approx 500$ Hz) and a coherence time of 85μs ($\mathrm{T}_c \approx 85\mu s$).

REF	Frequency [MHz]	Antenna (Elevation Beamwidth) UAV/Aircraft Omni.	UAV/Aircraft Direc.	GCS Omni.	GCS Direc.	(Antenna) Height [m] UAV/Aircraft: H_a	GCS: H_{GCS}	Ground Environment
[76]	960-977 5,000-5,100	✖	Cosine	✖	$2\times35°$ Antennas $2\times81°$ Antennas	$H_a^{max}=12,500$	3.5-18.3 + ?	Cleveland & Oxnard
[107]	1,510.5 1,460.5 2,344.5 2,360.5	✔	✖	✖	6° 6° 3° 6°	1,525/3,050 AMSL	2.5 (Antenna) + 700 AMSL 4.5 (Antenna) + 700 AMSL	Mountainous Desert
[90]	2,050	✔	✖	4-Array	✖	$450\leq H_a\leq 950$ AGL	GL	College Campus
[69]	5,120	✔	✖	✔	✖	5,000/8,000/11,000 AMSL	18 (Antenna) + 750 AMSL	Sonthofen (Germany)
[17]	5,135	✔	✖	✖	Dish (d=2.4 m)	Taxiing, Take-off, En-route	Airbus Saint-Martin site	Saint-Martin (Airbus)
[84]	5,700	✔	✖	✖	$2\times25°$ Antennas	370/970/1,830	2.10 + ?/7.65 + ?	Sea Surface

Table 1.10: *Wideband Configuration for Air-to-Ground Measurements (Vertical Polarization) [65]*

REF	N_m min	N_m max	τ_{RMS} [μs] average	τ_{RMS} [μs] max	Doppler Spectrum[kHz]	B_c^{min} [kHz]	T_c [μs]	Comments
[76]	≈ 3		-	0.050	-	4000	-	Oxnard C-band measurement case
[107]	3		0.074	-	-	-	-	-
[90]	≈ 8		0.09825	0.485	-	≈ 410	-	Use of elevation angles ε: 7.5°, 15°, 22.5°, 30°
[69]	1 (mainly LOS)		0.0384	0.398	[-5; 5]	≈ 500	≈ 85	$\|\vec{v}\|$=293 m/s, Bandwidth=20 MHz, STD (τ_{RMS})=0.021 μs
[17]	1		-	-	[-3.6; 4.1]	-	≈ 105	Time Delay MPC for en-route not considered.
[84]	2 or 3	7	-	0.480	-	≈ 420	-	Max RMS for Channel 2 (GCS Height: 2.10 m) and altitude 370 m

Table 1.11: *Resulting (Estimated) Channel Parameters [65]*

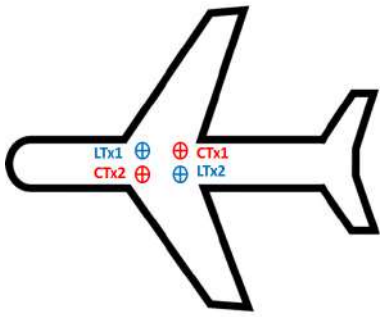

Figure 1.10: *Position of Tx/Rx antennas in underside of the aircraft.*

Other examples of wideband A2G channels are shown in Tables 1.10 and 1.11 presenting wideband configuration for each A2G channel example as well as the corresponding channel parameters.

1.4.2.6 Final expression of A2G channel

By using the definition of $\mathrm{K_{LOS}}$ factor, the expression of the A2G channel can be expressed by the following expression:

$$\mathrm{h}_a(t,\tau) = \sum_{n=0}^{\mathrm{N_m}-1} a_n(t)\ \delta(\tau-\tau_n) = \sqrt{\frac{\mathrm{K_{LOS}}}{1+\mathrm{K_{LOS}}}}\ \delta(\tau)\ +\ \frac{1}{\sqrt{1+\mathrm{K_{LOS}}}}\ \sum_{n=1}^{\mathrm{N_m}-1} \widetilde{a}_n(t)\ \delta(\tau-\tau_n) \tag{1.43}$$

Note that we consider a normalized aeronautical channel response:

$$\sum_{n=1}^{\mathrm{N_m}-1} \mathbb{E}\left\{|\widetilde{a}_n(t)|^2\right\} = 1 \tag{1.44}$$

1.4.3 MIMO technology for the aeronautical communications

One of the most promising avenues for achieving a constant and stable communication link is multi-antenna technology (MIMO). Multiple antennas allow the aircraft and Ground Stations to improve performance. Today the planes are able to communicate with ground stations in the two frequency bands allocated for UAS: in L-band from $960-977$ MHz and in C-band from $5030-5091$ MHz. For the mission link, signals will be transmitted via two antenna in the C-band CTX1 and CTx2 (respectively LTX1 and LTx2 in L-band). Figure 1.10 shows the location of the two receiver (Rx) antennas and the other two transmit antennas under the aircraft. The distance between L-band Rx1 and C-band Tx2 (or between C-band Rx1 and L band Tx2) antennas is 1.32 m[80].

In Multiple-Input Multiple-Output (MIMO) communication, we consider a number of $\mathrm{N_t}$ transmit antennas at emission and a number of $\mathrm{N_r}$ receive antennas at reception. The expression of the Single-Input Single-Output (SISO) A2G channel between the transmit antenna $1 \leq n_\mathrm{t} \leq \mathrm{N_t}$ element and the receive antenna $1 \leq n_\mathrm{r} \leq \mathrm{N_r}$ element is noted $\mathrm{h}_a^{(n_\mathrm{r},n_\mathrm{t})}(t,\tau)$ and its expression is deduced from (1.43) as:

$$\mathrm{h}_a^{(n_\mathrm{r},n_\mathrm{t})}(t,\tau) = \sqrt{\frac{\mathrm{K_{LOS}}}{1+\mathrm{K_{LOS}}}}\ \delta(\tau)\ +\ \frac{1}{\sqrt{1+\mathrm{K_{LOS}}}}\ \widetilde{h}_a^{(n_\mathrm{r},n_\mathrm{t})}(t,\tau) \tag{1.45}$$

where $\widetilde{h}_a^{(n_r,n_t)}(t,\tau)$ is a normalized channel referring the resulting ground reflected channel between the n_t transmit antenna element and the n_r receive antenna element:

$$\widetilde{h}_a^{(n_r,n_t)}(t,\tau) = \sum_{n=1}^{N_m-1} \widetilde{a}_n^{(n_r,n_t)}(t)\ \delta(\tau-\tau_n) \tag{1.46}$$

1.5 Summary

In this chapter, we presented an aeronautical communication system description which constitutes the core of our study. We considered three main links: the forward link, the return link and the mission link. For each link, a detailed link budget is provided. Two satellite data links are considered: the forward (uplink) and return (downlink) links. The role of the satellite in an aeronautical communication is specified. The satellite is assumed be transparent and geo-stationary. A special focus was given on the existing channel models. Three channel models are presented: a satellite-to-aircraft (S2A) channel model, a aircraft-to-satellite (A2S) channel model and a air-to-ground (A2G) channel model. For the two satellite data links, forward and return links, two satellite standards are available. An aeronautical ESA standard, ANTARES CS, and the traditional DVB-S2(X)/DVB-RCS(2). For the terrestrial link, we are interested in the mission link (data gathering link). Until today, no existing standard is proposed in that case for civil applications. Table 1.12 summarizes this chapter.

Link	Channel	Rquired SNR	Existing Standads	Comments
FWD	S2A channel expressed in (1.22) ($N_m = 3$) mainly two paths	3.8 dB	ANTARES CS	- Modulation: QPSK, 8-PSK, 16-APSK - IRA LDPC Codes (1/4,1/3,1/2, 2/3) - RRC Shaping filter β=0.2
			DVB-S2/S2x	- QPSK, 8-PSK, 16-APSK, 32-APSK - IRA LDPC Codes (from 1/4 to 9/10) - RRC: $\beta \in \{0.35, 0.25, 0.2, 0.15, 0.10, 0.05\}$
RTN	A2S channel expressed in (1.31) ($N_m = 1$) AWGN channel	3.8 dB	ANTARES CS	- Modulation: Dual-QPSK - Binary parallel TC (16 states) (1/3) - RRC Shaping filter β=0.2
			DVB-RCS(2)	- QPSK, 8-PSK, 16-QAM / CPM - TC (LM) / CC (CPM) - RRC/RC: β=0.2
Mission	A2G channel expressed in (1.43) ($N_m = 8$) Existing LOS path	14 dB	No existing standard for civil applications	- Characterized by LOS path. - Wide range K_{LOS} factor. - $K_{LOS} \in]-\infty, 15]$ dB - High-throughput data is required. - Possibility of MIMO communications - Problem of UAV endurance

Table 1.12: *Summary*

1.6 Recommendations

At this stage of the study, what can be said is no existing standard cope with all the requirements of the application. This means that since adaptations are required, it may be much easier to finally make a new waveform, instead of patching existing ones with no insurance of success and with a waveform that may not be scalable for the future. Moreover, making a new waveform will let the possibility to consider both the terrestrial and satellite links in a hybrid manner which will able the RPAS to use only one terminal for all links. This will be suitable for the equipment weight and for the power consumptions which are two issues for this application.

Chapter 2

Single-carrier communications over frequency selective channels

Sommaire

2.1 Introduction

There is a growing need for modern data communications in the aeronautical world with applications such as aircraft/Unmanned Aerial Vehicle (UAV), Air Traffic Control (AOC) and Airline Operational Control (ATC) communications. The growing capacity requirements of aeronautical applications has led to the design of new waveforms improving spectral efficiency ad with constraints on the complex envelope of the signal.
In this context, Single-Carrier waveforms are one of the considered solution. Indeed, SC linear modulations are practical waveforms for channels which are selective in frequency but with limited delay spread. Furthermore, SC guarantees a low Peak-to-Average Power Ratio (PAPR) which allows a more efficient use of High Power Amplifiers (HPAs).

Besides, several studies are launched to design new spectrally efficient waveforms. In satellite context, Single Carrier Orthogonal Frequency-Division Multiplexing (SC-OFDM) appears to be a promising waveform thanks to its low Peak-to-Average Power Ratio (PAPR) compared to OFDM [49]. Its construction in the frequency domain as OFDM is an advantage for low complexity frequency domain equalization. Recently, studies demonstrate that Extended Weighted SC-OFDM can offer better spectral occupancy than SC-OFDM by adding a spectral filtering to shape transmit symbols in the frequency domain. So, EW SC-OFDM is also an interesting waveform in the satellite context.

In order to study the viability of SC and EW SC-OFDM waveforms within UAV communication via satellite link, this chapter gives an overview of these two interesting waveforms and study existing algorithms in order to propose new adequate solutions. Moreover, SC and EW SC-OFDM waveforms are presented in both Nyquist and Faster-Than-Nyquist (FTN) contexts. The use of FTN signaling allows for the increase of the spectral efficiency.

2.2 Communication system model

For system model, we consider a frame based transmission. Moreover, we assume that each frame contains a number of N_f sub-frames and each sub-frame contains a number of N modulated data symbols. Furthermore, we assume that the digital communication system uses linear M-ary modulation. The considered M-ary constellations are drawn from a discrete alphabet $\chi = \{\mathcal{C}_1, \mathcal{C}_2, \ldots, \mathcal{C}_M\}$. Furthermore, we consider a Root Raised Cosine (RRC) shaping filter $h_e(t)$ as the transmit shaping filter with known parameters such as β, the

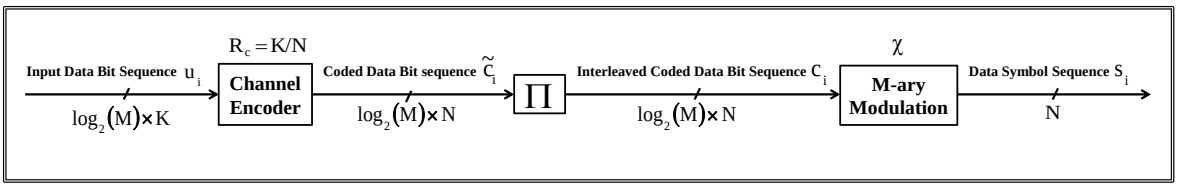

Figure 2.1: *M-ary Bit Interleaved Coded Modulation*

roll-off factor, and the Nyquist bandwidth B_h. The considered Nyquist bandwidth is expressed as follows:

$$\mathrm{B}_h = \frac{1+\beta}{\mathrm{T}_h} \tag{2.1}$$

where T_h is the Nyquist symbol duration.

At the transmitter, we consider an information bit sequence denoted by $\mathbf{u}_i = \left[u_{i,1}, u_{i,2}, \ldots, u_{i,K\times\log_2(M)}\right]^T$ of size $K \times \log_2(M)$ independent random bits, to be transmitted over a communication channel $\mathrm{h}_a(t,\tau)$. The transmission of the information bit sequence $\mathbf{u}_i$ follows the steps presented in Figure 2.1. First, $\mathbf{u}_i$ is encoded into N symbols using a M-ary Bit Interleaved Coded Modulation (BICM): $\mathbf{u}_i$ is encoded into a binary codeword $\widetilde{\mathbf{c}}_i = \left[\widetilde{c}_{i,1}, \widetilde{c}_{i,2}, \ldots, \widetilde{c}_{i,N\times\log_2(M)}\right]^T$ by using an error correcting code with rate $\mathrm{R}_c = K/N$, then $\widetilde{\mathbf{c}}_i$ is interleaved to obtain a bit sequence $\mathbf{c}_i = \left[c_{i,1}, c_{i,2}, \ldots, c_{i,N\times\log_2(M)}\right]$ and finally $\mathbf{c}_i$ is modulated using the M-ary modulation to give the data sequence denoted by $\mathbf{s}_i = [s_{i,1}, s_{i,2}, \ldots, s_{i,N}]$. The symbols $\{s_{i,n}\}$ are drawn from a discrete alphabet χ and having a symbol variance equal to σ_s^2. Furthermore, $\{s_{i,n}\}$ are separated by a symbol duration $\mathrm{T}_s = \nu.\mathrm{T}_h$. In order to improve the spectral efficiency, we assume using Nyquist/FTN signaling characterized by an acceleration factor denoted by ν and expressed as follows:

$$0 < \nu = \frac{\mathrm{T}_s}{\mathrm{T}_h} \leq 1 \tag{2.2}$$

The positive scalar ν denotes the acceleration factor and its values are taking between 0 and 1 ($0 < \nu \leq 1$). Note that, in the case where $\nu = 1$, we can assume Nyquist communication. For the other cases i.e. $\nu < 1$, Faster-than-Nyquist (FTN) communication is considered. The symbol variance σ_s^2, of the obtained data symbol, is calculated as follows:

$$\sigma_s^2 = \frac{1}{M}\sum_{m=1}^{M} |\mathcal{C}_m|^2 = \frac{\mathrm{E}_s}{\mathrm{T}_s} = \mathrm{E}_s \times \mathrm{R}_s \tag{2.3}$$

where $\mathrm{R}_s = \frac{1}{\mathrm{T}_s}$ is the symbol rate and $\mathrm{E}_s = \sigma_s^2 \times \mathrm{T}_s$ is the symbol energy.

On other hand, another sequence of $N_\mathrm{p} \leq N$ training symbols, denoted by $\mathbf{x} = \left[x_1, x_2, \ldots, x_{N_\mathrm{p}}\right]$, will be inserted in each transmitted sub-frame in order to estimate equivalent base-band channel response. Note that training symbols $x_1, x_2, \ldots, x_{N_\mathrm{p}}$ are perfectly known at the receiver. The symbol variance of the training sequence is noted σ_p^2 and is assumed to be equal to data symbol variance σ_s^2 i.e. $\sigma_p^2 = \sigma_s^2$. Additionally, for transmit data symbols, the sub-frame duration is equal to $N \times \mathrm{T}_s$ verifying:

$$\frac{1}{\mathrm{B}_c} \leq (N + N_\mathrm{p}) \times \mathrm{T}_s \leq \mathrm{T}_c \tag{2.4}$$

where, T_c and B_c denotes respectively the coherence time and the coherence bandwidth of the communication channel $\mathrm{h}_a(t,\tau)$.

For the i-th transmit sub-frame, by respecting its coherence time T_c, the communication channel, $\mathrm{h}_a(t,\tau)$, becomes a time-invariant channel:

$$\mathrm{h}_a(t,\tau) = \sum_{n=0}^{\mathrm{N_m}-1} a_n(t).\ \delta(\tau - \tau_n) \approx \sum_{n=0}^{\mathrm{N_m}-1} a_{i,n}.\ \delta(\tau - \tau_n) \approx \mathrm{h}_a(\tau) \tag{2.5}$$

where, $a_{i,n} \in \mathbb{C}$ and τ_n are respectively the attenuation and the delay of the n-th path and $\mathrm{N_m}$ is the number of considered paths. Moreover, we assume that we have $\tau_0 \leq \tau_1 \leq \ldots \leq \tau_{\mathrm{N_m}-1}$ and,

$$\sum_{n=0}^{\mathrm{N_m}-1} \mathbb{E}\left\{|a_{i,n}|^2\right\} = 1 \tag{2.6}$$

2.3 Classical Single-carrier waveform

Thanks to its low PAPR, SC waveform appears to be an interesting waveform in a satellite context. SC is a classical waveform which is considered for many communication systems notably in mobile networks. Furthermore, SC waveform is often considered where the channel impulse response (CIR) presents a weak delay spread. This is the case for the aeronautical channel response regarding the forward link. Therefore, SC can be a good candidate for forward link.

In this Section, we study SC waveform for both Nyquist/FTN signaling. The transmitter and the receiver structures are shown in Figure 2.2.

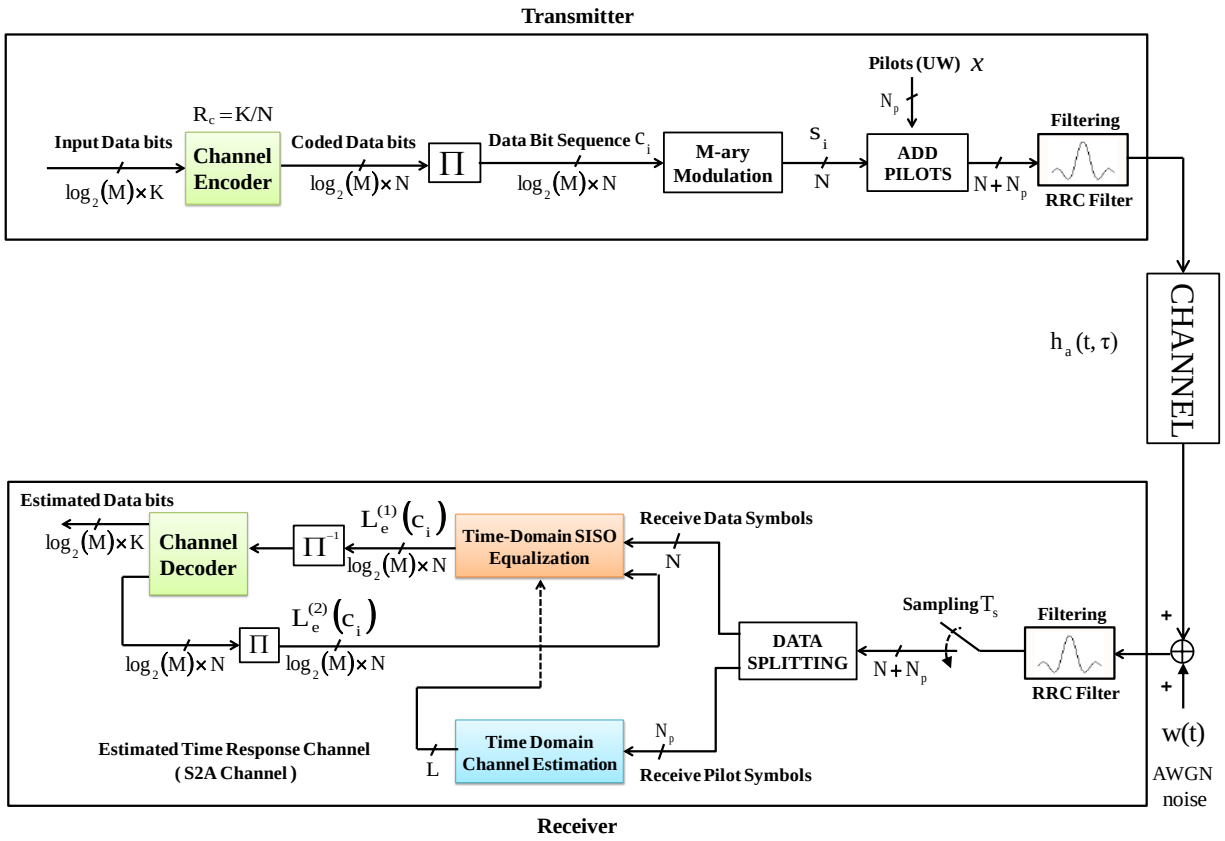

Figure 2.2: *Transmitter and receiver scheme for SC waveform*

2.3.1 Continuous equivalent baseband channel

At transmitter, the symbol sequence corresponding the i-th sub-frame and denoted by $\widetilde{\mathbf{s}}_i = [\mathbf{x}, \mathbf{s}_i]$ (or also we can assume this notation $\widetilde{\mathbf{s}}_i = \left[\widetilde{s}_{i,1}, \widetilde{s}_{i,2}, \ldots, \widetilde{s}_{i,N_\mathrm{p}+N}\right]$) is filtered by a normalized transmit shaping filter $\mathrm{h}_e(t)$ verifying:

$$\sum_{l=-\infty}^{+\infty} \left|h_e\left(l.\mathrm{T}_s\right)\right|^2 = \sum_{l=-\infty}^{+\infty} \left|h_e\left(l.\nu.\mathrm{T}_h\right)\right|^2 = 1 \qquad \forall \quad 0 < \nu \leq 1 \tag{2.7}$$

As a result, the expression of the transmitted signal corresponding to the i-th sub-frame is given as follows:

$$e_i\left(t\right) = \sum_{l=1}^{N+N_\mathrm{p}} h_e(t - l.\mathrm{T}_s)\ \widetilde{s}_{i,l} \tag{2.8}$$

The obtained transmitted signal will be sent over a time-invariant communication channel $\mathrm{h}_a(\tau)$. At the receiver, a zero-mean complex Additive White Gaussian Noise (AWGN) $w(t)$ will be added to receive signal. As a result, a received signal $r_i(t)$ corresponding to the i-th sub-frame is obtained. Then, after partial matched filtering, $r_i(t)$ is filtered by a RRC receive filter $h_r(t) = h_e^*(-t)$ before being sampled in each symbol duration T_s. After sampling two possible signals will be detected: the training symbol sequence and the data symbol sequence. The training symbol sequence will be used to estimate equivalent baseband channel. The received data symbol sequence will be used to detect transmit data symbol sequence $\mathbf{s}_i$.

The received signal $r_i(t)$ corresponding to the i-th frame can be written as follows:

$$r_i(t) = \left\{e_i(t) * \mathrm{h}_a(\tau)\right\}(t) + w(t) = \sum_{l=1}^{N+N_\mathrm{p}} \left\{h_e(t) * \mathrm{h}_a(\tau)\right\}(t - l.\mathrm{T}_s)\ \widetilde{s}_{i,l} + w(t) \tag{2.9}$$

where $*$ denotes the convolution operator and $w(t)$ is a centered complex AWGN noise with twosided spectral density equal to N_0.

The received signal $r_i(t)$ is filtered by a receive RRC filter $h_r(t) = h_e^*(-t)$. As a result, a continuous filtered signal $\widetilde{r}_i(t)$ is obtained and its expression is given as:

$$\begin{aligned}\widetilde{r}_i(t) = \left\{r_i(t) * h_r(t)\right\}(t) &= \sum_{l=1}^{N+N_\mathrm{p}} \left\{\mathrm{h}_e(t) * \mathrm{h}_a(\tau) * \mathrm{h}_r(t)\right\}(t - l.\mathrm{T}_s)\ \widetilde{s}_{i,l} + \left\{w(t) * h_r(t)\right\}(t) \\ &= \sum_{l=1}^{N+N_\mathrm{p}} \left\{\mathrm{h}_e(t) * \mathrm{h}_a(\tau) * \mathrm{h}_r(t)\right\}(t - l.\mathrm{T}_s)\ \widetilde{s}_{i,l} + w_c(t)\end{aligned} \tag{2.10}$$

where $w_c(t) = \left\{h_r(t) * w(t)\right\}(t)$ denoted the resulting additive filtered noise.

Considering linear modulation, the equivalent baseband channel is a time-invariant linear multipath channel. The continuous-time baseband channel corresponding to the i-th sub-frame is denoted by $\mathrm{h}_i(\tau)$ and is determinated as the convolution of the three filters in series; i.the RRC transmit shaping filter $\mathrm{h}_e(t)$, ii.the communication channel $\mathrm{h}_a(\tau)$ and iii. the receive RRC filter $\mathrm{h}_r(t)$. Thus, the expression of $h_i(\tau)$ can be given as:

$$\mathrm{h}_i(\tau) = \mathrm{h}_e(t) * \mathrm{h}_a(\tau) * \mathrm{h}_r(t) = \left\{\mathrm{h}_e(t) * \mathrm{h}_r(t)\right\}(t) * \mathrm{h}_a(\tau) = \mathrm{g}(t) * \mathrm{h}_a(\tau) = \sum_{n=0}^{\mathrm{N_m}-1} a_{i,n}.\ \mathrm{g}(t - \tau_n) \tag{2.11}$$

where $\mathrm{g}(t)$ is a Raised Cosine (RC) filter:

$$\mathrm{g}(t) = [\mathrm{h}_e(t) * \mathrm{h}_r(t)](t) \tag{2.12}$$

The coefficients of RC filter $\mathrm{g}(t)$ verify:

$$\mathrm{g}(0) = 1 \qquad \text{and} \qquad \mathrm{g}(l.\mathrm{T}_h) = 0 \qquad \forall \qquad l \in l \in \mathbb{Z}^* \tag{2.13}$$

After defining the continuous equivalent base-band channel $\mathrm{h}_i(\tau)$, the expression of the continuous-time filtered received signal $\widetilde{r}_i(t)$ can be reduced to:

$$\widetilde{r}_i(t) = \sum_{l=1}^{N+N_\mathrm{p}} \mathrm{h}_i(t - l.\mathrm{T}_s)\ \widetilde{s}_{i,l} + w_c(t) \tag{2.14}$$

2.3.2 Discrete-time equivalent baseband channel

The received signal $\widetilde{r}_i(t)$ is sampled in each symbol duration T_s. As a result, a sequence of $N + N_\mathrm{p}$ samples will be obtained. Each obtained sample $\widetilde{r}_{i,n}$ for $1 \leq n \leq N + N_\mathrm{p}$ can be expressed as:

$$\begin{aligned}\widetilde{r}_{i,n} = \widetilde{r}_i(n.\mathrm{T}_s) &= \sum_{l=1}^{N+N_\mathrm{p}} h_i([n-l].\mathrm{T}_s)\ \widetilde{s}_{i,l} + w_c(n.\mathrm{T}_s) = \sum_{l=-\infty}^{+\infty} h_i(l.\mathrm{T}_s)\ \widetilde{s}_{i,n-l} + w_c[n] \\ &\approx \sum_{l=-L/2}^{+L/2} h_i(l.\mathrm{T}_s)\ \widetilde{s}_{i,n-l} + w_c[n]\end{aligned} \tag{2.15}$$

The positive peer integer L specifies the memory of the system and is the smallest value such that $h_i(l.\mathrm{T}_s) = 0$, $|l| > L/2$.

The resulting additive noise vector $\mathbf{w}_c = (w_c[1], w_c[2], \ldots, w_c[N + N_\mathrm{p}])$ is a zero-mean Gaussian noise vector verifying:

$$\mathbb{E}\{w_c[n].w_c^*[n+l]\} = \mathrm{N}_0.\ \mathrm{R}_s.\ \mathrm{g}(l.\mathrm{T}_s) = \sigma_w^2.\ \mathrm{g}(l.\mathrm{T}_s) \tag{2.16}$$

with $\sigma_w^2 = \mathrm{N}_0.\ \mathrm{R}_s$ is the noise variance. Note that, in Nyquist signaling i.e. $\mathrm{T}_s = \mathrm{T}_h$ the additive noise vector $\mathbf{w}_c$ becomes white.

After sampling, we have a number of $N + N_\mathrm{p}$ received samples $\widetilde{r}_{i,1}, \widetilde{r}_2, \ldots, \widetilde{r}_{N+N_\mathrm{p}}$. The first N_p samples $\widetilde{r}_{i,1}, \widetilde{r}_2, \ldots, \widetilde{r}_{N_\mathrm{p}}$ correspond to the N_p transmitted training symbols. Whereas, the last N samples are correspond to the N transmitted data symbols. The first N_p samples and the last N samples will be splitted into two symbol blocs $\mathbf{y}_i^\mathrm{p}$ and $\mathbf{y}_i$ as follows:

$$\begin{cases} \mathbf{y}_i^\mathrm{p} = \left[\widetilde{r}_{i,L/2+1}, \widetilde{r}_{i,L/2+2}, \ldots, \widetilde{r}_{i,N_\mathrm{p}-L/2}\right]^T = \left[y_{i,1}^\mathrm{p}, y_{i,2}^\mathrm{p}, \ldots, y_{i,N_\mathrm{p}-L}^\mathrm{p}\right]^T & \text{received training sequence} \\ \mathbf{y}_i = \left[\widetilde{r}_{i,N_\mathrm{p}-L/2+1}, \widetilde{r}_{i,N_\mathrm{p}-L/2+2}, \ldots, \widetilde{r}_{i,N+N_\mathrm{p}-L/2}\right]^T = [y_{i,1}, y_{i,2}, \ldots, y_{i,N}]^T & \text{received data sequence} \end{cases} \tag{2.17}$$

with,

$$\begin{aligned} y_{i,n}^\mathrm{p} = \widetilde{r}_{i,n} &= \sum_{l=-L/2}^{+L/2} h_i(l.\mathrm{T}_s)\ x_{n-l} + w_c[n] && \text{for} \quad 1 \leq n \leq N_\mathrm{p} \\ y_{i,n} = \widetilde{r}_{i,N_\mathrm{p}+n} &= \sum_{l=-L/2}^{+L/2} h_i(l.\mathrm{T}_s)\ s_{i,n-l} + w_c[n] && \text{for} \quad 1 \leq n \leq N \end{aligned} \tag{2.18}$$

Moreover, the received training sequence $\mathbf{y}_i^{\mathrm{p}}$ can be written in this matrix form:

$$\mathbf{y}_i^{\mathrm{p}} = \begin{bmatrix} y_{i,1}^{\mathrm{p}} \\ y_{i,2}^{\mathrm{p}} \\ \vdots \\ y_{i,N_{\mathrm{p}}-L}^{\mathrm{p}} \end{bmatrix} = \begin{bmatrix} x_{L+1} & x_L & \cdots & x_1 \\ x_{L+2} & x_{L+1} & \cdots & x_2 \\ x_{L+3} & x_{L+2} & \cdots & x_3 \\ \vdots & \vdots & \cdots & \vdots \\ x_{N_{\mathrm{p}}} & x_{N_{\mathrm{p}}-1} & \cdots & x_{N_{\mathrm{p}}-L+1} \end{bmatrix} . \begin{bmatrix} h_i\left(-L/2.\mathrm{T}_s\right) \\ h_i\left((-L/2+1).\mathrm{T}_s\right) \\ \vdots \\ h_i\left(L/2.\mathrm{T}_s\right) \end{bmatrix} + \begin{bmatrix} w_c[L/2+1] \\ w_c[L/2+2] \\ \vdots \\ w_c[N_{\mathrm{p}}-L/2] \end{bmatrix}$$

$$= \mathbf{X}.\mathbf{h}_i + \mathbf{w}_c \tag{2.19}$$

with $\mathbf{X}$ denoting the corresponding Toeplitz matrix and $\mathbf{h}_i$ is the channel vector to be estimated:

$$\mathbf{X} = \begin{bmatrix} x_{L+1} & x_L & \cdots & x_1 \\ x_{L+2} & x_{L+1} & \cdots & x_2 \\ x_{L+3} & x_{L+2} & \cdots & x_3 \\ \vdots & \vdots & \cdots & \vdots \\ x_{N_{\mathrm{p}}} & x_{N_{\mathrm{p}}-1} & \cdots & x_{N_{\mathrm{p}}-L+1} \end{bmatrix} \quad \text{and} \quad \mathbf{h}_i = \begin{bmatrix} h_i\left(-L/2.\mathrm{T}_s\right) \\ h_i\left((-L/2+1).\mathrm{T}_s\right) \\ \vdots \\ h_i\left(L/2.\mathrm{T}_s\right) \end{bmatrix} \tag{2.20}$$

In the following, we further assume that we have an independent and identically distributed (i.i.d) training sequence satisfying:

$$\mathbf{X}^H\mathbf{X} \approx \left(N_{\mathrm{p}}-L\right).\,\sigma_p^2.\begin{bmatrix} 1 & 0 & \cdots & 0 \\ 0 & 1 & \cdots & 0 \\ \vdots & & \ddots & \vdots \\ 0 & 0 & \cdots & 1 \end{bmatrix} \tag{2.21}$$

The received training sequence $\mathbf{y}_i^{\mathrm{p}}$ contains a number of $N_{\mathrm{p}}-L$ symbols and will be used to estimate the discrete-time equivalent baseband channel. Whereas, the received data sequence $\mathbf{y}_i$ contains N received symbols and will be processed to detect transmit data symbol sequence $\mathbf{s}_i$.

Finally, we have:

$$y_{i,n} = \sum_{l=-L/2}^{+L/2} h_i\left(l.\mathrm{T}_s\right)\; s_{i,n-l} + w_c[n] \qquad \text{for} \qquad 1 \le n \le N \tag{2.22}$$

and,

$$\mathbf{y}_i^{\mathrm{p}} = \mathbf{X}.\mathbf{h}_i + \mathbf{w}_c \tag{2.23}$$

2.3.3 Existing time-domain channel equalization methods

In order to estimate the transmit data sequence $\mathbf{s}_i$, it is essential to equalize received sampled sequence. The equalization of the received signal is an important task for a signal receiver, especially in the presence of multiple paths.

Numerous equalization algorithms exist in the literature considering linear MMSE detection with *a priori* as in [124] or using turbo-equalization with interference canceler as in [43, 110] or others considering non-linear Decision Feedback Equalizer (DFE) [11] or trellis-based equalization methods (Viterbi Algorithm (VA) [45]) or a Maximum A Posteriori (MAP) detection (BCJR algorithm[9]). In this Section, we are interested in trellis-based equalization methods. The linear methods will be considered later in Section 2.4.2 for frequency-domain methods with circular channel matrix.

2.3.3.1 Nyquist signaling

In Nyquist signaling i.e. $\mathrm{T}_s = \mathrm{T}_h$, the noise variables $\{w_c[n]\}$ in Equation (2.16) are Gaussian and white. Thus, the model shown Equation (2.16) is a white-noise model and is commonly referred to as the *Forney's model*. In this case, a maximum-likelihood (ML) (Viterbi Algorithm (VA) [45]) or a Maximum A Posteriori (MAP) detection (BCJR algorithm[9]) are two optimum solutions.

Note that, time-domain equalization can introduce a high complexity when the channel present a «long» memory (large delay spread). In fact, considering a channel with a memory equal to L, we can observe that each sample $\widetilde{y}_{i,n}$ only depends on the current channel input $s_{i,n}$ and the L most recent channel inputs $s_{i,n-1}, s_{i,n-2}, \ldots, s_{i,n-L}$ (See Equation (2.22)). Therefore, the signal can be described by means of a trellis where each state is defined as $\sigma_{n-1} = \left(s_{i,n+L/2-1}, s_{i,n+L/2-2}, \ldots, s_{i,n-L/2}\right)$. Thus, the number of states is $|\chi|^L$. So, the computational complexity is exponentially proportional to the channel memory L.

Viterbi Algorithm The model shown in Equation (2.16) is a white-noise model and is commonly referred to as the *Forney's model*. In 1972, Forney showed that ML detection of $\mathbf{s}_i$ can be carried out by an application of the Viterbi algorithm (VA) [45]. Due to the fact that samples $\{y_{i,n}\}$ are conditionally independent, the conditional probability density function $\Pr(\mathbf{y}_i|\mathbf{s}_i)$ can be expressed in a recursive factorization of the form:

$$\Pr(\mathbf{y}_i|\mathbf{s}_i) = \prod_{n=1}^{N} \frac{1}{\pi\sigma_w^2} \exp\left(- \frac{\left| y_{i,n} - \sum_{l=-L/2}^{+L/2} h_i(l.\mathrm{T}_s)\ s_{i,n-l} \right|^2}{\sigma_w^2} \right) \tag{2.24}$$

Based on Equation (2.24), it is uncomplicated and easy to set up the VA. In fact, under the assumption of i.i.d constellation symbols $\{s_{i,n}\}$ and taking into account that the logarithm is a monotonic function, a MAP-based symbol detection can be expressed as:

$$\widehat{\mathbf{s}}_i = \underset{\mathbf{s}_i}{\operatorname{argmax}}\ \Pr(\mathbf{y}_i|\mathbf{s}_i) = \underset{\mathbf{s}_i}{\operatorname{argmax}}\ \log\{\Pr(\mathbf{y}_i|\mathbf{s}_i)\} = \underset{\mathbf{s}_i}{\operatorname{argmax}} \sum_{n=1}^{N} \mu_{i,n} \tag{2.25}$$

where $\mu_{i,n} = \left| y_{i,n} - \sum_{l=-L/2}^{+L/2} h_i(l.\mathrm{T}_s)\ s_{i,n-l} \right|^2$ is the so-called branch metric of the VA.

Note that in our definition, due to the sub-optimalely filtering, we do not have a strictly causal channel impulse as initially considered by Forney that considers matched filtering plus whitening. In our case, we will refer to *Forney model*, when the noise is white and the channel impulse is not symmetric. This implies that ML and MAP decoding introduce a decision delay due to the non-causal part of the channel.

Full-state BCJR-type algorithm In turbo equalization applications [31], one may resort to the MAP symbol detection. In this case, it is sufficient to replace the VA with the BCJR algorithm [9]. It will make use of the same branch metric $\mu_{i,n}$.

The BCJR algorithm takes in input an *a priori* bit LLR vector of length $\log_2(M) \times N$ and denoted by

$\mathrm{L}_a^{\mathrm{in}}(\mathbf{c}_i) = \left[\mathrm{L}_a^{\mathrm{in}}(c_{i,1}), \mathrm{L}_a^{\mathrm{in}}(c_{i,2}), \ldots, \mathrm{L}_a^{\mathrm{in}}\left(c_{i,\log_2(M)\times N}\right)\right]^T$ to calculate an *a priori* probability of the transmit data symbols $\{s_{i,n}\}$ $1 \leq n \leq N$. By assuming $\left[u_1^{(m)}, u_2^{(m)}, \ldots, u_{\log_2(M)}^{(m)}\right]$ is the transmit bit sequence corresponding to $s_{i,n} = \mathcal{C}_m$, the *a priori* symbol probability is calculated as:

$$\Pr\left(s_{i,n} = \mathcal{C}_m | \mathrm{L}_a^{\mathrm{in}}(\mathbf{c}_i)\right) = \prod_{q=1}^{\log_2(M)} \frac{\exp\left(-u_q^{(m)} \times \mathrm{L}_a^{\mathrm{in}}\left(c_{i,q+(n-1)\times\log_2(M)}\right)\right)}{1+\exp\left(-\mathrm{L}_a^{\mathrm{in}}\left(c_{i,q+(n-1)\times\log_2(M)}\right)\right)} \tag{2.26}$$

Under the assumption of i.i.d symbols $\{s_{i,n}\}$ drawn from a discrete alphabet χ i.e. $\{s_{i,n}\} \in \chi = \{\mathcal{C}_1, \mathcal{C}_2, \ldots, \mathcal{C}_M\}$ and taking into account the fact that the channel is convolutive, an Hidden Markov Model can be used according to a Markov state $\sigma_{n-1} = \left(s_1^{(m)}, s_2^{(m)}, \ldots, s_L^{(m)}\right)$ with $\left\{s_l^{(m)}\right\} \in \chi \quad \forall \quad 1 \leq l \leq L$. The number of states is $|\chi|^L$ i.e. $m \in \left\{1, 2, \ldots, M^L\right\}$.

Assuming $\sigma_{n-1} = \left(s_1^{(m')}, s_2^{(m')}, \ldots, s_L^{(m')}\right)$ and $\sigma_n = \left(s_1^{(m)}, s_2^{(m)}, \ldots, s_L^{(m)}\right)$ are respectively the previous and the next states with $m, m' \in \left\{1, 2, \ldots, M^L\right\}$. Moreover we define $x \in \chi$ as the entered symbol. Based on BCJR algorithm, the A Posteriori Probability (APP) of the transmit data symbols $\{s_{i,n}\}$ $1 \leq n \leq N$ can be computed based on the received data $\mathbf{y}_i = [y_{i,1}, y_{i,2}, \ldots, y_{i,N}]^T$ as follows:

$$\Pr\left(s_{i,n} = \mathcal{C}_q, \mathbf{y}_i\right) = \sum_{m,m'} \alpha_{n-1}(m') \,.\, \gamma_n(m', m, x = \mathcal{C}_q) \,.\, \beta_n(m) \tag{2.27}$$

Where the sum is performed over all possible pairs of state indexes m and m'. The quantity $\gamma_n(m', m, x)$ denotes the transition probability expressed as:

$$\begin{aligned}\gamma_n(m', m, x) &= \Pr\left(s_{i,n} = x | \mathrm{L}_a^{\mathrm{in}}(\mathbf{c}_i)\right) \,.\, \Pr\left(y_{i,n} \backslash \sigma_{n-1} = \left(s_1^{(m')}, s_2^{(m')}, \ldots, s_L^{(m')}\right), \sigma_n = \left(s_1^{(m)}, s_2^{(m)}, \ldots, s_L^{(m)}\right)\right) \\ &= \Pr\left(s_{i,n} = x\right) \,.\, \Pr\left(y_{i,n} \backslash \sigma_{n-1} = \left(s_1^{(m')}, s_2^{(m')}, \ldots, s_L^{(m')}\right), s_{i,n} = x\right) \,.\, \delta_{m' \mapsto m}(x)\end{aligned} \tag{2.28}$$

The signal can be described by means of a trellis. The possible transitions given by the constructed trellis are defined by the probability $\delta_{m' \mapsto m}(x)$ as follows:

$$\delta_{m' \mapsto m}(x) = \begin{cases} 1 & x = s_1^{(m)} \quad \text{and} \quad \left(s_2^{(m)}, \ldots, s_L^{(m)}\right) = \left(s_1^{(m')}, s_2^{(m')}, \ldots, s_{L-1}^{(m')}\right) \\ 0 & \text{otherwise.} \end{cases}$$

Given a previous state $\sigma_{n-1} = \left(s_1^{(m')}, s_2^{(m')}, \ldots, s_L^{(m')}\right)$ and an entered symbol $x \in \chi$, one can use a branch metric to calculate this conditional probability:

$$\Pr\left(y_{i,n} \backslash \sigma_{n-1} = \left(s_1^{(m')}, s_2^{(m')}, \ldots, s_L^{(m')}\right), s_{i,n} = x\right) \propto \exp\left(-\frac{\mu_{i,n}}{\sigma_w^2}\right) \tag{2.29}$$

where $\mu_{i,n} = \left| y_{i,n} - h_i(-L/2.\mathrm{T}_s) \,.\, x - \sum_{l=-L/2+1}^{+L/2} h_i(l.\mathrm{T}_s) \,.\, s_{L/2+l}^{(m')} \right|^2$ is the considered branch metric.

In Equation (2.27), the quantities $\alpha_n(m')$ and $\beta_n(m)$ can be computed by using this equations:

$$\alpha_n(m) = \Pr\left(\sigma_n = \left(s_1^{(m)}, s_2^{(m)}, \ldots, s_L^{(m)}\right), [y_{i,1}, y_{i,2}, \ldots, y_{i,n}]\right) = \sum_{m'} \alpha_{n-1}(m') \,.\, \sum_{x \in \chi} \gamma_n(m', m, x) \tag{2.30}$$

$$\beta_n(m) = \Pr\left([y_{i,n+1}, y_{i,n+2}, \ldots, y_{i,N}] \backslash \sigma_n = \left(s_1^{(m)}, s_2^{(m)}, \ldots, s_L^{(m)}\right)\right) = \sum_{m'} \beta_{n+1}(m') \,.\, \sum_{x \in \chi} \gamma_n(m, m', x) \tag{2.31}$$

At the output of BCJR algorithm, an *a posteriori* log-likelihood ratio (LLR) vector of the transmitted bit sequence $\mathbf{c}_i$ is generated. This *a posteriori* information is denoted $\mathrm{L}_a^{\mathrm{out}}(\mathbf{c}_i)$ and is written as $\mathrm{L}_a^{\mathrm{out}}(\mathbf{c}_i) = \left[\mathrm{L}_a^{\mathrm{out}}(c_{i,1}), \mathrm{L}_a^{\mathrm{out}}(c_{i,2}), \ldots, \mathrm{L}_a^{\mathrm{out}}\left(c_{i,\log_2(M)\times N}\right)\right]^T$. Each LLR bit component is calculated as follows:

$$\mathrm{L}_a^{\mathrm{out}}\left\{c_{i,q+(n-1)\times\log_2(M)}\right\} = \log\left\{\frac{\sum\limits_{m\in\mathbf{U}_q^0}\Pr\left(s_{i,n}=\mathcal{C}_m,\mathbf{y}_i\right)}{\sum\limits_{m\in\mathbf{U}_q^1}\Pr\left(s_{i,n}=\mathcal{C}_m,\mathbf{y}_i\right)}\right\} \tag{2.32}$$

The two sets of the constellation indexes $\mathbf{U}_q^0$ and $\mathbf{U}_q^1$ correspond to have respectively 0 and 1 entries at the q-th index position of constellation bits and verifying,

$$\mathbf{U}_q^0 \cup \mathbf{U}_q^1 = \{1,2,\ldots,M\} \quad ; \quad \mathbf{U}_q^0 \cap \mathbf{U}_q^1 = \oslash \tag{2.33}$$

Reduced-state MAP equalizers Given the channel is convolutive with a memory length L, the signal can be described by means of a trellis. By considering full-state BCJR-type algorithm, the constructed trellis contains a number $|\chi|^L$ states. In order to reduce the computational complexity, various versions of reduced-state MAP equalizers which employ channel-shortening method to «shorten» the channel memory L and then lower the resulting receiver complexity are described, for example, in [42]-[73]-[32] and references therein. Moreover, in [47] the decision-feedback approach has been also applied to reduce the complexity of the standard MAPSDs ([74] and references therein); the resulting MAP/DF equalizer reveals a structure similar to the DFE-MLSE of [33], the main difference being that a single feedback-filter is present in the MAP/DF receiver of [47] whereas in the DFE-MLSE of [51] each state of the trellis requires a feedback-filter. More recently, in [4], M-BCJR algorithms are proposed to reduce the BCJR algorithm. There exist several variations of the M-BCJR idea, but they follow closely the idea that both recursions should base their calculation on M major terms. It is not necessarily true that this is the best strategy for reducing the complexity of BCJR algorithm, but they have shown to have good performances.

MAP equalization for some specific channels In some case, the channel appears in a particular form. In order to exploit this particular form to propose reduced-complexity or tailored equalization structures, some studies are already available in the literature.

Two-tap channels For an ISI-channel with two taps, the channel memory is equal to 1 ($L=1$). This particular channel has interested some studies. For instance, in [112], it has been shown that two-tap channel is suitable to the use of matched decoding (MD) concept by introducing a non-linear representation of the trellis with significantly fewer states. Furthermore, the two-tap channel allows to have a reduced-complexity equalization. Indeed, with considering BCJR-type algorithms, it is clear that the number of states is reduced from $|\chi|^L$ to only $|\chi|$ i.e. $\sigma_{n-1} = s^{(m')}$ with $s^{(m')} \in \chi = \{\mathcal{C}_1, \mathcal{C}_2, \ldots, \mathcal{C}_M\}$ for $1 \leq m \leq M$. Moreover, in this case one can remark that the value of the next state which follows an entered symbol $x \in \chi$ is the only state

$\sigma_n = s^{(m)} = x$ and vice versa:

$$\gamma_n\left(m', m, x\right) = \begin{cases} \gamma_n(m', m, \mathcal{C}_m) \neq 0 & \text{if } x = \mathcal{C}_m \\ 0 & \text{if } x \neq \mathcal{C}_m \end{cases} \tag{2.34}$$

Consequently, the APP of the transmit data symbols $\{s_{i,n}\}\ 1 \leq n \leq N$ shown in Equation (2.27) can be reduced to:

$$\begin{aligned} \Pr\left(s_{i,n} = \mathcal{C}_q, \mathbf{y}_i\right) &= \sum_{m'=1}^{M} \sum_{m=1}^{M} \alpha_{n-1}\left(m'\right) . \gamma_n\left(m', m, x = \mathcal{C}_q\right) . \beta_n\left(m\right) \\ &= \left\{ \sum_{m'=1}^{M} \alpha_{n-1}\left(m'\right) . \gamma_n\left(m', m = q, x = \mathcal{C}_q\right) \right\} . \beta_n\left(q\right) = \alpha_n\left(q\right) . \beta_n\left(q\right) \end{aligned} \tag{2.35}$$

Considering a possible implementation of the BCJR algorithm in the logarithmic domain [108], it is straightforward to obtain APPs:

$$\log\left(\Pr\left(s_{i,n} = \mathcal{C}_q, \mathbf{y}_i\right)\right) = \log\left(\alpha_n\left(q\right)\right) + \log\left(\beta_n\left(q\right)\right) \tag{2.36}$$

Sparse channels Sparse channel equalization has been considered in several works [15]-[87] to exploit the sparsity, mainly using parallel trellis based detection algorithm such as Viterbi or MAP algorithms. For equalization of zero padded sparse channels, the parallel MAP receiver is shown to be optimal [72, 82, 87]. For more general sparse channels, interference cancellation has been taken into account by introducing inter-trellis interference mitigation between parallel trellises. This is done at the expense of additional complexity due to the need for proper scheduling [71, 88]. Several extensions of these works have been considered for application in turbo-equalization [72, 93, 94]. In these approaches, the interference mitigation is completely revised to enable an easy and efficient implementation. However, there is no consideration for a particular structure of the sparse channel.

Besides, the described methods are most often based on the implementation of a detection algorithm based on multiple parallel trellis, of Viterbi algorithm or MAP algorithm type. These algorithms have the drawback of considerable implementational complexity. On the other hand, some methods (described, for example, in references [82], and [87]) impose a channel model in which the secondary paths are of zero power, which amounts to an approximation that is not always realistic.

2.3.3.2 FTN signaling

In the FTN case, the spectral efficiency can be increased at the expense of an additional Inter-symbol Interference (ISI) compared to the Nyquist signaling case. In fact, by increasing the baud rate, $\mathrm{R}_s = 1/\mathrm{T}_s$ of the transmitted signal, a larger intentional ISI is introduced since the bandwidth of the shaping transmit filter, B_h, is fixed. Thus, the spectral efficiency is increased by introducing intentional ISI. To mitigate ISI, two models are used in the literature to equalize receive signal: the *Forney's model* invented by Forney in 1972 and the *Ungerboeck's model* invented by Ungerboeck in 1974. As FTN signaling can be seen as an ISI channel in the AWGN context, we review the main detectors in that context. Extensions to the MAP detection with ISI cancellation will be considered in the Chapter 3 since it is not be considered so far for trellis-based equalization.

Forney and Ungerboeck models We recall that Forney model is referred to white-noise model. In FTN signaling i.e. $T_s < T_h$, the noise variables $\{w_c[n]\}$ are still Gaussian, but are colored (See Equation (2.16)). Therefore, a MAP-based symbol detection, as given in Equation (2.25), considering as a starting point the samples $\{y_{i,n}\}$, given in Equation (2.22), without taking into account the noise correlation, is a highly suboptimal detection. Nevertheless, if the channel is symmetric, Ungerboeck has shown in 1974 that samples $\{y_{i,n}\}$ represent a sufficient statistic and can thus be employed for an optimal detection [125]. In this case, the model is commonly referred to as the *Ungerboeck's model*.

Symmetric channels In the case of symmetric channels, spectral factorization can be considered [24]. Without lack of generality, we are interested in trellis MAP-based symbol detection. In this context, due the fact that the obtained noise in Equation (2.22) is colored, two possible approaches are considered depending on the spectral properties of the colored noise. If spectral factorization is allowed (i.e. the power spectral density of the noise has not null-values or also $\nu \geq \frac{1}{1+\beta}$ expect at some specific values), then a whitening filter can be applied to the samples $\{y_{i,n}\}$. The new observation model is often referred to as *Forney's model*. Unfortunately, if the spectral factorization is not allowed, *Forney's model* strategy is not possible and one has to resort to the observation model as given initially in Equation (2.22), often referred to as *Ungerboeck's model*.

In the case of possible spectral factorization, Forney filtered the samples $\{y_{i,n}\}$ with a whitening filter $\left\{\widetilde{f}_l\right\}$ in order to obtain white noise. As a result we have:

$$z_{i,n} = \sum_l \widetilde{f}_l \; y_{i,n-l} = \sum_{k=0}^{L} h_k \; s_{i,n-k} + w[n] \tag{2.37}$$

In the previous observation model, the resulting additive noise $\{w[n]\}$ is Gaussian and white with variance σ_w^2. The channel impulse response $\{h_k\}$ is causal and verifies:

$$h_i\left(l.T_s\right) = \sum_{k=0}^{L} h_k^*.h_{l+k} \tag{2.38}$$

Based on BCJR algorithm, the A Posteriori Probability (APP) of the transmit data symbols $\{s_{i,n}\}$ $1 \leq n \leq N$ can be computed based on the received data $\mathbf{y}_i = [y_{i,1}, y_{i,2}, \ldots, y_{i,N}]^T$ as follows:

$$\Pr\left(s_{i,n} = \mathcal{C}_q, \mathbf{y}_i\right) = \sum_{m,m'} \alpha_{n-1}\left(m'\right) . \; \gamma_n\left(m', m, x = \mathcal{C}_q\right) . \; \beta_n\left(m\right) \tag{2.39}$$

Given a previous state $\sigma_{n-1} = \left(s_1^{(m')}, s_2^{(m')}, \ldots, s_L^{(m')}\right)$ and an entered symbol $x \in \chi$, one can use a branch metric to calculate this conditional probability:

$$\Pr\left(y_{i,n} \backslash \sigma_{n-1} = \left(s_1^{(m')}, s_2^{(m')}, \ldots, s_L^{(m')}\right), s_{i,n} = x\right) \propto \exp\left(-\frac{\mu_{i,n}}{\sigma_w^2}\right) \tag{2.40}$$

where $\mu_{i,n} = \left| z_{i,n} - \sum_{k=0}^{L} h_k \; s_{i,n-k} \right|^2$ is the considered branch metric.

In the case when spectral factorization is not allowed, *Ungerboeck's model* strategy is a solution. Indeed, thanks to the symmetric form of the channel, the noise color is irrelevant and the receive samples $\{y_{i,n}\}$

represent a sufficient statistic and can thus be employed for an optimal detection. By using the same trellis as considered for the *Forney's model*, a new expression of the branch metric will be considered (see [125] for further details):

$$\mu_{i,n} = -2.\ \Re\left\{ s^*_{i,n}.\left(y_{i,n} - \sum_{l=1}^{L} h_i\left(l.\mathrm{T}_s\right)\ s_{i,n-l} \right) \right\} + h_i\left(0\right).\left|s_{i,n}\right|^2 \tag{2.41}$$

It is interesting to note that while the BCJR already became available for the *Forney's model* by 1974 with [9], the story differs remarkably for the *Ungerboeck's model*. An equivalent algorithm to the BCJR that operates on the *Ungerboeck's model* and employs a branch metric equivalent to $\mu_{i,n}$ was demonstrated as late as 2005 in [27]. As a consequence, turbo equalization based on Ungerboeck's model was not available before 2005. The *Ungerboeck's model* has a number of strengths and has been rediscovered several times during the recent past. For instance, the *Ungerboeck's metric* can be used for BCJR turbo equalization in the case of using FTN signaling with small values of acceleration factor ν which are lower than the MAZO limit [81] ($\nu < \frac{1}{1+\beta}$ which means spectral factorization is not allowed).

To summarize, for symmetric channels, Ungerboeck's and Forney's ML sequence detectors involve different computations, but they traverse the very same trellis, and their final outputs are identical.

2.3.4 Existing time-domain channel estimation methods

In order to equalize the received data sequence, we need to estimate the impulse response of the equivalent baseband channel. Indeed, in the case of using SC waveform, all presented equalization algorithms suppose that the impulse channel response $\mathbf{h}_i$ is well known at the receiver. In order to have a realistic system performance, it is essential to take into consideration an efficient channel estimation method in order to have an accurate estimation of $\mathbf{h}_i$. To do it, we will investigate some existing channel estimation algorithms suitable for SC waveform.

In wireless communication systems, the estimation of the channel impulse response is necessary for the coherent demodulation. For this, it is common to introduce training sequences in the transmitted signal [114][28]. If the channel varies over time and if one knows the coherence time, one can then define the frames so that the channel can be assumed to be stationary on each. When estimating directly the equivalent discrete baseband channel impulse response, the use of the maximum likelihood (ML) criterion leads to an optimal solution. However, this estimation process can be very complex due to the memory channel which is generally high.

Following the pilot-observation model shown in Equation (2.23), the noise variables $\{w_c[n]\}$ are Gaussian and verifying $\mathbb{E}\{w_c[n].w_c^*[n+l]\} = \sigma_w^2.\ \mathrm{g}\left(l.\mathrm{T}_s\right)$. Assuming $\mathbf{w}_c$ is the corresponding additive noise in (2.23), we can write the following expression:

$$\mathbb{E}\left\{ \mathbf{w}_c.\mathbf{w}_c^H \right\} = \sigma_w^2.\ \mathbf{\Lambda} \tag{2.42}$$

where $\mathbf{\Lambda}$ denotes the corresponding correlation matrix which can be expressed as:

$$\mathbf{\Lambda} = \begin{bmatrix} \mathrm{g}(0) & \mathrm{g}(\mathrm{T}_s) & \mathrm{g}(2.\mathrm{T}_s) & \dots & \dots & \mathrm{g}([N_\mathrm{p}-L].\mathrm{T}_s) \\ \mathrm{g}(\mathrm{T}_s) & \mathrm{g}(0) & \mathrm{g}(\mathrm{T}_s) & \ddots & & \vdots \\ \mathrm{g}(2.\mathrm{T}_s) & \mathrm{g}(\mathrm{T}_s) & \ddots & \ddots & \ddots & \vdots \\ \vdots & \ddots & \ddots & \ddots & \mathrm{g}(\mathrm{T}_s) & \mathrm{g}(2.\mathrm{T}_s) \\ \vdots & & \ddots & \mathrm{g}(\mathrm{T}_s) & \mathrm{g}(0) & \mathrm{g}(\mathrm{T}_s) \\ \mathrm{g}([N_\mathrm{p}-L].\mathrm{T}_s) & \dots & \dots & \mathrm{g}(2.\mathrm{T}_s) & \mathrm{g}(\mathrm{T}_s) & \mathrm{g}(0) \end{bmatrix} \tag{2.43}$$

An optimum unbiased estimated channel vector is derived by using Maximum likelihood (ML) criterion. Under the assumption of i.i.d training symbols $\{x_n\}$ and taking into account that the logarithm is a monotonic function, a ML-based symbol detection can be expressed as:

$$\widehat{\mathbf{h}}_i^{\text{U-MLE}} = \underset{\mathbf{h}_i}{\text{argmax}}\ \Pr(\mathbf{y}_i^\mathrm{p}, \mathbf{h}_i) = \underset{\mathbf{h}_i}{\text{argmax}}\ \log\left\{\Pr\left(\mathbf{y}_i^\mathrm{p}, \mathbf{h}_i\right)\right\} \tag{2.44}$$

If matrix inversion of $\mathbf{\Lambda}$ is allowed, the logarithm value of conditional probability is given as:

$$\log\left\{\Pr\left(\mathbf{y}_i^\mathrm{p}, \mathbf{h}_i\right)\right\} = -\log\left(\mathrm{Det}\left(\pi.\sigma_w^2.\mathbf{\Lambda}\right)\right) - \frac{1}{\sigma_w^2}\ \left\{\left(\mathbf{y}_i^\mathrm{p} - \mathbf{X}\ \mathbf{h}_i\right).\mathbf{\Lambda}^{-1}.\left(\mathbf{y}_i^\mathrm{p} - \mathbf{X}\ \mathbf{h}_i\right)^H\right\} \tag{2.45}$$

The corresponding Fisher information matrix is expressed as follows:

$$\mathbf{F} = \mathbb{E}\left\{\nabla_{\mathbf{h}_i} \log\left\{\mathrm{P}(\mathbf{y}_i^\mathrm{p}, \mathbf{h}_i)\right\}\ \left[\nabla_{\mathbf{h}_i} \log\left\{\mathrm{P}\left(\mathbf{y}_i^\mathrm{p}, \mathbf{h}_i\right)\right\}\right]^H\right\} = \frac{1}{\sigma_w^2}\ \left(\mathbf{X}^H.\mathbf{\Lambda}^{-1}.\mathbf{X}\right) \tag{2.46}$$

Assuming that the correlation matrix $\mathbf{\Lambda}$ is invertible, the Equation (2.44) admits an unique unbiased optimal solution, $\widehat{\mathbf{h}}_i^{\text{U-MLE}}$ expressed as:

$$\widehat{\mathbf{h}}_i^{\text{U-MLE}} = \left(\mathbf{X}^H.\mathbf{\Lambda}^{-1}.\mathbf{X}\right)^{-1}.\mathbf{X}^H.\mathbf{\Lambda}^{-1}.\mathbf{y}_i^\mathrm{p} = \mathbf{h}_i + \left(\mathbf{X}^H.\mathbf{\Lambda}^{-1}.\mathbf{X}\right)^{-1}.\mathbf{X}^H.\mathbf{\Lambda}^{-1}.\mathbf{w}_c \tag{2.47}$$

The Mean Square Error (MSE) of the estimated channel vector is deduced as:

$$\mathrm{MSE}\left(\widehat{\mathbf{h}}_i^{\text{U-MLE}}\right) = tr\left\{\mathbb{E}\left\{\left(\widehat{\mathbf{h}}_i^{\text{U-MLE}} - \mathbf{h}_i\right).\left(\widehat{\mathbf{h}}_i^{\text{U-MLE}} - \mathbf{h}_i\right)^H\right\}\right\} = tr\left\{\sigma_w^2.\ \left(\mathbf{X}^H.\mathbf{\Lambda}^{-1}.\mathbf{X}\right)^{-1}\right\} = tr\{\mathbf{F}^{-1}\} \tag{2.48}$$

we denote $\mathrm{CRB}\left(\mathbf{h}_i\right) = \mathbf{F}^{-1}$ as the corresponding lower Cramer-Rao Bound [7]. One can observe that ML-based channel estimation can reach its corresponding Cramer-Rao Bound.

2.3.4.1 Nyquist signaling:

In Nyquist signaling i.e. $\mathrm{T}_s = \mathrm{T}_h$, the noise variables $\{w_c[n]\}$ in Equation (2.23) are Gaussian and white. Thus, the model shown Equation (2.23) is a white-noise model and the correlation matrix, $\mathbf{\Lambda}$, is equal to the identity matrix. In this case, Least Square (LS) [28] and ML channel estimation methods are equivalent and reach the same Cramer-Rao Bound.

Classical Unstructured LS estimator U-LSE: In the case of white-noise observation model, the unbiased ML estimator $\widehat{\mathbf{h}}_i^{\text{U-MLE}}$ is exactly the one given by the unbiased least-square (LS) solution $\widehat{\mathbf{h}}_i^{\text{U-LSE}}$ given by:

$$\widehat{\mathbf{h}}_i^{\text{U-LSE}} = \left[\mathbf{X}^H\mathbf{X}\right]^{-1}\mathbf{X}^H\ \mathbf{y}_i^\mathrm{p} \tag{2.49}$$

under the assumption of i.i.d constellation symbols $\{x_n\}$ as mentioned in Equation (2.21), a close form expression of the Mean Square Error of the unstructured Least Square is done:

$$\boxed{\text{MSE}\left(\widehat{\mathbf{h}}_i^{\text{U-LSE}}\right) = tr\left\{\sigma_w^2.\ \left(\mathbf{X}^H.\mathbf{X}\right)^{-1}\right\} = \frac{\sigma_w^2.\ (L+1)}{\sigma_p^2.\ (N_\text{p}-L)} = \frac{\sigma_w^2.\ (L+1)}{\sigma_s^2.\ (N_\text{p}-L)} = \frac{1}{N_\text{p}-L}.\ \frac{L+1}{(\text{E}_s/\text{N}_0)}} \tag{2.50}$$

Sparse channels: Joint Structured LS estimator (JSS-LSE): To some extent, the discrete impulse response of channel, $\mathbf{h}_i$, can be considered as sparse if some non-powerful coefficients are neglected. Starting with this assumption, we can use some estimation methods in the literature [10][30][8] which exploit the particular form of the channel.

In the case of the sparse channel, we can follow the work by Carbonelli and all [19]. The authors are interested in joint estimation of non-zero positions and the corresponding attenuation coefficients of a sparse multipath channel. For the sparse vector $\mathbf{h}_i$, we associate a binary position sparse vector $\mathbf{p} = [p_0, p_1, \ldots, p_L]$ which detects the non-zero positions obtained as [19]:

$$p_l = \begin{cases} 1 & \text{if } h_i\left((l-L/2).\text{T}_s\right) \neq 0 \\ 0 & \text{else} \end{cases} \tag{2.51}$$

Assuming $L'+1$ is the number of the considered non-zero coefficients in $\mathbf{h}_i$. Then,

$$\sum_{l=0}^{L} p_l = L'+1 \qquad \text{where} \qquad 2 \leq L'+1 \leq L+1 \tag{2.52}$$

Referring to the pilot-observation model shown in (2.23) and taking into account the sparse nature of the channel, a new observation model can be considered:

$$\mathbf{y}_i^\text{p} = \mathbf{X}.\ \mathbf{h}_i + \mathbf{w}_c = \mathbf{X}.\ \text{diag}\left(\mathbf{h}_i\right).\mathbf{p} + \mathbf{w}_c = \left\{\mathbf{X}.\ \text{diag}\left(\mathbf{p}\right)\right\}.\ \mathbf{h}_i + \mathbf{w}_c = \widetilde{\mathbf{X}}.\ \mathbf{h}_i + \mathbf{w}_c \tag{2.53}$$

According the new pilot-observation model shown in Equation (2.53), the channel estimation depends on the the value of the position vector $\mathbf{p}$. However, in the most cases, we have no *a priori* information about the position of the non-zero elements. For this kind of problem, in [19], the channel estimation is done within an iterative process. Two steps are considered: First, an estimation of the position vector $\widehat{\mathbf{p}}$ containing binary values i.e. either 0 or 1 is done. Secondly, estimation of the sparse channel, $\mathbf{h}_i$ is deduced. The channel estimation algorithm is given below in **Algorithm 1**.

To avoid the exhaustive research to estimate the position vector $\mathbf{p}$ and reduce the complexity of the problem, we can use for example the Viterbi algorithm[15]. Consequently, we can accurately identify the positions of non-zero coefficients of the channel considered as sparse.

Assuming a perfect estimation of the position vector $\mathbf{p}$, it is shown that Joint Structured LS estimator (JSS-LSE), exploiting the sparse form of the channel, gives better performance than the classical Unstructured LS estimator (U-LSE) in terms of mean square error (MSE):

$$\boxed{\text{MSE}\left(\widehat{\mathbf{h}}_i^{\text{JSS-LSE}}\right) = tr\left\{\sigma_w^2.\ \left(\widetilde{\mathbf{X}}^H.\widetilde{\mathbf{X}}\right)^{-1}\right\} = \frac{\sigma_w^2.\ \sum_{l=0}^{L} p_l}{\sigma_p^2.\ (N_\text{p}-L)} = \frac{1}{N_\text{p}-L}.\ \frac{L'+1}{(\text{E}_s/\text{N}_0)}} \tag{2.54}$$

Algorithm 1 Joint Structured LS estimator (JSS-LSE)

Initialization: $\widehat{\mathbf{h}}_i^{(0)} = \widehat{\mathbf{h}}_i^{\text{U-LSE}} = \left[\mathbf{X}^H\mathbf{X}\right]^{-1}\mathbf{X}^H\ \mathbf{y}_i^{\text{p}}$

for iter $\in \{1,...,\text{nIterMax}\}$ **do**

Estimate position vector: $\widehat{\mathbf{p}}^{(\text{iter})} = \underset{\mathbf{p}}{\text{argmax}}\left\{\left\|\mathbf{y}_i^{\text{p}} - \left[\mathbf{X}\ diag\left(\widehat{\mathbf{h}}_i^{(\text{iter}-1)}\right)\right].\mathbf{p}\right\|^2\right\}$

Update matrix $\widetilde{\mathbf{X}} = \mathbf{X}.diag\left(\widehat{\mathbf{p}}^{(\text{iter})}\right)$

LS Estimation of sparse channel $\widehat{\mathbf{h}}_i^{(\text{iter})} = \left[\widetilde{\mathbf{X}}^H.\widetilde{\mathbf{X}}\right]^{-1}.\widetilde{\mathbf{X}}^H.\mathbf{y}_i^{\text{p}}$

end for

Joint Structured LS estimation: $\widehat{\mathbf{h}}_i^{\text{JSS-LSE}} = \widehat{\mathbf{h}}_i^{(\text{nIterMax})}$

Joint Structured LS estimator with Multipath Parametric Model (JSMP-LSE): The present approach does not take into account any *a priori* information about the channel form. This approach considers a multipath parametric (MP) model. By considering MP model, the equivalent discrete channel impulse response, expressed in Equation (2.11), can be written in this matrix form:

$$\mathbf{h}_i = \mathbf{G}.\ \mathbf{a}_i \tag{2.55}$$

with,

$$\mathbf{G} = \begin{pmatrix} g\left(-\text{T}_s.L/2-\tau_0\right) & \dots & g\left(-\text{T}_s.L/2-\tau_{N_t-1}\right) \\ g\left(\text{T}_s.(-L/2+1)-\tau_0\right) & \dots & g\left(\text{T}_s.(-L/2+1)-\tau_{N_t-1}\right) \\ \vdots & \dots & \vdots \\ g\left(\text{T}_s.L/2-\tau_0\right) & \dots & g\left(\text{T}_s.L/2-\tau_{N_t-1}\right) \end{pmatrix} \quad \text{and} \quad \mathbf{a}_i = \begin{bmatrix} a_{i,1} \\ a_{i,2} \\ \vdots \\ a_{i,\text{N}_\text{m}} \end{bmatrix} \tag{2.56}$$

Referring to the pilot-observation model shown in (2.23) and taking into account the mutipath decomposition given in (2.55), a new observation model can be considered:

$$\mathbf{y}_i^{\text{p}} = \mathbf{X}.\mathbf{h}_i + \mathbf{w}_c = \{\mathbf{X}.\ \mathbf{G}\}.\ \mathbf{a}_i + \mathbf{w}_c = \mathbf{S}.\mathbf{a}_i + \mathbf{w}_c \tag{2.57}$$

In [113], it is shown that under some considerations, improvements can be achieved through an iterative estimation procedure if one are able to perform joint estimation of both attenuation vector $\mathbf{a}_i = \left[a_{i,1}, a_{i,2}, \dots, a_{i,\text{N}_\text{m}}\right]^T$ and delay vector $\tau = \left[\tau_1, \tau_2, \dots, \tau_{\text{N}_\text{m}}\right]^T$ of the discrete impulse response. These methods are based on a explicit multipath parametric model.

Referring to [113], the observation model is given in (2.57). By using this observation, channel estimation is reduced to an estimation of the combination $(\mathbf{a}_i, \tau)$. By taking into account joint estimation of the attenuation vector $\mathbf{a}_i$ and the delay propagation vector τ, an expression of Cramer-Rao Bound is done:

$$\text{CRB} = \mathbf{G}\ \text{CRB}\left(\mathbf{a}_i\right)\ \mathbf{G}^H + \left(\mathbf{G}.\left[\mathbf{S}^H.\mathbf{S}\right]^{-1}.\mathbf{S}^H.\mathbf{X}.\mathbf{V} + \mathbf{V}\right)\ \text{CRB}\left(\tau\right)\ \left(\mathbf{G}.\left[\mathbf{S}^H.\mathbf{S}\right]^{-1}.\mathbf{S}^H.\mathbf{X}.\mathbf{V} + \mathbf{V}\right)^H \tag{2.58}$$

where $\mathbf{V} = \dot{\mathbf{G}}.diag(\mathbf{a}_i)$ with $\dot{\mathbf{G}}$ is a differential matrix having the same size as the $\mathbf{G}$ matrix and defined as:

$$\left\{\dot{\mathbf{G}}\right\}_{l,p} = \frac{\partial}{\partial\tau_p}\left\{\mathbf{G}\right\}_{l,p} = \frac{\partial}{\partial\tau_p}g\left(l.\text{T}_s - \tau_p\right) \quad \text{for} \quad -L/2 \le l \le L/2 \quad \text{and} \quad 1 \le p \le \text{N}_\text{m} \tag{2.59}$$

The two matrices $\mathrm{CRB}(\mathbf{a}_i)$ and $\mathrm{CRB}(\tau)$ are respectively the CRB of the estimation of the attenuation vector $\mathbf{a}_i$ and the propagation delay vector τ given as:

$$\mathrm{CRB}(\mathbf{a}_i) = \sigma_w^2 \left[\mathbf{S}^H\mathbf{S}\right]^{-1} \tag{2.60}$$

$$\mathrm{CRB}(\tau) = \sigma_w^2 \left[2.\,\Re\left\{\mathbf{V}^H.\mathbf{X}^H.\mathbf{X}.\mathbf{V}\right\} - \mathbf{V}^H.\mathbf{X}^H.\mathbf{S}.\left[\mathbf{S}^H.\mathbf{S}\right]^{-1}.\mathbf{S}^H.\mathbf{X}.\mathbf{V}\right]^{-1} \tag{2.61}$$

Based on the expression of the Cramer-Rao bound given, we can deduce that:

$$\boxed{\mathrm{MSE}\left(\widehat{\mathbf{h}}_i^{\text{JSMP-LSE}}\right) \geq tr\left\{\mathbf{G}.\,\mathrm{CRB}(\mathbf{a}_i).\,\mathbf{G}^H\right\} = \frac{\sigma_w^2.\,tr\left\{\left[\mathbf{G}^H\mathbf{G}\right]^{-1}\,\mathbf{G}^H\mathbf{G}\right\}}{\sigma_p^2.\,(N_\mathrm{p}-L)} = \frac{1}{N_\mathrm{p}-L}.\,\frac{\mathrm{N_m}}{(\mathrm{E}_s/\mathrm{N}_0)}} \tag{2.62}$$

2.3.4.2 FTN signaling

In FTN signaling i.e. $\mathrm{T}_s < \mathrm{T}_h$, the noise variables $\{w_c[n]\}$ are still Gaussian, but are colored. Indeed, the correlation matrix Λ shown in (2.43) is no longer equal to the identity matrix. Consequently, a channel estimation using LS criterion and without taking into account the noise correlation is a highly suboptimal channel estimation. The optimal solution is given by the ML estimator as expressed in Equation (2.47). The ML solution suppose that the correlation matrix Λ is invertible. However, if matrix inversion is not allowed, it is not possible to achieve optimal solution and thus considering the observation model given in Equation (2.23) would not be the best strategy.

Note that if the spectral factorization is possible, it will be possible to apply the ML estimation as an optimal solution. For the case of system with low values of acceleration factor ν, ML estimation is not available and this estimation problem is still an issue. Only sub-optimal estimations are available (for example LS estimator).

2.4 EW SC-OFDM waveform

Block based circular waveforms have been considered in the satellite context for possible hybridization with terrestrial systems that are widely using OFDM based systems. Among the envisioned circular waveforms, EW SC-OFDM and SC-OFDM [14], the latter being a particular case with rectangular frequency frequency domain filtering (with circular cardinal sinus pulse shaping). The advantage of EW SC-OFDM waveform is that can offer a better PAPR level of the transmitted signal compared to OFDM and SC-OFDM.

In this Section, we present EW SC-OFDM and we further introduce its extension to the FTN case. Indeed, the use of FTN signaling allows the increase of the spectral efficiency. The FTN signaling sends pulse shaped data faster than the Nyquist criterion, and consequently there are inter-symbol interferences (ISI). In order to reduce complexity at the receiver, it is interesting to use a circular waveform. In this context, EW SC-OFDM waveform appears suitable to mitigate ISI by a simple Frequency Domain Equalization (FDE) implemented at the receiver. In this Section, EW SC-OFDM waveform will be studied for both Nyquist/FTN signaling. The transmitter and the receiver structures are shown in Figure 2.3.

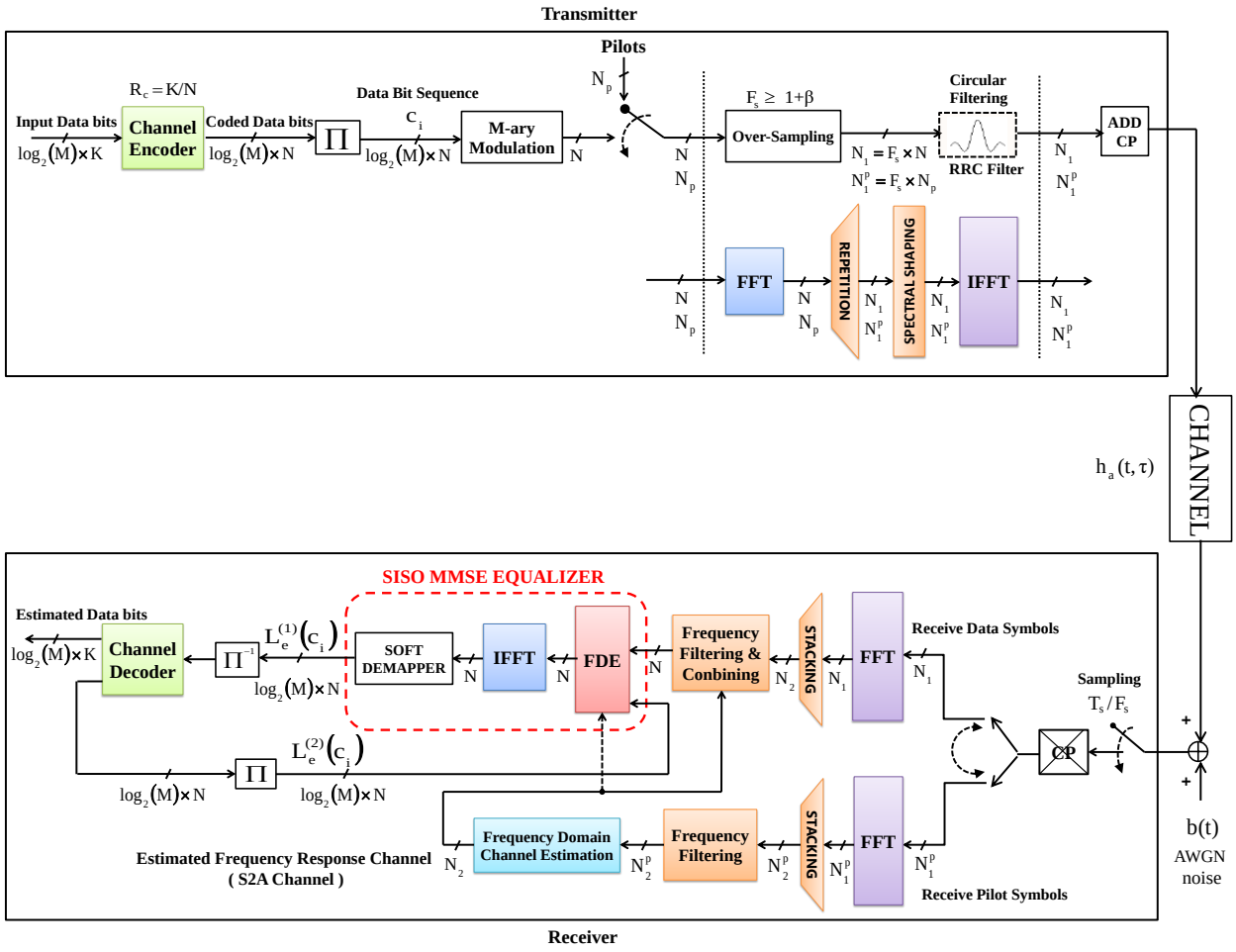

Figure 2.3: *Transmitter and receiver scheme for EW SC-OFDM waveform*

2.4.1 Expression of the received base-band signal

2.4.1.1 EW SC-OFDM transmitter

As for SC waveform, a sequence of $N_{\mathrm{p}} = (1/\Delta) \times N \leq N$ training symbols, denoted by $\mathbf{x} = \left[x_1, x_2, \ldots, x_{N_{\mathrm{p}}}\right]$, will be inserted in each transmitted sub-frame in order to estimate frequency response channel. The size of training sequence depends on a spacing factor $\Delta \in \{4; 8; 16; 32; \ldots\}$. The rational number $1/\Delta$ denotes the ratio between the size of the data sequence and the size of the training sequence. As shown in Figure 2.3, the training sequence is used alternately with the data sequence $\mathbf{s}_i$. Note that training symbols $x_1, x_2, \ldots, x_{N_{\mathrm{p}}}$ are perfectly known at the receiver and having a variance $\sigma_p^2 = \sigma_s^2$.

At the transmitter, each obtained data sequence $\mathbf{s}_i$ will be oversampled by a $\mathrm{F}_s \geq 1 + \beta$ factor before being *circularly* filtered by a RRC shaping filter $\mathrm{h}_e(\tau)$ with roll-off $0 \leq \beta \leq 1$ and a Nyquist bandwidth $\mathrm{B_h}$. A possible frequency implementation is considered in Figure 2.3. Indeed, over-sampling in time domain is equivalent to have a repetition in frequency domain. Also, considering circular shape filtering is equivalent to have a spectral shaping in the frequency domain. The ratio between the size of the second Inverse Fast Fourier Transform (IFFT) and the size of the first Fast Fourier Transform (FFT) is equal to the over-sampling factor F_s. Therefore, the size of the first FFT is equal to N and the size of the second IFFT is equal to $N_1 = \mathrm{F}_s \times N \geq N$. Respectively for training sequence, the size of the first FFT is equal to N_{p} and the size of the second IFFT is equal to $N_1^{\mathrm{p}} = \mathrm{F}_s \times N_{\mathrm{p}} \geq N_{\mathrm{p}}$. N_1 and N_1^{p} are two positive integers. Note that FFT sizes N,N_{p}, N_1^{p} and N_1 are assumed invariant during all the communication.

The expression of the transmitted signal corresponding to the i-th sub-frame is given as follows:

$$\mathbf{e}_i = \begin{bmatrix} e_{i,1} \\ e_{i,2} \\ \vdots \\ e_{i,N_1} \end{bmatrix} = \sqrt{\mathrm{F}_s} \times \mathbf{F}_{\mathrm{N}_1}^H . \mathbf{A} . \mathbf{F}_{\mathrm{N}} . \begin{bmatrix} s_{i,1} \\ s_{i,2} \\ \vdots \\ s_{i,N} \end{bmatrix} \tag{2.63}$$

The matrices $\mathbf{F}_{\mathrm{N}}$ and $\mathbf{F}_{\mathrm{N}_1}$ are two normalized Fourier matrices with sizes $N \times N$ and $N_1 \times N_1$, respectively. Additionally, The $\mathbf{A}$ matrix denotes an equivalent frequency transformation matrix and expressed as:

$$\mathbf{A} = \frac{1}{\mathrm{F}_s} . \; diag \begin{bmatrix} \mathrm{H}_e(1) \\ \mathrm{H}_e(2) \\ \vdots \\ \mathrm{H}_e(N_1) \end{bmatrix} . \begin{bmatrix} \mathrm{I}'' \\ \mathbf{I}_{N \times N} \\ \mathrm{I}' \end{bmatrix} \tag{2.64}$$

The complex coefficients $\mathrm{H}_e(1), \mathrm{H}_e(2), \ldots, \mathrm{H}_e(N_1)$ are the frequency responses of the RRC filter $h_e(\tau)$:

$$H_e(n) = \sum_{l=-\infty}^{+\infty} h_e(l.\frac{\mathrm{T}_s}{\mathrm{F}_s}) \; \exp\left(-2\pi j.l.\frac{\mathrm{T}_s}{\mathrm{F}_s}.f_n\right) \quad \text{with} \quad f_n = \frac{1}{\mathrm{T}_s/\mathrm{F}_s}.\left(\frac{n-1}{N_1} - \frac{1}{2}\right) \qquad \text{for} \qquad 1 \leq n \leq N_1 \tag{2.65}$$

A close expression for square of absolute value of the frequency response of the shaping filter $\mathrm{H}_e(n)$ is done:

$$|H_e(n)|^2 = \frac{(F_s)^2}{\nu} \times \begin{cases} 1, & |f_n| \leq \frac{1-\beta}{T_h} \\ \frac{1}{2}\left[1 + \cos\left(\frac{\pi T_h}{\beta}\left[|f_n| - \frac{1-\beta}{T_h}\right]\right)\right], & \frac{1-\beta}{T_h} < |f_n| \leq \frac{1+\beta}{T_h} \\ 0, & \text{otherwise} \end{cases} \tag{2.66}$$

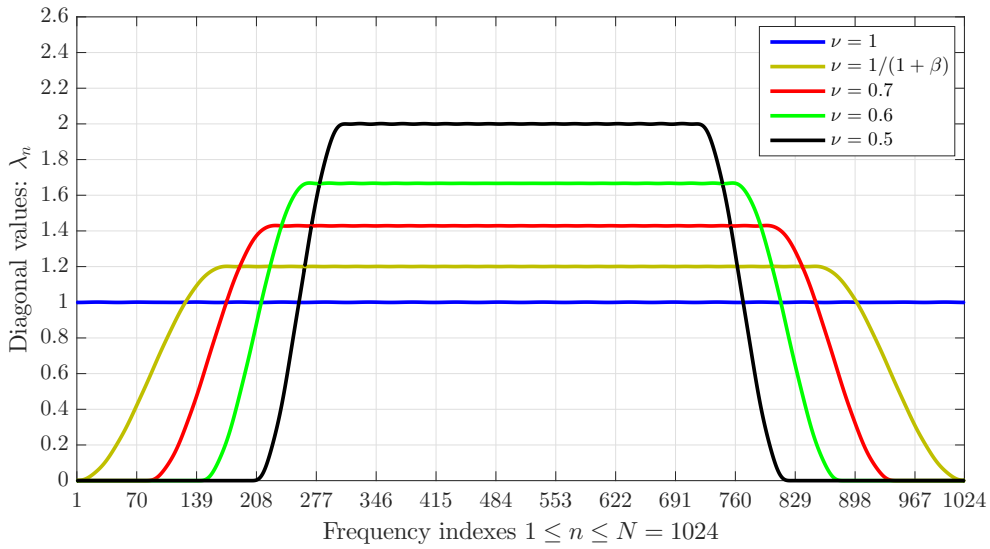

Figure 2.4: *Numerical values of diagonal values* $\{\lambda_n\}$ *in each frequency indexes* $1 \leq n \leq N = 1024$ *in the case of using RRC shaping filter with* $\beta = 0.20$.

we can verify that we have:

$$\frac{1}{N_1}\sum_{l=0}^{N_1}|H_e(n)|^2 = \sum_{l=-\infty}^{+\infty}\left|h_e\left(l.\frac{\mathrm{T}_s}{\mathrm{F}_s}\right)\right|^2 = \mathrm{F}_s \tag{2.67}$$

The two matrices $\mathrm{I}^{'}$ and $\mathrm{I}^{''}$ being two $\frac{N_1-N}{2} \times N$ matrices containing respectively the first $\frac{N_1-N}{2}$ and the last $\frac{N_1-N}{2}$ columns of the identity matrix $\mathbf{I}_{N\times N}$. The resulting matrix $\mathbf{A}$, having a size of $N_1 \times N$.
The $\mathbf{A}$ matrix is a pseudo-orthogonal matrix verifying:

$$\mathbf{A}^H.\mathbf{A} = \mathbf{A}^T.\mathbf{A}^* = \begin{bmatrix} \lambda_1 & 0 & \cdots & 0 \\ 0 & \lambda_2 & \cdots & 0 \\ \vdots & & \ddots & \vdots \\ 0 & 0 & \cdots & \lambda_N \end{bmatrix} \tag{2.68}$$

We note that the $\mathbf{A}$ matrix is perfectly known at the receiver. Furthermore, numerical values for $\lambda_1, \lambda_2, \ldots, \lambda_N$ are shown in Figure 2.4 for various values of acceleration factor ν. Due the fact that we consider a normalized transmit shaping filter, we can verify that we have:

$$\frac{1}{N}\sum_{n=1}^{N}\lambda_n = 1 \tag{2.69}$$

In Nyquist signaling, the real diagonal values $\{\lambda_n\}$ are equal to 1 i.e. $\lambda_1 = \lambda_2 = \ldots, \lambda_N = 1$. Whereas, in FTN signaling, the diagonal values are no longer equal to 1. Furthermore, for ν values grater than $1/(1+\beta)$, the eigenvalues are non-zero. Otherwise, there are a null values.

On other hand for the training sequence, the expression of transmitted signal is given as follows:

$$\mathbf{e}_{\mathrm{p}} = \begin{bmatrix} e_{p,1} \\ e_{p,2} \\ \vdots \\ e_{p,N_1^{\mathrm{p}}} \end{bmatrix} = \frac{1}{\sqrt{\mathrm{F}_s}} \times \mathbf{F}_{\mathrm{N}_1^{\mathrm{p}}}^{H} . diag \begin{bmatrix} \mathrm{H}_e(\Delta) \\ \mathrm{H}_e(2.\Delta) \\ \vdots \\ \mathrm{H}_e\left(N_1^{\mathrm{p}}.\Delta\right) \end{bmatrix} . \begin{bmatrix} \mathrm{I}_{\mathrm{p}}^{''} \\ \mathbf{I}_{N_{\mathrm{p}} \times N_{\mathrm{p}}} \\ \mathrm{I}_{\mathrm{p}}^{'} \end{bmatrix} . \begin{bmatrix} X_1 \\ X_2 \\ \vdots \\ X_{N_{\mathrm{p}}} \end{bmatrix} \tag{2.70}$$

The matrices $\mathbf{F}_{\mathrm{N_p}}$ and $\mathbf{F}_{\mathrm{N}_1^{\mathrm{p}}}$ are two normalized Fourier matrices with sizes $N_{\mathrm{p}} \times N_{\mathrm{p}}$ and $N_1^{\mathrm{p}} \times N_1^{\mathrm{p}}$, respectively. Additionally, the two matrices $\mathrm{I}_{\mathrm{p}}^{'}$ and $\mathrm{I}_{\mathrm{p}}^{''}$ being two $\frac{N_1^{\mathrm{p}} - \mathrm{N_p}}{2} \times \mathrm{N_p}$ matrices containing respectively the first $\frac{N_1^{\mathrm{p}} - \mathrm{N_p}}{2}$ and the last $\frac{N_1^{\mathrm{p}} - \mathrm{N_p}}{2}$ columns of the identity matrix $\mathbf{I}_{N_{\mathrm{p}} \times N_{\mathrm{p}}}$.

Further, The symbols $X_1, X_2, \ldots, X_{N_{\mathrm{p}}}$ denote the frequency responses of the transmit training sequence $\left[x_1, x_2, \ldots, x_{N_{\mathrm{p}}}\right]^T$ and are given as:

$$\left[X_1, X_2, \ldots, X_{N_{\mathrm{p}}}\right]^T = \mathbf{F}_{\mathrm{N_p}} . \left[x_1, x_2, \ldots, x_{N_{\mathrm{p}}}\right]^T \tag{2.71}$$

By assuming an independent and identically distributed (i.i.d) training symbols, we can deduce that the power spectrum density (PSD) of the considered training sequence is constant for all frequency elements and thus:

$$|X_n|^2 = \sigma_p^2 = \text{constant} \quad ; \quad \forall \quad 1 \leq n \leq N_{\mathrm{p}} \quad \text{(iid training symbol property)} \tag{2.72}$$

Finally, before transmitting the obtained time domain data signal $\mathbf{e}_i$ (respectively $\mathbf{e}_{\mathrm{p}}$ for training signal), a Cyclic Prefix (CP) of length T_g samples is inserted at the beginning of each resulting time domain data signal/training signal in order to cope with inter-symbol interference from the channel and to enable block circularization.

The obtained transmitted signal will be sent over a time-invariant communication channel $\mathrm{h}_a(\tau)$.

2.4.1.2 Expression of the received signal

Remove CP & down-Sampling: After removing the cyclic prefix (CP), $r(t)$ or $r_{\mathrm{p}}(t)$ will pass a down-sampling process with down-sampling factor equal to F_s. As a result, a sequence of N_1 (N_1^{p}) samples will be generated. The received sampled sequence is denoted by $\mathbf{r}_i = [r_{i,1}, r_{i,2}, \ldots, r_{i,N_1}]^T$ for receive data signal or $\mathbf{r}_i^{\mathrm{p}} = \left[r_{i,1}^{\mathrm{p}}, r_{i,2}^{\mathrm{p}}, \ldots, r_{i,N_1^{\mathrm{p}}}^{\mathrm{p}}\right]^T$ for receive training signal. Either $\mathbf{r}_i$ or $\mathbf{r}_i^{\mathrm{p}}$ can be expressed in this matrix forms:

$$\mathbf{r}_i = \begin{bmatrix} r_{i,1} \\ r_{i,2} \\ \vdots \\ r_{i,N_1} \end{bmatrix} = \begin{bmatrix} r\left([N_g+1].\frac{\mathrm{T}_s}{\mathrm{F}_s}\right) \\ r\left([N_g+2].\frac{\mathrm{T}_s}{\mathrm{F}_s}\right) \\ \vdots \\ r\left([N_g+N_1].\frac{\mathrm{T}_s}{\mathrm{F}_s}\right) \end{bmatrix} = \mathbf{F}_{\mathrm{N}_1}^{H} \times diag \begin{bmatrix} \mathrm{H}_a(1) \\ \mathrm{H}_a(2) \\ \vdots \\ \mathrm{H}_a(N_1) \end{bmatrix} \times \mathbf{F}_{\mathrm{N}_1} \times \begin{bmatrix} e_{i,1} \\ e_{i,2} \\ \vdots \\ e_{i,N_1} \end{bmatrix} + \begin{bmatrix} \widetilde{w}_1 \\ \widetilde{w}_2 \\ \vdots \\ \widetilde{w}_{N_1} \end{bmatrix} \tag{2.73}$$

or for the training signal,

$$\mathbf{r}_i^{\mathrm{p}} = \begin{bmatrix} r_{i,1}^{\mathrm{p}} \\ r_{i,2}^{\mathrm{p}} \\ \vdots \\ r_{i,N_1^{\mathrm{p}}}^{\mathrm{p}} \end{bmatrix} = \begin{bmatrix} r_{\mathrm{p}}\left([N_g+1].\frac{\mathrm{T}_s}{\mathrm{F}_s}\right) \\ r_{\mathrm{p}}\left([N_g+2].\frac{\mathrm{T}_s}{\mathrm{F}_s}\right) \\ \vdots \\ r_{\mathrm{p}}\left(\left[N_g+N_1^{\mathrm{p}}\right].\frac{\mathrm{T}_s}{\mathrm{F}_s}\right) \end{bmatrix} = \mathbf{F}_{\mathrm{N}_1^{\mathrm{p}}}^{H} \times diag \begin{bmatrix} \mathrm{H}_a(\Delta) \\ \mathrm{H}_a(2.\Delta) \\ \vdots \\ \mathrm{H}_a\left(N_1^{\mathrm{p}}.\Delta\right) \end{bmatrix} \times \mathbf{F}_{\mathrm{N}_1^{\mathrm{p}}} \times \begin{bmatrix} e_{p,1} \\ e_{p,2} \\ \vdots \\ e_{p,N_1^{\mathrm{p}}} \end{bmatrix} + \begin{bmatrix} \widetilde{w}_1 \\ \widetilde{w}_2 \\ \vdots \\ \widetilde{w}_{N_1^{\mathrm{p}}} \end{bmatrix} \tag{2.74}$$

The noise variables $\{\widetilde{w}_n\}$ are zero-mean complex AWGN with variance $\widetilde{\sigma}_w^2$ computed as:

$$\widetilde{\sigma}_w^2 = \mathrm{N}_0 \times \mathrm{F}_s \times \mathrm{R}_s = \mathrm{F}_s \times \sigma_w^2 \qquad \text{with} \qquad \sigma_w^2 = \mathrm{N}_0 \times \mathrm{R}_s \tag{2.75}$$

Additionally, $\mathrm{H}_a(1), \mathrm{H}_a(2), \ldots, \mathrm{H}_a(N_1)$ are the frequency responses the communication channel $\mathrm{h}_a(\tau)$:

$$\mathrm{H}_a(n) = \sum_{l=-\infty}^{+\infty} \mathrm{h}_a\left(l.\frac{\mathrm{T}_s}{\mathrm{F}_s}\right) \exp\left(-2\pi jl.\frac{\mathrm{T}_s}{\mathrm{F}_s}.f_n\right) = \sum_{l=0}^{+L_c} \mathrm{h}_a\left(l.\frac{\mathrm{T}_s}{\mathrm{F}_s}\right) \exp\left(-2\pi jl.\frac{\mathrm{T}_s}{\mathrm{F}_s}.f_n\right) \tag{2.76}$$

The positive integer L_c denotes the memory size of the discrete-time response of $\mathrm{h}_a(\tau)$ which is calculated as:

$$L_c = \left\lceil \frac{\tau_{\mathrm{N_m}-1}}{\mathrm{T}_s/\mathrm{F}_s} \right\rceil \tag{2.77}$$

where $\lceil(.)\rceil$ stands for the integer part of $(.)$.

Frequency domain processing: After sampling, the resulting sequences $\mathbf{r}_i$ and $\widetilde{\mathbf{r}}_i$ will pass to the frequency domain by using a Fast Fourier Transformation (FFT). This FFT transformation is equivalent to multiply the obtained down-sampled sequence by the Fourier matrix $\mathbf{F}_{\mathrm{N}_1}$ for data sequence and $\mathbf{F}_{\mathrm{N}_1^{\mathrm{p}}}$ for training sequence. As a result we have a frequency sequence denoted by $\mathbf{U}_i$ (respectively $\mathbf{U}_i^{\mathrm{p}}$ for training sequence). $\widetilde{\mathbf{Y}}_i$ and $\widetilde{\mathbf{Y}}_i^{\mathrm{p}}$ can be written in this matrix forms:

$$\widetilde{\mathbf{Y}}_i = \begin{bmatrix} \widetilde{Y}_{i,1} \\ \widetilde{Y}_{i,2} \\ \vdots \\ \widetilde{Y}_{i,N_1} \end{bmatrix} = \mathbf{F}_{\mathrm{N}_1}. \begin{bmatrix} r_{i,1} \\ r_{i,2} \\ \vdots \\ r_{i,N_1} \end{bmatrix} = \sqrt{\mathrm{F}_s} \times diag \begin{bmatrix} \mathrm{H}_a(1) \\ \mathrm{H}_a(2) \\ \vdots \\ \mathrm{H}_a(N_1) \end{bmatrix} . \mathbf{A}. \mathbf{F}_{\mathrm{N}}. \begin{bmatrix} s_{i,1} \\ s_{i,2} \\ \vdots \\ s_{i,N} \end{bmatrix} + \begin{bmatrix} \widetilde{w}_1 \\ \widetilde{w}_2 \\ \vdots \\ \widetilde{w}_{N_1} \end{bmatrix} \tag{2.78}$$

Similarly for receive training symbols, the expression of the frequency domain received signal is given as follows:

$$\widetilde{\mathbf{Y}}_i^{\mathrm{p}} = \begin{bmatrix} \widetilde{Y}_{i,1}^{\mathrm{p}} \\ \widetilde{Y}_{i,2}^{\mathrm{p}} \\ \vdots \\ \widetilde{Y}_{i,N_1^{\mathrm{p}}}^{\mathrm{p}} \end{bmatrix} = \frac{1}{\sqrt{\mathrm{F}_s}}. \; diag \begin{bmatrix} \mathrm{H}_a(\Delta) \\ \mathrm{H}_a(2.\Delta) \\ \vdots \\ \mathrm{H}_a\left(N_1^{\mathrm{p}}.\Delta\right) \end{bmatrix} .diag \begin{bmatrix} \mathrm{H}_e(\Delta) \\ \mathrm{H}_e(2.\Delta) \\ \vdots \\ \mathrm{H}_e\left(N_1^{\mathrm{p}}.\Delta\right) \end{bmatrix} . \begin{bmatrix} \mathrm{I}_{\mathrm{p}}'' \\ \mathbf{I}_{N_{\mathrm{p}} \times N_{\mathrm{p}}} \\ \mathrm{I}_{\mathrm{p}}' \end{bmatrix} . \begin{bmatrix} X_1 \\ X_2 \\ \vdots \\ X_{N_{\mathrm{p}}} \end{bmatrix} + \begin{bmatrix} \widetilde{w}_1 \\ \widetilde{w}_2 \\ \vdots \\ \widetilde{w}_{N_1^{\mathrm{p}}} \end{bmatrix} \tag{2.79}$$

2.4.2 Existing frequency-domain channel equalization methods

In linear model, as given in Equation (2.78), a Minimum Mean Square Error (MMSE) criterion is often used to equalize received data sequence. The term MMSE refers more specifically to the detection in a Bayesian parameter with a quadratic cost function $\mathbf{J}$ expressed as:

$$\mathbf{J} = \mathbb{E}\left\{\|\mathbf{s}_i - \mathbf{z}_i\|^2\right\} = \mathbb{E}\left\{\left\|\mathbf{s}_i - \mathbf{W}.\widetilde{\mathbf{Y}}_i\right\|^2\right\} \tag{2.80}$$

where $\widetilde{\mathbf{Y}}_i$ is a random observation vector from the channel given through the linear model (2.78):

$$\widetilde{\mathbf{Y}}_i = \sqrt{\mathrm{F}_s} \times \left\{ diag \begin{bmatrix} \mathrm{H}_a(1) \\ \mathrm{H}_a(2) \\ \vdots \\ \mathrm{H}_a(N_1) \end{bmatrix} . \mathbf{A} \right\} . \mathbf{F}_{\mathrm{N}}. \begin{bmatrix} s_{i,1} \\ s_{i,2} \\ \vdots \\ s_{i,N} \end{bmatrix} + \begin{bmatrix} \widetilde{w}_1 \\ \widetilde{w}_2 \\ \vdots \\ \widetilde{w}_{N_1} \end{bmatrix} = \sqrt{\mathrm{F}_s} \times \mathbf{A}_i. \mathbf{F}_{\mathrm{N}}. \begin{bmatrix} s_{i,1} \\ s_{i,2} \\ \vdots \\ s_{i,N} \end{bmatrix} + \begin{bmatrix} \widetilde{w}_1 \\ \widetilde{w}_2 \\ \vdots \\ \widetilde{w}_{N_1} \end{bmatrix} \tag{2.81}$$

The noise variables $\{\widetilde{w}_n\}$ are zero-mean complex AWGN with variance $\widetilde{\sigma}_w^2$ computed as:

$$\widetilde{\sigma}_w^2 = \mathrm{N}_0 \times \mathrm{F}_s \times \mathrm{R}_s = \mathrm{F}_s \times \sigma_w^2 \qquad \text{with} \qquad \sigma_w^2 = \mathrm{N}_0 \times \mathrm{R}_s \tag{2.82}$$

MMSE with *a priori* in the case of general channel matrix form: In [122, 124], it is shown that is possible to enhance the performances of the MMSE linear equalizer by considering some *a priori* information on the distribution of the transmitted constellation symbols $\mathbf{s}_i$ to be estimated, notably the mean symbol vector $\bar{\mathbf{s}}_i = [\bar{s}_{i,1}, \bar{s}_{i,2}, \ldots, \bar{s}_{i,N}]^T$ and the soft symbol variance $\bar{v}_s$ $(0 \leq \bar{v}_s/\sigma_s^2 \leq 1)$. Thereupon, solving this kind of problem amounts to solving a linear system with minimization of the cost function.

$$\mathbf{W}_i^{\text{opt}} = \underset{\mathbf{W}_i}{\operatorname{argmin}} \{\mathbf{J}\} = \underset{\mathbf{W}_i}{\operatorname{argmin}} \left\{ \mathbb{E}\left\{ \left\| \mathbf{s}_i - \mathbf{W}_i . \widetilde{\mathbf{Y}}_i \right\|^2 \right\} \right\} \tag{2.83}$$

The mean symbol vector $\bar{\mathbf{s}}_i$ and soft symbol variance $\bar{v}_s$ are computed from a given *a priori* information vector denoted by $\mathrm{L}_a^{\text{in}}(\mathbf{c}_i)$ which contains a number of $N \times \log_2(M)$ bit Log-Likelihood Ratio values:

$$\mathrm{L}_a^{\text{in}}(\mathbf{c}_i) = \left[\mathrm{L}_a^{\text{in}}(c_{i,1}), \mathrm{L}_a^{\text{in}}(c_{i,2}), \ldots, \mathrm{L}_a^{\text{in}}\left(c_{i,\log_2(M)\times N}\right) \right] \tag{2.84}$$

By assuming $\left[u_1^{(m)}, u_2^{(m)}, \ldots, u_{\log_2(M)}^{(m)}\right]$ is the transmit bit sequence corresponding to $s_{i,n} = \mathcal{C}_m$, a soft mapper (cf.2.5) is able to compute $\bar{\mathbf{s}}_i$ and $\bar{v}_s$ in two steps:

- First, a conditional probability denoted by $\Pr\left\{s_{i,n} = \mathcal{C}_m | \mathrm{L}_a^{\text{in}}(\mathbf{c}_i)\right\}$ is derived as follows:

$$\Pr\left\{s_{i,n} = \mathcal{C}_m | \mathrm{L}_a^{\text{in}}(\mathbf{c}_i)\right\} = \prod_{q=1}^{\log_2(M)} \frac{\exp\left(-u_q^{(m)} \times \mathrm{L}_a^{\text{in}}\left[c_{i,q+(n-1)\times\log_2(M)}\right]\right)}{1+\exp\left(-\mathrm{L}_a^{\text{in}}\left[c_{i,q+(n-1)\times\log_2(M)}\right]\right)} \tag{2.85}$$

- Second, The mean symbol vector $\bar{\mathbf{s}}_i$ and soft symbol variance $\bar{v}_s$ are deduced as follows:

$$\begin{aligned} \bar{s}_{i,n} &= \sum_{m=1}^{M} \Pr\left\{s_{i,n} = \mathcal{C}_m | \mathrm{L}_a^{\text{in}}(\mathbf{c}_i)\right\} \times \mathcal{C}_m \\ \bar{v}_s &= \frac{1}{N} \sum_{n=1}^{N} \left[\sum_{m=1}^{M} \Pr\left\{s_{i,n} = \mathcal{C}_m | \mathrm{L}_a^{\text{in}}(\mathbf{c}_i)\right\} \times |\mathcal{C}_m - \bar{s}_{i,n}|^2 \right] \end{aligned} \tag{2.86}$$

Note that $\bar{v}_s$ values are taken between 0 and σ_s^2 i.e. $0 \leq \bar{v}_s \leq \sigma_s^2$. In the case of zero *a priori*, we have $\bar{v}_s = \sigma_s^2$. However, in perfect *a priori* case, we have $\bar{v}_s = 0$.

In linear model (2.81), the noise variable $\{\widetilde{w}_n\}$ are zero-mean complex AWGN with variance $\widetilde{\sigma}_w^2 = \mathrm{F}_s \times \sigma_w^2$. Furthermore, the constellation symbols $\{s_{i,n}\}$ are assumed i.id with variance equal to σ_s^2. After a linear

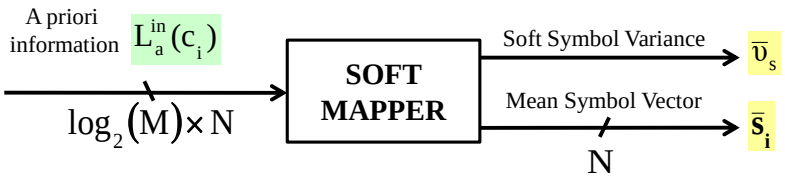

Figure 2.5: *Considered Soft Mapper scheme*

resolution of the equation (2.83) taking into account *a priori* information i.e. $\bar{\mathbf{s}}_i$ and $\bar{v}_s$, the MMSE with *a priori* can still been computed using the same steps as in [124]. We denote $\mathbf{z}_i = [z_{i,1}, z_{i,2}, \ldots, z_{i,N}]^T$ as the output MMSE equalization vector which is a soft estimate of $\mathbf{s}_i = [s_{i,1}, s_{i,2}, \ldots, s_{i,N}]^T$ and is obtained by considering MMSE criterion and resolving the equation (2.83) using the following linear equation:

$$\mathbf{z}_i = \mathbf{W}_i^{\text{opt}}.\widetilde{\mathbf{Y}}_i = \mathbf{F}_{\text{N}}^H.\Sigma^{-1}.\mathbf{A}_i^H.\left(\frac{1}{\sqrt{\text{F}_s}}.\ \widetilde{\mathbf{Y}}_i - \mathbf{A}_i.\mathbf{F}_{\text{N}}.\bar{\mathbf{s}}_i\right) + \mu_i = \mathbf{F}_{\text{N}}^H.\Sigma^{-1}.\left(\mathbf{Y}_i - \bar{\mathbf{Y}}_i\right) + \mu_i \tag{2.87}$$

where $\mathbf{Y}_i = \frac{1}{\sqrt{\text{F}_s}}.\ \mathbf{A}_i^H.\widetilde{\mathbf{Y}}_i$ is the output frequency domain observation after being filtered by a receive matched filter. Furthermore, The three quantities Σ^{-1}, μ_i and $\bar{\mathbf{Y}}_i$ denote the three MMSE equalization parameters to be computed for a given *a priori* information $(\bar{v}_s, \bar{\mathbf{s}}_i)$ and they are expressed as:

$$\Sigma^{-1} \triangleq \frac{1}{1+[1-(\bar{v}_s/\sigma_s^2)].\ \varrho_i}.\left[\left(\bar{v}_s/\sigma_s^2\right).\ \mathbf{A}_i^H.\mathbf{A}_i + \left(\sigma_w^2/\sigma_s^2\right).\ \mathbf{I}_{N\times N}\right]^{-1} \tag{2.88}$$

$$\bar{\mathbf{Y}}_i \triangleq \mathbf{A}_i^H.\mathbf{A}_i.\mathbf{F}_{\text{N}}.\bar{\mathbf{s}}_i \tag{2.89}$$

$$\mu_i \triangleq \frac{\varrho_i}{1+[1-(\bar{v}_s/\sigma_s^2)].\ \varrho_i}.\ \bar{\mathbf{s}}_i = \alpha_i.\ \bar{\mathbf{s}}_i \tag{2.90}$$

By taking into account an *a priori* information, the values of the two real positive scalars, ϱ_i and α_i, depend on the given symbol variance values $\bar{v}_s$ as follows:

$$\varrho_i \triangleq \frac{1}{N}.\ tr\left\{\left[\left(\bar{v}_s/\sigma_s^2\right).\ \mathbf{A}_i^H.\mathbf{A}_i + \left(\sigma_w^2/\sigma_s^2\right).\ \mathbf{I}_{N\times N}\right]^{-1}.\mathbf{A}_i^H.\mathbf{A}_i\right\} \quad \text{and} \quad \alpha_i \triangleq \frac{\varrho_i}{1+[1-(\bar{v}_s/\sigma_s^2)].\ \varrho_i} \tag{2.91}$$

In general form of channel matrix, the implementation of MMSE with *a priori* equalization would require an online inversion of Σ having a size of $N \times N$ in each transmitted sub-frame. This is clearly impractical for large N. However, in the case of circular channel matrix, the matrix inversion is no longer a problem. Indeed, in our case, we can show that the matrix $\mathbf{A}_i^H.\mathbf{A}_i$ is a $N \times N$ diagonal matrix and $\text{H}_{i,1}, \text{H}_{i,2}, \ldots, \text{H}_{i,N}$ are its real diagonal values:

$$\mathbf{A}_i^H.\mathbf{A}_i = \mathbf{A}^H\, diag\begin{bmatrix} |\text{H}_a(1)|^2 \\ |\text{H}_a(2)|^2 \\ \vdots \\ |\text{H}_a(N_1)|^2 \end{bmatrix}.\ \mathbf{A} = diag\begin{bmatrix} \text{H}_{i,1} \\ \text{H}_{i,2} \\ \vdots \\ \text{H}_{i,N} \end{bmatrix} \tag{2.92}$$

As a favorable result, the channel equalization is simplified to a channel inversion operation on each sub-carrier:

$$\Sigma^{-1} = \frac{\sigma_s^2}{1+[1-(\bar{v}_s/\sigma_s^2)].\ \varrho_i}.diag\begin{bmatrix} \frac{1}{\bar{v}_s.\ \text{H}_{i,1}+\sigma_w^2} \\ \frac{1}{\bar{v}_s.\ \text{H}_{i,2}+\sigma_w^2} \\ \vdots \\ \frac{1}{\bar{v}_s.\ \text{H}_{i,N}+\sigma_w^2} \end{bmatrix} \quad \text{with} \quad \varrho_i = \frac{1}{N}\sum_{n=1}^{N}\frac{\text{H}_{i,n}}{(\bar{v}_s/\sigma_s^2).\ \text{H}_{i,n}+(\sigma_w^2/\sigma_s^2)} \tag{2.93}$$

Thus, the complexity of the receiver is significantly reduced and matrix inversion is no longer a problem. Moreover, the expression of $\bar{\mathbf{Y}}_i$ and μ_i can be reduced to:

$$\bar{\mathbf{Y}}_i = diag\begin{bmatrix} \text{H}_{i,1} \\ \text{H}_{i,2} \\ \vdots \\ \text{H}_{i,N} \end{bmatrix}.\mathbf{F}_{\text{N}}.\begin{bmatrix} \bar{s}_{i,1} \\ \bar{s}_{i,2} \\ \vdots \\ \bar{s}_{i,N} \end{bmatrix} \quad \text{and} \quad \mu_i = \alpha_i.\begin{bmatrix} \bar{s}_{i,1} \\ \bar{s}_{i,2} \\ \vdots \\ \bar{s}_{i,N} \end{bmatrix} \tag{2.94}$$

Referring to [70], it is shown that $\widetilde{\mathbf{z}}_i$ is a biased estimation of $\mathbf{s}_i$ and its expression can be approximated to:

$$\mathbf{z}_i = \begin{bmatrix} z_{i,1} \\ z_{i,2} \\ \vdots \\ z_{i,N} \end{bmatrix} = \mathbf{F}_{\mathrm{N}}^{H}.\Sigma^{-1}.\left(\mathbf{Y}_i - \bar{\mathbf{Y}}_i\right) + \mu_i \approx \alpha_i \left\{ \begin{bmatrix} s_{i,1} \\ s_{i,2} \\ \vdots \\ s_{i,N} \end{bmatrix} + \frac{1}{\sqrt{\gamma_i}} \begin{bmatrix} w_{i,1} \\ w_{i,2} \\ \vdots \\ w_{i,N} \end{bmatrix} \right\} \tag{2.95}$$

where $\mathbf{w} = [w_1, w_2, \ldots, w_N]^T$ is a zero-mean complex AWGN noise vector and symbols $\{w_n\}$ having a variance equal to σ_w^2. Additionally, the positive scalar γ_i denotes the MMSE equalization gain and is referred to the reduced signal-to-noise ratio (SNR). The expression of γ_i is given as the following:

$$\gamma_i = \left(\sigma_w^2/\sigma_s^2\right).\frac{\alpha_i}{1-\alpha_i} = \left(\sigma_w^2/\sigma_s^2\right).\frac{\varrho_i}{1-\left(\bar{v}_s/\sigma_s^2\right).\varrho_i} \tag{2.96}$$

Referring to the the previous expression (2.96), we can deduce that the value of γ_i depends on the shape of the channel frequency response and also on the value of the *a priori* information and notably the symbol variance $\bar{v}_s$. Indeed, we can show that γ_i values are inversely proportional to $\bar{v}_s$ values and channel selectivity level. Assuming that the channel frequency response still invariant for all sub-frame duration, for all $\bar{v}_s$ between 0 and σ_s^2, γ_i values are delimited between two finite extreme values $\gamma_i^{\min}$ and $\gamma_i^{\max}$. $\gamma_i^{\min}$ denotes the lower bound of γ_i values and is obtained in the case of zero *a priori* ($\bar{v}_s = \sigma_s^2$). However, $\gamma_i^{\max}$ denotes the upper bound of γ_i values and is obtained on the case of perfect *a priori* ($\bar{v}_s = 0$):

$$0 < \underbrace{\gamma_i^{\min}}_{\text{zero a priori}} \leq \gamma_i \leq \underbrace{\gamma_i^{\max}}_{\text{perfect a priori}} \tag{2.97}$$

Note that in the case of circular channel matrix form, by using Equation (2.96), a close expression of the MMSE equalization gain, γ_i, is given by:

$$\gamma_i = \frac{\left(\sigma_w^2/\sigma_s^2\right).\varrho_i}{1-\left(\bar{v}_s/\sigma_s^2\right).\varrho_i} = \begin{cases} \left(\frac{1}{N}\sum_{n=1}^{N}\frac{1}{\mathrm{H}_{i,n}+\left(\sigma_w^2/\sigma_s^2\right)}\right)^{-1} - \left(\sigma_w^2/\sigma_s^2\right) = \gamma_i^{\min} & \text{for} \quad \bar{v}_s = \sigma_s^2 \quad \text{(zero a priori)} \\ \left(\sigma_s^2/\bar{v}_s\right).\left\{\left(\frac{1}{N}\sum_{n=1}^{N}\frac{1}{\left(\bar{v}_s/\sigma_s^2\right).\mathrm{H}_{i,n}+\left(\sigma_w^2/\sigma_s^2\right)}\right)^{-1} - \left(\sigma_w^2/\sigma_s^2\right)\right\} & \text{for} \quad 0 < \bar{v}_s < \sigma_s^2 \\ \frac{1}{N}\sum_{n=1}^{N}\mathrm{H}_{i,n} = \gamma_i^{\max} \approx 1 & \text{for} \quad \bar{v}_s = 0 \quad \text{(Perfect a priori)} \end{cases} \tag{2.98}$$

Besides, owing to the Gaussian model given in Equation (2.95) and for the sake of simplicity, we introduce an equivalent reduced output equalized sequence denoted by $\widetilde{\mathbf{s}}_i = [\widetilde{s}_{i,1}, \widetilde{s}_{i,2}, \ldots, \widetilde{s}_{i,N}]^T$ and can be written as a function of the output equalized sequence $\mathbf{z}_i$. The introduced equalized sequence $\widetilde{\mathbf{s}}_i$ is expressed as:

$$\widetilde{\mathbf{s}}_i = \begin{bmatrix} \widetilde{s}_{i,1} \\ \widetilde{s}_{i,2} \\ \vdots \\ \widetilde{s}_{i,N} \end{bmatrix} = \sqrt{\frac{\gamma_i}{\alpha_i^2}}\,\mathbf{z}_i = \sqrt{\frac{\gamma_i}{\alpha_i^2}} \begin{bmatrix} z_{i,1} \\ z_{i,2} \\ \vdots \\ z_{i,N} \end{bmatrix} = \sqrt{\gamma_i} \begin{bmatrix} s_{i,1} \\ s_{i,2} \\ \vdots \\ s_{i,N} \end{bmatrix} + \begin{bmatrix} w_{i,1} \\ w_{i,2} \\ \vdots \\ w_{i,N} \end{bmatrix} \tag{2.99}$$

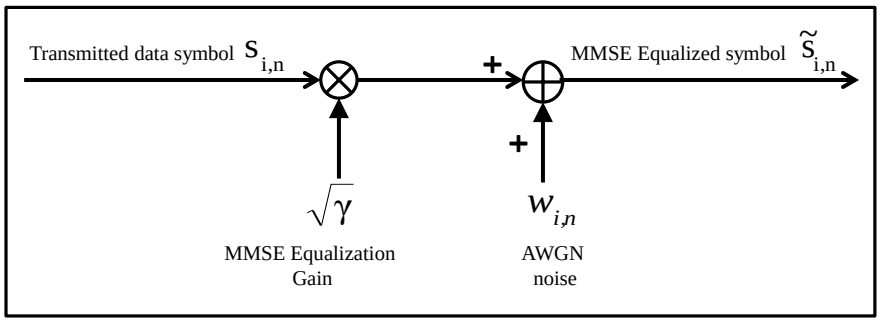

Figure 2.6: *Gaussian approximation of MMSE estimated symbols*

Given the additive noise is «uncorrelated», each MMSE estimated symbol $\widetilde{s}_{i,n}$ can be independently modeled by an equivalent scheme shown in Figure 2.6.

Finally, by using (2.87) and given that observation samples $\{Y_{i,n}\}$ represent a sufficient statistic (matched filtering), we can consider a simplified MMSE equalization structure that taking at a starting point the samples $\{Y_{i,n}\}$ as shown in Figure 2.7. At the output of MMSE equalization, an extrinsic LLR vector is generated. The considered extrinsic LLR vector contains $N \times \log_2(M)$ bit LLR values and is denoted by $\mathrm{L}_e^{\mathrm{out}}(\mathbf{c}_i) = \left[\mathrm{L}_e^{\mathrm{out}}(c_{i,1}), \mathrm{L}_e^{\mathrm{out}}(c_{i,2}), \ldots, \mathrm{L}_e^{\mathrm{out}}\left(c_{i,\log_2(M)\times N}\right)\right]$. At the bit position $p = q + (n-1) \times \log_2(M)$ with $1 \leq q \leq \log_2(M)$, the expression of $\mathrm{L}_e^{\mathrm{out}}\left(c_{i,q+(n-1)\times\log_2(M)}\right)$ is given as:

$$\mathrm{L}_e^{\mathrm{out}}\left[c_{i,q+(n-1)\times\log_2(M)}\right] = \mathrm{L}_a^{\mathrm{out}}\left(c_{i,q+(n-1)\times\log_2(M)}\right) - \mathrm{L}_a^{\mathrm{in}}\left(c_{i,q+(n-1)\times\log_2(M)}\right) \tag{2.100}$$

where $\mathrm{L}_a^{\mathrm{in}}\left(c_{i,q+(n-1)\times\log_2(M)}\right)$ is the *a priori* information vector given in Equation (2.84) and $\mathrm{L}_a^{\mathrm{out}}\left[c_{i,q+(n-1)\times\log_2(M)}\right]$ is the *a posteriori* information of the coded bit $c_{i,q+(n-1)\times\log_2(M)}$ which is derived by using the following expression:

$$\mathrm{L}_a^{\mathrm{out}}\left[c_{i,q+(n-1)\times\log_2(M)}\right] = \log\left\{\frac{\sum_{m\in\mathbf{U}_q^0}\Pr\left(s_{i,n}=\mathcal{C}_m|\mathrm{L}_a^{\mathrm{in}}(\mathbf{c}_i)\right)\Pr(\widetilde{s}_{i,n}|s_{i,n}=\mathcal{C}_m)}{\sum_{m\in\mathbf{U}_q^1}\Pr\left(s_{i,n}=\mathcal{C}_m|\mathrm{L}_a^{\mathrm{in}}(\mathbf{c}_i)\right)\Pr(\widetilde{s}_{i,n}|s_{i,n}=\mathcal{C}_m)}\right\} \tag{2.101}$$

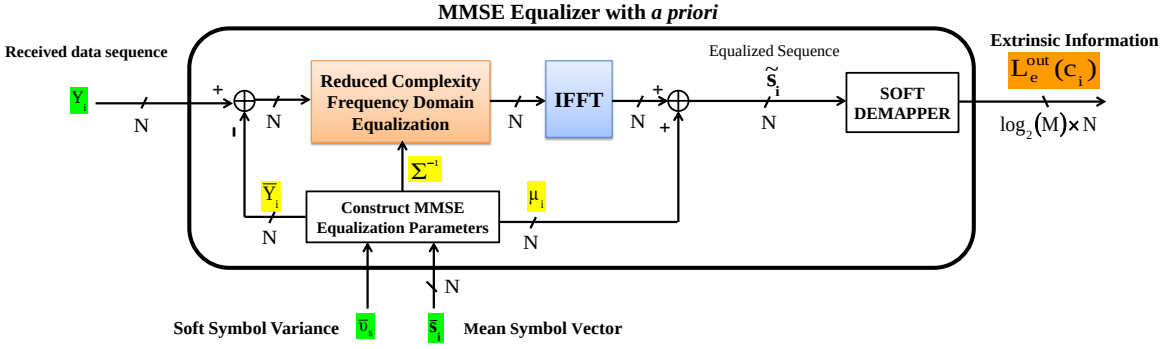

Figure 2.7: *The considered Linear MMSE equalizer using a priori information.*

MOD	$\mathrm{D}_{\min}$	σ_s^2	$\mathrm{D}_{\min}^2/(2.\sigma_s^2)$	N_v
M-PSK	$2\times\sin(\frac{\pi}{M})$	1	$2\times\sin^2(\frac{\pi}{M})$	2
M-QAM	2	$2\times(M-1)/3$	$3/(M-1)$	$4\times\left(\sqrt{M}-1\right)/\sqrt{M}$

Table 2.1: *Numerical values of N_v and D_{min} for each considered linear modulation.*

The two sets of the constellation indexes $\mathbf{U}_q^0$ and $\mathbf{U}_q^1$ correspond to have respectively 0 and 1 entries at the q-th index position of constellation bits and verifying,

$$\mathbf{U}_q^0 \cup \mathbf{U}_q^1 = \{1,2,\ldots,M\} \qquad ; \qquad \mathbf{U}_q^0 \cap \mathbf{U}_q^1 = \oslash \tag{2.102}$$

Referring to (2.99), the conditional probability $\Pr(\widetilde{s}_{i,n}|s_{i,n}=\mathcal{C}_m)$ is given by the following expression:

$$\Pr(\widetilde{s}_{i,n}|s_{i,n}=\mathcal{C}_m) = \frac{1}{\pi.\sigma_w^2}\exp\left(-\frac{\left|\widetilde{s}_{i,n}-\sqrt{\gamma_i}\,\mathcal{C}_m\right|^2}{\sigma_w^2}\right)$$

2.4.2.1 The uncoded case:

In the uncoded case, we did not consider *a priori* information i.e $\gamma_i = \gamma_i^{\min}$. In general case, $\gamma_i^{\min}$ is a complex random variable depending on the instantaneous channel response i.e the channel matrix $\mathbf{A}_i$. In this case, the theoretical average Symbol Error Rate (SER) can be determinated as follows:

$$\text{Average SER} = \int \text{SER}\left(\gamma_i^{\min}\right)\ \text{PDF}\left(\gamma_i^{\min}\right)\ d\gamma_i^{\min} \tag{2.103}$$

with

$$\begin{aligned}\text{SER}\left(\gamma_i^{\min}\right) &= \mathrm{N}_v \times Q\left(\sqrt{\frac{\gamma_i^{\min}.\mathrm{D}_{\min}^2}{2\ \sigma_w^2}}\right) = \mathrm{N}_v \times Q\left(\sqrt{\gamma_i^{\min}.\left(\frac{\mathrm{D}_{\min}^2}{2.\sigma_s^2}\right).\mathrm{E}_s/\mathrm{N}_0}\right)\\ &= \mathrm{N}_v \times Q\left(\sqrt{\gamma_i^{\min}.\left(\frac{\mathrm{D}_{\min}^2}{2.\sigma_s^2}\right).\mathrm{R}_c.\log_2(M).\mathrm{E}_b/\mathrm{N}_0}\right)\end{aligned} \tag{2.104}$$

where $Q(x)$ stands for the Q-function. $\mathrm{D}_{\min}$ is defined as the minimum distance between two arbitrary constellation points and N_v is the mean number of possible neighbors constellation points having a distance equal to $\mathrm{D}_{\min}$. Table 2.1 shows some values taken by N_v and $\mathrm{D}_{\min}$ in linear modulation.

By considering Gray mapping [50], it is shown that we have only one erroneous bit in each erroneous mapping constellation symbol. Thus, the theoretical average Bit Error Rate can be expressed as:

$$\text{Average BER} \cong \frac{1}{\log_2(M)} \times \text{Average SER} \tag{2.105}$$

2.4.2.2 The coded case: using turbo-equalization

In coded case, after MMSE equalization process, a soft channel decoding structure is added in series to decode received data bits. In order to improve performance system, MMSE equalization and channel decoding will be operated in iterative process to maximize the reliability of transmitted bits. As as result, a

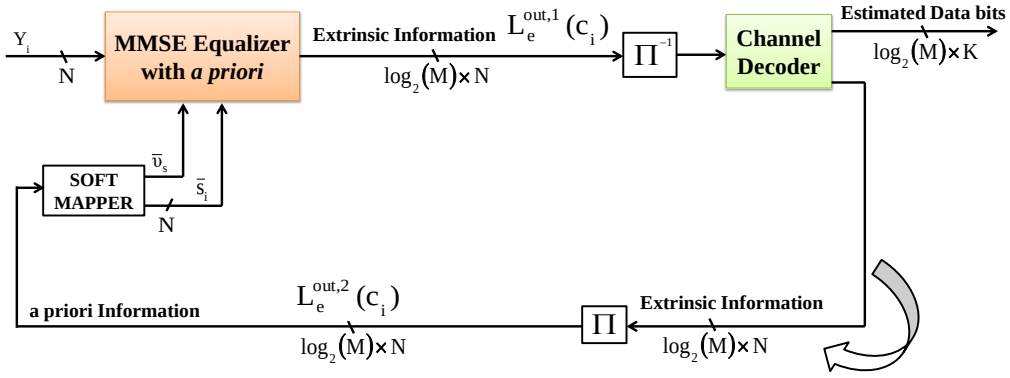

Figure 2.8: *Considered iterative equalization structure.*

turbo equalization is performed. For each iteration, the MMSE equalizer will generate an extrinsic bit information denoted by $\mathrm{L}_e^{\mathrm{out},1}(\mathbf{c}_i) = \left[\mathrm{L}_e^{\mathrm{out},1}(c_{i,1}), \mathrm{L}_e^{\mathrm{out},1}(c_{i,2}), \ldots, \mathrm{L}_e^{\mathrm{out},1}\left(c_{i,\log_2(M)\times N}\right)\right]^T$ corresponding to each symbol assigned by the channel. Then this extrinsic information will be sent to LDPC/convolutional decoder, which does not require the calculation of an observation, not an estimate of the noise variance on this observation. At the output of decoding, another extrinsic bit information denoted by $\mathrm{L}_e^{\mathrm{out},2}(\mathbf{c}_i) = \left[\mathrm{L}_e^{\mathrm{out},2}(c_{i,1}), \mathrm{L}_e^{\mathrm{out},2}(c_{i,2}), \ldots, \mathrm{L}_e^{\mathrm{out},2}\left(c_{i,\log_2(M)\times N}\right)\right]^T$ will be generated. The latter will be used in the next iteration as *a priori* information for Bayesian MMSE equalization. The iterative receiver diagram is shown in Figure 2.8.

2.4.3 Existing frequency-domain channel estimation methods

In order to equalize received data sequence, we need to estimate the frequency response of the baseband channel. Indeed, in the case of using EW SC-OFDM waveform, it is assumed that frequency channel response vector $\mathbf{H}_a$ is fully known at the receiver. In order to have a realistic system performance, it is essential to take into consideration an accurate estimation of the frequency channel vector $\mathbf{H}_a$ at the receiver. To do it, we will investigate some existing channel estimation algorithms suitable for EW SC-OFDM waveform.

Until today, it is common to use pilot-based channel estimation algorithms, including LS (Least Squares), Minimum Mean Square Error (MMSE), and channel estimation based on transformation domain, etc. [52] proposed a symbol decision algorithm for fast time-varying channel estimation, but its accuracy is not good enough; [130] presented a combination channel estimation algorithm that has good performance when SNR is between 7∼15dB, but it decreases when SNR takes other values; [56, 104] made a research on LS, MMSE and decision feedback algorithm,the simulation results show that MMSE has a better performance; R-LS (Regularization-LS) algorithm and M-MMSE(Mismatch-MMSE) algorithm are respectively proposed in [3, 54], the feasibility of the theoretical analysis is verified by simulation results.

Besides, for time-slotted mobile communication systems, [92] presented reduced-rank LS (rr-LS) channel estimation algorithm. It has been shown that reduced rank methods allow to improve the estimate accuracy

by reducing the set of unknown parameters (rank reduction) [92] [55].

2.5 Conclusion

In this chapter, we presented two waveforms; Single carrier and Extended Weighted Single Carrier Orthogonal Frequency-Division Multiplexing EW SC-OFDM which are suitable to satellite context. For both SC and EW SC-OFDM, a system model is described considering a generalized form of the propagation channel. In order to mitigate ISI introduced by the channel, we presented various equalization methods which are classified according to the channel form (sparse, two-taps, symmetric, etc.) or also according to the type of signaling (FTN/Nyquist) and also according to the shape of the waveform (circular/non-circular). In a first time, for equalization algorithms, we supposed that channel coefficients are perfectly known at the receiver. Later, an overview of existing channel estimation methods is given. Channel estimation methods are also classified according to the type of waveform (Time-domain or Frequency-domain), according to the channel form and also according to the type of signaling.

For channel equalization methods, we are interested in BCJR-based symbol detection for both Nyquist and FTN signaling. In Nyquist signaling, *Forney's model* can give an optimal MAP-based symbol detection for which sparse structure can be exploited. However, for FTN signaling, the noise correlation is a problem. It makes MAP-based symbol detection, according to the *Forney's model*, a sub-optimal detection. If the channel is symmetric, one may resort to the *Ungerboeck's model* to have an optimal detection.

For channel estimation methods, there are two main classes: Time-domain and frequency-domain channel estimation methods. In Nyquist signaling, there are no noise correlation. In this case, LS estimators are equivalent to ML estimators and can achieve the lower Cramer-Rao Bound (CRB). However, in FTN signaling the noise becomes correlated and it is a serious problem for time-domain channel estimation methods. Indeed, in some cases for time-domain channel estimation methods, if the covariance matrix of the additive noise is not invertible, an optimal solution is not possible and this case remains an open problem.

Chapter 3

Forward link: Channel estimation & Channel equalization

Sommaire

3.1 Introduction

In Chapter 1, we studied different possible UAV/aircraft links that can be considered in aeronautical communications. Mainly, there are three possible links; two satellite links which are the forward link and the return link and one terrestrial link which is the mission link. Because of the presence of satellite link, we considered two low PAPR linear waveforms : classical Single-Carrier (SC) waveform and Extended Weighted Single-Carrier Orthogonal Frequency-Division Multiplexing (EW SC-OFDM) waveform. These two waveforms have been studied in Chapter 2 with a generalized form of the propagation channel. Knowing the explicit expression of the satellite-to-aircraft (S2A) propagation channel, this chapter aims to study the viability of these two waveforms for the forward link. Moreover, thanks to the particular form of S2A channel, it is possible to propose new tailored solutions for both channel estimation and channel equalization tasks.

3.2 Classical Single-Carrier (SC) waveform

In this Section, we are interested in classical SC waveform. Based on the expression of received symbols (data symbols and training symbols) initially given in Equations (2.22) and (2.23), this section aims to give the corresponding system model in the case of aeronautical channel and especially for the forward link. We recall that the expression of the satellite-to-aircraft (S2A) channel is initially done in Equation (1.22). By introducing the particular form of S2A channel, it may be possible to propose new efficient and appropriate solutions. Especially, for channel estimation and channel equalization.

3.2.1 Expression of impulse response of the satellite-to-aircraft (S2A) channel

In Chapter 2, we studied the system model for both SC and EW SC-OFDM waveforms for a general form of the propagation channel $\mathrm{h}_a(t,\tau)$. For the forward link, it has been shown in Chapter 1 that the S2A channel (propagation channel) has a particular form. This channel contains only three main paths with two delays $\tau_0 = 0$ and τ_2. Its expression is initially given in (1.22) as:

$$\mathrm{h}_a(t,\tau) = \sum_{n=0}^{\mathrm{N_m}-1} a_n(t).\ \delta(\tau-\tau_n) = (\mathrm{A_{LOS}} + \ a_1(t))\,.\ \delta(\tau)\ +\ a_2(t).\ \delta(\tau-\tau_2) \tag{3.1}$$

Note that we consider a normalized aeronautical channel response:

$$|\mathrm{A_{LOS}}|^2 + \mathbb{E}\left\{|a_1(t)|^2\right\} + \mathbb{E}\left\{|a_2(t)|^2\right\} = |\mathrm{A_{LOS}}|^2 + \mathrm{P}_1 + \mathrm{P}_2 = 1 \tag{3.2}$$

where $\mathrm{A_{LOS}}$ is a constant scalar given by the line of sight (LOS) path which is present most of the time and P_1 and P_2 are the powers of others paths verifying:

$$\begin{cases} \mathrm{P}_1 & = \mathbb{E}\left\{|a_1(t)|^2\right\} = 10^{-1.42}.\ |\mathrm{A_{LOS}}|^2 \\ \mathrm{P}_2 & = \mathbb{E}\left\{|a_2(t)|^2\right\} = (1+\mathrm{C/M})^{-1} \end{cases} \tag{3.3}$$

The A2S channel is characterized by a C/M factor with depends on the UAV/aircraft position (elevation angle ε). Its expression is initially introduced in Equation (1.24) as:

$$\mathrm{C/M\ [dB]} = 10.\log_{10}\left(\frac{|\mathrm{A_{LOS}}|^2 + \mathrm{P_1}}{\mathrm{P_2}}\right) \tag{3.4}$$

Table 3.1 shows some numerical values of C/M in decibels as a function of the UAV/aircraft position.

ε	5°	20°	25°	35°	55°
UAV/aircraft height	10 (km)	10 (km)	10 (km)	10 (km)	10 (km)
Ground surface	Ice water	Wet Ground	Medium dry ground	Very dry ground	Dry Ground
Location	Groenland	Royaume-Uni	France	Senegal	South-africa
C/M [dB]	6	15	20	27	40

Table 3.1: *C/M as a function of ε*

If the channel varies over time and if one knows its coherence time, one can then define the frames so that the channel can be assumed to be stationary on each. In the following, we assume a frame-based communication and we suppose that frame duration does not exceed the coherence time, T_c, of the propagation channel. The expression of the A2S channel becomes:

$$\mathrm{h}_a(t,\tau) \approx \mathrm{h}_a(\tau) = (\mathrm{A_{LOS}} + a_{i,1})\ \delta(\tau) + a_{i,2}\ \delta(\tau - \tau_2) \tag{3.5}$$

By applying central limit theorem, the complex variables $a_{i,1}$ and $a_{i,2}$ are two independent zero-mean complex Gaussian variables with variances P_1 and P_2, respectively.

3.2.2 System model

For the system model, we consider a frame based transmission. Moreover, we assume that each frame contains a number of N_f sub-frames and each sub-frame contains a number of N modulated data symbols. Furthermore, we assume that the digital communication system uses linear M-ary modulation. Furthermore, we consider a Root Raised Cosine (RRC) shaping filter $h_e(\tau)$ as a transmit shaping filter with known parameters such as β, the roll-off factor, and the Nyquist bandwidth B_h. The considered Nyquist bandwidth is expressed as follows:

$$\mathrm{B}_h = \frac{1+\beta}{\mathrm{T}_h} \tag{3.6}$$

where T_h is the Nyquist symbol duration and is a fixed value depending on the considered frequency plan and on the reserved bandwidth. For instance, in AMS(R)S L-band, a bandwidth of 300 kHz is considered. It means a Nyquist symbol duration $\mathrm{T}_h = 6.6\mu s$. Also, we note that roll-off factors are defined by the existing standards. For example for DVB-S2/S2x standard we have $\beta \in \{0.35, 0.25, 0.2, 0.15, 0.10, 0.05\}$, whereas, for ANTARES CS standard we have $\beta = 0.2$. The transmitter/receiver scheme is illustrated in Figure 3.1.

At the transmitter, bit sequence $\mathbf{u}_i$ is encoded on to N symbols by using a M-ary Bit Interleaved Coded Modulation (BICM) scheme as shown in Figure 2.1. As a result, a sequence of N data modulated symbols

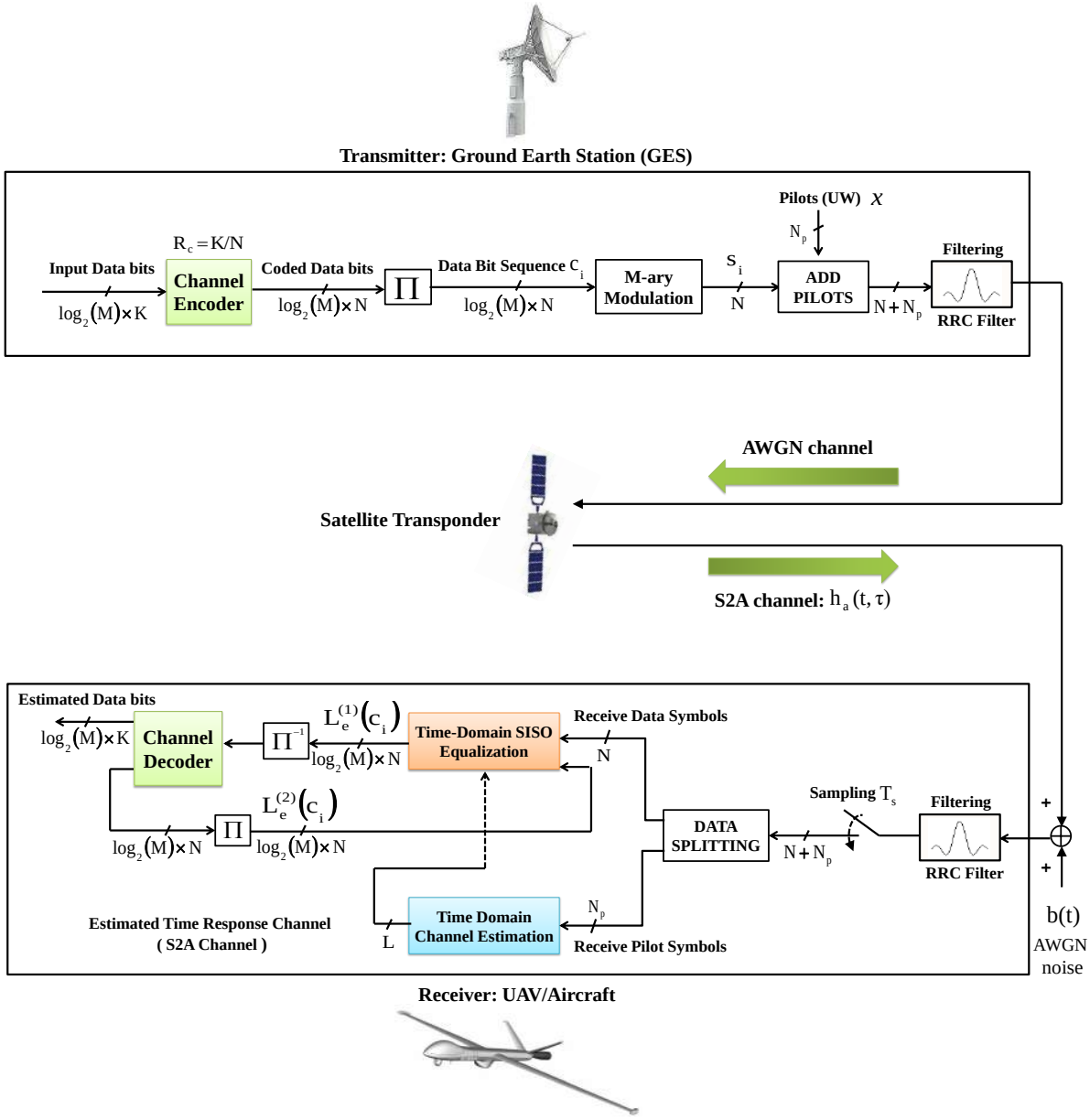

Figure 3.1: *GES transmitter and UAV/Aircraft receiver using SC waveform for the forward link*

is generated denoted by $\mathbf{s}_i = [s_{i,1}, s_{i,2}, \ldots, s_{i,N}]$. The symbols $\{s_{i,n}\}$ are drawn from a discrete alphabet $\chi = \{\mathcal{C}_1, \mathcal{C}_2, \ldots, \mathcal{C}_M\}$. The obtained data modulated symbols have a variance equal to σ_s^2 and have a symbol duration $\mathrm{T}_s = \nu.\mathrm{T}_h$. In order to improve the spectral efficiency, we assume using Nyquist/FTN signaling characterized by an acceleration factor denoted by ν and expressed as follows:

$$0 < \nu = \frac{\mathrm{T}_s}{\mathrm{T}_h} \leq 1 \tag{3.7}$$

The values of ν are taking between 0 and 1 ($0 < \nu \leq 1$). Note that, in the case where $\nu = 1$, we can assume Nyquist communication. For the other cases i.e. $\nu < 1$, Faster-than-Nyquist (FTN) communication is considered.

On other hand, another sequence of $N_{\mathrm{p}} \leq N$ i.i.d training symbols which is denoted by $\mathbf{x} = \left[x_1, x_2, \ldots, x_{N_{\mathrm{p}}}\right]$ is inserted in each transmitted sub-frame and will be used to estimate the channel response. Note that training symbols $x_1, x_2, \ldots, x_{N_{\mathrm{p}}}$ are fully known at the receiver and have the same variance as data modulated symbols i.e. $\sigma_p^2 = \sigma_s^2$.

At the receiver, two signals are detected: a received data signal and a received training signal. The received data signal will be processed to detect transmit data modulated sequence $\mathbf{s}_i$. Whereas, the received training signal is used to estimate the channel response. For SC waveform, we associate received data sequence $\mathbf{y}_i = [y_{i,1}, y_{i,2}, \ldots, y_{i,N}]^T$ to received data signal and received training sequence $\mathbf{y}_i^{\mathrm{p}} = \left[y_{i,1}^{\mathrm{p}}, y_{i,2}^{\mathrm{p}}, \ldots, y_{i,N_{\mathrm{p}}-L}^{\mathrm{p}}\right]^T$ to received training signal. Referring to Equations (2.22) and (2.23), the expression of received data symbols $\{y_{i,n}\}$ and received training symbols $\left\{y_{i,n}^{\mathrm{p}}\right\}$ are given by:

$$y_{i,n} = \sum_{l=-L/2}^{+L/2} h_i\left(l.\mathrm{T}_s\right)\ s_{i,n-l} + w_c[n] \qquad \text{for} \qquad 1 \leq n \leq N \tag{3.8}$$

and,

$$\mathbf{y}_i^{\mathrm{p}} = \mathbf{X}.\mathbf{h}_i + \mathbf{w}_c \tag{3.9}$$

with $h_i(\tau)$ denotes the continuous equivalent baseband channel expressed in (2.11) as:

$$\mathrm{h}_i(\tau) = \sum_{n=0}^{\mathrm{N_m}-1} a_{i,n}.\ \mathrm{g}(\tau - \tau_n) = \left(\mathrm{A_{LOS}} + a_{i,1}\right)\ \mathrm{g}(\tau) + a_{i,2}\ \mathrm{g}(\tau - \tau_2) \tag{3.10}$$

where $\mathrm{g}(\tau)$ is a Raised Cosine (RC) filter verifying:

$$\mathrm{g}(0) = 1 \qquad \text{and} \qquad \mathrm{g}\left(l.\mathrm{T}_h\right) = 0 \qquad \forall \qquad l \in l \in \mathbb{Z}^* \tag{3.11}$$

An example of continuous/discrete channel impulse response response $\mathrm{h}_i(\tau)$ is given in Figure 3.2 for $\nu = 1$ (Nyquist case) and also in Figure 3.3 for $\nu = 0.7$ (FTN case).

The channel vector $\mathbf{h}_i = \left[h_i\left(-L/2.\mathrm{T}_s\right), h_i\left((-L/2+1).\mathrm{T}_s\right), \ldots, h_i\left(L/2.\mathrm{T}_s\right)\right]^T$ denotes the discrete-time equivalent baseband channel to be estimated and equalized later. The positive odd integer L specifies the memory of the system and is the smallest value such that $h_i\left(l.\mathrm{T}_s\right) = 0$, $|l| > L/2$.

The resulting additive noise vector $\mathbf{w}_c = (w_c[1], w_c[2], \ldots, w_c[N_{\mathrm{p}} - L])$ is a zero-mean Gaussian noise vector verifying:

$$\mathbb{E}\left\{w_c[n].w_c^*[n+l]\right\} = \mathrm{N}_0.\ \mathrm{R}_s.\ \mathrm{g}\left(l.\mathrm{T}_s\right) = \sigma_w^2.\ \mathrm{g}\left(l.\mathrm{T}_s\right) \tag{3.12}$$

with $\sigma_w^2 = \mathrm{N}_0.\ \mathrm{R}_s$ is the noise variance. Note that, in Nyquist signaling i.e. $\mathrm{T}_s = \mathrm{T}_h$ the additive noise vector $\mathbf{w}_c$ becomes white.

Finally, The matrix $\mathbf{X}$ corresponding to the received training sequence is initially defined in (2.20) and is a Toeplitz matrix containing transmit training symbols $\{x_n\}$ and having a size of $(N_{\mathrm{p}} - L) \times (L+1)$. Due the

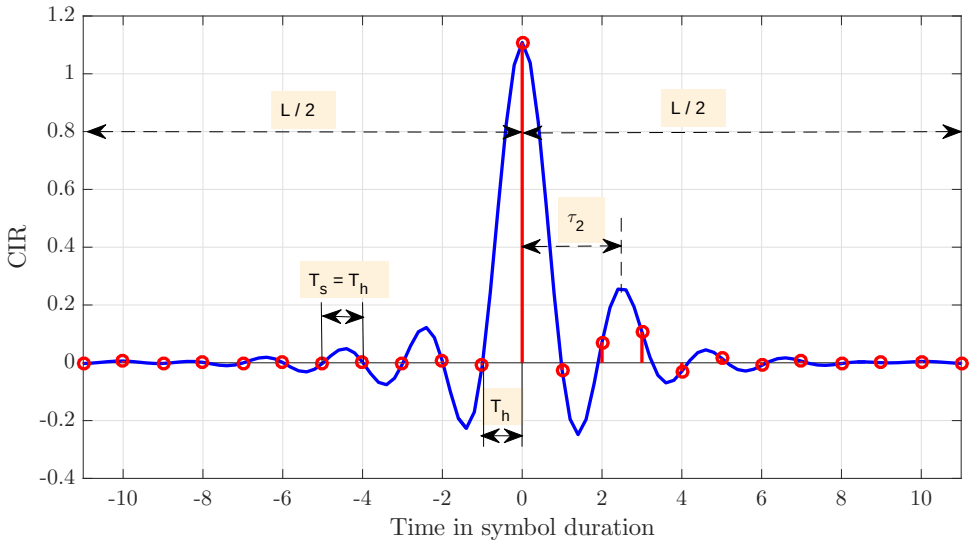

Figure 3.2: *CIR in Nyquist signaling ($\nu = 1$)*

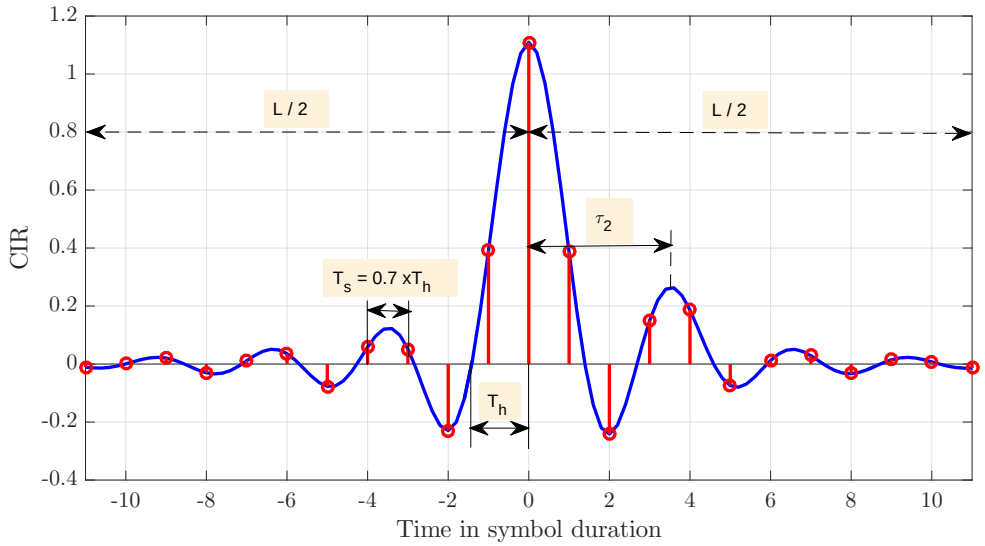

Figure 3.3: *CIR in FTN signaling ($\nu = 0.7$)*

fact that we consider i.i.d training sequence, it is shown in Equation (2.21) that matrix $\mathbf{X}$ satisfies the following expression:

$$\mathbf{X}^H\mathbf{X} \approx (N_\mathrm{p} - L)\,.\,\sigma_p^2.\,\mathbf{I}_{\mathrm{L+1\times L+1}} \tag{3.13}$$

with $\mathbf{I}_{\mathrm{L+1\times L+1}}$ being the identity matrix with size $(\mathrm{L}+1)\times(\mathrm{L}+1)$.

3.2.3 Reduced-complexity MAP-based time-domain channel equalization:

The equalization of the received signal is an important task for a signal receiver, especially when the propagation channel is disrupted by the presence of multiple paths. For instance, in high-bit-rate data transmissions, the transceiver encounters an equivalent base-band channel with large delay-spreads. Then the communication system is subject to severe inter-symbol interference (ISI) impairment which, in principle, could be well compensated by resorting to equalizers based on minimum mean-square-error (MMSE) criterion or Bayesian MAP criterion to detect transmit constellation symbols. The MAP equalizer (or a maximum likelihood sequence estimator, MLSE) still provides improved performance over a MMSE equalizer. However, the computational complexity of the MAP-based equalization grows exponentially with the channel memory length, so that considerable efforts have been undertaken to develop reduced-Complexity versions of MAP equalizers suitable for the application on transmission channels with large delay-spreads [73][33][47].
In this Section, we investigate a sub-optimal but efficient equalization method proposed for the forward link. The proposed equalization method is shown to be very efficient while significantly decreasing the complexity compared to a Full-complexity MAP receiver that does not exploit the particular form of the equivalent baseband channel.

3.2.3.1 All proposed equalization structure:

The present contribution aims to overcome the drawbacks of the equalization methods that are known from the prior state of the art by proposing an equalization method suited for channels with Exponential-Decay PDPs, shown in Figure 3.4, and more specially for sparse channels with equally spaced coefficients as given in Figure 3.5. The main idea proposed in [95, 100] is to design an architecture combining the benefits of a decision feedback equalizer (DFE) with a maximum-a-posteriori (MAP) equalizer (or a maximum likelihood sequence estimator, MLSE) which performs equalization in a time-forward or time-reversed manner based on the particular form of the baseband channel to provide an equalization device with significantly lower complexity than a full-state MAP device, but which still provides improved performance over a conventional DFE.
The proposed equalization architecture includes two block DFE-like structures; a forward block and a backward block (see Figures 3.4). The forward block forms tentative symbol decisions with a MAP criterion considering a mismatched truncated channel response. Whereas, the backward block is used thereafter to reduce the channel response to the desired truncated channel used in the first structure. The signal is then processed through a finite number of «self-iterations». We denote $N_{s\text{-}i}$, the number of considered «self-iterations». For each «self-iteration» process we have two equalization steps:

- a first equalization step, given by the forward block, for so called mismatched processing: equalizing each block of N received symbols using a Maximum A posteriori (MAP) equalization algorithm.
- a second step given by the backward structure consists of removing instances of interference that are linked to paths other than powerful paths. To do so, we generate an estimate of the interference term

resulting from the interference on equalized symbols, of all paths of the transmission channel except selected powerful paths and then subtracting interference term from the received sequence of N symbols.

The first equalization step and the second equalization step are both executed iteratively.

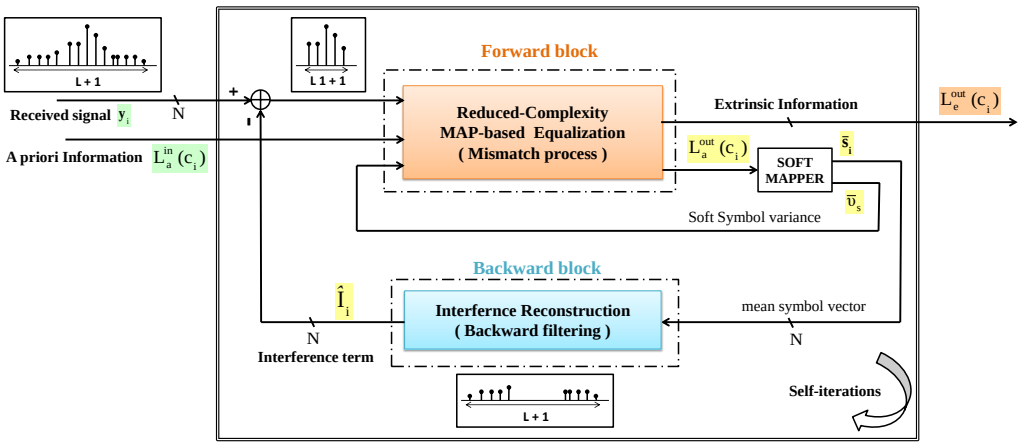

Figure 3.4: *Equalization Structure (I): Proposed reduced complexity MAP-based channel equalization structure with interference cancellation for channels with exponential-decay PDPs.*

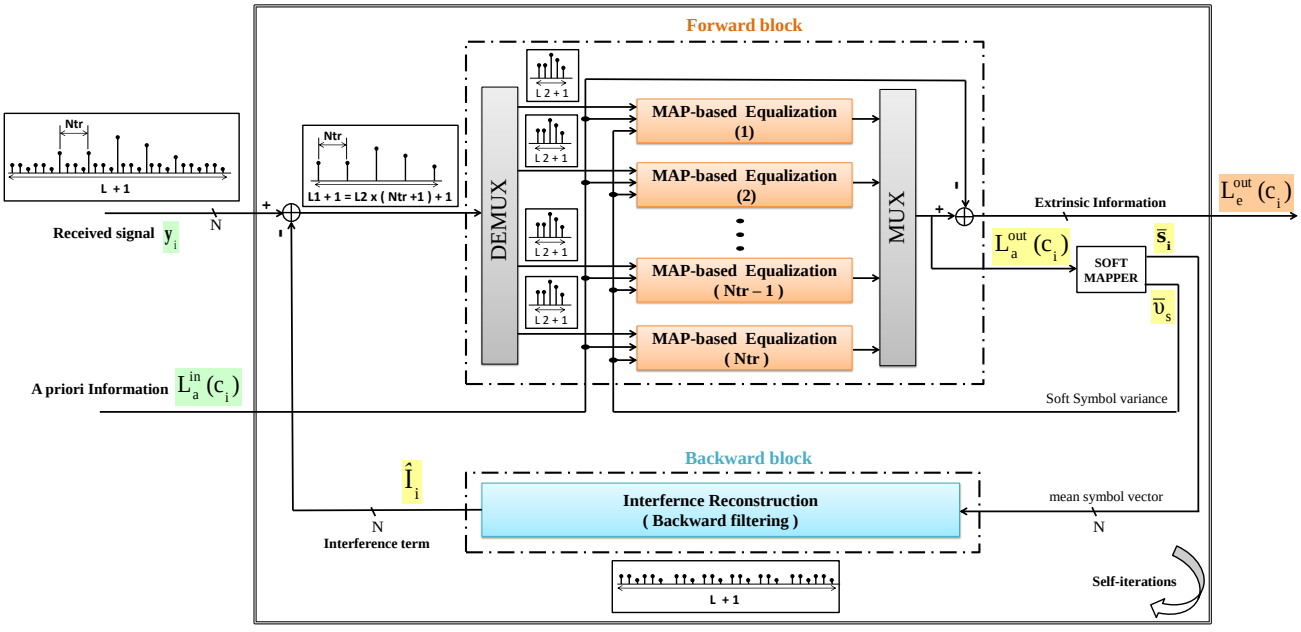

Figure 3.5: *Equalization Structure (II): Proposed reduced complexity parallel MAP-based channel equalization structure with interference cancellation for sparse channels with equally spaced coefficients.*

3.2.3.2 Aeronautical channel in Nyquist signaling: Proposed Parallel-trellis MAP-based channel equalization structure (Equalization Structure (II))

In this Section we are interested in a special class of ISI channels: sparse channels with equally spaced powerful coefficients. These channels present some number of powerful coefficients and other secondary coefficients. Moreover, the powerful coefficients are equally spaced. Moreover, the powerful coefficients are equally spaced. This type of channels has interested several studies [83, 87, 91]. The main advantage of this type of channels is that it allow us to consider parallel processing [15, 72, 82, 88].

Note that sparse channel equalization has still been considered in several works [15, 15, 71, 82], exploiting the sparsity mainly using parallel trellis based detection algorithm such as Viterbi or MAP algorithms. For equalization of zero padded sparse channels, the parallel MAP receiver is shown to be optimal [72, 82, 87]. For more general sparse channels, interference cancellation has been taken into account by introducing inter-trellis interference mitigation between parallel trellises, but at the expense of additional complexity due to the need for proper scheduling [71, 88].

In this context, we propose an enhanced channel equalization structure taking into account the sparsity form of the channel in order decrease the computational complexity at the receiver. In general form of sparse channels with equally spaced powerful coefficients, the proposed equalization structure is presented in Figure 3.5. For this contribution, the interference mitigation is completely revised to enable an easy and efficient implementation.

Proposed Parallel-trellis MAP-based channel equalization structure In Nyquist case ($\mathrm{T}_s = \mathrm{T}_h$), Figure 3.2 shows that the equivalent baseband channel has two powerful coefficients and other secondary paths and thus we can consider that the channel is sparse. Moreover, since we only have two powerful coefficients, it is straightforward to deduce that the considered channel is sparse with equally spaced coefficients.

At the receiver, the observation model is given by the following expression:

$$y_{i,n} = \sum_{l=-L/2}^{+L/2} h_i\left(l.\mathrm{T}_s\right)\ s_{i,n-l} + w_n = \underbrace{\sum_{l\in\mathcal{I}}^{L/2} h_i\left(l.\mathrm{T}_s\right)\ s_{i,n-l}}_{\text{Powerful component}} + \underbrace{\sum_{\substack{l=-L/2 \\ l\notin\mathcal{I}}}^{L/2} h_i\left(l.\mathrm{T}_s\right)\ s_{i,n-l}}_{\text{low powered component: } \mathrm{I}_{i,n}} + w_n$$

$$= h_i\left(0\right)\ s_{i,n} + h_i\left(\mathrm{N_{tr}}.\mathrm{T}_s\right)\ s_{i,n-\mathrm{N_{tr}}} + \mathrm{I}_{i,n} + w_n \qquad \text{for} \qquad 1 \le n \le N \tag{3.14}$$

where $h_i\left(0\right)$ and $h_i\left(\mathrm{N_{tr}}.\mathrm{T}_s\right)$ are the two powerful coefficients $\mathcal{I} = \{0, \mathrm{N_{tr}}\}$ is the set of their indexes. The positive integer $\mathrm{N_{tr}}$ denoted the spacing factor. Based on geometrical considerations, the value of $\mathrm{N_{tr}}$ is given by:

$$\mathrm{N_{tr}} = \left\lceil \frac{\tau_2}{\mathrm{T}_s} \right\rceil = \left\lceil \frac{2.\mathrm{H}_a.\sin\varepsilon}{3.10^8.\mathrm{T}_h} \right\rceil \tag{3.15}$$

Referring to (3.14), the equivalent baseband channel can be well represented by a «strong» sparse channel component plus some low power interference residual terms. The memory of the sparse channel is equal to $\mathrm{N_{tr}}$. In order to reduce the memory channel to one, a serial-to-parallel processing is considered. As a result,

a number of $\mathrm{N_{tr}}$ streams of the received signal is obtained as follows:

$$\begin{bmatrix} \mathbf{y}_i^{(1)} \\ \mathbf{y}_i^{(2)} \\ \vdots \\ \mathbf{y}_i^{(\mathrm{N_{tr}})} \end{bmatrix} = \begin{bmatrix} y_{i,1} & y_{i,1+\mathrm{N_{tr}}} & \cdots & y_{i,1+(Q-1).\mathrm{N_{tr}}} \\ y_{i,2} & y_{i,2+\mathrm{N_{tr}}} & \cdots & y_{i,2+(Q-1).\mathrm{N_{tr}}} \\ \vdots & \vdots & \ddots & \vdots \\ y_{i,\mathrm{N_{tr}}} & y_{i,2.\mathrm{N_{tr}}} & \cdots & y_{i,N} \end{bmatrix} = \begin{bmatrix} y_{i,1}^{(1)} & y_{i,2}^{(1)} & \cdots & y_{i,Q}^{(1)} \\ y_{i,1}^{(2)} & y_{i,2}^{(2)} & \cdots & y_{i,Q}^{(2)} \\ \vdots & \vdots & \ddots & \vdots \\ y_{i,1}^{(\mathrm{N_{tr}})} & y_{i,2}^{(\mathrm{N_{tr}})} & \cdots & y_{i,Q}^{(\mathrm{N_{tr}})} \end{bmatrix} \tag{3.16}$$

Here, $N = \mathrm{N_{tr}} \times Q$. For $1 \leq n_{\mathrm{tr}} \leq \mathrm{N_{tr}}$, the parallel observed sequence $\mathbf{y}_i^{(n_{\mathrm{tr}})} = \left[y_{i,1}^{(n_{\mathrm{tr}})}, y_{i,2}^{(n_{\mathrm{tr}})}, \ldots, y_{i,Q}^{(n_{\mathrm{tr}})}\right]$ can be considered as the result of convolution with a one memory channel plus plus some low powered interference residual terms:

$$y_{i,n}^{(n_{\mathrm{tr}})} = \underbrace{h_i(0)\ s_{i,n}^{(n_{\mathrm{tr}})} + h_i(\mathrm{N_{tr}}.\mathrm{T}_s)\ s_{i,n-1}^{(n_{\mathrm{tr}})} + w_n^{(n_{\mathrm{tr}})}}_{\text{Mismatched observation Model}} + \underbrace{\mathrm{I}_{i,n}^{(n_{\mathrm{tr}})}}_{\text{ISI Term}} = z_{i,n}^{(n_{\mathrm{tr}})} + \mathrm{I}_{i,n}^{(n_{\mathrm{tr}})} + w_n^{(n_{\mathrm{tr}})} \qquad \text{for} \qquad 1 \leq n \leq Q \tag{3.17}$$

with $z_{i,n}^{(n_{\mathrm{tr}})} = h_i(0)\ s_{i,n}^{(n_{\mathrm{tr}})} + h_i(\mathrm{N_{tr}}.\mathrm{T}_s)\ s_{i,n-1}^{(n_{\mathrm{tr}})}$ is the output mismatched channel model considering that the secondary coefficients are zero and $s_{i,n}^{(n_{\mathrm{tr}})} = s_{i,n_{\mathrm{tr}}+(n-1)\times \mathrm{N_{tr}}}$. The additional term $\mathrm{I}_{i,n}^{(n_{\mathrm{tr}})}$ denotes the ISI term observed in each received parallel signal and can be written in this matrix form:

$$\begin{bmatrix} \mathrm{I}_{i,1}^{(1)} & \mathrm{I}_{i,2}^{(1)} & \cdots & \mathrm{I}_{i,Q}^{(1)} \\ \mathrm{I}_{i,1}^{(2)} & \mathrm{I}_{i,2}^{(2)} & \cdots & \mathrm{I}_{i,Q}^{(2)} \\ \vdots & \vdots & \ddots & \vdots \\ \mathrm{I}_{i,1}^{(\mathrm{N_{tr}})} & \mathrm{I}_{i,2}^{(\mathrm{N_{tr}})} & \cdots & \mathrm{I}_{i,Q}^{(\mathrm{N_{tr}})} \end{bmatrix} = \begin{bmatrix} \mathrm{I}_{i,1} & \mathrm{I}_{i,1+\mathrm{N_{tr}}} & \cdots & \mathrm{I}_{i,1+(Q-1).\mathrm{N_{tr}}} \\ \mathrm{I}_{i,2} & \mathrm{I}_{i,2+\mathrm{N_{tr}}} & \cdots & \mathrm{I}_{i,2+(Q-1).\mathrm{N_{tr}}} \\ \vdots & \vdots & \ddots & \vdots \\ \mathrm{I}_{i,\mathrm{N_{tr}}} & \mathrm{I}_{i,2.\mathrm{N_{tr}}} & \cdots & \mathrm{I}_{i,N} \end{bmatrix} = \begin{bmatrix} \mathbf{I}_i^{(1)} \\ \mathbf{I}_i^{(2)} \\ \vdots \\ \mathbf{I}_i^{(\mathrm{N_{tr}})} \end{bmatrix} \tag{3.18}$$

Based on this model, a simple but efficient equalization structure is derived. The proposed equalization structure is presented in Figure 3.5. The proposed equalization architecture includes two DFE-like structures; a forward block and a backward block. The forward block contains a number $\mathrm{N_{tr}}$ parallel trellises. Each parallel trellis forms tentative symbol decisions with a MAP criterion considering a mismatch observation model expressed as $y_{i,n}^{(n_{\mathrm{tr}})} = z_{i,n}^{(n_{\mathrm{tr}})} + w_n^{(n_{\mathrm{tr}})}$. Concerning backward block, it is designed to be matched to zero padded sparse channel (i.e. $\mathrm{I}_{i,n} = 0 \quad \forall \quad 1 \leq n \leq N$). The backward block iteratively generates an estimation of residual interference sequence $[\mathrm{I}_{i,1}, \mathrm{I}_{i,2}, \ldots, \mathrm{I}_{i,N}]$ based on hard/soft outputs from parallel MAP equalizers. By using (3.18), for $1 \leq n_{\mathrm{tr}} \leq \mathrm{N_{tr}}$, an estimation of the additional ISI sequence $\mathbf{I}_i^{(n_{\mathrm{tr}})}$ denoted by $\widehat{\mathbf{I}}_i^{(n_{\mathrm{tr}})}$, is deduced as:

$$\widehat{\mathbf{I}}_i^{(n_{\mathrm{tr}})} = \left[\widehat{\mathrm{I}}_{i,1}^{(n_{\mathrm{tr}})}, \widehat{\mathrm{I}}_{i,2}^{(n_{\mathrm{tr}})}, \ldots, \widehat{\mathrm{I}}_{i,Q}^{(n_{\mathrm{tr}})}\right] = \left[\widehat{\mathrm{I}}_{i,n_{\mathrm{tr}}}, \widehat{\mathrm{I}}_{i,n_{\mathrm{tr}}+\mathrm{N_{tr}}}, \ldots, \widehat{\mathrm{I}}_{i,n_{\mathrm{tr}}+(Q-1).\mathrm{N_{tr}}}\right] \tag{3.19}$$

The backward block will operate in iterative process and the resulting equalized signal is given through a finite number of «self-iterations». For each «self-iteration», three main steps are considered. In the first step, the signal to be equalized is passed by the upper block composed of independent parallel Maximum A Posteriori (MAP) equalizers, which considers the incoming block symbols as the result of convolution with a one memory channel. Thus, we intentionally consider a mismatched decoding by neglecting the effect of the residual interference. This is motivated by the power distribution properties of the considered channels. At the second step, the second block (Feed-back) estimates and generates the interference term taking into consideration a decision of outgoing symbols of the first block. After generating the remaining interference,

it is canceled from the incoming signal before feeding to the parallel equalizers. In the third step, the signal with reduced residual interference will be detected using the parallel MAP equalizers. The detection and interference cancellation steps are iteratively processed. The three steps are detailed as:

- *Interference cancellation step*: This steps consists to iteratively mitigate the residual interference. Given an estimation of ISI term, $\left[\widehat{\mathrm{I}}_{i,1},\widehat{\mathrm{I}}_{i,2},\ldots,\widehat{\mathrm{I}}_{i,N}\right]$, an estimated interference matrix $\left[\widehat{\mathbf{I}}_i^{(1)},\widehat{\mathbf{I}}_i^{(2)},\ldots,\widehat{\mathbf{I}}_i^{(\mathrm{N_{tr}})}\right]^T$ is constructed by using (3.19) (serial-to-parallel processing). Then, the obtained estimated interference matrix is removed from the parallel received signal $\left[\mathbf{y}_i^{(1)},\mathbf{y}_i^{(2)},\ldots,\mathbf{y}_i^{(\mathrm{N_{tr}})}\right]^T$ as the following:

$$\begin{bmatrix}\widetilde{\mathbf{y}}_i^{(1)}\\ \widetilde{\mathbf{y}}_i^{(2)}\\ \vdots\\ \widetilde{\mathbf{y}}_i^{(\mathrm{N_{tr}})}\end{bmatrix}=\begin{bmatrix}\mathbf{y}_i^{(1)}\\ \mathbf{y}_i^{(2)}\\ \vdots\\ \mathbf{y}_i^{(\mathrm{N_{tr}})}\end{bmatrix}-\begin{bmatrix}\widehat{\mathbf{I}}_i^{(1)}\\ \widehat{\mathbf{I}}_i^{(2)}\\ \vdots\\ \widehat{\mathbf{I}}_i^{(\mathrm{N_{tr}})}\end{bmatrix} \tag{3.20}$$

  The main objective of this step is enhance the signal-to-noise ratio (SNR) at the input of the forward block. Indeed, assuming $0\leq\bar{v}_s\leq\sigma_s^2$ is the soft variance of the estimated symbols, the expression of obtained SNR ratio in decibels after interference cancellation step is given by the following expression:

$$\mathrm{SNR}^{\min}\leq\mathrm{SNR}=10\log_{10}\left(\sigma_s^2.\sum_{l\in\mathcal{I}}\left|h_i\left(l.\mathrm{T}_s\right)\right|^2\right)-10\log_{10}\left(\mathrm{Var}\left\{\mathrm{I}_{i,n}^{(n_{\mathrm{tr}})}-\widehat{\mathrm{I}}_{i,n}^{(n_{\mathrm{tr}})}\right\}+\sigma_w^2\right)\leq\mathrm{SNR}^{\max}$$

  Here, it is clear that SNR ratio values are taken between two extreme values $\mathrm{SNR}^{\min}$ and $\mathrm{SNR}^{\max}$. $\mathrm{SNR}^{\max}$ corresponds to have $\mathrm{Var}\left\{\mathrm{I}_{i,n}^{(n_{\mathrm{tr}})}-\widehat{\mathrm{I}}_{i,n}^{(n_{\mathrm{tr}})}\right\}=0$ which is the case with perfect interference cancellation (i.e. $\mathrm{I}_{i,n}^{(n_{\mathrm{tr}})}=\widehat{\mathrm{I}}_{i,n}^{(n_{\mathrm{tr}})}$). Whereas, $\mathrm{SNR}^{\min}$ corresponds to have $\mathrm{Var}\left\{\mathrm{I}_{i,n}^{(n_{\mathrm{tr}})}-\widehat{\mathrm{I}}_{i,n}^{(n_{\mathrm{tr}})}\right\}=\sigma_s^2.\sum\limits_{\substack{l=-L/2\\ l\notin\mathcal{I}}}^{L/2}\left|h_i\left(l.\mathrm{T}_s\right)\right|^2$ which is the case without considering interference cancellation step (i.e. $\widehat{\mathrm{I}}_{i,n}^{(n_{\mathrm{tr}})}=0$).

- *Mismatch parallel trellis-based equalization step (forward block)*: This steps corresponds to the parallel MAP-based detection. To do it, the considered observation model is expressed as:

$$\begin{bmatrix}\widetilde{\mathbf{y}}_i^{(1)}\\ \widetilde{\mathbf{y}}_i^{(2)}\\ \vdots\\ \widetilde{\mathbf{y}}_i^{(\mathrm{N_{tr}})}\end{bmatrix}=\begin{bmatrix}z_{i,1}^{(1)} & z_{i,2}^{(1)} & \cdots & z_{i,Q}^{(1)}\\ z_{i,1}^{(2)} & z_{i,2}^{(2)} & \cdots & z_{i,Q}^{(2)}\\ \vdots & \vdots & \ddots & \vdots\\ z_{i,1}^{(\mathrm{N_{tr}})} & z_{i,2}^{(\mathrm{N_{tr}})} & \cdots & z_{i,Q}^{(\mathrm{N_{tr}})}\end{bmatrix}+\left\{\begin{bmatrix}\mathbf{I}_i^{(1)}\\ \mathbf{I}_i^{(2)}\\ \vdots\\ \mathbf{I}_i^{(\mathrm{N_{tr}})}\end{bmatrix}-\begin{bmatrix}\widehat{\mathbf{I}}_i^{(1)}\\ \widehat{\mathbf{I}}_i^{(2)}\\ \vdots\\ \widehat{\mathbf{I}}_i^{(\mathrm{N_{tr}})}\end{bmatrix}\right\}+\begin{bmatrix}\mathbf{w}^{(1)}\\ \mathbf{w}^{(2)}\\ \vdots\\ \mathbf{w}^{(\mathrm{N_{tr}})}\end{bmatrix} \tag{3.21}$$

  Based on this observation model, a BCJR algorithm is performed in each parallel trellis. The considered branch metric, $\mu_{i,n}$ is expressed as follows:

$$\boxed{\mu_{i,n}=\left|\widetilde{y}_{i,n}^{(n_{\mathrm{tr}})}-\left[h_i\left(0\right).\mathcal{C}_m+h_i\left(\mathrm{N_{tr}}.\mathrm{T}_s\right).\mathcal{C}_{m'}\right]\right|^2} \tag{3.22}$$

  The α-values and β-values denote the state-probabilities. Their expressions are initially given in (2.31)

and are recursively determinated by using the following expressions:

$$\alpha_n(m) = \sum_{m'=1}^{M} \alpha_{n-1}(m') \,.\, \sum_{x\in\chi} \gamma_n(m',m,x) = \sum_{m'=1}^{M} \alpha_{n-1}(m') \,.\, \gamma_n(m',m,\mathcal{C}_m) \tag{3.23}$$

$$\beta_n(m) = \sum_{m'=1}^{M} \beta_{n+1}(m') \,.\, \sum_{x\in\chi} \gamma_n(m,m',x) = \sum_{m'=1}^{M} \beta_{n+1}(m') \,.\, \gamma_n(m',m,\mathcal{C}_m) \tag{3.24}$$

where $\gamma_n(m',m,x)$ is the transition probability initially defined in (2.28). Furthermore, By assuming that the interference term $\mathrm{I}_{i,n}^{(n_{\mathrm{tr}})} - \widehat{\mathrm{I}}_{i,n}^{(n_{\mathrm{tr}})}$ in (3.21), varies according a centered Gaussian distribution with variance equal to κ, a final expression of the transition probability is given by:

$$\gamma_n(m',m,x) = \begin{cases} \gamma_n(m',m,\mathcal{C}_m) = \Pr\left(s_{i,n}^{(n_{\mathrm{tr}})} = \mathcal{C}_m | \mathrm{L}_a^{\mathrm{in}}(\mathbf{c}_i)\right) . \frac{1}{\pi\,(\sigma_w^2+\kappa)} . \exp\left(-\frac{\mu_{i,n}}{\sigma_w^2+\kappa}\right) & \text{if } x = \mathcal{C}_m \\ 0 & \text{if } x \neq \mathcal{C}_m. \end{cases} \tag{3.25}$$

The BCJR algorithm takes in input an *a priori* information vector of $\log_2(M)\times N$ bit LLRs, $\mathrm{L}_a^{\mathrm{in}}(\mathbf{c}_i) = \left[\mathrm{L}_a^{\mathrm{in}}(c_{i,1}), \mathrm{L}_a^{\mathrm{in}}(c_{i,2}), \ldots, \mathrm{L}_a^{\mathrm{in}}\left(c_{i,\log_2(M)\times N}\right)\right]^T$ to calculate an *a priori* probability of the transmit data symbols $\{s_{i,n}\}$ $1 \leq n \leq N$. By assuming $\left[u_1^{(m)}, u_2^{(m)}, \ldots, u_{\log_2(M)}^{(m)}\right]$ is the transmit bit sequence corresponding to $s_{i,n} = \mathcal{C}_m$, the *a priori* symbol probability is calculated as:

$$\Pr\left(s_{i,n} = \mathcal{C}_m | \mathrm{L}_a^{\mathrm{in}}(\mathbf{c}_i)\right) = \prod_{q=1}^{\log_2(M)} \frac{\exp\left(-u_q^{(m)} \times \mathrm{L}_a^{\mathrm{in}}\left(c_{i,q+(n-1)\times\log_2(M)}\right)\right)}{1+\exp\left(-\mathrm{L}_a^{\mathrm{in}}\left(c_{i,q+(n-1)\times\log_2(M)}\right)\right)} \tag{3.26}$$

In (3.25), $\Pr\left(s_{i,n}^{(n_{\mathrm{tr}})} = \mathcal{C}_m | \mathrm{L}_a^{\mathrm{in}}(\mathbf{c}_i)\right)$ denotes the *a priori* probability and is calculated as:

$$\Pr\left(s_{i,n}^{(n_{\mathrm{tr}})} = \mathcal{C}_m | \mathrm{L}_a^{\mathrm{in}}(\mathbf{c}_i)\right) = \Pr\left(s_{i,n_{\mathrm{tr}}+(n-1)\times \mathrm{N_{tr}}} = \mathcal{C}_m | \mathrm{L}_a^{\mathrm{in}}(\mathbf{c}_i)\right) \tag{3.27}$$

In each parallel trellis, the BCJR algorithm operates on a trellis. Here, the considered channel is a one-memory channel. For this particular case, it is shown in (2.35) that the calculation of the *a posteriori* symbol probability is reduced to a simple multiplication of α-values and β-values or also, more simply, an addition of α-values and β-values when we consider log-BCJR algorithm:

$$\Pr\left(s_{i,n}^{(n_{\mathrm{tr}})} = \mathcal{C}_m, \widetilde{\mathbf{y}}_i^{(n_{\mathrm{tr}})}\right) = \alpha_n(m) \,.\, \beta_n(m) \tag{3.28}$$

At the output of each parallel MAP-based detection, an *a postoriori* bit LLR vector, denoted by $\left[\mathrm{LLR}_1^{(n_{\mathrm{tr}})}, \mathrm{LLR}_2^{(n_{\mathrm{tr}})}, \ldots, \mathrm{LLR}_{\log_2(M)\times Q}^{(n_{\mathrm{tr}})}\right]$, is generated. Each LLR bit component is calculated as follows:

$$\mathrm{LLR}_{k+(q-1)\times\log_2(M)}^{(n_{\mathrm{tr}})} = \log\left\{ \frac{\sum_{m\in\mathbf{U}_k^0} \Pr\left(s_{i,q}^{(n_{\mathrm{tr}})} = \mathcal{C}_m, \widetilde{\mathbf{y}}_i^{(n_{\mathrm{tr}})}\right)}{\sum_{m\in\mathbf{U}_k^1} \Pr\left(s_{i,q}^{(n_{\mathrm{tr}})} = \mathcal{C}_m, \widetilde{\mathbf{y}}_i^{(n_{\mathrm{tr}})}\right)} \right\} \tag{3.29}$$

The two sets of the constellation indexes $\mathbf{U}_k^0$ and $\mathbf{U}_k^1$ correspond to have respectively 0 and 1 entries at the k-th index position of constellation bits and verifying,

$$\mathbf{U}_k^0 \cup \mathbf{U}_k^1 = \{1,2,\ldots,M\} \quad ; \quad \mathbf{U}_k^0 \cap \mathbf{U}_k^1 = \oslash \tag{3.30}$$

By considering all parallel MAP-based detectors, an *a postoriori* LLR bit matrix, **APP**, is obtained as follows:

$$\mathbf{APP} = \begin{bmatrix} \mathrm{LLR}_1^{(1)} & \mathrm{LLR}_2^{(1)} & \dots & \mathrm{LLR}_{\log_2(M)\times Q}^{(1)} \\ \mathrm{LLR}_{i,1}^{(2)} & \mathrm{LLR}_2^{(2)} & \dots & \mathrm{LLR}_{\log_2(M)\times Q}^{(2)} \\ \vdots & \vdots & \ddots & \vdots \\ \mathrm{LLR}_1^{(\mathrm{N_{tr}})} & \mathrm{LLR}_2^{(\mathrm{N_{tr}})} & \dots & \mathrm{LLR}_{\log_2(M)\times Q}^{(\mathrm{N_{tr}})} \end{bmatrix} \tag{3.31}$$

Finally, by applying a parallel-to-serial process, a total *a postoriori* bit LLR vector is constructed. This *a posteriori* information is denoted $\mathrm{L}_a^{\mathrm{out}}(\mathbf{c}_i)$ and is written as:

$$\mathrm{L}_a^{\mathrm{out}}(\mathbf{c}_i) = \left[\mathrm{L}_a^{\mathrm{out}}(c_{i,1}), \mathrm{L}_a^{\mathrm{out}}(c_{i,2}), \dots, \mathrm{L}_a^{\mathrm{out}}\left(c_{i,\log_2(M)\times N}\right)\right]^T \tag{3.32}$$

- *Update interference sequence step (backward block)*: This step consists to generate an updated estimation of residual interference sequence denoted by $\left[\widehat{\mathrm{I}}_{i,1}, \widehat{\mathrm{I}}_{i,2}, \dots, \widehat{\mathrm{I}}_{i,N}\right]$. This estimation will be associated to an error soft variance κ calculated from $\mathrm{L}_a^{\mathrm{out}}(\mathbf{c}_i)$.

  Given $\mathrm{L}_a^{\mathrm{out}}(\mathbf{c}_i)$, a soft mapper (see Figures 3.4 and 3.5) is able to compute an *a posteriori* probability of the transmit data symbols $\{s_{i,n}\}$ $1 \le n \le N$ by using the following expression:

$$\Pr(s_{i,n} = \mathcal{C}_m, \mathbf{y}_i) = \prod_{q=1}^{\log_2(M)} \frac{\exp\left(-u_q^{(m)} \times \mathrm{L}_a^{\mathrm{out}}\left(c_{i,q+(n-1)\times\log_2(M)}\right)\right)}{1+\exp\left(-\mathrm{L}_a^{\mathrm{out}}\left(c_{i,q+(n-1)\times\log_2(M)}\right)\right)} \tag{3.33}$$

At the output of soft mapping, a mean symbol vector $\bar{\mathbf{s}}_i = [\bar{s}_{i,1}, \bar{s}_{i,2}, \dots, \bar{s}_{i,N}]$ and a soft symbol variance $\bar{v}_s$ are derived as follows:

$$\begin{aligned} \bar{s}_{i,n} &= \sum_{m=1}^{M} \Pr(s_{i,n} = \mathcal{C}_m, \mathbf{y}_i) \times \mathcal{C}_m \\ \bar{v}_s &= \frac{1}{N} \sum_{n=1}^{N} \left[\sum_{m=1}^{M} \Pr(s_{i,n} = \mathcal{C}_m, \mathbf{y}_i) \times |\mathcal{C}_m - \bar{s}_{i,n}|^2 \right] \end{aligned} \tag{3.34}$$

The soft symbol variance $\bar{v}_s$ is re-injected into the forward for updating transition probabilities. Whereas, the mean symbol vector $\bar{\mathbf{s}}_i$ is re-used by the backward block to estimate an interference sequence of N symbols (block-based interference estimation), $\left[\widehat{\mathrm{I}}_{i,1}, \widehat{\mathrm{I}}_{i,2}, \dots, \widehat{\mathrm{I}}_{i,N}\right]$. Each interference element $\widehat{\mathrm{I}}_{i,n}$ is calculated as follows:

$$\widehat{\mathrm{I}}_{i,n} = \sum_{\substack{l=-L/2 \\ l \notin \mathcal{I}}}^{L/2} h_i(l.\mathrm{T}_s)\ \bar{s}_{i,n-l} \qquad \text{for} \qquad 1 \le n \le N \tag{3.35}$$

In each «self-iterations», the estimate interference is removed from received data sequence. Thus, the variance of the residual interference is updated. Under assumption of zero-mean interference term, the new value of residual interference variance is calculated as:

$$\kappa = \mathrm{Var}\left\{\mathrm{I}_{i,n}^{(n_{\mathrm{tr}})} - \widehat{\mathrm{I}}_{i,n}^{(n_{\mathrm{tr}})}\right\} = \mathrm{Var}\left\{\mathrm{I}_{i,n} - \widehat{\mathrm{I}}_{i,n}\right\} = \mathbb{E}\left\{\left|\mathrm{I}_{i,n} - \widehat{\mathrm{I}}_{i,n}\right|^2\right\} = \bar{v}_s. \sum_{\substack{l=-L/2 \\ l \notin \mathcal{I}}}^{L/2} |h_i(l.\mathrm{T}_s)|^2 \tag{3.36}$$

Finally, at the end of $N_{s\text{-}i}$ «self-iterations», the equalization structure generates an extrinsic LLR vector $L_e^{out}(\mathbf{c}_i)$ calculated as:

$$L_e^{out}(\mathbf{c}_i) = L_a^{out}(\mathbf{c}_i) - L_a^{in}(\mathbf{c}_i) \tag{3.37}$$

To conclude, by Considering this proposed channel equalization structure, we can verify that the corresponding computational complexity is significantly reduced. Indeed, comparing to the classical full-state MAP-based equalization, the overall complexity is reduced from $\mathcal{O}\left(|\chi|^L\right)$ to $\mathcal{O}\left(N_{s\text{-}i} \times N_{tr} \times |\chi|^{L_2}\right)$, where L_2+1 is the number of powerful coefficients. In aeronautical channel case, there are only two powerful coefficients or also $L_2 = 1$. So, the computational complexity for the aeronautical channel is given by:

$$\boxed{\text{Complexity} = \mathcal{O}(N_{s\text{-}i} \times N_{tr} \times |\chi|) \ll \mathcal{O}\left(|\chi|^L\right)} \tag{3.38}$$

As a result, one can remark that the complexity of equalization becomes linear with the modulation order M. Thus, it possible to set up a digital communication systems employing high-order modulation schemes.
Finally, we note that it is common to use parallel trellis based detection algorithms for sparse channels with equally spaced coefficients. The main contribution of the proposed structure is that it can offer a reduced hardware complexity for easy implementation. Indeed, for the proposed structure the parallel MAP detectors not only use the same trellis but also operate independently of each other. Which is not the case for other proposed structures [71, 88].

3.2.3.3 Aeronautical channel in FTN signaling: Proposed reduced complexity MAP-based channel equalization structure (Equalization Structure (I))

For the FTN signaling, the equivalent baseband channel is no longer sparse and is its shape is presented in Figure 3.3. As can can see, the ISI channels presents some powerful centered coefficients and others low-powered coefficients. For this kind of channels, no parallel processing is possible and the proposed structure, «Structure II», becomes non suitable to equalize this channel. In addition, the main weakness of these channels is that they have a large memory length and taking into account a complete MAP equalization is a serious problem in terms of computational complexity. In order to perform an efficient channel equalization process with a reasonable computational complexity, a new sub-optimal but efficient equalization structure is proposed to equalize this type of channels. The proposed structure uses a trellis-based MAP detection and is previously presented in Figure 3.4. For this structure, we can consider two possible models: *Forney's model* and *Ungerboeck's model*.

Forney's model: We recall that *Forney's model* is referred to a white-noise model. In FTN signaling i.e. $T_s < T_h$, the noise variables $\{w_c[n]\}$ are still Gaussian, but are colored (See Equation (3.12)). Therefore, a MAP-based symbol detection considering as a starting point the samples $\{y_{i,n}\}$, given in Equation (3.8), without taking into account the noise correlation, is a highly suboptimal detection. If spectral factorization is allowed, one can resort to the *Forney's model* by applying a whitening filter. Then, in order to reduce the complexity at the receiver, we propose to use the proposed equalization structure, presented in Figure 3.4, to reduce the computational complexity at the receiver. Otherwise, if

spectral factorization is not possible, the *Forney's model* is not available and one can resort to the *Ungerboeck's model* applied to the proposed equalization structure.

Ungerboeck's model: The observation model as given in (3.8) can not be used directly for *Ungerboeck's model*. To overcome this problem, it is essential to consider another observation model with a symmetric channel. This new considered observation model is given as:

$$\widetilde{y}_{i,n} = \sum_{k} \mathrm{h}_a^*((k-n).\mathrm{T}_s)\ y_{i,k} \approx \sum_{l=-L}^{+L} \widetilde{h}_i(l.\mathrm{T}_s)\ s_{i,n-l} + \widetilde{w}_c[n] \qquad \text{for} \qquad 1 \leq n \leq N \tag{3.39}$$

where $\widetilde{w}_c[n] = \sum_{k} \mathrm{h}_a^*((k-n).\mathrm{T}_s)\ w_c[k]$ is an additive Gaussian noise and $\widetilde{h}_i(\tau)$ is a continuous-time symmetric channel expressed as:

$$\begin{aligned}\widetilde{h}_i(\tau) &= h_i(\tau) * \mathrm{h}_a^*(-\tau) = \{(\mathrm{A_{LOS}} + a_{i,1})\ g(\tau) + a_{i,2}\ g(\tau-\tau_2)\} * \left\{\left(\mathrm{A_{LOS}} + a_{i,1}^*\right)\ \delta(\tau) + a_{i,2}^*\ \delta(\tau+\tau_2)\right\} \\ &= \left(|\mathrm{A_{LOS}} + a_{i,1}|^2 + |a_{i,2}|^2\right)\ g(\tau) + \mathrm{A_{LOS}}\ \left\{a_{i,1}^*\ a_{i,2}\ g(\tau-\tau_2) + a_{i,1}\ a_{i,2}^*\ g(\tau+\tau_2)\right\}\end{aligned} \tag{3.40}$$

An example of channel impulse response of the new considered symmetric channel is shown in Figure 3.6.

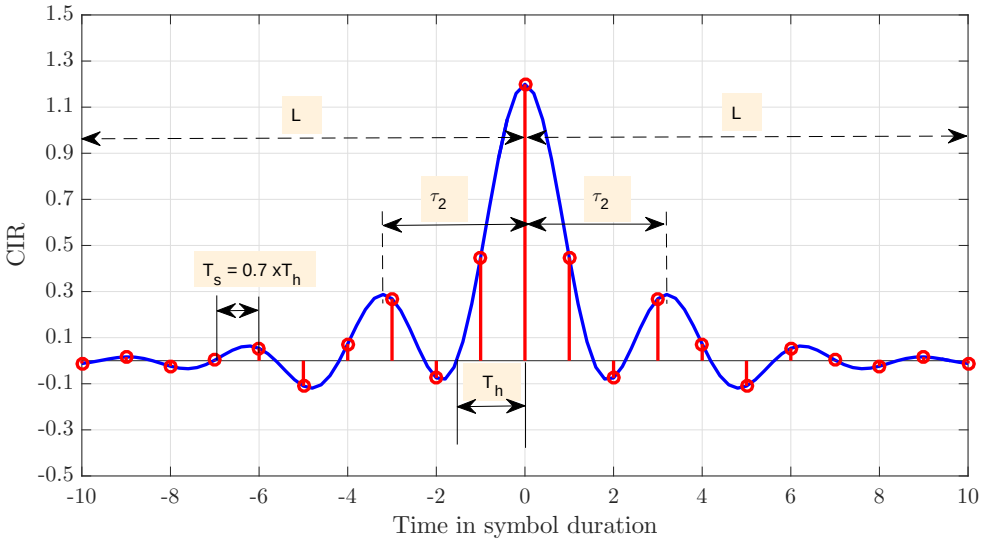

Figure 3.6: *Symmetric CIR in FTN signaling ($\nu = 0.7$)*

The new observation model, given in Equation (3.39), represents a sufficient statistic and can thus be used for an optimal detection [125]. In this case, the branch metric, $\mu_{i,n}$, is derived as the following:

$$\mu_{i,n} = -2.\ \Re\left\{s_{i,n}^*.\left(\widetilde{y}_{i,n} - \sum_{l=1}^{L} \widetilde{h}_i(l.\mathrm{T}_s)\ s_{i,n-l}\right)\right\} + \widetilde{h}_i(0).|s_{i,n}|^2 \tag{3.41}$$

The new considered symmetric channel expressed in (3.40) and shown in Figure 3.6, having an Exponential-Decay PDPs. Thus, one may resort to the proposed equalization structure presented in Figure 3.4. In

this case, the branch metric, given in (3.41), becomes:

$$\mu_{i,n} = -2.\ \Re\left\{ s^*_{i,n}.\left[\left(\widetilde{y}_{i,n} - \widehat{\mathrm{I}}_{i,n}\right) - \sum_{l=1}^{L_1} \widetilde{h}_i\left(l.\mathrm{T}_s\right)\ s_{i,n-l}\right]\right\} + \widetilde{h}_i\left(0\right).\left|s_{i,n}\right|^2 \tag{3.42}$$

where $\widehat{\mathbf{I}}_i = \left[\widehat{\mathrm{I}}_{i,1}, \widehat{\mathrm{I}}_{i,2}, \ldots, \widehat{\mathrm{I}}_{i,N}\right]^T$, is the obtained interference in each «self-iteration». Each interference element $\widehat{I}_{i,n}$ is calculated as follows:

$$\widehat{\mathrm{I}}_{i,n} = \sum_{|l|>L_1} \widetilde{h}_i\left(l.\mathrm{T}_s\right)\ \bar{s}_{i,n-l} \qquad \text{for} \qquad 1 \leq n \leq N \tag{3.43}$$

In each «self-iteration», the estimate interference is removed from received data sequence. Thus, the variance of the residual interference is updated. Under assumption of zero-mean interference term, the new value of residual interference variance is calculated as:

$$\kappa = \mathrm{Var}\left\{\mathrm{I}_{i,n} - \widehat{\mathrm{I}}_{i,n}\right\} = \mathbb{E}\left\{\left|\mathrm{I}_{i,n} - \widehat{\mathrm{I}}_{i,n}\right|^2\right\} = \bar{v}_s.\ \sum_{|l|>L_1}\left|\widetilde{h}_i\left(l.\mathrm{T}_s\right)\right|^2 \tag{3.44}$$

Furthermore, we assume that residual interference term varies according to zero-mean Gaussian distribution with variance equal to κ. The variance κ and the branch metric $\mu_{i,n}$ are used to calculate the transition probability for the BCJR algorithm implemented in the forward block. Note that in particular case when the memory length is equal to 1 i.e. $L_1 = 1$, the expression of the transition probability is given in (3.25).

It is important to note that *Forney's model* can be also considered for the new observation model, shown in (3.39), when spectral factorization is allowed.

Proposed reduced-complexity MAP-based qualization structure: Structure (I) For the proposed equalization structure (I) presented in Figure 3.4, we are interested in a special class of ISI channels: ISI channels with exponential-decay PDPs. For this kind of channels, we give a sufficient condition that insures that the impulse response of a channel is of exponential-decay power delay profile (PDP). Assuming an ISI channel with memory length L, the condition is that the power spectral density of the L_1+1 paths with indexes $\in \mathcal{I} = \{-L_1/2; -L_1/2+1; \ldots; L_1/2-1; L_1/2\}$ be larger than the other $L-L_1$ subsequent paths where $L_1 \leq L$ is a positive integer. Establishing a lower bound to the first path energy, this condition is more likely to be met if transmitter and receiver are in line-of-sight. As a particular case, for low values of L_1, the channel is a assumed be a minimum-phase channel [20].

Based on the same principle as presented for the equalization structure (II), the proposed equalized (I) exploits the particular form of the ISI channel in order to reduce the computational complexity of the receiver. Based on the particular form of the ISI channel, we propose « Structure (I) » to be suitable for ISI channels with exponential-decay PDPs or also for non-sparse ISI channels. This structure contains two block DFE-like structures: a forward block and backward block. The forward block is a detection block and considers only the central powerful channel coefficients. Whereas the backward block consists of removing instances of interference that are linked to others neglected non-central paths. The proposed structure is presented in Figure 3.4.

In this structure, the residual interference term is iteratively mitigated by considering block-based interference estimation based on hard/soft outputs from forward block. For forward block, a MAP-based equalization is considered. This block is matched to channels presenting only L_1+1 paths (memory length of L_1) and is mainly associated to a mismatch process.
The proposed equalization structure is able to reduce the overall complexity compared to the full-state BCJR equalization. The computational complexity is assumed to be:

$$\boxed{\text{Complexity} = \mathcal{O}\left(\mathrm{N_{s\text{-}i}} \times |\chi|^{L_1}\right) \ll \mathcal{O}\left(|\chi|^{L}\right)} \tag{3.45}$$

Furthermore, the proposed equalization structure can achieve a good trade-off between computational complexity and simplicity of design.

3.2.4 Symbol detection: simulation results

In this section we study the performance of transmit symbol detection for the uncoded case. For the forward link, the aeronautical channel is characterized by a C/M factor almost taking a values between 5 dB and 40 dB. We recall that C/M values are also proportional to ε values.

For the simulation results, we consider QPSK (Quadrature Phase-Shift Keying) and 8-PSK (Phase-Shift Keying) modulations. At transmitter, the considered shaping filter is RRC with $\beta = 0.20$. At the UAV/aircraft receiver, we assume a perfect channel estimation.
For SC waveform, we proposed two equalization structures (I) and (II). The first one is suitable to sparse channels which is the case in Nyquist signaling. However, the second structure is designed for non-sparse channels and it is used for the FTN case. In order to reduce the complexity of the receiver, we consider a memory length of 1 for the two equalization structures and thus we can deduce that the computational complexity is heavily reduced. The two proposed equalization structure contains two blocks: a forward block and a backward block. The forward block forms tentative symbol decisions with a MAP criterion considering a mismatch truncated channel response. Whereas, the backward block is used thereafter to reduce the channel response to the desired truncated channel used in the forward block.
For simulation results, we study system performance in terms of BER (Bit Error Rate) for QPSK and 8-PSK modulations in Nyquist and FTN signaling.
For the uncoded case, we assume using MAP-based equalization with zero *a priori*
i.e. $\Pr\left(s_{i,n} = \mathcal{C}_m | \mathrm{L}_a^{\mathrm{in}}(\mathbf{c}_i)\right) = 1/M$. After a few number of «self-iterations», the estimated transmit symbol is determinated as the most likely symbol as follows:

$$\widehat{x}_{i,n} = \underset{\mathcal{C}_m \in \chi}{\operatorname{argmax}} \Pr\left(s_{i,n} = \mathcal{C}_m, \mathbf{y}_i\right) \qquad 1 \leq n \leq N \tag{3.46}$$

Scenario with high values of C/M: In this scenario we assume that C/M values taking a values grater than 20 dB which correspond to $\varepsilon \geq 25°$ and thus we can verify that we have $\mathrm{N_{tr}} \geq 4$. For this range of C/M values, it is assumed that the channel is not very selective. This particular case is studied for the worst case corresponding to C/M=20 dB. We note that all simulations results still valid for C/M $\geq$ 20 dB.

- *Case of Nyquist signaling* In Nyquist signaling, it is shown that the equivalent baseband channel has a sparse form. This particular form is exploited to reduce the complexity of the receiver when considering MAP-based symbol detection. The considered equalization structure is «Structure (II)». In this structure, the forward block contains a finite number of independent and parallel trellis. It is shown in (3.15) that the number of considered trellis, $\mathrm{N_{tr}}$, is proportional to the delay τ_2 and the elevation angle ε as:

$$\mathrm{N_{tr}} = \left\lceil \frac{\tau_2}{\mathrm{T}_s} \right\rceil = \left\lceil \frac{2.\mathrm{H}_a.\sin\varepsilon}{3.10^8.\mathrm{T}_h} \right\rceil \tag{3.47}$$

By considering «Structure (II)», uncoded BER performance considering BPSK and 8-PSK modulations are presented in Figure 3.7. For solid curves, we assume a simple parallel MAP equalizer i.e we only consider the forward block. The dashed curves represent the case where residual interference is perfectly removed by the backward block (perfect feedback case). It can be seen that we are achieving the perfect feedback case for QPSK modulation. The same kind of results are observed for 8-PSK modulation. For lower modulation order, such as QPSK and 8-PSK, these results are expected because of the low power of the residual interference term. In fact, in High C/M values, the residual interference can be neglected. As a consequence, in order to have a low-complexity system it would be better to use an equalizer without a feedback block. The residual interference being low-powered, it does not have a visible effect on the performance of the uncoded QPSK and 8-PSK modulation. It is important to note that this result is not valid for higher order modulations such as 16-APSK and 32-APSK modulations.

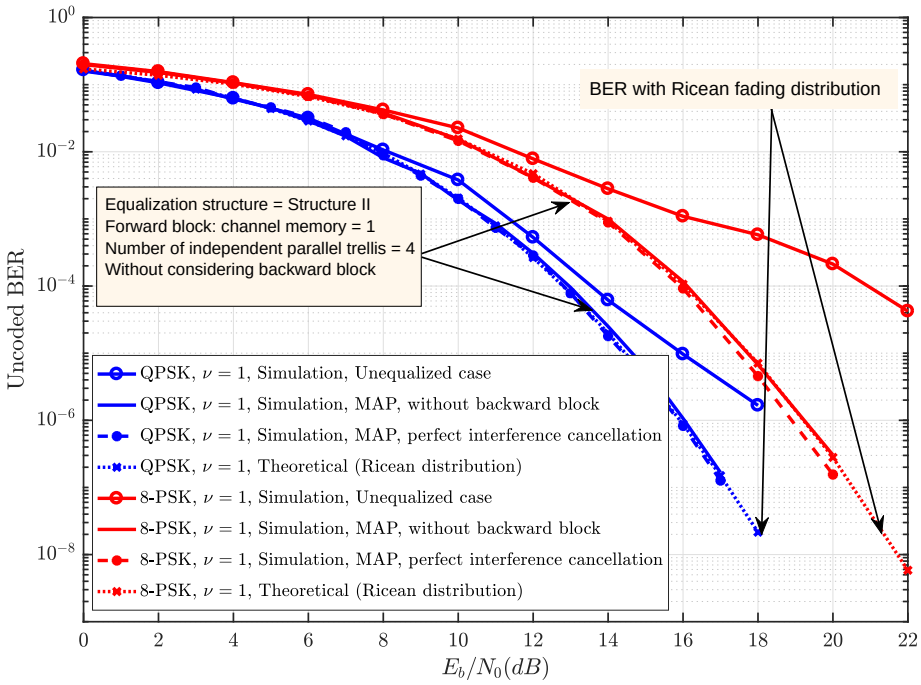

Figure 3.7: *Scenario with high ratio C/M: Uncoded BER performances vs. E_b/N_0 in dB with using the proposed equalization structure (II) for QPSK/8-PSK modulation in Nyquist signaling. The considered C/M value is equal to 20 dB and $R_c = 1/2$.*

- *Case of FTN signaling*

Scenario with low values of C/M: The scenario is characterized by low values of elevation angle between 6° and 12° which corresponds also to low values of C/M taken between 5 dB and 10 dB. In this range, the S2A channel is supposed to be very selective.

- *Case of Nyquist signaling:*

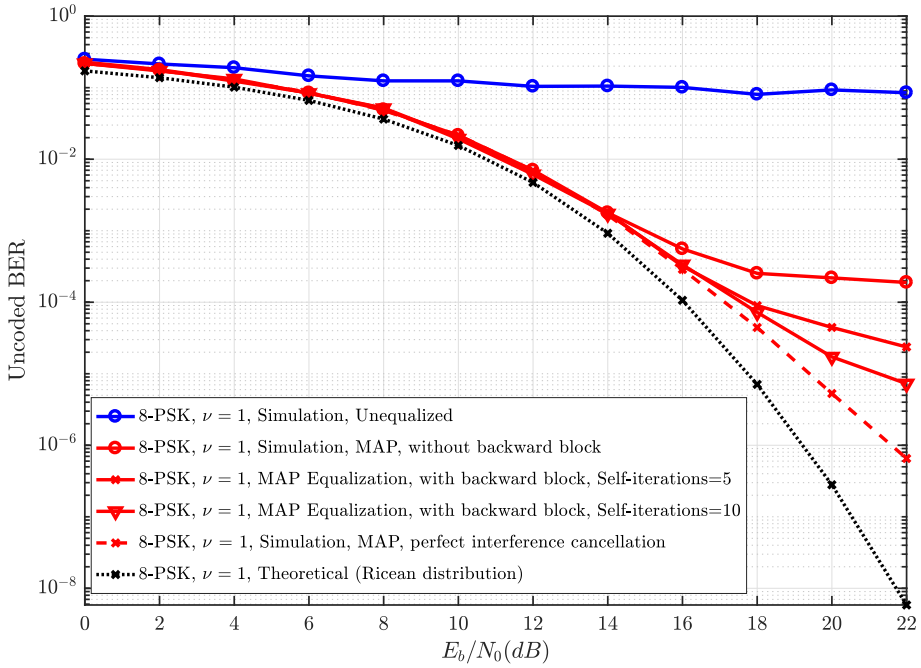

Figure 3.8: *Scenario with low ratio C/M: Uncoded BER performances vs. E_b/N_0 in dB with using the proposed equalization structure (II) for 8-PSK modulation in Nyquist signaling. The considered C/M value is equal to 5 dB and $R_c = 1/2$.*

In Figure 3.8, we present the performance in terms of BER for an uncoded 8-PSK modulation. Performance shown by the blue curve represents the unequalized case. For the red curves, we assume a simple parallel MAP equalizer (mismatched decoder). As we can see, all simulation results are lower bounded by the case with Rice fading distribution shown in black curve.

For the equalized case (shown in red curves), we present the effect of the number of «self-iterations» on the BER performances. To do it, we consider three numbers of «self-iterations» : $N_{s\text{-}i} = 0$ (without backward bloc), $N_{s\text{-}i} = 5$ and $N_{s\text{-}i} = 10$. As a result, It can be seen that uncoded BER performances increase with the number of «self-iterations». The higher the number of «self-iterations», the better are the uncoded BER performance. Indeed, the add of a feedback block allows us to iteratively mitigate the effects of residual interference after a finite number of «self-iterations» and thus enhance system

performances. However, This performance gain is done at the expense of additional complexity at the receiver.

To conclude, for low values of C/M ratio, the residual interference term can not be neglected and thus it is essential add a feedback block to iteratively mitigate the effects of residual interference after a finite number of «self-iterations». Referring to simulation results, considering only a number of 5 «self-iterations» appears sufficient to achieve a good trade-off between performance and complexity. Note that for the case of an QPSK modulation, the same kinds of results are observed.

- *Case of FTN signaling:* In FTN signaling, the equivalent baseband channel is no longer sparse. That's why another equalization structure is designed to equalize receive signals. The considered equalization structure is «Structure (I)».

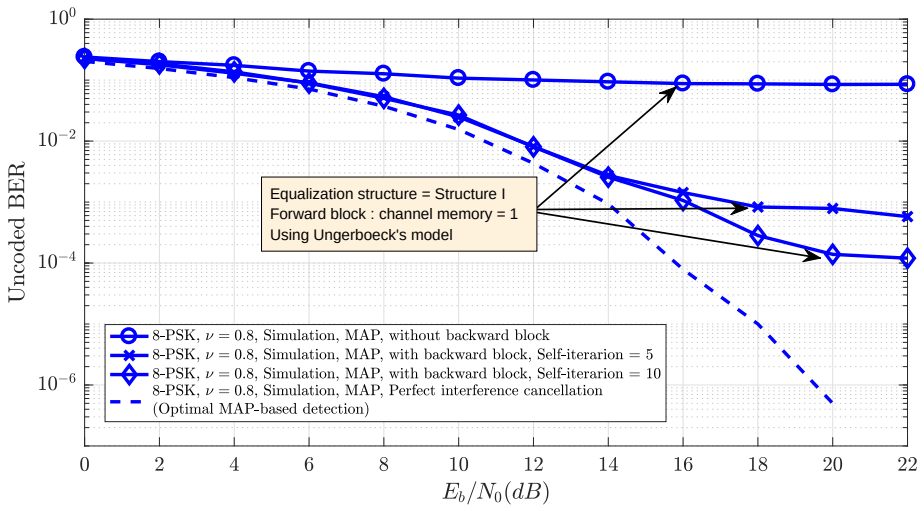

Figure 3.9: *Scenario with high ratio C/M: Uncoded BER performances vs. E_b/N_0 in dB with using the proposed equalization structure (I) for 8-PSK modulation in FTN signaling. The considered C/M is equal to 15 dB and $R_c = 1/2$.*

As for «Structure (II)», the proposed equalization structure contains a forward block and a backward block. In order to reduce the computational complexity of the forward block, we consider a channel memory of 1. Furthermore, we assume a trellis-based detection using *Ungerboeck model*.

In Figure 3.9, we present the performance in terms of BER for an uncoded 8-PSK modulation. As we can see, despite the high values of C/M and the low modulation order, the residual interference term can not be neglected in the case of FTN signaling. Indeed, without considering backward block, simulations results show that BER performances are heavily decreased compared to the case with perfect feedback (dashed curve).

In order to enhance BER performance, a backward block is considered to mitigate the effects of residual interference in few «self-iterations». In the same Figure 3.9, we present the effect of the number of

«self-iterations» on the BER performances. For simulation results, we consider two numbers of «self-iterations» : 5 and 10. As a result, It can be seen that uncoded BER performances decrease with the number of «self-iterations». The higher the number of «self-iterations», the better are the uncoded BER performance. However, This performance gain is done at the expense of additional complexity at the receiver. Considering only a number of 5 «self-iterations», can achieve a good trade-off between performance and complexity.

3.2.5 Proposed Position based time-domain channel estimation:

In this Section, we investigate on some efficient channel estimation methods for discrete equivalent baseband channel. The proposed methods exploit both the particular form of the channel impulse response and *a priori* knowledge of some parameters (mainly delays) that can be inferred from geometrical considerations based on geolocation. The first estimation method is based on a parametric multipath channel model while the second tries to exploit the relative sparsity of the channel impulse response. In both cases, this reduces the number of variables to be estimated and provides better performance compared to a direct classical least-square estimation of the discrete equivalent channel impulse response.
In wireless communication systems, the estimation of the channel impulse response is necessary for the coherent demodulation. For this, it is common to introduce training sequences in the transmitted signal[114][28]. In own case, we consider pilot-aided channel estimation methods. For SC waveform, the considered pilot-observation model is given in (3.9). Whereas, for EW SC-OFDM, the corresponding pilot-observation model is given by (3.70). When estimating directly the equivalent discrete baseband channel impulse response, the use of the maximum likelihood (ML) criterion leads to an optimal solution. However, this estimation process can be very complex due to the memory channel which is generally high. Fortunately, if the observation model is a white-noise model, using simple Least-square criterion is sufficient to avoid high complexity ML-based channel estimation without loss of performance.

3.2.5.1 UAV/aircraft position assumption

Taking into account the geometrical properties of the scene, it is possible to estimate τ_2 if some *a priori* information on the position of the aircraft is available, which can be achieved by using some geolocation techniques. An estimate of τ_2 can be calculated from the knowledge of the elevation angle ε between the UAV/aircraft and a GEO satellite. Indeed, refer to Equation (1.20), an expression of the delay τ_2 is:

$$\tau_2 = \frac{2.\mathrm{H}_a.\sin\varepsilon}{3.10^8} \tag{3.48}$$

By using GPS measurements [68], the value of the elevation angle ε can be calculated from geolocation data or GPS coordinates such as the longitude, the latitude and the altitude. Let $(\Psi_a, \varphi_a, \mathrm{H}_a)$ and $(\Psi_s, \varphi_s, \mathrm{H}_s)$ are the latitude, the longitude and the altitude of an UAV/aircraft and a GEO satellite, respectively. According to the geometry of satellite and aircraft and referring to (1.25), the elevation angle ε between them can be

expressed as:

$$\varepsilon = \arctan\left\{\frac{\varpi - \frac{R_e+H_a}{R_e+H_s}}{\sqrt{1-\varpi^2}}\right\} \qquad \text{with} \qquad \varpi = \cos(\Psi_a)\cos(\Psi_s)\cos(\varphi_s-\varphi_a)+\sin(\Psi_a)\sin(\Psi_s) \tag{3.49}$$

where $R_e = 6371\ km$ being the radius of the earth. The GEO satellite coordinates (Ψ_s, φ_s, H_s) can be assumed well known at the UAV receiver. Given an accurate estimation of UAV/aircraft coordinates (Ψ_a, φ_a, H_a) with a position error less than 15 m, we assume that the value of the elevation angle ε is perfectly known at the receiver.

3.2.5.2 Case of Nyquist signaling

In Nyquist signaling, the additive noise is Gaussian and white and thus the pilot-observation model given in (3.9) is a white-Gaussian model. In the presence of white-Gaussian noise (AWGN), ML estimation becomes equivalent to the least square criterion (LS) [28] and reaches the Cramer-Rao bound (CRB)[8]. Under some considerations, improvements can be achieved if one are able to perform joint estimation of both attenuations and delays of the continuous impulse response which is generally practically achieved through an iterative estimation procedure [113]. These methods are based on a explicit multipath parametric model. However, in some transmission systems, such as aeronautical communication systems, some parameters for the continuous channel can be determined in a very accurate manner, such as the delays of the different paths, based on some geometrical considerations from geolocation techniques[119]. This extra *a priori* allows us to further reduce the unknown of our system and leads to more efficient multipath parametric based estimation methods. Only the attenuation coefficients of the multipath channel will be estimated. This has to be compared with the classical estimation of all taps of the discrete equivalent channel as usually done. Other features could be exploited such as the sparsity of the channel [19].

As shown in Figure 3.10, the impulse response of the equivalent channel presents some powerful coefficients and the others are negligible. The impulse channel response can be considered as «sparse». The estimation method proposed in [19] can be considered. In [19] a position vector is considered and will be estimated through an iterative process. Taking in account the perfect knowledge of the delay τ_2, the position vector is fully known at the receiver and thus the channel estimation can be significantly improved. However, the method proposed by [19] imposes a channel model in which the secondary paths are of zero power. Unfortunately, this is not the case for the aeronautical channel i.e. the secondary paths are negligible but not zero. Because of this mismatch model, the choice of sparse channel estimation method, is not the best strategy. Therefore, in this section, we are interested in channel estimation methods based on an explicit multipath parametric (MP) model, which presents a better strategy.

By applying parametric multipath model, we propose simple but efficient channel estimation methods that benefit from a known position of the UAV/aircraft receiver. The proposed methods exploit both the particular form of the channel impulse response and *a priori* knowledge of some parameters (mainly delays) that can be inferred from geometrical considerations based on geolocalization. The first estimation method is based on a parametric multipath channel model while the second method tries to exploit the relative sparsity of the

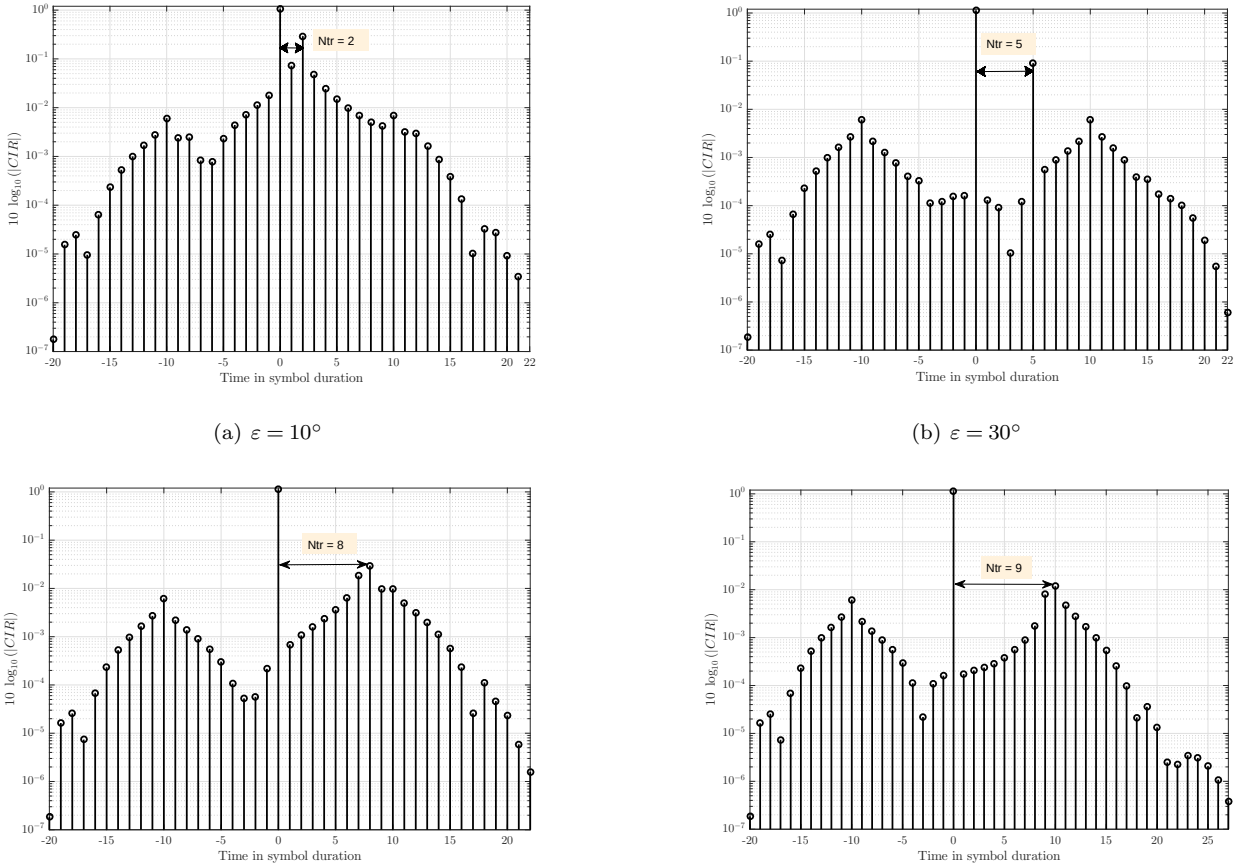

(a) $\varepsilon = 10°$ (b) $\varepsilon = 30°$

(c) $\varepsilon = 50°$ (d) $\varepsilon = 70°$

Figure 3.10: *CIR in Nyquist signaling ($\nu = 1$)*

channel impulse response. In both cases, this reduces the number of variables to be estimated and provides better performance compared to a direct classical least-square estimation of the discrete equivalent channel impulse response.

By considering mutipath parametric (MP) model as given in Section 2.3.4.1, the channel impulse response can be written in this matrix form:

$$\mathbf{h}_i = \mathbf{G}.\ \mathbf{a}_i \tag{3.50}$$

with,

$$\mathbf{G} = \begin{pmatrix} g(-\mathrm{T}_s.L/2) & g(-\mathrm{T}_s.L/2-\tau_2) \\ g(\mathrm{T}_s.(-L/2+1)) & g(\mathrm{T}_s.(-L/2+1)-\tau_2) \\ \vdots & \vdots \\ g(\mathrm{T}_s.L/2) & g(\mathrm{T}_s.L/2-\tau_2) \end{pmatrix} \quad \text{and} \quad \mathbf{a}_i = \begin{bmatrix} \mathrm{A}_{\mathrm{LOS}} + a_{i,1} \\ a_{i,2} \end{bmatrix} \tag{3.51}$$

Without *a priori* knowledge of the delay τ_2, such estimation method, based on a explicit multipath parametric model, should be able to perform joint estimation of both attenuation vector $\mathbf{a}_i$ and delay vector $\tau = [\tau_0, \tau_2]^T$ through an iterative estimation procedure [113]. If it is possible to set up this joint estimation,

the MSE for the structured mutipath LS estimator (SMP-LSE) is lower bounded by (see Equation (2.58)):

$$\text{MSE}\left(\widehat{\mathbf{h}}_i^{\text{SMP-LSE}}\right) \geq tr\{\text{CRB}\} = tr\left\{\mathbf{G}\ \text{CRB}\left(\mathbf{a}_i\right)\ \mathbf{G}^H\right\} + tr\left\{\left(\mathbf{G}.\left[\mathbf{S}^H.\mathbf{S}\right]^{-1}.\mathbf{S}^H.\mathbf{X}.\mathbf{V}+\mathbf{V}\right)\ \text{CRB}\left(\tau\right)\ \left(\mathbf{G}.\left[\mathbf{S}^H.\mathbf{S}\right]^{-1}.\mathbf{S}^H.\mathbf{X}.\mathbf{V}+\mathbf{V}\right)^H\right\} \quad (3.52)$$

where $\text{CRB}\left(\mathbf{a}_i\right)$ and $\text{CRB}\left(\tau\right)$ are respectively the Cramer-Rao Bound of the attenuation vector $\mathbf{a}_i$ and the delay vector τ. The matrices $\mathbf{S}=\mathbf{X}.\ \mathbf{G}$ and $\mathbf{V}=\dot{\mathbf{G}}.diag(\mathbf{a}_i)$ are initially defined in Equation (2.58). The matrix $\dot{\mathbf{G}}$ is a differential matrix having the same size as the $\mathbf{G}$ matrix (see Equation (2.59)).

Referring to Equation (3.52), it is clearly shown that channel estimation is highly penalized when the delay vector τ is non-perfectly estimated. However, in perfect knowledge of the delay vector $\tau=[\tau_0,\tau_2]^T$ i.e. $\text{CRB}\left(\tau\right)=\mathbf{0}$, channel estimation can be significantly improved and a new lower bound can be achieved:

$$\text{MSE}\left(\widehat{\mathbf{h}}_i^{\text{SMP-LSE}}\right) \geq tr\left\{\mathbf{G}\ \text{CRB}\left(\mathbf{a}_i\right)\ \mathbf{G}^H\right\} \quad (3.53)$$

Fortunately, in the case of aeronautical communication, the delay vector can be perfectly estimated thanks to geometrical considerations. Indeed, given an accurate estimation of UAV/aircraft coordinates $(\Psi_a,\varphi_a,\text{H}_a)$, the delay τ_2 is fully known at the receiver by substituting (3.49) in (3.48). Additionally, all delays are measured relative to the first detectable signal at the receiver at $\tau_0=0$.

Thanks to the perfect knowledge of the delay vector, one can reach the lower Cramer-Rao bound without the need for considering joint estimation. Only a simple LS estimation is enough. Indeed, by knowing the delays τ_0 and τ_2, to estimate the channel impulse response is equivalent to estimate the attenuation vector $\mathbf{a}_i$. Given the noise is AWGN, considering LS estimation is equivalent to considering optimal ML estimation. In this case, an estimate of the discrete equivalent baseband channel can be done in two steps as follows [96, 101]:

$$\begin{cases} \text{Step 1: } \underline{\text{LS estimation of attenuation vector:}} \quad \widehat{\mathbf{a}}_i^{\text{LS}} = \left(\mathbf{S}^H.\ \mathbf{S}\right)^{-1}.\ \mathbf{S}^H.\ \mathbf{y}_i^{\text{p}} \qquad \text{with} \qquad \mathbf{S}=\mathbf{X}.\ \mathbf{G} \\ \text{Step 2: } \underline{\text{Channel reconstruction using multipath parametric (MP) model:}} \quad \widehat{\mathbf{h}}_i^{\text{SMP-LSE}} = \mathbf{G}\ \widehat{\mathbf{a}}_i \end{cases}$$

by considering this channel estimation method, one can reach the Cramer-Rao bound expressed in Equation (3.53):

$$\boxed{\text{MSE}\left(\widehat{\mathbf{h}}_i^{\text{SMP-LSE}}\right) = tr\left\{\mathbf{G}\ \text{CRB}\left(\mathbf{a}_i\right)\ \mathbf{G}^H\right\} = \frac{\sigma_w^2.\ tr\left\{\left[\mathbf{G}^H\mathbf{G}\right]^{-1}\ \mathbf{G}^H\mathbf{G}\right\}}{\sigma_p^2.\ (N_{\text{p}}-L)} = \frac{1}{N_{\text{p}}-L}.\ \frac{2}{(\text{E}_s/\text{N}_0)}} \quad (3.54)$$

Compared to the classical unstructured LS estimator (U-LSE), the proposed structured multipath LS estimator (SMP-LSE) can offer a significant gain in terms of MSE. Indeed, the obtained MSE for the unstructured LS estimator is initially derived in Equation (2.50):

$$\text{MSE}\left(\widehat{\mathbf{h}}_i^{\text{U-LSE}}\right) = tr\left\{\sigma_w^2.\ \left(\mathbf{X}^H.\mathbf{X}\right)^{-1}\right\} = \frac{\sigma_w^2.\ (L+1)}{\sigma_p^2.\ (N_{\text{p}}-L)} = \frac{\sigma_w^2.\ (L+1)}{\sigma_s^2.\ (N_{\text{p}}-L)} = \frac{1}{N_{\text{p}}-L}.\ \frac{L+1}{(\text{E}_s/\text{N}_0)} \quad (3.55)$$

By comparing the two MSE equations given in (3.54) and (3.55), the obtained gain is calculated as the following:

$$\text{Gain [dB]} = 10.\log_{10}\left(\frac{\text{MSE}\left(\widehat{\mathbf{h}}_i^{\text{U-LSE}}\right)}{\text{MSE}\left(\widehat{\mathbf{h}}_i^{\text{SMP-LSE}}\right)}\right) = 10.\log_{10}\left(\frac{L+1}{2}\right) \quad (3.56)$$

Assuming a memory length $L = 21$, one can obtain a gain of 11 dB.

For different values of $\mathrm{E}_s/\mathrm{N}_0$, table 3.2 gives some values of MSE for both unstructured and structured LS estimation methods.

		$\varepsilon = 10°$	$\varepsilon = 30°$	$\varepsilon = 50°$	$\varepsilon = 70°$
Memory length L		20	21	22	22
Number pilot symbols $\mathrm{N_p}$		24	24	24	24
Classical unstructured LS estimator MSE $\left(\widehat{\mathbf{h}}_i^{\text{U-LSE}}\right)$	$\mathrm{E}_s/\mathrm{N}_0$=5 dB	1.6602	2.319	3.6366	3.6366
	$\mathrm{E}_s/\mathrm{N}_0$=10 dB	0.5250	0.7333	1.15	1.15
	$\mathrm{E}_s/\mathrm{N}_0$=15 dB	0.1660	0.2319	0.3637	0.3637
Proposed structured multipath LS estimator (SMP-LSE) exploiting *a priori* UAV/aircraft position MSE $\left(\widehat{\mathbf{h}}_i^{\text{SMP-LSE}}\right)$	$\mathrm{E}_s/\mathrm{N}_0$=5 dB	0.1581	0.1581	0.1581	0.1581
	$\mathrm{E}_s/\mathrm{N}_0$=10 dB	0.05	0.05	0.05	0.05
	$\mathrm{E}_s/\mathrm{N}_0$=15 dB	0.0158	0.0158	0.0158	0.0158

Table 3.2: *Simulation parameters & simulation results of proposed channel estimation method in the case of Nyquist signaling for SC waveform*

3.2.5.3 Case of Faster-than-Nyquist (FTN) signaling

In the case of FTN signaling, the equivalent baseband channel seems to be a selective channel presenting many non-negligible "taps". For instance, in the case of $\beta = 0.25$ and $\nu = 0.7$, Figure 3.11 presents an example of the obtained equivalent baseband channel.

For FTN signaling using the pilot-observation model (3.9), the additive noise is still Gaussian but colored. The considered correlation matrix is noted $\mathbf{\Lambda}$ and expressed in (2.43) as:

$$\mathbf{\Lambda} = \begin{bmatrix} \mathrm{g}(0) & \mathrm{g}(\mathrm{T}_s) & \mathrm{g}(2.\mathrm{T}_s) & \dots & \dots & \mathrm{g}([N_\mathrm{p}-L].\mathrm{T}_s) \\ \mathrm{g}(\mathrm{T}_s) & \mathrm{g}(0) & \mathrm{g}(\mathrm{T}_s) & \ddots & & \vdots \\ \mathrm{g}(2.\mathrm{T}_s) & \mathrm{g}(\mathrm{T}_s) & \ddots & \ddots & \ddots & \vdots \\ \vdots & \ddots & \ddots & \ddots & \mathrm{g}(\mathrm{T}_s) & \mathrm{g}(2.\mathrm{T}_s) \\ \vdots & & \ddots & \mathrm{g}(\mathrm{T}_s) & \mathrm{g}(0) & \mathrm{g}(\mathrm{T}_s) \\ \mathrm{g}([N_\mathrm{p}-L].\mathrm{T}_s) & \dots & \dots & \mathrm{g}(2.\mathrm{T}_s) & \mathrm{g}(\mathrm{T}_s) & \mathrm{g}(0) \end{bmatrix} \tag{3.57}$$

In this case LS estimation method is a sub-optimal solution. That's why, we consider ML-based channel estimation methods. Again, considering mutipath parametric (MP) model, it is possible to enhance channel estimation performance. Indeed, with assuming a perfect estimation of the delay τ_2, we improve the estimate accuracy by reducing the set of unknown parameters. In fact, instead of estimating all channel coefficients, it is sufficient to estimate only the attenuation vector $\mathbf{a}_i$.

Assuming that the correlation matrix $\mathbf{\Lambda}$ is invertible and considering the MP model given in (3.50), an estimation of the attenuation vector, $\mathbf{a}_i$, according to ML criterion is given as follows:

$$\widehat{\mathbf{a}}_i^{\text{ML}} = \left(\mathbf{S}^H.\mathbf{\Lambda}^{-1}.\mathbf{S}\right)^{-1}.\mathbf{S}^H.\mathbf{\Lambda}^{-1}.\mathbf{y}_i^{\text{p}} \tag{3.58}$$

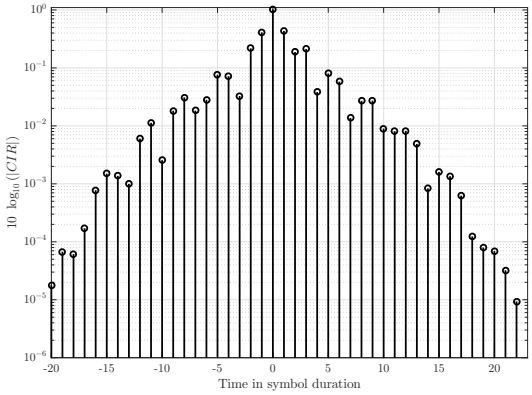

(a) $\varepsilon = 10°$

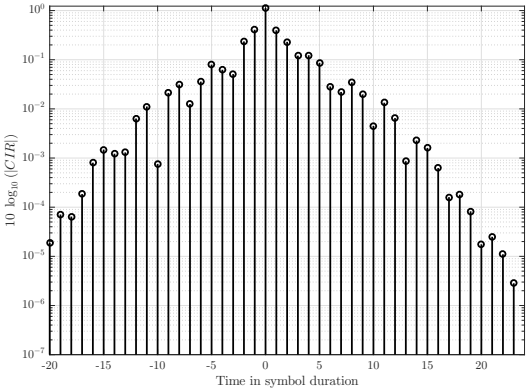

(b) $\varepsilon = 30°$

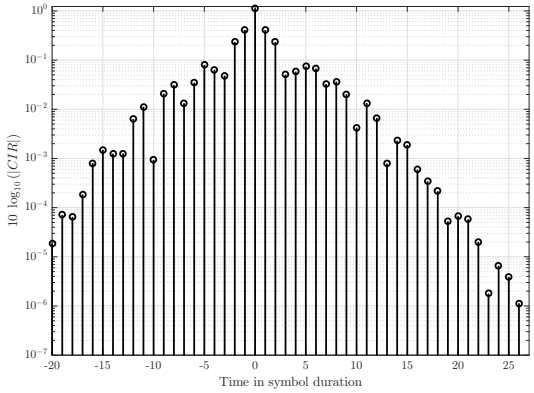

(c) $\varepsilon = 50°$

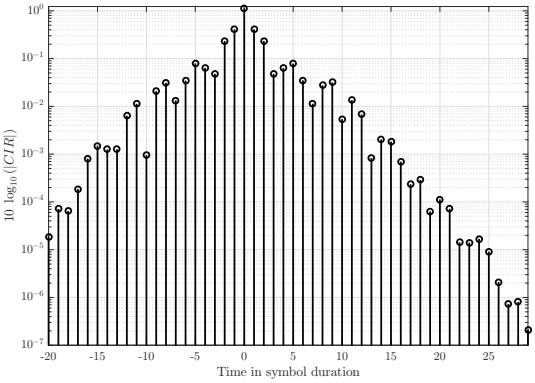

(d) $\varepsilon = 70°$

Figure 3.11: *CIR in Fast-Than-Nyquist (FTN) signaling ($\nu = 0.7$)*

Then, an estimate of the channel impulse response $\mathbf{h}_i$ can be deduced by using MP model (channel reconstruction):

$$\widehat{\mathbf{h}}_i^{\text{SMP-MLE}} = \mathbf{G}\ \widehat{\mathbf{a}}_i^{\text{ML}} \tag{3.59}$$

Thus, an estimate of the discrete equivalent baseband channel can be done in two steps as follows:

$$\begin{cases} \text{Step 1: } \underline{\text{ML estimation of attenuation vector:}} \quad \widehat{\mathbf{a}}_i^{\text{ML}} = \left(\mathbf{S}^H.\mathbf{\Lambda}^{-1}.\mathbf{S}\right)^{-1}.\mathbf{S}^H.\mathbf{\Lambda}^{-1}.\mathbf{y}_i^{\text{p}} \qquad \text{with} \qquad \mathbf{S} = \mathbf{X}.\ \mathbf{G} \\ \text{Step 2: } \underline{\text{Channel reconstruction using multipath parametric (MP) model:}} \quad \widehat{\mathbf{h}}_i^{\text{SMP-LSE}} = \mathbf{G}.\ \widehat{\mathbf{a}}_i^{\text{ML}} \end{cases}$$

by considering this channel estimation method, one can reach its corresponding Cramer-Rao bound as follows:

$$\text{MSE}\left(\widehat{\mathbf{h}}_i^{\text{SMP-MLE}}\right) = tr\{\text{CRB}\} = tr\Big\{\mathbf{G}.\ \text{CRB}\left(\mathbf{a}_i\right).\ \mathbf{G}^H\Big\} \tag{3.60}$$

with $\text{CRB}\left(\mathbf{a}_i\right)$ denotes the Cramer-Rao bound of the attenuation vector estimation at it is expressed as:

$$\text{CRB}\left(\mathbf{a}_i\right) = \sigma_w^2.\ \left(\mathbf{S}^H.\mathbf{\Lambda}^{-1}.\mathbf{S}\right)^{-1} = \sigma_w^2.\ \left(\mathbf{G}^H.\ \mathbf{X}^H.\ \mathbf{\Lambda}^{-1}.\ \mathbf{X}.\ \mathbf{G}\right)^{-1} \tag{3.61}$$

By substituting (3.60) in (3.61), the expression of the MSE is done as

$$\boxed{\text{MSE}\left(\widehat{\mathbf{h}}_i^{\text{SMP-MLE}}\right) = \sigma_w^2.\ tr\left\{\left(\mathbf{G}^H.\ \mathbf{X}^H.\mathbf{\Lambda}^{-1}.\mathbf{X}.\mathbf{G}\right)^{-1}.\ \mathbf{G}^H.\ \mathbf{G}\right\}} \tag{3.62}$$

Compared to the classical unstructured ML estimator (U-MLE), we can verify that the proposed structured multipath ML estimator (SMP-MLE) can offer a significant gain in terms of MSE. The obtained MSE for the unstructured ML estimator is initially derived in Equation (2.48):

$$\text{MSE}\left(\widehat{\mathbf{h}}_i^{\text{U-MLE}}\right) = \sigma_w^2.\ tr\left\{\left(\mathbf{X}^H.\mathbf{\Lambda}^{-1}.\mathbf{X}\right)^{-1}\right\} \tag{3.63}$$

Figure 3.12 shows that proposed U-MLE channel estimation method reaches the lower Cramer-Rao bound (CRB). Moreover, it is shown that for each value of ν, a new CRB is obtained. Also, we can see that MSE performance increase with ν values. For instance, compared to the classical unstructured ML estimation, we can have a gain of 14 dB for $\nu = 1$ and a gain of 10 dB for $\nu = 0.4$ for the same simulation parameters.

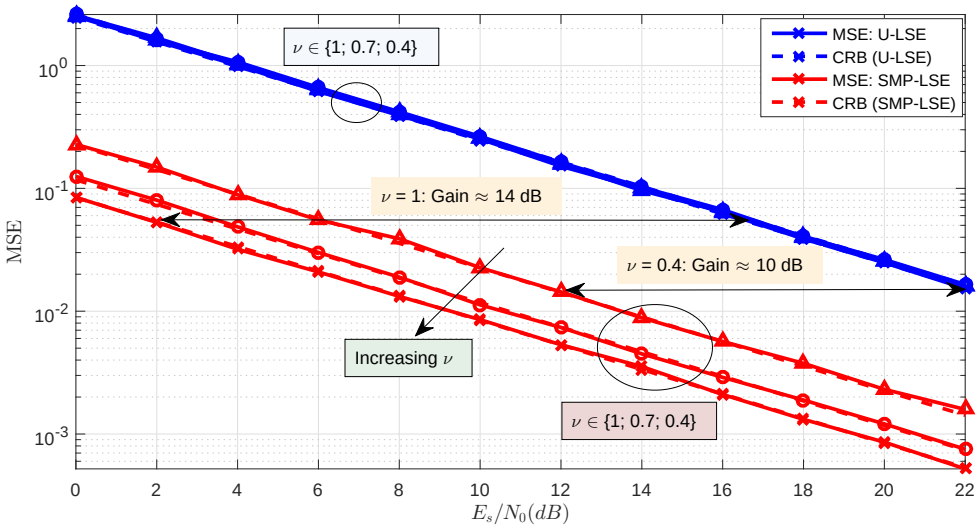

Figure 3.12: *MSE and Cramer-Rao bound for proposed channel estimation method compared to the classical unstructured LS estimation method.* $N_p = 52$ *and* $L = 27$

3.3 EW SC-OFDM waveform

In this Section, we are interested in EW SC-OFDM waveform. Based on the expression of received symbols (data symbols and training symbols) initially given in Equations (2.78) and (2.79), this section aims to give the corresponding system model in the case of aeronautical channel and especially for the forward link. The objective of this Section is to study the system performances with considering frequency-domain channel estimation and channel equalization methods.

3.3.1 Expression of frequency response of the satellite-to-aircraft (S2A) channel

By assuming a frame-based communication and supposing that frame duration does not exceed the coherence time, T_c, of the propagation channel. The expression of the A2S channel is given in (3.5) as:

$$\mathrm{h}_a(t,\tau) \approx \mathrm{h}_a(\tau) = (\mathrm{A}_{\mathrm{LOS}} + a_{i,1})\ \delta(\tau) + a_{i,2}\ \delta(\tau - \tau_2) \tag{3.64}$$

The frequency response of S2A channel in each frequency indexes $1 \leq n \leq N_1$ is given by:

$$\mathrm{H}_a(n) = (\mathrm{A}_{\mathrm{LOS}} + a_{i,1}) + a_{i,2}.\ \exp(-2\pi j f_n \bar{\tau}_2) \qquad \text{for} \qquad 1 \leq n \leq N_1 \tag{3.65}$$

where f_n is the n-th frequency element and $\bar{\tau}_2 = L_c \times (\mathrm{T}_s/\mathrm{F}_s)$. The positive integer L_c denotes the memory size of the discrete-time response of $\mathrm{h}_a(\tau)$ which is calculated as:

$$L_c = \left\lceil \frac{\tau_2}{\mathrm{T}_s/\mathrm{F}_s} \right\rceil \qquad \text{where } \lceil(.)\rceil \text{ stands for the integer part of } (.). \tag{3.66}$$

Note that we consider zero-centered frequency elements $\{f_n\}$. Each one is expressed as:

$$f_n = \frac{1}{\mathrm{T}_s/\mathrm{F}_s}.\left(\frac{n-1}{N_1} - \frac{1}{2}\right) \qquad \text{for} \qquad 1 \leq n \leq N_1 \tag{3.67}$$

with $\mathrm{F}_s \geq 1+\beta$ denotes the considered over-sampling factor and $N_1 = N \times \mathrm{F}_s$ is the total number of frequency elements.

By considering the expression of the frequency response of the S2A channel given in (3.65), a close expression for square of absolute value of each frequency response $\mathrm{H}_a(n)$ can be deduced as:

$$|\mathrm{H}_a(n)|^2 = \left(|\mathrm{A}_{\mathrm{LOS}} + a_{i,1}|^2 + |a_{i,2}|^2\right) + 2.\ \mathrm{A}_{\mathrm{LOS}}.\ \Re\left\{a_{i,1}^*.\ a_{i,2}.\ \exp(2\pi j f_n \bar{\tau}_2)\right\} \tag{3.68}$$

we recall that $\mathrm{A}_{\mathrm{LOS}}$ is a constant value and the complex variables $a_{i,1}$ and $a_{i,2}$ are two independent zero-mean complex Gaussian variables with variances P_1 and P_2, respectively.

3.3.2 System model

As for SC waveform, a sequence of $N_{\mathrm{p}} = (1/\Delta) \times N \leq N$ training symbols, denoted by $\mathbf{x} = [x_1, x_2, \ldots, x_{N_{\mathrm{p}}}]$, will be inserted in each transmitted sub-frame in order to estimate frequency response channel. The size of training sequence depends on a spacing factor $\Delta \in \{4; 8; 16; 32; \ldots\}$. The rational number $1/\Delta$ denotes the ratio between the size of the data sequence and the size of the training sequence. As shown in Figure 2.3, the

training sequence is used alternately with the data sequence $\mathbf{s}_i$. Note that training symbols $x_1, x_2, \ldots, x_{N_\mathrm{p}}$ are perfectly known at the receiver and having a variance $\sigma_p^2 = \sigma_s^2$.

At the transmitter, each obtained data sequence $\mathbf{s}_i$ will be oversampled by a $\mathrm{F}_s \geq 1+\beta$ factor before being *circularly* filtered by a RRC shaping filter $\mathrm{h}_e(\tau)$ with roll-off $0 \leq \beta \leq 1$ and a Nyquist bandwidth $\mathrm{B_h}$. A possible frequency implementation is considered in Figure 3.13. Indeed, over-sampling in time domain is equivalent to have a repetition in frequency domain. Also, considering circular shape filtering is equivalent to have a spectral shaping in the frequency domain. The ratio between the size of the second Inverse Fast Fourier Transform (IFFT) and the size of the first Fast Fourier Transform (FFT) is equal to the over-sampling factor F_s. Therefore, the size of the first FFT is equal to N and the size of the second IFFT is equal to $N_1 = \mathrm{F}_s \times N \geq N$. Respectively for training sequence, the size of the first FFT is equal to N_p and the size of the second IFFT is equal to $N_1^\mathrm{p} = \mathrm{F}_s \times N_\mathrm{p} \geq N_\mathrm{p}$. N_1 and N_1^p are two positive integers. Note that FFT sizes N,N_p, N_1^p and N_1 are assumed invariant during all the communication.

Similarity to SC waveform, for EW SC-OFDM waveform the received data signal and the received training signal are detected at the reception. The received data signal will be processed to detect transmit data modulated sequence $\mathbf{s}_i$. Whereas, the received training signal is used to estimate the channel response. The frequency received data sequence corresponding to received data signal is denoted by $\widetilde{\mathbf{Y}}_i = \left[\widetilde{Y}_{i,1}, \widetilde{Y}_{i,2}, \ldots, \widetilde{Y}_{i,N_1}\right]^T$. Whereas, the frequency received training sequence corresponding to the received training signal is denoted by $\widetilde{\mathbf{Y}}_i^\mathrm{p} = \left[\widetilde{Y}_{i,1}^\mathrm{p}, \widetilde{Y}_{i,2}^\mathrm{p}, \ldots, \widetilde{Y}_{i,N_1^\mathrm{p}}^\mathrm{p}\right]^T$. Refer to Equations (2.78) and (2.79), the expression of received data symbols $\left\{\widetilde{Y}_{i,n}\right\}$ and received training symbols $\left\{\widetilde{Y}_{i,n}^\mathrm{p}\right\}$ are given by:

$$\widetilde{\mathbf{Y}}_i = \begin{bmatrix} \widetilde{Y}_{i,1} \\ \widetilde{Y}_{i,2} \\ \vdots \\ \widetilde{Y}_{i,N_1} \end{bmatrix} = \sqrt{\mathrm{F}_s} \times diag \begin{bmatrix} \mathrm{H}_a(1) \\ \mathrm{H}_a(2) \\ \vdots \\ \mathrm{H}_a(N_1) \end{bmatrix} . \mathbf{A} . \mathbf{F}_\mathrm{N} . \begin{bmatrix} s_{i,1} \\ s_{i,2} \\ \vdots \\ s_{i,N} \end{bmatrix} + \begin{bmatrix} \widetilde{w}_1 \\ \widetilde{w}_2 \\ \vdots \\ \widetilde{w}_{N_1} \end{bmatrix} \tag{3.69}$$

and,

$$\widetilde{\mathbf{Y}}_i^\mathrm{p} = \begin{bmatrix} \widetilde{Y}_{i,1}^\mathrm{p} \\ \widetilde{Y}_{i,2}^\mathrm{p} \\ \vdots \\ \widetilde{Y}_{i,N_1^\mathrm{p}}^\mathrm{p} \end{bmatrix} = \frac{1}{\sqrt{\mathrm{F}_s}} . \; diag \begin{bmatrix} \mathrm{H}_a(\Delta) \\ \mathrm{H}_a(2.\Delta) \\ \vdots \\ \mathrm{H}_a\left(N_1^\mathrm{p}.\Delta\right) \end{bmatrix} . diag \begin{bmatrix} \mathrm{H}_e(\Delta) \\ \mathrm{H}_e(2.\Delta) \\ \vdots \\ \mathrm{H}_e\left(N_1^\mathrm{p}.\Delta\right) \end{bmatrix} . \begin{bmatrix} \mathrm{I}_\mathrm{p}'' \\ \mathbf{I}_{N_\mathrm{p} \times N_\mathrm{p}} \\ \mathrm{I}_\mathrm{p}' \end{bmatrix} . \begin{bmatrix} X_1 \\ X_2 \\ \vdots \\ X_{N_\mathrm{p}} \end{bmatrix} + \begin{bmatrix} \widetilde{w}_1 \\ \widetilde{w}_2 \\ \vdots \\ \widetilde{w}_{N_1^\mathrm{p}} \end{bmatrix} \tag{3.70}$$

The noise variables $\{\widetilde{w}_n\}$ are zero-mean complex AWGN with variance $\widetilde{\sigma}_w^2$ computed as:

$$\widetilde{\sigma}_w^2 = \mathrm{N}_0 \times \mathrm{F}_s \times \mathrm{R}_s = \mathrm{F}_s \times \sigma_w^2 \qquad \text{with} \qquad \sigma_w^2 = \mathrm{N}_0 \times \mathrm{R}_s \tag{3.71}$$

3.3.3 Classical MMSE-based frequency-domain channel equalization

In linear observation model given in Equation (3.69), the noise variables $\{\widetilde{w}_n\}$ are Gaussian and white. Furthermore, the constellation symbols $\{s_{i,n}\}$ are assumed i.i.d with variance equal to σ_s^2. By applying a linear MMSE equalization *a priori* [122], we can obtain a biased estimation of the transmitted data sequence

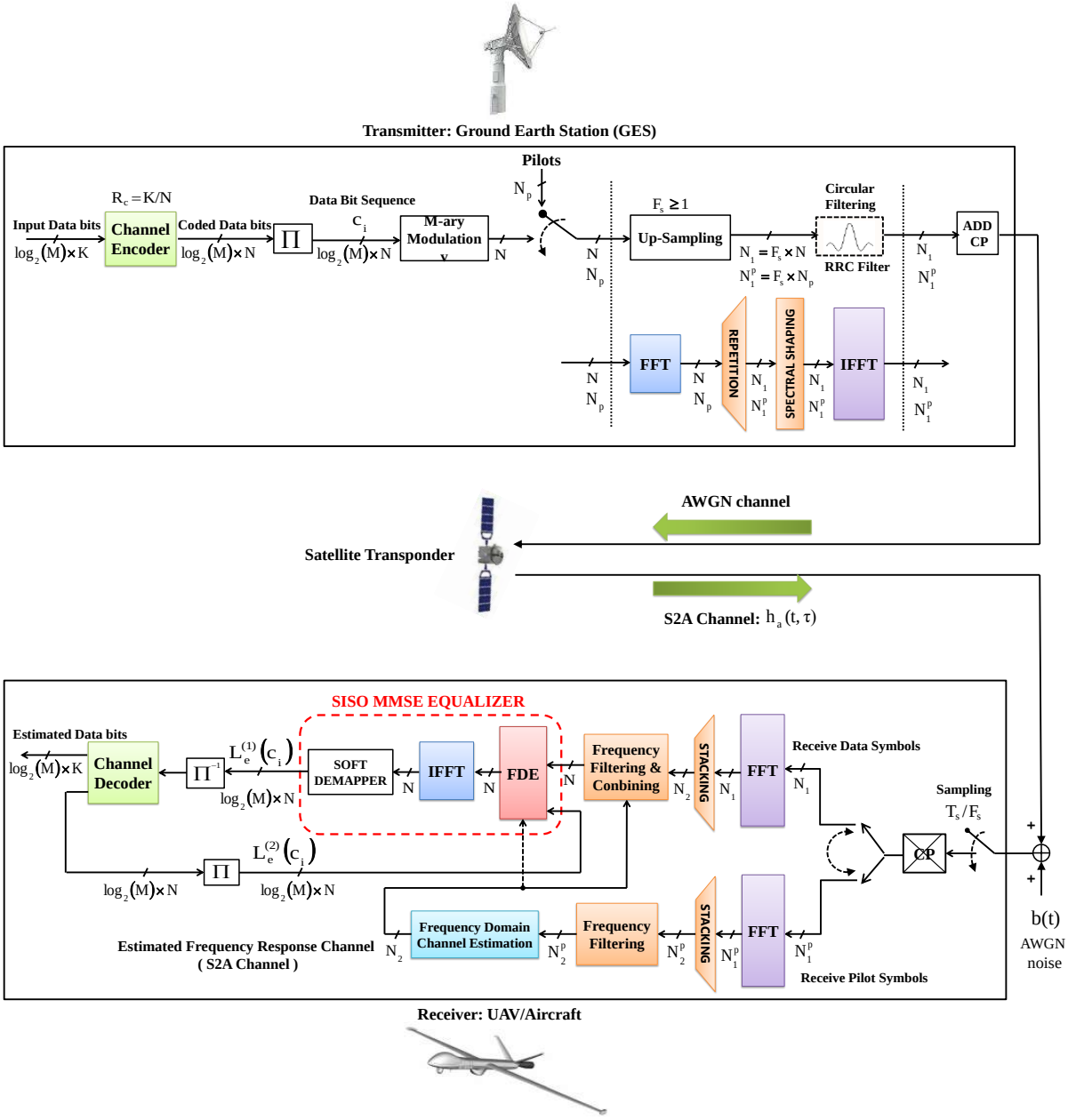

Figure 3.13: *GES transmitter and UAV/Aircraft receiver using EW SC-OFDM waveform for the forward link*

$\mathbf{s}_i = [s_{i,1}, s_{i,2}, \ldots, s_{i,N}]^T$. We denote $\mathbf{z}_i = [z_{i,1}, z_{i,2}, \ldots, z_{i,N}]^T$ as the output MMSE equalization vector which is expressed as:

$$\mathbf{z}_i = \mathbf{F}_{\mathrm{N}}^H . \Sigma^{-1} . \mathbf{A}_i^H . \left(\frac{1}{\sqrt{\mathrm{F}_s}} . \widetilde{\mathbf{Y}}_i - \mathbf{A}_i . \mathbf{F}_{\mathrm{N}} . \bar{\mathbf{s}}_i \right) + \mu_i = \mathbf{F}_{\mathrm{N}}^H . \Sigma^{-1} . \left(\mathbf{Y}_i - \bar{\mathbf{Y}}_i \right) + \mu_i \tag{3.72}$$

where $\mathbf{Y}_i$ is the output frequency domain observation after being filtered by a receive matched filter:

$$\mathbf{Y}_i = \frac{1}{\sqrt{\mathrm{F}_s}} . \mathbf{A}_i^H . \widetilde{\mathbf{Y}}_i \tag{3.73}$$

Furthermore, The three quantities Σ^{-1}, μ_i and $\bar{\mathbf{Y}}_i$ denote the three MMSE equalization parameters to be computed for a given *a priori* information $(\bar{v}_s, \bar{\mathbf{s}}_i)$ and they are expressed as:

$$\Sigma^{-1} \triangleq \frac{1}{1+[1-(\bar{v}_s/\sigma_s^2)].\ \varrho_i}.\left[(\bar{v}_s/\sigma_s^2).\ \mathbf{A}_i^H.\mathbf{A}_i + (\sigma_w^2/\sigma_s^2).\ \mathbf{I}_{N\times N}\right]^{-1} \tag{3.74}$$

$$\bar{\mathbf{Y}}_i \triangleq \mathbf{A}_i^H.\mathbf{A}_i.\mathbf{F}_{\mathrm{N}}.\bar{\mathbf{s}}_i \tag{3.75}$$

$$\mu_i \triangleq \frac{\varrho_i}{1+[1-(\bar{v}_s/\sigma_s^2)].\ \varrho_i}.\ \bar{\mathbf{s}}_i = \alpha_i.\ \bar{\mathbf{s}}_i \tag{3.76}$$

By taking into account an *a priori* information, the values of the two real positive scalars, ϱ_i and α_i, depend on the given symbol variance values $\bar{v}_s$ as follows:

$$\varrho_i \triangleq \frac{1}{N}.\ tr\left\{\left[(\bar{v}_s/\sigma_s^2).\ \mathbf{A}_i^H.\mathbf{A}_i + (\sigma_w^2/\sigma_s^2).\ \mathbf{I}_{N\times N}\right]^{-1}.\mathbf{A}_i^H.\mathbf{A}_i\right\} \quad \text{and} \quad \alpha_i \triangleq \frac{\varrho_i}{1+[1-(\bar{v}_s/\sigma_s^2)].\ \varrho_i} \tag{3.77}$$

Besides, we can show that the matrix $\mathbf{A}_i^H.\mathbf{A}_i$ is a $N\times N$ diagonal matrix and $\mathrm{H}_{i,1}, \mathrm{H}_{i,2}, \ldots, \mathrm{H}_{i,N}$ are its real diagonal values. By using the explicit expression of the square of absolute value of each frequency response $\mathrm{H}_a(n)$ given in (3.68), an explicit expression of the diagonal matrix $\mathbf{A}_i^H.\mathbf{A}_i$ is given:

$$\mathbf{A}_i^H.\mathbf{A}_i = diag\begin{bmatrix}\mathrm{H}_{i,1}\\ \mathrm{H}_{i,2}\\ \vdots\\ \mathrm{H}_{i,N}\end{bmatrix} = \left(|\mathrm{A}_{\mathrm{LOS}}+a_{i,1}|^2+|a_{i,2}|^2\right).\ diag\begin{bmatrix}\lambda_1\\ \lambda_2\\ \vdots\\ \lambda_N\end{bmatrix} + 2.\ \mathrm{A}_{\mathrm{LOS}}.\ \Re\left\{a_{i,1}^*.\ a_{i,2}.\ diag\begin{bmatrix}\Phi_1\\ \Phi_2\\ \vdots\\ \Phi_N\end{bmatrix}\right\} \tag{3.78}$$

the diagonal values $\Phi_1, \Phi_2, \ldots, \Phi_N$ are also invariant for all received sub-frames. They only depend on the chosen shaping filter $h_e(\tau)$, the acceleration factor $0<\nu\leq 1$ and also on the delay τ_2 given by the S2A channel. These diagonal values can be obtained as follows:

$$diag\begin{bmatrix}\Phi_1\\ \Phi_2\\ \vdots\\ \Phi_N\end{bmatrix} = \frac{1}{(\mathrm{F}_s)^2}.\begin{bmatrix}\mathrm{I}''\\ \mathbf{I}_{N\times N}\\ \mathrm{I}'\end{bmatrix}^H.diag\begin{bmatrix}|\mathrm{H}_e(1)|^2.\exp(-2\pi j f_1\bar{\tau}_2)\\ |\mathrm{H}_e(2)|^2.\exp(-2\pi j f_2\bar{\tau}_2)\\ \vdots\\ |\mathrm{H}_e(N_1)|^2.\exp(-2\pi j f_{N_1}\bar{\tau}_2)\end{bmatrix}.\begin{bmatrix}\mathrm{I}''\\ \mathbf{I}_{N\times N}\\ \mathrm{I}'\end{bmatrix} \tag{3.79}$$

Thus, by considering Equation (3.78), one can deduce the following expression:

$$\mathrm{H}_{i,n} = \left(|\mathrm{A}_{\mathrm{LOS}}+a_{i,1}|^2+|a_{i,2}|^2\right).\ \lambda_n + 2.\ \mathrm{A}_{\mathrm{LOS}}.\ \Re\left\{a_{i,1}^*.\ a_{i,2}.\ \Phi_n\right\} \tag{3.80}$$

The values of frequency responses $\{\mathrm{H}_{i,n}\}$ vary in each received sub-frame. The mean values of each frequency responses $\mathrm{H}_{i,n}$ is calculated as:

$$\mathbb{E}\{\mathrm{H}_{i,n}\} = \lambda_n.\ \mathbb{E}\left\{|\mathrm{A}_{\mathrm{LOS}}+a_{i,1}|^2+|a_{i,2}|^2\right\} = \lambda_n.\ \left(\mathrm{A}_{\mathrm{LOS}}^2+\mathrm{P}_1+\mathrm{P}_2\right) = \lambda_n \tag{3.81}$$

Numerical values for diagonal frequency responses $\mathrm{H}_{i,1}, \mathrm{H}_{i,2}, \ldots, \mathrm{H}_{i,N}$ are shown in Figure 3.14 for various values of the acceleration factor ν.

Given the fact that $\mathbf{A}_i^H.\mathbf{A}_i$ is a diagonal matrix, the expression of ϱ_i in (3.77), and Σ^{-1} in (3.76) can be reduced to:

$$\varrho_i = \frac{1}{N}\sum_{n=1}^{N}\frac{\mathrm{H}_{i,n}}{(\bar{v}_s/\sigma_s^2).\ \mathrm{H}_{i,n}+(\sigma_w^2/\sigma_s^2)} \quad \text{and} \quad \Sigma^{-1} = \frac{\sigma_s^2}{1+[1-(\bar{v}_s/\sigma_s^2)].\ \varrho_i}.diag\begin{bmatrix}\frac{1}{\bar{v}_s.\ \mathrm{H}_{i,1}+\sigma_w^2}\\ \frac{1}{\bar{v}_s.\ \mathrm{H}_{i,2}+\sigma_w^2}\\ \vdots\\ \frac{1}{\bar{v}_s.\ \mathrm{H}_{i,N}+\sigma_w^2}\end{bmatrix} \tag{3.82}$$

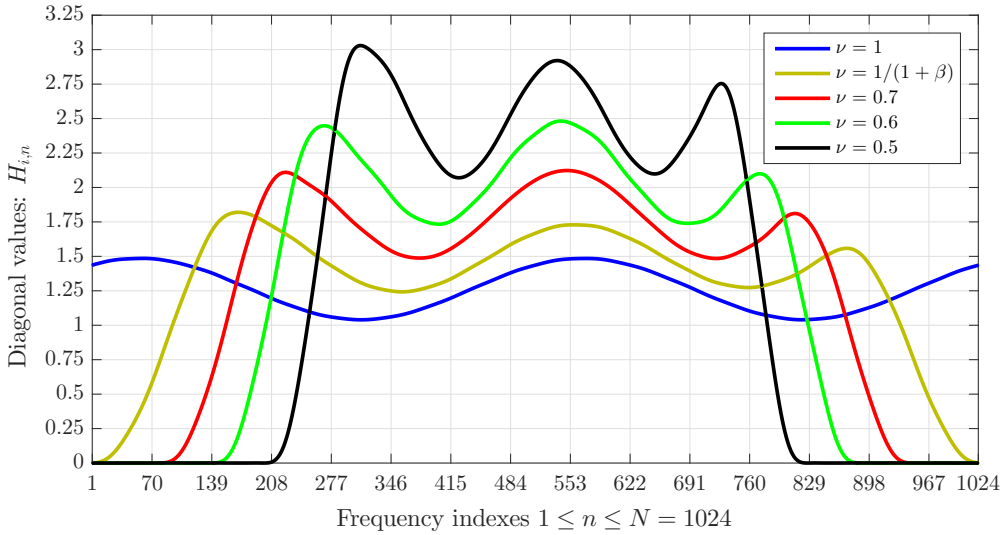

Figure 3.14: *Numerical values of diagonal values* $\{H_{i,n}\}$ *in each frequency indexes* $1 \leq n \leq N = 1024$ *in the case of using RRC shaping filter with* $\beta = 0.20$. $A_{LOS} = 0.9767$ *;* $a_{i,1} = 0.1904$. $e^{j\pi/4}$ *and* $a_{i,2} = 0.0994$. $e^{j\pi/4}$

Thus, the complexity of the receiver is significantly reduced and matrix inversion is no longer a problem. As a consequence, it is possible to consider Frequency Domain Equalization (FDE) based on MMSE criterion as shown in Figure 3.15.

Referring to [70], it is shown that the output MMSE equalized vector, $\widetilde{\mathbf{s}}_i$, is a biased estimation of $\mathbf{s}_i$ and its expression can be reduced to:

$$\widetilde{\mathbf{s}}_i = \sqrt{\frac{\gamma_i}{\alpha_i^2}}\,\mathbf{z}_i \approx \sqrt{\gamma_i}\,\mathbf{s}_i + \mathbf{w} \tag{3.83}$$

where $\mathbf{w} = [w_1, w_2, \ldots, w_N]^T$ is a zero-mean complex AWGN noise vector and symbols $\{w_n\}$ have a variance equal to σ_w^2. The positive scalar γ_i denotes the MMSE equalization gain and its expression is initially given in (2.98) as:

$$\gamma_i = \begin{cases} \left(\frac{1}{N} \sum_{n=1}^{N} \frac{1}{\mathrm{H}_{i,n} + (\sigma_w^2/\sigma_s^2)} \right)^{-1} - (\sigma_w^2/\sigma_s^2) = \gamma_i^{\min} & \text{for} \quad \bar{v}_s = \sigma_s^2 \quad \text{(zero a priori)} \\ (\sigma_s^2/\bar{v}_s) \cdot \left\{ \left(\frac{1}{N} \sum_{n=1}^{N} \frac{1}{(\bar{v}_s/\sigma_s^2).\mathrm{H}_{i,n} + (\sigma_w^2/\sigma_s^2)} \right)^{-1} - (\sigma_w^2/\sigma_s^2) \right\} & \text{for} \quad 0 < \bar{v}_s < \sigma_s^2 \\ \frac{1}{N} \sum_{n=1}^{N} \mathrm{H}_{i,n} = \gamma_i^{\max} & \text{for} \quad \bar{v}_s = 0 \quad \text{(Perfect a priori)} \end{cases} \tag{3.84}$$

In Figure 3.15, an extrinsic LLR vector of size $N \times \log_2(M)$, $\mathrm{L}_e^{\mathrm{out}}(\mathbf{c}_i)$, is generated and calculated as follows:

$$\mathrm{L}_e^{\mathrm{out}}(\mathbf{c}_i) = \mathrm{L}_a^{\mathrm{out}}(\mathbf{c}_i) - \mathrm{L}_a^{\mathrm{in}}(\mathbf{c}_i) \tag{3.85}$$

where $\mathrm{L}_a^{\mathrm{out}}(\mathbf{c}_i)$ is an *a posteriori* LLR vector and its expression is initially given in Equation (2.101).

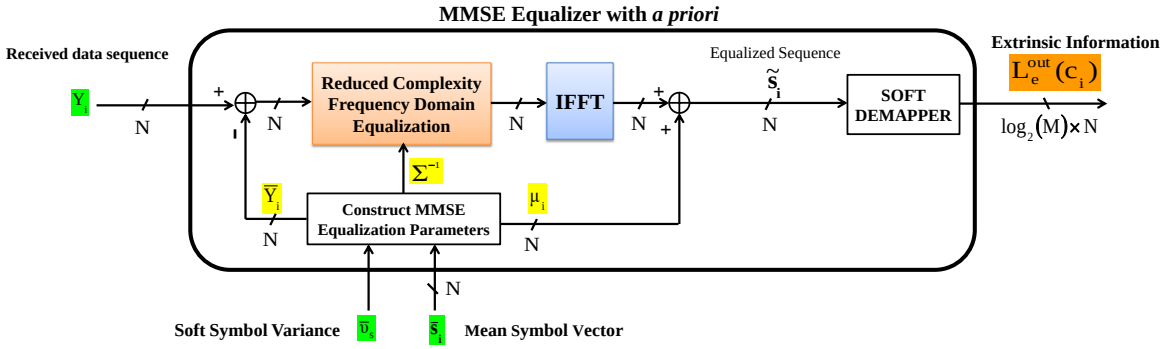

Figure 3.15: *The considered Linear MMSE equalizer using a priori information.*

3.3.4 Symbol detection: simulation results

In this section we study the performance of transmit symbol detection for the uncoded and the coded cases. According to the value of C/M ratio, uncoded and coded BER performances are plotted. For the simulation results, we consider QPSK (Quadrature Phase-Shift Keying) and 8-PSK (Phase-Shift Keying) modulations. At transmitter, the considered shaping filter is RRC with $\beta = 0.20$. At the UAV/aircraft receiver, we assume a perfect channel estimation.

3.3.4.1 The uncoded case

For the uncoded case, we assume using MMSE equalization with zero *a priori* i.e. $\gamma_i = \gamma_i^{\min}$. The estimated transmit symbol is determinated as the most likely symbol as follows:

$$\widehat{x}_{i,n} = \underset{\mathcal{C}_m \in \chi}{\operatorname{argmin}} \left| \widetilde{s}_{i,n} - \sqrt{\gamma_i^{\min}}.\, \mathcal{C}_m \right|^2 \qquad 1 \leq n \leq N \tag{3.86}$$

By using the expression of $\gamma_i^{\min}$, given in Equation (3.84), and by taking into account the expression the channel frequency responses $\{\mathrm{H}_{i,n}\}$, given in Equation (3.80), a close expression of $\gamma_i^{\min}$ is done as follows:

$$\begin{aligned} \gamma_i^{\min} &= \left(\frac{1}{N} \sum_{n=1}^{N} \frac{1}{\mathrm{H}_{i,n} + (\sigma_w^2/\sigma_s^2)} \right)^{-1} - (\sigma_w^2/\sigma_s^2) \qquad (3.87) \\ &= \left(\frac{1}{N} \sum_{n=1}^{N} \frac{1}{\left(|\mathrm{A_{LOS}} + a_{i,1}|^2 + |a_{i,2}|^2 \right).\, \lambda_n + 2.\, \mathrm{A_{LOS}}.\, \Re\left\{ a_{i,1}^*.\, a_{i,2}.\, \Phi_n \right\} + (\sigma_w^2/\sigma_s^2)} \right)^{-1} - (\sigma_w^2/\sigma_s^2) \end{aligned}$$

By considering Gray mapping [50], it is shown that we have only one erroneous bit in each erroneous mapping constellation symbol. Thus, the theoretical average Bit Error Rate can be expressed as:

$$\mathrm{BER} \cong \frac{\mathrm{N}_v}{\log_2(M)} \times \int Q\left(\sqrt{\gamma_i^{\min}}.\sqrt{\left(\frac{\mathrm{D}_{\min}^2}{2.\sigma_s^2} \right).\mathrm{R}_c.\log_2(M).\mathrm{E}_b/\mathrm{N}_0} \right) \mathrm{PDF}\left(\sqrt{\gamma_i^{\min}} \right) d\sqrt{\gamma_i^{\min}} \tag{3.88}$$

where $\mathrm{PDF}\left(\sqrt{\gamma_i^{\min}}\right)$ denotes the the probability density function of square root values of variables $\gamma_i^{\min}$. The minimum distance, $\mathrm{D}_{\min}$, and the mean number of possible neighbors constellation points N_v are initially defined in Table 2.1.

Scenario with high value of C/M

- *Nyquist signaling*: In Nyquist signaling we have $\lambda_1 = \lambda_2 = \ldots, \lambda_N = 1$. As a result, we can verify that we have:

$$\sqrt{\gamma_i^{\min}} \approx |\mathrm{A_{LOS}} + a_{i,1}| \tag{3.89}$$

Given the complex fading coefficient $a_{i,1}$ varying according to zero-mean Gaussian distribution with variance equal to $\mathrm{P_1} = 10^{1.42}.\mathrm{A_{LOS}^2}$, we can deduce that $\sqrt{\gamma_i^{\min}}$ values varie according to a Rician distribution with a high Rice factor of approximately 14.2 dB. The probability density function is:

$$\mathrm{PDF}\left(\sqrt{\gamma_i^{\min}}\right) = \frac{\sqrt{\gamma_i^{\min}}}{\mathrm{P_1}} \exp\left(\frac{-\left(\gamma_i^{\min} + \mathrm{A_{LOS}^2}\right)}{2\mathrm{P_1}}\right) I_0\left(\frac{\mathrm{A_{LOS}}\sqrt{\gamma_i^{\min}}}{\mathrm{P_1}}\right) \tag{3.90}$$

where $I_0(x)$ is the modified Bessel function of the first kind with order zero.

As expected, simulation results, given in Fig. 3.16, confirm the analytical expression of BER given in Equation (3.88). Indeed, we can see that simulated uncoded BER (solid curves) and theoretical uncoded BER (dashed curves) are almost identical for both QPSK (Quadrature Phase-Shift Keying) and 8-PSK (Phase-Shift Keying) modulations. As a consequence, uncoded BER performances are given according to a Ricean distribution of channel fading. This result is only valid for the Nyquist case and in high C/M values i.e C/M $\geq$ 20 dB.

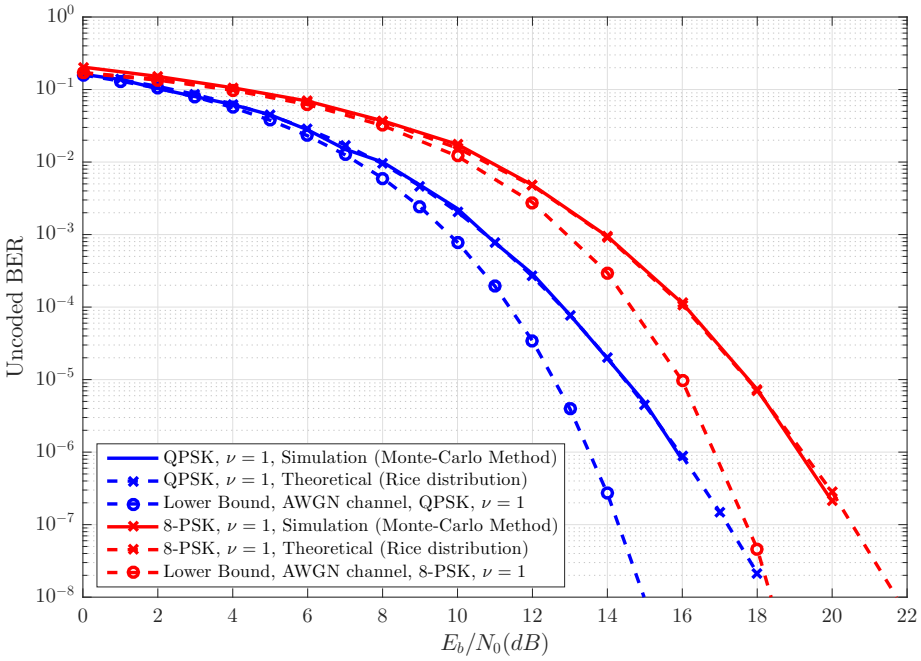

Figure 3.16: *Scenario with high ratio C/M: Uncoded BER performances vs. E_b/N_0 in dB with MMSE equalization using the proposed equalization structure (I) for QPSK and 8-PSK modulation in Nyquist signaling. The considered C/M value is equal to 20 dB and $R_c = 1/2$.*

Furthermore, simulation results show a performance degradation compared to the AWGN case where the S2A channel is assumed AWGN when considering Nyquist signaling. The considered loss of performance is expected because of the presence of fading S2A channel. This loss is about 2 dB for both QPSK and 8-PSK modulations.

- *FTN signaling*: For FTN signaling, we still neglect the contribution of fading coefficients $a_{i,2}$. However, $\{\lambda_n\}$ values are different from 1. Thus, we can not consider Equation (3.89) and the probability density function is no longer a Ricean one. In order to extend the study for different values of ν, Figure 3.17 shows the performances in terms of uncoded BER of 8-PSK modulation. Again, as we can see, simulation results confirm the analytical expression of the uncoded BER given in Equation (3.88). Indeed, we can see that simulated uncoded BER (solid curves) and theoretical uncoded BER (dashed curves) are almost identical for different values of ν.

  We notice that the uncoded BER performances decrease with the use of FTN signaling. This result is expected. Indeed, by considering FTN signaling, the frequency channel becomes more selective and MMSE equalization becomes not able to mitigate inter-symbol-interference (ISI). This effect is more impacting for low values of ν. For instance, for $\nu = 0.90$, we have a small degradation of BER performance compared to the Nyquist case. However, for $\nu = 0.80$, the performance degradation is very significant.

Despite the degradation of the BER performance compared to Nyquist signaling shown in Figure 3.17,

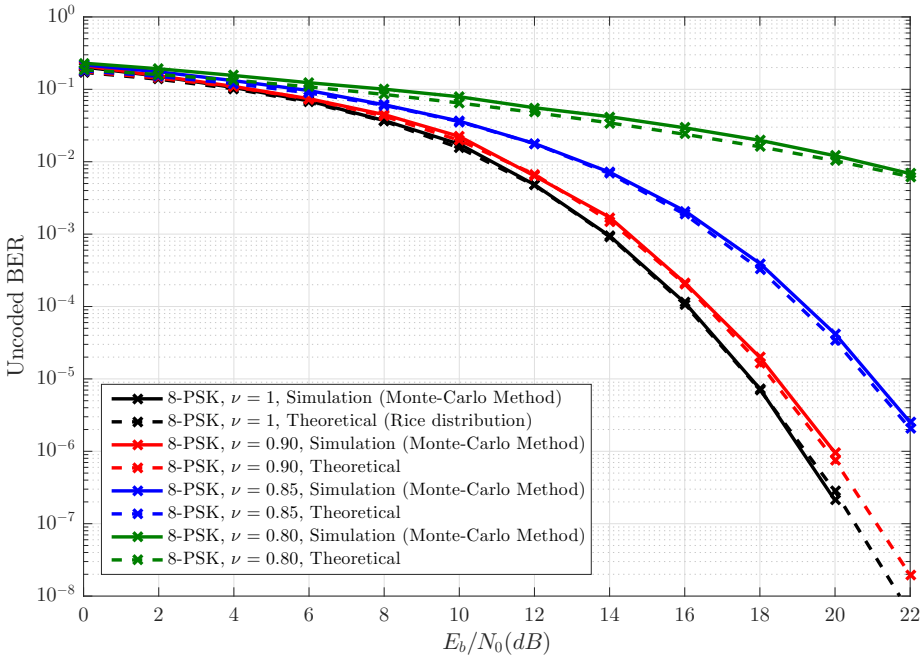

Figure 3.17: *Scenario with high ratio C/M: Uncoded BER performances vs. E_b/N_0 in dB with MMSE equalization using the proposed equalization structure (I) for 8-PSK modulation in FTN signaling. The considered C/M value is equal to 20 dB and $R_c = 1/2$.*

using FTN signaling has a great interest in terms of spectral efficiency. Indeed, for low values of acceleration factor ν, the achievable spectral efficiency can reach high values. Its expression can be given as:

$$\eta = \frac{\text{Throughput}}{\text{Bandwidth}} = \frac{\mathrm{R}_c \ \log_2(M) \ \mathrm{R}_s}{\mathrm{B}_h} = \frac{\mathrm{R}_c \ \log_2(M)}{\mathrm{T}_s \ \mathrm{B}_h} = \frac{\mathrm{R}_c \ \log_2(M)}{(\mathrm{T}_s/\mathrm{T}_h) \ (1+\beta)} = \frac{\mathrm{R}_c \ \log_2(M)}{\nu \ (1+\beta)} \tag{3.91}$$

The spectral efficiency percentage gain corresponding to the use of FTN signaling compared to the Nyquist case, is expressed as the following:

$$\text{Gain } [\%] = \frac{\eta^{\text{FTN}} - \eta^{\text{Nyquist}}}{\eta^{\text{Nyquist}}} \times 100 = \left(\frac{1}{\nu} - 1\right) \times 100 \tag{3.92}$$

Assuming a ν value of 0.8, one can obtain a gain of 25% in terms of spectral efficiency compared to the Nyquist case.

Scenario with low values of C/M The scenario is characterized by low values of elevation angle between 6° and 12° which corresponds also to low values of C/M taken between 5 dB and 10 dB. In this range, the S2A channel is supposed to be very selective. This particular case will be studied for SC and EW SC-OFDM waveforms.

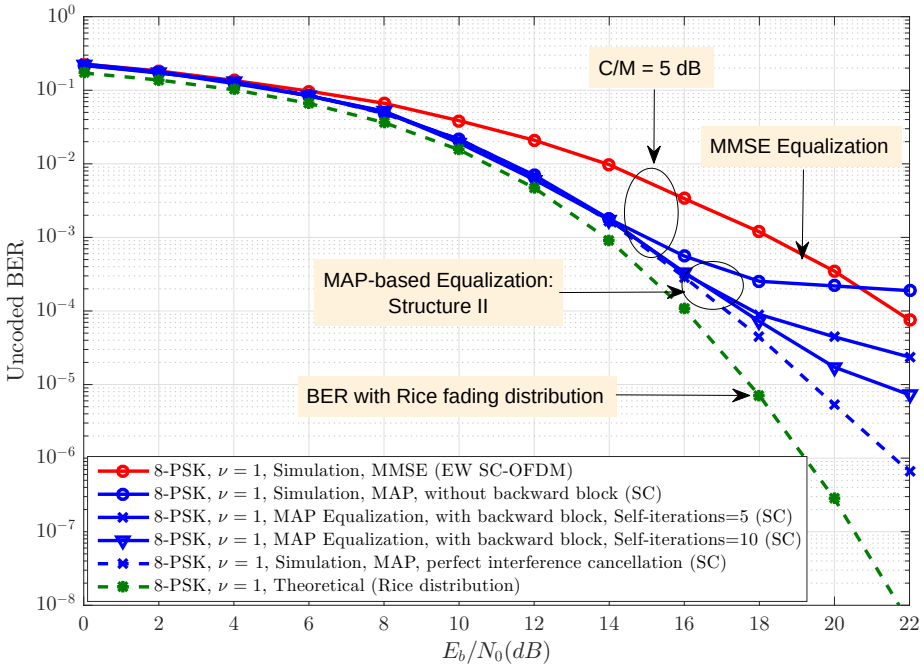

Figure 3.18: *Scenario with low ratio C/M: Uncoded BER performances vs. E_b/N_0 in dB with using MMSE/MAP equalization for 8-PSK modulation in Nyquist signaling. The considered C/M is equal to 5 dB and $R_c = 1/2$.*

In FTN signaling, we have a simple degradation of performance and the same kinds of results can be obtained. However, in Nyquist signaling, there are some differences compared to the case with high C/M

values. First, there are a performance degradation compared to the case where the channel fading is assumed varying according to a Rice distribution. This result is valid for both SC and EW SC-OFDM waveforms. Second, we can observe that MAP and MMSE equalization have no longer the same performance. Another major difference can be observed when we equalize SC signals: the use of the forward block without considering backward block becomes not sufficient to achieve the perfect feedback case. Indeed, because of the increased power of ground reflected path, the power of the residual interference is no longer negligible.
As we can see in Figure 3.18, the uncoded performance are lower bounded by the case with Rice fading distribution. Furthermore, Simulation results show that the MAP equalizer provides improved performance over a MMSE equalizer. For the proposed MAP-based equalization structure, « Structure (II) », it is clear that the case without considering backward block provides a loss of performance compared to the case with perfect interference cancellation (perfect feedback). By adding a backward block, we can iteratively mitigate the effects of residual interference at the end of a finite number of «self-iterations». In the same Figure 3.18, simulation results show that uncoded BER performance increases with the number of considered «self-iterations».

3.3.4.2 The coded case: using Turbo-equalization

In this Chapter, we considered Soft-Input Soft-Output (SISO) MMSE/MAP equalizers using an *a priori* information of transmitted bits. In the uncoded case, this *a priori* input is not taken into account for equalization step. In order to improve symbol detection, it is highly recommended to benefit from this *a priori* information especially in the FTN case. As a solution, one may resort to the turbo-equalization approach. For turbo-equalization, an equalizer and an associated channel decoding will be operated in iterative process to maximize the reliability of transmitted bits at the input of the equalizer. In this case, choosing the right channel code is a determinant step.

EXIT Chart analysis: In order to predict system's convergence, we adopt EXIT CHARTs analysis. EXIT CHARTs represent the exchange of extrinsic information between the considered MAP equalizer structure and the associated channel decoder. For such iterative process, the convergence threshold can be determined as the lowest E_b/N_0 for which there is no intersection point between the equalizer and decoder curves.
In Figure 3.19, EXIT CHARTs of MAP/MMSE equalizer are provided for 8-PSK modulation. EXIT CHARTs of the associated Soft-Input Soft-Output (SISO) convolutional decoder is also plotted. For FTN signaling ($\nu < 1$), we consider MMSE equalization using *a priori* for EW SC-OFDM signals. Whereas, for SC signals, the proposed equalization structure, «Structure I», is considered as reduced complexity MAP equalizer. For both MMSE and MAP equalization, the EXIT CHART diagram presents an increasing curve. As a result, by considering turbo-equalization, one can obtain a gain compared to the case when we only consider serial channel equalization and channel decoding. In fact, in the general case, the obtained gain increases with the slop of the EXIT curve.
Besides, for turbo-equalization, we notice that the number of considered « Turbo-iterations » depends on the shape of the obtained EXIT CHART curves at the output of both the equalizer and the corresponding channel

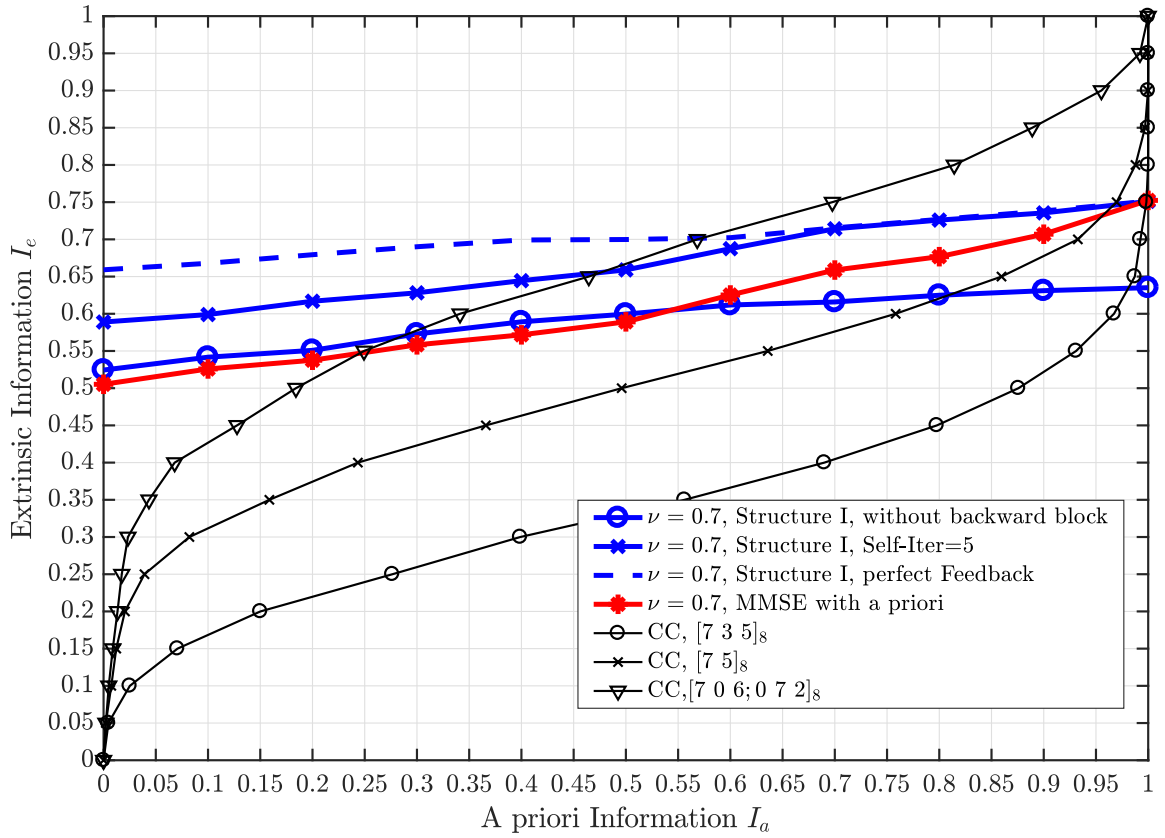

Figure 3.19: *EXIT CHARTs of MMSE/MAP equalizer for 8-PSK modulation at* $E_b/N_0 = 5$ *dB in Nyquist/FTN signaling. A fixed S2A channel is considered:* $A_{LOS} = 0.9358$*;* $a_{i,1} = 0.1825.\ e^{j\pi/4}$*;* $a_{i,2} = 0.3015.\ e^{j\pi/4}$*. C/M*$= 10$ *dB and* $\beta = 0.20$

decoder. For instance, for 8-PSK modulation with $\nu = 0.7$, by considering a convolutional code $[7\ 5]_8$, we need more turbo iterations for MMSE equalization than MAP equalization to have the same performance. Also, we note that EXIT CHART curves allow us to select the right channel code an avoid other ones for a considered operation point. Indeed, EXIT curves show that, for 8-PSK modulation with $\nu = 0.7$, a convolutional code having a rate of 2/3 is not the right channel coder that will be chosen to decode properly data symbols at $E_b/N_0 = 5$ dB. However, a convolutional code, with a rate 1/2 or 1/3, can be selected as an associated channel decoder for a turbo-equalization process.

Coded BER performances: Simulation performances in term of coded BER are given in Figures 3.20 for 8-PSK modulation and for $\nu = 0.7$. For the two simulations, we consider a convolutional decoder CC $(7,5)_8$ with rate equal to 1/2. The blue curves present the MMSE-based receiver. Whereas, the red curves present the MAP-based receiver. In FTN signaling, simulation results, presented in Figure 3.20, show that coded BER performance considering turbo-equalization are considerably better than the ones without considering

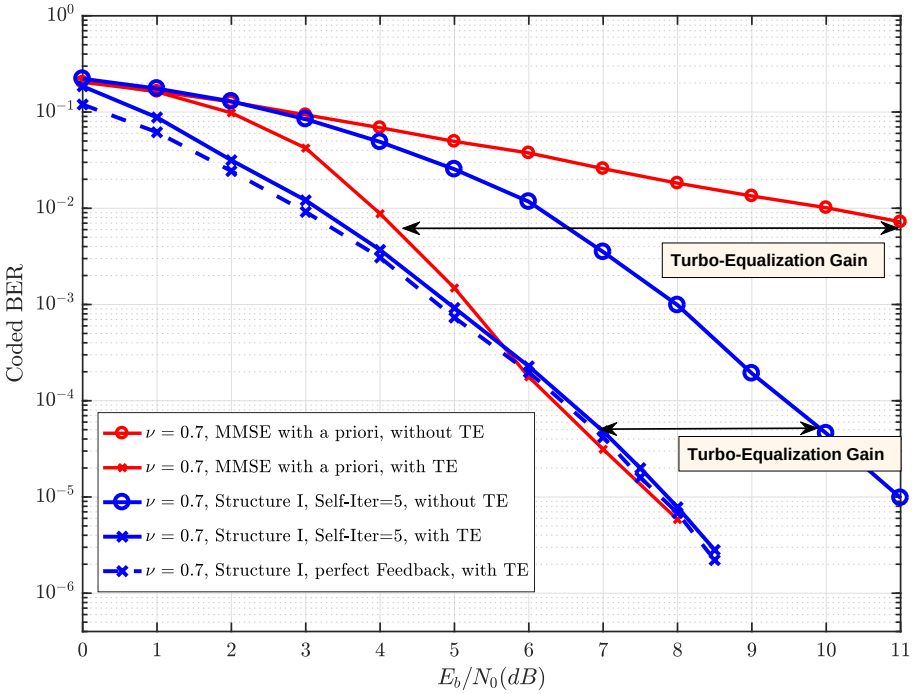

Figure 3.20: *Coded BER performances vs.* E_b/N_0 *in dB using (7,5) convolutional code for 8-PSK modulation in FTN signaling for MMSE equalization. The number of considered « Turbo-iterations » is equal to 10. A fixed S2A channel is considered:* $A_{LOS} = 0.9358$*;* $a_{i,1} = 0.1825$*.* $e^{j\pi/4}$*;* $a_{i,2} = 0.3015$*.* $e^{j\pi/4}$*.* C/M= 10 *and* $\beta = 0.20$

turbo-equalization process. This performance improvement is expected when we observe the increasing EXIT CHART curve for both MAP/MMSE equalizers as shown in Figure 3.19.

For the case without considering turbo-equalization process, simulation results show that the MAP equalizer still provides improved performance over a MMSE equalizer. However, when we consider turbo-equalization process, coded BER performances for both MMSE and MAP equalization are almost identical are reach the matched filter bound (the Nyquist case). This result is very interesting. It means that we can increase spectral efficiency values without loss of performance compared to the Nyquist case. In this case, the gain in percentage of spectral efficiency is about 42,85% compared to the Nyquist case. In conclusion, for the FTN case, one need using iterative equalization to improve system performance.

3.4 Conclusion

In this chapter, SC and EW SC-OFDM waveforms are considered for the forward link. It has been show that the satellite-to-aircraft (S2A) channel model contains only two paths. As a consequence, the equivalent baseband channel has a particular form. This particular form is exploited to propose new adequate solutions for both channel estimation and channel equalization tasks.

For channel estimation task, we proposed some efficient channel estimation exploiting both the particular form of the channel impulse response and *a priori* knowledge of the delay τ_2. Indeed, it has been shown that the delay τ_2 can be determined by geometrical considerations. Thanks to this *a priori* knowledge, the proposed channels estimation methods can provide better performances. In fact, with considering this *a priori* knowledge, it is possible to reduce the number of variables to be estimated and thus we can obtain better performances compared to the existing channel estimation algorithms that do not exploit this knowledge.

For channel equalization task, a MAP-based equalization is considered to detect transmit data symbols for SC signals. However, it is shown that the computational complexity of MAP equalizers is exponentially increased with the memory length of the baseband channel. Given the presented baseband channel presenting a long memory length, it is essential to design a new reduced-complexity equalization method. Consequently, we have investigated an efficient implementation of channel equalization and two equalization structures are proposed: « Structure (I) » and « Structure (II) » .The first one, « Structure (I) », is suitable for non-sparse channels while the second one, « Structure (II) », is designed for sparse channels with equally spaced coefficients.

- *Nyquist signaling*: In Nyquist signaling, the discrete equivalent channel can be decomposed in a strong sparse channel component with additional low power interference residual terms. Based on this model, « Structure (II) » implements some independent parallel MAP equalizers with proper iterative interference cancellation. The proposed scheme is able to reduce the complexity of the receiver and it is shown than it can exhibit interesting performance.

- *FTN signaling*: In FTN signaling, the baseband channel is no longer sparse. In order to equalize received SC signals with reasonable complexity, « Structure (I) » appears suitable for this kind of channels. As for « Structure (II) », « Structure (I) » contains two blocks: a forward block a backward block. The forward block forms tentative symbol decisions with a MAP criterion considering a mismatch truncated channel response. Whereas, the backward block is used thereafter to reduce the channel response to the desired truncated channel used in the forward block. The system performance are lower-bounded by the case with perfect interference cancellation (perfect feedback). Given that proposed scheme uses *Ungerboeck model* with symmetric channel for the forward block, the case with perfect feedback would be optimal for detecting transmit symbols.

On other hand, for EW SC-OFDM waveform, a low complexity MMSE equalization is considered to detect transmit data symbols in FTN/Nyquist signaling. As a result, a linear model is obtained and analytical performances are derived. Simulation results show that the SC waveform using a MAP equalizer still provides improved performance over EW SC-OFDM using a MMSE equalizer.

For simulation results, we considered the uncoded case for different ranges of C/M values. Two scenarios are distinguished: scenario with high C/M values and scenario with low C/M values. For the first one, it is shown that uncoded BER performance, in Nyquist signaling, can be approximated to the case with Rice fading distribution. Whereas, for the second scenario, uncoded performances are lower bounded by the same

case with Rice fading distribution.

In order to enhance data symbol detection, we consider turbo-equalization process. Consequently, Coded BER performance are compared for both SC and EW SC-OFDM waveform using MAP and MMSE equalization, respectively. As a result, The proposed MAP equalization structure still provides improved performance over a MMSE equalizer.

Finally, it has been shown that using FTN signaling can increase the spectral efficiency of transmitter/receiver system for some values of ν. For these considered ν values, MAP equalization provides a good trade-off between spectral efficiency gain and performance degradation, compared to MMSE equalization.

Chapter 4

The return link

Sommaire

4.1 Introduction

In the previous chapter we investigate the issue of mitigating the inter-symbol interference (ISI) resulting from using Faster-than-Nyquist signaling in the presence of frequency selective satellite-to-aircraft channel. In this chapter, we are interested to the return link i.e. the uplink between the UAV/aircraft as a transmitter and the ground earth station (GES) as a receiver. This link will be established via a GEO satellite and the considered prorogation channel is assumed AWGN.

For the return link, we are interested in two waveform candidates: SC and EW SC-OFDM waveforms. SC is a practical waveform for channels which are not very selective and allows us to consider optimal MAP-based detection at the receiver. Whereas EW SC-OFDM waveform is an interesting linear waveform offering a flexible generation of transmitted signals given by a simple frequency domain implementation as well as a low complexity MMSE-based detection at the receiver. For the return link, the two waveforms, SC and EW SC-OFDM, are studied for both FTN/Nyquist signaling. the aim is to evaluate spectral efficiency improvement in the case of FTN signaling. In this context, some new receivers are proposed.

4.2 Classical Single-Carrier (SC) waveform

In this Section, we are interested in classical SC waveform. Based on the expression of received symbols initially given in Equations (4.3), this section aims to give the corresponding system model in the case of aeronautical channel and especially for return link. It is shown in Equation (1.31) that the aircraft-to-satellite (A2S) is assumed be an AWGN channel:

$$\mathrm{h}_a(t,\tau) = \mathrm{h}_a(\tau) = \delta(\tau) \tag{4.1}$$

The considered transmitter/receiver scheme is illustrated in Figure 4.1.

4.2.1 System model

For system model, we consider a frame based transmission. Moreover, we assume that each frame contains a number of N_f sub-frames and each sub-frame contains a number of N modulated data symbols. Furthermore, we assume that the digital communication system uses linear M-ary modulation. In addition, we consider a Root Raised Cosine (RRC) shaping filter $h_e(\tau)$ as a transmit shaping filter with known parameters such as β, the roll-off factor, and the Nyquist bandwidth B_h. The considered Nyquist bandwidth is expressed as follows:

$$\mathrm{B}_h = \frac{1+\beta}{\mathrm{T}_h} \tag{4.2}$$

At the transmitter, bit sequence $\mathbf{u}_i$ is encoded into N symbols by using a M-ary Bit Interleaved Coded Modulation (BICM) scheme as shown in Figure 2.1. As a result, a sequence of N data modulated symbols is generated denoted by $\mathbf{s}_i = [s_{i,1}, s_{i,2}, \ldots, s_{i,N}]$. The symbols $\{s_{i,n}\}$are drawn from a discrete alphabet $\chi = \{\mathcal{C}_1, \mathcal{C}_2, \ldots, \mathcal{C}_M\}$. The obtained data modulated symbols have a variance equal to σ_s^2 and have a symbol duration $\mathrm{T}_s = \nu.\mathrm{T}_h$. In order to improve the spectral efficiency, we assume using Nyquist/FTN signaling characterized

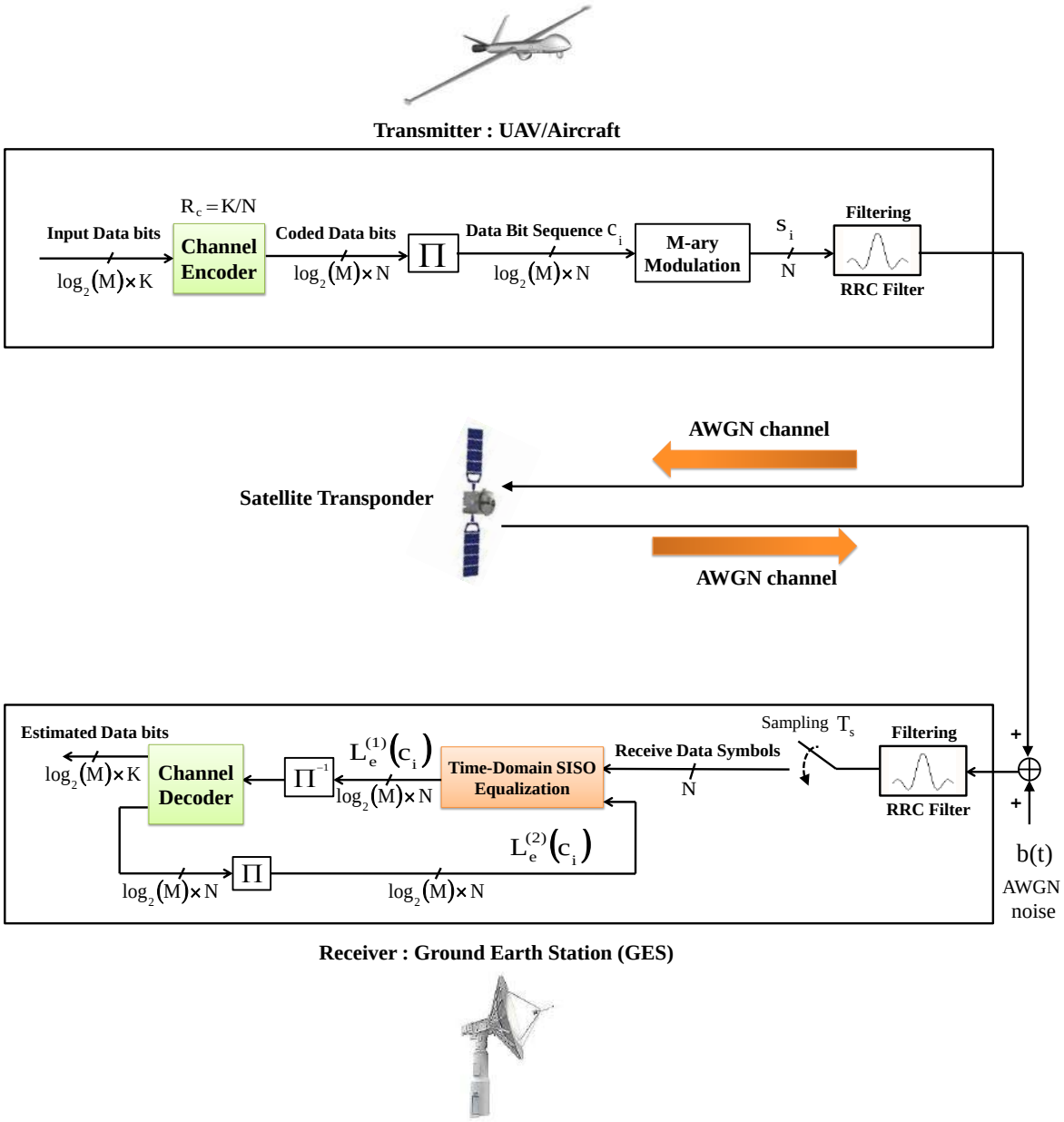

Figure 4.1: *UAV/Aircraft transmitter and GES receiver using SC waveform for the return link*

by an acceleration factor $\frac{T_s}{T_h}$ taking a values between 0 and 1. At the receiver, the expression of received data symbols $\{y_{i,n}\}$ are given by:

$$y_{i,n} = \sum_{l=-L}^{+L} g\left(l.T_s\right)\ s_{i,n-l} + w_c[n] \qquad \text{for} \qquad 1 \leq n \leq N \tag{4.3}$$

where $g(t)$ is the equivalent base-band filter defined as:

$$g(t) = h_e(t) * h_r(t) \qquad \text{where} \qquad h_r(t) = h_e^*(-t) \tag{4.4}$$

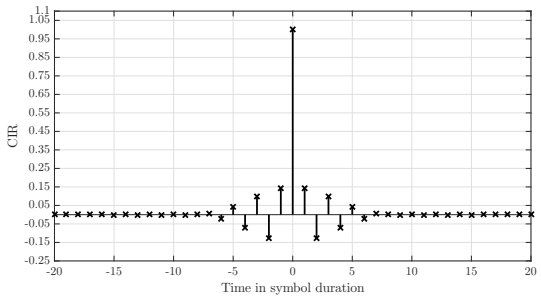

(a) $\nu = 0.87$

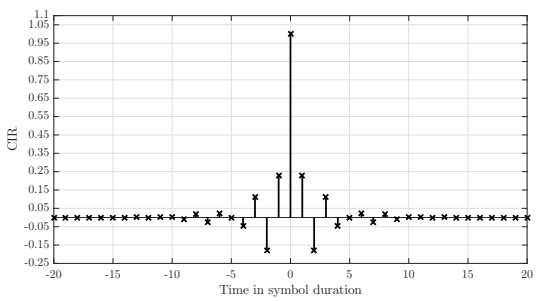

(b) $\nu = 0.8$

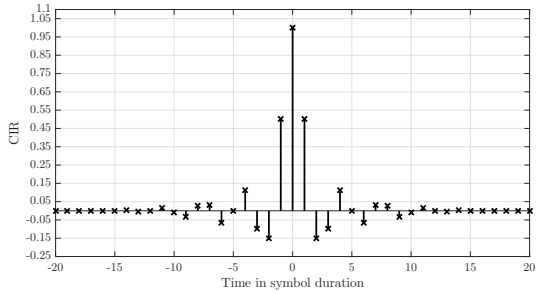

(c) $\nu = 0.6$

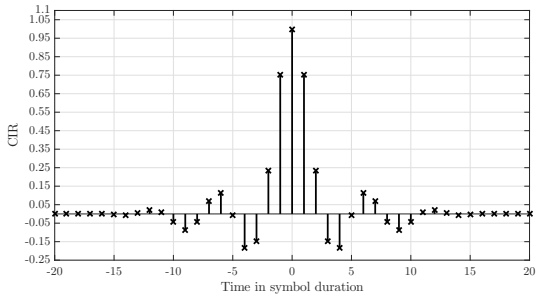

(d) $\nu = 0.4$

Figure 4.2: *CIR for various values of acceleration factor ν. The considered roll-off is equal to* 0.20 *($\beta = 0.20$)*

we can verify that each coefficient $g(l.\mathrm{T}_s)$ can verify:

$$\mathrm{g}(0) = 1 \qquad \text{and} \qquad \mathrm{g}(l.\mathrm{T}_h) = 0 \qquad \forall \qquad l \in l \in \mathbb{Z}^* \tag{4.5}$$

Thus, in Nyquist signaling the equivalent baseband channel is reduced to an AWGN channel. Whereas, in FTN signaling the channel is presented as a multipath channel with a memory length L. The channel vector $\mathbf{g} = [g(-L/2.\mathrm{T}_s), g((-L/2+1).\mathrm{T}_s), \ldots, g(L/2.\mathrm{T}_s)]^T$ denotes the discrete-time equivalent baseband channel. The positive peer integer L specifies the memory of the system and is the smallest value such that $g(l.\mathrm{T}_s) = 0$, $|l| > L/2$. An example of the discrete channel impulse response response is given in Figure 3.2 for $\nu = 1$ (Nyquist case) and also in Figure 4.2 for different values of ν. The noise variables $\{w_c[n]\}$ vary according to a complex zero-mean Gaussian distribution and verifying:

$$\mathbb{E}\{w_c[n].w_c^*[n+l]\} = \mathrm{N}_0.\ \mathrm{R}_s.\ \mathrm{g}(l.\mathrm{T}_s) = \sigma_w^2.\ \mathrm{g}(l.\mathrm{T}_s) \tag{4.6}$$

with $\sigma_w^2 = \mathrm{N}_0.\ \mathrm{R}_s$ is the noise variance. Note that, in Nyquist signaling i.e. $\mathrm{T}_s = \mathrm{T}_h$, the noise variables $\{w_c[n]\}$ are white.

4.2.2 Data symbol detection in Nyquist signaling:

In Nyquist signaling ($\mathrm{T}_s = \mathrm{T}_h$), we do not need to consider channel equalization. Indeed, by using the expression of the received signal given in (4.3) and also by considering considering the property of the equivalent

RC filter $g(t)$ given in (4.5), we can deduce the expression of the received samples can be reduced to:

$$y_{i,n} = s_{i,n} + w_n \qquad \text{for} \qquad 1 \leq n \leq N \tag{4.7}$$

The variable $\{w_n\}$ are Gaussian and white.

The Nyquist case will be the reference case since we are interested in spectral efficiency improvement in the return channel.

4.2.2.1 The uncoded case

For the uncoded case, the estimated transmit symbol is determinated as the most likely symbol as follows:

$$\widehat{s}_{i,n} = \underset{\mathcal{C}_m \in \chi}{\operatorname{argmin}} \left\{ |y_{i,n} - \mathcal{C}_m|^2 \right\} \tag{4.8}$$

The theoretical Symbol Error Rate (SER) can be determinated as follows:

$$\mathrm{SER} = \mathrm{N}_v \times Q\left(\sqrt{\left(\frac{\mathrm{D}^2_{\min}}{2.\sigma_s^2} \right) .\mathrm{R}_c . \log_2(M) . \mathrm{E}_b/\mathrm{N}_0} \right) \tag{4.9}$$

with $Q(x)$ represents the Q-function. The minimum distance, $\mathrm{D}_{\min}$, and the mean number of possible neighbors constellation points N_v are initially defined in Table 2.1.

By considering Gray mapping [50], it is shown that we have only one erroneous bit in each erroneous mapping constellation symbol. Thus, the Bit Error Rate can be expressed as:

$$\mathrm{BER} \cong \frac{1}{\log_2(M)} \times \mathrm{SER} = \frac{\mathrm{N}_v}{\log_2(M)} \times Q\left(\sqrt{\left(\frac{\mathrm{D}^2_{\min}}{2.\sigma_s^2} \right) .\mathrm{R}_c . \log_2(M) . \mathrm{E}_b/\mathrm{N}_0} \right) \tag{4.10}$$

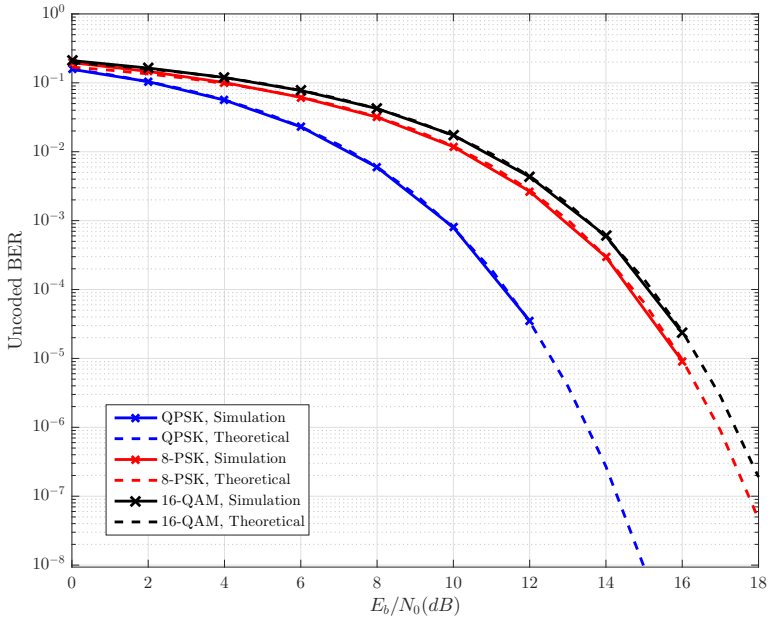

Figure 4.3: *Uncoded BER performance for Nyquist signaling.*

$\beta = 0.20$ 50 LDPC iterations (ARJA Codes)					
Modulation	τ	**Rate**	E_b/N_0**[dB] @ BER=**10^{-6}	$(E_b/N_0)_{\mathbf{min}}$**[dB]**	η**[bit/s/Hz]**
QPSK	1	2/7	1.1	-1.1	0.4762
		2/5	1.95	-0.6	0.6667
		4/7	2.7	0.5	0.9524
		8/11	3.6	1.4	1.2121
16-QAM	1	8/11	6.8	4.75	2.4243

Table 4.1: *Achievable spectral efficiency and E_b/N_0 values corresponding to BER equal to 10^{-6} in Nyquist signaling case for both SC and EW SC-OFDM waveform.*

As expected, in Figure 4.3, we can see that simulation results shown in solid curves confirm the analytical expression given in (4.10) and shown in dashed curves.

4.2.2.2 The coded case

For the coded case, we only consider a channel decoding. In Figure 4.4, we consider a coded QPSK and 16-QAM modulations using ARJA (Accumulate Repeat Jagged Accumulate) protograph based low-density parity-check (LDPC) codes of rates $\mathrm{R}_c \in \{2/7, 2/5, 4/7, 8/11\}$ with information length $K = 2048$ bits. Based on simulation results in the coded case, one can deduct the following Table 4.1 which summarizes the corresponding spectral efficiency values η:

$$\eta = \mathrm{R}_c \times \frac{\log_2(M)}{\nu \times (1+\beta)} \tag{4.11}$$

Considering $\beta = 0.20$, Table 4.1 summarizes the spectral efficiency η for BER $= 10^{-6}$. Note that for the coded case, we don't consider an optimized LDPC coding. Indeed, with considering high performance optimized

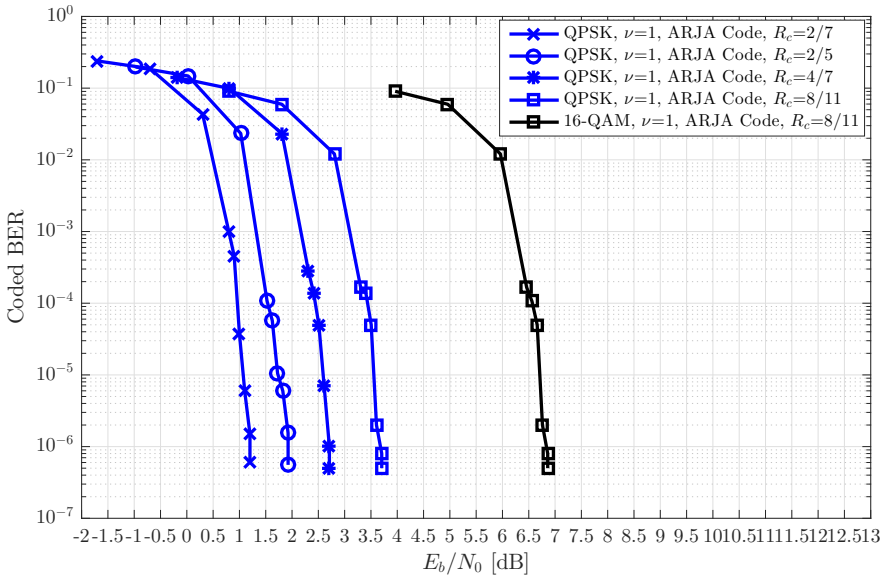

Figure 4.4: *Coded BER performance for Nyquist signaling.*

LDPC code, it is shown that we can even obtain smaller values of E_b/N_0 which are closer to $(E_b/N_0)_{\min}$.

4.2.3 Data symbol detection in FTN signaling:

4.2.3.1 MAP-based symbol detection

For FTN signaling, the baseband channel is a symmetric channel with a memory length $2 \times L$ and the additive noise is still Gaussian but colored. Since the channel is symmetric, one can resort to the *Ungerboeck's model*. Indeed, referring to *Ungerboeck's model*, the samples $\{y_{i,n}\}$ represent a sufficient statistic and can thus be employed for an optimal detection [125]. The considered branch metric for the full complexity *Ungerboeck's model* is derived as the following:

$$\mu_{i,n} = -2\ \Re\left\{ s^*_{i,n}.\left(y_{i,n} - \sum_{l=1}^{L} g\left(l.\mathrm{T}_s\right)\ s_{i,n-l} \right) \right\} + g\left(0\right).\left|s_{i,n}\right|^2 \tag{4.12}$$

For channel equalization task, a MAP-based equalization is considered to detect transmit data symbols for SC signals. However, it is shown that the computational complexity of MAP equalizers is exponentially increased with the memory length of the baseband channel. Since the presented baseband channel presenting a long memory length L, it is essential to design new reduced-complexity equalization structure. As shown in Figure 4.2, the baseband channel has an Exponential-Decay PDPs. On other hand, in Chapter 3, a modified equalization structure is proposed to equalize these types of channels. The considered equalization structure is denoted « Structure (I) » and is presented in (4.5).

This equalization is suitable for channels with Exponential-Decay PDPs. As a result, it is possible to apply this structure for own case. We recall that « Structure (I) » contains two blocks: a forward block a backward block. The forward block forms tentative symbol decisions with a MAP criterion considering a mismatch truncated channel response with memory length $L_1 \leq L$ in order to reduce the computational complexity of the receiver. Whereas, the backward block is used thereafter to reduce the channel response to the desired truncated channel used in the forward block. The system performance are lower-bounded by the case with

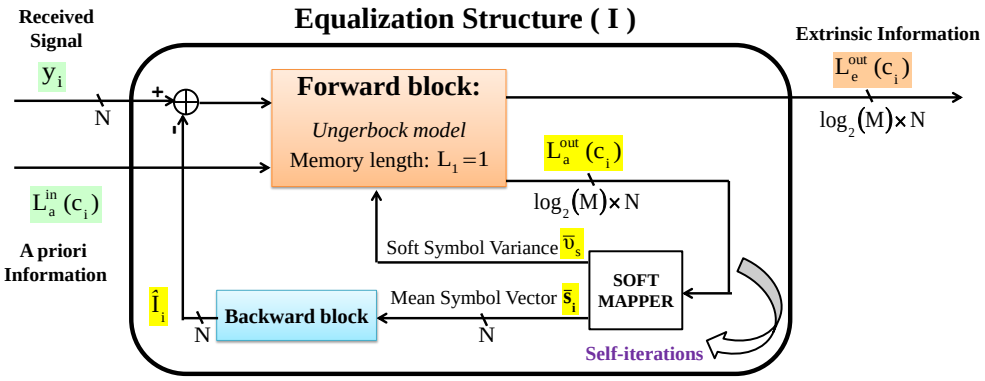

Figure 4.5: *The proposed equalization structure « Structure (I) ». For the forward block, Ungerboeck model is considered and the memory length is equal to 1.*

perfect interference cancellation (perfect feedback).

By considering the proposed equalization structure, « Structure (I) », the new branch metric is expressed as:

$$\mu_{i,n} = -2\ \Re\left\{ s^*_{i,n}.\left[\left(y_{i,n} - \widehat{\mathrm{I}}_{i,n}\right) - \sum_{l=1}^{L_1} g\left(l.\mathrm{T}_s\right)\ s_{i,n-l}\right]\right\} + g\left(0\right).\left|s_{i,n}\right|^2 \tag{4.13}$$

where $\widehat{\mathbf{I}}_i = \left[\widehat{\mathrm{I}}_{i,1}, \widehat{\mathrm{I}}_{i,2}, \ldots, \widehat{\mathrm{I}}_{i,N}\right]^T$, is the obtained interference in each «self-iterations». Each interference element $\widehat{I}_{i,n}$ is calculated as follows:

$$\widehat{\mathrm{I}}_{i,n} = \sum_{|l|>L_1} g\left(l.\mathrm{T}_s\right)\ \bar{s}_{i,n-l} \qquad \text{for} \qquad 1 \leq n \leq N \tag{4.14}$$

In each «self-iterations», the estimate interference is removed from received data sequence. Thus, the variance of the residual interference is updated. Under assumption of zero-mean interference term, the new value of residual interference variance is calculated as:

$$\kappa = \mathrm{Var}\left\{\mathrm{I}_{i,n} - \widehat{\mathrm{I}}_{i,n}\right\} = \mathbb{E}\left\{\left|\mathrm{I}_{i,n} - \widehat{\mathrm{I}}_{i,n}\right|^2\right\} = \bar{v}_s.\sum_{|l|>L_1}\left|g\left(l.\mathrm{T}_s\right)\right|^2 \tag{4.15}$$

For simplification reasons, we assume that residual interference term varies according to zero-mean Gaussian distribution with variance equal to κ. The variance κ and the branch metric $\mu_{i,n}$ are used to calculate the transition probability for the BCJR algorithm implemented in the forward block. Additionally, we notice that the proposed structure will use *Ungerboeck model* for the forward block (see Equation (4.18)) . As a result, one can deduce that the case with perfect feedback $(\mathrm{I}_{i,n} - \widehat{\mathrm{I}}_{i,n})$ provides an optimal detection of transmit symbols.

In Equations (4.14) and (4.15), $\bar{\mathbf{s}}_i = [\bar{s}_{i,1}, \bar{s}_{i,2}, \ldots, \bar{s}_{i,N}]$ and $\bar{v}_s$ are respectively the mean symbol vector and the soft symbol variance which are calculated as follows:

$$\begin{aligned}
\bar{s}_{i,n} &= \sum_{m=1}^{M} \Pr\left(s_{i,n} = \mathcal{C}_m, \mathbf{y}_i\right) \times \mathcal{C}_m \\
\bar{v}_s &= \frac{1}{N}\sum_{n=1}^{N}\left[\sum_{m=1}^{M} \Pr\left(s_{i,n} = \mathcal{C}_m, \mathbf{y}_i\right) \times \left|\mathcal{C}_m - \bar{s}_{i,n}\right|^2\right]
\end{aligned} \tag{4.16}$$

with $\Pr\left(s_{i,n} = \mathcal{C}_m, \mathbf{y}_i\right)$ is the the *a posteriori* symbol probability obtained at the output of MAP detection. In particular case when the memory length is equal to 1 i.e. $L_1 = 1$, the expression of the transition probability is given as:

$$\gamma_n\left(m', m, x\right) = \begin{cases} \gamma_n(m', m, \mathcal{C}_m) \neq 0 & \text{if } x = \mathcal{C}_m \\ 0 & \text{if } x \neq \mathcal{C}_m. \end{cases} \tag{4.17}$$

with,

$$\gamma_n(m', m, \mathcal{C}_m) = \Pr\left(s_{i,n} = \mathcal{C}_m | \mathrm{L}_a^{\mathrm{in}}\left(\mathbf{c}_i\right)\right).\ \frac{1}{\pi\ \left(\sigma_w^2 + \kappa\right)}.\ e^{-\frac{\mu_{i,n}}{\sigma_w^2 + \kappa}} \tag{4.18}$$

By considering BCJR algorithm for the forward block, the *a posteriori* symbol probability is reduced to a simple multiplication of α-values and β-values:

$$\Pr\left(s_{i,n} = \mathcal{C}_m, \mathbf{y}_i\right) = \alpha_n\left(m\right).\beta_n\left(m\right) \tag{4.19}$$

The α-values and β-values are recursively computed by using the following expressions:

$$\alpha_n(m) = \sum_{m'=1}^{M} \alpha_{n-1}(m') \,.\, \gamma_n(m', m, \mathcal{C}_m) \tag{4.20}$$

$$\beta_n(m) = \sum_{m'=1}^{M} \beta_{n+1}(m') \,.\, \gamma_n(m', m, \mathcal{C}_m) \tag{4.21}$$

The BCJR algorithm takes in input an *a priori* information vector of $\log_2(M) \times N$ bit LLRs, $\mathrm{L}_a^{\mathrm{in}}(\mathbf{c}_i) = \left[\mathrm{L}_a^{\mathrm{in}}(c_{i,1}), \mathrm{L}_a^{\mathrm{in}}(c_{i,2}), \ldots, \mathrm{L}_a^{\mathrm{in}}\left(c_{i,\log_2(M)\times N}\right)\right]^T$ to calculate an *a priori* probability of the transmit data symbols $\{s_{i,n}\}$ $1 \leq n \leq N$. By assuming $\left[u_1^{(m)}, u_2^{(m)}, \ldots, u_{\log_2(M)}^{(m)}\right]$ is the transmit bit sequence corresponding to $s_{i,n} = \mathcal{C}_m$, the *a priori* symbol probability is calculated as:

$$\Pr\left(s_{i,n} = \mathcal{C}_m | \mathrm{L}_a^{\mathrm{in}}(\mathbf{c}_i)\right) = \prod_{q=1}^{\log_2(M)} \frac{\exp\left(-u_q^{(m)} \times \mathrm{L}_a^{\mathrm{in}}\left(c_{i,q+(n-1)\times\log_2(M)}\right)\right)}{1+\exp\left(-\mathrm{L}_a^{\mathrm{in}}\left(c_{i,q+(n-1)\times\log_2(M)}\right)\right)} \tag{4.22}$$

Strengths: By considering the proposed one-state equalization structure, we can significantly reduce the computational complexity. Indeed, with the considered modified structure, the complexity is linear with the modulation order M. Moreover, the considered modification allows us to apply MAP equalization for the case of linear modulations with high modulation order i.e 64-QAM and 256-QAM.

Weaknesses: The proposed assumes a mismatched channel model. It means that the symbol detection is based on the first iteration of the equalization process i.e. if the equalizer can not detect transmit symbols in the first iterations, then it was necessary to do more «self-iterations». In addition, if the channel is very selective, the equalizer may not be able to converge.

4.2.3.2 The uncoded case

For the uncoded case, we assume using MAP-based equalization with zero *a priori*
i.e. $\Pr\left(s_{i,n} = \mathcal{C}_m | \mathrm{L}_a^{\mathrm{in}}(\mathbf{c}_i)\right) = 1/M$. After a few number of «self-iterations», the estimated transmit symbol is determinated as the most likely symbol as follows:

$$\widehat{x}_{i,n} = \underset{\mathcal{C}_m \in \chi}{\operatorname{argmax}} \Pr\left(s_{i,n} = \mathcal{C}_m, \mathbf{y}_i\right) \qquad 1 \leq n \leq N \tag{4.23}$$

Since it difficult to derive theoretical performances, uncoded system performances will be studied on the basis of simulation results. As results, Figures 4.6, 4.7 and 4.8 show some uncoded BER performances for FTN signaling. For the two simulations results, the considered shaping filter is RRC with $\beta = 0.20$.

In Figure 4.6, performance in terms of uncoded Bit Error Rate (BER) in the case of 8-PSK modulation is plotted. The considered acceleration factor is equal to 0.8 ($\nu = 0.8$). Moreover, three values of number of «self-iterations» are considered: 1, 5 and 10.

Simulations results show that system performance increases with the number of considering «self-iterations». The higher «self-iterations» are, the better the system performances are. Again, simulation results show that it is necessary to consider «self-iterations». Indeed, we can see that without considering self-iteration (blue curve), the equalizer is not able to remove the interference term.

Figure 4.7 performs the uncoded BER for 8-PSK modulation in FTN signaling for various values of acceleration factor ν: 0.6,0.7,0.8 and 0.9. The considered number of «self-iterations» is equal to 5.

As expected, simulations results show that system uncoded BER performance decrease with use of FTN signaling. Indeed by considering FTN signaling, an additional inter-symbol interference (ISI) will appear. The lower the acceleration factor ν is, the higher ISI power is. Considering different linear modulation types, Figure 4.8 give simulation results for uncoded BER performances for QPSK, 8-PSK, 32-QAM and 64-QAM in FTN

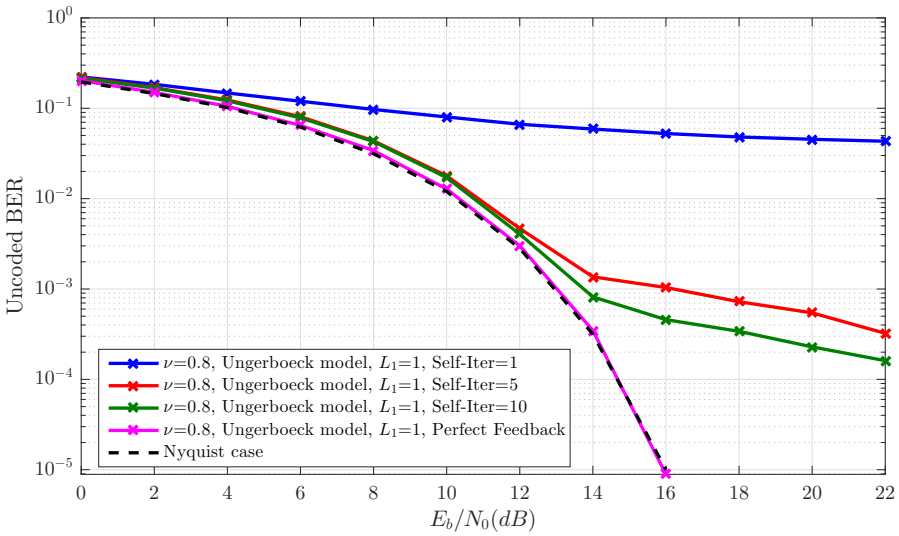

Figure 4.6: *Uncoded BER performances vs. E_b/N_0 for 8-PSK modulation in Faster-Than-Nyquist case using one-sate Ungerboeck model for various number of self-iterations*

signaling. The considered The considered number of «self-iterations» is equal to 5.

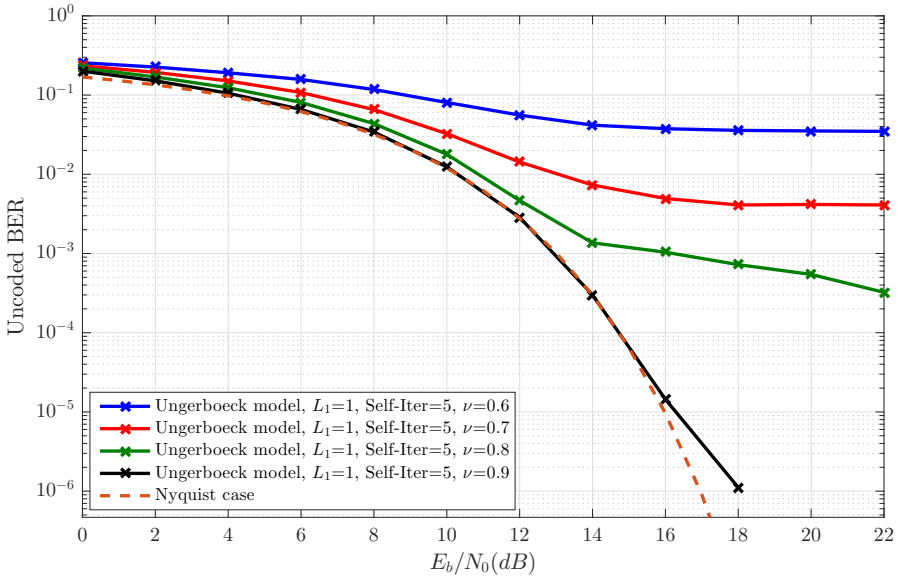

Figure 4.7: *Uncoded BER performances vs. E_b/N_0 for 8-PSK modulation in Faster-Than-Nyquist case using one-sate Ungerboeck model for various values of ν*

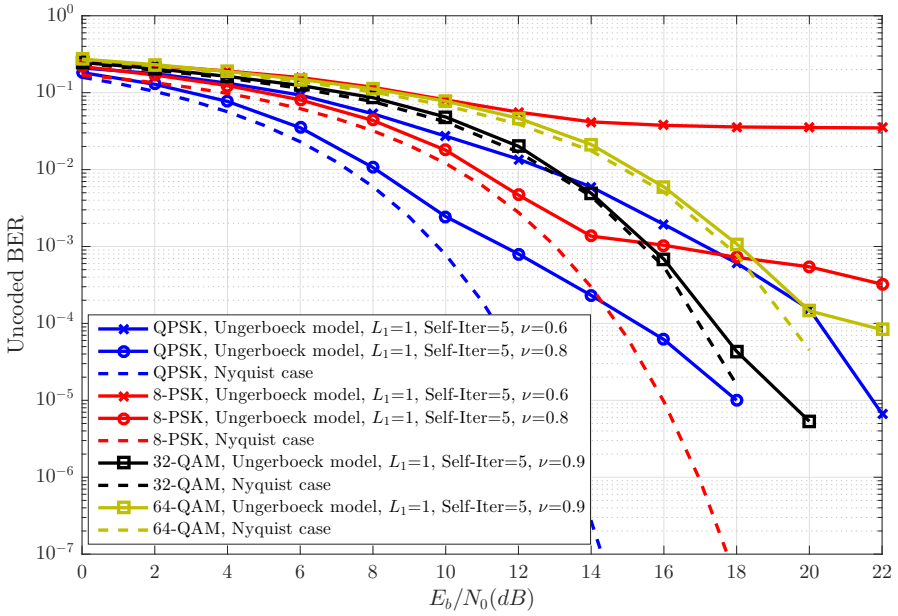

Figure 4.8: *Uncoded BER performances vs. E_b/N_0 in Faster-Than-Nyquist case using one-sate Ungerboeck model for various values of ν*

4.2.3.3 EXIT CHART Analysis:

In Figure 4.9, we give the EXtrinsic Information Transfer (EXIT) charts for the proposed MMSE equalizer for $\nu = \{1; 0.8; 0.6\}$ for a Signal to Noise Ratio $E_b/N_0 = 5$ dB. The Nyquist case ($\nu = 1$) is presented in dashed curve.

In perfect *a priori*, we observe the same kind of results as given by the MMSE equalization for the EW SC-OFDM system. Indeed, all extrinsic information values, for both QPSK and 16-QAM modulation, converge to a single value which is the extrinsic information value given by the Nyquist case.

Compared to MMSE equalization, the main difference for the proposed MAP equalization structure is the obtained extrinsic information value in *a priori*. In fact, compared to EXIT chart's curves given in Figure 4.21, simulation results in Figure 4.9 show an improved extrinsic information values in zero *a priori* and this for only 5 «self-iterations».

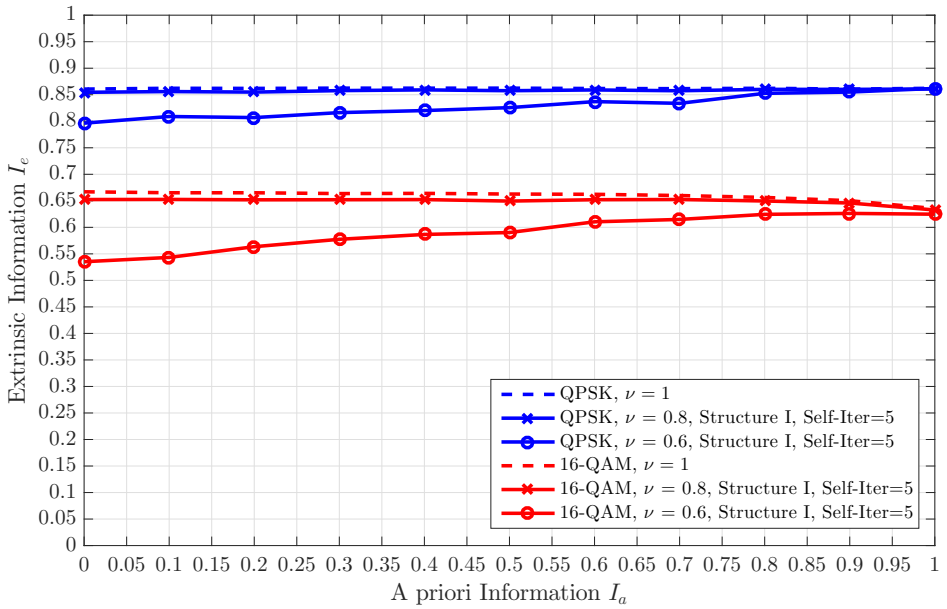

Figure 4.9: *EXIT CHARTs of the proposed MAP equalization structure « Structure (I) » for QPSK and 16-QAM modulations at $E_b/N_0 = 5$ dB in Nyquist/FTN signaling with $\beta = 0.20$. The considered memory length for the forward block is equal to 1.*

4.2.3.4 The coded case: using turbo-equalization

In coded case, after MAP equalization process, an associated soft channel decoding structure is added in series to decode received data bits. In order to improve performance system, MAP equalization structure and associated channel decoding will be operated in iterative process to maximize the reliability of transmitted bits. As as result, a turbo equalization is considered.

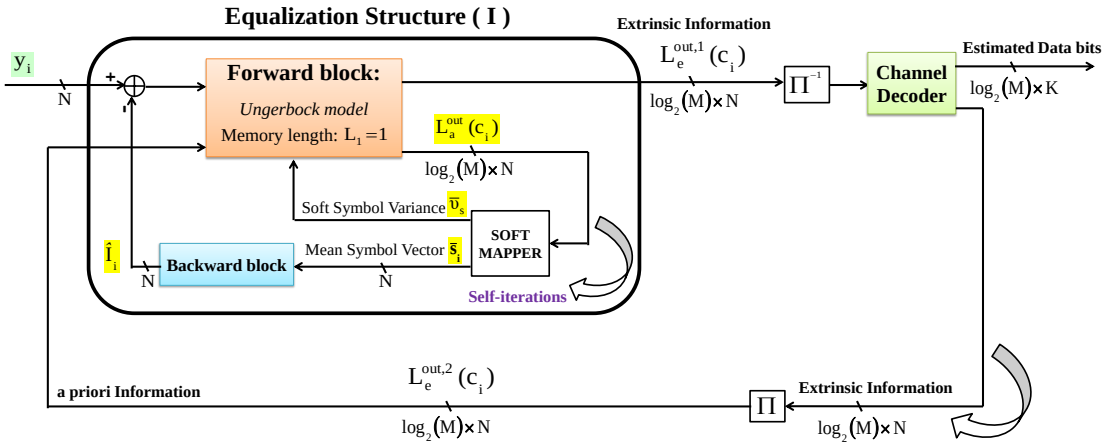

Figure 4.10: *Considered iterative equalization structure.*

For each iteration, in order to remove interference term, the proposed equalization structure realizes a few number of self-iterations. At the output of equalization, a first intrinsic information LLR sequence will be generated. Then this LLR sequence will be sent to LDPC/convolutional decoder. At the output of decoding, a second extrinsic information LLR sequence will be generated. This obtained LLR sequence will be sent to MAP equalization structure for the next iteration.

The iterative receiver diagrams for one-state Ungerboeck model are shown in Figure 4.10.

Coded BER performance: Simulation performance in term of coded BER are given in Figures 4.11 and 4.12 for both QPSK and 16-QAM modulations, respectively. For the simulation, we consider ARJA (Accumulate Repeat Jagged Accumulate) protograph based low-density parity-check (LDPC) codes of rates $R_c \in \{2/7; 2/5; 4/7; 8/11\}$ with information length $K = 2048$ bits. For one-state MAP equalization, the number of number of «self-iterations» is equal to 5. Furthermore, the number of turbo-iterations is equal to 50.

In the case of using QPSK (Quaternary Phase Shift Keying) modulation, Figure 4.11 performs the coded BER for different values of acceleration factor ν: $\nu \in \{1; 0.8; 0.6\}$. For each chosen value ν, four code rates are considered i.e. $R_c \in \{2/7; 2/5; 4/7; 8/11\}$. The Nyquist case ($\nu = 1$) is shown in dashed curves.

In the case of using 16-QAM (Quadrature Amplitude Modulation) modulation, Figure 4.12 performs the coded BER for different values of acceleration factor ν: $\nu \in \{1; 0.95; 0.9; 0.85; 0.8; 0.75\}$. The considered code rate is equal to 8/11 ($R_c = 8/11$). Similarly to the QPSK case, the Nyquist case is shown in dashed curve.

As expected, simulations results show that system uncoded BER performance decrease with use of FTN signaling. Additionally, we can see that with the use use of turbo-equalization, we can reach the Nyquist case for both (QPSK,0.8) and (16-QAM,0.95).

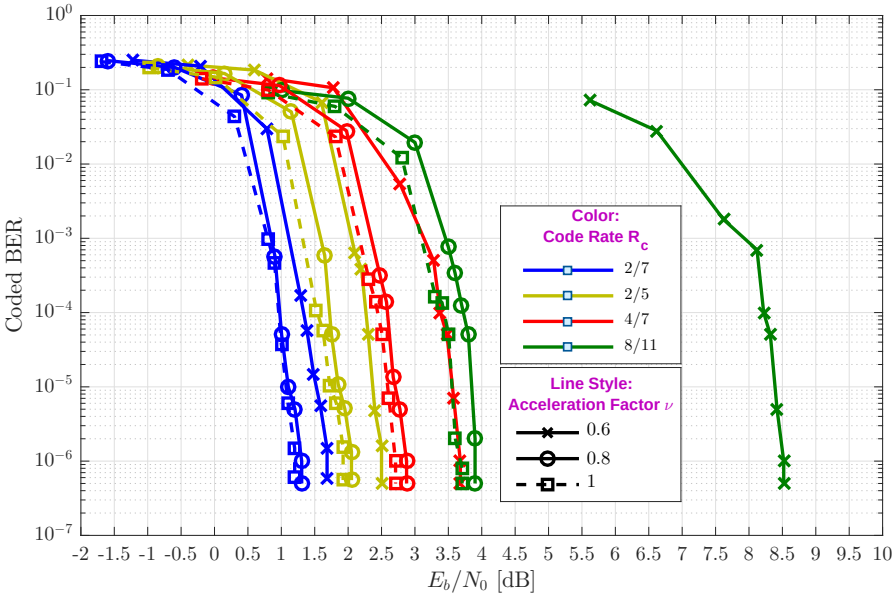

Figure 4.11: *Coded BER performances vs. E_b/N_0 in dB Coded BER performances vs. E_b/N_0 of system using One-state MAP equalization with Ungerboeck model for QPSK modulation.*

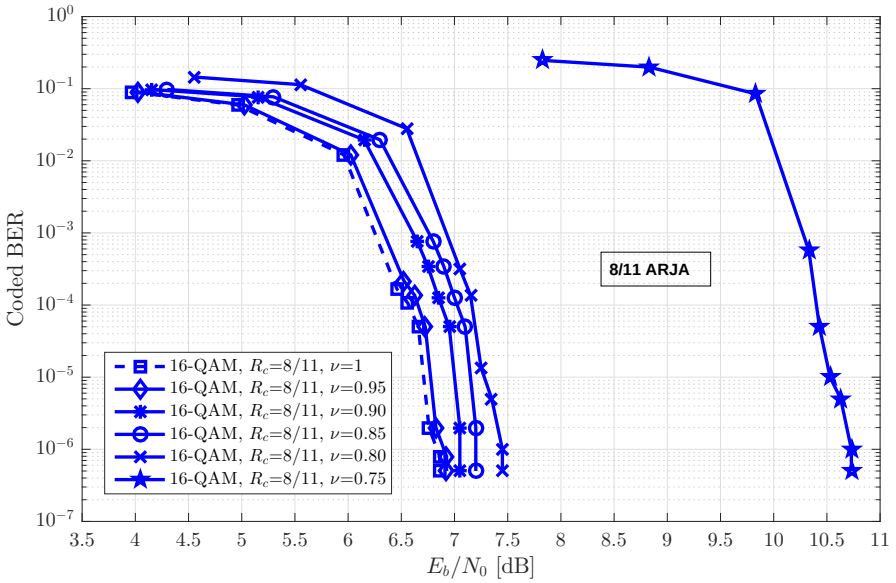

Figure 4.12: *Coded BER performances vs. E_b/N_0 in dB Coded BER performances vs. E_b/N_0 of system using One-state MAP equalization with Ungerboeck model for 16-QAM modulation.*

Spectral efficiency: Despite the degradation of the BER performance compared to Nyquist signaling shown in Figure 4.11 and Figure 4.12, FTN signaling is of great interest in terms of spectral efficiency. Furthermore, the proposed one-state equalizer offers the possibility of communicating with low values of ν. This makes it possible to achieve a maximum spectral efficiency twice as high as that using Nyquist signaling ($\tau = 1$).

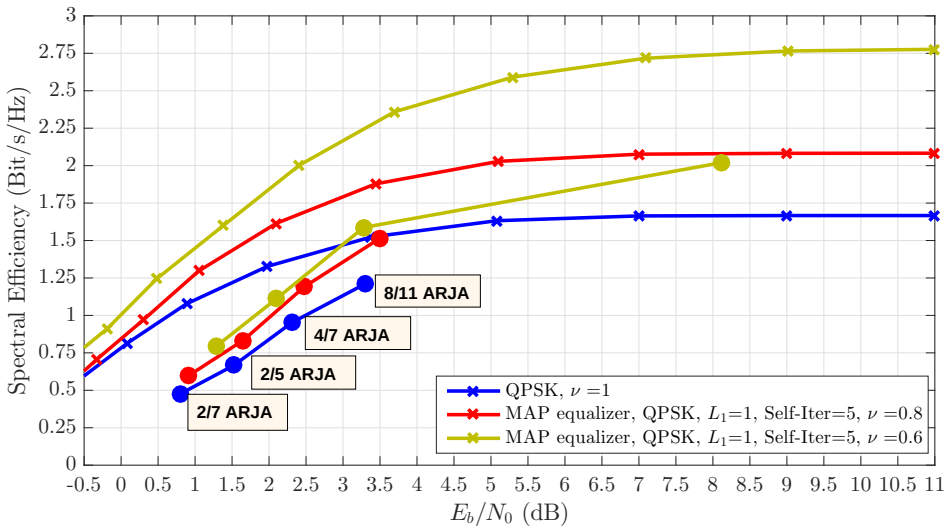

Figure 4.13: *Achievable spectral efficiency of system using MAP equalization with Ungerboeck model for QPSK case.*

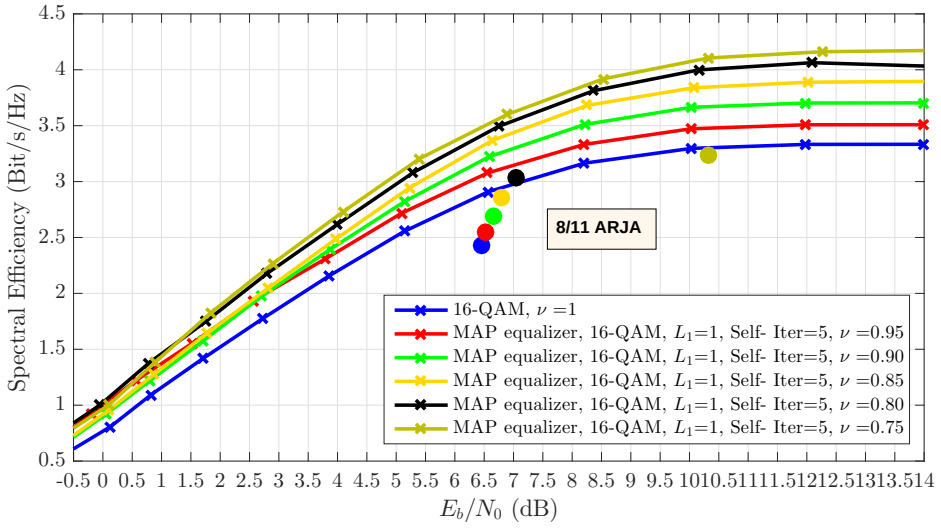

Figure 4.14: *Achievable spectral efficiency of system using MAP equalization with Ungerboeck model for 16-QAM case.*

Figures 4.13 and 4.14 show the achievable spectral efficiency. We define the achievable spectral efficiency for such system as the maximum spectral efficiency for which the decoding error probability is taken equal to 10^{-6}. In the QPSK, we consider foor code rates $\mathrm{R}_c = \{2/7; 2/5; 4/7; 8/11\}$ and fir each considered code rate, we consider three acceleration factor values $\nu = \{1; 0.8; 0.6\}$. On other hand, in the case of 16-QAM modulation, we consider one code rate $\mathrm{R}_c = 8/11$ and five acceleration factor values $\nu = \{1; 0.95; 0.9; 0.85; 0.8; 0.75\}$. In all cases, ARJA codes is used and the number of turbo-iterations is fixed to 50. For the two Figures 4.13 and 4.14, the dashed curves present the theoretical achievable spectral efficiency and are used to determinate the

$\beta = 0.20$ 50 LDPC iterations (ARJA Codes)					
Modulation	τ	**Rate**	E_b/N_0**[dB] @ BER=**10^{-6}	$(E_b/N_0)_{\mathbf{min}}$**[dB]**	η**[bit/s/Hz]**
QPSK	1	2/7	1.1	-1.1	0.4762
		2/5	1.95	-0.6	0.6667
		4/7	2.7	0.5	0.9524
		8/11	3.6	1.4	1.2121
	0.8	2/7	1.205	-0.8	0.5953
		2/5	2.075	-0.05	0.8333
		4/7	2.865	0.67	1.1905
		8/11	3.795	1.6	1.5152
	0.6	2/7	1.585	-0.42	0.7937
		2/5	2.525	0.43	1.1111
		4/7	3.67	1.47	1.5873
		8/11	8.415	2.55	2.0202
16-QAM	1	8/11	6.8	4.75	2.4243
	0.95	8/11	6.865	4.815	2.5518
	0.90	8/11	6.99	4.94	2.6936
	0.85	8/11	7.14	5.09	2.8521
	0.80	8/11	7.39	5.34	3.0303
	0.75	8/11	10.67	5.8	2.6936

Table 4.2: *Achievable spectral efficiency and E_b/N_0 values corresponding to BER equal to 10^{-6} in FTN signaling case corresponding to one-state MAP equalization (SC waveform).*

minimum possible E_b/N_0 denoted by $(E_b/N_0)_{\min}$.

For FTN signaling, the spectral efficiency increases compared to the Nyquist signaling case. For instance, in Figure 4.13, the spectral efficiency increases from $\eta = 0.6667$ bit/s/Hz at $E_b/N_0 = 1.95$ dB for the combination (QPSK ; $\nu = 1$; 2/5) to $\eta = 0.8333$ bit/s/Hz at $E_b/N_0 = 2.075$ dB for the combination (QPSK ; $\nu = 0.8$; 2/5). Similarly in the case of 16-QAM modulation shown in Figure 4.14, the spectral efficiency increases from $\eta = 2.4243$ bit/s/Hz at $E_b/N_0 = 6.8$ dB for the combination (16-QAM ; $\nu = 1$; 8/11) to $\eta = 3.0303$ bit/s/Hz at $E_b/N_0 = 7.39$ dB for the combination (16-QAM ; $\nu = 0.8$; 8/11).

Based on simulation results in the coded case, one can deduct the following Table 4.2 which summarizes the spectral efficiency η at BER = 10^{-6} for $\beta = 0.20$. Finally, we note that the achievable spectral efficiency can be improved by optimizing the considered LDPC code and choosing the most efficient configuration in each case.

4.3 EW SC-OFDM waveform

In this Section, EW SC-OFDM waveform will be studied for both Nyquist/FTN signaling and for the return link. Based on the expression of received symbols given in Equations (4.24), this section aims to give the corresponding system model in the case of aeronautical channel and especially for return link. For the return link the aeronautical channel is assumed AWGN. The UAV/aircraft transmitter and the receiver structures are shown in Figure 4.15.

4.3.1 System model

For system model, we consider a frame based transmission. Moreover, we assume that each frame contains a number of N_f sub-frames and each sub-frame contains a number of N modulated data symbols. Furthermore, we assume that the digital communication system uses linear M-ary modulation.

At the transmitter, each obtained data sequence $\mathbf{s}_i$ will be oversampled by a $\mathrm{F}_s \geq 1+\beta$ factor before being *circularly* filtered by a RRC shaping filter $\mathrm{h}_e(\tau)$ with roll-off $0 \leq \beta \leq 1$ and a Nyquist bandwidth $\mathrm{B_h}$. A possible frequency implementation is considered in Figure 3.13. Indeed, over-sampling in time domain is equivalent to have a repetition in frequency domain. Also, considering circular shape filtering is equivalent to have a spectral shaping in the frequency domain. The ratio between the size of the second Inverse Fast Fourier Transform (IFFT) and the size of the first Fast Fourier Transform (FFT) is equal to the over-sampling factor $\mathrm{F}_s \geq 1+\beta$. Therefore, the size of the first FFT is equal to N and the size of the second IFFT is equal to $N_1 = \mathrm{F}_s \times N \geq N$. N_1 is a positive integers. Note that FFT sizes N and N_1 are assumed invariant during all the communication.

At the receiver, the expression of the received frequency domain data sequence $\widetilde{\mathbf{Y}}_i = \left[\widetilde{Y}_{i,1}, \widetilde{Y}_{i,2}, \ldots, \widetilde{Y}_{i,N_1}\right]^T$ is given by:

$$\widetilde{\mathbf{Y}}_i = \begin{bmatrix} \widetilde{Y}_{i,1} \\ \widetilde{Y}_{i,2} \\ \vdots \\ \widetilde{Y}_{i,N_1} \end{bmatrix} = \sqrt{\mathrm{F}_s} \times \mathbf{A}.\ \mathbf{F}_{\mathrm{N}}.\begin{bmatrix} s_{i,1} \\ s_{i,2} \\ \vdots \\ s_{i,N} \end{bmatrix} + \begin{bmatrix} \widetilde{w}_1 \\ \widetilde{w}_2 \\ \vdots \\ \widetilde{w}_{N_1} \end{bmatrix} \tag{4.24}$$

The noise variables $\{\widetilde{w}_n\}$ are zero-mean complex AWGN with variance $\widetilde{\sigma}_w^2$ computed as:

$$\widetilde{\sigma}_w^2 = \mathrm{N}_0 \times \mathrm{F}_s \times \mathrm{R}_s = \mathrm{F}_s \times \sigma_w^2 \qquad \text{with} \qquad \sigma_w^2 = \mathrm{N}_0 \times \mathrm{R}_s \tag{4.25}$$

The $\mathbf{A}$ is initially introduced in (2.68) and is perfectly known at the receiver. Also, we recall that the $\mathbf{A}$ matrix is a pseudo-orthogonal matrix verifying:

$$\mathbf{A}^H.\mathbf{A} = \mathbf{A}^T.\mathbf{A}^* = \begin{bmatrix} \lambda_1 & 0 & \cdots & 0 \\ 0 & \lambda_2 & \cdots & 0 \\ \vdots & & \ddots & \vdots \\ 0 & 0 & \cdots & \lambda_N \end{bmatrix} \tag{4.26}$$

In Nyquist signaling, the real diagonal values $\{\lambda_n\}$ are equal to 1 i.e. $\lambda_1 = \lambda_2 = \ldots, \lambda_N = 1$. Whereas, in FTN signaling, the diagonal values are no longer equal to 1. Due the fact that we consider a normalized transmit

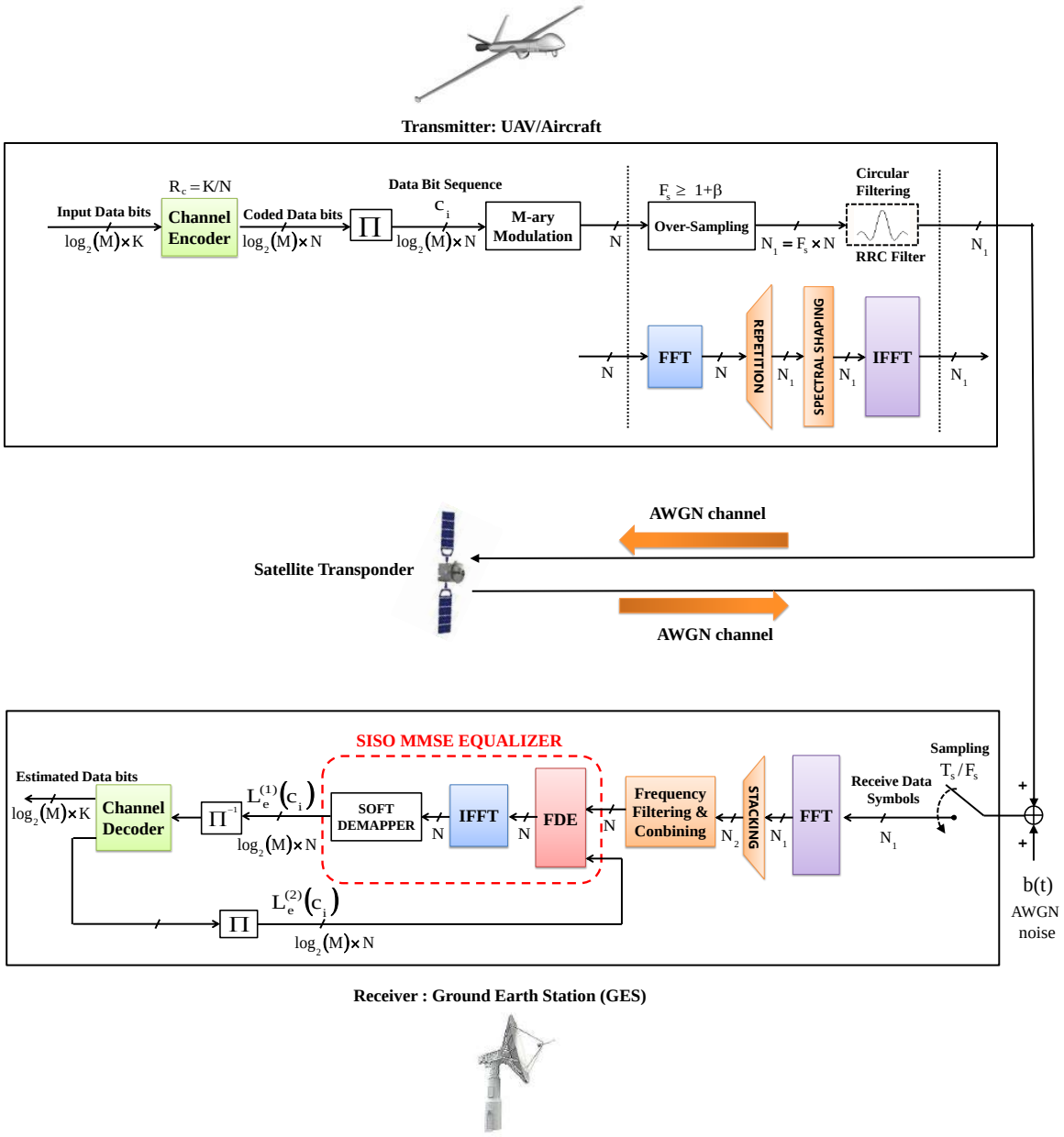

Figure 4.15: *UAV/Aircraft transmitter and GES receiver using EW SC-OFDM waveform for the return link*

shaping filter, we can verify that we have:

$$\frac{1}{N}\sum_{n=1}^{N}\lambda_n = 1 \tag{4.27}$$

numerical values for $\lambda_1, \lambda_2, \ldots, \lambda_N$ are shown in Figure 4.16 for various values of acceleration factor ν.

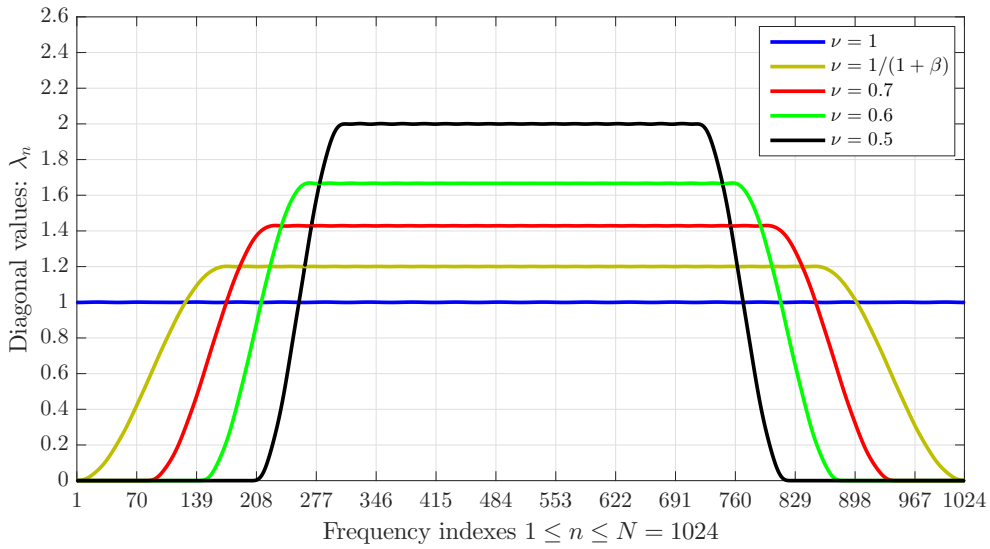

Figure 4.16: *Numerical values of diagonal values* $\{\lambda_n\}$ *in each frequency indexes* $1 \leq n \leq N = 1024$ *in the case of using RRC shaping filter with* $\beta = 0.20$.

4.3.2 Data symbol detection in Nyquist signaling:

In Nyquist signaling ($T_s = T_h$), we do not need to consider channel equalization. Indeed, applying a matched filtering to the received frequency symbols $\widetilde{\mathbf{Y}}_i$ is sufficient to obtain an optimal detection at the receiver:

$$\mathbf{y}_i = \frac{1}{\sqrt{F_s}}.\ \mathbf{F}_N^H.\ \mathbf{A}^H.\widetilde{\mathbf{Y}}_i = \begin{bmatrix} s_{i,1} \\ s_{i,2} \\ \vdots \\ s_{i,N} \end{bmatrix} + \begin{bmatrix} w_1^c \\ w_2^c \\ \vdots \\ w_N^c \end{bmatrix} \tag{4.28}$$

In general case, the noise vector $\mathbf{w}_c = [w_1^c, w_2^c, \ldots, w_N^c]^T$ is a centered colored Gaussian noise with a covariance matrix calculated as follows:

$$\mathbb{E}\left\{\mathbf{w}_c.\mathbf{w}_c^H\right\} = \sigma_w^2.\ diag \begin{bmatrix} \lambda_1 \\ \lambda_2 \\ \vdots \\ \lambda_N \end{bmatrix} \tag{4.29}$$

Due to the fact that the diagonal values $\{\lambda_n\}$ are equal to 1 in Nyquist signaling, we can deduce that the additive noise is AWGN and and the expression of the detected samples can be reduced to:

$$y_{i,n} = s_{i,n} + w_n \qquad \text{for} \qquad 1 \leq n \leq N \tag{4.30}$$

where the noise variables $\{w_n\}$ are Gaussian, white and having a variance equal to σ_w^2.
Finally, by using (4.30), we can deduce that in the presence of AWGN channel and by using Nyquist signaling, system performances for both SC and EW SC-OFDM are equivalent, which is trivial.

4.3.3 Data symbol detection in FTN signaling:

In linear observation model given in Equation (4.24), the noise variables $\{\widetilde{w}_n\}$ are Gaussian and white. Furthermore, the constellation symbols $\{s_{i,n}\}$ are assumed i.i.d with variance equal to σ_s^2. By applying a linear MMSE equalization *a priori* [122], we can obtain a biased estimation of the transmitted data sequence $\mathbf{s}_i = [s_{i,1}, s_{i,2}, \ldots, s_{i,N}]^T$. We denote $\mathbf{z}_i = [z_{i,1}, z_{i,2}, \ldots, z_{i,N}]^T$ as the output MMSE equalization vector which is expressed as:

$$\mathbf{z}_i = \mathbf{F}_{\mathrm{N}}^H.\Sigma^{-1}.\mathbf{A}^H.\left(\frac{1}{\sqrt{\mathrm{F}_s}}.\ \widetilde{\mathbf{Y}}_i - \mathbf{A}.\mathbf{F}_{\mathrm{N}}.\bar{\mathbf{s}}_i\right) + \mu_i = \mathbf{F}_{\mathrm{N}}^H.\Sigma^{-1}.\left(\mathbf{Y}_i - \bar{\mathbf{Y}}_i\right) + \mu_i \tag{4.31}$$

where $\mathbf{Y}_i$ is the output frequency domain observation after being filtered by a receive matched filter:

$$\mathbf{Y}_i = \frac{1}{\sqrt{\mathrm{F}_s}}.\ \mathbf{A}^H.\widetilde{\mathbf{Y}}_i \tag{4.32}$$

Furthermore, The three quantities Σ^{-1}, μ_i and $\bar{\mathbf{Y}}_i$ denote the three MMSE equalization parameters to be computed for a given *a priori* information $(\bar{v}_s, \bar{\mathbf{s}}_i)$ and they are expressed as:

$$\Sigma^{-1} \triangleq \frac{1}{1+[1-(\bar{v}_s/\sigma_s^2)].\ \varrho}.\left[(\bar{v}_s/\sigma_s^2).\ \mathbf{A}_i^H.\mathbf{A}_i + (\sigma_w^2/\sigma_s^2).\ \mathbf{I}_{N\times N}\right]^{-1} \tag{4.33}$$

$$\bar{\mathbf{Y}}_i \triangleq \mathbf{A}_i^H.\mathbf{A}_i.\mathbf{F}_{\mathrm{N}}.\bar{\mathbf{s}}_i \tag{4.34}$$

$$\mu_i \triangleq \frac{\varrho}{1+[1-(\bar{v}_s/\sigma_s^2)].\ \varrho}.\ \bar{\mathbf{s}}_i = \alpha_i.\ \bar{\mathbf{s}}_i \tag{4.35}$$

By taking into account an *a priori* information, the values of the two real positive scalars, ϱ and α_i, depend on the given symbol variance values $\bar{v}_s$ as follows:

$$\varrho \triangleq \frac{1}{N}.\ tr\left\{\left[(\bar{v}_s/\sigma_s^2).\ \mathbf{A}_i^H.\mathbf{A}_i + (\sigma_w^2/\sigma_s^2).\ \mathbf{I}_{N\times N}\right]^{-1}.\mathbf{A}_i^H.\mathbf{A}_i\right\} \quad \text{and} \quad \alpha \triangleq \frac{\varrho}{1+[1-(\bar{v}_s/\sigma_s^2)].\ \varrho} \tag{4.36}$$

Besides, it is previously shown in (4.26), that the matrix $\mathbf{A}^H.\mathbf{A}$ is a $N \times N$ diagonal matrix and $\lambda_1, \lambda_2, \ldots, \lambda_N$ are its real diagonal values:

$$\mathbf{A}^H.\mathbf{A} = diag\begin{bmatrix}\lambda_1\\ \lambda_2\\ \vdots\\ \lambda_N\end{bmatrix} \tag{4.37}$$

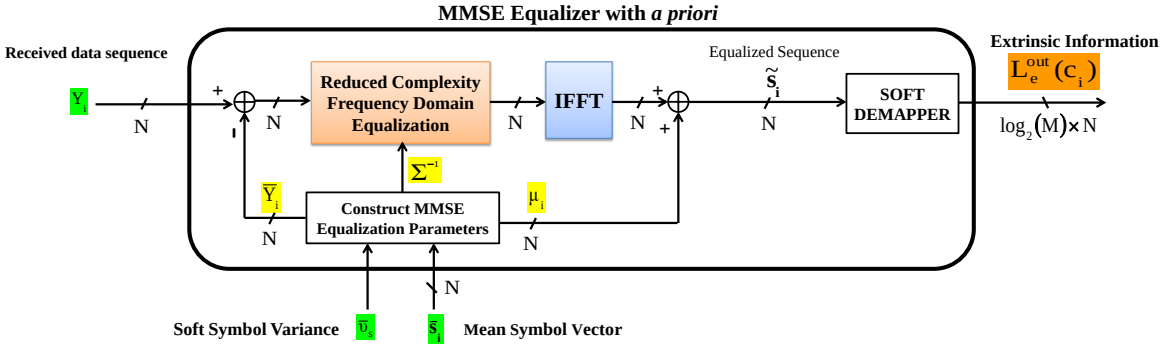

Figure 4.17: *The considered Linear MMSE equalizer using a priori information.*

Given the fact that $\mathbf{A}^H.\mathbf{A}$ is a diagonal matrix, the expression of ϱ in (4.36), and Σ^{-1} in (4.35) can be reduced to:

$$\varrho = \frac{1}{N}\sum_{n=1}^{N}\frac{\lambda_n}{(\bar{v}_s/\sigma_s^2).\ \lambda_n + (\sigma_w^2/\sigma_s^2)} \qquad \text{and} \qquad \Sigma^{-1} = \frac{\sigma_s^2}{1+[1-(\bar{v}_s/\sigma_s^2)].\ \varrho}.diag\begin{bmatrix}\frac{1}{\bar{v}_s.\ \lambda_1+\sigma_w^2}\\ \frac{1}{\bar{v}_s.\ \lambda_2+\sigma_w^2}\\ \vdots \\ \frac{1}{\bar{v}_s.\ \lambda_n+\sigma_w^2}\end{bmatrix} \tag{4.38}$$

Thus, the complexity of the receiver is significantly reduced and matrix inversion is no longer a problem. As a consequence, it is possible to consider Frequency Domain Equalization (FDE) based on MMSE criterion as shown in Figure 4.17.

Referring to [70], it is shown that the output MMSE equalized vector, $\widetilde{\mathbf{s}}_i$, is a biased estimation of $\mathbf{s}_i$ and its expression can be reduced to:

$$\widetilde{\mathbf{s}}_i = \sqrt{\frac{\gamma}{\alpha^2}}\ \mathbf{z}_i \approx \sqrt{\gamma}\ \mathbf{s}_i + \mathbf{w} \tag{4.39}$$

where $\mathbf{w} = [w_1, w_2, \ldots, w_N]^T$ is a zero-mean complex AWGN noise vector and symbols $\{w_n\}$ having a variance equal to σ_w^2. The positive scalar γ denotes the MMSE equalization gain and its expression is initially given in

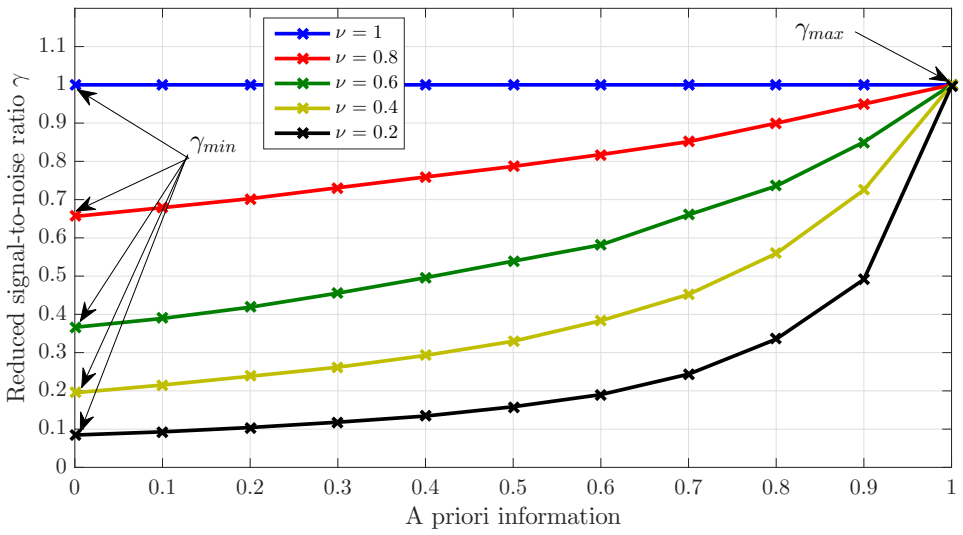

Figure 4.18: *Numerical values of γ as function of a priori information for $E_s/N_0 = 5$ dB.*

(2.98) as:

$$\gamma = \begin{cases} \left(\frac{1}{N} \sum_{n=1}^{N} \frac{1}{\lambda_n + (\sigma_w^2/\sigma_s^2)} \right)^{-1} - (\sigma_w^2/\sigma_s^2) = \gamma^{\min} & \text{for} \quad \bar{v}_s = \sigma_s^2 \quad \text{(zero a priori)} \\ (\sigma_s^2/\bar{v}_s) . \left\{ \left(\frac{1}{N} \sum_{n=1}^{N} \frac{1}{(\bar{v}_s/\sigma_s^2) . \lambda_n + (\sigma_w^2/\sigma_s^2)} \right)^{-1} - (\sigma_w^2/\sigma_s^2) \right\} & \text{for} \quad 0 < \bar{v}_s < \sigma_s^2 \\ \frac{1}{N} \sum_{n=1}^{N} \lambda_n = 1 = \gamma^{\max} & \text{for} \quad \bar{v}_s = 0 \quad \text{(Perfect a priori)} \end{cases} \tag{4.40}$$

Some Numerical values of γ as function of *a priori* information for $\mathrm{E}_s/\mathrm{N}_0 = 5$ dB are given in Figure 4.18. In Figure 4.17, an extrinsic LLR vector of size $N \times \log_2(M)$, $\mathrm{L}_e^{\mathrm{out}}(\mathbf{c}_i)$, is generated and calculated as follows:

$$\mathrm{L}_e^{\mathrm{out}}(\mathbf{c}_i) = \mathrm{L}_a^{\mathrm{out}}(\mathbf{c}_i) - \mathrm{L}_a^{\mathrm{in}}(\mathbf{c}_i) \tag{4.41}$$

where $\mathrm{L}_a^{\mathrm{out}}(\mathbf{c}_i)$ is an *a posteriori* LLR vector and its expression is initially given in Equation (2.101).

4.3.3.1 The uncoded case

For the uncoded case, we assume using MMSE equalization with zero *a priori* i.e. $\gamma = \gamma^{\min}$. The estimated transmit symbol is determinated as the most likely symbol as follows:

$$\widehat{x}_{i,n} = \underset{\mathcal{C}_m \in \chi}{\operatorname{argmin}} \left| \widetilde{s}_{i,n} - \sqrt{\gamma^{\min}} . \mathcal{C}_m \right|^2 \qquad 1 \leq n \leq N \tag{4.42}$$

By considering Gray mapping [50], it is shown that we have only one erroneous bit in each erroneous mapping constellation symbol. Thus, the theoretical average Bit Error Rate can be expressed as:

$$\mathrm{BER} \cong \frac{\mathrm{N}_v}{\log_2(M)} \times Q \left(\sqrt{\gamma^{\min} . \left(\frac{\mathrm{D}_{\min}^2}{2.\sigma_s^2} \right) . \mathrm{R}_c . \log_2(M) . \mathrm{E}_b/\mathrm{N}_0} \right) \tag{4.43}$$

As expected, in Figure 4.19, we can see that simulation results in the case of 8-PSK (Phase-Shift Keying) modulation shown in solid curves confirm the analytical expression given in (4.43) and shown in dashed curves. By considering different linear modulation types, Figure 4.20 give simulation results for uncoded BER performances for QPSK, 8-PSK and 16-QAM in FTN signaling. As expected, simulations results show that system uncoded BER performance decrease with use of FTN signaling. Indeed by considering FTN signaling, the frequency channel becomes selective. The more the acceleration factor ν is low, the more the channel selectivity is high.

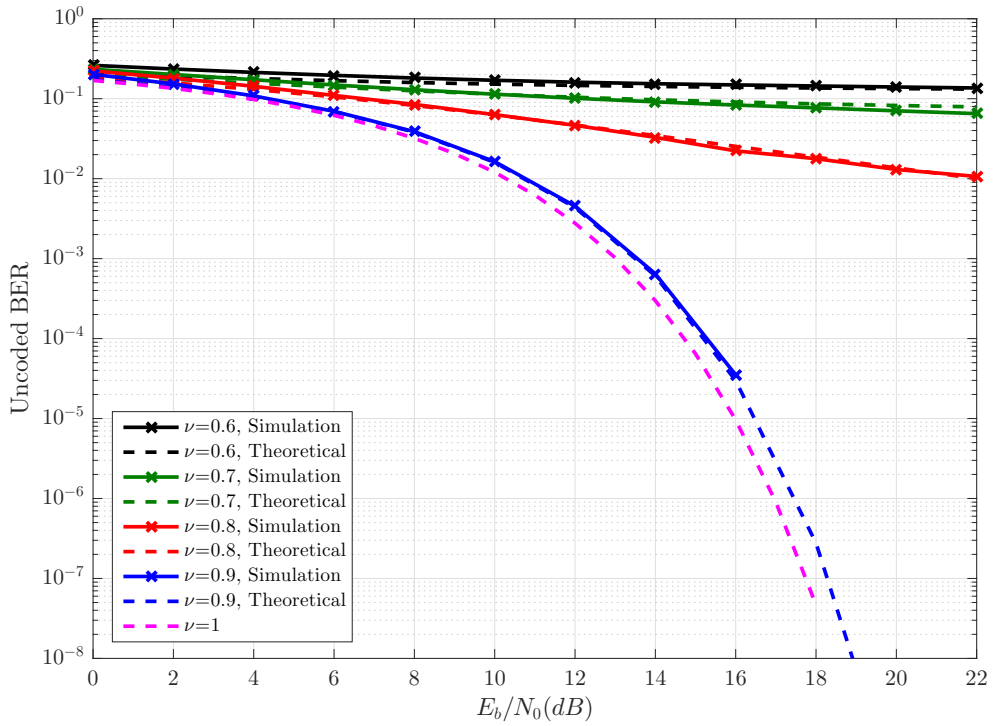

Figure 4.19: *Uncoded BER performance in the case of 8-PSK modulation of system using EW-SC-OFDM waveform as function of acceleration factor ν. The shaping filter is RRC with $\beta = 0.20$.*

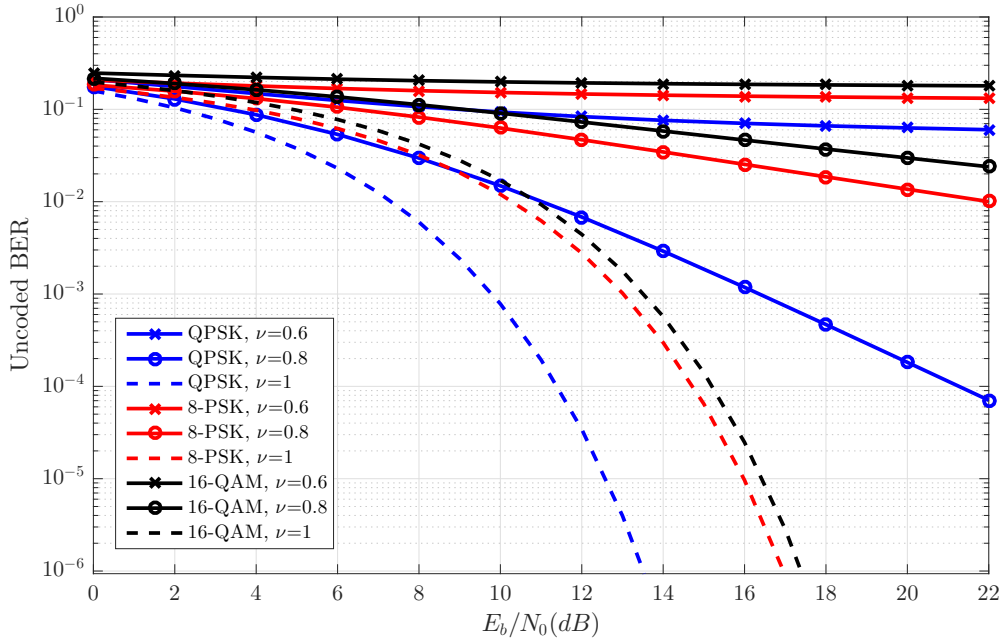

Figure 4.20: *Uncoded BER performance of system using EW-SC-OFDM waveform as function of acceleration factor ν. The shaping filter is RRC with $\beta = 0.20$.*

4.3.3.2 EXIT CHART Analysis:

In Figure 4.21, we give the EXtrinsic Information Transfer (EXIT) charts for the proposed MMSE equalizer for $\nu = \{1; 0.8; 0.6\}$ for a Signal to Noise Ratio $E_b/N_0 = 5$ dB. The Nyquist case ($\nu = 1$) is presented in dashed curve.

As we can observe, in perfect *a priori*, all extrinsic information values, for both QPSK and 16-QAM modulation, converge to a single value which is the extrinsic information value given by the Nyquist case. This result is expected. Indeed, by using Gaussian approximation, it is shown in Equation (4.39) that the expression of the equalized sequence is reduced to:

$$\widetilde{\mathbf{s}}_i = \sqrt{\gamma}.\ \mathbf{s}_i + \mathbf{w} \tag{4.44}$$

The elements of the noise vector $\mathbf{w}$ are additive white Gaussian noise (AWGN) and independent and identically distributed (i.i.d) with the variance equal to σ_w^2.

Furthermore, in the case of perfect *a priori*, it is shown in Equation (4.40) that we have:

$$\gamma = \gamma^{\max} = \frac{1}{N}\sum_{n=1}^{N} \lambda_n = 1 \qquad \text{for all values of } \nu \in]0,1]. \tag{4.45}$$

Thus, by using (4.44) and (4.45), we can deduce that in the case of perfect *a priori*, the system performances are equivalent to the Nyquist case.

Besides, in the case of zero *a priori*, it is shown in Equation (4.40) that we have:

$$\gamma = \gamma^{\min} = \left(\frac{1}{N}\sum_{n=1}^{N} \frac{1}{\lambda_n + (\sigma_w^2/\sigma_s^2)}\right)^{-1} - (\sigma_w^2/\sigma_s^2) \leq 1 \tag{4.46}$$

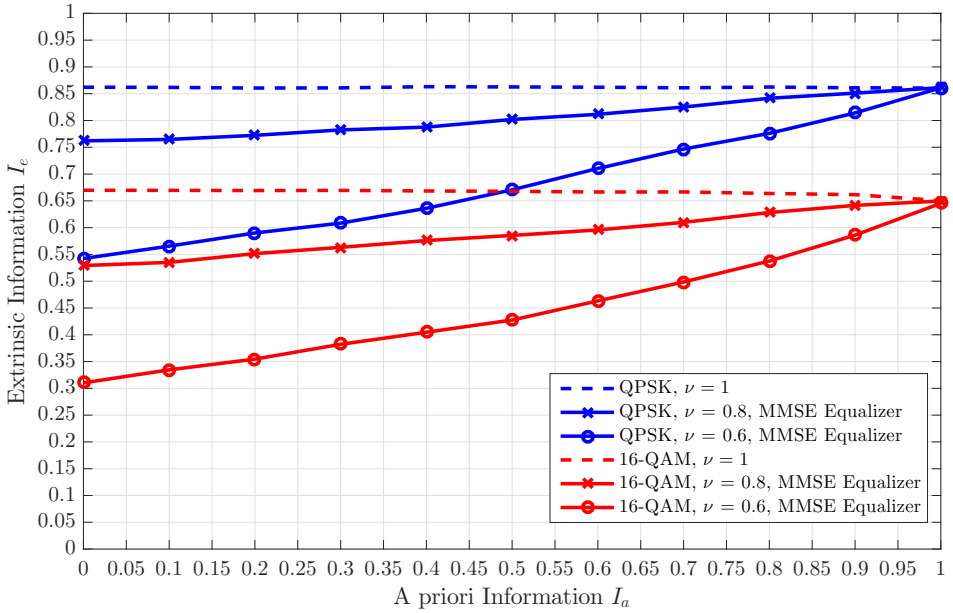

Figure 4.21: *EXIT CHARTs of MMSE equalizer for QPSK and 16-QAM modulations at $E_b/N_0 = 5$ dB in Nyquist/FTN signaling with $\beta = 0.20$*

Some Numerical values of $\gamma^{\min}$ for $\mathrm{E}_s/\mathrm{N}_0 = 5$ dB are given in Figure 4.18. Given the fact that $\gamma \leq 1$, we can deduce a system performance degradation compared to the Nyquist case. This behavior is corroborated by the uncoded Bit Error Rate curves given in Figures (4.19) and (4.20).

4.3.3.3 The coded case: using turbo-equalization

In coded case, after MMSE equalization process, a soft channel decoding structure is added in series to decode received data bits. In order to improve performance system, MMSE equalization and channel decoding will be operated in iterative process to maximize the reliability of transmitted bits. As as result, turbo equalization is performed.

For each iteration, the MMSE equalizer will generate an extrinsic bit information denoted by $\mathrm{L}_e^{\mathrm{out},1}(\mathbf{c}_i) =$

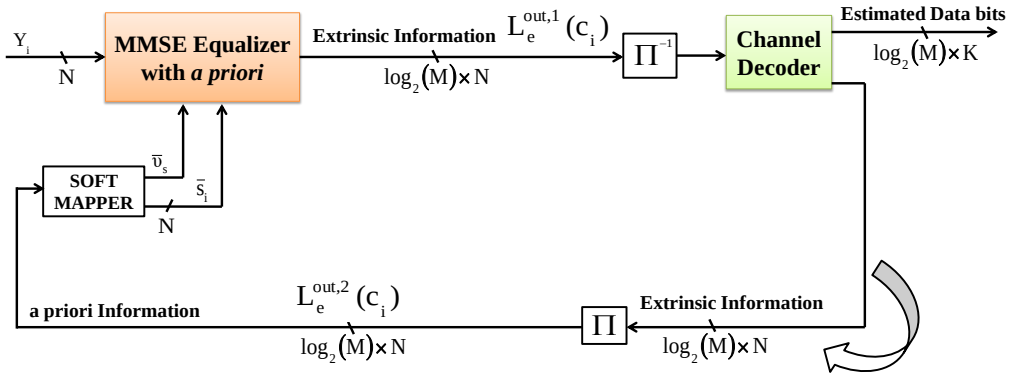

Figure 4.22: *Considered iterative equalization structure.*

$\left[\mathrm{L}_e^{\mathrm{out},1}(c_{i,1}), \mathrm{L}_e^{\mathrm{out},1}(c_{i,2}), \ldots, \mathrm{L}_e^{\mathrm{out},1}\left(c_{i,\log_2(M)\times N}\right)\right]^T$ corresponding to each symbol assigned by the channel. Then this extrinsic information will be sent to LDPC/convolutional decoder, which does not require the calculation of an observation, not an estimate of the noise variance on this observation. At the output of decoding, another extrinsic bit information denoted by $\mathrm{L}_e^{\mathrm{out},2}(\mathbf{c}_i) = \left[\mathrm{L}_e^{\mathrm{out},2}(c_{i,1}), \mathrm{L}_e^{\mathrm{out},2}(c_{i,2}), \ldots, \mathrm{L}_e^{\mathrm{out},2}\left(c_{i,\log_2(M)\times N}\right)\right]^T$ will be generated. The latter will be used in the next iteration as *a priori* information for Bayesian MMSE equalization. The iterative receiver diagram is shown in Figure 4.22.

Coded BER performance: Simulation performance in term of coded BER are given in Figures 4.23 and 4.24 for both QPSK and 16-QAM modulations, respectively. For the simulation, we consider ARJA (Accumulate Repeat Jagged Accumulate) protograph based low-density parity-check (LDPC) codes of rates $R_c \in \{2/7; 2/5; 4/7; 8/11\}$ with information length $K = 2048$ bits. The number of turbo-iterations is equal to 50.

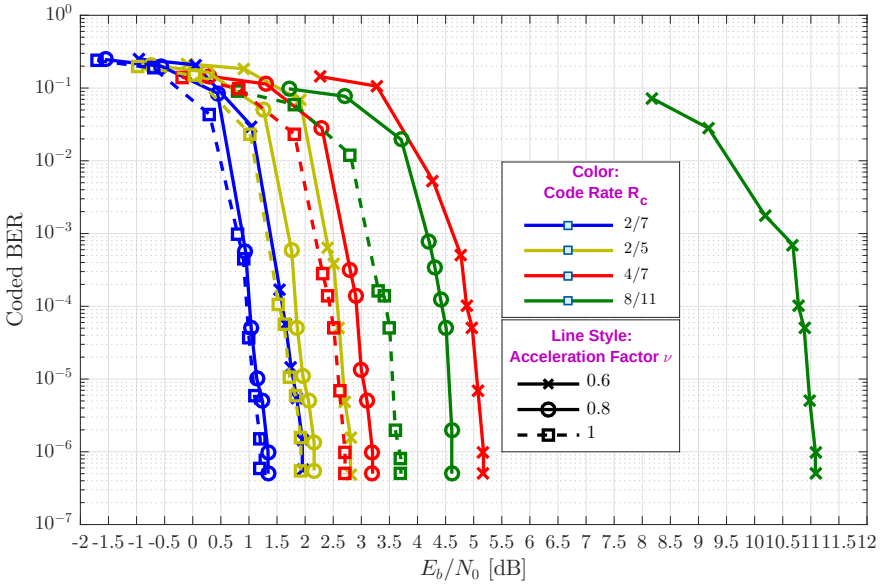

Figure 4.23: *Coded BER performances vs. E_b/N_0 in dB of system using Bayesian MMSE equalization for QPSK modulation.*

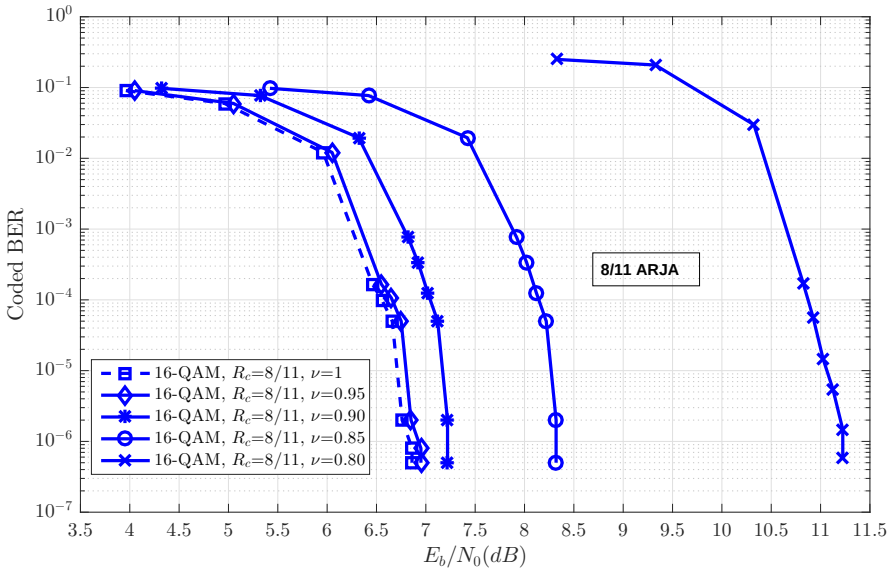

Figure 4.24: *Coded BER performances vs. E_b/N_0 of system using Bayesian MMSE equalization for 16-QAM modulation.*

In the case of using QPSK (Quaternary Phase Shift Keying) modulation, Figure 4.23 performs the coded BER for different values of acceleration factor ν: $\nu \in \{1; 0.8; 0.6\}$. For each chosen value ν, for code rates are considered i.e. $\mathrm{R}_c \in \{2/7; 2/5; 4/7; 8/11\}$. The Nyquist case ($\nu = 1$) is shown in dashed curves.
In the case of using 16-QAM (Quadrature Amplitude Modulation) modulation, Figure 4.24 performs the coded BER for different values of acceleration factor ν: $\nu \in \{1; 0.95; 0.9; 0.85; 0.8\}$. The considered code rate is equal to 8/11 ($\mathrm{R}_c = 8/11$). Similarly to the QPSK case, the Nyquist case is shown in dashed curve.
As expected, simulations results show that system coded BER performance decrease with use of FTN signaling. Additionally, simulation results show that with the use use of turbo-equalization, we can reach the Nyquist case for both combinations (QPSK ; 0.8) and (16-QAM ; 0.95).

Spectral efficiency: Despite the degradation of the BER performance compared to Nyquist signaling shown in Figure 4.23 and Figure 4.24, FTN signaling is of great interest in terms of spectral efficiency. Furthermore, the proposed one-state equalizer offers the possibility of communicating with low values of ν. This makes it possible to achieve a maximum spectral efficiency twice as high as that using Nyquist signaling ($\tau = 1$).
The considered spectral efficiency denoted by η and calculated as follows:

$$\eta = \mathrm{R}_c \times \frac{\log_2(M)}{\nu \times (1+\beta)} \tag{4.47}$$

As mentioned in (4.47), the spectral efficiency inversely proportional to the acceleration factor ν.

Figures 4.25 and 4.26 show the achievable spectral efficiency. We define the achievable spectral efficiency for such system as the maximum spectral efficiency for which the decoding error probability is taken equal to 10^{-6}. In the QPSK, we consider four code rates $\mathrm{R}_c = \{2/7; 2/5; 4/7; 8/11\}$ and fir each considered code rate, we consider three acceleration factor values $\nu = \{1; 0.8; 0.6\}$. On other hand, in the case of 16-QAM modulation,

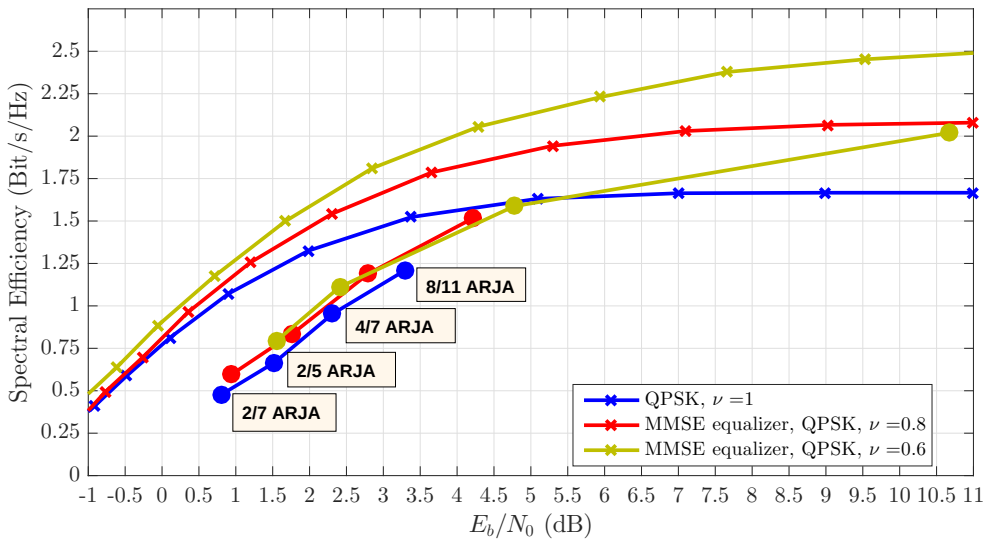

Figure 4.25: *Achievable spectral efficiency of system using Bayesian MMSE equalization for QPSK modulation.*

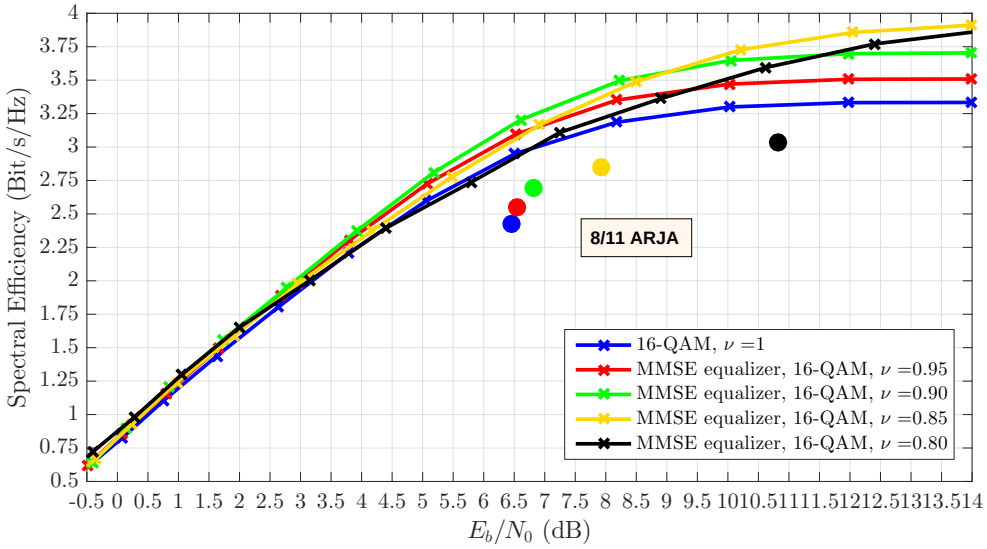

Figure 4.26: *Achievable spectral efficiency of system using Bayesian MMSE equalization for 16-QAM modulation.*

we consider one code rate $R_c = 8/11$ and five acceleration factor values $\nu = \{1; 0.95; 0.9; 0.85; 0.8; 0.75\}$. In all cases, ARJA codes is used and the number of turbo-iterations is fixed to 50. For the two Figures 4.25 and 4.26, the dashed curves present the theoretical achievable spectral efficiency and are used to determinate the minimum possible E_b/N_0 denoted by $(E_b/N_0)_{\min}$.

For FTN signaling, the spectral efficiency increases compared to the Nyquist signaling case. For instance, in Figure 4.25 , the spectral efficiency increases from $\eta = 0.6667$ bit/s/Hz at $E_b/N_0 = 1.95$ dB for the combination (QPSK ; $\nu = 1$; 2/5) to $\eta = 0.8333$ bit/s/Hz at $E_b/N_0 = 2.185$ dB for the combination (QPSK ; $\nu = 0.8$; 2/5). Similarly in the case of 16-QAM modulation shown in Figure 4.26, the spectral efficiency increases from $\eta = 2.4243$ bit/s/Hz at $E_b/N_0 = 6.8$ dB for the combination (16-QAM ; $\nu = 1$; 8/11) to $\eta = 3.0303$ bit/s/Hz at $E_b/N_0 = 11.165$ dB for the combination (16-QAM ; $\nu = 0.8$; 8/11).

Based on simulation results in the coded case, one can deduct the following Table 4.3 which summarizes the spectral efficiency η at BER $= 10^{-6}$ for $\beta = 0.20$. Finally, we note that the achievable spectral efficiency can be improved by optimizing the considered LDPC code and choosing the most efficient configuration in each case.

$\beta = 0.20$ 50 LDPC iterations (ARJA Codes)					
Modulation	τ	**Rate**	E_b/N_0**[dB] @ BER=**10^{-6}	$(E_b/N_0)_{\mathbf{min}}$**[dB]**	η**[bit/s/Hz]**
QPSK	1	2/7	1.1	-1.1	0.4762
		2/5	1.95	-0.6	0.6667
		4/7	2.7	0.5	0.9524
		8/11	3.6	1.4	1.2121
	0.8	2/7	1.24	-0.765	0.5953
		2/5	2.185	0.06	0.8333
		4/7	3.19	1	1.1905
		8/11	4.505	2.35	1.5152
	0.6	2/7	1.85	-0.3	0.7937
		2/5	2.833	0.738	1.1111
		4/7	5.165	2.2	1.5873
		8/11	10.976	4.48	2.0202
16-QAM	1	8/11	6.8	4.75	2.4243
	0.95	8/11	6.89	4.85	2.5518
	0.90	8/11	7.16	5.11	2.6936
	0.85	8/11	8.26	6	2.8521
	0.80	8/11	11.165	7.2	3.0303

Table 4.3: *Achievable spectral efficiency and E_b/N_0 values corresponding to BER equal to 10^{-6} in FTN signaling case corresponding to MMSE equalization (EW SC-OFDM waveform).*

4.4 Comparison of system performance: SC waveform vs EW SC-OFDM waveform

In this Section, we will compare system performance for both SC and EW SC-OFDM waveforms.

In Nyquist signaling, it has been shown that system performances for both SC and EW SC-OFDM are equivalent and are shown in Table 4.1 in Section 4.2.2.

In FTN signaling case, for the SC waveform, we have investigated low complexity MAP equalizer. However, for EW SC-OFDM waveform, Bayesian frequency domain MMSE equalized is considered. System performances corresponding to MAP equalization are shown in Table 4.2 in Section 4.2.3. Concerning MMSE equalization, system performances are shown in Table 4.3 in Section 4.3.3.

By combining all result, Table 4.4 summarizes system performance for all considered case.

$\beta = 0.20$ 50 LDPC iterations (ARJA Codes)							
MOD	τ	**Rate**	E_b/N_0**[dB] @ BER=**10^{-6}		$(E_b/N_0)_{\mathbf{min}}$**[dB]**		η**[bit/s/Hz]**
			SC	EW SC-OFDM	SC	EW SC-OFDM	
QPSK	1	2/7	1.1	1.1	-1.1	-1.1	0.4762
		2/5	1.95	1.95	-0.6	-0.6	0.6667
		4/7	2.7	2.7	0.5	0.5	0.9524
		8/11	3.6	3.6	1.4	1.4	1.2121
	0.8	2/7	1.205	1.24	-0.8	-0.765	0.5953
		2/5	2.075	2.185	-0.05	0.06	0.8333
		4/7	2.865	3.19	0.67	1	1.1905
		8/11	3.795	4.505	1.6	2.35	1.5152
	0.6	2/7	1.585	1.85	-0.42	-0.3	0.7937
		2/5	2.525	2.833	0.43	0.738	1.1111
		4/7	3.67	5.165	1.47	2.2	1.5873
		8/11	8.415	10.976	2.55	4.48	2.0202
16-QAM	1	8/11	6.8	6.8	4.75	4.75	2.4243
	0.95	8/11	6.865	6.89	4.815	4.85	2.5518
	0.90	8/11	6.99	7.16	4.94	5.11	2.6936
	0.85	8/11	7.14	8.26	5.09	6	2.8521
	0.80	8/11	7.39	11.165	5.34	7.2	3.0303
	0.75	8/11	10.67	-	5.8	-	3.2323

Table 4.4: *Comparison of the achievable spectral efficiency and E_b/N_0 values corresponding to BER equal to 10^{-6} in Nyquist/FTN signaling case for both SC and EW SC-OFDM waveforms.*

4.5 Conclusion

In this chapter, we are interested in the Return link. In order to compare system performance for different waveform, we have investigated two possible waveform: Single Carrier (SC) waveform and the Extended Weighted Single Carrier Orthogonal Frequency Division Multiplexing (EW SC-OFDM) waveforms. These two waveforms are studied in two contexts: Nyquist and Faster-Than-Nyquist (FTN) signaling.

In Nyquist signaling, it has been shown that system performances for both SC and EW SC-OFDM are equivalent which is trivial. However, in FTN signaling case, There are an additive ISI term and therefore we need to design a reduced complexity equalizer. To do it, we have investigated reduced complexity equalizers for both SC and EW SC-OFDM waveforms. EW SC-OFDM offers an interesting low complexity frequency domain equalization abilities and thus low complexity Bayesian Minimum Mean Square Error (MMSE) equalization is considered. For SC waveform, an optimum detection scheme is given by considering Maximum A Posteriori (MAP) criterion, but it has been shown that the computational complexity of MAP equalizers exponentially increases with the memory of the equivalent base-band channel. To cope with this problem, we have investigated an efficient reduced-state implementation of MAP equalization.

Finally, performance system for SC and EW SC-OFDM waveform, using respectively MAP and MMSE equalization, are compared. As a result, The proposed reduced-state MAP equalization structure for SC waveform give a better performance compared the one using MMSE equalization for EW SC-OFDM waveform especially at high spectral efficiencies.

Chapter 5

Spatial Modulation vs SIMO techniques: State-of-the-art

Sommaire

5.1 SM vs SIMO techniques

Nowadays, several studies are launched for the design of highly reliable and cost-effective communications systems that introduce Unmanned Aerial Vehicle (UAV), this paves the way for UAV networks to play an important role in a lot of applications. Indeed, thanks to UAVs, many complex mission will be feasible, such as the collection of information in areas humans cannot reach, either because of safety issues (like working within a radioactive cloud), or other issues related to human beings (like working over enemy places) [18] [41]. The mission link required a very large amount of data (live video, images etc.), this link requires a high bit rate. In some environments [79], UAVs can fly in a rich multipath environments (NLOS). In this case, it is interesting to take advantage of using Multi-Input-Multi-Output (MIMO) techniques, since it exploit the decorrelation of received signals to improve symbol detection at the receiver. Since UAV architecture envisages the implantation of two antennas placed at wings. So, it is straightforwardly recommended to use these two antennas in order to increase diversity gain.

However, the use of these two antennas can affect UAV/aircraft endurance. In fact, doubling the number of active antennas means reducing half of endurance time. In order to reduce the energy consumption at the transmitter, one may resort to the use of the Single-Input Multiple-Output (SIMO) system. For the SIMO system, only one transmit antenna is considered. The SIMO solution presents a trade-off between reducing energy consumption and increasing diversity gain given by the use of the second transmit antenna. This solution is the most envisaged until the appearance of a new technique called spatial modulation (SM). SM allows us to benefit from the diversity offered by the two antennas without affecting endurance. This new modulation technique SM selects active transmit antenna in an alternative manner and thus it makes possible to increase the diversity gain at the reception. Since transmit active antenna is selected in an alternative manner, from a budgetary point of view, this is equivalent to having a permanent single transmit active antenna. So, in terms of energy consumption, this is equivalent to the SIMO case. Consequently, the SM system can achieve a good trade-off between energy consumption and diversity gain compared to the SIMO system. Moreover, SM technique uses antenna position as a source of information and a part of the information bits are carried by a selection of the active antennas. As a result, SM technique allows us to increase the spectral efficiency compared to SIMO technique. For the same modulation order M, the considered spectral efficiency percentage gain is expressed as:

$$\text{Gain } [\%] = \frac{\eta^{\text{SM}} - \eta^{\text{SIMO}}}{\eta^{\text{SIMO}}} \times 100 = \frac{\log_2(\text{N}_\text{t})}{\log_2(M)} \times 100 \tag{5.1}$$

where N_t is the number of considered transmit antennas.

This spectral efficiency gain is done at the expense of performance degradation given by the presence of estimation errors of active transmit antennas at rthe receiver. In SM system, BER performance heavily depends on the active transmit antennas selection and enhancing active transmit antennas is challenging task. Indeed, sometimes a poor selection of active transmit antennas can cause an entire erroneous sub-frame. If it possible to perfectly estimate the considered active transmit antennas, the BER performance can be considerably improved and one can obtain a BER performance gain compared to the SIMO system. The

considered gain in decibels can be expressed as:

$$\text{BER Gain [dB]} = 10\ \log_{10}\left(\frac{\text{BER}^{\text{SIMO}}}{\text{BER}^{\text{SM}}}\right) = 10\ \log_{10}\left(1+\frac{\log_2(\text{N}_\text{t})}{\log_2(M)}\right) \tag{5.2}$$

In this case, SM system presents an improved performances compared to the SIMO system in terms of spectral efficiency and also in terms of BER performances. Therefore, it is interesting to investigate new modified SM structures that enhance active antenna selection.

On other hand, for both SM and SIMO systems, the use of the maximum likelihood (ML) criterion at the reception leads to an optimal solution. For the transmitter, Orthogonal Frequency Division Multiplexing (OFDM) is considered [106][85][86]. However, high peak to average power ratio (PAPR) at the OFDM transmitter caused by the Inverse Fast Fourier Transform (IFFT) operation implemented in each transmit antenna which makes the design of High Power Amplifier (HPA) a challenging task. In this context, a design of a new modified reduced PAPR SM/SIMO structure is required.

Besides, a lot of recent researches give a great interest to the communication channel between UAVs and the Ground Control Station (GCS) as it has a great effect on the performance of system [127] [116] . In this context, this chapter starts to give an analyze of the performance of SM/SIMO system, taking into account the different effects introduced real-world channels is studied. In fact, a simplified model of spatially correlated Ricean MIMO channels is given and a three dimensional channel model is derived. Based on the considered space diversity model, it is shown in [86] that when the distance in wavelengths separating two adjacent transmit antennas, d_e, and the distance in wavelengths separating two adjacent receive antennas, d_r, are both sufficiently large than $\frac{1}{2}$ i.e. $d_e > \frac{1}{2}$ and $d_r > \frac{1}{2}$, we can assume that the signals relative to multipath component become spatially uncorrelated. In this case, the system performance heavily depends on the Rice factor K_{LOS} given by the observed air-to-ground (A2G) channel and consequently, it is important to study the use cases of spatial modulation in relation to the nature of the environment (non Line-of-Sight/Line-of-Sight) below the flying UAV/aircraft. According to the characteristics of the actual communications environment of UAV/aircraft, we study the performance analysis of the classical CP-aided OFDM-SM-ML and CP-aided OFDM-SIMO-ML systems over spatially correlated Ricean MIMO channels for different values of K_{LOS}.

5.2 Expression of Air-to-ground MIMO channel

Assuming a number of $\mathrm{N_t}$ transmit antennas at emission and a number of $\mathrm{N_r}$ receive antennas at the receiver, the Single-Input Single-Output (SISO) A2G channel between the transmit antenna $1 \leq n_\mathrm{t} \leq \mathrm{N_t}$ element and the receive antenna $1 \leq n_\mathrm{r} \leq \mathrm{N_r}$ element is noted $\mathrm{h}_a^{(n_\mathrm{r},n_\mathrm{t})}(t,\tau)$ and previously expressed in (1.45) as:

$$\mathrm{h}_a^{(n_\mathrm{r},n_\mathrm{t})}(t,\tau) = \sqrt{\frac{\mathrm{K_{LOS}}}{1+\mathrm{K_{LOS}}}}\,\delta(\tau) \;+\; \frac{1}{\sqrt{1+\mathrm{K_{LOS}}}}\,\widetilde{h}_a^{(n_\mathrm{r},n_\mathrm{t})}(t,\tau) \tag{5.3}$$

In MIMO communication, we define a space correlated MIMO channel matrix having this form:

$$\mathbf{H}_{i,n} = \begin{bmatrix} \mathrm{H}_{i,n}^{(1,1)} & \mathrm{H}_{i,n}^{(1,2)} & \dots & \mathrm{H}_{i,n}^{(1,\mathrm{N_t})} \\ \mathrm{H}_{i,n}^{(2,1)} & \mathrm{H}_{i,n}^{(2,2)} & \dots & \mathrm{H}_{i,n}^{(2,\mathrm{N_t})} \\ \vdots & \vdots & \ddots & \vdots \\ \mathrm{H}_{i,n}^{(\mathrm{N_r},1)} & \mathrm{H}_{i,n}^{(\mathrm{N_r},2)} & \dots & \mathrm{H}_{i,n}^{(\mathrm{N_r},\mathrm{N_t})} \end{bmatrix} = \sqrt{\frac{\mathrm{K_{LOS}}}{1+\mathrm{K_{LOS}}}} + \frac{1}{\sqrt{1+\mathrm{K_{LOS}}}} \times \mathbf{R}_{\mathrm{H,Rx}}^{\frac{1}{2}} \,.\widetilde{\mathbf{H}}_n.\, \mathbf{R}_{\mathrm{H,Tx}}^{\frac{1}{2}} \tag{5.4}$$

The channel matrix $\widetilde{\mathbf{H}}_n$ is a stochastic full-rank $\mathrm{N_r} \times \mathrm{N_t}$ matrix with complex Gaussian elements:

$$\widetilde{\mathbf{H}}_n = \begin{bmatrix} \widetilde{\mathrm{H}}_{i,n}^{(1,1)} & \widetilde{\mathrm{H}}_{i,n}^{(1,2)} & \dots & \widetilde{\mathrm{H}}_{i,n}^{(1,\mathrm{N_t})} \\ \widetilde{\mathrm{H}}_{i,n}^{(2,1)} & \widetilde{\mathrm{H}}_{i,n}^{(2,2)} & \dots & \widetilde{\mathrm{H}}_{i,n}^{(2,\mathrm{N_t})} \\ \vdots & \vdots & \ddots & \vdots \\ \widetilde{\mathrm{H}}_{i,n}^{(\mathrm{N_r},1)} & \widetilde{\mathrm{H}}_{i,n}^{(\mathrm{N_r},2)} & \dots & \widetilde{\mathrm{H}}_{i,n}^{(\mathrm{N_r},\mathrm{N_t})} \end{bmatrix} \quad \text{with} \quad \widetilde{\mathrm{H}}_{i,n}^{(n_\mathrm{r},n_\mathrm{t})} = \sum_{l=-\infty}^{+\infty} \widetilde{h}_a^{(n_\mathrm{r},n_\mathrm{t})}(l)\; e^{-2\pi j \frac{ln}{N}} \tag{5.5}$$

Each element of the matrix $\widetilde{\mathrm{H}}_{i,n}^{(n_\mathrm{r},n_\mathrm{t})}$ represents the frequency response at the frequency index n of the impulse response $\widetilde{h}_a^{(n_\mathrm{r},n_\mathrm{t})}(t,\tau)$ between the transmit antenna n_t element and the receive antenna n_r element. Furthermore, the frequency responses $\left\{\widetilde{\mathrm{H}}_{i,n}^{(n_\mathrm{r},n_\mathrm{t})}\right\}$ are assumed decorrelated and varying according a zero-mean normalized Gaussian distribution to verify:

$$\mathbb{E}\left\{\widetilde{\mathrm{H}}_{i,n}^{(n_\mathrm{r},n_\mathrm{t})}\right\} = 0 \qquad \mathbb{E}\left\{\left|\widetilde{\mathrm{H}}_{i,n}^{(n_\mathrm{r},n_\mathrm{t})}\right|^2\right\} = 1 \qquad \text{and} \qquad \mathbb{E}\left\{\widetilde{\mathbf{H}}_n^H.\widetilde{\mathbf{H}}_n\right\} = \mathrm{N_r} \times \begin{bmatrix} 1 & 0 & \cdots & 0 \\ 0 & 1 & \cdots & 0 \\ \vdots & & \ddots & \vdots \\ 0 & 0 & \cdots & 1 \end{bmatrix} \tag{5.6}$$

The space correlation matrices $\mathbf{R}_{\mathrm{H,Tx}}$ and $\mathbf{R}_{\mathrm{H,Rx}}$ are calculated as a function of the distance between the receiving and transmitting elements [126]. A short description follows assuming that the $\mathbf{R}_{\mathrm{H,Tx}}$, $\mathbf{R}_{\mathrm{H,Rx}}$ matrices have the form:

$$\mathbf{R}_{\mathrm{H,Tx}} = \begin{bmatrix} 1 & r_T & r_T^2 & \dots & r_T^{N_\mathrm{t}-1} \\ r_T & 1 & r_T & \dots & \vdots \\ r_T^2 & r_T & 1 & \dots & r_T^2 \\ \vdots & \ddots & \ddots & \ddots & r_T \\ r_T^{N_\mathrm{t}-1} & \dots & r_T^2 & r_T & 1 \end{bmatrix} \quad ; \quad \mathbf{R}_{\mathrm{H,Rx}} = \begin{bmatrix} 1 & r_R & r_R^2 & \dots & r_R^{N_\mathrm{r}-1} \\ r_R & 1 & r_R & \dots & \vdots \\ r_R^2 & r_R & 1 & \dots & r_R^2 \\ \vdots & \ddots & \ddots & \ddots & r_R \\ r_R^{N_\mathrm{r}-1} & \dots & r_R^2 & r_R & 1 \end{bmatrix} \tag{5.7}$$

where r_T and r_R are the fading correlation between two adjacent transmit antenna elements and receive antenna elements respectively. The expressions r_T and r_R are approximated by [126]:

$$r_T = \exp(-23.\Lambda_e.d_e^2) \qquad \text{and} \qquad r_R = \exp(-23.\Lambda_r.d_r^2) \tag{5.8}$$

d_e and d_r are respectively the distance in wavelengths between two adjacent transmit antenna elements and receive antenna elements. For each antenna element, the angular spread for the transmitted signals is noted $0 \leq \Lambda_e \leq 1$, respectively $0 \leq \Lambda_r \leq 1$ for the arriving signals at the receiver [34, 126].

5.3 Communication system assumptions

For the propagation MIMO channel, we assume that the distance in wavelengths separating two adjacent transmit antenna elements, d_e, and two adjacent receive antenna elements, d_r, is sufficiently large than $\frac{1}{2}$ i.e. $d_e > \frac{1}{2}$ and $d_r > \frac{1}{2}$. As a result, by considering Equation (5.8), the signals relative to multipath component become spatially uncorrelated. In this case, we can deduce that both the transmit and the receive correlation matrices $\mathbf{R}_{\mathrm{H,Tx}}$ and $\mathbf{R}_{\mathrm{H,Rx}}$ can be approximated to the identity matrix and the expanded expression of the spatially uncorrelated Ricean channel matrix $\mathbf{H}_{i,n}$, given in Equation (5.4), can be reduced to:

$$\mathbf{H}_{i,n} = \sqrt{\frac{\mathrm{K_{LOS}}}{1+\mathrm{K_{LOS}}}} + \frac{1}{\sqrt{1+\mathrm{K_{LOS}}}} \times \widetilde{\mathbf{H}}_n = \left[\mathbf{h}_{i,n}^{(1)}, \mathbf{h}_{i,n}^{(2)}, \ldots, \mathbf{h}_{i,n}^{(\mathrm{N_t})}\right] \tag{5.9}$$

with $\widetilde{\mathbf{H}}_n$ is a stochastic $\mathrm{N_r} \times \mathrm{N_t}$ matrix with uncorrelated normalized complex Gaussian elements and verifying (5.6). In the following, we assume that channel matrix $\widetilde{\mathbf{H}}_n$ is fully known at the receiver. The value of the $\mathrm{K_{LOS}}$ factor depends on the nature of environment. In fact, for rich environment (Urban, Mountainous etc.), the $\mathrm{K_{LOS}}$ factor takes low values. Whereas, for open environment (Flat desert, Rural etc.), the $\mathrm{K_{LOS}}$ factor takes high values. Also, we note that the value of the $\mathrm{K_{LOS}}$ factor is proportional to the UAV altitude. The higher the UAV altitude, the higher $\mathrm{K_{LOS}}$ is. The maximum value of the $\mathrm{K_{LOS}}$ factor is 15 dB for UAV altitude of 30 Km.

5.4 Classical CP-aided OFDM-SM system vs classical CP-aided OFDM-SIMO system

5.4.1 Classical CP-aided OFDM-SM system

Orthogonal frequency division multiplexing (OFDM) is also a well-known communication technique which has already been included in many wireless standards such as 802.11n [29], digital video broadcasting (DVB) and long term evolution (LTE) due to its high spectrum efficiency and robustness against frequency-selective channels. The combination of OFDM and MIMO appears as an competitive alternative for the next generation mobile communications [5]. The attempt to introduce SM to OFDM systems is made by [63, 85, 86, 106] and is termed as CP-aided OFDM-SM, which exhibits enhanced error performance as compared with classical MIMO-OFDM schemes. Furthermore, CP-aided OFDM-SM conveys additional information by active antenna indices of subcarriers, and thus achieves enhanced data rate and robustness against inter-antenna interference within subcarriers. However, this comes at the expense of an increase in hardware complexity, where the number of radio frequency (RF) chains is equal to the number of transmit antennas. Moreover, the implementation of an Inverse Fast Fourier Transform (IFFT) operation in each transmit antenna causes a high peak to average

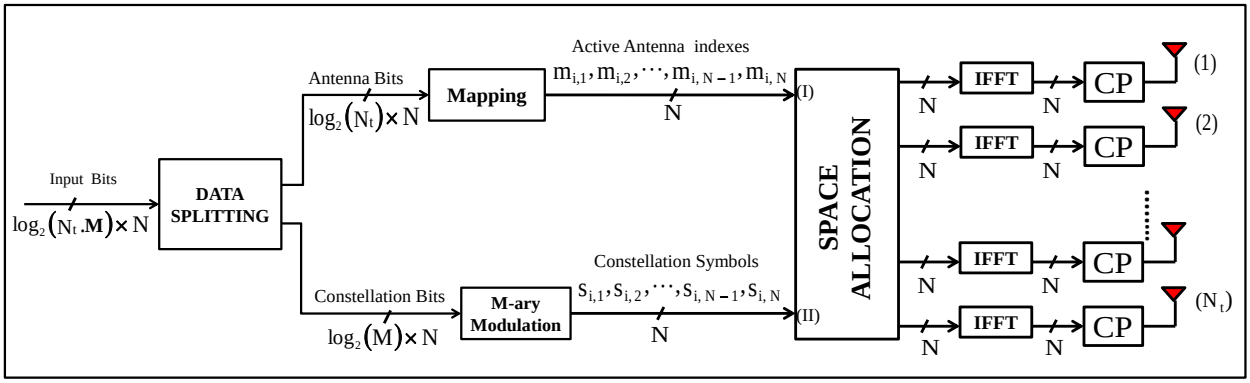

Figure 5.1: *Uncoded transmitter for the classical CP-aided OFDM-SM structure.*

power ratio (PAPR) which makes the design of High Power Amplifier (HPA) a challenging task [63].
For the CP-aided OFDM-SM receiver, different detection techniques are possible, including linear frequency-domain equalization (FDE) detection techniques such as zero forcing (ZF), minimum mean square error (MMSE) and maximum ratio combining (MRC) as a sub-optimal but reduced complexity solutions. The optimal solution is given by the maximum likelihood (ML) detector.

5.4.1.1 Transmitter SM structure

We consider a multiple input-multiple output (MIMO) communication system with $\mathrm{N_t}$ transmit antennas and $\mathrm{N_r}$ receive antennas. The transmitter of the classical CP-aided OFDM-SM is given in Figure 5.1.
We consider MIMO communication system with $\mathrm{N_t}$ transmit antennas and $\mathrm{N_r}$ receive antennas. Let us consider a sequence of independent random bits to be transmitted over a uncorrelated Ricean MIMO channel. Furthermore, we consider a frame based transmission with a symbol period $\mathrm{T_s}$ and a modulation order M. The considered M-ary constellation symbols are drawn from a discrete alphabet $\chi = \{\mathcal{C}_1, \mathcal{C}_2, \ldots, \mathcal{C}_M\}$.
Each frame contains a number of N_f sub-frames. The size of each sub-frame is $N \times \log_2(M.\mathrm{N_t})$ bits, where N is a non-zero positive integer which denotes the number of modulated symbols in each transmit sub-frame.

Data splitting and frequency domain processing: For each transmit sub-frame $1 \leq i \leq N_f$, the transmitter starts to split the bit sequence $\mathbf{u}_i$ into two bit blocks $\mathbf{u}_i^a$ and $\mathbf{u}_i^d$ verifying $\mathbf{u}_i = [\mathbf{u}_i^a, \mathbf{u}_i^d]$. The first bit block $\mathbf{u}_i^a$ contains $N \times \log_2(\mathrm{N_t})$ bits and it is designed to select the active transmit antennas. The second bit block $\mathbf{u}_i^d$ contains $N \times \log_2(M)$ bits and it is designed to transmit constellation symbols. The two blocks will be processed as follows:

- The first bit block $\mathbf{u}^a$ being mapped to generate a select antenna vector $\underline{\mathbf{m}}_i = [m_{i,1}, m_{i,2}, \ldots, m_{i,N}]^T$ containing the transmit antenna index $m_{i,n} \in \{1, \ldots, \mathrm{N_t}\}$ for each symbol duration $\mathrm{T_s}$.
- The second bit block $\mathbf{u}_i^d$ will be modulated into a M-ary constellation to provide a sequence of N symbols denoted by $\underline{\mathbf{s}}_i = [s_{i,1}, s_{i,2}, \ldots, s_{i,N}]^T$ where $s_{i,n} = \mathcal{C}_q \in \chi$ and $\mathbb{E}\{s_{i,n}\} = \sigma_s^2 = \frac{1}{M}\sum_{q=1}^{M} |\mathcal{C}_q|^2 = \mathrm{E_s} \times \mathrm{R_s}$ with

$\mathrm{R}_s = 1/\mathrm{T}_s$ is the considered symbol rate and E_s is the symbol energy.

Space allocation in the frequency domain: By using the resulting transmit antenna index sequence $\underline{\mathbf{m}}_i = [m_{i,1}, m_{i,2}, \ldots, m_{i,N}]^T$ and also the resulting modulated sequence $\underline{\mathbf{s}}_i = [s_{i,1}, s_{i,2}, \ldots, s_{i,N}]^T$, a simple antenna coding is used: For each couple $(s_{i,n}, m_{i,n})$ we associate a column vector $\mathbf{x}_{i,n}$ obtained as follows:

$$\mathbf{x}_{i,n} = \begin{bmatrix} x_{i,n}^{(1)} \\ x_{i,n}^{(2)} \\ \vdots \\ x_{i,n}^{(\mathrm{N_t})} \end{bmatrix} = [\underbrace{0,\ldots,0}_{(m_{i,n}-1)}, s_{i,n}, \underbrace{0,\ldots,0}_{\mathrm{N_t}-m_{i,n}}]^T = [\underbrace{0,\ldots,0}_{(m_{i,n}-1)}, \mathcal{C}_q, \underbrace{0,\ldots,0}_{\mathrm{N_t}-m_{i,n}}]^T \tag{5.10}$$
$$\forall \quad 1 \leq n \leq N \qquad \text{and} \qquad \forall \quad 1 \leq i \leq N_f$$

Time domain processing: The resulting matrix $[\mathbf{x}_{i,1}, \mathbf{x}_{i,2}, \ldots, \mathbf{x}_{i,N}]$ is transformed to the time domain by using an Inverse Fast Fourier Transform (IFFT) operation. Using the Fourier matrix $\mathbf{F}_N$ of size $N \times N$, the resulting matrix $\mathbf{E}_i = \left[\mathbf{e}_i^{(1)}, \mathbf{e}_i^{(2)}, \ldots, \mathbf{e}_i^{(\mathrm{N_t})}\right]^T$ is obtained as follows:

$$\mathbf{E}_i = \begin{bmatrix} \mathbf{e}_i^{(1)} \\ \mathbf{e}_i^{(2)} \\ \vdots \\ \mathbf{e}_i^{(\mathrm{N_t})} \end{bmatrix} = \begin{bmatrix} e_{i,1}^{(1)} & e_{i,2}^{(1)} & \ldots & e_{i,N}^{(1)} \\ e_{i,1}^{(2)} & e_{i,2}^{(2)} & \ldots & e_{i,N}^{(2)} \\ \vdots & \vdots & \ldots & \vdots \\ e_{i,1}^{(\mathrm{N_t})} & e_{i,2}^{(\mathrm{N_t})} & \ldots & e_{i,N}^{(\mathrm{N_t})} \end{bmatrix} = \begin{bmatrix} x_{i,1}^{(1)} & x_{i,2}^{(1)} & \ldots & x_{i,N}^{(1)} \\ x_{i,1}^{(2)} & x_{i,2}^{(2)} & \ldots & x_{i,N}^{(2)} \\ \vdots & \vdots & \ldots & \vdots \\ x_{i,1}^{(\mathrm{N_t})} & x_{i,2}^{(\mathrm{N_t})} & \ldots & x_{i,N}^{(\mathrm{N_t})} \end{bmatrix} . \mathbf{F}_{\mathrm{N}}^H \tag{5.11}$$

In the following, we assume a normalized Fourier matrix $\mathbf{F}_N$ verifying $\mathbf{F}_N . \mathbf{F}_N^H = \mathbf{F}_N^H . \mathbf{F}_N = \mathbf{I}_{N \times N}$ with $\mathbf{I}_{N \times N}$ is the identity matrix with size $N \times N$.

Add Cyclic Prefix: For all transmit antennas, a Cyclic Prefix (CP) block matrix of size $\mathrm{N_t} \times N_g$ is inserted at the beginning of each resulting matrix $\mathbf{E}_i$ in order to cope with inter-symbol interference from the channel and maintain sub-carriers orthogonality.

5.4.1.2 Receiver SM structure

At the receiver $\mathrm{N_r}$ receive antennas is considered. After sampling and removing CP, the resulting time-domain received symbol matrix, associated with frame $1 \leq i \leq N_f$, can be written as:

$$\mathbf{R}_i = \begin{bmatrix} \mathbf{r}_i^{(1)} \\ \mathbf{r}_i^{(2)} \\ \vdots \\ \mathbf{r}_i^{(\mathrm{N_r})} \end{bmatrix} = \begin{bmatrix} r_{i,1}^{(1)} & r_{i,2}^{(1)} & \ldots & r_{i,N}^{(1)} \\ r_{i,1}^{(2)} & r_{i,2}^{(2)} & \ldots & r_{i,N}^{(2)} \\ \vdots & \vdots & \ldots & \vdots \\ r_{i,1}^{(\mathrm{N_r})} & r_{i,2}^{(\mathrm{N_r})} & \ldots & r_{i,N}^{(\mathrm{N_r})} \end{bmatrix} \tag{5.12}$$

Thanks to the add of a circular prefix at the transmitter, the MIMO channel has a circular form. Thus, the time-domain received sample sequence for each receive antenna $1 \leq n_{\mathrm{r}} \leq \mathrm{N_r}$ can be given as follows:

$$\mathbf{r}_i^{(n_{\mathrm{r}})} = \begin{bmatrix} r_{i,1}^{(n_{\mathrm{r}})} \\ r_{i,2}^{(n_{\mathrm{r}})} \\ \vdots \\ r_{i,N}^{(n_{\mathrm{r}})} \end{bmatrix}^T = \sum_{n_{\mathrm{t}}=1}^{\mathrm{N_t}} \mathbf{e}_i^{(n_{\mathrm{t}})} . \left\{ \mathbf{F}_{\mathrm{N}} . diag \begin{bmatrix} \mathrm{H}_{i,1}^{(n_{\mathrm{r}},n_{\mathrm{t}})} \\ \mathrm{H}_{i,2}^{(n_{\mathrm{r}},n_{\mathrm{t}})} \\ \vdots \\ \mathrm{H}_{i,N}^{(n_{\mathrm{r}},n_{\mathrm{t}})} \end{bmatrix} . \mathbf{F}_{\mathrm{N}}^H \right\} + \begin{bmatrix} w_1^{(n_{\mathrm{r}})} \\ w_2^{(n_{\mathrm{r}})} \\ \vdots \\ w_N^{(n_{\mathrm{r}})} \end{bmatrix}^T \tag{5.13}$$

where the resulting noise vector is $\mathbf{w}^{(n_r)} = \left[w_1^{(n_r)}, w_2^{(n_r)}, \ldots, w_N^{(n_r)}\right]^T$ is a centered complex AWGN noise with two-sided spectral density equal to N_0 and the noise variable $\left\{w_n^{(n_r)}\right\}$ having a variance σ_w^2 calculated as:

$$\sigma_w^2 = \mathrm{N}_0 \times \mathrm{R}_s \qquad \text{with} \qquad \mathrm{R}_s = 1/\mathrm{T}_s \tag{5.14}$$

By using the expanded matrix form of the expression of the transmitted vector $\mathbf{e}_i^{(n_t)}$ given in Equation (5.11), the Equation (5.13) can be re-written as the following:

$$\mathbf{r}_i^{(n_r)} = \begin{bmatrix} r_{i,1}^{(n_r)} \\ r_{i,2}^{(n_r)} \\ \vdots \\ r_{i,N}^{(n_r)} \end{bmatrix}^T = \sum_{n_t=1}^{\mathrm{N_t}} \begin{bmatrix} x_{i,1}^{(n_t)} \\ x_{i,2}^{(n_t)} \\ \vdots \\ x_{i,N}^{(n_t)} \end{bmatrix}^T .diag \begin{bmatrix} \mathrm{H}_{i,1}^{(n_r,n_t)} \\ \mathrm{H}_{i,2}^{(n_r,n_t)} \\ \vdots \\ \mathrm{H}_{i,N}^{(n_r,n_t)} \end{bmatrix} .\mathbf{F}_{\mathrm{N}}^H + \begin{bmatrix} w_1^{(n_r)} \\ w_2^{(n_r)} \\ \vdots \\ w_N^{(n_r)} \end{bmatrix}^T \tag{5.15}$$

For each receive antenna $1 \leq n_r \leq \mathrm{N_r}$, the receiver starts to transform the resulting received sequence $\mathbf{r}_i^{(n_r)}$ to the frequency domain by using a Fast Fourier Transform (FFT) operation as follows:

$$\mathbf{y}_i^{(n_r)} = \begin{bmatrix} y_{i,1}^{(n_r)} \\ y_{i,2}^{(n_r)} \\ \vdots \\ y_{i,N}^{(n_r)} \end{bmatrix}^T = \mathbf{r}_i^{(n_r)}.\mathbf{F}_{\mathrm{N}} = \sum_{n_t=1}^{\mathrm{N_t}} \begin{bmatrix} x_{i,1}^{(n_t)} \\ x_{i,2}^{(n_t)} \\ \vdots \\ x_{i,N}^{(n_t)} \end{bmatrix}^T .diag \begin{bmatrix} \mathrm{H}_{i,1}^{(n_r,n_t)} \\ \mathrm{H}_{i,2}^{(n_r,n_t)} \\ \vdots \\ \mathrm{H}_{i,N}^{(n_r,n_t)} \end{bmatrix} + \begin{bmatrix} w_1^{(n_r)} \\ w_2^{(n_r)} \\ \vdots \\ w_N^{(n_r)} \end{bmatrix}^T \tag{5.16}$$

The previous expression of the received frequency domain symbols, can be also re-written in the following form given in each frequency index $1 \leq n \leq N$ as follows:

$$\mathbf{y}_{i,n} = \begin{bmatrix} y_{i,n}^{(1)} \\ y_{i,n}^{(2)} \\ \vdots \\ y_{i,n}^{(\mathrm{N_r})} \end{bmatrix} = \begin{bmatrix} \mathrm{H}_{i,n}^{(1,1)} & \mathrm{H}_{i,n}^{(1,2)} & \ldots & \mathrm{H}_{i,n}^{(1,\mathrm{N_t})} \\ \mathrm{H}_{i,n}^{(2,1)} & \mathrm{H}_{i,n}^{(2,2)} & \ldots & \mathrm{H}_{i,n}^{(2,\mathrm{N_t})} \\ \vdots & \vdots & \ddots & \vdots \\ \mathrm{H}_{i,n}^{(\mathrm{N_r},1)} & \mathrm{H}_{i,n}^{(\mathrm{N_r},2)} & \ldots & \mathrm{H}_{i,n}^{(\mathrm{N_r},\mathrm{N_t})} \end{bmatrix} . \begin{bmatrix} x_{i,n}^{(1)} \\ x_{i,n}^{(2)} \\ \vdots \\ x_{i,n}^{(\mathrm{N_t})} \end{bmatrix} + \begin{bmatrix} w_n^{(1)} \\ w_n^{(2)} \\ \vdots \\ w_n^{(\mathrm{N_r})} \end{bmatrix} = \mathbf{H}_{i,n}.\mathbf{x}_{i,n} + \mathbf{w}_n = s_{i,n}\, \mathbf{h}_{i,n}^{(m_{i,n})} + \mathbf{w}_n \tag{5.17}$$

Optimal detector: ML-based receiver Let us assume that the transmitted signals are equally likely. As in [64], the optimal detector based on ML criterion is given as:

$$[\widehat{m}, \widehat{q}] = \underset{\substack{m \in \{1,2,\ldots,\mathrm{N_t}\} \\ q \in \{1,2,\ldots,M\}}}{\operatorname{argmax}} \Pr\left(\mathbf{y}_{i,n} | \mathbf{H}_{i,n}, \mathbf{x}_{i,n}\right) \qquad \text{with} \qquad \Pr\left(\mathbf{y}_{i,n} | \mathbf{H}_{i,n}, \mathbf{x}_{i,n}\right) \propto \exp\left(- \frac{\left\| \mathbf{y}_{i,n} - \mathcal{C}_q\ \mathbf{h}_{i,n}^{(m)} \right\|^2}{\sigma_w^2} \right) \tag{5.18}$$

where the conditional probability density function (pdf) is represented by $\Pr\left(\mathbf{y}_{i,n} | \mathbf{H}_{i,n}, \mathbf{x}_{i,n}\right)$. Antenna indexes and constellation data symbols are recovered by the joint detection as given in Equation (5.18):

$$\widehat{m}_{i,n} = \widehat{m} \qquad \text{and} \qquad \widehat{s}_{i,n} = \mathcal{C}_{\hat{q}} \qquad \forall \quad 1 \leq n \leq N \tag{5.19}$$

The computational complexity of the SM–ML receiver in Equation (5.18) is evaluated in [129] and is equal to:

$$\text{Complexity} = \mathcal{O}\left(8 \times \mathrm{N_r} \times (\mathrm{N_t} \times M) \times N\right) \tag{5.20}$$

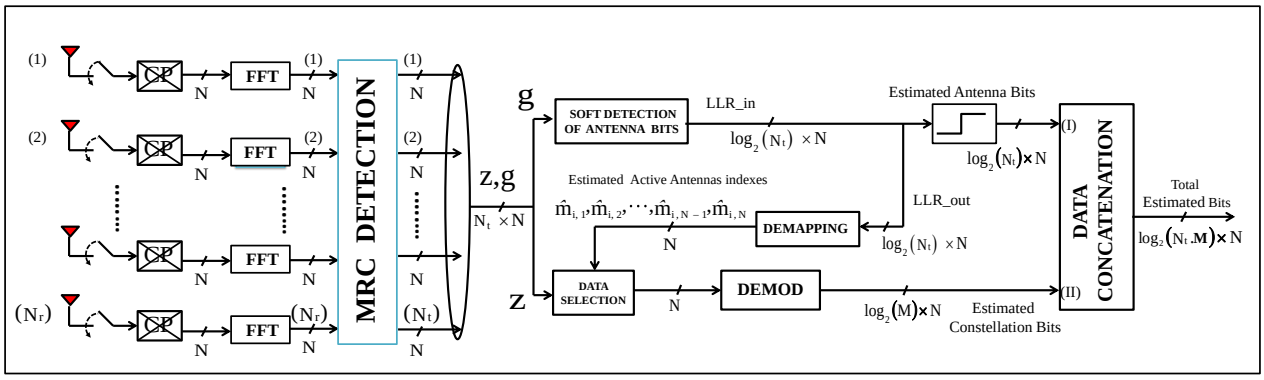

Figure 5.2: *Uncoded receiver based on MRC detection for the classical CP-aided OFDM-SM structure.*

The complexity is computed as the number of real multiplicative operations $(\times, \div)$ needed. As as the ML detector searches through the whole transmit and receive search spaces. Note, evaluating the Euclidean distance $\left\|\mathbf{y}_{i,n} - \mathcal{C}_q\ \mathbf{h}_{i,n}^{(m)}\right\|^2$ which is considered as the sum of $\mathrm{N_r}$ absolute squared complex subtractions $\left\|y_{i,n}^{(n_r)} - \mathcal{C}_q\ \mathrm{H}_{i,n}^{(n_r,n_t)}\right\|^2$ and the latter requires 2 complex multiplications, where each complex multiplication requires 4 real multiplications. As a result, each Euclidean distance $\left\|\mathbf{y}_{i,n} - \mathcal{C}_q\ \mathbf{h}_{i,n}^{(m)}\right\|^2$ requires a number of $8 \times \mathrm{N_r}$ real multiplications.

Sub-optimal MRC-based receiver For the MRC detection, the considered receiver is presented in Figure 5.2. The Maximum Ratio Combining (MRC) detector [75] is a sub-optimal linear detector used to detect the active transmit antenna indexes and the transmitted constellation symbols. After MRC decoding, a resulting output vector $\mathbf{z}_{i,n}$ is obtained which is expressed as:

$$\mathbf{z}_{i,n} = \begin{bmatrix} z_{i,n}^{(1)} \\ z_{i,n}^{(2)} \\ \vdots \\ z_{i,n}^{(\mathrm{N_t})} \end{bmatrix} = \begin{bmatrix} \left\|\mathbf{h}_{i,n}^{(1)}\right\|^2 & 0 & \cdots & 0 \\ 0 & \left\|\mathbf{h}_{i,n}^{(2)}\right\|^2 & \cdots & 0 \\ \vdots & & \ddots & \vdots \\ 0 & 0 & \cdots & \left\|\mathbf{h}_{i,n}^{(\mathrm{N_t})}\right\|^2 \end{bmatrix}^{-1} .\mathbf{H}_{i,n}^{H}.\mathbf{y}_{i,n} \qquad \text{for} \qquad 1 \leq n \leq N \tag{5.21}$$

The output vector $\mathbf{z}_{i,n}$ is an estimation of the transmitted SM vector $\mathbf{x}_{i,n}$. Furthermore, the output vector $\mathbf{z}_{i,n}$ is used to estimate the active transmit antenna indexes. Indeed, in the presence of AWGN noise and spatial correlation, the antenna indexes should be estimated prior to detection of the transmitted constellation symbols. By finding the maximum value of the obtained vector elements, $\left\{\left\|\mathbf{h}_{i,n}^{(n_t)}\right\|\ z_{i,n}^{(n_t)}\right\}$, an estimation of the antenna index is obtained as the following:

$$\widehat{m}_{i,n} = \underset{n_t \in \{1,2,\ldots,\mathrm{N_t}\}}{\operatorname{argmax}} \left\{\left\|\mathbf{h}_{i,n}^{(n_t)}\right\|^2 \left|z_{i,n}^{(n_t)}\right|^2\right\} \qquad 1 \leq n \leq N \tag{5.22}$$

In particular case when we consider a normalized channel matrix $\left\|\mathbf{h}_{i,n}^{(n_t)}\right\| = 1$ for $1 \leq n_t \leq \mathrm{N_t}$ as given in [86], the expression of output MRC is reduced to:

$$\mathbf{z}_{i,n} = \mathbf{H}_{i,n}^{H}.\mathbf{y}_{i,n} \qquad \text{for} \qquad 1 \leq n \leq N \tag{5.23}$$

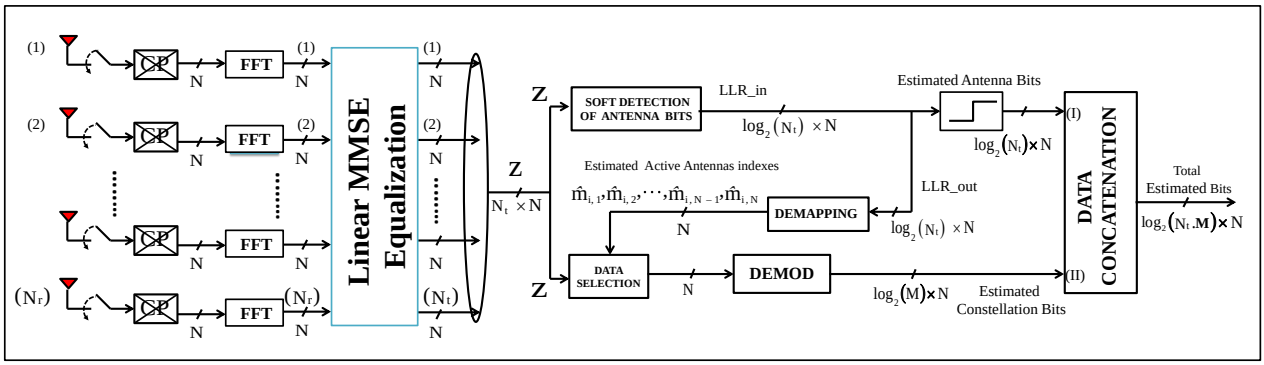

Figure 5.3: *Uncoded receiver based on MMSE detection for the classical CP-aided OFDM-SM structure.*

and the active antenna detection is reduced to find the the maximum value of the $\mathbf{z}_{i,n}$ elements.
Then, for data symbol detection, we can demodulate the transmitted constellation symbols $s_{i,n}$ by quantizing the corresponding maximum value $z_{i,n}^{(\widehat{m}_{i,n})}$ as in [86]:

$$\widehat{s}_{i,n} = \underset{\mathcal{C}_q \in \chi}{\operatorname{argmin}} \left| \widetilde{z}_{i,n}^{(\widehat{m}_{i,n})} - \mathcal{C}_q \right|^2 \qquad 1 \leq n \leq N \tag{5.24}$$

Finally, at this stage of the study, what can be said is that the MRC detector can offer a simple detection and compared to the MMSE-based of the ZF-based detector, the channel equalization is simplified to a channel inversion operation on each sub-carrier.

Sub-optimal MMSE-based detection For the MMSE detection, the considered receiver is presented in Figure 5.3. By using Minimum Mean Square Error (MMSE) criterion, a sub-optimal detection can be considered to detect the active transmit antenna indexes and the transmitted constellation symbols. The MMSE detector can be expressed as:

$$\mathbf{z}_{i,n} = \begin{bmatrix} z_{i,n}^{(1)} \\ z_{i,n}^{(2)} \\ \vdots \\ z_{i,n}^{(\mathrm{N_t})} \end{bmatrix} = \mathbf{W}_{i,n}.\mathbf{y}_{i,n} = \left[\mathbf{H}_{i,n}^H.\mathbf{H}_{i,n} + \frac{\sigma_w^2}{(\sigma_s^2/\mathrm{N_t})} \times \mathbf{I}_{\mathrm{N_t} \times \mathrm{N_t}} \right]^{-1} .\mathbf{H}_{i,n}^H.\mathbf{y}_{i,n} \qquad \text{for} \qquad 1 \leq n \leq N \tag{5.25}$$

As for the MRC detector, the MMSE detector follows two steps. First, an estimation of the active antenna index is given by finding the maximum value of the output vector $\mathbf{z}_{i,n}$. Second, the vector element having the maximum value will demodulated to detect the transmitted constellation symbol. The two steps are expressed as the following:

$$\begin{cases} \text{Step 1: } \underline{\text{Estimate antenna indexes:}} & \widehat{m}_{i,n} = \underset{n_t \in \{1,2,\ldots,\mathrm{N_t}\}}{\operatorname{argmax}} \left| z_{i,n}^{(n_t)} \right|^2 \qquad 1 \leq n \leq N \\ \text{Step 2: } \underline{\text{Estimate constellation symbols:}} & \widehat{s}_{i,n} = \underset{\mathcal{C}_q \in \chi}{\operatorname{argmin}} \left| \widetilde{z}_{i,n}^{(\widehat{m}_{i,n})} - \mathcal{C}_q \right|^2 \qquad 1 \leq n \leq N \end{cases}$$

Finally, at this stage of the study, what can be said is that the MMSE detector allows us to consider SISO channel decoder. Furthermore, MMSE-based decoder can offer a simple detection with reasonable computational complexity compared to the optimal ML-based detector. The complexity of the MMSE detector is

evaluated in [128] and is equal to:

$$\text{Complexity} = \mathcal{O}\left(\mathrm{N_r} \times \mathrm{N_t^2} \times N\right) + \mathcal{O}\left(\mathrm{N_t^3} \times N\right) \tag{5.26}$$

5.4.2 Classical CP-aided OFDM-SIMO system

5.4.2.1 Transmitter SIMO structure

We consider a number of $\mathrm{N_t}$ of transmit antennas. Only a single transmit antenna, having a antenna index $m_0 \in \{1,\ldots,\mathrm{N_t}\}$, is activated during all transmitted sub-frames. The transmitter of the classical CP-aided OFDM-SIMO is given in Figure 5.4.

Let us consider a sequence of independent random bits to be transmitted over a uncorrelated Ricean MIMO channel. Furthermore, we consider a frame based transmission with a symbol period $\mathrm{T_s}$ and a modulation order M. Each frame contains a number of N_f sub-frames. The size of each sub-frame is $N \times \log_2(M)$ bits. The considered M-ary constellation symbols are drawn from a discrete alphabet $\chi = \{\mathcal{C}_1, \mathcal{C}_2, \ldots, \mathcal{C}_M\}$.

The input bit block $\mathbf{u}_i^d$ will be modulated into a M-ary constellation to provide a sequence of N constellation symbols denoted by $\underline{\mathbf{s}}_i = [s_{i,1}, s_{i,2}, \ldots, s_{i,N}]^T$ where $s_{i,n} = \mathcal{C}_q \in \chi$

Space allocation in the frequency domain: Assuming m_0 is the index of the selected active transmit antenna, the obtained constellation sequence $\underline{\mathbf{s}}_i$ will be transmitted via the m_0 transmit antenna. As a result, we have:

$$\begin{bmatrix} x_{i,1}^{(1)} & x_{i,2}^{(1)} & \ldots & x_{i,N}^{(1)} \\ \vdots & \vdots & \ldots & \vdots \\ x_{i,1}^{(m_0)} & x_{i,2}^{(m_0)} & \ldots & x_{i,N}^{(m_0)} \\ \vdots & \vdots & \ldots & \vdots \\ x_{i,1}^{(\mathrm{N_t})} & x_{i,2}^{(\mathrm{N_t})} & \ldots & x_{i,N}^{(\mathrm{N_t})} \end{bmatrix} = \begin{bmatrix} 0 & 0 & \ldots & 0 \\ \vdots & \vdots & \ldots & \vdots \\ s_{i,1} & s_{i,2} & \ldots & s_{i,N} \\ \vdots & \vdots & \ldots & \vdots \\ 0 & 0 & \ldots & 0 \end{bmatrix} \tag{5.27}$$

Time domain processing: The resulting matrix $[\mathbf{x}_{i,1}, \mathbf{x}_{i,2}, \ldots, \mathbf{x}_{i,N}]$ is transformed to the time domain by using an Inverse Fast Fourier Transform (IFFT) operation. Using the Fourier matrix $\mathbf{F}_N$ of size $N \times N$, the resulting matrix $\mathbf{E}_i = \left[\mathbf{e}_i^{(1)}, \mathbf{e}_i^{(2)}, \ldots, \mathbf{e}_i^{(\mathrm{N_t})}\right]^T$ is obtained as follows:

$$\mathbf{E}_i = \begin{bmatrix} \mathbf{e}_i^{(1)} \\ \mathbf{e}_i^{(2)} \\ \vdots \\ \mathbf{e}_i^{(\mathrm{N_t})} \end{bmatrix} = \begin{bmatrix} e_{i,1}^{(1)} & e_{i,2}^{(1)} & \ldots & e_{i,N}^{(1)} \\ e_{i,1}^{(2)} & e_{i,2}^{(2)} & \ldots & e_{i,N}^{(2)} \\ \vdots & \vdots & \ldots & \vdots \\ e_{i,1}^{(\mathrm{N_t})} & e_{i,2}^{(\mathrm{N_t})} & \ldots & e_{i,N}^{(\mathrm{N_t})} \end{bmatrix} = \begin{bmatrix} x_{i,1}^{(1)} & x_{i,2}^{(1)} & \ldots & x_{i,N}^{(1)} \\ x_{i,1}^{(2)} & x_{i,2}^{(2)} & \ldots & x_{i,N}^{(2)} \\ \vdots & \vdots & \ldots & \vdots \\ x_{i,1}^{(\mathrm{N_t})} & x_{i,2}^{(\mathrm{N_t})} & \ldots & x_{i,N}^{(\mathrm{N_t})} \end{bmatrix} . \mathbf{F}_{\mathrm{N}}^H \tag{5.28}$$

Add Cyclic Prefix: For all transmit antennas, a Cyclic Prefix (CP) block matrix of size $\mathrm{N_t} \times N_g$ is inserted at the beginning of each resulting matrix $\mathbf{E}_i$ in order to cope with inter-symbol interference from the channel and maintain sub-carriers orthogonality.

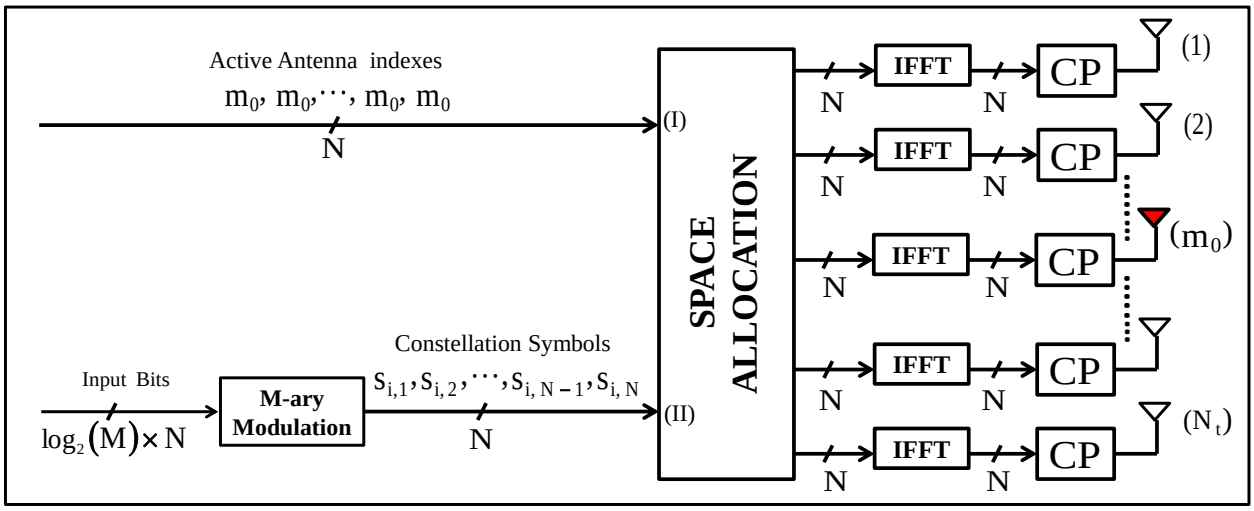

Figure 5.4: *Uncoded transmitter for the classical CP-aided OFDM-SIMO structure.*

5.4.2.2 Receiver SIMO structure

At the receiver a number of $\mathrm{N_r}$ receive antennas are considered. Thanks to the add of a circular prefix at the transmitter, the MIMO channel has a circular form. Thus, the time-domain received sample sequence for each receive antenna $1 \leq n_{\mathrm{r}} \leq \mathrm{N_r}$ can be given as follows:

$$\begin{aligned}\mathbf{r}_i^{(n_{\mathrm{r}})} = \begin{bmatrix} r_{i,1}^{(n_{\mathrm{r}})} \\ r_{i,2}^{(n_{\mathrm{r}})} \\ \vdots \\ r_{i,N}^{(n_{\mathrm{r}})} \end{bmatrix}^T &= \sum_{n_{\mathrm{t}}=1}^{\mathrm{N_t}} \begin{bmatrix} x_{i,1}^{(n_{\mathrm{t}})} \\ x_{i,2}^{(n_{\mathrm{t}})} \\ \vdots \\ x_{i,N}^{(n_{\mathrm{t}})} \end{bmatrix}^T . \left\{ \mathbf{F}_{\mathrm{N}} . diag \begin{bmatrix} \mathrm{H}_{i,1}^{(n_{\mathrm{r}},n_{\mathrm{t}})} \\ \mathrm{H}_{i,2}^{(n_{\mathrm{r}},n_{\mathrm{t}})} \\ \vdots \\ \mathrm{H}_{i,N}^{(n_{\mathrm{r}},n_{\mathrm{t}})} \end{bmatrix} . \mathbf{F}_{\mathrm{N}}^H \right\} + \begin{bmatrix} w_1^{(n_{\mathrm{r}})} \\ w_2^{(n_{\mathrm{r}})} \\ \vdots \\ w_N^{(n_{\mathrm{r}})} \end{bmatrix}^T \\ &= \begin{bmatrix} s_{i,1} \\ s_{i,2} \\ \vdots \\ s_{i,N} \end{bmatrix}^T . diag \begin{bmatrix} \mathrm{H}_{i,1}^{(n_{\mathrm{r}},m_0)} \\ \mathrm{H}_{i,2}^{(n_{\mathrm{r}},m_0)} \\ \vdots \\ \mathrm{H}_{i,N}^{(n_{\mathrm{r}},m_0)} \end{bmatrix} . \mathbf{F}_{\mathrm{N}}^H + \begin{bmatrix} w_1^{(n_{\mathrm{r}})} \\ w_2^{(n_{\mathrm{r}})} \\ \vdots \\ w_N^{(n_{\mathrm{r}})} \end{bmatrix}^T \end{aligned} \tag{5.29}$$

Optimal detector: ML-based receiver and MRC-based receiver For the ML-based and the MRC based detection, the receiver starts to transform the received signal to the frequency domain by using by using a Fast Fourier Transform (FFT) operation. As a result, the obtained frequency-domain received sequence can be expressed as:

$$\mathbf{y}_i^{(n_{\mathrm{r}})} = \begin{bmatrix} y_{i,1}^{(n_{\mathrm{r}})} \\ y_{i,2}^{(n_{\mathrm{r}})} \\ \vdots \\ y_{i,N}^{(n_{\mathrm{r}})} \end{bmatrix}^T = \mathbf{r}_i^{(n_{\mathrm{r}})} . \mathbf{F}_{\mathrm{N}} = \begin{bmatrix} s_{i,1} \\ s_{i,2} \\ \vdots \\ s_{i,N} \end{bmatrix}^T . diag \begin{bmatrix} \mathrm{H}_{i,1}^{(n_{\mathrm{r}},m_0)} \\ \mathrm{H}_{i,2}^{(n_{\mathrm{r}},m_0)} \\ \vdots \\ \mathrm{H}_{i,N}^{(n_{\mathrm{r}},m_0)} \end{bmatrix} + \begin{bmatrix} w_1^{(n_{\mathrm{r}})} \\ w_2^{(n_{\mathrm{r}})} \\ \vdots \\ w_N^{(n_{\mathrm{r}})} \end{bmatrix}^T \tag{5.30}$$

On other hand, the previous expression of the received frequency domain symbols, can be also re-written in the following form given in each frequency index $1 \leq n \leq N$ as follows:

$$\mathbf{y}_{i,n} = \begin{bmatrix} y_{i,n}^{(1)} \\ y_{i,n}^{(2)} \\ \vdots \\ y_{i,n}^{(\mathrm{N_r})} \end{bmatrix} = s_{i,n} \begin{bmatrix} \mathrm{H}_{i,n}^{(1,m_0)} \\ \mathrm{H}_{i,n}^{(2,m_0)} \\ \vdots \\ \mathrm{H}_{i,n}^{(\mathrm{N_r},m_0)} \end{bmatrix} + \begin{bmatrix} w_n^{(1)} \\ w_n^{(2)} \\ \vdots \\ w_n^{(\mathrm{N_r})} \end{bmatrix} = s_{i,n}\ \mathbf{h}_{i,n}^{(m_0)} + \mathbf{w}_n \tag{5.31}$$

1. ML-based receiver: Let us assume that the transmitted signals are equally likely, the optimal detector based on ML is given as:

$$\begin{aligned} \widehat{s}_{i,n}^{\mathrm{ML}} = \underset{\mathcal{C}_q \in \chi}{\operatorname{argmin}} \left\| \mathbf{y}_{i,n} - \mathcal{C}_q\ \mathbf{h}_{i,n}^{(m_0)} \right\|^2 &= \underset{\mathcal{C}_q \in \chi}{\operatorname{argmin}} \left\{ \left\| \mathbf{h}_{i,n}^{(m_0)} \right\|^2 \left(|\mathcal{C}_q|^2 - 2\Re \left\{ \mathcal{C}_q^* \frac{\left[\mathbf{h}_{i,n}^{(m_0)} \right]^H . \mathbf{y}_{i,n}}{\left\| \mathbf{h}_{i,n}^{(m_0)} \right\|^2} \right\} \right) \right\} \\ &= \underset{\mathcal{C}_q \in \chi}{\operatorname{argmin}} \left\{ |\mathcal{C}_q|^2 - 2\Re \left\{ \mathcal{C}_q^* \frac{\left[\mathbf{h}_{i,n}^{(m_0)} \right]^H . \mathbf{y}_{i,n}}{\left\| \mathbf{h}_{i,n}^{(m_0)} \right\|^2} \right\} \right\} \qquad 1 \leq n \leq N \end{aligned} \tag{5.32}$$

2. MRC-based receiver: The MRC receiver is presented in Figure 5.5. In SIMO system MRC-based detector is equivalent to ML-based-based detector. At the output of MRC decoding, a vector $\mathbf{z}_{i,n} = \left[z_{i,n}^{(1)}, z_{i,n}^{(2)}, \ldots, z_{i,n}^{(\mathrm{N_t})} \right]^T$ where each vector component $z_{i,n}^{(n_t)}$ is expressed as:

$$z_{i,n}^{(n_t)} = \frac{\left[\mathbf{h}_{i,n}^{(n_t)} \right]^H . \mathbf{y}_{i,n}}{\left\| \mathbf{h}_{i,n}^{(n_t)} \right\|^2} \tag{5.33}$$

Then, by knowing the index of the active transmit antenna, m_0, the receiver selects the received symbols corresponding to the m_0-th transmit antenna as follows:

$$[z_{i,1}, z_{i,2}, \ldots, z_{i,N}]^T = \left[z_{i,1}^{(m_0)}, z_{i,2}^{(m_0)}, \ldots, z_{i,N}^{(m_0)} \right]^T \tag{5.34}$$

Finally, we can demodulate the transmitted constellation symbols $s_{i,n}$ by quantizing the corresponding maximum value as:

$$\begin{aligned} \widehat{s}_{i,n}^{\mathrm{MRC}} = \underset{\mathcal{C}_q \in \chi}{\operatorname{argmin}} \left| z_{i,n} - \mathcal{C}_q \right|^2 &= \underset{\mathcal{C}_q \in \chi}{\operatorname{argmin}} \left\{ |\mathcal{C}_q|^2 - 2\Re \left\{ \mathcal{C}_q^*\ z_{i,n} \right\} \right\} \\ &= \underset{\mathcal{C}_q \in \chi}{\operatorname{argmin}} \left\{ |\mathcal{C}_q|^2 - 2\Re \left\{ \mathcal{C}_q^* \frac{\left[\mathbf{h}_{i,n}^{(m_0)} \right]^H . \mathbf{y}_{i,n}}{\left\| \mathbf{h}_{i,n}^{(m_0)} \right\|^2} \right\} \right\} = \widehat{s}_{i,n}^{\mathrm{ML}} \qquad 1 \leq n \leq N \end{aligned} \tag{5.35}$$

Sub-optimal MMSE-based detection The MMSE receiver is a sub-optimal receiver for which the detection is done in two steps as shown in Figure 5.6.

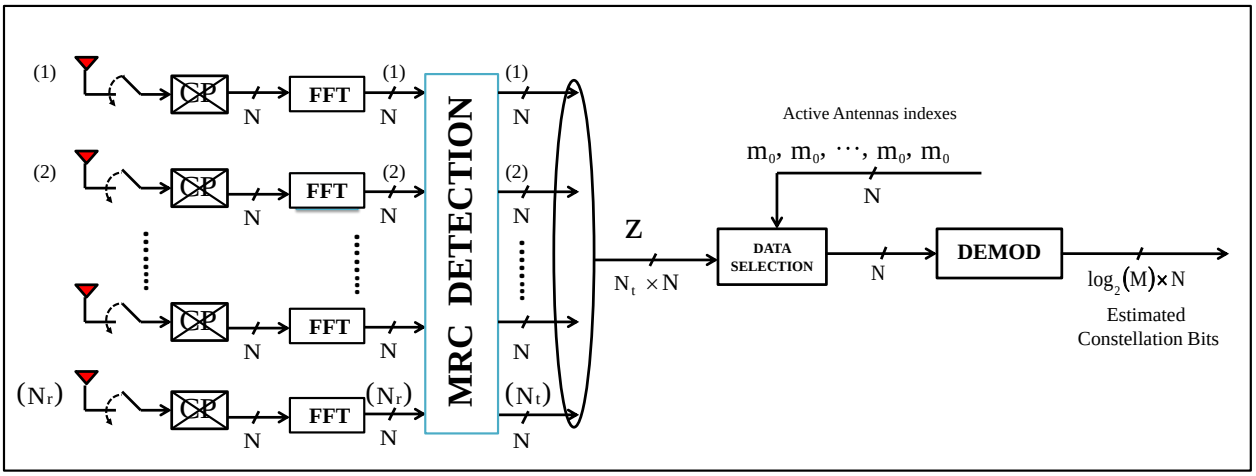

Figure 5.5: *Uncoded receiver based on MRC detection for the classical CP-aided OFDM-SIMO structure.*

- *Frequency-domain transform and averaging*: At first, the receiver calculates the average value of the frequency transform of the $\mathrm{N_r}$ received signals:

$$\mathbf{y}_i = \begin{bmatrix} y_{i,1} \\ y_{i,2} \\ \vdots \\ y_{i,N} \end{bmatrix}^T = \frac{1}{\mathrm{N_r}} \sum_{n_\mathrm{r}=1}^{\mathrm{N_r}} \mathbf{r}_i^{(n_\mathrm{r})} . \mathbf{F}_\mathrm{N} = \begin{bmatrix} s_{i,1} \\ s_{i,2} \\ \vdots \\ s_{i,N} \end{bmatrix}^T . \left\{ \frac{1}{\mathrm{N_r}} \sum_{n_\mathrm{r}=1}^{\mathrm{N_r}} diag \begin{bmatrix} \mathrm{H}_{i,1}^{(n_\mathrm{r},m_0)} \\ \mathrm{H}_{i,2}^{(n_\mathrm{r},m_0)} \\ \vdots \\ \mathrm{H}_{i,N}^{(n_\mathrm{r},m_0)} \end{bmatrix} \right\} + \left\{ \frac{1}{\mathrm{N_r}} \sum_{n_\mathrm{r}=1}^{\mathrm{N_r}} \begin{bmatrix} w_1^{(n_\mathrm{r})} \\ w_2^{(n_\mathrm{r})} \\ \vdots \\ w_N^{(n_\mathrm{r})} \end{bmatrix}^T \right\}$$

$$= \begin{bmatrix} s_{i,1} \\ s_{i,2} \\ \vdots \\ s_{i,N} \end{bmatrix}^T . diag \begin{bmatrix} \mathrm{H}_{i,1}^{(m_0)} \\ \mathrm{H}_{i,2}^{(m_0)} \\ \vdots \\ \mathrm{H}_{i,N}^{(m_0)} \end{bmatrix} + \begin{bmatrix} w_{i,1} \\ w_{i,2} \\ \vdots \\ w_{i,N} \end{bmatrix}^T = \begin{bmatrix} s_{i,1} \\ s_{i,2} \\ \vdots \\ s_{i,N} \end{bmatrix}^T . \mathbf{H}_{i,m_0} + \mathbf{w}_i \tag{5.36}$$

As a result, an equivalent baseband channel $\mathbf{H}_{i,m_0}$ is identified. Moreover, the variance of noise elements of the resulting zero-mean AWGN noise vector $\mathbf{w}_i$ is reduced by the number of the receive antennas:

$$\mathbb{E}\left\{ |w_{i,n}|^2 \right\} = \frac{\sigma_w^2}{\mathrm{N_r}} \qquad \forall \qquad 1 \le n \le N \tag{5.37}$$

- *Linear Frequency-domain MMSE equalization*: For the second step, the receiver applies a reduced complexity linear MMSE equalization in order to generate a biased estimation of the transmitted constellation sequence, $\underline{\mathbf{s}}_i = [s_{i,1}, s_{i,2}, \ldots, s_{i,N}]^T$, denoted by $\mathbf{z}_i$ and calculated as follows:

$$\mathbf{z}_i = \begin{bmatrix} z_{i,1} \\ z_{i,2} \\ \vdots \\ z_{i,N} \end{bmatrix}^T = \mathbf{y}_i . \mathbf{W}_{i,m_0} \approx \alpha^{(m_0)} \left\{ \begin{bmatrix} s_{i,1} \\ s_{i,2} \\ \vdots \\ s_{i,N} \end{bmatrix}^T + \frac{1}{\sqrt{\gamma^{(m_0)}}} \begin{bmatrix} w_{i,1} \\ w_{i,2} \\ \vdots \\ w_{i,N} \end{bmatrix}^T \right\} \tag{5.38}$$

where $\mathbf{W}_{i,m_0} = \mathbf{H}_{i,m_0}^H . \left[\mathbf{H}_{i,m_0} . \mathbf{H}_{i,m_0}^H + \frac{\sigma_w^2}{\mathrm{N_r} . \sigma_s^2} \right]^{-1}$ is a diagonal equalization matrix. The two positive

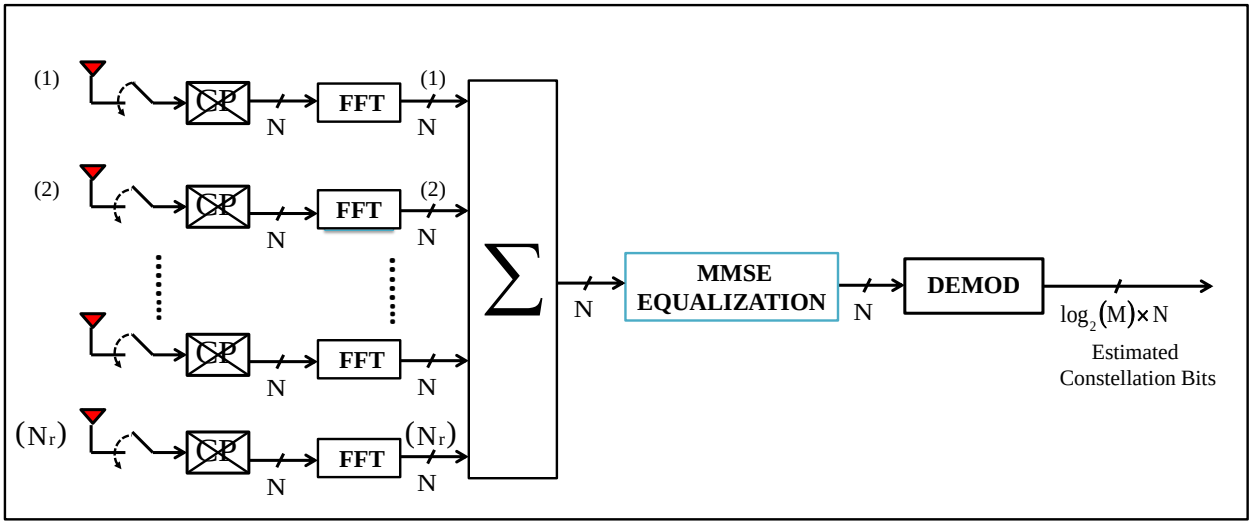

Figure 5.6: *Uncoded receiver based on MMSE detection for the classical CP-aided OFDM-SIMO structure.*

scalars $\alpha^{(m_0)}$ and $\gamma^{(m_0)}$ are defined as:

$$\alpha^{(m_0)} = \frac{1}{N}.\ tr\{\mathbf{H}_{i,m_0}.\mathbf{W}_{i,m_0}\} = \frac{1}{N}\sum_{n=1}^{N} \frac{\left|\mathrm{H}_{i,n}^{(m_0)}\right|^2}{\left|\mathrm{H}_{i,n}^{(m_0)}\right|^2 + \frac{\sigma_w^2}{\mathrm{N_r}.\sigma_s^2}} \qquad \text{and} \qquad \gamma^{(m_0)} = \frac{\sigma_w^2}{\mathrm{N_r}.\sigma_s^2}\left(\frac{\alpha^{(m_0)}}{1-\alpha^{(m_0)}}\right) \tag{5.39}$$

Finally, we can demodulate the transmitted constellation symbols $s_{i,n}$ by quantizing the corresponding maximum value as:

$$\widehat{s}_{i,n}^{\mathrm{MMSE}} = \underset{\mathcal{C}_q \in \chi}{\mathrm{argmin}} \left| z_{i,n} - \alpha^{(m_0)}\ \mathcal{C}_q \right|^2 \tag{5.40}$$

5.4.3 Uncoded BER performances for CP-aided OFDM-SM/CP-aided OFDM-SIMO system

Let us consider a MIMO system with a number of 2 of transmit antennas ($\mathrm{N_t} = 2$) and a number of 4 of receive antennas ($\mathrm{N_r} = 4$). Moreover, two configuration are considered: SM and SIMO configuration. Further, we consider a OFDM waveform at the transmitter.

Assuming that the Rice factor $\mathrm{K_{LOS}}$ of the Ricean MIMO channel is perfectly known, a simulation of the uncoded BER performance is done in Figure 5.7 for both the SM and the SIMO configurations. For simulation results, we assume a linear 16-QAM modulation (Quadrature Amplitude Modulation) and a number of two transmit transmit for the SM configuration. Whereas, for SIMO configuration, we assume a linear 32-QAM modulation and only one transmit antenna is selected to convey the transmitted constellation symbols. Consequently, the SM and the SIMO system offer the same system efficiency of 5 bit/s/channel use (bpcu).

At the receiver, a ML-based, a MRC-based and a MMSE-based detections are considered for SM and SIMO configurations. The considered signal-to-noise ratio (SNR) is equal to 14 dB ($\mathrm{E}_s/\mathrm{N}_0 = 14$ dB).

As we can see in Figure 5.7, the uncoded BER performance for the CP-aided OFDM-SM system is shown

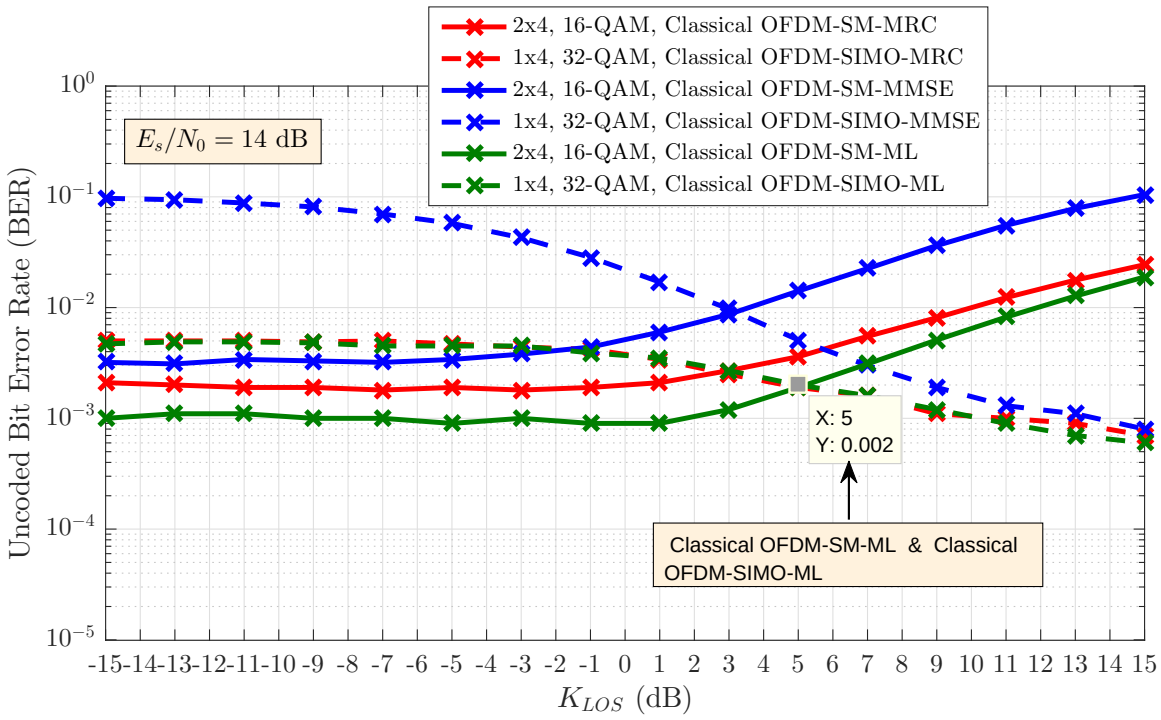

Figure 5.7: *Uncoded BER performance for the classical OFDM-SM / OFDM-SIMO structure as a function of the Rice factor K_{LOS} and for different detection techniques at the receiver.*

in solid curve. Whereas, the uncoded BER performance for the CP-aided OFDM-SIMO system is plotted in dashed curve. For ML-based, MRC-based and MMSE-based detections, simulation results are plotted in black, red and blue curves, respectively.

In Figure 5.7, simulation results show that for low values of $\mathrm{K_{LOS}}$, the uncoded BER performances for OFDM-SM system are better that those for the SC-SIMO system. However, for high values of $\mathrm{K_{LOS}}$, OFDM-SIMO system can offer a good uncoded BER performances which are better than OFDM-SM system. Indeed, from $\mathrm{K_{LOS}} \geq 5$ dB (for the ML receiver), the OFDM-SM system suffer from a BER degradation and it no longer offers a better uncoded BER performance than those for OFDM-SIMO system. This is due the fact that the diversity gain is inversely proportional to $\mathrm{K_{LOS}}$ factor. On the contrary, for high values of $\mathrm{K_{LOS}}$, the equivalent baseband channel, for the SC-SIMO system, presents a low selectivity and thus the uncoded BER performances are improved. In order to ensure good performances in terms of uncoded BER for all values of $\mathrm{K_{LOS}}$ factor, OFDM-SM and OFDM-SIMO systems could be operated in an alternate manner. Referring to the simulation results given in Figure 5.7, three values of $\mathrm{K_{LOS}}$ can be distinguished: 3, 3.1 and 5 dB for MMSE-based, MRC-based and ML-based detection, respectively. In fact, simulation results show that for MMSE-based receiver, it is better to consider OFDM-SM for $\mathrm{K_{LOS}} \leq 3$ dB. However, for $\mathrm{K_{LOS}} \geq 3$ dB, it is preferable to consider OFDM-SIMO system. The same kind of results is obtained for MRC-based and ML-based receiver for $\mathrm{K_{LOS}} = 3.1$ dB and $\mathrm{K_{LOS}} = 5$ dB, respectively.

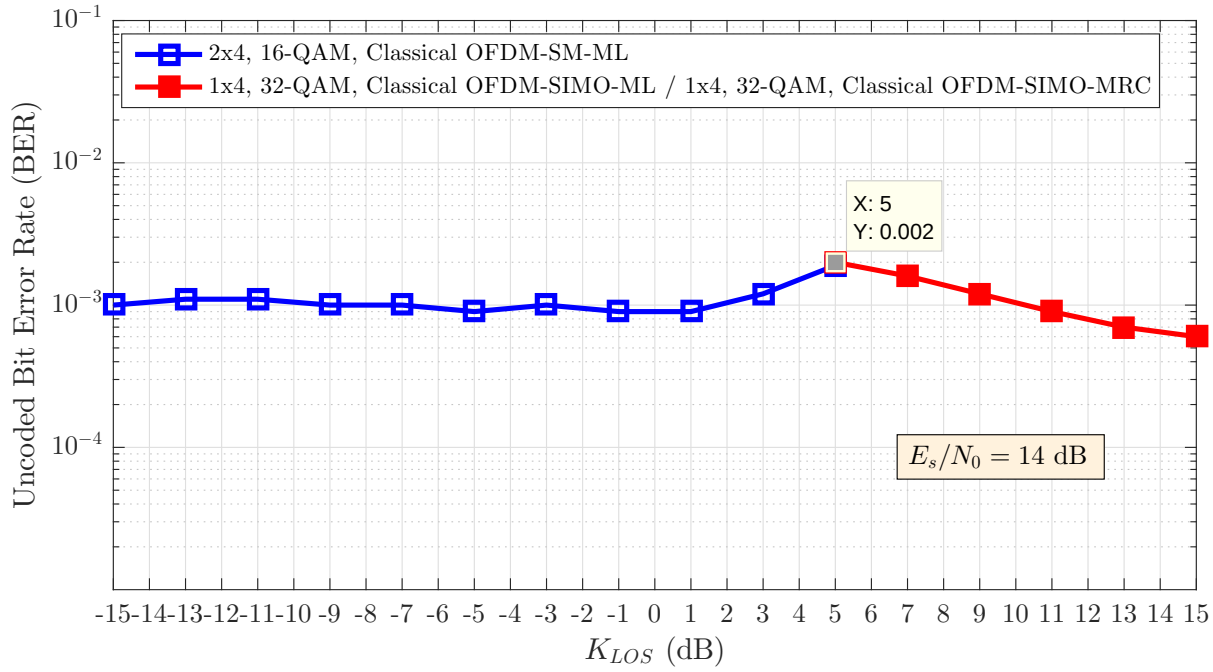

Figure 5.8: *Uncoded BER performances for the better combination for both the classical CP-aided OFDM-SM/SIMO for different values of K_{LOS}.*

Considering an adaptive configuration based on $\mathrm{K_{LOS}}$ values, we can obtain an enhanced uncoded BER performance as given in Figure 5.8.

As we can observe in Figure 5.8, for $\mathrm{E}_s/\mathrm{N}_0 = 14$ dB, the uncoded BER values are lower that 10^{-2} for all values of $\mathrm{K_{LOS}}$ factor between -15 and 15 dB.

5.5 Classical CP-aided SC-SM system vs Classical CP-aided SC-SIMO system

5.5.1 Classical CP-aided SC-SM system

By combining SM technique with single-carrier (SC) transmission systems, CP-aided SC-SM systems can overcome the shortcoming of high peak to average power ratio (PAPR) for the CP-aided OFDM-SM systems. Indeed, owing to its inherent SC structure, the transmit signals of CP-aided SC-SM have attractive peak power characteristics. On other hand, since CP-aided SC-SM uses the same concept as CP-aided OFDM-SM of using the transmit antenna number as an additional source of information, the benefit of the increased bit rate is maintained, while a high MIMO diversity gain can be achieved. Moreover, thanks to the use of SC waveform instead to OFDM, CP-aided SC-SM systems presented a reduced hardware complexity and the number of radio frequency (RF) chains can be reduced to one. However, the non-use of shaping filter at the transmitter for the classical CP-aided SC-SM structure makes the design of spectrally efficient transmitter a challenging task. Indeed, the transmitted signals have a non-finite power density function (psd) and the

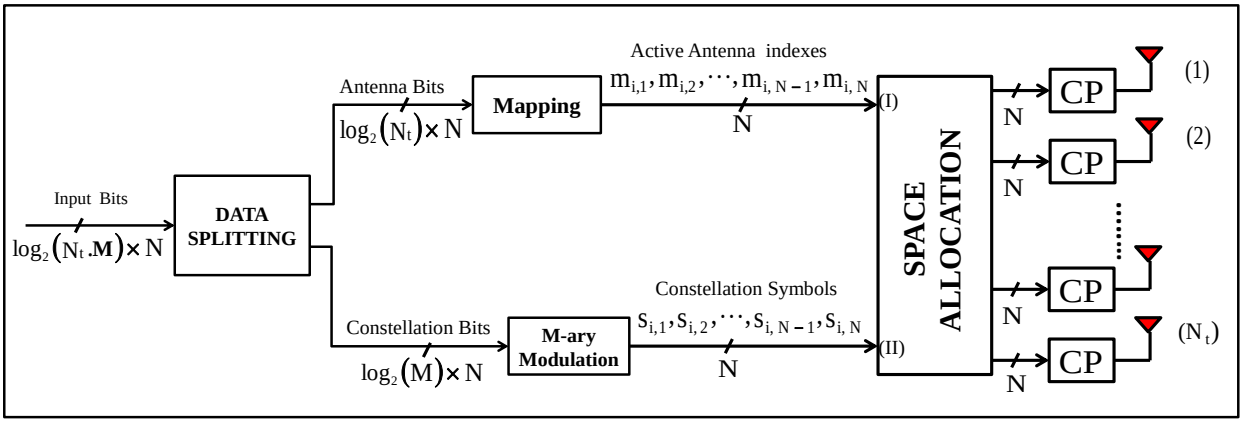

Figure 5.9: *Uncoded transmitter for the classical CP-aided SC-SM structure.*

spectral occupancy is not well tailored.

For the CP-aided SC-SM receiver, different detection techniques are possible, including linear frequency-domain equalization (FDE) detection techniques such as zero forcing (ZF) and minimum mean square error (MMSE), a hybrid time-frequency decision feedback equalizer (DFE) detection [66] and maximum likelihood (ML) detection employing QR decomposition and M algorithm (QRM-MLD) [58].

5.5.1.1 Transmitter SM structure

We consider a multiple input-multiple output (MIMO) communication system with $\mathrm{N_t}$ transmit antennas and $\mathrm{N_r}$ receive antennas. The transmitter of the classical CP-aided SC-SM is given in Figure 5.9.

Let us consider a sequence of independent random bits to be transmitted over a uncorrelated Ricean MIMO channel. Furthermore, we consider a frame based transmission with a symbol period $\mathrm{T_s}$ and a modulation order M. The considered M-ary constellation symbols are drawn from a discrete alphabet $\chi = \{\mathcal{C}_1, \mathcal{C}_2, \ldots, \mathcal{C}_M\}$. Each frame contains a number of N_f sub-frames. The size of each sub-frame is $N \times \log_2(M.\mathrm{N_t})$ bits, where N is a non-zero positive integer which denotes the number of modulated symbols in each transmit sub-frame.

Data splitting and frequency domain processing: For each transmit sub-frame $1 \leq i \leq N_f$, the transmitter starts to split the bit sequence $\mathbf{u}_i$ into two bit blocks $\mathbf{u}_i^a$ and $\mathbf{u}_i^d$ verifying $\mathbf{u}_i = [\mathbf{u}_i^a, \mathbf{u}_i^d]$. The first bit block $\mathbf{u}_i^a$ contains $N \times \log_2(\mathrm{N_t})$ bits and it is designed to select the active transmit antennas. The second bit block $\mathbf{u}_i^d$ contains $N \times \log_2(M)$ bits and it is designed to transmit constellation symbols. The two blocks will be processed as follows:

- The first bit block $\mathbf{u}_i^d$ being mapped to generate a select antenna vector $\underline{\mathbf{m}}_i = [m_{i,1}, m_{i,2}, \ldots, m_{i,N}]^T$ containing transmit antenna indexes $m_{i,n} \in \{1, \ldots, \mathrm{N_t}\}$. Note that only one transmit antenna index is selected in each symbol duration $\mathrm{T_s} = \mathrm{T_h}$.
- The second bit block $\mathbf{u}_i^d$ will be modulated using a M-ary constellation to provide a sequence of N symbols denoted by $\underline{\mathbf{s}}_i = [s_{i,1}, s_{i,2}, \ldots, s_{i,N}]^T$. The considered M-ary constellation symbols are drawn

from a discrete alphabet $\chi = \{\mathcal{C}_1, \mathcal{C}_2, \ldots, \mathcal{C}_M\}$.

Space allocation in the time domain: By using the resulting transmit antenna index sequence $\underline{\mathbf{m}}_i = [m_{i,1}, m_{i,2}, \ldots, m_{i,N}]^T$ and also the resulting modulated sequence $\underline{\mathbf{s}}_i = [s_{i,1}, s_{i,2}, \ldots, s_{i,N}]^T$, a simple antenna coding is used: For each combination $(s_{i,n}, m_{i,n})$ we associate a column vector $\mathbf{x}_{i,n}$ obtained as follows:

$$\mathbf{x}_{i,n} = \begin{bmatrix} x_{i,n}^{(1)} \\ x_{i,n}^{(2)} \\ \vdots \\ x_{i,n}^{(\mathrm{N_t})} \end{bmatrix} = [\underbrace{0,\ldots,0}_{(m_{i,n}-1)}, s_{i,n}, \underbrace{0,\ldots,0}_{\mathrm{N_t}-m_{i,n}}]^T \quad \forall \quad 1 \leq n \leq N \qquad \text{and} \qquad \forall \quad 1 \leq i \leq N_f \tag{5.41}$$

For each transmitted sub-frame, a resulting matrix $\mathbf{E}_i = \left[\mathbf{e}_i^{(1)}, \mathbf{e}_i^{(2)}, \ldots, \mathbf{e}_i^{(\mathrm{N_t})}\right]^T$ is obtained, which represents the transmitted symbols over all transmit antennas:

$$\mathbf{E}_i = \begin{bmatrix} \mathbf{e}_i^{(1)} \\ \mathbf{e}_i^{(2)} \\ \vdots \\ \mathbf{e}_i^{(\mathrm{N_t})} \end{bmatrix} = \begin{bmatrix} e_{i,1}^{(1)} & e_{i,2}^{(1)} & \ldots & e_{i,N}^{(1)} \\ e_{i,1}^{(2)} & e_{i,2}^{(2)} & \ldots & e_{i,N}^{(2)} \\ \vdots & \vdots & \ldots & \vdots \\ e_{i,1}^{(\mathrm{N_t})} & e_{i,2}^{(\mathrm{N_t})} & \ldots & e_{i,N}^{(\mathrm{N_t})} \end{bmatrix} = \begin{bmatrix} x_{i,1}^{(1)} & x_{i,2}^{(1)} & \ldots & x_{i,N}^{(1)} \\ x_{i,1}^{(2)} & x_{i,2}^{(2)} & \ldots & x_{i,N}^{(2)} \\ \vdots & \vdots & \ldots & \vdots \\ x_{i,1}^{(\mathrm{N_t})} & x_{i,2}^{(\mathrm{N_t})} & \ldots & x_{i,N}^{(\mathrm{N_t})} \end{bmatrix} \tag{5.42}$$

Add Cyclic Prefix: Before transmitting, a Cyclic Prefix (CP) block matrix of size $\mathrm{N_t} \times N_g$ is inserted at the beginning of each resulting matrix $\mathbf{E}_i$ in order to cope with inter-symbol interference from the MIMO channel and maintain sub-carriers orthogonality.

5.5.1.2 Receiver SM structure

At the receiver $\mathrm{N_r}$ receive antennas is considered. After sampling and removing CP, the resulting time-domain received symbol matrix can be written as:

$$\mathbf{R}_i = \begin{bmatrix} \mathbf{r}_i^{(1)} \\ \mathbf{r}_i^{(2)} \\ \vdots \\ \mathbf{r}_i^{(\mathrm{N_r})} \end{bmatrix} = \begin{bmatrix} r_{i,1}^{(1)} & r_{i,2}^{(1)} & \ldots & r_{i,N}^{(1)} \\ r_{i,1}^{(2)} & r_{i,2}^{(2)} & \ldots & r_{i,N}^{(2)} \\ \vdots & \vdots & \ldots & \vdots \\ r_{i,1}^{(\mathrm{N_r})} & r_{i,2}^{(\mathrm{N_r})} & \ldots & r_{i,N}^{(\mathrm{N_r})} \end{bmatrix} \tag{5.43}$$

Thanks to the add of a circular prefix at the transmitter, the MIMO channel has a circular form. Thus, the time-domain received sample sequence for each receive antenna $1 \leq n_\mathrm{r} \leq \mathrm{N_r}$ can be given as follows:

$$\mathbf{r}_i^{(n_\mathrm{r})} = \begin{bmatrix} r_{i,1}^{(n_\mathrm{r})} \\ r_{i,2}^{(n_\mathrm{r})} \\ \vdots \\ r_{i,N}^{(n_\mathrm{r})} \end{bmatrix}^T = \sum_{n_\mathrm{t}=1}^{\mathrm{N_t}} \begin{bmatrix} x_{i,1}^{(n_\mathrm{t})} \\ x_{i,2}^{(n_\mathrm{t})} \\ \vdots \\ x_{i,N}^{(n_\mathrm{t})} \end{bmatrix}^T . \left\{ \mathbf{F}_\mathrm{N} . diag \begin{bmatrix} \mathrm{H}_{i,1}^{(n_\mathrm{r},n_\mathrm{t})} \\ \mathrm{H}_{i,2}^{(n_\mathrm{r},n_\mathrm{t})} \\ \vdots \\ \mathrm{H}_{i,N}^{(n_\mathrm{r},n_\mathrm{t})} \end{bmatrix} . \mathbf{F}_\mathrm{N}^H \right\} + \begin{bmatrix} w_1^{(n_\mathrm{r})} \\ w_2^{(n_\mathrm{r})} \\ \vdots \\ w_N^{(n_\mathrm{r})} \end{bmatrix}^T \tag{5.44}$$

the resulting noise vector is $\mathbf{w}^{(n_\mathrm{r})} = \left[w_1^{(n_\mathrm{r})}, w_2^{(n_\mathrm{r})}, \ldots, w_N^{(n_\mathrm{r})}\right]^T$ is a centered complex AWGN noise with two-sided spectral density equal to $\mathrm{N_0}$ and the noise variable $\left\{w_n^{(n_\mathrm{r})}\right\}$ having a variance σ_w^2 calculated as:

$$\sigma_w^2 = \mathrm{N_0} \times \mathrm{R}_s \qquad \text{with} \qquad \mathrm{R}_s = 1/\mathrm{T}_s \tag{5.45}$$

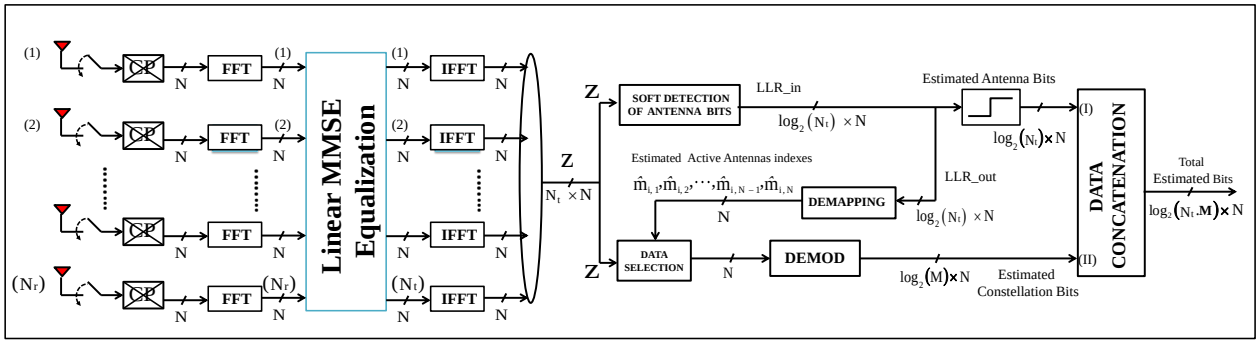

Figure 5.10: *Uncoded receiver based on MMSE detection for the classical CP-aided SC-SM structure.*

Optimal detector: ML-based receiver In [118], an optimal ML detector was proposed for CP-aided SC-SM schemes, which carries out an exhaustive search for finding the global optimum in the entire transmit signal space. This detector jointly detects the entire transmission frame to retrieve the original transmitted bit block $\mathbf{u}_i = [\mathbf{u}_i^a, \mathbf{u}_i^d]$ containing $N \times \log_2(M \times \mathrm{N_t})$ bits. The complexity of the ML detector is evaluated in [128] as:

$$\text{Complexity} = \mathcal{O}\left((M \times \mathrm{N_t})^N\right) \tag{5.46}$$

The advantages of the ML detector over the ZF and the MMSE detectors were evaluated for the CP-aided SC-SM schemes. However, as both the transmission rate and N increase, the complexity of the ML detector becomes excessive.

Sub-optimal detector: MMSE-based detection For the MMSE detection, the considered receiver is presented in Figure 5.10. At the receiver, the selection of the active transmit antennas and the detection of the transmit constellation symbols follow the following steps:

- *Frequency domain processing*: For each receive antenna $1 \leq n_\mathrm{r} \leq \mathrm{N_r}$, the receiver starts to transform the resulting received sequence $\mathbf{r}_i^{(n_\mathrm{r})}$ to the frequency domain by using a Fast Fourier Transform (FFT) operation as follows:

$$\mathbf{y}_i^{(n_\mathrm{r})} = \begin{bmatrix} y_{i,1}^{(n_\mathrm{r})} \\ y_{i,2}^{(n_\mathrm{r})} \\ \vdots \\ y_{i,N}^{(n_\mathrm{r})} \end{bmatrix}^T = \mathbf{r}_i^{(n_\mathrm{r})}.\mathbf{F}_\mathrm{N} = \sum_{n_\mathrm{t}=1}^{\mathrm{N_t}} \begin{bmatrix} \widetilde{x}_{i,1}^{(n_\mathrm{t})} \\ \widetilde{x}_{i,2}^{(n_\mathrm{t})} \\ \vdots \\ \widetilde{x}_{i,N}^{(n_\mathrm{t})} \end{bmatrix}^T .diag \begin{bmatrix} \mathrm{H}_{i,1}^{(n_\mathrm{r},n_\mathrm{t})} \\ \mathrm{H}_{i,2}^{(n_\mathrm{r},n_\mathrm{t})} \\ \vdots \\ \mathrm{H}_{i,N}^{(n_\mathrm{r},n_\mathrm{t})} \end{bmatrix} + \begin{bmatrix} w_1^{(n_\mathrm{r})} \\ w_2^{(n_\mathrm{r})} \\ \vdots \\ w_N^{(n_\mathrm{r})} \end{bmatrix}^T \tag{5.47}$$

with the data vector $\left[\widetilde{x}_{i,1}^{(n_\mathrm{t})}, \widetilde{x}_{i,2}^{(n_\mathrm{t})}, \ldots, \widetilde{x}_{i,N}^{(n_\mathrm{t})}\right]$ denotes the frequency version of the transmitted vector $\left[x_{i,1}^{(n_\mathrm{t})}, x_{i,2}^{(n_\mathrm{t})}, \ldots, x_{i,N}^{(n_\mathrm{t})}\right]$ for $1 \leq n_\mathrm{t} \leq \mathrm{N_t}$:

$$\left[\widetilde{x}_{i,1}^{(n_\mathrm{t})}, \widetilde{x}_{i,2}^{(n_\mathrm{t})}, \ldots, \widetilde{x}_{i,N}^{(n_\mathrm{t})}\right] = \left[x_{i,1}^{(n_\mathrm{t})}, x_{i,2}^{(n_\mathrm{t})}, \ldots, x_{i,N}^{(n_\mathrm{t})}\right].\mathbf{F}_\mathrm{N} \tag{5.48}$$

In Equation (5.47), the expression of the received frequency domain symbols can be also re-written in

the following form given in each frequency index $1 \leq n \leq N$ as follows:

$$\mathbf{y}_{i,n} = \begin{bmatrix} y_{i,n}^{(1)} \\ y_{i,n}^{(2)} \\ \vdots \\ y_{i,n}^{(\mathrm{N_r})} \end{bmatrix} = \begin{bmatrix} \mathrm{H}_{i,n}^{(1,1)} & \mathrm{H}_{i,n}^{(1,2)} & \dots & \mathrm{H}_{i,n}^{(1,\mathrm{N_t})} \\ \mathrm{H}_{i,n}^{(2,1)} & \mathrm{H}_{i,n}^{(2,2)} & \dots & \mathrm{H}_{i,n}^{(2,\mathrm{N_t})} \\ \vdots & \vdots & \ddots & \vdots \\ \mathrm{H}_{i,n}^{(\mathrm{N_r},1)} & \mathrm{H}_{i,n}^{(\mathrm{N_r},2)} & \dots & \mathrm{H}_{i,n}^{(\mathrm{N_r},\mathrm{N_t})} \end{bmatrix} . \begin{bmatrix} \widetilde{x}_{i,n}^{(1)} \\ \widetilde{x}_{i,n}^{(2)} \\ \vdots \\ \widetilde{x}_{i,n}^{(\mathrm{N_t})} \end{bmatrix} + \begin{bmatrix} w_n^{(1)} \\ w_n^{(2)} \\ \vdots \\ w_n^{(\mathrm{N_r})} \end{bmatrix} = \mathbf{H}_{i,n} . \widetilde{\mathbf{x}}_{i,n} + \mathbf{w}_n \tag{5.49}$$

- *Linear MMSE equalization in the Space-frequency domain*:Typically in literature [98, 117], a linear MMSE channel equalization is considered in the frequency domain to detect the transmitted SM symbols. By applying Linear MMSE equalization, The filter linearly combines the received samples to form an estimation of the frequency response of transmitted symbols as follows:

$$\widetilde{\mathbf{z}}_{i,n} = \begin{bmatrix} \widetilde{z}_{i,n}^{(1)} \\ \widetilde{z}_{i,n}^{(2)} \\ \vdots \\ \widetilde{z}_{i,n}^{(\mathrm{N_t})} \end{bmatrix} = \mathbf{W}_{i,n} . \mathbf{y}_{i,n} = \left[\mathbf{H}_{i,n}^H . \mathbf{H}_{i,n} + \frac{\sigma_w^2}{(\sigma_s^2/\mathrm{N_t})} \times \mathbf{I}_{\mathrm{N_t} \times \mathrm{N_t}} \right]^{-1} . \mathbf{H}_{i,n}^H . \mathbf{y}_{i,n} \qquad \text{for} \qquad 1 \leq n \leq N \tag{5.50}$$

- *Time-domain transform*: The resulting sequence corresponding to the estimated sequence transmitted through the n_t antenna element is denoted by $\widetilde{\mathbf{z}}_i^{(n_\mathrm{t})} = \left[\widetilde{z}_{i,1}^{(n_\mathrm{t})}, \widetilde{z}_{i,2}^{(n_\mathrm{t})}, \dots, \widetilde{z}_{i,N}^{(n_\mathrm{t})} \right]$ and contains N equalized frequency symbols. For $1 \leq n_\mathrm{t} \leq \mathrm{N_t}$, the equalized sequence $\widetilde{\mathbf{z}}_i^{(n_\mathrm{t})}$ will be transformed to the time domain by Inverse Fast Fourier Transform (IFFT):

$$[\mathbf{z}_{i,1}, \mathbf{z}_{i,2}, \dots, \mathbf{z}_{i,N}] = \begin{bmatrix} z_{i,1}^{(1)} & z_{i,2}^{(1)} & \dots & z_{i,N}^{(1)} \\ z_{i,1}^{(2)} & z_{i,2}^{(2)} & \dots & z_{i,N}^{(2)} \\ \vdots & \vdots & \dots & \vdots \\ z_{i,1}^{(\mathrm{N_t})} & z_{i,2}^{(\mathrm{N_t})} & \dots & z_{i,N}^{(\mathrm{N_t})} \end{bmatrix} = [\widetilde{\mathbf{z}}_{i,1}, \widetilde{\mathbf{z}}_{i,2}, \dots, \widetilde{\mathbf{z}}_{i,N}] . \mathbf{F}_\mathrm{N}^H \tag{5.51}$$

The equalized vector $\mathbf{z}_{i,n}$ is an estimation of the transmitted SM vector $\mathbf{x}_{i,n}$ and it is used to detect the active transmit antenna indexes and the transmitted constellation symbols. To do it, the receiver sequentially follows two steps: first, an estimation of the active antenna index is given by finding the maximum value of the output vector $\mathbf{z}_{i,n}$. Second, the vector element having the maximum value will demodulated to detect the transmitted constellation symbol. The two steps are expressed as the following:

$$\begin{cases} \text{Step 1: } \underline{\text{Estimate antenna indexes:}} & \widehat{m}_{i,n} = \underset{n_\mathrm{t} \in \{1,2,\dots,\mathrm{N_t}\}}{\operatorname{argmax}} \left| z_{i,n}^{(n_\mathrm{t})} \right|^2 \qquad 1 \leq n \leq N \\ \text{Step 2: } \underline{\text{Estimate constellation symbols:}} & \widehat{s}_{i,n} = \underset{\mathcal{C}_q \in \chi}{\operatorname{argmin}} \left| \widetilde{z}_{i,n}^{(\widehat{m}_{i,n})} - \mathcal{C}_q \right|^2 \qquad 1 \leq n \leq N \end{cases}$$

Finally, at this stage of the study, what can be said is that the MMSE detector allows us to consider SISO channel decoder. Further, MMSE-based decoder can offer a simple detection with reasonable computational complexity compared to the optimal ML-based detector. The complexity of the MMSE detector is evaluated in [128] and is equal to:

$$\text{Complexity} = \mathcal{O}\left(\mathrm{N_r} \times \mathrm{N_t}^2 \times N\right) + \mathcal{O}\left(\mathrm{N_t}^3 \times N\right) + \mathcal{O}\left(\mathrm{N_t} \times N^2\right) + \mathcal{O}\left(\mathrm{N_t}^2 \times N \times M\right) \tag{5.52}$$

5.5.2 Classical CP-aided SC-SIMO system

5.5.2.1 Transmitter SIMO structure

We consider a number of $\mathrm{N_t}$ of transmit antennas. Only a single transmit antenna, having a antenna index $m_0 \in \{1,\ldots,\mathrm{N_t}\}$, is activated during all transmitted sub-frames. The transmitter of the classical CP-aided SC-SIMO is given in Figure 5.11.

Let us consider a sequence of independent random bits to be transmitted over a uncorrelated Ricean MIMO channel. Furthermore, we consider a frame based transmission with a symbol period $\mathrm{T_s}$ and a modulation order M. Each frame contains a number of N_f sub-frames. The size of each sub-frame is $N \times \log_2(M)$ bits. The considered M-ary constellation symbols are drawn from a discrete alphabet $\chi = \{\mathcal{C}_1, \mathcal{C}_2, \ldots, \mathcal{C}_M\}$.

The input bit block $\mathbf{u}_i^d$ will be modulated into a M-ary constellation to provide a sequence of N constellation symbols denoted by $\underline{\mathbf{s}}_i = [s_{i,1}, s_{i,2}, \ldots, s_{i,N}]^T$ where $s_{i,n} = \mathcal{C}_q \in \chi$

Space allocation in the frequency domain: Assuming m_0 is the index of the selected active transmit antenna, the obtained constellation sequence $\underline{\mathbf{s}}_i$ will be transmitted via the m_0 transmit antenna. As a result, we have:

$$\mathbf{E}_i = \begin{bmatrix} e_{i,1}^{(1)} & e_{i,2}^{(1)} & \ldots & e_{i,N}^{(1)} \\ \vdots & \vdots & \ldots & \vdots \\ e_{i,1}^{(m_0)} & e_{i,2}^{(m_0)} & \ldots & e_{i,N}^{(m_0)} \\ \vdots & \vdots & \ldots & \vdots \\ e_{i,1}^{(\mathrm{N_t})} & e_{i,2}^{(\mathrm{N_t})} & \ldots & e_{i,N}^{(\mathrm{N_t})} \end{bmatrix} = \begin{bmatrix} x_{i,1}^{(1)} & x_{i,2}^{(1)} & \ldots & x_{i,N}^{(1)} \\ \vdots & \vdots & \ldots & \vdots \\ x_{i,1}^{(m_0)} & x_{i,2}^{(m_0)} & \ldots & x_{i,N}^{(m_0)} \\ \vdots & \vdots & \ldots & \vdots \\ x_{i,1}^{(\mathrm{N_t})} & x_{i,2}^{(\mathrm{N_t})} & \ldots & x_{i,N}^{(\mathrm{N_t})} \end{bmatrix} = \begin{bmatrix} 0 & 0 & \ldots & 0 \\ \vdots & \vdots & \ldots & \vdots \\ s_{i,1} & s_{i,2} & \ldots & s_{i,N} \\ \vdots & \vdots & \ldots & \vdots \\ 0 & 0 & \ldots & 0 \end{bmatrix} \tag{5.53}$$

Add Cyclic Prefix: For all transmit antennas, a Cyclic Prefix (CP) block matrix of size $\mathrm{N_t} \times N_g$ is inserted at the beginning of each resulting matrix $\mathbf{E}_i$ in order to cope with inter-symbol interference from the channel and maintain sub-carriers orthogonality.

5.5.2.2 Receiver SIMO structure

At the receiver a number of $\mathrm{N_r}$ receive antennas are considered.

Thanks to the add of a circular prefix at the transmitter, the MIMO channel has a circular form. Thus, the time-domain received sample sequence for each receive antenna $1 \leq n_\mathrm{r} \leq \mathrm{N_r}$ can be given as follows:

$$\begin{aligned} \mathbf{r}_i^{(n_\mathrm{r})} = \begin{bmatrix} r_{i,1}^{(n_\mathrm{r})} \\ r_{i,2}^{(n_\mathrm{r})} \\ \vdots \\ r_{i,N}^{(n_\mathrm{r})} \end{bmatrix}^T &= \sum_{n_\mathrm{t}=1}^{\mathrm{N_t}} \begin{bmatrix} x_{i,1}^{(n_\mathrm{t})} \\ x_{i,2}^{(n_\mathrm{t})} \\ \vdots \\ x_{i,N}^{(n_\mathrm{t})} \end{bmatrix}^T . \left\{ \mathbf{F}_\mathrm{N} . diag \begin{bmatrix} \mathrm{H}_{i,1}^{(n_\mathrm{r},n_\mathrm{t})} \\ \mathrm{H}_{i,2}^{(n_\mathrm{r},n_\mathrm{t})} \\ \vdots \\ \mathrm{H}_{i,N}^{(n_\mathrm{r},n_\mathrm{t})} \end{bmatrix} . \mathbf{F}_\mathrm{N}^H \right\} + \begin{bmatrix} w_1^{(n_\mathrm{r})} \\ w_2^{(n_\mathrm{r})} \\ \vdots \\ w_N^{(n_\mathrm{r})} \end{bmatrix}^T \\ &= \begin{bmatrix} s_{i,1} \\ s_{i,2} \\ \vdots \\ s_{i,N} \end{bmatrix}^T . \left\{ \mathbf{F}_\mathrm{N} . diag \begin{bmatrix} \mathrm{H}_{i,1}^{(n_\mathrm{r},m_0)} \\ \mathrm{H}_{i,2}^{(n_\mathrm{r},m_0)} \\ \vdots \\ \mathrm{H}_{i,N}^{(n_\mathrm{r},m_0)} \end{bmatrix} . \mathbf{F}_\mathrm{N}^H \right\} + \begin{bmatrix} w_1^{(n_\mathrm{r})} \\ w_2^{(n_\mathrm{r})} \\ \vdots \\ w_N^{(n_\mathrm{r})} \end{bmatrix}^T \end{aligned} \tag{5.54}$$

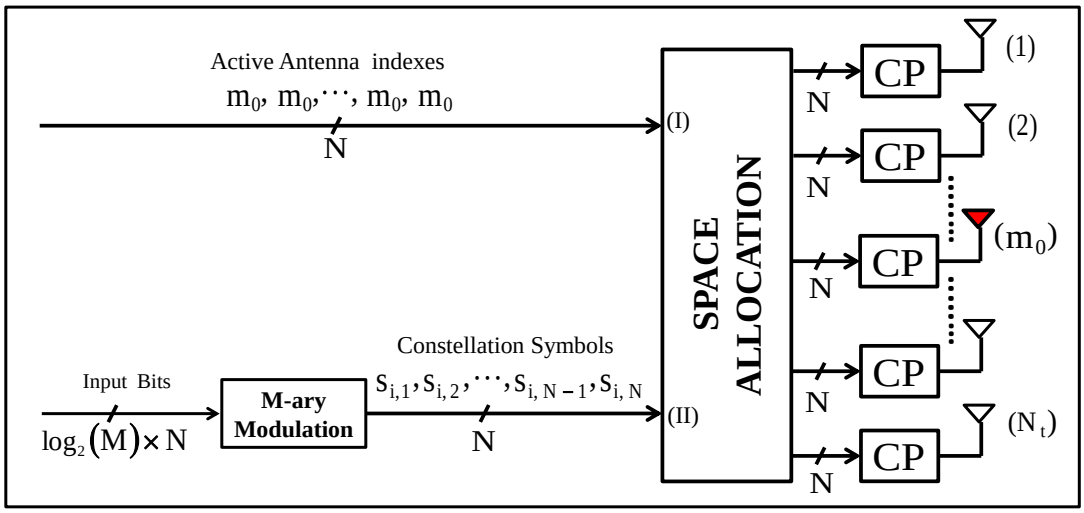

Figure 5.11: *Uncoded transmitter for the classical CP-aided SC-SIMO structure.*

the resulting noise vector $\mathbf{w}^{(n_r)} = \left[w_1^{(n_r)}, w_2^{(n_r)}, \ldots, w_N^{(n_r)}\right]^T$ is a centered complex AWGN noise with two-sided spectral density equal to N_0 and the noise variable $\left\{w_n^{(n_r)}\right\}$ having a variance σ_w^2 calculated as:

$$\sigma_w^2 = N_0 \times R_s \qquad \text{with} \qquad R_s = 1/T_s \tag{5.55}$$

For each receive antenna $1 \leq n_r \leq N_r$, the receiver starts to transform the resulting received sequence $\mathbf{r}_i^{(n_r)}$ to the frequency domain by using a Fast Fourier Transform (FFT) operation as follows:

$$\mathbf{y}_i^{(n_r)} = \begin{bmatrix} y_{i,1}^{(n_r)} \\ y_{i,2}^{(n_r)} \\ \vdots \\ y_{i,N}^{(n_r)} \end{bmatrix}^T = \mathbf{r}_i^{(n_r)}.\mathbf{F}_{N_1} = \begin{bmatrix} S_{i,1} \\ S_{i,2} \\ \vdots \\ S_{i,N} \end{bmatrix}^T .diag \begin{bmatrix} H_{i,1}^{(n_r,m_0)} \\ H_{i,2}^{(n_r,m_0)} \\ \vdots \\ H_{i,N}^{(n_r,m_0)} \end{bmatrix} + \begin{bmatrix} w_1^{(n_r)} \\ w_2^{(n_r)} \\ \vdots \\ w_N^{(n_r)} \end{bmatrix}^T \tag{5.56}$$

where $\mathbf{S}_i = [S_{i,1}, S_{i,2}, \ldots, S_{i,N}]$ is the frequency response of the transmitted data symbol sequence. By using Equation (6.31), the expression of $\mathbf{S}_i$ is done:

$$\begin{bmatrix} S_{i,1} \\ S_{i,2} \\ \vdots \\ S_{i,N} \end{bmatrix}^T = \begin{bmatrix} s_{i,1} \\ s_{i,2} \\ \vdots \\ s_{i,N} \end{bmatrix}^T .\mathbf{F}_N \tag{5.57}$$

On other hand, the expression of the received frequency domain symbols, can be also re-written in the following form given in each frequency index $1 \leq n \leq N$ as follows:

$$\mathbf{y}_{i,n} = \begin{bmatrix} y_{i,n}^{(1)} \\ y_{i,n}^{(2)} \\ \vdots \\ y_{i,n}^{(N_r)} \end{bmatrix} = S_{i,n} \begin{bmatrix} H_{i,n}^{(1,m_0)} \\ H_{i,n}^{(2,m_0)} \\ \vdots \\ H_{i,n}^{(N_r,m_0)} \end{bmatrix} + \begin{bmatrix} w_n^{(1)} \\ w_n^{(2)} \\ \vdots \\ w_n^{(N_r)} \end{bmatrix} = S_{i,n}\ \mathbf{h}_{i,n}^{(m_0)} + \mathbf{w}_n \tag{5.58}$$

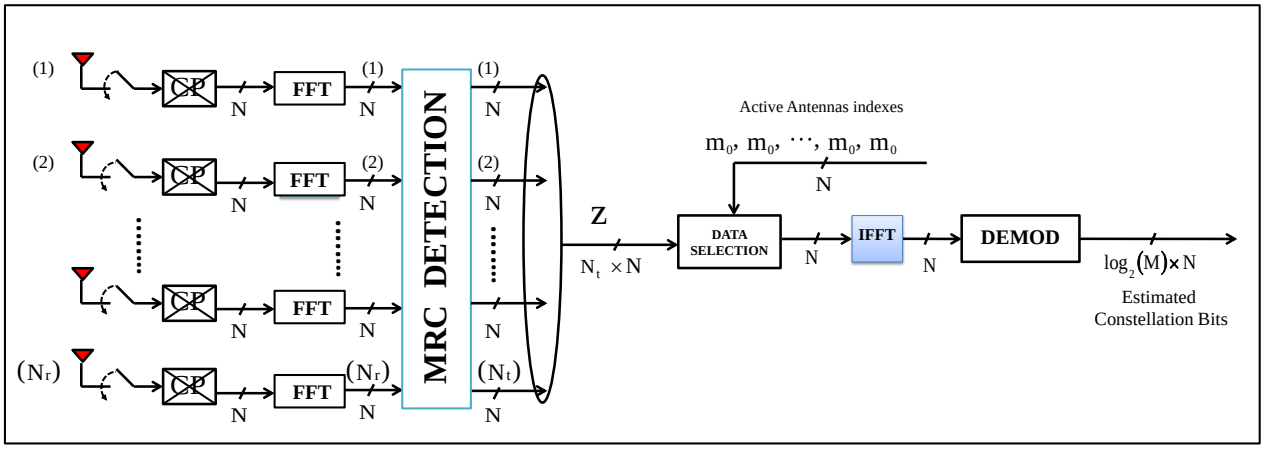

Figure 5.12: *Uncoded receiver based on MRC detection for the classical CP-aided SC-SIMO structure.*

Sub-optimal MRC-based receiver The Maximum Ratio Combining (MRC) detector is a sub-optimal linear detector and is presented in Figure 5.12. After MRC decoding, a resulting output vector $\mathbf{z}_{i,n} = \left[z_{i,n}^{(1)}, z_{i,n}^{(2)}, \ldots, z_{i,n}^{(m_0)}, \ldots, z_{i,n}^{(\mathrm{N_t})}\right]^T$ is obtained for $1 \leq n \leq N$. Then, by knowing that the index of the active transmit antenna is equal to m_0, the receiver selects the symbols corresponding to the m_0 transmit antenna. As a result, a sequence of N symbols, denoted by $\mathbf{z}_i = \left[z_{i,1}^{(m_0)}, z_{i,2}^{(m_0)}, \ldots, z_{i,N}^{(m_0)}\right]$, is obtained. Each element $z_{i,n}^{(m_0)}$ is expressed as:

$$z_{i,n}^{(m_0)} = \frac{\left[\mathbf{h}_{i,n}^{(m_0)}\right]^H . \mathbf{y}_{i,n}}{\left\|\mathbf{h}_{i,n}^{(m_0)}\right\|^2} = S_{i,n} + \frac{\left[\mathbf{h}_{i,n}^{(m_0)}\right]^H . \mathbf{w}_n}{\left\|\mathbf{h}_{i,n}^{(m_0)}\right\|^2} \qquad \text{for} \qquad 1 \leq n \leq N \tag{5.59}$$

After selecting data symbols, the selected frequency domain sequence must pass through a spectral filter matched to the transmit filter, in order to maximize the useful received power in the Nyquist bandwidth. Then, the obtained filtered sequence will be transformed to the time-domain by using an IFFT operation in order to recover the transmitted constellation symbols:

$$\begin{bmatrix} \widetilde{s}_{i,1} \\ \widetilde{s}_{i,2} \\ \vdots \\ \widetilde{s}_{i,N} \end{bmatrix} = \mathbf{F}_{\mathrm{N}}^H . \begin{bmatrix} z_{i,1}^{(m_0)} \\ z_{i,2}^{(m_0)} \\ \vdots \\ z_{i,N}^{(m_0)} \end{bmatrix} \tag{5.60}$$

Then we can demodulate the transmitted constellation symbols $s_{i,n}$ by quantizing the corresponding maximum value as:

$$\widehat{s}_{i,n} = \underset{\mathcal{C}_q \in \chi}{\operatorname{argmin}} \ |\widetilde{s}_{i,n} - \mathcal{C}_q|^2 \qquad 1 \leq n \leq N \tag{5.61}$$

Sub-optimal MMSE-based detection The MMSE receiver is a sub-optimal receiver at the detection is done in three steps as shown in Figure 5.13.

- *Frequency-domain transform and averaging*: At first, the receiver calculates the average value of the

frequency transform of the $\mathrm{N_r}$ received signal:

$$\mathbf{y}_i = \begin{bmatrix} y_{i,1} \\ y_{i,2} \\ \vdots \\ y_{i,N} \end{bmatrix}^T = \frac{1}{\mathrm{N_r}} \sum_{n_\mathrm{r}=1}^{\mathrm{N_r}} \mathbf{r}_i^{(n_\mathrm{r})}.\mathbf{F}_\mathrm{N} = \begin{bmatrix} s_{i,1} \\ s_{i,2} \\ \vdots \\ s_{i,N} \end{bmatrix}^T .\mathbf{F}_\mathrm{N}.\left\{ \frac{1}{\mathrm{N_r}} \sum_{n_\mathrm{r}=1}^{\mathrm{N_r}} diag \begin{bmatrix} \mathrm{H}_{i,1}^{(n_\mathrm{r},m_0)} \\ \mathrm{H}_{i,2}^{(n_\mathrm{r},m_0)} \\ \vdots \\ \mathrm{H}_{i,N}^{(n_\mathrm{r},m_0)} \end{bmatrix} \right\} + \left\{ \frac{1}{\mathrm{N_r}} \sum_{n_\mathrm{r}=1}^{\mathrm{N_r}} \begin{bmatrix} w_1^{(n_\mathrm{r})} \\ w_2^{(n_\mathrm{r})} \\ \vdots \\ w_N^{(n_\mathrm{r})} \end{bmatrix}^T \right\}$$

$$= \begin{bmatrix} s_{i,1} \\ s_{i,2} \\ \vdots \\ s_{i,N} \end{bmatrix}^T .\mathbf{F}_\mathrm{N}.diag \begin{bmatrix} \mathrm{H}_{i,1}^{(m_0)} \\ \mathrm{H}_{i,2}^{(m_0)} \\ \vdots \\ \mathrm{H}_{i,N}^{(m_0)} \end{bmatrix} + \begin{bmatrix} w_{i,1} \\ w_{i,2} \\ \vdots \\ w_{i,N} \end{bmatrix}^T = \begin{bmatrix} s_{i,1} \\ s_{i,2} \\ \vdots \\ s_{i,N} \end{bmatrix}^T .\mathbf{F}_\mathrm{N}.\mathbf{H}_{i,m_0} + \mathbf{w}_i \tag{5.62}$$

As a result, an equivalent baseband channel $\mathbf{H}_{i,m_0}$ is identified. Moreover, the variance of noise elements of the resulting zero-mean AWGN noise vector $\mathbf{w}_i$ is reduced by the number of the receive antennas:

$$\mathbb{E}\left\{ |w_{i,n}|^2 \right\} = \frac{\sigma_w^2}{\mathrm{N_r}} \qquad \forall \qquad 1 \leq n \leq N \tag{5.63}$$

- *Linear Frequency-domain MMSE equalization*: For the second step, the receiver applies a reduced complexity frequency domain linear MMSE equalization in order to generate a biased estimation of the frequency response of the transmitted constellation sequence. As a result, we obtain frequency domain vector denoted by $\widetilde{\mathbf{z}}_i$ and expressed as:

$$\widetilde{\mathbf{z}}_i = \begin{bmatrix} \widetilde{z}_{i,1} \\ \widetilde{z}_{i,2} \\ \vdots \\ \widetilde{z}_{i,N} \end{bmatrix}^T = \mathbf{y}_i.\mathbf{W}_{i,m_0} \approx \alpha^{(m_0)} \left\{ \begin{bmatrix} s_{i,1} \\ s_{i,2} \\ \vdots \\ s_{i,N} \end{bmatrix}^T .\mathbf{F}_\mathrm{N} + \frac{1}{\sqrt{\gamma^{(m_0)}}} \begin{bmatrix} w_{i,1} \\ w_{i,2} \\ \vdots \\ w_{i,N} \end{bmatrix}^T \right\} \tag{5.64}$$

where $\mathbf{W}_{i,m_0} = \mathbf{H}_{i,m_0}^H.\left[\mathbf{H}_{i,m_0}.\mathbf{H}_{i,m_0}^H + \frac{\sigma_w^2}{\mathrm{N_r}.\sigma_s^2}\right]^{-1}$ is a diagonal equalization matrix. The two positive scalars $\alpha^{(m_0)}$ and $\gamma^{(m_0)}$ are initially defined in Equation (5.39).

- *Time-domain transform*: For the third step, the output MMSE equalized vector $\widetilde{\mathbf{z}}_i$ will be transformed to the time domain to generate a biased estimation of the transmitted constellation sequence, $\underline{\mathbf{s}}_i = [s_{i,1}, s_{i,2}, \ldots, s_{i,N}]^T$, as the following:

$$\mathbf{z}_i = \begin{bmatrix} z_{i,1} \\ z_{i,2} \\ \vdots \\ z_{i,N} \end{bmatrix}^T = \begin{bmatrix} \widetilde{z}_{i,1} \\ \widetilde{z}_{i,2} \\ \vdots \\ \widetilde{z}_{i,N} \end{bmatrix}^T .\mathbf{F}_\mathrm{N}^H = \alpha^{(m_0)} \left\{ \begin{bmatrix} s_{i,1} \\ s_{i,2} \\ \vdots \\ s_{i,N} \end{bmatrix}^T + \frac{1}{\sqrt{\gamma^{(m_0)}}} \begin{bmatrix} w_{i,1} \\ w_{i,2} \\ \vdots \\ w_{i,N} \end{bmatrix}^T \right\} \tag{5.65}$$

Finally, we can demodulate the transmitted constellation symbols $s_{i,n}$ by quantizing the corresponding maximum value as:

$$\widehat{s}_{i,n}^{\mathrm{MMSE}} = \underset{\mathcal{C}_q \in \chi}{\mathrm{argmin}} \left| z_{i,n} - \alpha^{(m_0)}\, \mathcal{C}_q \right|^2 \tag{5.66}$$

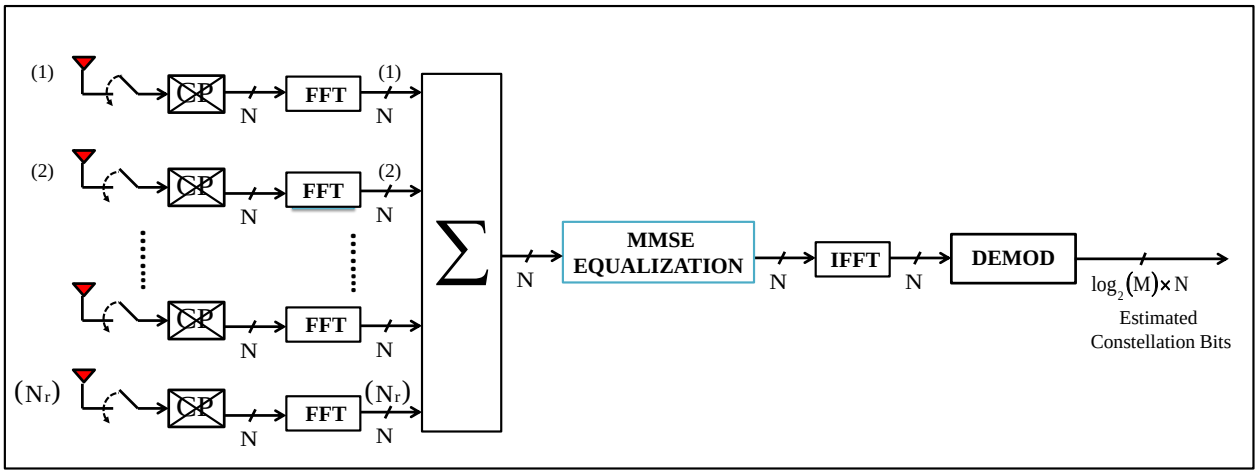

Figure 5.13: *Uncoded receiver based on MMSE detection for the classical CP-aided SC-SIMO structure.*

5.5.3 Uncoded BER performances for CP-aided SC-SM/SC-SIMO system

Let us consider a MIMO system with a number of 2 of transmit antennas ($N_t = 2$) and a number of 4 of receive antennas ($N_r = 4$). Moreover, two configuration are considered: SM and SIMO configuration. Further, we consider a SC waveform at the transmitter.

Assuming that the Rice factor K_{LOS} of the Ricean MIMO channel is perfectly known, a simulation of the uncoded BER performance is done in Figure 5.14 for both the SM and the SIMO configuration. For simulation results, we assume a linear 16-QAM modulation (Quadrature Amplitude Modulation) and a number of two transmit for SM configuration. Whereas, for SIMO configuration, we assume a linear 32-QAM modulation and only one transmit antenna is selected to convey the transmitted constellation symbols. Consequently, the SM and the SIMO system offer the same bit rate of 5 bpcu.

For the sake of simplicity, at the receiver, we consider a MMSE-based detection for both SM and SIMO configurations. The considered signal-to-noise ratio (SNR) is equal to 14 dB ($E_s/N_0 = 14$ dB).

As we can see in Figure 5.14, the uncoded BER performances for the CP-aided SC-SM system are shown in solid curve. Whereas, the uncoded BER performances for the CP-aided SC-SIMO system are plotted in dashed curve.

In Figure 5.14, simulation results show that for low values of K_{LOS}, the uncoded BER performances for SC-SM system are better that those for the SC-SIMO system. However, for high values of K_{LOS}, SC-SIMO system can offer a good uncoded BER performances which are better than the SC-SM system. Indeed, from $K_{LOS} \geq 3$ dB, the SC-SM system suffer from a BER degradation and it no longer offers a better uncoded BER performance than those for SC-SIMO system. This is due the fact that the diversity gain is inversely proportional to the K_{LOS} factor. On the contrary, for high values of K_{LOS}, the equivalent baseband channel, for the SC-SIMO system, presents a low selectivity and thus the uncoded BER performances are improved. In order to ensure good performances in terms of uncoded BER for all values of K_{LOS} factor, SC-SM and SC-SIMO systems could be operated in an alternate manner. Indeed, for $K_{LOS} \leq 3$ dB, SC-SM is considered. Whereas, for $K_{LOS} \geq 3$

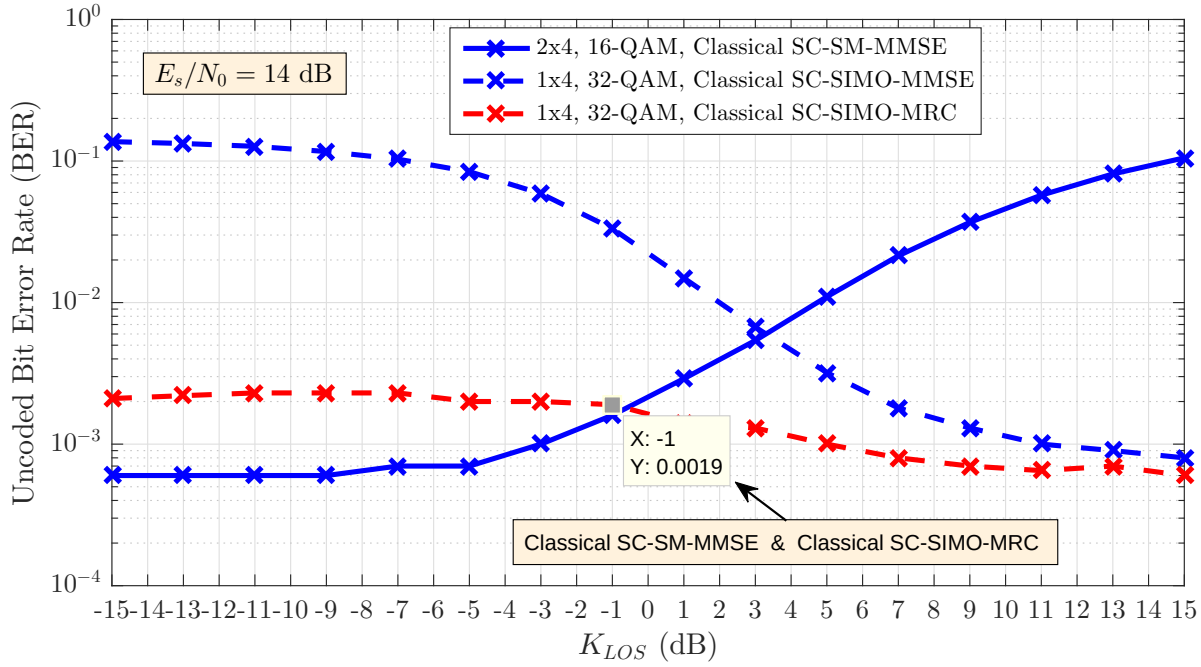

Figure 5.14: *Uncoded BER performance for the classical SC-SM / SC-SIMO structure as a function of the Rice factor K_{LOS} and for different detection techniques at the receiver.*

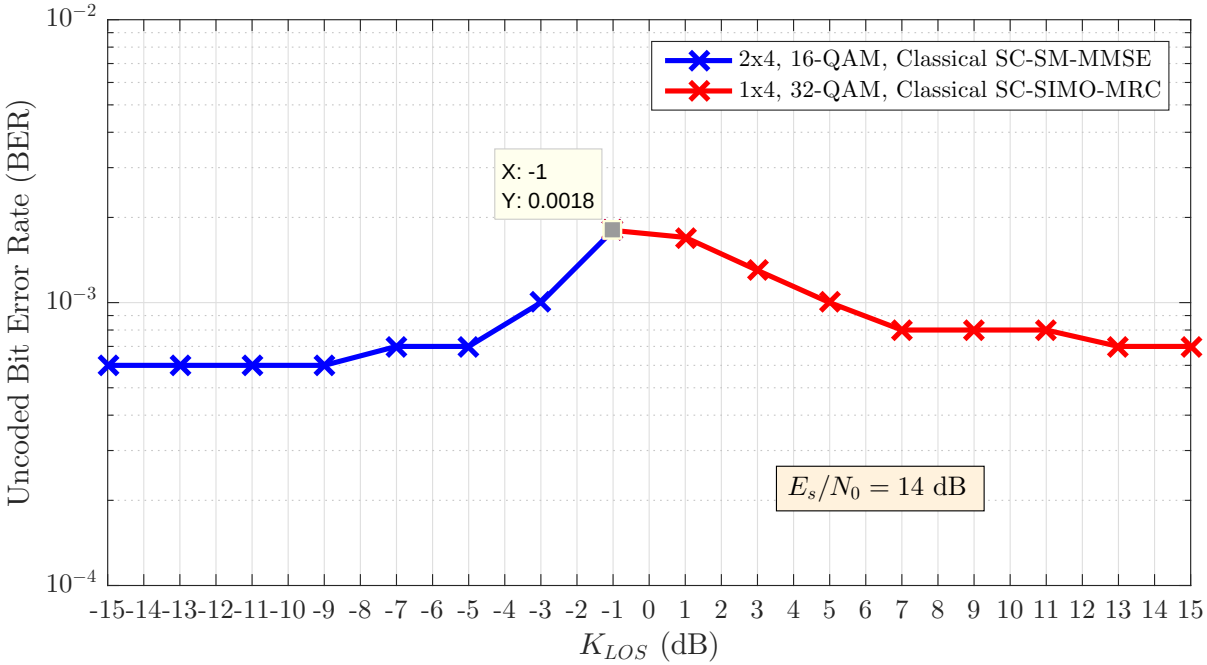

Figure 5.15: *Uncoded BER performances for the better combination for both the classical CP-aided SC-SM/SIMO for different values of K_{LOS}.*

dB, it preferable to use SC-SIMO system. Referring to the simulation results given in Figure 5.14, we can

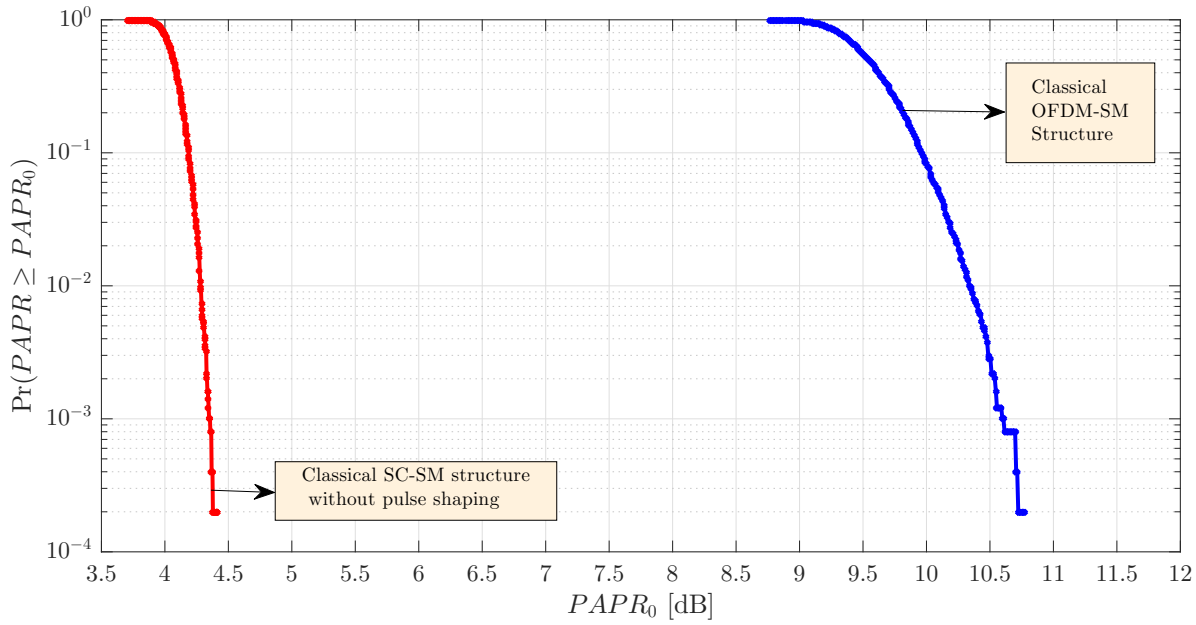

Figure 5.16: *PAPR level of the classical CP-aided OFDM-SM compared to the classical CP-aided SC-SM structure at the output of each transmit antenna element.*

obtain an enhanced uncoded BER performance given in Figure 5.15.

As we can observe in Figure 5.15, for $E_s/N_0 = 14$ dB, the uncoded BER values are lower that 10^{-2} for all values of K_{LOS} factor between -15 and 15 dB.

To conclude, SM technique is usefull for low K_{LOS} factor (Rayleigh fading context or Ricean fading with small K_{LOS} factor). Whereas, SIMO technique is a good solution for high K_{LOS} factor (LOS communication context).

5.6 PAPR level Comparison between CP-aided SC-SM/SC-SIMO and CP-aided OFDM-SM/OFDM-SIMO systems

Based on the transmit signal model, the corresponding complementary cumulative distribution functions (CCDFs) of the PAPR of both CP-aided SC-SM and CP-aided OFDM-SM systems are shown in Figure 5.16. Given that the nature of transmitted signal is similar for all transmit antenna elements, we only give the CCDF result of the PAPR for the signal vector transmitted over one of the N_t transmit antenna elements. The CCDF explicitly shows the probability of having a PAPR, which is higher than a certain PAPR threshold of $PAPR_0$, namely that we have $\Pr(PAPR \geq PAPR_0)$.

As observed in Figure 5.16, in the absence of pulse shaping, the PAPR of the classical CP-aided SC-SM scheme is about 6.5 dB lower than that of the classical SC-OFDM scheme at a CCDF of 10^{-3}. As a further metric, the PAPR of the transmitted CP-aided SC-SM signals only has a 1% probability of being above 4.2 dB.

5.7 Conclusion

In this Chapter we look at some existing multi-antenna system communications such as: SM and SIMO techniques. Moreover, in order to ensure a simple frequency domain equalization at the receiver, we are considered a CP-aided communication. For this, we presented two classical CP-aided uncoded SM/SIMO systems: CP-aided OFDM-SM/OFDM-SIMO and CP-aided SC-SM/SC-SIMO systems.

CP-aided OFDM-SM/OFDM-SIMO is an interesting MIMO system which can offer a good spectral occupancy at the transmitter and allows us to consider an optimal ML-based detection at the receiver with a reasonable computational complexity. However, the use of OFDM technique at the transmitter makes the design of High Power Amplifier (HPA) a challenging task.

On other hand, CP-aided SC-SM/SC-SIMO is an interesting system is also an interesting MIMO system offering a good PAPR level at the transmitter and allow us to consider a sub-optimal but reduced complexity MMSE-based/MRC-based detection. However, in the absence of pulse shaping at the transmitter, the transmitted signals may occupy a bandwidth larger than the reserved bandwidth.

Besides, considering a spatially uncorrelated Ricean MIMO channel matrix, SM system performances are compared to those for SIMO system for different values of Rice factor, K_{LOS}. As a result, SM technique can realize a considerable gain compared to the SIMO technique for low values of K_{LOS}. In fact, for low values of K_{LOS} SM provides a better performance in terms of BER. However, for high values of K_{LOS}, it is shown that BER/SER performances for the SM system are subject to severe degradations and thus it is preferable to consider the SIMO configuration. This result is expected given the poor diversity gain of the MIMO channel matrix in high K_{LOS} values. This result is confirmed for CP-aided OFDM-SM/OFDM-SIMO and CP-aided SC-SM/SC-SIMO systems.

In aeronautical communication context, the mission link required a very large amount of data (live video, images etc.), this link requires a high date rate. As a solution, it is interesting to take advantage of using MIMO techniques in order to exploit the diversity gain or the increase of the data rate. However, it essential to design a new SM/SIMO transmitter structure that can reach a better trade-off between PAPR level and spectral occupancy to have a low PAPR level at the transmitter and a better power efficiency to ensure a good UAV endurance.

Chapter 6

Mission link : Spatial Modulation technique

Sommaire

6.1 Introduction

In Chapter 5, two SM systems are introduced: classical CP-aided OFDM-SM system and classical CP-aided SC-SM system. The two classical SM schemes are suitable for two possible configurations: SM configuration and SIMO configuration. In SIMO configuration, the index of the active antenna takes all time the same value and this value is perfectly known at the receiver. However, in SM configuration, the index of the active antenna takes new value at each symbol duration, which makes it possible to convey extra information and increase the bit rate by the base two logarithm of the number of transmit antennas, compared to the SIMO configuration. In Chapter 5, the two classical SM systems are applied in aeronautical communication context. In the presence of Ricean MIMO channel with low values of Rice factor K_{LOS}, SM appears as an interesting modulation technique and gives better performance than SIMO technique. Or the contrary, for high values of K_{LOS} factor, the channel presents a poor diversity gain at the reception and the SIMO technique is a better solution.

Despite the fact that classical CP-aided OFDM-SM transmitter offers a good spectral occupancy, the use of OFDM modulation causes a high PAPR level and this makes the design of High Power Amplifier (HPA) a challenging task. On the contrary, classical CP-aided SC-SM transmitter, in the absence of pulse shaping, offers a low PAPR level at the expense of large bandwidth excess. In order to achieve a good trade-off between PAPR level and spectral occupancy, this chapter proposes two modified SM structures as illustrated in Figure 6.1: the first one is named « code-aided spectrally shaped DFT-Precoded OFDM-SM » and is referred to the CP-aided OFDM-SM system. Whereas, the second one is named « code-aided EW SC-OFDM-SM » and is

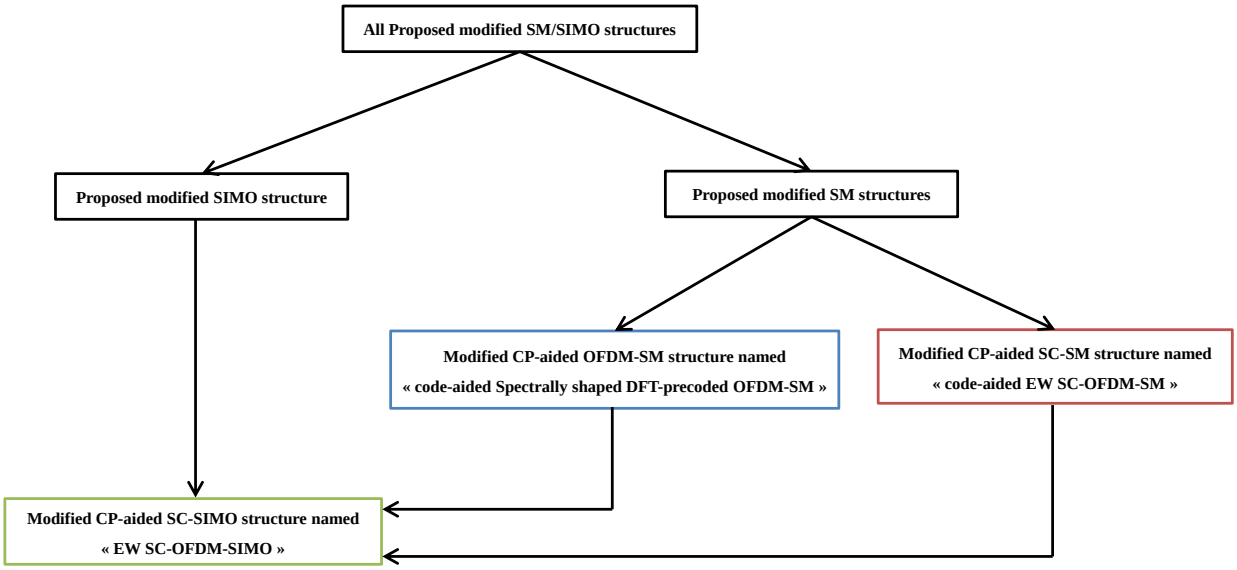

Figure 6.1: *All proposed modified structures: a modified CP-aided OFDM-SM structure and a modified CP-aided SC-SM structure for SM configuration and a common modified CP-aided SC-SIMO structure for the SIMO configuration.*

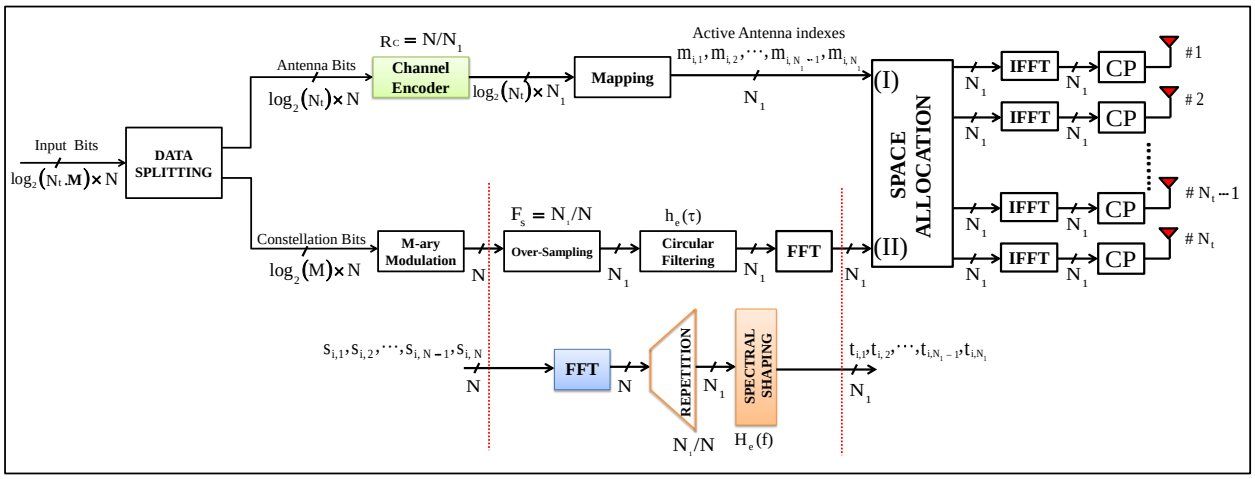

Figure 6.2: *Uncoded transmitter for the proposed code-aided spectrally shaped DFT-Precoded OFDM-SM structure*

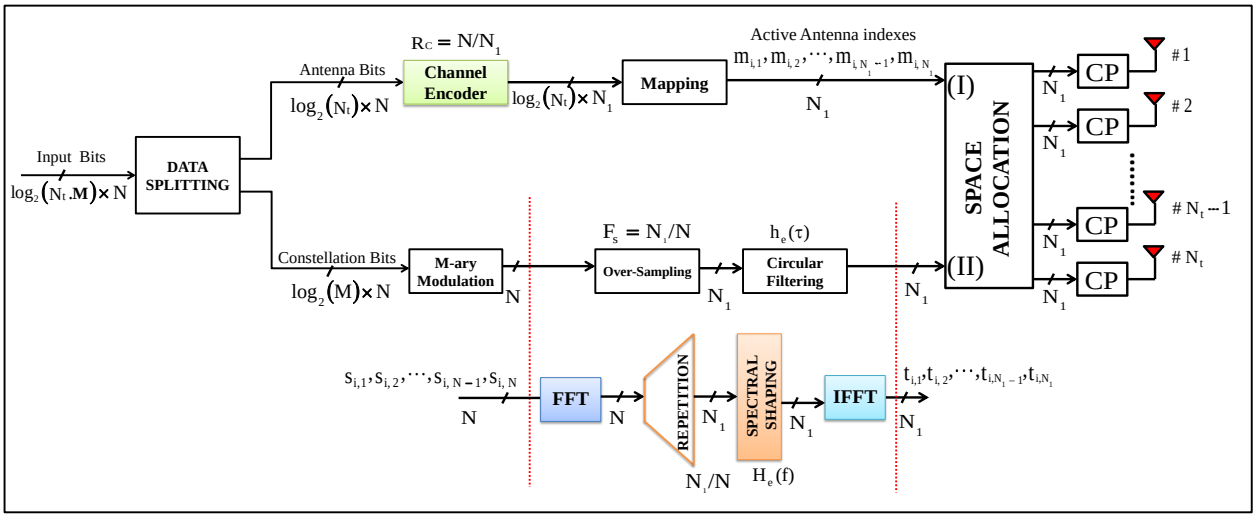

Figure 6.3: *Uncoded transmitter for the proposed code-aided EW SC-OFDM-SM structure*

referred to the CP-aided SC-SM system. The two proposed modified SM structures are presented in Figures 6.2 and 6.3, respectively. The proposed « code-aided spectrally shaped SC-OFDM structure » aims to reduce the PAPR level compared to the classical OFDM-SM structure. This done by adding a DFT operation just before selecting active transmit antennas, hence the name « DFT-precoded ». Moreover, in order to enhance active antenna selection at reception, the proposed structure uses a spectral root raised cosine (RRC) filtering with a roll-off factor β. The RRC filter extends the bandwidth by an excess bandwidth factor of $1+\beta$. This bandwidth expansion is exploited to associate a high performance error correcting code with rate $\mathrm{R}_c = 1/(1+\beta)$ for the antenna bits. The associated code allows us to protect antenna bits and thus enhances active antenna selection at the reception.

Besides, for the proposed « code-aided EW SC-OFDM-SM » structure, the main objective is to reduce the

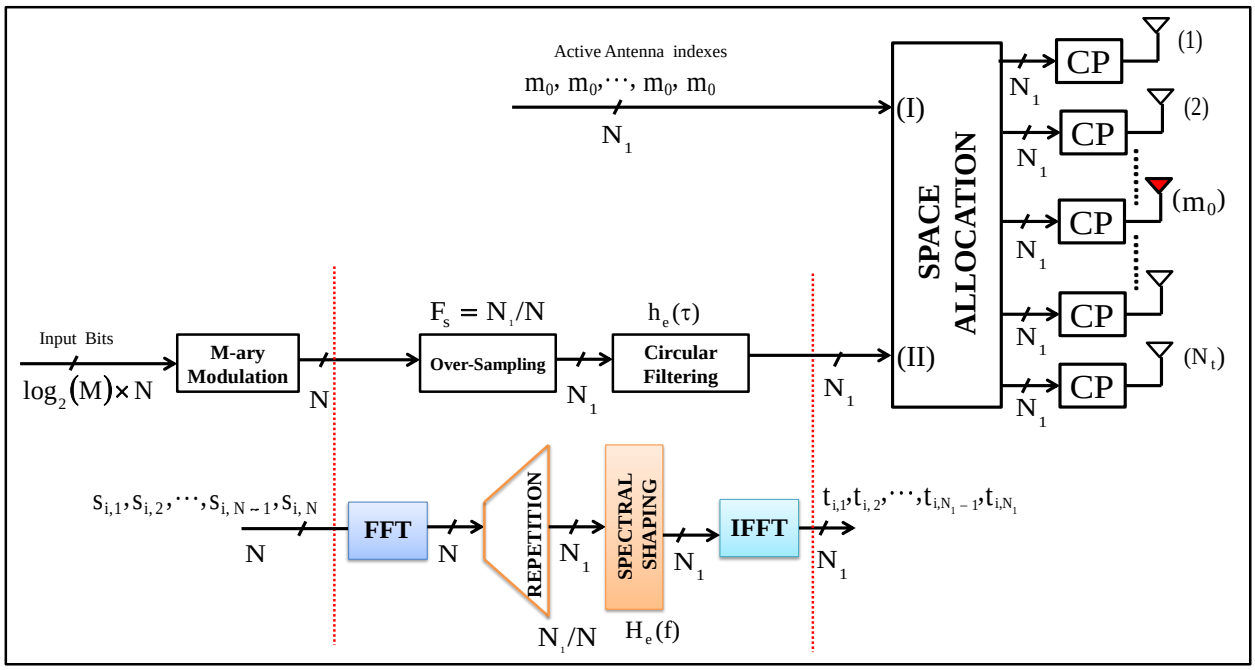

Figure 6.4: *Uncoded transmitter for the proposed EW SC-OFDM-SIMO structure*

spectral occupancy compared to the classical CP-aided SC-SM structure while maintaining the single-RF benefits of the SC-SM transmitter. This done by adding a pulse shaping filter at the transmitter. Moreover, in order to adopt a simple low complexity frequency domain equalization, we consider a EW SC-OFDM using a circular RRC pulse shaping at the transmitter.

Furthermore, we note that the two proposed modified SM structures allow us to choose between two possible configurations: SM configuration (Figures 6.2 and 6.3) and SIMO configuration (Figure 6.4). The SIMO configuration is done by choosing all time the same transmit antenna index denoted by $m_0 \in \{1,\ldots,\mathrm{N_t}\}$ i.e. $m_{i,n} = m_0 \forall 1 \leq n \leq N_1$ and $1 \leq i \leq N_f$, where $\mathrm{N_t}$, N_1 and N_f denote the number of transmit antennas, the sub-frame size and the number of sub-frames, respectively.

Finally, according the value of the $\mathrm{K_{LOS}}$ factor, this chapter discusses the favorable $\mathrm{K_{LOS}}$ value range for using the SM configuration and that for switching to SIMO configuration.

6.2 Expression of the Ricean MIMO channel for the mission link

For the mission link, refer to (5.9), the expression of the Ricean MIMO channel is expressed as:

$$\mathbf{H}_{i,n} = \sqrt{\frac{\mathrm{K_{LOS}}}{1+\mathrm{K_{LOS}}}} + \frac{1}{\sqrt{1+\mathrm{K_{LOS}}}} \times \widetilde{\mathbf{H}}_n = \left[\mathbf{h}_{i,n}^{(1)}, \mathbf{h}_{i,n}^{(2)}, \ldots, \mathbf{h}_{i,n}^{(\mathrm{N_t})}\right] \tag{6.1}$$

with $\widetilde{\mathbf{H}}_n$ is a stochastic $\mathrm{N_r} \times \mathrm{N_t}$ matrix with uncorrelated normalized complex Gaussian elements and verifying (5.6). In the following, we assume that channel matrix $\widetilde{\mathbf{H}}_n$ is fully known at the receiver. The value of the $\mathrm{K_{LOS}}$ factor depends on the nature of environment. In fact, for rich environment (Urban, Mountainous etc.),

the K_{LOS} factor takes low values. Whereas, for open environment (Flat desert, Rural etc.), the K_{LOS} factor takes high values. Also, we note that the value of the K_{LOS} factor is proportional to the UAV altitude. The higher the UAV altitude, the higher the K_{LOS} is. The maximum value of the K_{LOS} factor is 15 dB for UAV altitude of 30 Km.

6.3 Proposed modified SM/SIMO structures

In this Section, we are interested in a modified CP-aided OFDM-SM and SC-SM systems. For CP-aided OFDM-SM system, the aims is to reduce the PAPR level of the transmitted signals and ensure a good selection of active transmit antennas. Whereas, for the CP-aided SC-SM systems, the objective is to propose a new modified CP-aided SC-SM structures using a shaping filter at the transmitter in order to ensure a good spectrum occupancy.

Considering OFDM in OFDM-SM systems has attracted substantial interests because it offers a powerful and practical means to mitigate the effects of ISI in high-throughput MIMO transmissions [48]. However, the DFT operation based modulation at the transmitter disperses each sub-carrier's modulated signal across the entire DFT-block and hence erodes the single-RF benefits of SM-MIMO [121], whilst simultaneously resulting in a high PAPR.

By contrast, SC-SM is capable of retaining all the benefits of SM, whilst exhibiting a lower PAPR than its OFDM-based counterpart [102, 121, 131]. As a result, the performance of SM is less affected by the transmitter's power amplifier non-linearities. However, the absence of pulse shaping for the classical CP-aided SC-SM structure makes the transmitted signals not practical. Indeed, with the non design of pulse shaping the PSD of the transmitted occupies a large bandwidth.

6.3.1 Proposed modified CP-aided OFDM-SM structure with reduced PAPR level

In order to reduce the PAPR level, we propose a new non linear pre-coding OFDM-SM structure, named « code-aided spectrally shaped DFT-Precoded OFDM-SM » and presented in Figure 6.2. In the proposed scheme only one precoding FFT block is considered (instead of one per antenna) and SM mapping is done in the frequency domain. This enables a PAPR level reduction at the transmitter.

In SM, a good active antenna detection is required and it is often mentioned that poor detection has a detrimental effect on the system performance [103]. In order to enhance active antenna selection at the receiver, we propose to associate an error correcting code to protect the antenna bits. In fact, thanks to the use of spectral root raised cosine (RRC) shaping with roll-off β, we can associate a high performance channel coder with rate $R_c = \frac{1}{1+\beta}$ for the antenna bits. Indeed, the association of channel coding is done at the expense of a bandwidth expansion of $1+\beta$. Nevertheless, this extra redundancy can be exploited by enabling the use of redundancy on the bit antenna selection stream. As a result, we can reduce the active antenna detection error and even, we can reach the perfect active antenna selection case. Of course, all bits can be previously

coded by an error correcting code in a coded context. In this Section, we point out the fact that we consider an uncoded structure: the proposed code here is part of the modulated scheme that can be seen as a code-aided DFT-precoded OFDM-SM scheme and we focus on the performance of the uncoded structure.
Compared to the classical CP-aided OFDM-SM structure, the proposed structure operates at an oversampled rate $\mathrm{F}_s = 1+\beta$, so that the bandwidth is expanded by a factor of $1+\beta$. In the structure proposed in [117] and [100] an expansion of the bandwidth is also considered but it can not be used to increase the system bit rate. Indeed, structure proposed in [117] and [100] has a bit rate which is the same as that of OFDM-SM system. The main idea is to design a structure that provides a bandwidth extension just before the selection of active antennas. In that case, the structure is able to increase the system bit rate by a factor equal to $1+(\mathrm{F}_s-1)\times\frac{\log_2(\mathrm{N_t})}{\log_2(\mathrm{N_t})+\log_2(M)}$ compared to the OFDM-SM system, where $\mathrm{N_t}$ represents the number of transmit and the number of receive antennas. However a better strategy can be used. Indeed, the bandwidth expansion can be exploited in order to improve the detection of active antennas, which is a limiting factor, while keeping the same information bit rate as that of the OFDM-SM system. This is done by adding a high rate error correcting code (with rate equal to $\frac{1}{1+\beta}$) for the antenna selection bits, allowing to improve the detection of active antennas, while the information bit rate remains the same as that of OFDM-SM system.

6.3.1.1 Transmitter structure

For the transmitter structure shown in Figure 6.2, we assume a number of $\mathrm{N_t}$ transmit antennas. Let us consider a sequence of independent random bits to be transmitted over a uncorrelated Ricean MIMO channel. Furthermore, we consider a frame based transmission with a symbol period $\mathrm{T_s}$ and a modulation order M. The considered M-ary constellation are drawn from a discrete alphabet $\chi = \{\mathcal{C}_1, \mathcal{C}_2, \ldots, \mathcal{C}_M\}$.
Each frame contains a number of N_f sub-frames. The size of each sub-frame is $N \times \log_2(M.\mathrm{N_t})$ bits, where N is a non-zero positive integer which denotes the number of modulated symbols in each transmit sub-frame. For each transmit sub-frame $1 \leq i \leq N_f$, the transmitter starts to split the bit sequence $\mathbf{u}_i$ into two bit blocks $\mathbf{u}_i^a$ and $\mathbf{u}_i^d$ verifying $\mathbf{u}_i = [\mathbf{u}_i^a, \mathbf{u}_i^d]$. The first bit block $\mathbf{u}_i^a$ contains $N \times \log_2(\mathrm{N_t})$ bits and it is designed to select the active transmit antennas. The second bit block $\mathbf{u}_i^d$ contains $N \times \log_2(M)$ bits and it is designed to transmit constellation symbols. The two blocks will be processed as follows:

- The first antenna bit block $\mathbf{u}^a = \left[u_{i,1}^a, u_{i,1}^a, \ldots, u_{i,N\times\log_2(\mathrm{N_t})}^a\right]^T$ will be passed to an error correcting code with a Rate $R_c^a = 1/(1+\beta)$ to generate a coded bit sequence with size $(1+\beta)\times N \times \log_2(\mathrm{N_t})$ which denoted by $\mathbf{c}_i^a = \left[c_{i,1}^a, c_{i,1}^a, \ldots, c_{i,N_1\times\log_2(\mathrm{N_t})}^a\right]$. Then, $\mathbf{c}_i^a$ will be mapped to give a sequence of N_1 selected transmit antenna indexes, $\underline{\mathbf{m}}_i = [m_{i,1}, m_{i,2}, \ldots, m_{i,N_1}]^T$. Each transmit antenna index is noted $m_{i,n} \in \{1, \ldots, \mathrm{N_t}\}$.

- The second bit block $\mathbf{u}_i^d$ will be modulated into a M-ary constellation to provide a sequence of N symbols denoted by $\underline{\mathbf{s}}_i = [s_{i,1}, s_{i,2}, \ldots, s_{i,N}]^T$ where $s_{i,n} = \mathcal{C}_q \in \chi$. The N obtained symbols will be oversampled by an oversampling factor, $\mathrm{F}_s = 1+\beta$. As a result, a number of $N_1 = (1+\beta)\times N$ symbols are obtained. Then, the N_1 obtained symbols being circularly shaped by a RRC shaping filter, $h_e(\tau)$, before being

transformed to the frequency domain by using a FFT operation. As a result, the obtained spectrally shaped frequency domain sequence can be can be written in this matrix form:

$$\begin{bmatrix} t_{i,1} \\ t_{i,2} \\ \vdots \\ t_{i,N_1} \end{bmatrix} = \sqrt{\mathrm{F}_s} \times \mathbf{A}.\mathbf{F}_{\mathrm{N}}. \begin{bmatrix} s_{i,1} \\ s_{i,2} \\ \vdots \\ s_{i,N} \end{bmatrix} \tag{6.2}$$

with $\mathbf{A}$ denotes an equivalent frequency transformation matrix and expressed as:

$$\mathbf{A} = \frac{1}{\mathrm{F}_s}.\ diag \begin{bmatrix} \mathrm{H}_e(1) \\ \mathrm{H}_e(2) \\ \vdots \\ \mathrm{H}_e(N_1) \end{bmatrix} . \begin{bmatrix} \mathrm{I}^{''} \\ \mathbf{I}_{N\times N} \\ \mathrm{I}^{'} \end{bmatrix} \tag{6.3}$$

The complex coefficients $\mathrm{H}_e(1), \mathrm{H}_e(2), \ldots, \mathrm{H}_e(N_1)$ are the frequency responses of the RRC filter $h_e(\tau)$:

$$H_e(n) = \sum_{l=-\infty}^{+\infty} h_e(l.\frac{\mathrm{T}_s}{\mathrm{F}_s}) \exp\left(-2\pi j.l.\frac{\mathrm{T}_s}{\mathrm{F}_s}.f_n\right) \quad \text{with} \quad f_n = \frac{\mathrm{F}_s}{\mathrm{T}_s}.\left(\frac{n-1}{N_1} - \frac{1}{2}\right) \quad \text{for} \quad 1 \le n \le N_1 \tag{6.4}$$

Since $\mathrm{F}_s = 1+\beta$, the frequency responses $\{\mathrm{H}_e(n)\}$ are assumed non-zero and verifying:

$$\frac{1}{N_1}\sum_{l=0}^{N_1} |H_e(n)|^2 = \sum_{l=-\infty}^{+\infty} \left| h_e\left(l.\frac{\mathrm{T}_s}{\mathrm{F}_s}\right)\right|^2 = \mathrm{F}_s = 1+\beta \tag{6.5}$$

The two matrices $\mathrm{I}^{'}$ and $\mathrm{I}^{''}$ being two $\frac{N_1-N}{2} \times N$ matrices containing respectively the first $\frac{N_1-N}{2}$ and the last $\frac{N_1-N}{2}$ columns of the identity matrix $\mathbf{I}_{N\times N}$. The resulting matrix $\mathbf{A}$, having a size of $N_1 \times N$. Considering Nyquist signaling, the $\mathbf{A}$ matrix is a pseudo-orthogonal matrix verifying:

$$\mathbf{A}^H.\mathbf{A} = \mathbf{A}^T.\mathbf{A}^* = \begin{bmatrix} \lambda_1 & 0 & \cdots & 0 \\ 0 & \lambda_2 & \cdots & 0 \\ \vdots & & \ddots & \vdots \\ 0 & 0 & \cdots & \lambda_N \end{bmatrix} = \begin{bmatrix} 1 & 0 & \cdots & 0 \\ 0 & 1 & \cdots & 0 \\ \vdots & & \ddots & \vdots \\ 0 & 0 & \cdots & 1 \end{bmatrix} = \mathbf{I}_{\mathrm{N}\times\mathrm{N}} \tag{6.6}$$

We note that the $\mathbf{A}$ matrix is perfectly known at the receiver.

By using the resulting transmit antenna index sequence $\underline{\mathbf{m}}_i = [m_{i,1}, m_{i,2}, \ldots, m_{i,N_1}]^T$ and also the resulting frequency filtered sequence $\underline{\mathbf{t}}_i = [t_{i,1}, t_{i,2}, \ldots, t_{i,N_1}]^T$, a spatial allocation in the frequency domain is considered by using a simple antenna coding: For each combination $(t_{i,n}, m_{i,n})$ we associate a column vector $\mathbf{x}_{i,n}$ obtained as follows:

$$\mathbf{x}_{i,n} = \begin{bmatrix} x_{i,n}^{(1)} \\ x_{i,n}^{(2)} \\ \vdots \\ x_{i,n}^{(\mathrm{N_t})} \end{bmatrix} = [\underbrace{0,\ldots,0}_{(m_{i,n}-1)}, t_{i,n}, \underbrace{0,\ldots,0}_{\mathrm{N_t}-m_{i,n}}]^T \quad \forall \quad 1 \le n \le N_1 \qquad \text{and} \qquad \forall \quad 1 \le i \le N_f \tag{6.7}$$

Then, the resulting matrix $[\mathbf{x}_{i,1}, \mathbf{x}_{i,2}, \ldots, \mathbf{x}_{i,N_1}]$ is transformed to the time domain by using an Inverse Fast Fourier Transform (IFFT) operation. Using the Fourier matrix $\mathbf{F}_{\mathrm{N}_1}$ of size $N_1 \times N_1$, the resulting matrix

$\mathbf{E}_i = \left[\mathbf{e}_i^{(1)}, \mathbf{e}_i^{(2)}, \ldots, \mathbf{e}_i^{(\mathrm{N_t})}\right]^T$ is obtained as follows:

$$\mathbf{E}_i = \begin{bmatrix} \mathbf{e}_i^{(1)} \\ \mathbf{e}_i^{(2)} \\ \vdots \\ \mathbf{e}_i^{(\mathrm{N_t})} \end{bmatrix} = \begin{bmatrix} e_{i,1}^{(1)} & e_{i,2}^{(1)} & \ldots & e_{i,N_1}^{(1)} \\ e_{i,1}^{(2)} & e_{i,2}^{(2)} & \ldots & e_{i,N_1}^{(2)} \\ \vdots & \vdots & \ldots & \vdots \\ e_{i,1}^{(\mathrm{N_t})} & e_{i,2}^{(\mathrm{N_t})} & \ldots & e_{i,N_1}^{(\mathrm{N_t})} \end{bmatrix} = \begin{bmatrix} x_{i,1}^{(1)} & x_{i,2}^{(1)} & \ldots & x_{i,N_1}^{(1)} \\ x_{i,1}^{(2)} & x_{i,2}^{(2)} & \ldots & x_{i,N_1}^{(2)} \\ \vdots & \vdots & \ldots & \vdots \\ x_{i,1}^{(\mathrm{N_t})} & x_{i,2}^{(\mathrm{N_t})} & \ldots & x_{i,N_1}^{(\mathrm{N_t})} \end{bmatrix} . \mathbf{F}_{\mathrm{N_1}}^H \tag{6.8}$$

In the following, we assume a normalized Fourier matrix $\mathbf{F}_{\mathrm{N_1}}$ verifying $\mathbf{F}_{\mathrm{N_1}} . \mathbf{F}_{\mathrm{N_1}}^H = \mathbf{F}_{\mathrm{N_1}}^H . \mathbf{F}_{\mathrm{N_1}} = \mathbf{I}_{\mathrm{N_1} \times \mathrm{N_1}}$ with $\mathbf{I}_{\mathrm{N_1} \times \mathrm{N_1}}$ is the identity matrix with size $N_1 \times N_1$.

Finally, a Cyclic Prefix (CP) of size $\mathrm{N_t} \times N_g$ is inserted at the beginning of each resulting matrix $\mathbf{E}_i$ in order to cope with inter-symbol interference from the A2G channel and maintain sub-carriers orthogonality.

6.3.1.2 Receiver structure

At the receiver $\mathrm{N_r}$ receive antennas are considered. In each receive antenna $1 \leq n_\mathrm{r} \leq \mathrm{N_r}$, after sampling and removing CP, the resulting symbols are transformed to the frequency domain by using a Fast Fourier Transform (FFT) operation. The resulting received sequence can be expressed as:

$$\mathbf{y}_i^{(n_\mathrm{r})} = \begin{bmatrix} y_{i,1}^{(n_\mathrm{r})} \\ y_{i,2}^{(n_\mathrm{r})} \\ \vdots \\ y_{i,N_1}^{(n_\mathrm{r})} \end{bmatrix}^T = \mathbf{r}_i^{(n_\mathrm{r})} . \mathbf{F}_{\mathrm{N_1}} = \sum_{n_\mathrm{t}=1}^{\mathrm{N_t}} \begin{bmatrix} x_{i,1}^{(n_\mathrm{t})} \\ x_{i,2}^{(n_\mathrm{t})} \\ \vdots \\ x_{i,N_1}^{(n_\mathrm{t})} \end{bmatrix}^T . diag \begin{bmatrix} \mathrm{H}_{i,1}^{(n_\mathrm{r},n_\mathrm{t})} \\ \mathrm{H}_{i,2}^{(n_\mathrm{r},n_\mathrm{t})} \\ \vdots \\ \mathrm{H}_{i,N_1}^{(n_\mathrm{r},n_\mathrm{t})} \end{bmatrix} + \begin{bmatrix} \widetilde{w}_1^{(n_\mathrm{r})} \\ \widetilde{w}_2^{(n_\mathrm{r})} \\ \vdots \\ \widetilde{w}_{N_1}^{(n_\mathrm{r})} \end{bmatrix}^T \tag{6.9}$$

the resulting noise vector $\widetilde{\mathbf{w}}^{(n_\mathrm{r})} = \left[\widetilde{w}_1^{(n_\mathrm{r})}, \widetilde{w}_2^{(n_\mathrm{r})}, \ldots, \widetilde{w}_{N_1}^{(n_\mathrm{r})}\right]^T$ is a centered complex AWGN noise with two-sided spectral density equal to $\mathrm{N_0}$ and the noise variable $\left\{\widetilde{w}_n^{(n_\mathrm{r})}\right\}$ having a variance $\widetilde{\sigma}_w^2$ calculated as:

$$\widetilde{\sigma}_w^2 = \mathrm{N_0} \times \mathrm{F}_s \times \mathrm{R}_s = \mathrm{F}_s \times \sigma_w^2 \qquad \text{with} \qquad \sigma_w^2 = \mathrm{N_0} \times \mathrm{R}_s \tag{6.10}$$

For the receiver, we consider two sub-optimal detectors: MRC-based detector and MMSE-based detector. The code-aided MRC receiver is presented in Figure 6.5. Whereas, the code-aided MMSE receiver is shown in Figure 6.6. Given the expression of the received signal, the *a posteriori* log-likelihood ratio (LLR) vector for the transmitted coded antenna bit sequence $\mathbf{c}_i^a$ can be derived for all bit positions p. Indeed, for the p-th bit position verifying $p = q + (n-1) \times \log_2(\mathrm{N_t})$ with $1 \leq q \leq \log_2(\mathrm{N_t})$, the corresponding *a posteriori* LLR can be expressed as:

- *MRC receiver*: At the output of MRC detection, a $\mathrm{N_t} \times N_1$ matrix is generated and is denoted by $\mathbf{z} = [\mathbf{z}_{i,1}, \mathbf{z}_{i,2}, \ldots, \mathbf{z}_{i,N_1}]$. This output equalized matrix is used to detect the N_1 transmitted constellation symbols.

  Furthermore, in order to give a soft detection of the active transmit antennas, the receiver can take as a starting point the received vector $\mathbf{y}_{i,n} = \left[y_{i,n}^{(1)}, y_{i,n}^{(2)}, \ldots, y_{i,n}^{(\mathrm{N_r})}\right]^T$ to calculate the *a posteriori* log-likelihood ratio (LLR) vector of the transmitted coded antenna bit sequence $\mathbf{c}_i^a$. The resulting LLR vector having a size of $\log_2(\mathrm{N_t}) \times N_1$ *a posteriori* bit LLRs. At the p-th bit position verifying $p = q + (n-1) \times \log_2(\mathrm{N_t})$

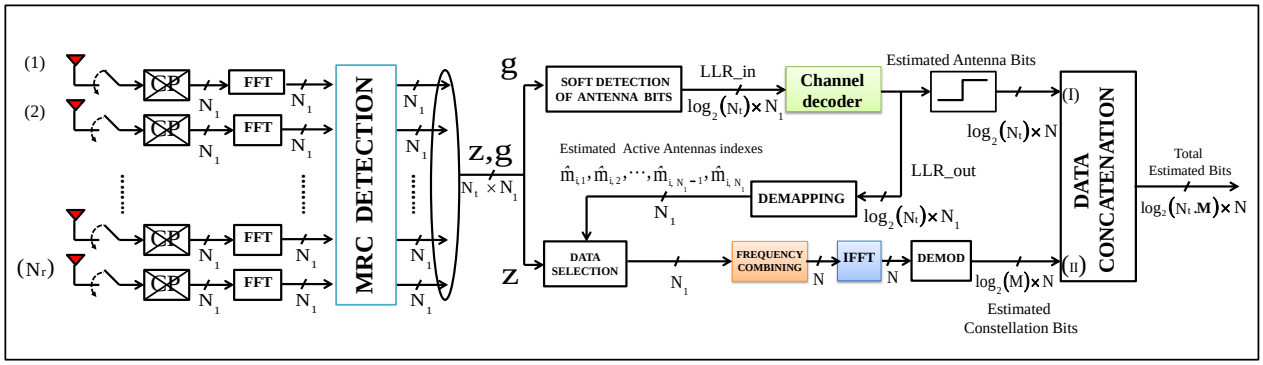

Figure 6.5: *Uncoded receiver based on MRC detection for the proposed code-aided spectrally shaped DFT-Precoded OFDM-SM structure.*

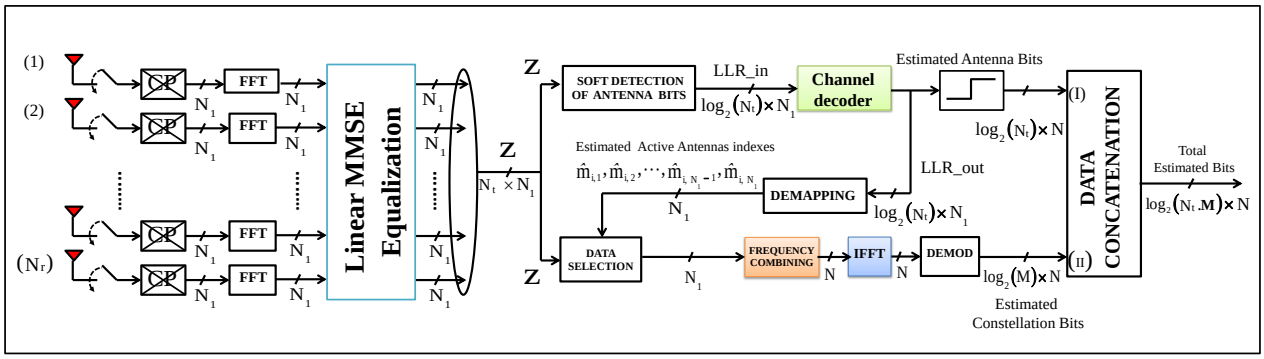

Figure 6.6: *Uncoded receiver based on MMSE detection for the proposed code-aided spectrally shaped DFT-Precoded OFDM-SM structure.*

with $1 \leq q \leq \log_2(\mathrm{N_t})$, the considered *a posteriori* LLR is expressed as:

$$\mathrm{LLR}\left\{c^{a}_{i,q+(n-1)\times\log_2(\mathrm{N_t})}\right\} = \log\left\{\frac{\sum\limits_{n_\mathrm{t}\in\mathbf{U}^0_q}\Pr\left(m_{i,n}=n_\mathrm{t}\right)\Pr\left(\mathbf{y}_{i,n}|m_{i,n}=n_\mathrm{t},t_{i,n}=\widehat{t}_{i,n},\mathbf{H}_{i,n}\right)}{\sum\limits_{n_\mathrm{t}\in\mathbf{U}^1_q}\Pr\left(m_{i,n}=n_\mathrm{t}\right)\Pr\left(\mathbf{y}_{i,n}|m_{i,n}=n_\mathrm{t},t_{i,n}=\widehat{t}_{i,n},\mathbf{H}_{i,n}\right)}\right\} \tag{6.11}$$

The two sets of the transmit antenna indexes $\mathbf{U}^0_q$ and $\mathbf{U}^1_q$ correspond to have respectively 0 and 1 entries at the q-th index position of antenna bits and verifying,

$$\mathbf{U}^0_q \cup \mathbf{U}^1_q = \{1,2,\ldots,\mathrm{N_t}\} \quad ; \quad \mathbf{U}^0_q \cap \mathbf{U}^1_q = \oslash \tag{6.12}$$

In addition, $\Pr\left(\mathbf{y}_{i,n}|m_{i,n}=n_\mathrm{t},t_{i,n}=\widehat{t}_{i,n},\mathbf{H}_{i,n}\right)$ denotes the conditional probability and its expression is detailed in Section 6.4.1.2.

- *MMSE receiver*: Similarly to the CP-aided OFDM-SM receiver, at the output of MMSE detection, a $\mathrm{N_t}\times N_1$ matrix is generated and is denoted by $\mathbf{z}=[\mathbf{z}_{i,1},\mathbf{z}_{i,2},\ldots,\mathbf{z}_{i,N_1}]$. This output equalized matrix is used to detect the N_1 transmitted constellation symbols.

  Similarly to the MRC receiver, the receiver can take as a starting point the received vector $\mathbf{y}_{i,n}=$

$\left[y_{i,n}^{(1)}, y_{i,n}^{(2)}, \ldots, y_{i,n}^{(\mathrm{N_r})}\right]^T$ to calculate the *a posteriori* log-likelihood ratio (LLR) vector of the transmitted coded antenna bit sequence $\mathbf{c}_i^a$. As a result, a LLR vector is generated for all bit positions $1 \leq p \leq \log_2(\mathrm{N_t}) \times N_1$. At the p-th bit position verifying $p = q + (n-1) \times \log_2(\mathrm{N_t})$ with $1 \leq q \leq \log_2(\mathrm{N_t})$, the *a posteriori* LLR is expressed as:

$$\mathrm{LLR}\left\{c_{i,q+(n-1)\times\log_2(\mathrm{N_t})}^a\right\} = \log\left\{\frac{\sum\limits_{n_\mathrm{t}\in\mathbf{U}_q^0} \Pr\left(m_{i,n}=n_\mathrm{t}\right)\Pr\left(\mathbf{y}_{i,n}|m_{i,n}=n_\mathrm{t}, t_{i,n}=\widehat{t}_{i,n}, \mathbf{H}_{i,n}\right)}{\sum\limits_{n_\mathrm{t}\in\mathbf{U}_q^1} \Pr\left(m_{i,n}=n_\mathrm{t}\right)\Pr\left(\mathbf{y}_{i,n}|m_{i,n}=n_\mathrm{t}, t_{i,n}=\widehat{t}_{i,n}, \mathbf{H}_{i,n}\right)}\right\} \tag{6.13}$$

As another possible strategy, the receiver can take as a starting point the output MMSE vector $\mathbf{z}_{i,n} = \left[z_{i,n}^{(1)}, z_{i,n}^{(2)}, \ldots, z_{i,n}^{(\mathrm{N_t})}\right]^T$ to compute the *a posteriori* log-likelihood ratio (LLR) vector. In this case, the expression of the *a posteriori* LLR at the p-th bit position becomes:

$$\mathrm{LLR}\left\{c_{i,q+(n-1)\times\log_2(\mathrm{N_t})}^a\right\} = \log\left\{\frac{\sum\limits_{n_\mathrm{t}\in\mathbf{U}_q^0} \Pr\left(m_{i,n}=n_\mathrm{t}\right)\Pr\left(\mathbf{z}_{i,n}|m_{i,n}=n_\mathrm{t}, t_{i,n}=\widehat{t}_{i,n}, \mathbf{H}_{i,n}\right)}{\sum\limits_{n_\mathrm{t}\in\mathbf{U}_q^1} \Pr\left(m_{i,n}=n_\mathrm{t}\right)\Pr\left(\mathbf{z}_{i,n}|m_{i,n}=n_\mathrm{t}, t_{i,n}=\widehat{t}_{i,n}, \mathbf{H}_{i,n}\right)}\right\} \tag{6.14}$$

For the two conditional probability, $\Pr\left(\mathbf{y}_{i,n}|m_{i,n}=n_\mathrm{t}, t_{i,n}=\widehat{t}_{i,n}, \mathbf{H}_{i,n}\right)$ and $\Pr\left(\mathbf{z}_{i,n}|m_{i,n}=n_\mathrm{t}, t_{i,n}=\widehat{t}_{i,n}, \mathbf{H}_{i,n}\right)$, two close expressions are detailed in in Section 6.4.1.3.

In order to improve the antenna bit detection, we consider a high performance low-density parity check (LDPC) code using belief propagation (BP) decoding and having a code rate $\mathrm{R}_c = \frac{1}{1+\beta}$ with β is roll-off factor of the transmit RRC shaping filter. For instance for $\beta = 0.375$, the considered code rate is $\mathrm{R}_c = 8/11$.
After feeding the obtained LLRs to the BP decoder, an a posteriori LLR vector of length $\log_2(\mathrm{N_t}) \times N_1$ is generated. The p-th element of the latter generated vector is denoted $\mathrm{LLR}^{\mathrm{ldpc}}\left\{c_{i,p}^a\right\}$ for $1 \leq p \leq \log_2(\mathrm{N_t}) \times N_1$. Then a hard decision of the coded block is deduced by the sign of the LLR vector generated by the LDPC decoder as follows:

$$\widehat{c}_{i,q+(n-1)\times\log_2(\mathrm{N_t})}^a = \begin{cases} 0, & \text{if } \mathrm{LLR}^{\mathrm{ldpc}}\left\{c_{i,q+(n-1)\times\log_2(\mathrm{N_t})}^a\right\} > 0. \\ 1, & \text{else.} \end{cases} \tag{6.15}$$

$$1 \leq q \leq \log_2(\mathrm{N_t}) \quad \text{and} \quad 1 \leq n \leq N_1$$

Given an estimation of bit values of the coded antenna bit block, an estimation of the active antennas is deduced as:

$$\widehat{m}_{i,n} = \sum_{q=1}^{\log_2(\mathrm{N_t})} 2^{q-1}.\ \widehat{c}_{i,q+(n-1)\times\log_2(\mathrm{N_t})}^a \quad ; \quad 1 \leq n \leq N_1 \tag{6.16}$$

After estimating the active transmit antennas for each transmitted sub-frame $1 \leq i \leq N_f$, an estimated antenna index sequence is generated, $\underline{\widehat{\mathbf{m}}}_i = [\widehat{m}_{i,1}, \widehat{m}_{i,2}, \ldots, \widehat{m}_{i,N_1}]^T$. This index sequence will be used to select the

transmitted symbols as follows:

$$\begin{bmatrix} \widetilde{t}_{i,1} \\ \widetilde{t}_{i,2} \\ \vdots \\ \widetilde{t}_{i,N_1} \end{bmatrix} = \begin{bmatrix} z_{i,1}^{(\widehat{m}_{i,1})} \\ z_{i,2}^{(\widehat{m}_{i,2})} \\ \vdots \\ z_{i,N_1}^{(\widehat{m}_{i,N_1})} \end{bmatrix} \tag{6.17}$$

After selecting data symbols, the selected frequency domain sequence must pass through a spectral filter matched to the transmit filter, in order to maximize the useful received power in the Nyquist bandwidth. Then, the obtained filtered sequence will be transformed to the time-domain by using an IFFT operation in order to recover the transmitted constellation symbols:

$$\begin{bmatrix} \widetilde{s}_{i,1} \\ \widetilde{s}_{i,2} \\ \vdots \\ \widetilde{s}_{i,N} \end{bmatrix} = \frac{1}{\sqrt{\mathrm{F}_s}} \times \mathbf{F}_{\mathrm{N}}^{H}.\ \mathbf{A}^{H}.\ \begin{bmatrix} \widetilde{t}_{i,1} \\ \widetilde{t}_{i,2} \\ \vdots \\ \widetilde{t}_{i,N_1} \end{bmatrix} \tag{6.18}$$

Then we can demodulate the transmitted constellation symbols $s_{i,n}$ by quantizing the corresponding maximum value $\widetilde{s}_{i,n}$ as:

$$\widehat{s}_{i,n} = \begin{cases} \underset{\mathcal{C}_q \in \chi}{\operatorname{argmin}} \ |\widetilde{s}_{i,n} - \mathcal{C}_q|^2 & 1 \leq n \leq N \quad \text{MRC-based detector} \\ \underset{\mathcal{C}_q \in \chi}{\operatorname{argmin}} \ |\widetilde{s}_{i,n} - \alpha_{i,n}\ \mathcal{C}_q|^2 & 1 \leq n \leq N \quad \text{MMSE-based detector} \end{cases} \tag{6.19}$$

where $\alpha_{i,n}$ denotes the resulting bias after considering MMSE equalization and its expression will be later detailed in (6.56).

6.3.2 Proposed modified CP-aided SC-SM structure with circular pulse shaping

The absence of pulse shaping for the classical CP-aided SC-SM structure makes the transmitted signals are not practical. Indeed, with the non design of pulse shaping at the transmitter, we observe an out-of-band transmitted signals. Therefore, in order to maintain the single-RF benefits of the SC-SM transmitter, it is essential to design a new modified SC-SM transmitter structure using a pulse shaping. Indeed, with the use of pulse shaping, we can have a good spectrum occupancy. However, it is shown in [128] that using a shaping filter causes an increasing PAPR. Therefore, designing the right waveform with ensuring a reasonable PAPR is a challenging task. This kind of problem has interested several studies [97, 98, 117, 128]. Recently, a detailed overview of the SM in Single Carrier modulations has been given in [128], addressing the issue of PAPR level and studying the effect of pulse shaping to reduce it compared to OFDM-SM systems. In [117], a modification of SM, named LPSM (Low PAPR SM), has been proposed to decrease the PAPR. It relies on a pre-coding scheme based on Fast Fourier Transforms (FFT) added on each transmit antenna to consider SC-OFDM waveform. Of course, the complexity increases with the number of considered antennas. In order to further reduce the PAPR with a reasonable increased complexity, in [98], we propose a modified CP-aided SC-SM structure using EW SC-OFDM waveform with considering circular RRC pulse shaping just before SM mapping. the proposed SM structure is presented Figure 6.3 and is named « code-aided EW SC-OFDM-SM

».

In the proposed scheme only one EW SC-OFDM waveform is implemented (instead of one per antenna) and is done before selecting active transmit antennas. This enables a low hardware complexity at the transmitter while still allowing PAPR reduction. Furthermore, since EW SC-OFDM operates with an over-sampling factor $\mathrm{F}_s \geq 1+\beta$, this modified structure offers the ability to associate a high performance error correcting code of rate $\mathrm{R}_c = 1/\mathrm{F}_s$ and thus it is possible to enhance active antenna selection at the receiver and reach the perfect active antenna selection case. For the proposed structure, we point out the fact that we consider an uncoded structure: the proposed code here is part of the modulated scheme that can be seen as a code-aided EW SC-OFDM-SM scheme and we focus on the performance of the uncoded structure.

6.3.2.1 Transmitter structure

For the transmitter structure shown in Figure 6.3, we assume a number of $\mathrm{N_t}$ transmit antennas. Let us consider a sequence of independent random bits to be transmitted over a uncorrelated Ricean MIMO channel. Furthermore, we consider a frame based transmission with a symbol period $\mathrm{T_s}$ and a modulation order M. The considered M-ary constellation are drawn from a discrete alphabet $\chi = \{\mathcal{C}_1, \mathcal{C}_2, \ldots, \mathcal{C}_M\}$.
Each frame contains a number of N_f sub-frames. The size of each sub-frame is $N \times \log_2(M.\mathrm{N_t})$ bits, where N is a non-zero positive integer which denotes the number of modulated symbols in each transmit sub-frame. For each transmit sub-frame $1 \leq i \leq N_f$, the transmitter starts to split the bit sequence $\mathbf{u}_i$ into two bit blocks $\mathbf{u}_i^a$ and $\mathbf{u}_i^d$ verifying $\mathbf{u}_i = [\mathbf{u}_i^a, \mathbf{u}_i^d]$. The first bit block $\mathbf{u}_i^a$ contains $N \times \log_2(\mathrm{N_t})$ bits and it is designed to select the active transmit antennas. The second bit block $\mathbf{u}_i^d$ contains $N \times \log_2(M)$ bits and it is designed to transmit constellation symbols. The two blocks will be processed as follows:

- The first antenna bit block $\mathbf{u}^a = \left[u_{i,1}^a, u_{i,1}^a, \ldots, u_{i,N\times\log_2(\mathrm{N_t})}^a\right]^T$ will be passed to an error correcting code with a Rate $R_c^a = 1/\mathrm{F}_s$ to generate a coded bit sequence with size $\mathrm{F}_s \times N \times \log_2(\mathrm{N_t})$ which denoted by $\mathbf{c}_i^a = \left[c_{i,1}^a, c_{i,1}^a, \ldots, c_{i,N_1\times\log_2(\mathrm{N_t})}^a\right]$. Then, $\mathbf{c}_i^a$ will be mapped to give a sequence of N_1 selected transmit antenna indexes, $\underline{\mathbf{m}}_i = [m_{i,1}, m_{i,2}, \ldots, m_{i,N_1}]^T$. Each transmit antenna index is noted $m_{i,n} \in \{1, \ldots, \mathrm{N_t}\}$.

- The second bit block $\mathbf{u}_i^d$ will be modulated into a M-ary constellation to provide a sequence of N symbols denoted by $\underline{\mathbf{s}}_i = [s_{i,1}, s_{i,2}, \ldots, s_{i,N}]^T$ where $s_{i,n} = \mathcal{C}_q \in \chi$. The N obtained symbols will be oversampled by an oversampling factor, $\mathrm{F}_s \geq 1+\beta$. As a result, a number of $N_1 = \mathrm{F}_s \times N$ symbols are obtained. Then, the N_1 obtained symbols being circularly shaped by a RRC shaping filter, $h_e(\tau)$, before being transformed to the frequency domain by using a FFT operation. As a result, the obtained spectrally shaped frequency domain sequence can be can be written in this matrix form:

$$\begin{bmatrix} t_{i,1} \\ t_{i,2} \\ \vdots \\ t_{i,N_1} \end{bmatrix} = \sqrt{\mathrm{F}_s} \times \mathbf{F}_{\mathrm{N_1}}^H . \mathbf{A} . \mathbf{F}_{\mathrm{N}} . \begin{bmatrix} s_{i,1} \\ s_{i,2} \\ \vdots \\ s_{i,N} \end{bmatrix} \tag{6.20}$$

By using the resulting transmit antenna index sequence $\underline{\mathbf{m}}_i = [m_{i,1}, m_{i,2}, \ldots, m_{i,N_1}]^T$ and also the resulting frequency filtered sequence $\underline{\mathbf{t}}_i = [t_{i,1}, t_{i,2}, \ldots, t_{i,N_1}]^T$, a spatial allocation in the frequency domain is considered by using a simple antenna coding: For each combination $(t_{i,n}, m_{i,n})$ we associate a column vector $\mathbf{x}_{i,n}$ obtained as follows:

$$\mathbf{x}_{i,n} = \begin{bmatrix} x_{i,n}^{(1)} \\ x_{i,n}^{(2)} \\ \vdots \\ x_{i,n}^{(\mathrm{N_t})} \end{bmatrix} = [\underbrace{0,\ldots,0}_{(m_{i,n}-1)}, t_{i,n}, \underbrace{0,\ldots,0}_{\mathrm{N_t}-m_{i,n}}]^T \quad \forall \quad 1 \leq n \leq N_1 \qquad \text{and} \qquad \forall \quad 1 \leq i \leq N_f \tag{6.21}$$

Then, the resulting matrix $[\mathbf{x}_{i,1}, \mathbf{x}_{i,2}, \ldots, \mathbf{x}_{i,N_1}]$ is transformed to the time domain by using an Inverse Fast Fourier Transform (IFFT) operation. Using the Fourier matrix $\mathbf{F}_{\mathrm{N_1}}$ of size $N_1 \times N_1$, the resulting matrix $\mathbf{E}_i = \left[\mathbf{e}_i^{(1)}, \mathbf{e}_i^{(2)}, \ldots, \mathbf{e}_i^{(\mathrm{N_t})}\right]^T$ is obtained as follows:

$$\mathbf{E}_i = \begin{bmatrix} \mathbf{e}_i^{(1)} \\ \mathbf{e}_i^{(2)} \\ \vdots \\ \mathbf{e}_i^{(\mathrm{N_t})} \end{bmatrix} = \begin{bmatrix} e_{i,1}^{(1)} & e_{i,2}^{(1)} & \ldots & e_{i,N_1}^{(1)} \\ e_{i,1}^{(2)} & e_{i,2}^{(2)} & \ldots & e_{i,N_1}^{(2)} \\ \vdots & \vdots & \ldots & \vdots \\ e_{i,1}^{(\mathrm{N_t})} & e_{i,2}^{(\mathrm{N_t})} & \ldots & e_{i,N_1}^{(\mathrm{N_t})} \end{bmatrix} = \begin{bmatrix} x_{i,1}^{(1)} & x_{i,2}^{(1)} & \ldots & x_{i,N_1}^{(1)} \\ x_{i,1}^{(2)} & x_{i,2}^{(2)} & \ldots & x_{i,N_1}^{(2)} \\ \vdots & \vdots & \ldots & \vdots \\ x_{i,1}^{(\mathrm{N_t})} & x_{i,2}^{(\mathrm{N_t})} & \ldots & x_{i,N_1}^{(\mathrm{N_t})} \end{bmatrix} \tag{6.22}$$

Finally, a Cyclic Prefix (CP) of size $\mathrm{N_t} \times N_g$ is inserted at the beginning of each resulting matrix $\mathbf{E}_i$ in order to cope with inter-symbol interference from the A2G channel and maintain sub-carriers orthogonality.

6.3.2.2 Receiver structure

At the receiver $\mathrm{N_r}$ receive antennas are considered. In each receive antenna $1 \leq n_\mathrm{r} \leq \mathrm{N_r}$, after sampling and removing CP, the resulting symbols are transformed to the frequency domain by using a Fast Fourier Transform (FFT) operation. The resulting received sequence can be expressed as:

$$\mathbf{y}_i^{(n_\mathrm{r})} = \begin{bmatrix} y_{i,1}^{(n_\mathrm{r})} \\ y_{i,2}^{(n_\mathrm{r})} \\ \vdots \\ y_{i,N_1}^{(n_\mathrm{r})} \end{bmatrix}^T = \mathbf{r}_i^{(n_\mathrm{r})}.\mathbf{F}_{\mathrm{N_1}} = \sum_{n_\mathrm{t}=1}^{\mathrm{N_t}} \begin{bmatrix} x_{i,1}^{(n_\mathrm{t})} \\ x_{i,2}^{(n_\mathrm{t})} \\ \vdots \\ x_{i,N_1}^{(n_\mathrm{t})} \end{bmatrix}^T .\mathbf{F}_{\mathrm{N_1}}.diag \begin{bmatrix} \mathrm{H}_{i,1}^{(n_\mathrm{r},n_\mathrm{t})} \\ \mathrm{H}_{i,2}^{(n_\mathrm{r},n_\mathrm{t})} \\ \vdots \\ \mathrm{H}_{i,N_1}^{(n_\mathrm{r},n_\mathrm{t})} \end{bmatrix} + \begin{bmatrix} \widetilde{w}_1^{(n_\mathrm{r})} \\ \widetilde{w}_2^{(n_\mathrm{r})} \\ \vdots \\ \widetilde{w}_{N_1}^{(n_\mathrm{r})} \end{bmatrix}^T \tag{6.23}$$

The resulting noise vector $\widetilde{\mathbf{w}}^{(n_\mathrm{r})} = \left[\widetilde{w}_1^{(n_\mathrm{r})}, \widetilde{w}_2^{(n_\mathrm{r})}, \ldots, \widetilde{w}_{N_1}^{(n_\mathrm{r})}\right]^T$ is a centered complex AWGN noise with two-sided spectral density equal to $\mathrm{N_0}$ and the noise variable $\left\{\widetilde{w}_n^{(n_\mathrm{r})}\right\}$ having a variance $\widetilde{\sigma}_w^2$ calculated as:

$$\widetilde{\sigma}_w^2 = \mathrm{N_0} \times \mathrm{F}_s \times \mathrm{R}_s = \mathrm{F}_s \times \sigma_w^2 \qquad \text{with} \qquad \sigma_w^2 = \mathrm{N_0} \times \mathrm{R}_s \tag{6.24}$$

For the receiver, we consider a sub-optimal MMSE-based detector and the code-aided MMSE receiver is shown in Figure 6.7. At the output of MMSE detection, a $\mathrm{N_t} \times N_1$ matrix is generated, $\mathbf{z} = [\mathbf{z}_{i,1}, \mathbf{z}_{i,2}, \ldots, \mathbf{z}_{i,N_1}]$. This output equalized matrix is used for both the active transmit antenna detection and the transmitted constellation symbol detection. Assuming $\mathbf{z}_{i,n} = \left[z_{i,n}^{(1)}, z_{i,n}^{(2)}, \ldots, z_{i,n}^{(\mathrm{N_t})}\right]^T$, the *a posteriori* log-likelihood ratio (LLR) vector for the transmitted coded antenna bit sequence $\mathbf{c}_i^a$ can be derived for all bit positions p. Indeed,

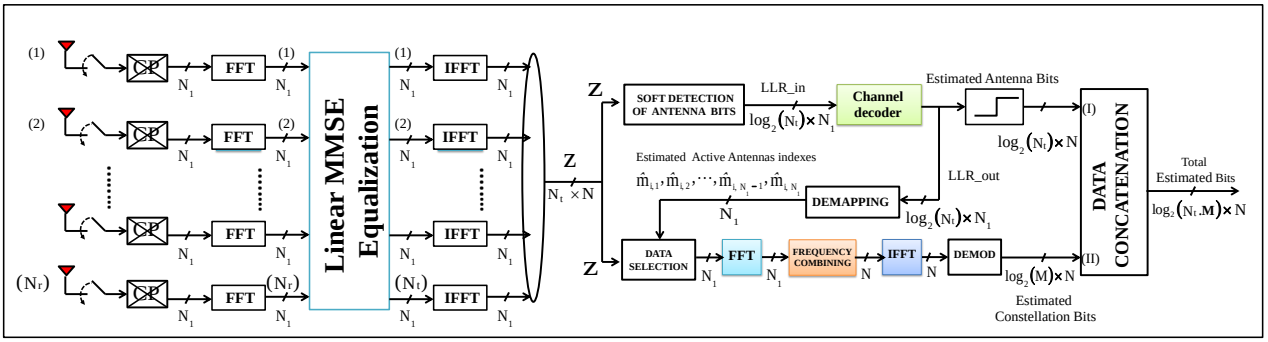

Figure 6.7: *Uncoded receiver based on MMSE detection for the proposed code-aided EW SC-OFDM-SM structure.*

for the p-th bit position verifying $p = q + (n-1) \times \log_2(\mathrm{N_t})$ with $1 \leq q \leq \log_2(\mathrm{N_t})$, the corresponding *a posteriori* LLR can be expressed as:

$$\mathrm{LLR}\left\{c^a_{i,q+(n-1)\times\log_2(\mathrm{N_t})}\right\} = \log\left\{\frac{\sum\limits_{n_\mathrm{t}\in\mathbf{U}^0_q}\Pr\left(m_{i,n}=n_\mathrm{t}\right)\Pr\left(\mathbf{z}_{i,n}|m_{i,n}=n_\mathrm{t},t_{i,n}=\widehat{t}_{i,n},\mathbf{H}_i\right)}{\sum\limits_{n_\mathrm{t}\in\mathbf{U}^1_q}\Pr\left(m_{i,n}=n_\mathrm{t}\right)\Pr\left(\mathbf{z}_n|m_{i,n}=n_\mathrm{t},t_{i,n}=\widehat{t}_{i,n},\mathbf{H}_i\right)}\right\} \tag{6.25}$$

where $\Pr\left(\mathbf{z}_{i,n}|m_{i,n}=n_\mathrm{t},t_{i,n}=\widehat{t}_{i,n},\mathbf{H}_i\right)$ denotes the conditional probability when we take as a starting point the output vector $\mathbf{z}_{i,n}$. The expression of the conditional probability is detailed in Section 6.4.2.2.

In order to improve the antenna bit detection, we consider a high performance low-density parity check (LDPC) code using belief propagation (BP) decoding and having a code rate $\mathrm{R}_c = 1/\mathrm{F}_s$ with $\mathrm{F}_s \geq 1+\beta$ is the considered oversampling factor.

After feeding the obtained LLRs to the BP decoder, an a posteriori LLR vector of length $\log_2(\mathrm{N_t}) \times N_1$ is generated. The p-th element of the latter generated vector is denoted $\mathrm{LLR}^{\mathrm{ldpc}}\left\{c^a_{i,p}\right\}$ for $1 \leq p \leq \log_2(\mathrm{N_t}) \times N_1$. Then a hard decision of the coded block is deduced by the sign of the LLR vector generated by the LDPC decoder as follows:

$$\widehat{c}^a_{i,q+(n-1)\times\log_2(\mathrm{N_t})} = \begin{cases} 0, & \text{if } \mathrm{LLR}^{\mathrm{ldpc}}\left\{c^a_{i,q+(n-1)\times\log_2(\mathrm{N_t})}\right\} > 0. \\ 1, & \text{else.} \end{cases} \tag{6.26}$$

$$1 \leq q \leq \log_2(\mathrm{N_t}) \quad \text{and} \quad 1 \leq n \leq N_1$$

Given an estimation of bit values of the coded antenna bit block, an estimation of the active antennas is deduced as:

$$\widehat{m}_{i,n} = \sum_{q=1}^{\log_2(\mathrm{N_t})} 2^{q-1}.\ \widehat{c}^a_{i,q+(n-1)\times\log_2(\mathrm{N_t})} \quad ; \quad 1 \leq n \leq N_1 \tag{6.27}$$

After estimating the active transmit antennas for each transmitted sub-frame $1 \leq i \leq N_f$, an estimated antenna index sequence is generated, $\underline{\widehat{\mathbf{m}}}_i = [\widehat{m}_{i,1}, \widehat{m}_{i,2}, \ldots, \widehat{m}_{i,N_1}]^T$. This index sequence will be used to select the

transmitted symbols as follows:

$$\begin{bmatrix} \widetilde{t}_{i,1} \\ \widetilde{t}_{i,2} \\ \vdots \\ \widetilde{t}_{i,N_1} \end{bmatrix} = \begin{bmatrix} z_{i,1}^{(\widehat{m}_{i,1})} \\ z_{i,2}^{(\widehat{m}_{i,2})} \\ \vdots \\ z_{i,N_1}^{(\widehat{m}_{i,N_1})} \end{bmatrix} \tag{6.28}$$

After selecting data symbols, the selected frequency domain sequence must pass through a spectral filter matched to the transmit filter, in order to maximize the useful received power in the Nyquist bandwidth. Then, the obtained filtered sequence will be transformed to the time-domain by using an IFFT operation in order to recover the transmitted constellation symbols:

$$\begin{bmatrix} \widetilde{s}_{i,1} \\ \widetilde{s}_{i,2} \\ \vdots \\ \widetilde{s}_{i,N} \end{bmatrix} = \frac{1}{\sqrt{\mathrm{F}_s}} \times \mathbf{F}_{\mathrm{N}}^{H} . \mathbf{A}^{H} . \mathbf{F}_{\mathrm{N}_1} . \begin{bmatrix} \widetilde{t}_{i,1} \\ \widetilde{t}_{i,2} \\ \vdots \\ \widetilde{t}_{i,N_1} \end{bmatrix} \tag{6.29}$$

Then we can demodulate the transmitted constellation symbols $s_{i,n}$ by quantizing the corresponding maximum value $\widetilde{s}_{i,n}$ as:

$$\widehat{s}_{i,n} = \underset{\mathcal{C}_q \in \chi}{\operatorname{argmin}} \ |\widetilde{s}_{i,n} - \mathcal{C}_q|^2 \qquad 1 \leq n \leq N \tag{6.30}$$

where α_i denotes the resulting bias after considering MMSE equalization and its expression will be later detailed in (6.75).

6.3.3 Proposed modified CP-aided SC-SIMO structure with circular pulse shaping

6.3.3.1 Transmitter SIMO structure

We consider a number of $\mathrm{N_t}$ of transmit antennas. Only a single transmit antenna, having a antenna index $m_0 \in \{1, \ldots, \mathrm{N_t}\}$, is activated during all transmitted sub-frames. The transmitter of the classical CP-aided OFDM-SIMO is given in Figure 6.4.

Let us consider a sequence of independent random bits to be transmitted over a uncorrelated Ricean MIMO channel. Furthermore, we consider a frame based transmission with a symbol period $\mathrm{T_s}$ and a modulation order M. Each frame contains a number of N_f sub-frames. The size of each sub-frame is $N \times \log_2(M)$ bits. The considered M-ary constellation are drawn from a discrete alphabet $\chi = \{\mathcal{C}_1, \mathcal{C}_2, \ldots, \mathcal{C}_M\}$.

The input bit block $\mathbf{u}_i^d$ will be modulated into a M-ary constellation to provide a sequence of N constellation symbols denoted by $\underline{\mathbf{s}}_i = [s_{i,1}, s_{i,2}, \ldots, s_{i,N}]^T$ where $s_{i,n} = \mathcal{C}_q \in \chi$. The N obtained symbols will be oversampled by an oversampling factor, $\mathrm{F}_s \geq 1 + \beta$. As a result, a number of $N_1 = \mathrm{F}_s \times N$ symbols are obtained. Then, the N_1 obtained symbols being circularly shaped by a RRC shaping filter, $h_e(\tau)$, before being transformed to the frequency domain by using a FFT operation. As a result, the obtained spectrally shaped frequency domain

sequence can be can be written in this matrix form:

$$\begin{bmatrix} t_{i,1} \\ t_{i,2} \\ \vdots \\ t_{i,N_1} \end{bmatrix} = \sqrt{\mathrm{F}_s} \times \mathbf{F}_{\mathrm{N}_1}^{H}.\ \mathbf{A}.\ \mathbf{F}_{\mathrm{N}}.\ \begin{bmatrix} s_{i,1} \\ s_{i,2} \\ \vdots \\ s_{i,N} \end{bmatrix} \tag{6.31}$$

Space allocation in the frequency domain: Assuming m_0 is the index of the selected active transmit antenna, the obtained constellation sequence $\underline{\mathbf{s}}_i$ will be transmitted via the m_0 transmit antenna. As a result, we have:

$$\mathbf{E}_i = \begin{bmatrix} e_{i,1}^{(1)} & e_{i,2}^{(1)} & \dots & e_{i,N_1}^{(1)} \\ \vdots & \vdots & \dots & \vdots \\ e_{i,1}^{(m_0)} & e_{i,2}^{(m_0)} & \dots & e_{i,N_1}^{(m_0)} \\ \vdots & \vdots & \dots & \vdots \\ e_{i,1}^{(\mathrm{N_t})} & e_{i,2}^{(\mathrm{N_t})} & \dots & e_{i,N_1}^{(\mathrm{N_t})} \end{bmatrix} = \begin{bmatrix} x_{i,1}^{(1)} & x_{i,2}^{(1)} & \dots & x_{i,N_1}^{(1)} \\ \vdots & \vdots & \dots & \vdots \\ x_{i,1}^{(m_0)} & x_{i,2}^{(m_0)} & \dots & x_{i,N_1}^{(m_0)} \\ \vdots & \vdots & \dots & \vdots \\ x_{i,1}^{(\mathrm{N_t})} & x_{i,2}^{(\mathrm{N_t})} & \dots & x_{i,N_1}^{(\mathrm{N_t})} \end{bmatrix} = \begin{bmatrix} 0 & 0 & \dots & 0 \\ \vdots & \vdots & \dots & \vdots \\ t_{i,1} & t_{i,2} & \dots & t_{i,N_1} \\ \vdots & \vdots & \dots & \vdots \\ 0 & 0 & \dots & 0 \end{bmatrix} \tag{6.32}$$

Add Cyclic Prefix: In each transmit antenna, a Cyclic Prefix (CP) of size $\mathrm{N_t} \times N_g$ is inserted at the beginning of each resulting matrix $\mathbf{E}_i$ in order to cope with inter-symbol interference from the channel and maintain sub-carriers orthogonality.

6.3.3.2 Receiver SM structure

For the receiver, we consider a sub-optimal MMSE-based detector and the MMSE receiver is shown in Figure 6.9. At the receiver a number of $\mathrm{N_r}$ receive antennas are considered.

Thanks to the add of a circular prefix at the transmitter, the A2G channel has a circular form. Thus, the time-domain received sample sequence for each receive antenna $1 \leq n_{\mathrm{r}} \leq \mathrm{N_r}$ can be given as follows:

$$\begin{aligned} \mathbf{r}_i^{(n_{\mathrm{r}})} = \begin{bmatrix} r_{i,1}^{(n_{\mathrm{r}})} \\ r_{i,2}^{(n_{\mathrm{r}})} \\ \vdots \\ r_{i,N_1}^{(n_{\mathrm{r}})} \end{bmatrix}^T &= \sum_{n_{\mathrm{t}}=1}^{\mathrm{N_t}} \begin{bmatrix} x_{i,1}^{(n_{\mathrm{t}})} \\ x_{i,2}^{(n_{\mathrm{t}})} \\ \vdots \\ x_{i,N_1}^{(n_{\mathrm{t}})} \end{bmatrix}^T . \left\{ \mathbf{F}_{\mathrm{N}_1}.diag \begin{bmatrix} \mathrm{H}_{i,1}^{(n_{\mathrm{r}},n_{\mathrm{t}})} \\ \mathrm{H}_{i,2}^{(n_{\mathrm{r}},n_{\mathrm{t}})} \\ \vdots \\ \mathrm{H}_{i,N_1}^{(n_{\mathrm{r}},n_{\mathrm{t}})} \end{bmatrix} .\mathbf{F}_{\mathrm{N}_1}^{H} \right\} + \begin{bmatrix} \widetilde{w}_1^{(n_{\mathrm{r}})} \\ \widetilde{w}_2^{(n_{\mathrm{r}})} \\ \vdots \\ \widetilde{w}_{N_1}^{(n_{\mathrm{r}})} \end{bmatrix}^T \\ &= \begin{bmatrix} t_{i,1} \\ t_{i,2} \\ \vdots \\ t_{i,N_1} \end{bmatrix}^T . \left\{ \mathbf{F}_{\mathrm{N}_1}.diag \begin{bmatrix} \mathrm{H}_{i,1}^{(n_{\mathrm{r}},m_0)} \\ \mathrm{H}_{i,2}^{(n_{\mathrm{r}},m_0)} \\ \vdots \\ \mathrm{H}_{i,N_1}^{(n_{\mathrm{r}},m_0)} \end{bmatrix} .\mathbf{F}_{\mathrm{N}_1}^{H} \right\} + \begin{bmatrix} \widetilde{w}_1^{(n_{\mathrm{r}})} \\ \widetilde{w}_2^{(n_{\mathrm{r}})} \\ \vdots \\ \widetilde{w}_{N_1}^{(n_{\mathrm{r}})} \end{bmatrix}^T \end{aligned} \tag{6.33}$$

the resulting noise vector $\widetilde{\mathbf{w}}^{(n_{\mathrm{r}})} = \left[\widetilde{w}_1^{(n_{\mathrm{r}})}, \widetilde{w}_2^{(n_{\mathrm{r}})}, \dots, \widetilde{w}_{N_1}^{(n_{\mathrm{r}})}\right]^T$ is a centered complex AWGN noise with twosided spectral density equal to $\mathrm{N_0}$ and the noise variable $\left\{\widetilde{w}_n^{(n_{\mathrm{r}})}\right\}$ having a variance $\widetilde{\sigma}_w^2$ calculated as:

$$\widetilde{\sigma}_w^2 = \mathrm{N_0} \times \mathrm{F}_s \times \mathrm{R}_s = \mathrm{F}_s \times \sigma_w^2 \qquad \text{with} \qquad \sigma_w^2 = \mathrm{N_0} \times \mathrm{R}_s \tag{6.34}$$

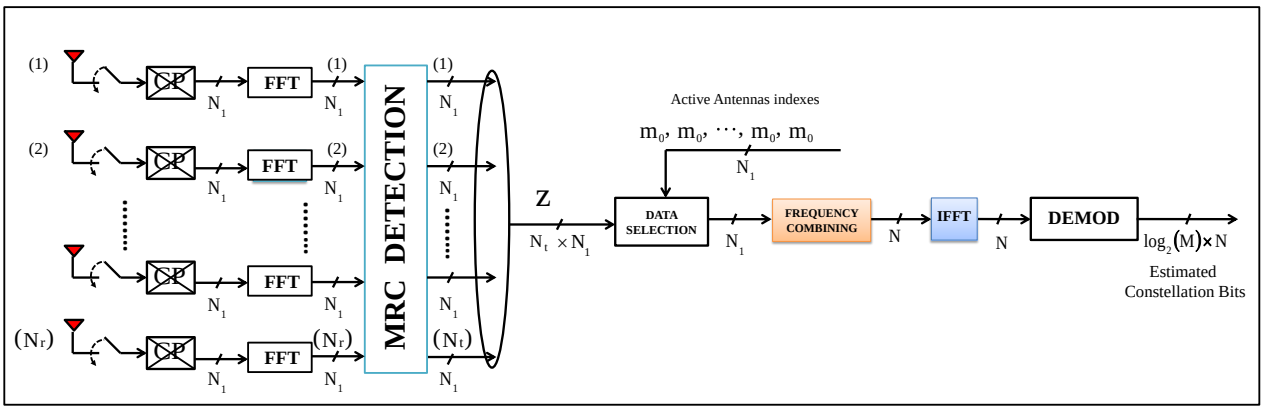

Figure 6.8: *Uncoded receiver based on MRC detection for the proposed EW SC-OFDM-SIMO.*

For each receive antenna $1 \leq n_{\mathrm{r}} \leq \mathrm{N_r}$, the receiver starts to transform the resulting received sequence $\mathbf{r}_i^{(n_{\mathrm{r}})}$ to the frequency domain by using a Fast Fourier Transform (FFT) operation as follows:

$$\mathbf{y}_i^{(n_{\mathrm{r}})} = \begin{bmatrix} y_{i,1}^{(n_{\mathrm{r}})} \\ y_{i,2}^{(n_{\mathrm{r}})} \\ \vdots \\ y_{i,N_1}^{(n_{\mathrm{r}})} \end{bmatrix}^T = \mathbf{r}_i^{(n_{\mathrm{r}})}.\mathbf{F}_{\mathrm{N}_1} = \begin{bmatrix} T_{i,1} \\ T_{i,2} \\ \vdots \\ T_{i,N_1} \end{bmatrix}^T .diag \begin{bmatrix} \mathrm{H}_{i,1}^{(n_{\mathrm{r}},m_0)} \\ \mathrm{H}_{i,2}^{(n_{\mathrm{r}},m_0)} \\ \vdots \\ \mathrm{H}_{i,N_1}^{(n_{\mathrm{r}},m_0)} \end{bmatrix} + \begin{bmatrix} \widetilde{w}_1^{(n_{\mathrm{r}})} \\ \widetilde{w}_2^{(n_{\mathrm{r}})} \\ \vdots \\ \widetilde{w}_{N_1}^{(n_{\mathrm{r}})} \end{bmatrix}^T \tag{6.35}$$

where $\mathbf{T}_i = [T_{i,1}, T_{i,2}, \ldots, T_{i,N_1}]$ is the frequency response of the transmitted data symbol sequence . By using Equation (6.31), the expression of $\mathbf{T}_i$ is done:

$$\begin{bmatrix} T_{i,1} \\ T_{i,2} \\ \vdots \\ T_{i,N_1} \end{bmatrix}^T = \begin{bmatrix} t_{i,1} \\ t_{i,2} \\ \vdots \\ t_{i,N_1} \end{bmatrix}^T .\mathbf{F}_{\mathrm{N}_1} = \sqrt{\mathrm{F}_s} \times \begin{bmatrix} s_{i,1} \\ s_{i,2} \\ \vdots \\ s_{i,N_1} \end{bmatrix}^T .\mathbf{F}_{\mathrm{N}}.\ \mathbf{A} \tag{6.36}$$

On other hand, the expression of the received frequency domain symbols, can be also re-written in the following form given in each frequency index $1 \leq n \leq N_1$ as follows:

$$\mathbf{y}_{i,n} = \begin{bmatrix} y_{i,n}^{(1)} \\ y_{i,n}^{(2)} \\ \vdots \\ y_{i,n}^{(\mathrm{N_r})} \end{bmatrix} = T_{i,n} \begin{bmatrix} \mathrm{H}_{i,n}^{(1,m_0)} \\ \mathrm{H}_{i,n}^{(2,m_0)} \\ \vdots \\ \mathrm{H}_{i,n}^{(\mathrm{N_r},m_0)} \end{bmatrix} + \begin{bmatrix} \widetilde{w}_n^{(1)} \\ \widetilde{w}_n^{(2)} \\ \vdots \\ \widetilde{w}_n^{(\mathrm{N_r})} \end{bmatrix} = T_{i,n}\ \mathbf{h}_{i,n}^{(m_0)} + \widetilde{\mathbf{w}}_n \tag{6.37}$$

Optimal detector: MRC-based receiver The Maximum Ratio Combining (MRC) detector is a sub-optimal linear detector and is presented in Figure 6.8. After MRC decoding, a resulting output vector $\mathbf{z}_{i,n} = \left[z_{i,n}^{(1)}, z_{i,n}^{(2)}, \ldots, z_{i,n}^{(m_0)}, \ldots, z_{i,n}^{(\mathrm{N_t})}\right]^T$ is obtained for $1 \leq n \leq N_1$. Then, by knowing that the index of the active transmit antenna is equal to m_0, the receiver selects the symbols corresponding to the m_0 transmit antenna. As a result, a sequence of N_1symbols, denoted by $\mathbf{z}_i = \left[z_{i,1}^{(m_0)}, z_{i,2}^{(m_0)}, \ldots, z_{i,N_1}^{(m_0)}\right]$, is obtained. Each element

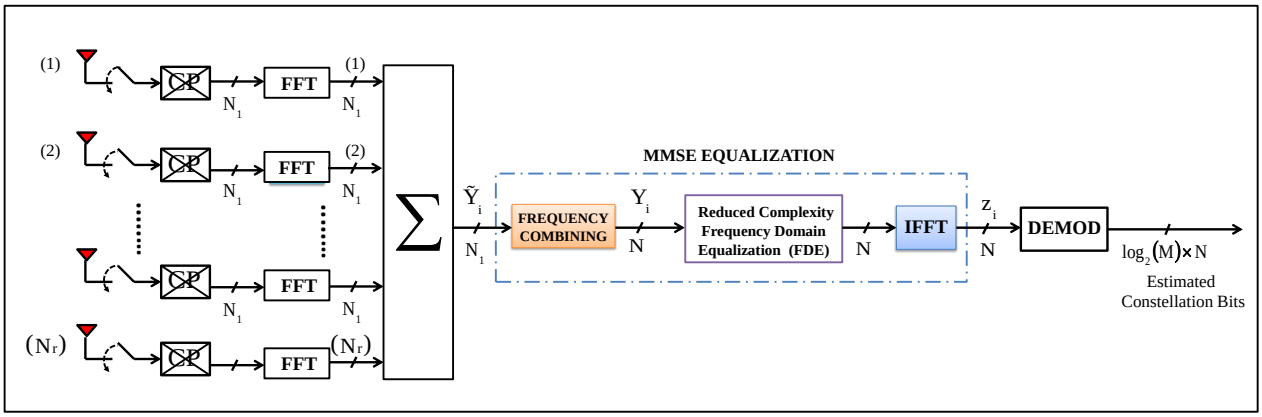

Figure 6.9: *Uncoded receiver based on MMSE detection for the proposed EW SC-OFDM-SIMO structure.*

$z_{i,n}^{(m_0)}$ is expressed as:

$$z_{i,n}^{(m_0)} = \frac{\left[\mathbf{h}_{i,n}^{(m_0)}\right]^H . \mathbf{y}_{i,n}}{\left\|\mathbf{h}_{i,n}^{(m_0)}\right\|^2} = T_{i,n} + \frac{\left[\mathbf{h}_{i,n}^{(m_0)}\right]^H . \widetilde{\mathbf{w}}_n}{\left\|\mathbf{h}_{i,n}^{(m_0)}\right\|^2} \qquad \text{for} \qquad 1 \leq n \leq N_1 \tag{6.38}$$

After selecting data symbols, the selected frequency domain sequence must pass through a spectral filter matched to the transmit filter, in order to maximize the useful received power in the Nyquist bandwidth. Then, the obtained filtered sequence will be transformed to the time-domain by using an IFFT operation in order to recover the transmitted constellation symbols:

$$\begin{bmatrix} \widetilde{s}_{i,1} \\ \widetilde{s}_{i,2} \\ \vdots \\ \widetilde{s}_{i,N} \end{bmatrix} = \frac{1}{\sqrt{\mathrm{F}_s}} \times \mathbf{F}_{\mathrm{N}}^H . \mathbf{A}^H . \begin{bmatrix} z_{i,1}^{(m_0)} \\ z_{i,2}^{(m_0)} \\ \vdots \\ z_{i,N_1}^{(m_0)} \end{bmatrix} \tag{6.39}$$

Then we can demodulate the transmitted constellation symbols $s_{i,n}$ by quantizing the corresponding maximum value $\widetilde{s}_{i,n}$ as:

$$\widehat{s}_{i,n} = \underset{\mathcal{C}_q \in \chi}{\operatorname{argmin}} \ |\widetilde{s}_{i,n} - \mathcal{C}_q|^2 \qquad 1 \leq n \leq N \tag{6.40}$$

Sub-optimal detector: MMSE-based receiver The MMSE-based receiver is a sub-optimal receiver and is presented in Figure 6.9. For the MMSE-based receiver, the received sequence is obtained by computing the average received sequence over the $\mathrm{N_r}$ receive antenna, $\mathbf{y}_i^{(n_r)}$. As a result, an average frequency received sequence N_1 samples is obtained and denoted by $\widetilde{\mathbf{Y}}_i$. Moreover, by using (6.35) and (6.36), the expression of

the obtained received frequency-domain sequence is expressed as:

$$\widetilde{\mathbf{Y}}_i^T = \frac{1}{\mathrm{N_r}}\sum_{n_\mathrm{r}=1}^{\mathrm{N_r}} \mathbf{y}_i^{(n_\mathrm{r})} = \sqrt{\mathrm{F}_s}\times \begin{bmatrix} s_{i,1} \\ s_{i,2} \\ \vdots \\ s_{i,N_1} \end{bmatrix}^T .\mathbf{F}_\mathrm{N}.\ \mathbf{A}.\ \left\{ \frac{1}{\mathrm{N_r}}\sum_{n_\mathrm{r}=1}^{\mathrm{N_r}} diag \begin{bmatrix} \mathrm{H}_{i,1}^{(n_\mathrm{r},m_0)} \\ \mathrm{H}_{i,2}^{(n_\mathrm{r},m_0)} \\ \vdots \\ \mathrm{H}_{i,N_1}^{(n_\mathrm{r},m_0)} \end{bmatrix} \right\} + \left\{ \frac{1}{\mathrm{N_r}}\sum_{n_\mathrm{r}=1}^{\mathrm{N_r}} \begin{bmatrix} \widetilde{w}_1^{(n_\mathrm{r})} \\ \widetilde{w}_2^{(n_\mathrm{r})} \\ \vdots \\ \widetilde{w}_{N_1}^{(n_\mathrm{r})} \end{bmatrix}^T \right\}$$

$$= \sqrt{\mathrm{F}_s}\times \begin{bmatrix} s_{i,1} \\ s_{i,2} \\ \vdots \\ s_{i,N_1} \end{bmatrix}^T .\mathbf{F}_\mathrm{N}.\ \mathbf{A}_{i,m_0} + \begin{bmatrix} \widetilde{w}_1 \\ \widetilde{w}_2 \\ \vdots \\ \widetilde{w}_{N_1} \end{bmatrix}^T \tag{6.41}$$

the resulting additive noise vector $\widetilde{\mathbf{w}} = [\widetilde{w}_1, \widetilde{w}_2, \ldots, \widetilde{w}_{N_1}]$ is a centered complex AWGN noise and the noise variable $\{w_n\}$ are decorrelated and having a variance equal to $\mathrm{F}_s \times \sigma_w^2/\mathrm{N_r}$. On other hand, the $N \times N_1$ matrix, $\mathbf{A}_{i,m_0}$, is an equivalent frequency domain transformation matrix expressed as:

$$\mathbf{A}_{i,m_0} = \mathbf{A}.\ \left\{ \frac{1}{\mathrm{N_r}}\sum_{n_\mathrm{r}=1}^{\mathrm{N_r}} diag \begin{bmatrix} \mathrm{H}_{i,1}^{(n_\mathrm{r},m_0)} \\ \mathrm{H}_{i,2}^{(n_\mathrm{r},m_0)} \\ \vdots \\ \mathrm{H}_{i,N_1}^{(n_\mathrm{r},m_0)} \end{bmatrix} \right\} \qquad \text{verifying} \qquad \mathbf{A}_{i,m_0}^H.\mathbf{A}_{i,m_0} = diag \begin{bmatrix} \bar{\mathrm{H}}_{i,1}^{(m_0)} \\ \bar{\mathrm{H}}_{i,2}^{(m_0)} \\ \vdots \\ \bar{\mathrm{H}}_{i,N}^{(m_0)} \end{bmatrix} \tag{6.42}$$

Given the additive noise is AWGN, by applying a MMSE criterion in order to generate a biased estimation of the frequency response of the transmitted constellation sequence, a reduced complexity frequency domain equalization is considered. As a result, a time-domain vector denoted by $\mathbf{z}_i$ is obtained and expressed as:

$$\mathbf{z}_i = \begin{bmatrix} z_{i,1} \\ z_{i,2} \\ \vdots \\ z_{i,N} \end{bmatrix} = \mathbf{F}_\mathrm{N}^H.\left\{ \left[\left(\mathrm{F}_s \times \mathbf{A}_{i,m_0}^H.\mathbf{A}_{i,m_0} \right) + \frac{\mathrm{F}_s\ \sigma_w^2}{\mathrm{N_r}\ \sigma_s^2} \times \mathbf{I}_{N\times N} \right]^{-1} .\left(\sqrt{\mathrm{F}_s} \times \mathbf{A}_{i,m_0}^H \right) \right\}.\ \widetilde{\mathbf{Y}}_i$$

$$= \mathbf{F}_\mathrm{N}^H.\left\{ \left[\left(\mathbf{A}_{i,m_0}^H.\mathbf{A}_{i,m_0} \right) + \frac{\sigma_w^2}{\mathrm{N_r}\ \sigma_s^2} \times \mathbf{I}_{N\times N} \right]^{-1} .\left(\frac{1}{\sqrt{\mathrm{F}_s}} \times \mathbf{A}_{i,m_0}^H \right) \right\}.\ \widetilde{\mathbf{Y}}_i$$

$$= \mathbf{F}_\mathrm{N}^H.\Sigma^{-1}.\mathbf{Y}_i \tag{6.43}$$

where Σ^{-1} is a diagonal equalization matrix and $\mathbf{Y}_i$ is an output filtered vector:

$$\Sigma^{-1} = \left[\left(\mathbf{A}_{i,m_0}^H.\mathbf{A}_{i,m_0} \right) + \frac{\sigma_w^2}{\mathrm{N_r}\ \sigma_s^2} \times \mathbf{I}_{N\times N} \right]^{-1} \qquad \text{and} \qquad \mathbf{Y}_i = \frac{1}{\sqrt{\mathrm{F}_s}} \times \mathbf{A}_{i,m_0}^H.\ \widetilde{\mathbf{Y}}_i \tag{6.44}$$

By considering a Gaussian approximation, the output MMSE vector, $\mathbf{z}_i$, can be re-written as:

$$\mathbf{z}_i = \begin{bmatrix} z_{i,1} \\ z_{i,2} \\ \vdots \\ z_{i,N} \end{bmatrix} = \mathbf{F}_\mathrm{N}^H.\Sigma^{-1}.\mathbf{Y}_i \approx \alpha_i^{(m_0)} \left\{ \begin{bmatrix} s_{i,1} \\ s_{i,2} \\ \vdots \\ s_{i,N} \end{bmatrix} + \frac{1}{\sqrt{\gamma_i^{(m_0)}}} \begin{bmatrix} w_{i,1} \\ w_{i,2} \\ \vdots \\ w_{i,N} \end{bmatrix} \right\} \tag{6.45}$$

the additive noise vector $\mathbf{w} = [w_1, w_2, \ldots, w_N]^T$ is a centered complex AWGN noise and the noise variable $\{w_n\}$ having a variance equal to $\sigma_w^2/\mathrm{N_r}$. Furthermore, the two positive scalars α_{m_0} and γ_{m_0} are defined as:

$$\alpha_i^{(m_0)} = \frac{1}{N}\sum_{n=1}^{N} \frac{\bar{\mathrm{H}}_{i,n}^{(m_0)}}{\bar{\mathrm{H}}_{i,n}^{(m_0)} + \frac{\sigma_w^2}{\mathrm{N_r}.\sigma_s^2}} \qquad \text{and} \qquad \gamma_i^{(m_0)} = \frac{\sigma_w^2}{\mathrm{N_r}.\sigma_s^2} \left(\frac{\alpha_i^{(m_0)}}{1-\alpha_i^{(m_0)}} \right) \tag{6.46}$$

Finally, we can demodulate the transmitted constellation symbols $s_{i,n}$ by quantizing the corresponding maximum value $\widetilde{s}_{i,n}$ as:

$$\widehat{s}_{i,n} = \underset{\mathcal{C}_q \in \chi}{\operatorname{argmin}} \left| z_{i,n} - \alpha_i^{(m_0)} \, \mathcal{C}_q \right|^2 \tag{6.47}$$

6.4 Proposed soft antenna selection for the proposed modified SM structures

In [57], it is reported the performance of SM combined with soft detection of active transmit antenna indexes. The soft decision is quite desirable to apply powerful forward error correction (FEC) such as Turbo or low density parity check (LDPC) codes for the SM system in order to enhance active antenna selection. In order to have enhanced performance for antenna selection at the receiver, we need to derive a new soft output detector for the transmit antenna indexes, enabling the use of efficient Soft-Input Soft-Output (SISO) channel decoder.

6.4.1 Soft antenna selection for the code-aided spectrally shaped DFT-Precoded OFDM-SM structure

Given the expression of the received signal, the *a posteriori* log-likelihood ratio (LLR) vector for the transmitted coded antenna bit sequence $\mathbf{c}_i^a$ can be derived for all bit positions p. Indeed, for the p-th bit position verifying $p = q + (n-1) \times \log_2(\mathrm{N_t})$ with $1 \leq q \leq \log_2(\mathrm{N_t})$, the corresponding *a posteriori* LLR can be expressed as:

$$\mathrm{LLR}\left\{c^a_{i,q+(n-1)\times\log_2(\mathrm{N_t})}\right\} = \log\left\{\frac{\sum\limits_{n_\mathrm{t}\in\mathbf{U}_q^0} \Pr\left(m_{i,n}=n_\mathrm{t}\right)\Pr\left(\mathbf{y}_{i,n}|m_{i,n}=n_\mathrm{t},t_{i,n}=\widehat{t}_{i,n},\mathbf{H}_{i,n}\right)}{\sum\limits_{n_\mathrm{t}\in\mathbf{U}_q^1} \Pr\left(m_{i,n}=n_\mathrm{t}\right)\Pr\left(\mathbf{y}_{i,n}|m_{i,n}=n_\mathrm{t},t_{i,n}=\widehat{t}_{i,n},\mathbf{H}_{i,n}\right)}\right\} \tag{6.48}$$

The two sets of the transmit antenna indexes $\mathbf{U}_q^0$ and $\mathbf{U}_q^1$ correspond to have respectively 0 and 1 entries at the q-th index position of antenna bits and verifying,

$$\mathbf{U}_q^0 \cup \mathbf{U}_q^1 = \{1, 2, \ldots, \mathrm{N_t}\} \qquad ; \qquad \mathbf{U}_q^0 \cap \mathbf{U}_q^1 = \oslash \tag{6.49}$$

In addition, $\Pr\left(\mathbf{y}_{i,n}|m_{i,n}=n_\mathrm{t},t_{i,n}=\widehat{t}_{i,n},\mathbf{H}_{i,n}\right)$ denotes the conditional probability.
On other hand, for MMSE-based detection and by considering a Gaussian approximation for the received output MMSE vector $\mathbf{z}_{i,n}$expressed in (6.55), another expression of the *a posteriori* LLR vector can be derived as:

$$\mathrm{LLR}\left\{c^a_{i,q+(n-1)\times\log_2(\mathrm{N_t})}\right\} = \log\left\{\frac{\sum\limits_{n_\mathrm{t}\in\mathbf{U}_q^0} \Pr\left(m_{i,n}=n_\mathrm{t}\right)\Pr\left(\mathbf{z}_{i,n}|m_{i,n}=n_\mathrm{t},t_{i,n}=\widehat{t}_{i,n},\mathbf{H}_{i,n}\right)}{\sum\limits_{n_\mathrm{t}\in\mathbf{U}_q^1} \Pr\left(m_{i,n}=n_\mathrm{t}\right)\Pr\left(\mathbf{z}_{i,n}|m_{i,n}=n_\mathrm{t},t_{i,n}=\widehat{t}_{i,n},\mathbf{H}_{i,n}\right)}\right\} \tag{6.50}$$

where $\Pr\left(\mathbf{z}_{i,n}|m_{i,n}=n_\mathrm{t},t_{i,n}=\widehat{t}_{i,n},\mathbf{H}_{i,n}\right)$ denotes the conditional probability when we consider as a starting point the output MMSE vector $\mathbf{z}_{i,n}$.

6.4.1.1 Expression of the received signal

In the proposed modified CP-aided OFDM-SM system, the expression of the received frequency-domain sequence is written in this matrix form:

$$\mathbf{y}_{i,n} = \begin{bmatrix} y_{i,n}^{(1)} \\ y_{i,n}^{(2)} \\ \vdots \\ y_{i,n}^{(\mathrm{N_r})} \end{bmatrix} = \mathbf{H}_{i,n}\ \mathbf{x}_{i,n} + \begin{bmatrix} \widetilde{w}_n^{(1)} \\ \widetilde{w}_n^{(2)} \\ \vdots \\ \widetilde{w}_n^{(\mathrm{N_r})} \end{bmatrix} = t_{i,n}\ \mathbf{H}_{i,n}.\ \mathbf{p}^{(m_{i,n})} + \widetilde{\mathbf{w}}_n = t_{i,n}\ \mathbf{h}_{i,n}^{(m_{i,n})} + \widetilde{\mathbf{w}}_n \tag{6.51}$$

with $\mathbf{p}^{(m_{i,n})} = [\underbrace{0,\ldots,0}_{(m_{i,n}-1)}, 1, \underbrace{0,\ldots,0}_{\mathrm{N_t}-m_{i,n}}]^T$ is a position vector and $\widetilde{\mathbf{w}}_n$ is a noise vector and its elements are additive white Gaussian noise (AWGN) and independent and identically distributed (i.i.d) with a variance $\widetilde{\sigma}_w^2 = \mathrm{F}_s \times \sigma_w^2$. Furthermore, the complex symbols $\{t_{i,n}\}$ are the transmitted data symbols and are defined in (6.2) for the proposed « code-aided spectrally shaped DFT-Precoded OFDM-SM structure ».

MRC-based detector In SM, Maximum Ratio Combining (MRC) is a sub-optimal linear detector used to detect both the active transmit antenna indexes and the transmitted constellation symbols. At the output of MRC decoding, an output vector, $\mathbf{z}_{i,n}$, is generated for $1 \leq n \leq N_1$ and is expressed as:

$$\mathbf{z}_{i,n} = \begin{bmatrix} z_{i,n}^{(1)} \\ z_{i,n}^{(2)} \\ \vdots \\ z_{i,n}^{(\mathrm{N_t})} \end{bmatrix} = \begin{bmatrix} \left\|\mathbf{h}_{i,n}^{(1)}\right\|^2 & 0 & \cdots & 0 \\ 0 & \left\|\mathbf{h}_{i,n}^{(2)}\right\|^2 & \cdots & 0 \\ \vdots & & \ddots & \vdots \\ 0 & 0 & \cdots & \left\|\mathbf{h}_{i,n}^{(\mathrm{N_t})}\right\|^2 \end{bmatrix}^{-1} .\mathbf{H}_{i,n}^H.\mathbf{y}_{i,n} \qquad \text{for} \qquad 1 \leq n \leq N \tag{6.52}$$

The output vector, $\mathbf{z}_{i,n}$, is an unbiased estimation of the transmitted SM vector $\mathbf{x}_{i,n}$ and,

$$\boxed{z_{i,n}^{(n_t)} = \frac{\left[\mathbf{h}_{i,n}^{(n_t)}\right]^H .\mathbf{y}_{i,n}}{\left\|\mathbf{h}_{i,n}^{(n_t)}\right\|^2} = \frac{\left[\mathbf{h}_{i,n}^{(n_t)}\right]^H .\mathbf{h}_{i,n}^{(m_{i,n})}}{\left\|\mathbf{h}_{i,n}^{(n_t)}\right\|^2}\ t_{i,n}\ +\ \frac{\left[\mathbf{h}_{i,n}^{(n_t)}\right]^H .\widetilde{\mathbf{w}}_n}{\left\|\mathbf{h}_{i,n}^{(n_t)}\right\|^2} \qquad \text{for} \qquad 1 \leq n_t \leq \mathrm{N_t}} \tag{6.53}$$

MMSE-based detector By using Minimum Mean Square Error (MMSE) criterion, a sub-optimal detection can be considered to detect both the active transmit antenna indexes and the transmitted constellation symbols. At the output of MMSE equalization, an output vector, $\mathbf{z}_{i,n}$, is generated for $1 \leq n \leq N_1$ and is expressed as:

$$\mathbf{z}_{i,n} = \begin{bmatrix} z_{i,n}^{(1)} \\ z_{i,n}^{(2)} \\ \vdots \\ z_{i,n}^{(\mathrm{N_t})} \end{bmatrix} = \mathbf{W}_{i,n}.\mathbf{y}_{i,n} \qquad \text{with} \qquad \mathbf{W}_{i,n} = \left[\mathbf{H}_{i,n}^H.\mathbf{H}_{i,n} + \frac{\widetilde{\sigma}_w^2}{(\sigma_s^2/\mathrm{N_t})} \times \mathbf{I}_{\mathrm{N_t}\times\mathrm{N_t}}\right]^{-1} .\mathbf{H}_{i,n}^H \tag{6.54}$$

The output vector $\mathbf{z}_{i,n}$ is a biased estimation of the transmitted SM vector $\mathbf{x}_{i,n}$. Indeed, we can assume that we have:

$$\boxed{\mathbf{z}_{i,n} \approx \alpha_{i,n}\ \mathbf{x}_{i,n} + \frac{\alpha_{i,n}}{\sqrt{\gamma_{i,n}}}\ \widetilde{\mathbf{w}}_n = \alpha_{i,n}\ t_{i,n}\ \mathbf{p}^{(m_{i,n})} + \frac{\alpha_{i,n}}{\sqrt{\gamma_{i,n}}}\ \widetilde{\mathbf{w}}_n \qquad \text{for} \qquad 1 \leq n \leq N_1} \tag{6.55}$$

where $\alpha_{i,n}$ and $\gamma_{i,n}$ are two positive scalars defined as:

$$\alpha_{i,n} \triangleq \frac{1}{\mathrm{N_t}}.\ tr\{\mathbf{W}_{i,n}.\mathbf{H}_{i,n}\} \qquad \text{and} \qquad \gamma_{i,n} = \frac{\widetilde{\sigma}_w^2}{(\sigma_s^2/\mathrm{N_t})}\ \frac{\alpha_{i,n}}{1-\alpha_{i,n}} \in]0,1] \tag{6.56}$$

6.4.1.2 Expression of the conditional probability for the MRC-based detector

To generate an output *a posteriori* log-likelihood ratio (LLR), the soft detector starts to derive an expression of the corresponding conditional probability $\Pr\left(\mathbf{y}_{i,n}|m_{i,n}=n_\mathrm{t},\mathbf{H}_{i,n}\right)$. Given the additive noise $\widetilde{\mathbf{w}}_n$ in Equation (6.51) is AWGN, the conditional probability is expressed as:

$$\Pr\left(\mathbf{y}_{i,n}|m_{i,n}=n_\mathrm{t},t_{i,n}=\widehat{t}_{i,n},\mathbf{H}_{i,n}\right) \propto \exp\left(-\frac{\left\|\mathbf{y}_{i,n}-\widehat{t}_{i,n}.\mathbf{h}_{i,n}^{(n_\mathrm{t})}\right\|^2}{\widetilde{\sigma}_w^2}\right) \tag{6.57}$$

where $\widehat{t}_{i,n}$ is an estimation of the transmitted symbol $t_{i,n}$.

6.4.1.3 Expression of the conditional probability for the MMSE-based detector

As mentioned for the MRC detector, given the expression of the received signal, the *a posteriori* log-likelihood ratio (LLR) vector for the transmitted coded antenna bit sequence $\mathbf{u}_i^a$ can be derived for all bit positions p. Indeed, for the p-th bit position verifying $p=q+(n-1)\times\log_2(\mathrm{N_t})$ with $1\leq q\leq\log_2(\mathrm{N_t})$, the corresponding *a posteriori* LLR is expressed as given in (6.48) with $\Pr\left(\mathbf{y}_{i,n}|m_{i,n}=n_\mathrm{t},\mathbf{H}_{i,n}\right)$ is the conditional probability:

$$\Pr\left(\mathbf{y}_{i,n}|m_{i,n}=n_\mathrm{t},t_{i,n}=\widehat{t}_{i,n},\mathbf{H}_{i,n}\right) \propto \exp\left(-\frac{\left\|\mathbf{y}_{i,n}-\widehat{t}_{i,n}.\mathbf{h}_{i,n}^{(n_\mathrm{t})}\right\|^2}{\widetilde{\sigma}_w^2}\right) \tag{6.58}$$

On other hand, by considering as a starting point the output MMSE vector $\mathbf{z}_{i,n}$ expressed in (6.55), another expression of the conditional probability $\Pr\left(\mathbf{z}_{i,n}|m_{i,n}=n_\mathrm{t},\mathbf{H}_{i,n}\right)$ can be derived as:

$$\begin{aligned}\Pr\left(\mathbf{z}_{i,n}|m_{i,n}=n_\mathrm{t},t_{i,n}=\widehat{t}_{i,n},\mathbf{H}_{i,n}\right) &\propto \exp\left(-\frac{\left\|\mathbf{z}_{i,n}-\alpha_{i,n}\ \widehat{t}_{i,n}.\mathbf{p}^{(n_\mathrm{t})}\right\|^2}{\left(\alpha_{i,n}^2/\gamma_{i,n}\right)\times\widetilde{\sigma}_w^2}\right)\\ = \exp\left(-\frac{\|\mathbf{z}_{i,n}\|^2-\left|z_{i,n}^{(n_\mathrm{t})}\right|^2+\left|z_{i,n}^{(n_\mathrm{t})}-\alpha_{i,n}\ \widehat{t}_{i,n}\right|^2}{\left(\alpha_{i,n}^2/\gamma_{i,n}\right)\times\widetilde{\sigma}_w^2}\right) &\propto \exp\left(+\frac{\left|z_{i,n}^{(n_\mathrm{t})}\right|^2-\left|z_{i,n}^{(n_\mathrm{t})}-\alpha_{i,n}\ \widehat{t}_{i,n}\right|^2}{\left(\alpha_{i,n}^2/\gamma_{i,n}\right)\times\widetilde{\sigma}_w^2}\right)\end{aligned} \tag{6.59}$$

6.4.1.4 Proposed self-iterative soft detector

Classically in CP-aided OFDM-SM system, the transmitted data symbols $\{t_{i,n}\}$ are drawn from a finite known alphabet χ. In this case, no estimation of $\{t_{i,n}\}$ is required. Indeed, it is sufficient to marginalize the symbols $\{t_{i,n}\}$ into χ and thus the expression of the optimal soft detector can be derived as:

$$\Pr\left(\mathbf{y}_{i,n}|m_{i,n}=n_\mathrm{t},\mathbf{H}_{i,n}\right) \propto \sum_{x\in\chi}\Pr\left(t_{i,n}=x\right)\ \exp\left(-\frac{\left\|\mathbf{y}_{i,n}-x.\mathbf{h}_{i,n}^{(n_\mathrm{t})}\right\|^2}{\widetilde{\sigma}_w^2}\right) \tag{6.60}$$

Or also for MMSE-based detector, the optimal soft detector is expressed as:

$$\Pr\left(\mathbf{z}_{i,n}|m_{i,n}=n_{\mathrm{t}},\mathbf{H}_{i,n}\right)\propto\sum_{x\in\chi}\Pr\left(t_{i,n}=x\right)\ \exp\left(+\frac{\left|z_{i,n}^{(n_{\mathrm{t}})}\right|^{2}-\left|z_{i,n}^{(n_{\mathrm{t}})}-\alpha_{i,n}\ x\right|^{2}}{\left(\alpha_{i,n}^{2}/\gamma_{i,n}\right)\times\widetilde{\sigma}_{w}^{2}}\right)\tag{6.61}$$

Unfortunately, for the proposed modified CP-aided OFDM-SM structure, the transmitted data symbols $\{t_{i,n}\}$ are no longer drawn from a finite known alphabet χ. As a consequence, it is highly recommended to give an accurate unbiased estimation of the transmitted data symbol sequence $[t_{i,1},t_{i,2},\ldots,t_{i,N_1}]^T$. To do it, we propose a sub-optimal self-iterative soft detector. In the proposed soft detector, an estimation of the transmitted data symbol sequence, $\left[\widehat{t}_{i,1},\widehat{t}_{i,2},\ldots,\widehat{t}_{i,N_1}\right]^T$, is given after a number of $NbrSelfIter$ self-iterations. The proposed self-iterated block processing is presented in Figure 6.10. and the different steps of the proposed sub-optimal self-iterative soft detector are detailed in **Algorithm 2**.

Finally, we note that the performance of the proposed sub-optimal soft detector is lower bounded by the case

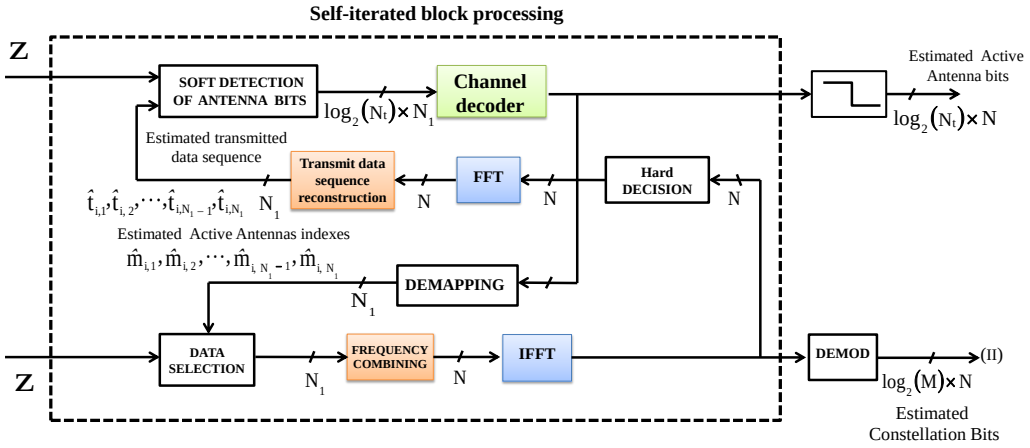

Figure 6.10: *The proposed self-iterated block processing*

with a perfect estimation of the transmitted data symbol sequence.

6.4.1.5 Expression of the soft detector in the first iteration

Given an estimation of the transmitted data symbols $\left\{\widehat{t}_{i,n}\right\}$, a sub-optimal soft detector for active antenna selection is given in Equation (6.57) for MRC-based detector and in (6.59) for MMSE-based detector. In order to obtain an accurate unbiased estimation of $\{t_{i,n}\}$, an iterative process is proposed in Section 6.4.1.4. At the initialization step, an initialized value of $\left\{\widehat{t}_{i,n}\right\}$, denoted by $\left\{\widehat{t}_{i,n}^{(0)}\right\}$, is required. This Section aims to give an explicit expression of $\widehat{t}_{i,n}^{(0)}$ for MRC-based and MMSE-based detectors.

MRC detector : After MRC detection, an expanded expression of the received symbols is done in Equation (6.53). It is shown that the output MRC vector, $\mathbf{z}_{i,n}$, is an unbiased estimation of the transmitted SM vector $\mathbf{x}_{i,n}$. Thus, the output MRC symbols can be taken as an estimation of the transmitted data symbols as follows:

$$\widehat{t}_{i,n}^{(0)} = z_{i,n}^{(n_t)} = \frac{\left[\mathbf{h}_{i,n}^{(n_t)}\right]^H . \mathbf{y}_{i,n}}{\left\|\mathbf{h}_{i,n}^{(n_t)}\right\|^2} \tag{6.62}$$

As a result, a new expression of the conditional probability is derived as:

$$\Pr\left(\mathbf{y}_{i,n}|m_{i,n}=n_t, t_{i,n}=\widehat{t}_{i,n}^{(0)}, \mathbf{H}_{i,n}\right) \propto \exp\left(-\frac{\left\|\mathbf{y}_{i,n}-z_{i,n}^{(n_t)}.\mathbf{h}_{i,n}^{(n_t)}\right\|^2}{\widetilde{\sigma}_w^2}\right) = \exp\left(-\frac{\|\mathbf{y}_{i,n}\|^2-\left\|\mathbf{h}_{i,n}^{(n_t)}\right\|^2\left|z_{i,n}^{(n_t)}\right|^2}{\widetilde{\sigma}_w^2}\right)$$
$$\propto \exp\left(+\frac{\left\|\mathbf{h}_{i,n}^{(n_t)}\right\|^2\left|z_{i,n}^{(n_t)}\right|^2}{\widetilde{\sigma}_w^2}\right) \tag{6.63}$$

At the first self-iteration, we notice that this soft detector is equivalent to the classical MRC-based hard detector initially defined in (5.22) and expressed as:

$$\widehat{m}_{i,n} = \underset{n_t\in\{1,2,\ldots,N_t\}}{\text{argmax}} \left\{\left\|\mathbf{h}_{i,n}^{(n_t)}\right\|^2\left|z_{i,n}^{(n_t)}\right|^2\right\} \tag{6.64}$$

MMSE detector : After MMSE detection, an expanded expression of the received symbols is done in Equation (6.55). It is shown that the output MMSE vector, $\mathbf{z}_{i,n}$, is a biased estimation of the transmitted SM vector $\mathbf{x}_{i,n}$. For each output MMSE symbol $z_{i,n}^{(n_t)}$ the corresponding bias is equal to $\alpha_{i,n}$. Therefore, the symbols $\left\{\frac{1}{\alpha_{i,n}}\, z_{i,n}^{(n_t)}\right\}$ can be considered as an unbiased estimation of the transmitted data symbols $\{t_{i,n}\}$ as follows:

$$\widehat{t}_{i,n}^{(0)} = \frac{1}{\alpha_{i,n}}\, z_{i,n}^{(n_t)} \tag{6.65}$$

By considering as a starting point the received output MMSE vector $\mathbf{z}_{i,n}$, the expression of the conditional probability can be expressed as:

$$\Pr\left(\mathbf{z}_{i,n}|m_{i,n}=n_t, t_{i,n}=\widehat{t}_{i,n}^{(0)}, \mathbf{H}_{i,n}\right) \propto \exp\left(+\frac{\left|z_{i,n}^{(n_t)}\right|^2-\left|z_{i,n}^{(n_t)}-\alpha_{i,n}\,\left(\frac{1}{\alpha_{i,n}}\, z_{i,n}^{(n_t)}\right)\right|^2}{\left(\alpha_{i,n}^2/\gamma_{i,n}\right)\times\widetilde{\sigma}_w^2}\right)$$
$$= \exp\left(+\frac{\left|z_{i,n}^{(n_t)}\right|^2}{\left(\alpha_{i,n}^2/\gamma_{i,n}\right)\times\widetilde{\sigma}_w^2}\right) \tag{6.66}$$

At the first self-iteration, we notice that this soft soft detector is equivalent to the classical MMSE-based hard detector initially defined in (5.26) and expressed as:

$$\widehat{m}_{i,n} = \underset{n_t\in\{1,2,\ldots,N_t\}}{\text{argmax}} \left|z_{i,n}^{(n_t)}\right|^2 \tag{6.67}$$

6.4.2 Soft antenna selection for the code-aided EW SC-OFDM-SM structure

Given the expression of the received signal, the *a posteriori* log-likelihood ratio (LLR) vector for the transmitted coded antenna bit sequence $\mathbf{c}_i^a$ can be derived for all bit positions p. Indeed, for the p-th bit position

Algorithm 2 self-iterative soft detector for active antenna selection for the code-aided spectrally shaped DFT-precoded OFDM-SM structure

Initialization: $\left[\widehat{t}_{i,1},\widehat{t}_{i,2},\ldots,\widehat{t}_{i,N_1}\right]^T=\left[\widehat{t}_{i,1}^{(0)},\widehat{t}_{i,2}^{(0)},\ldots,\widehat{t}_{i,N_1}^{(0)}\right]^T$

for iter $\in\{0,...,NbrSelfIter\}$ **do**

(1) Given $\widehat{t}_{i,n}$, we can derive an expression of the conditional probability: MRC (6.57), MMSE (6.59).

(2) Applying SISO channel decoding :⇒ generate bit LLRs, $\mathrm{LLR}^{\mathrm{ldpc}}\left\{c^a_{i,q+(n-1)\times\log_2(\mathrm{N_t})}\right\}$.

(3) Give an estimation of the active antenna index sequence as in (6.16) :⇒ $\left[\widehat{m}_{i,1}^{(iter)},\widehat{m}_{i,2}^{(iter)},\ldots,\widehat{m}_{i,N_1}^{(iter)}\right]^T$.

(4) Select an estimation sequence of the transmitted data sequence as given in (6.17).

(5) Generate an estimation of the transmitted constellation sequence as given in (6.18).

(6) Quantize the obtained estimated constellation sequence as in (6.19) :⇒ $\left[\widehat{s}_{i,1}^{(iter)},\widehat{s}_{i,2}^{(iter)},\ldots,\widehat{s}_{i,N}^{(iter)}\right]^T$.

(7) Update the values of $\widehat{t}_{i,n}$ by using the following expression:

$$\left[\widehat{t}_{i,1},\widehat{t}_{i,2},\ldots,\widehat{t}_{i,N_1}\right]^T=\left[\widehat{t}_{i,1}^{(iter)},\widehat{t}_{i,2}^{(iter)},\ldots,\widehat{t}_{i,N_1}^{(iter)}\right]^T=\sqrt{\mathrm{F}_s}\times\mathbf{A}.\,\mathbf{F}_{\mathrm{N}}.\left[\widehat{s}_{i,1}^{(iter)},\widehat{s}_{i,2}^{(iter)},\ldots,\widehat{s}_{i,N}^{(iter)}\right]^T \tag{6.68}$$

end for

After a number of $NbrSelfIter$ self-iterations we have:

$$\begin{cases}\left[\widehat{m}_{i,1},\widehat{m}_{i,2},\ldots,\widehat{m}_{i,N}\right]^T=\left[\widehat{m}_{i,1}^{(NbrSelfIter)},\widehat{m}_{i,2}^{(NbrSelfIter)},\ldots,\widehat{m}_{i,N}^{(NbrSelfIter)}\right]^T\\ \left[\widehat{s}_{i,1},\widehat{s}_{i,2},\ldots,\widehat{s}_{i,N}\right]^T=\left[\widehat{s}_{i,1}^{(NbrSelfIter)},\widehat{s}_{i,2}^{(NbrSelfIter)},\ldots,\widehat{s}_{i,N}^{(NbrSelfIter)}\right]^T\end{cases} \tag{6.69}$$

verifying $p = q + (n-1) \times \log_2(\mathrm{N_t})$ with $1 \leq q \leq \log_2(\mathrm{N_t})$, the corresponding *a posteriori* LLR can be expressed as:

$$\mathrm{LLR}\left\{c^a_{i,q+(n-1)\times\log_2(\mathrm{N_t})}\right\} = \log\left\{\frac{\sum\limits_{n_t \in \mathbf{U}^0_q} \Pr\left(m_{i,n}=n_t\right)\Pr\left(\mathbf{z}_{i,n}|m_{i,n}=n_t, t_{i,n}=\widehat{t}_{i,n}, \mathbf{H}_i\right)}{\sum\limits_{n_t \in \mathbf{U}^1_q} \Pr\left(m_{i,n}=n_t\right)\Pr\left(\mathbf{z}_n|m_{i,n}=n_t, t_{i,n}=\widehat{t}_{i,n}, \mathbf{H}_i\right)}\right\} \tag{6.70}$$

where, $\mathbf{H}_i = [\mathbf{H}_{i,1}, \mathbf{H}_{i,2}, \ldots, \mathbf{H}_{i,N_1}]$

6.4.2.1 Expression of the received signal

For SC-SM system, a suboptimal but simple linear MMSE frequency domain equalization (FDE) is typically used to detect both the active transmit antenna indexes and the transmitted constellation symbols. At the output of MMSE detection, a $\mathrm{N_t} \times N_1$ matrix is generated and is denoted by $\mathbf{z} = [\mathbf{z}_{i,1}, \mathbf{z}_{i,2}, \ldots, \mathbf{z}_{i,N_1}]$ and expressed as:

$$[\mathbf{z}_{i,1}, \mathbf{z}_{i,2}, \ldots, \mathbf{z}_{i,N_1}] = [\widetilde{\mathbf{z}}_{i,1}, \widetilde{\mathbf{z}}_{i,2}, \ldots, \widetilde{\mathbf{z}}_{i,N_1}].\mathbf{F}^H_{\mathrm{N}_1} \qquad \text{with} \qquad \widetilde{\mathbf{z}}_{i,n} = \mathbf{W}_{i,n}.\mathbf{y}_{i,n} \qquad \text{for} \qquad 1 \leq n \leq N_1 \tag{6.71}$$

By applying Linear MMSE equalization, The filter linearly combines the received samples to form an estimation of the frequency response of transmitted symbols to obtain $\widetilde{\mathbf{z}}_{i,n} = \mathbf{W}_{i,n}.\mathbf{y}_{i,n}$. Moreover, by considering a Gaussian approximation of the obtained MMSE equalized vector, we can assume that we have $\widetilde{\mathbf{z}}_{i,n} \approx \alpha_{i,n}\, \widetilde{\mathbf{x}}_{i,n} + \frac{\alpha_{i,n}}{\sqrt{\gamma_n}}\, \widetilde{\mathbf{w}}_n$, where $\alpha_{i,n}$ and $\gamma_{i,n}$ are previously defined in Equation (6.56). Consequently, by grouping together all obtained MMSE equalized vectors $\widetilde{\mathbf{z}}_{i,1}, \widetilde{\mathbf{z}}_{i,2}, \ldots, \widetilde{\mathbf{z}}_{i,N}$, we can obtain the following matrix form:

$$[\widetilde{\mathbf{z}}_{i,1}, \widetilde{\mathbf{z}}_{i,2}, \ldots, \widetilde{\mathbf{z}}_{i,N}] = [\widetilde{\mathbf{x}}_{i,1}, \widetilde{\mathbf{x}}_{i,2}, \ldots, \widetilde{\mathbf{x}}_{i,N}].diag\begin{bmatrix}\alpha_{i,1}\\ \alpha_{i,2}\\ \vdots\\ \alpha_{i,N_1}\end{bmatrix} + [\mathbf{w}_{i,1}, \mathbf{w}_{i,2}, \ldots, \mathbf{w}_{i,N}].diag\begin{bmatrix}\alpha_{i,1}/\sqrt{\gamma_{i,1}}\\ \alpha_{i,2}/\sqrt{\gamma_{i,2}}\\ \vdots\\ \alpha_{i,N_1}/\sqrt{\gamma_{i,N_1}}\end{bmatrix} \tag{6.72}$$

where $[\widetilde{\mathbf{x}}_{i,1}, \widetilde{\mathbf{x}}_{i,2}, \ldots, \widetilde{\mathbf{x}}_{i,N}] = [\mathbf{x}_{i,1}, \mathbf{x}_{i,2}, \ldots, \mathbf{x}_{i,N}].\mathbf{F}_{\mathrm{N}}$ is the frequency domain representation of the transmitted time-domain SM symbols.

In order, to detect the transmitted time-domain SM symbols, a simple time-domain transformation is considered. As a result, the expression of the received time-domain SM symbols can be written in this matrix form:

$$[\mathbf{z}_{i,1}, \mathbf{z}_{i,2}, \ldots, \mathbf{z}_{i,N}] = [\widetilde{\mathbf{z}}_{i,1}, \widetilde{\mathbf{z}}_{i,2}, \ldots, \widetilde{\mathbf{z}}_{i,N}].\mathbf{F}^H_{\mathrm{N}} \tag{6.73}$$

Again, by using a Gaussian approximation of the obtained received vectors, $\mathbf{z}_{i,n}$, we can show that we have this approximation:

$$\boxed{\mathbf{z}_{i,n} = \alpha_i\ \mathbf{x}_{i,n} + \frac{\alpha_i}{\sqrt{\gamma_i}}\ \widetilde{\mathbf{w}}_n = \alpha_i\ t_{i,n}\ \mathbf{p}^{(m_{i,n})} + \frac{\alpha_i}{\sqrt{\gamma_i}}\ \widetilde{\mathbf{w}}_n \qquad \text{for} \qquad 1 \leq n \leq N_1} \tag{6.74}$$

where α_i and γ_i are two positive scalars which are expressed as the following:

$$\alpha_i = \frac{1}{N_1}\sum_{n=1}^{N_1}\alpha_{i,n} \qquad \text{and} \qquad \gamma_i = \frac{\widetilde{\sigma}^2_w}{(\sigma^2_s/\mathrm{N_t})}\ \frac{\alpha_i}{1-\alpha_i} \in]0,1] \tag{6.75}$$

Furthermore, the complex symbols $\{t_{i,n}\}$ are the transmitted data symbols and are defined in (6.20) for the proposed « code-aided EW SC-OFDM-SM structure ».

6.4.2.2 Expression of the conditional probability for the MMSE-based detector

By considering as a starting point the output MMSE vector $\mathbf{z}_{i,n}$ expressed in (6.74), another expression of the conditional probability $\Pr\left(\mathbf{z}_{i,n}|m_{i,n}=n_{\mathrm{t}},\mathbf{H}_{i,n}\right)$ can be derived as:

$$\Pr\left(\mathbf{z}_{i,n}|m_{i,n}=n_{\mathrm{t}},t_{i,n}=\widehat{t}_{i,n},\mathbf{H}_i\right)\propto\exp\left(+\frac{\left|z_{i,n}^{(n_{\mathrm{t}})}\right|^2-\left|z_{i,n}^{(n_{\mathrm{t}})}-\alpha_i\ \widehat{t}_{i,n}\right|^2}{\left(\alpha_i^2/\gamma_i\right)\times\widetilde{\sigma}_w^2}\right) \tag{6.76}$$

6.4.2.3 Proposed self-iterative soft detector

For the proposed modified CP-aided SC-SM structure, the transmitted data symbols $\{t_{i,n}\}$ are not drawn from a finite known alphabet χ. Therefore, for the same reasons as given in Section 6.4.1.4, we propose another sub-optimal self-iterative soft detector in order to give an accurate unbiased estimation of the transmitted data symbol sequence $[t_{i,1},t_{i,2},\ldots,t_{i,N_1}]^T$ and thus improve the active antenna selection at the receiver. The proposed sub-optimal self-iterative soft detector follows the same steps as given in Section 6.4.1.4. The different steps are illustrated in **Algorithm 3**.

6.4.2.4 Expression of the soft detector in the first iteration

Given an estimation of the transmitted data symbols $\left\{\widehat{t}_{i,n}\right\}$, a sub-optimal soft detector for active antenna selection is given in Equation (6.59) for MMSE-based detector. In order to obtain an accurate unbiased estimation of $\{t_{i,n}\}$, an iterative process is proposed in Section 6.4.2.3. At the initialization step, an initialized value of $\left\{\widehat{t}_{i,n}\right\}$, denoted by $\left\{\widehat{t}_{i,n}^{(0)}\right\}$, is required. This Section aims to give an explicit expression of $\widehat{t}_{i,n}^{(0)}$ for the MMSE-based detector.

After MMSE detection, an expanded expression of the received symbols is done in Equation (6.74). It is shown that the output MMSE vector, $\mathbf{z}_{i,n}$, is a biased estimation of the transmitted SM vector $\mathbf{x}_{i,n}$. For the received MMSE symbol sequence, the corresponding bias is equal to α_i. Therefore, the symbols $\left\{\frac{1}{\alpha_i}\ z_{i,n}^{(n_{\mathrm{t}})}\right\}$ can be considered as an unbiased estimation of the transmitted data symbols $\{t_{i,n}\}$ as follows:

$$\widehat{t}_{i,n}^{(0)}=\frac{1}{\alpha_i}\ z_{i,n}^{(n_{\mathrm{t}})} \tag{6.77}$$

By considering as a starting point the received vector $\mathbf{z}_{i,n}$, the expression of the conditional probability shown in Equation (6.76) becomes:

$$\begin{aligned}\Pr\left(\mathbf{z}_{i,n}|m_{i,n}=n_{\mathrm{t}},t_{i,n}=\widehat{t}_{i,n}^{(0)},\mathbf{H}_i\right)&\propto\exp\left(+\frac{\left|z_{i,n}^{(n_{\mathrm{t}})}\right|^2-\left|z_{i,n}^{(n_{\mathrm{t}})}-\alpha_i\ \left(\frac{1}{\alpha_i}\ z_{i,n}^{(n_{\mathrm{t}})}\right)\right|^2}{\left(\alpha_i^2/\gamma_i\right)\times\widetilde{\sigma}_w^2}\right)\\&=\exp\left(+\frac{\left|z_{i,n}^{(n_{\mathrm{t}})}\right|^2}{\left(\alpha_i^2/\gamma_i\right)\times\widetilde{\sigma}_w^2}\right)\end{aligned} \tag{6.78}$$

At the first self-iteration, we notice that this soft soft detector is equivalent to the classical MMSE-based hard detector initially defined in (5.52) and expressed as:

$$\widehat{m}_{i,n}=\underset{n_{\mathrm{t}}\in\{1,2,\ldots,\mathrm{N_t}\}}{\operatorname{argmax}}\left|z_{i,n}^{(n_{\mathrm{t}})}\right|^2 \tag{6.79}$$

Algorithm 3 Proposed self-iterative soft detector for the code-aided EW SC-OFDM-SM structure

Initialization: $\left[\widehat{t}_{i,1},\widehat{t}_{i,2},\ldots,\widehat{t}_{i,N_1}\right]^T=\left[\widehat{t}_{i,1}^{(0)},\widehat{t}_{i,2}^{(0)},\ldots,\widehat{t}_{i,N_1}^{(0)}\right]^T$

for iter $\in\{0,...,NbrSelfIter\}$ **do**

(1) Given $\widehat{t}_{i,n}$, we can derive an expression of the conditional probability: MMSE (6.76).

(2) Applying SISO channel decoding :⇒ generate bit LLRs, $\mathrm{LLR}^{\mathrm{ldpc}}\left\{c^{a}_{i,q+(n-1)\times\log_2(\mathrm{N_t})}\right\}$.

(3) Give an estimation of the active antenna index sequence as in (6.27) :⇒ $\left[\widehat{m}_{i,1}^{(iter)},\widehat{m}_{i,2}^{(iter)},\ldots,\widehat{m}_{i,N_1}^{(iter)}\right]^T$.

(4) Select an estimation sequence of the transmitted data sequence as given in (6.28).

(5) Generate an estimation of the transmitted constellation sequence as given in (6.29).

(6) Quantize the obtained estimated constellation sequence as in (6.30) :⇒ $\left[\widehat{s}_{i,1}^{(iter)},\widehat{s}_{i,2}^{(iter)},\ldots,\widehat{s}_{i,N}^{(iter)}\right]^T$.

(7) Update the values of $\widehat{t}_{i,n}$ by using the following expression:

$$\left[\widehat{t}_{i,1},\widehat{t}_{i,2},\ldots,\widehat{t}_{i,N_1}\right]^T=\left[\widehat{t}_{i,1}^{(iter)},\widehat{t}_{i,2}^{(iter)},\ldots,\widehat{t}_{i,N_1}^{(iter)}\right]^T=\sqrt{\mathrm{F}_s}\times\mathbf{F}_{\mathrm{N}_1}^{H}.\,\mathbf{A}.\,\mathbf{F}_{\mathrm{N}}.\left[\widehat{s}_{i,1}^{(iter)},\widehat{s}_{i,2}^{(iter)},\ldots,\widehat{s}_{i,N}^{(iter)}\right]^T \tag{6.80}$$

end for

After a number of $NbrSelfIter$ self-iterations we have:

$$\begin{cases}\left[\widehat{m}_{i,1},\widehat{m}_{i,2},\ldots,\widehat{m}_{i,N}\right]^T=\left[\widehat{m}_{i,1}^{(NbrSelfIter)},\widehat{m}_{i,2}^{(NbrSelfIter)},\ldots,\widehat{m}_{i,N}^{(NbrSelfIter)}\right]^T\\ \left[\widehat{s}_{i,1},\widehat{s}_{i,2},\ldots,\widehat{s}_{i,N}\right]^T=\left[\widehat{s}_{i,1}^{(NbrSelfIter)},\widehat{s}_{i,2}^{(NbrSelfIter)},\ldots,\widehat{s}_{i,N}^{(NbrSelfIter)}\right]^T\end{cases} \tag{6.81}$$

6.5 System performance analysis

6.5.1 Proposed modified CP-aided OFDM-SM/OFDM-SIMO structure

6.5.1.1 PAPR level

In order to compare the different SM systems in terms of PAPR level, we simulate the measured PAPR level of the transmitted signal at the output of all transmit antennas elements for the proposed code-aided spectrally shaped DFT-precoded OFDM-SM structure. The simulated PAPR level is compared to that for classical OFDM-SM structure. For both the classical and the proposed structure, we assume of bit rate of 5 bpcu.

Based on the transmit signal model, the corresponding complementary cumulative distribution functions (CCDFs) of the PAPR level of both the proposed and the claccical OFDM-SM systems are shown in Figure 6.11. Given that the nature of transmitted signal is similar for all transmit antenna elements, we only give the CCDF result of the PAPR for the signal vector transmitted over one of the $\mathrm{N_t}$ transmit antenna elements. The CCDF explicitly shows the probability of having a PAPR, which is higher than a certain PAPR threshold of PAPR_0, namely that we have $\Pr\left(\mathrm{PAPR}\geq\mathrm{PAPR}_0\right)$. As expected and observed in Figure 6.11, in the presence of DFT operation in each transmit antenna, the PAPR level of the classical OFDM system takes high values and this makes the design of High Power Amplifier (HPA) is a challenging task. In order to reduce the PAPR level, the use of a DFT-precoding block before selecting the active transmit antennas can

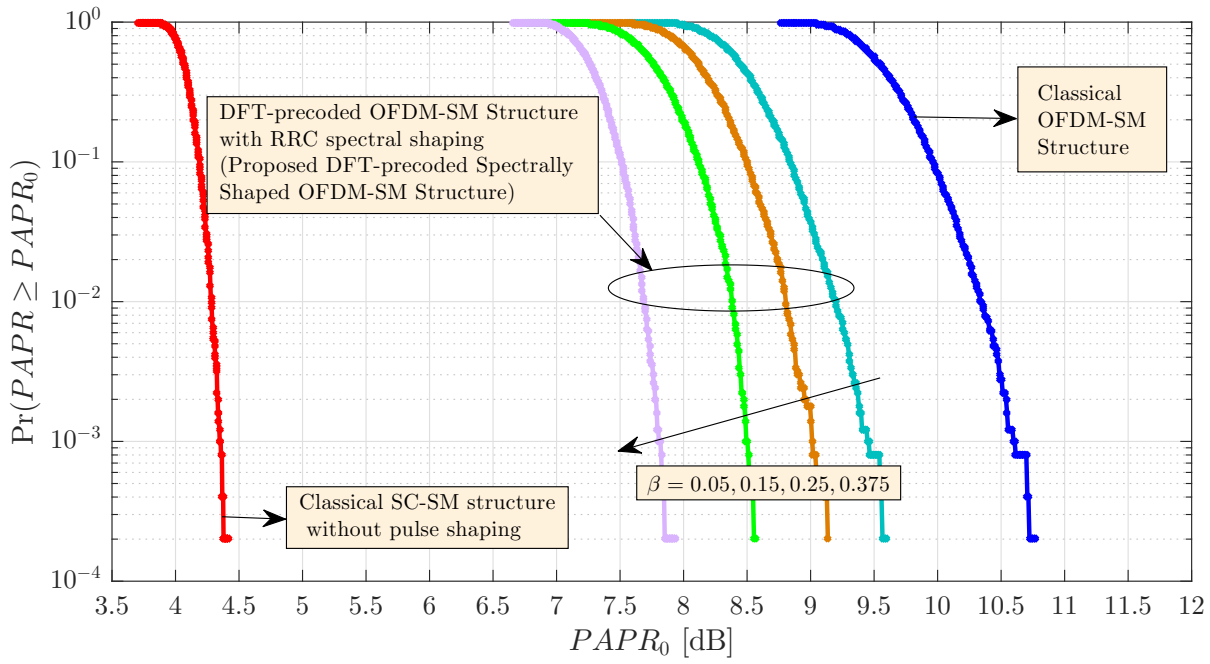

Figure 6.11: *PAPR level of the proposed spectrally shaped DFT-precoded OFDM-SM compared to the classical OFDM-SM structure at the output of each transmit antenna element*

be considered as a straightforward solution. Indeed, for all values of roll-off factor, β, for proposed code-aided spectrally shaped DFT-precoded OFDM-SM structure can offer a reduced PAPR level. Moreover, it clearly shown that for the proposed modified OFDM-SM structure, the PAPR level decreases with the value of β. Finally, we notice that, in the absence of pulse shaping, the classical SC-SM system still offer the lower PAPR level at the expense of the presence of out-of-band transmit signals.

6.5.1.2 Uncoded BER performances over Ricean MIMO channel

Assuming a number of 2 of transmit antennas ($N_t = 2$) and a number of 4 of receive antennas ($N_r = 4$), the simulation of uncoded Bit Error Rate (BER) for the proposed modified OFDM-SM/OFDM-SIMO system over a 2×4 Ricean channel matrix is given in Figure 6.12 for different values of K_{LOS} values. For MMSE-based detection, the uncoded BER performances are shown in blue curves. Whereas, for MRC-based detection, the uncoded BER performances are shown in red curves. For SM system, the case with perfect active transmit antenna selection is shown with dashed curves. For all simulation performances, we assume a linear 16-QAM modulation (Quadrature Amplitude Modulation) for SM system and linear 32-QAM modulation for SIMO system. As a result, for both SM and SIMO systems, the considered bit rate is equal to 5 bpcu.
The main objective is to determinate which is the possible (transmitter structure $\in \{SM, SIMO\}$, receiver detector $\in \{MMSE, MRC\}$) combination that can offer the better performances in terms of uncoded BER for all values of K_{LOS} between -15 dB and 15 dB. As we can see in Figure 6.12, until the value of 6 dB of K_{LOS} factor, the combination considering code-aided sprectrally shaped DFT-precoded OFDM-SM as a transmitter

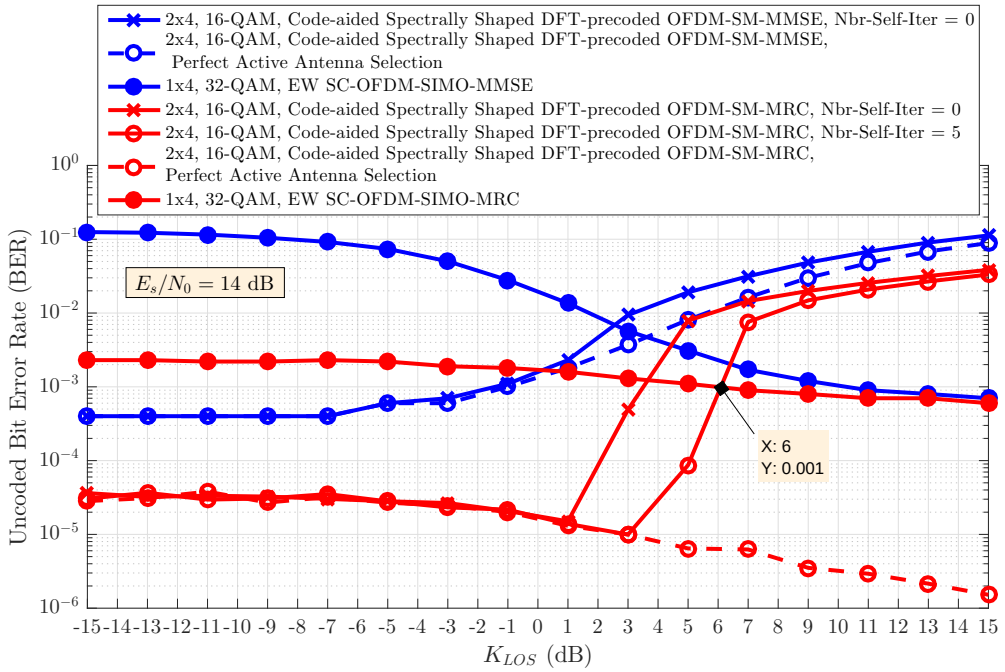

Figure 6.12: *Uncoded BER performance for the proposed spectrally shaped DFT-precoded OFDM-SM/ EW SC-OFDM-SIMO structure as a function of the Rice factor K_{LOS} and for different detection techniques at the receiver.*

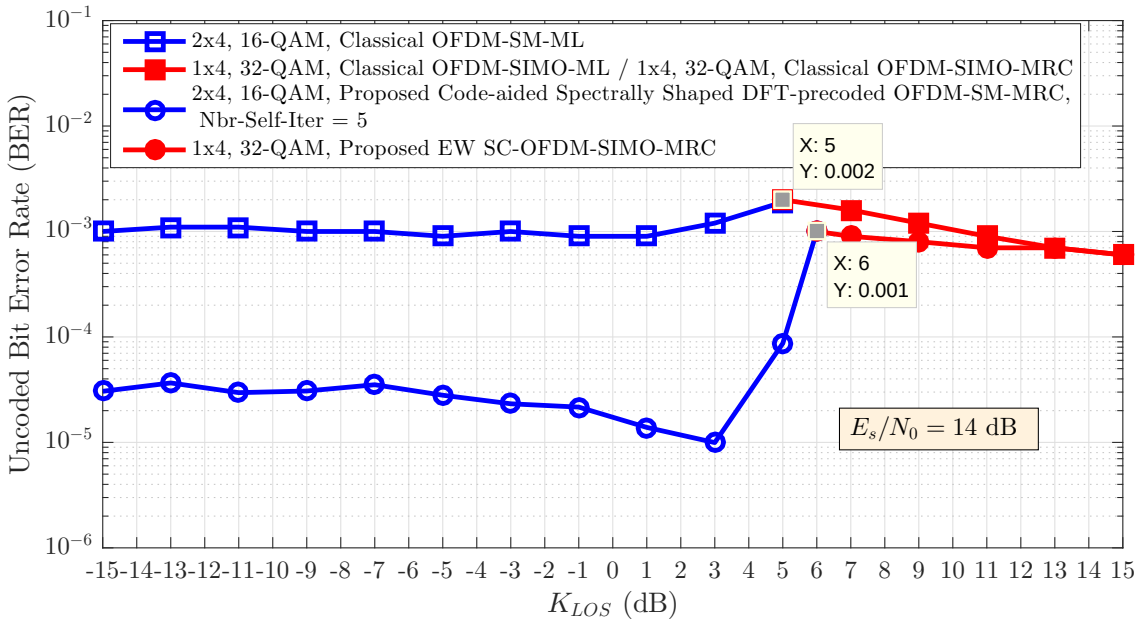

Figure 6.13: *Comparison between the better combination for both the proposed modified CP-aided OFDM-SM/SIMO and the classical CP-aided SC-SM/SIMO structures in terms of uncoded BER and for different values of K_{LOS}.*

structure and using MRC-based detection at the receiver and taking into account a number of 5 self-iterations for active antenna selection, can offer the better performances in terms of uncoded BER. Whereas, from the value of of 6 dB of K_{LOS} factor, the SIMO configuration using MRC-based detection at the receiver is the better one. This better combination is selected and separately shown in Figure 6.13.

In order to compare the better combination for both the proposed modified CP-aided OFDM-SM/SIMO and the classical CP-aided SC-SM/SIMO structures in terms of uncoded BER, Figure 6.13 shows the simulation results for the two better combinations. As we can observe in Figure 6.13, the proposed SM/SIMO structure can offer a better performances in terms of uncoded BER for all values of K_{LOS} factor between -15 dB and 15 dB. Indeed, thanks to the add of a code-aided block, the uncoded BER for the proposed SM structure can operate with a perfect antenna selection at the receiver and reach a value of 10^{-5} for $-15 \text{ dB} \leq K_{LOS} \leq 3 \text{ dB}$. This is not the case for the classical OFDM-SM-ML structure and that's why there are low values of uncoded BER for the proposed code-aided spectrally shaped DFT-precoded OFDM-SM structure.

Besides, from the value of of 6 dB of K_{LOS} factor, there are a considerable uncoded BER degradation for the proposed SM structure and it is shown that is preferable to using the SIMO configuration using MRC-based detection. In this case, the uncoded BER performances for both classical OFDM-SIMO and proposed OFDM-SIMO structures are almost identical.

6.5.1.3 Case of Rayleigh MIMO channels: comparison of uncoded BER performances

By considering Rayleigh fading MIMO channels ($K_{LOS} = -\infty$), we evaluate the impact of antenna selection error on system performances in terms of uncoded BER for the two best combinations for the proposed spectrally shaped DFT-precoded OFDM-SM system and the classical OFDM-SM system. To do it, we assume a number of 2 of transmit antennas ($N_t = 2$) and a number of 4 of receive antennas ($N_r = 4$). Furthermore, we assume a linear 16-QAM modulation. As a result, the two SM systems offer the same bit rate of 5 bpcu. For OFDM-SM system a ML receiver is considered. Whereas, for DFT-precoded OFDM-SM system, a MRC-based detection is considered.

Additionally, for the proposed spectrally shaped DFT-precoded OFDM-SM structure, we consider a transmit RRC filter with a roll-off $\beta = 0.375$ which corresponds to a rate value of $8/11$ for the associated error correcting code. To protect antenna bits, we consider ARJA (Accumulate Repeat Jagged Accumulate) protograph based low-density parity-check (LDPC) codes.

Simulation results are shown in Figure 6.14. In Figure 6.14, we point out the fact that we consider an uncoded structure: the use of channel coding for the antenna bits is part of the modulated scheme that can be seen as a code-aided DFT-precoded OFDM-SM scheme and we focus on the performance of the uncoded structure. Besides, it is shown that the uncoded BER performances of the proposed spectrally shaped DFT-precoded OFDM-SM (red and blue curves) are lower bounded by the case of perfect active antenna selection (dashed curves). Furthermore, simulation results confirm that it important to associate high performance error correcting to reach the perfect antenna selection case. In fact, without considering a code-aided processing, the receiver suffers from an erroneous detection of the active antennas. That's why it essential to exploit excess

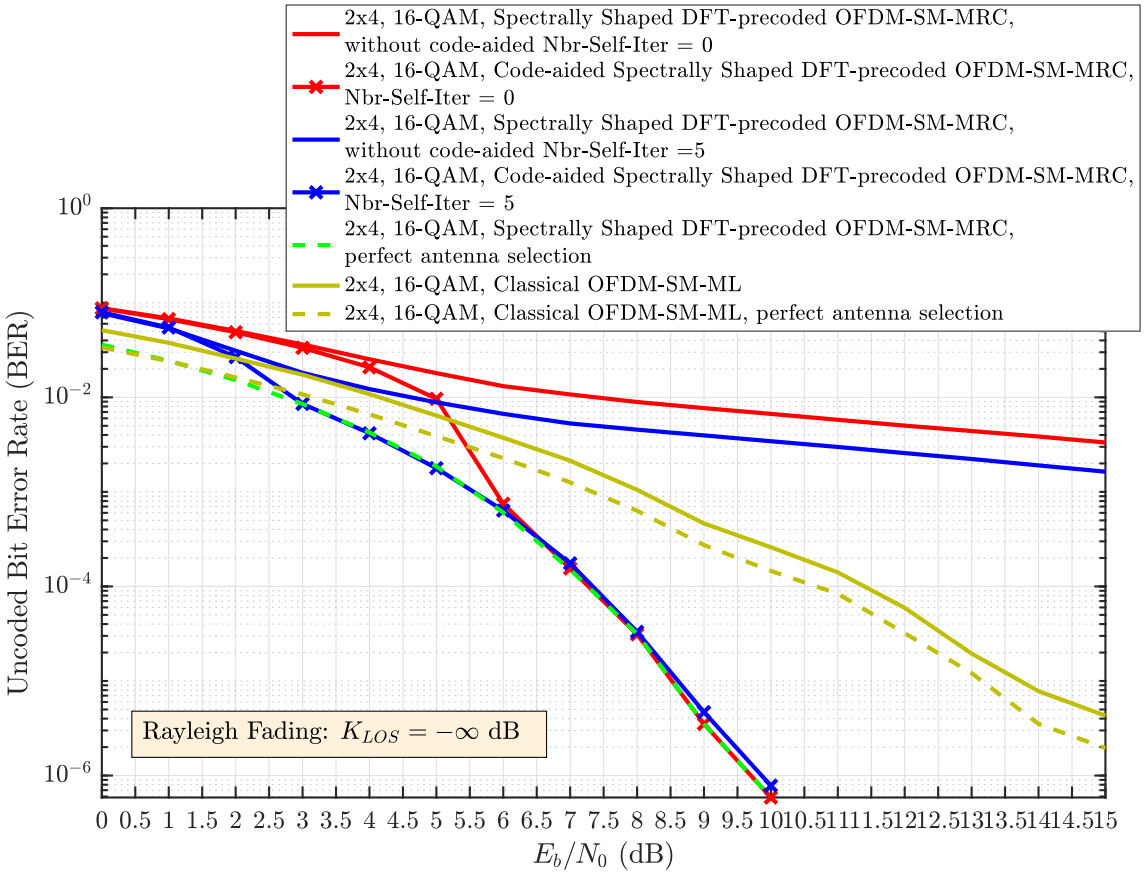

Figure 6.14: *Uncoded BER performance for the proposed spectrally shaped DFT-precoded OFDM-SM structure compared to the classical OFDM-SM-ML structure for Rayleigh fading channels*

bandwidth to associate an error correcting code in order to enhance antenna selection. Indeed, we can see that with associating high performance error correcting, uncoded BER performances are considerably improved and we can reach the perfect antenna selection case.

Moreover, in the same Figure 6.14, we can clearly see the advantage of considering a self-iterated process at the receiver. Indeed, by considering a self iterated receiver, we can considerably reduce antenna selection errors and thus reach the perfect antenna case in lower operating point compared to the case without using a self-iterated processing at the receiver. Compared to the classical OFDM-SM system using ML-based detection, the proposed structure can offer a better asymptotic uncoded BER performance. However, for low SNR values, OFDM-SM-ML still offering a slightly better performances Than the proposed spectrally shaped DFT-precoded OFDM-SM.

In conclusion, in first time, it is shown that we can enhance uncoded BER performances by associating a high performance error correcting code. As a result, we can reach the perfect antenna selection case. Second, it is shown that considering a self-iterated receiver leads to enhance antenna selection and thus improve the overall system performance. Finally, for E_b/N_0 values grater than 2 dB, the proposed structure can offer an uncoded BER performance improvement compared to classical OFDM-SM-ML.

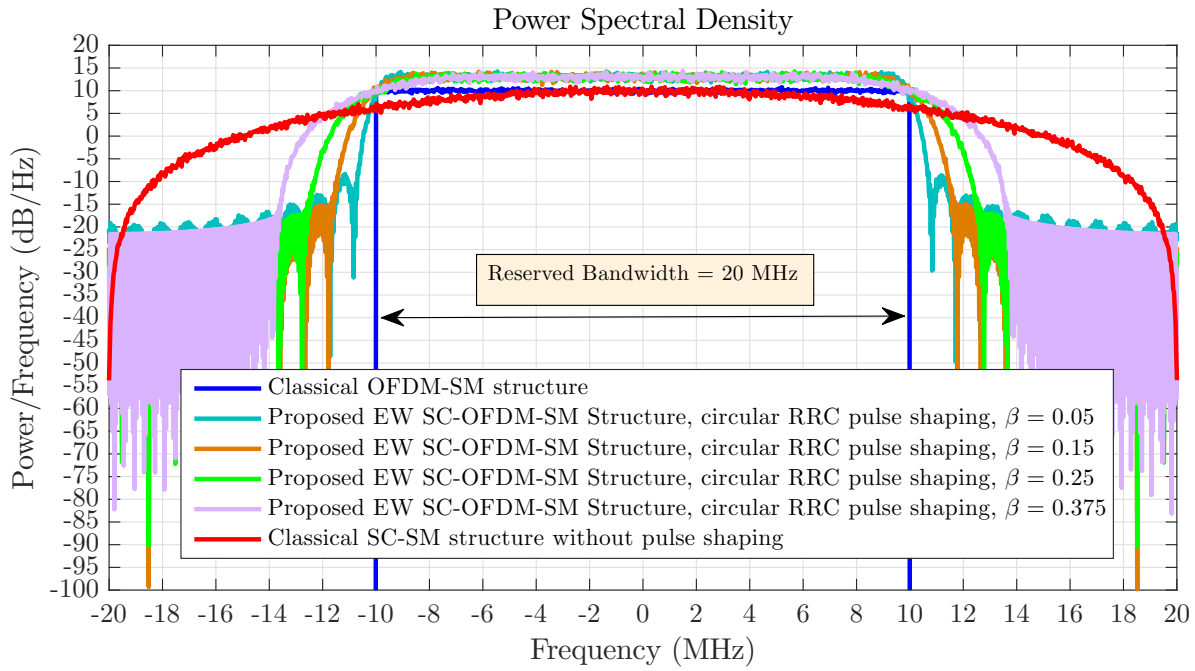

Figure 6.15: *Power Spectrum Density of the transmitted signals for both the proposed EW SC-OFDM-SM and the classical SC-SM structures for a same reserved bandwidth of 20 MHz*

6.5.2 Proposed modified CP-aided SC-SM/SC-SIMO structure

6.5.2.1 Spectral occupancy

In order to evaluate the performances in terms of spectral occupancy of the proposed EW SC-OFDM-SM/SIMO structure, Figure 6.15 simulates the Power Spectral Density (PSD) for the proposed modified SC-SM structure for different values of roll-off factor $\beta \in \{0.05, 0.15, 0.25, 0.375\}$. Furthermore, simulation results are compared to that for the classical CP-aided SC-SM structure with absence of pulse shaping.

As expected and observed in Figure 6.15, the classical CP-aided SC-SM system (shown in red curve) presents the worst case of out-of-band transmitted signals. Indeed, in the absence of pulse shaping filter, the transmitted signals occupy twice the reserved bandwidth. Consequently, the classical CP-aided SC-SM system is not a good candidate for multi-user communications because of the presence of adjacent-band interference coming from the adjacent users. In order to make a better spectral occupancy, it is straightforwardly recommended to consider a pulse shaping at the transmitter with maintaining the single-RF benefits of the SC-SM transmitter. As a solution, EW SC-OFDM-SM structure is proposed. Indeed, with the presence of circular RRC pulse shaping with roll-off $0 < \beta < 1$, the proposed EW SC-OFDM-SM structure can offer a better spectral occupancy compared to the classical CP-aided SC-SM structure and the excess bandwidth factor becomes equal to $1+\beta$ instead of 2. In fact, it clearly shown that for the proposed EW SC-OFDM-SM, the spectral occupancy increases with the value of β.

Finally, we notice that the classical CP-aided OFDM-SM system still offer the best spectral occupancy at the

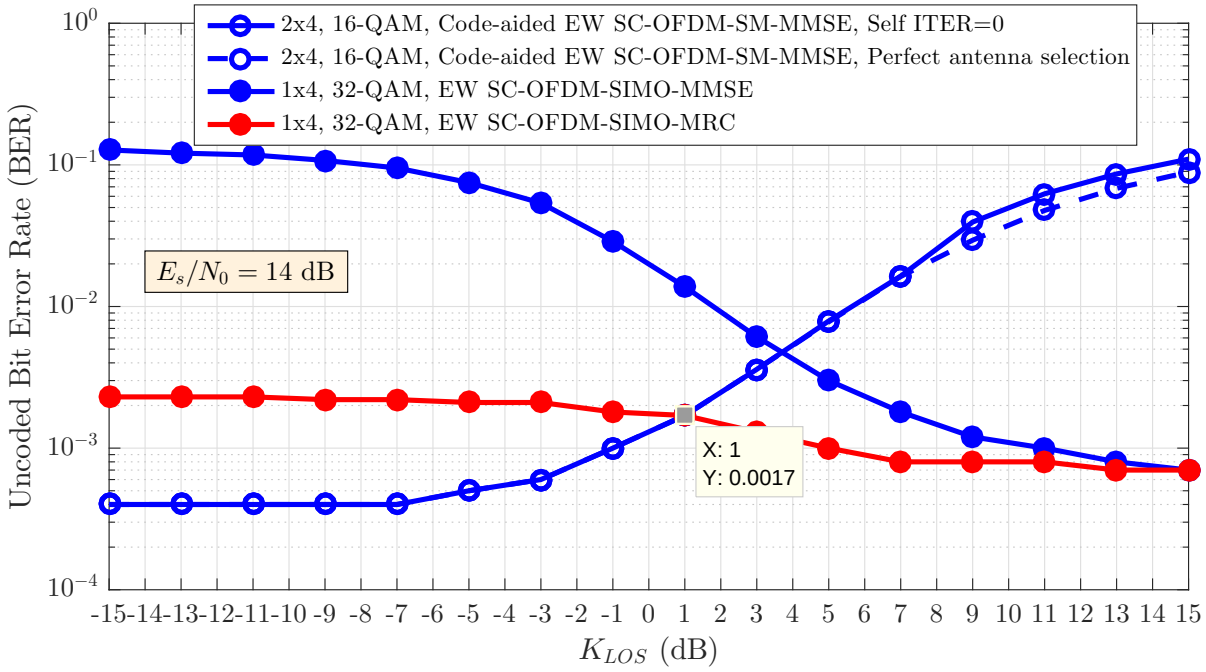

Figure 6.16: *Uncoded BER performance for the proposed EW SC-OFDM-SM / EW SC-OFDM-SIMO structure as a function of the Rice factor K_{LOS} and for different detection techniques at the receiver.*

expense of high PAPR level.

6.5.2.2 Uncoded BER performances over Ricean MIMO channel

Assuming a number of 2 of transmit antennas ($N_t = 2$) and a number of 4 of receive antennas ($N_r = 4$), the simulation of uncoded Bit Error Rate (BER) for the proposed modified SC-SM/SC-SIMO system over a 2×4 Ricean channel matrix is given in Figure 6.16 for different values of K_{LOS} values. For MMSE-based detection, the uncoded BER performances are shown in blue curves. Whereas, for MRC-based detection, the uncoded BER performances are shown in red curves. For all simulation performances, we assume a linear 16-QAM modulation (Quadrature Amplitude Modulation) for SM system and linear 32-QAM modulation for SIMO system. As a result, for both SM and SIMO systems, the considered bit rate is equal to 5 bpcu.

The main objective is to determinate which is the possible (transmitter structure $\in \{SM, SIMO\}$, receiver detector $\in \{MMSE, MRC\}$) combination that can offer the better performances in terms of uncoded BER for all values of K_{LOS} between -15 dB and 15 dB. As we can see in Figure 6.16, until the value of 1 dB of K_{LOS} factor, the SM configuration considering code-aided EW SC-OFDM-SM as a transmitter structure and using MMSE-based detection at the receiver with taking into account a number of 5 self-iterations for active antenna selection, can offer the better performances in terms of uncoded BER. Whereas, from the value of of 1 dB of K_{LOS} factor, the SIMO configuration using MRC-based detection at the receiver (red curve) is the better SIMO configuration. This better combination is selected and separately shown in Figure 6.17.

In order to compare the better combination for both the proposed modified CP-aided SC-SM/SIMO and

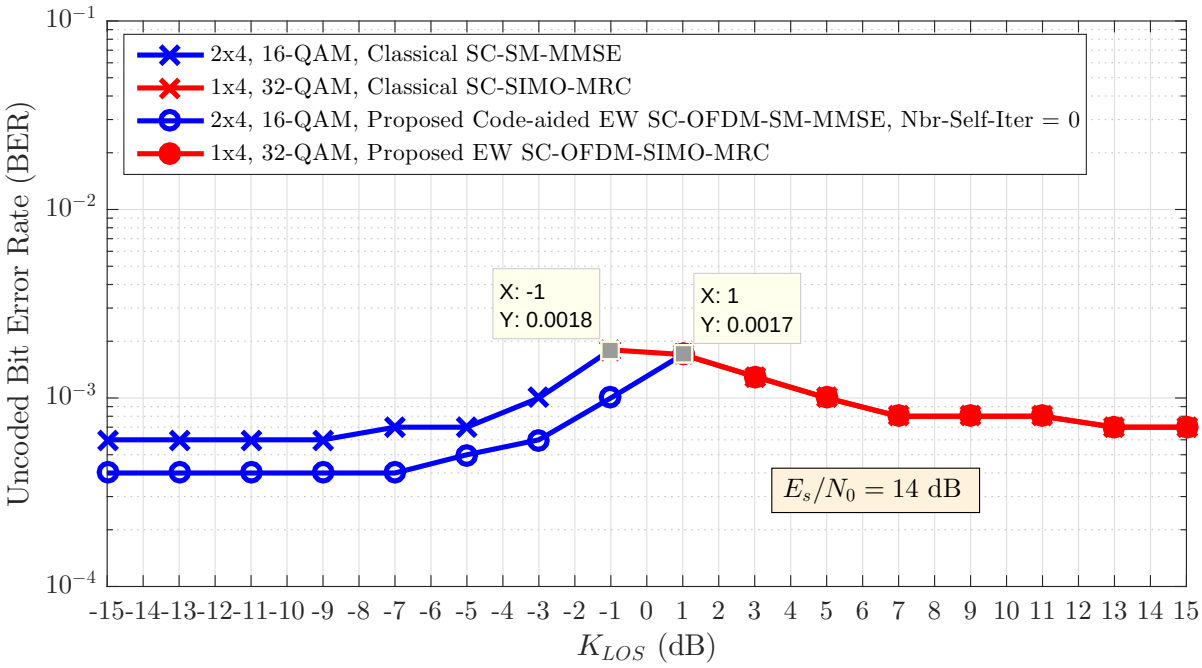

Figure 6.17: *Comparison between the better combination for both the proposed modified CP-aided SC-SM/SIMO and the classical CP-aided SC-SM/SIMO structures in terms of uncoded BER and for different values of K_{LOS}.*

the classical CP-aided SC-SM/SIMO structures, Figure 6.17 shows the simulation results for the two better combinations. As we can observe in Figure 6.17, the proposed SC-SM/SIMO structure can offer a better performances in terms of uncoded BER for all values of $\mathrm{K_{LOS}}$ factor between -15 dB and 15 dB. Indeed, thanks to the add of a code-aided block, the uncoded BER for the proposed SM structure can operate with a perfect antenna selection at the receiver and thus the uncoded BER performances are improved compared the classical SC-SM-MMSE structure.

Besides, from the value of of 1 dB of $\mathrm{K_{LOS}}$ factor, there are a considerable uncoded BER degradation for the proposed SM structure and it is shown that is preferable to using the SIMO configuration using MRC-based detection. In this case, the uncoded BER performances for both classical CP-aided SC-SIMO-MRC and proposed EW SC-OFDM-SIMO-MRC structures are identical.

6.6 Conclusion

In this chapter, we are interested in the mission link and we are proposed two modified CP-aided SM systems: « code-aided Spectrally shaped DFT-precoded OFDM-SM » and « code-aided EW SC-OFDM-SM systems ». These two modified SM system can also operated in SIMO configuration to give a proposed modified SIMO structure named « EW SC-OFDM-SIMO ». The proposed « code-aided Spectrally shaped DFT-precoded OFDM-SM » structure uses a DFT-precoded block before active antenna selection in order to reduce the PAPR level compared to the classical CP-aided OFDM-SM structure. Whereas, The proposed « code-aided

EW SC-OFDM-SM systems » used a circular RRC pulse shaping with a roll-off $0 < \beta < 1$ at the transmitter in order to reduce the spectral occupancy. As a result, the two proposed SM structures can reach a good trade-off between PAPR level and spectral occupancy.

Furthermore, the two proposed SM structures operate at an oversampled rate $\mathrm{F}_s \leq 1+\beta$ and thus the bandwidth is expanded by a factor of $1+\beta$. In order to protect the antenna bits, the two proposed SM structures exploit the bandwidth expansion to associate a high performance error correcting code with a rate $R_{\mathrm{c}} = \frac{1}{\mathrm{F}_s}$ at the transmitter. As a result, the active antenna selection is improved at the receiver and we can reach the perfect antenna selection case for low values of Rice factor $\mathrm{K}_{\mathrm{LOS}}$. However, for $\mathrm{K}_{\mathrm{LOS}}$ values grater than a studied critical value, it is shown that BER/SER performances for the SM system are subject to severe degradation and thus it is preferable to switch to the SIMO configuration using the proposed « EW SC-OFDM-SIMO » structure. The critical value of $\mathrm{K}_{\mathrm{LOS}}$ is studied for the the two proposed SM structures. As a result, it is shown that for the « code-aided Spectrally shaped DFT-precoded OFDM-SM » structure, the critical value of $\mathrm{K}_{\mathrm{LOS}}$ is equal to 6 dB instead to 5 dB for the classical CP-aided OFDM-SM system. Whereas, for the « code-aided EW SC-OFDM-SM systems » structure, the critical value is equal to 1 dB instead of -1 dB for the classical CP-aided SC-SM system.

To conclude, Thanks to the associated code-aided bloc, the two proposed SM structure allow us to enhance the active selection at the receiver an thus reach improve system performances in terms of uncoded BER compared to the classical SM structure. Moreover, the two SM structure can reach a good trade-off between PAPR level and spectral occupancy compared to the two classical SM structures: OFDM-SM and SC-SM.

Chapter 7

Conclusions and perspectives

7.1 Conclusions

7.1.1 Thesis Summary

In this thesis, we were interested in the design of viable communication for UAV links. Indeed, the future UAV communications will require an increasing throughput and with spectrum scarcity, increasing the throughput is usually tied with the rise or the increase of Inter Symbol Interference (ISI) in the received demodulated signals. The objective of this thesis was to suggest adequate waveforms and mitigation techniques to cope with the aeronautical aeronautical channel interference for the three possible UAV links: the forward link, the return link and the mission link.

First, we have studied advanced waveforms and receivers to cope with ISI for UAV communication. Second, we have investigated Spatial Modulation (SM) technique which can offer a diversity gain at the reception and can reach a good trade-off between energy consumption and bit rate. The SM technique is an interesting technique, but it requires a good antenna selection at the reception. However, in the presence of wideband Ricean MIMO channel characterized by a K_{LOS} factor, the active antenna selection at the reception can be heavily affected and consequently, the system performances in terms of BER are subject to severe degradation. According to the value of K_{LOS} between -15 dB and 15 dB, SM technique is studied and compared to SIMO technique for the mission link.

For two satellite data links i.e. the forward link and the return link, the on-board High Power Amplifiers (HPAs) are usually preferred to operate near or at saturation, which yields non linear interference due to the increased envelope fluctuation of transmitted signals. In order to avoid non-linear interference and make a more efficient use of HPAs, we are interested to low Peak-to-Average Power Ratio (PAPR) linear waveforms such as classical Single-Carrier (SC) waveform and Extended Weighted Single Carrier Orthogonal Frequency-Division Multiplexing (EW SC-OFDM) waveform. SC is a practical waveform for channels which are not very selective and allows us to consider optimal MAP-based detection at the receiver. Whereas EW SC-OFDM waveform is an interesting linear waveform offering a flexible generation of transmitted signals given by a simple frequency domain implementation as well as a low complexity MMSE-based detection at the receiver. For forward and return links, The two waveforms, SC and EW SC-OFDM, are studied for Nyquist and FTN signaling. Further, in order to maintain the advantages of the low PAPR level at the transmitter and reduced complexity detection at the receiver, EW SC-OFDM waveform is also proposed for the mission link and is combined with SM/SIMO technique enabling also a possible hybridization with terrestrial systems.

7.1.2 Thesis contribution

In this thesis, we are interested in UAV communication system and the main contributions are focused on three main UAV links: the forward link, the return link and the mission link. We recall that the forward link and the return link are two satellite links. Whereas, the mission link is a terrestrial link.

7.1.2.1 Main contributions for the satellite link

***Proposed reduced-complexity equalization structure using trellis-based detection*:** Despite the envisaged low modulation order (QPSK and 8-PSK) for the forward link (control link), the complexity of the optimal MAP-based equalizer at the receiver, still provides a serious problem for SC system. For SC receiver, the MAP equalizer still provides improved performance over a MMSE equalizer. However, the computational complexity of the MAP-based equalization grows (at least) exponentially with length of equivalent baseband channel. For the forward link, the equivalent baseband channel presents a large memory length ($L > 20$) and considering full-state MAP equalizer is no longer possible. That's why it is necessary to propose new reduced-complexity equalization structures in order to achieve a reasonable complexity at the receiver and maintain the benefits of the SC waveform at the transmitter. In this context, two proposed trellis-based equalization structures are proposed. The first one (I) is proposed for for non-sparse channels. Whereas the second one (II) is dedicated for for sparse channels for sparse channels with equally spaced coefficients.
The two proposed equalization structures (I) and (II) exploit the particular form of the discrete-time equivalent baseband channel in order to reduce the complexity at the receiver. In aeronautical communications, it is shown that for Nyquist signaling, the resulting discrete-time equivalent baseband channel is sparse with equally spaced coefficients and in this case, it is shown that the proposed equalization structure (II) is able to perform efficient channel equalization with reduced computational complexity. On the other hand, for FTN signaling, it is shown that the equivalent baseband channel is no longer sparse and having a long memory length. In this case, the proposed equalization structure (I) appears suitable for this kind of channels. By considering this structure, it is shown that we can reach a good trade-off between computational complexity and system performance.

***Proposed efficient channel estimation method using parametric model*:** In wireless communication systems, the estimation of the channel impulse response is necessary for the coherent demodulation. For channel estimation, it is shown that the performance of the unstructured LS estimator decreases with the number of random variables to be estimated i.e. the channel length. Since, in some cases, the aeronautical channel presents a long memory length, it is clear that using the classical unstructured LS estimator is not sufficient to give an accurate estimation of the baseband channel. In order to enhance channel estimation accuracy, we proposed a simple and efficient channel estimation method based on UAV position. Indeed, by taking into account some geometrical considerations, some channel parameters (essentially delays) can be well known at the receiver. For instance, for the aeronautical channel, if we exactly know the UAV coordinates (latitude, longitude, altitude), we can exactly determinate all delay values. By exploiting this *a priori*, it is shown that

the proposed channel estimator is able to greatly enhance the estimation performance. Based on a parametric model, the proposed channel estimation methods allow us to reduce the number of variables to be estimated to only two random complex variables $a_{i,1}$ and $a_{i,2}$ which are the two complex fading of the aeronautical channel for the forward link. As a result, in terms of Minimum Square Error (MSE), the obtained estimation gain in decibels is about 10 $\log_{10}(L/2)$ compared to the classical unstructured LS estimator. Assuming a typical channel length of 20 ($L = 20$), one can obtain a channel estimation gain of approximately 10 dB.

7.1.2.2 Main contributions for the mission link

***Proposed reduced PAPR SM structure based on DFT-Precoding for OFDM Signals*:** a code-aided OFDM-SM structure is proposed. The modified proposed SM structure aims to reduce the PAPR level at the transmitter compared to the classical OFDM-SM structure. By adding a DFT-precoded block, it is shown that we can reduce the PAPR level at the transmitter. Note that the idea of adding DFT-precoding to reduce the PAPR level of SM system is considered in some works in the literature. The main difference is that we propose to use a DFT-precoding block just before antenna selection and not in each transmit antenna. This choice not only allows us a hardware complexity reduction (only one DFT-precoded bloc instead of many ones implemented for all transmitted antenna), but also leads to a system performance improvement. Indeed, by using DFT-precoded block with an expanded bandwidth (DFT-precoded spectrally shaped block), it is possible to exploit excess bandwidth to improve antenna bit protection and thus enhancing system performances.

***Proposed SM structure combining EW SC-OFDM waveform and SM modulation*:** a code-aided SC-SM structure is proposed. The main advantage of this structure is that operates with only one Radio Frequency (RF) chain which leads to hardware complexity reduction at the transmitter. Compared to the classical SC-SM structure, the proposed structure uses a circular pulse shaping. This design aims to reduce the spectral occupancy of the transmitted signals and thus enhance the spectral efficiency of the system. Furthermore, the proposed structure combines EW SC-OFDM waveform to SM technique. The choice of EW SC-OFDM waveform as circular waveform allows us to benefit from a reduced complexity Frequency Domain Equalization (FDE) at the receiver. Moreover, since EW SC-OFDM operates with an oversampling factor or also with an excess bandwidth, it is shown than we can exploit bandwidth expansion to protect antenna bits at the transmitter and thus enhance system performances at the receiver. Also, compared to others circular waveforms such as SC-OFDM and OFDM, EW SC-OFDM provides a reduced PAPR at the transmitter. Besides, the considered SM structure is perfectly suitable to Faster-than-Nyquist (FTN) signaling and thus it is possible to increase more the spectral efficiency of the system.

7.2 Perspectives

Several perspectives can be envisaged as the opening of this work on future lines of research. We summarize them as follows:

7.2.1 Non-Linear effect

In the satellite communication context, resorting to the linear model to evaluate the spectral efficiency improvement is not sufficient to assess the effectiveness of the FTN signaling. Indeed, the introduced ISI will lead to higher envelop fluctuations. The resulting non linear distortion introduced by the payload should be carefully analyzed in this context. Therefore, the non-linear regime should be addressed and associated equivalent base-band models have to be considered.

7.2.2 Frequency and clock synchronization

One of the main assumptions used in this thesis was a perfect time and frequency synchronization. In reality, there are usually residual synchronization errors, which it will be interesting to include in our system model. It would also be interesting to derive fractional spaced equalizers and evaluate their ability to account for timing synchronization.

7.2.3 Channel estimation for SC signals using FTN signaling

In this thesis, we have assumed that the channel response is perfectly known to the receiver. In practice, channel response must be estimated at the receiver. Generally, the channel response is often taken with an estimation error. For this reason, it would be interesting to evaluate the impact of this error on system performance.

Furthermore, in this thesis we have investigated efficient channel equalization structures without taking into consideration channel estimation constraints. Indeed, For SC signals using FTN signaling, it is shown that, if the spectral factorization is allowed, i.e. the correlation matrix $\mathbf{\Lambda}$ is non-invertible, it will be possible to apply the ML estimation as an optimal solution. Otherwise, optimal ML estimation is not available and this estimation problem is still an issue. Only sub-optimal estimations are available (for example, LS estimator). In the case of non-possible spectral factorization, one had to wonder if FTN signaling is really an interesting strategy or no? For this issue, it would be interesting to evaluate the trade-off between spectral efficiency improvement and system performance degradation with considering sub-optimal channel estimators.

7.2.4 Interference term modeling for MAP equalization with successive interference cancellation (SIC) for FTN signaling

In this thesis, we have investigated two reduced-complexity MAP-based equalization structure. For the two proposed structures, the expression of the observation model is broken into a powerful useful part, a low-powered interference part, and a noise part, in the form:

$$y_{i,n} = \sum_{l=-L/2}^{+L/2} h_l \; s_{i,n-l} + w_n = \underbrace{\sum_{l \in \mathcal{I}}^{L/2} h_i\,(l.\mathrm{T}_s) \; s_{i,n-l}}_{\text{Powerful component}} + \underbrace{\sum_{\substack{l=-L/2 \\ l \notin \mathcal{I}}}^{L/2} h_l \; s_{i,n-l}}_{\text{Interference term}} + \underbrace{w_n}_{noise}$$

Here, the interference term is modeled as Gaussian and having the same statistics (notably the covariance matrix) as the additive noise w_n. In Nyquist signaling, we can show that this assumption still valid. However, for FTN signaling, it is not necessarily the case. Fortunately, if the interference term is low-powered (the case of high value of acceleration factor ν), we can safety adopt this assumption and we can neglect this mismatch modeling of the interference term given the fact that the latter is lower-powered and its impact on system performance is not significant. However, if the case low values of ν, the interference term is no longer low-powered and this mismatch modeling can impact system performances. Indeed, in this case, the decoder is mismatched with its input signal (mismatched model) and the symbol detection is commonly referred to as *mismatch decoding*. So, in order to enhance symbol detection for lower values of ν, it is highly recommended to take into consideration this mismatch modeling when considering trellis-based equalization for the proposed Structures (I) and (II).

7.2.5 Using FTN signaling for SM system

In this thesis, we are proposed a modified SC-SM structure named «EW SC-OFDM-SM». This structure is operating with one RF chain and is perfectly suitable to Faster-than-Nyquist (FTN) signaling. In order to increase more the spectral efficiency of the system, it is possible to maintain the benefits of SM modulation and using FTN signaling at the transmitter. At the receiver, one can resort to consider turbo-equalization in order to enhance symbol detection. Since the proposed uses a circular shaping at the transmitter, one of the possible solutions is considering MMSE equalizer with *a priori* at the receiver.

Bibliography

[1] DVB-S2/RCS Transparent Mesh Overlay Network. Technical report. Available at http://arquivo.pt/wayback/20160522190813/http://telecom.esa.int/telecom/media/document/ASN%20Mesh%20Presentation.pdf.

[2] ANTARES CS standard (DRAFT). Technical report. Available at https://artes.esa.int/sites/default/files/IRIS-AN-CP-TNO-612-ESA-C1.pdf.

[3] A. Ancora, C. Bona, and D. T. Slock. Down-sampled impulse response least-squares channel estimation for LTE OFDMA. In *Acoustics, Speech and Signal Processing, 2007. ICASSP 2007. IEEE International Conference on*, volume 3, pages III–293. IEEE, 2007.

[4] J. B. Anderson and A. Prlja. Turbo equalization and an M-BCJR algorithm for strongly narrowband intersymbol interference. In *2010 International Symposium On Information Theory Its Applications*, pages 261–266, Oct 2010.

[5] J. G. Andrews, S. Buzzi, W. Choi, S. V. Hanly, A. Lozano, A. C. Soong, and J. C. Zhang. What will 5G be? *IEEE Journal on selected areas in communications*, 32(6):1065–1082, 2014.

[6] R. Austin. *Unmanned Aircraft Systems: UAVS Design, Development and Deployment (Aerospace Series)*. Wiley, 2011. Available at https://www.amazon.com/Unmanned-Aircraft-Systems-Development-Deployment-ebook/dp/B005UQLG0C?SubscriptionId=0JYN1NVW651KCA56C102&tag=techkie-20&linkCode=xm2&camp=2025&creative=165953&creativeASIN=B005UQLG0C.

[7] B. Babadi, N. Kalouptsidis, and V. Tarokh. Asymptotic achievability of the Cramér–Rao bound for noisy compressive sampling. *IEEE Transactions on Signal Processing*, 57(3):1233–1236, 2009.

[8] B. Babadi, N. Kalouptsidis, and V. Tarokh. Asymptotic Achievability of the Cramer-Rao Bound for Noisy Compressive Sampling. *IEEE Transactions on Signal Processing*, 57(3):1233–1236, March 2009.

[9] L. Bahl, J. Cocke, F. Jelinek, and J. Raviv. Optimal decoding of linear codes for minimizing symbol error rate (Corresp.). *IEEE Transactions on Information Theory*, 20(2):284–287, Mar 1974.

[10] W. U. Bajwa, J. Haupt, A. M. Sayeed, and R. Nowak. Compressed Channel Sensing: A New Approach to Estimating Sparse Multipath Channels. *Proceedings of the IEEE*, 98(6):1058–1076, June 2010.

[11] C. A. Belfiore and J. H. Park. Decision feedback equalization. *Proceedings of the IEEE*, 67(8):1143–1156, 1979.

[12] P. Bello. Aeronautical channel characterization. *IEEE Transactions on Communications*, 21(5):548–563, 1973.

[13] B. Benammar. *Formes d'ondes avancées et traitements itératifs pour les canaux non linéaires satellites*. PhD thesis, 2014.

[14] B. Benammar, N. Thomas, M.-L. Boucheret, C. Poulliat, and M. Dervin. Analytical expressions of power spectral density for general spectrally shaped sc-fdma systems. In *Signal Processing Conference (EUSIPCO), 2013 Proceedings of the 21st European*, pages 1–5. IEEE, 2013.

[15] N. Benvenuto and R. Marchesani. The Viterbi algorithm for sparse channels. *IEEE Transactions on Communications*, 44(3):287–289, Mar 1996.

[16] S. Blandino, F. Kaltenberger, and M. Feilen. Wireless Channel Simulator Testbed for Airborne Receivers. In *2015 IEEE Globecom Workshops (GC Wkshps)*, pages 1–6, Dec 2015.

[17] C. Bluemm, C. Heller, B. Fourestie, and R. Weigel. Wideband aeronautical channel sounding and modeling for C-band telemetry. In *Personal Indoor and Mobile Radio Communications (PIMRC), 2013 IEEE 24th International Symposium on*, pages 264–269. IEEE, 2013.

[18] D. C. Callaghan. Everyone has an unmanned aircraft: The control, de-confliction and coordination of Unmanned Aircraft in the future battlespace. Master's thesis, Faculty of the U.S. Army Command and General Staff College, Embry-Riddle Aeronautical Univ, Kansas, USA, 2007.

[19] C. Carbonelli, S. Vedantam, and U. Mitra. Sparse Channel Estimation with Zero Tap Detection. *IEEE Transactions on Wireless Communications*, 6(5):1743–1763, May 2007.

[20] D. Cassioli and A. Mecozzi. Minimum-phase impulse response channels. *IEEE Transactions on Communications*, 57(12), 2009.

[21] M. K. Caswell. Need for Vertical Delineation of Air Space: Can Google's Project Loon Survive without It. *Tul. J. Int'l & Comp. L.*, 24:205, 2015.

[22] V. Center. Unmanned Aircraft System (UAS) Service Demand 2015-2035: Literature Review & Projections of Future Usage, 2013.

[23] Y. A. Chau and S.-H. Yu. Space modulation on wireless fading channels. In *Vehicular Technology Conference, 2001. VTC 2001 Fall. IEEE VTS 54th*, volume 3, pages 1668–1671 vol.3, 2001.

[24] J. M. Cioffi, G. P. Dudevoir, M. V. Eyuboglu, and G. D. Forney. MMSE decision-feedback equalizers and coding. I. Equalization results. *IEEE transactions on Communications*, 43(10):2582–2594, 1995.

[25] I. Cir. 328: Unmanned Aircraft Systems (UAS). *International Civil Aviation Organization*, 2011.

[26] R. Clarke. A statistical theory of mobile-radio reception. *Bell Labs Technical Journal*, 47(6):957–1000, 1968.

[27] G. Colavolpe and A. Barbieri. On MAP symbol detection for ISI channels using the Ungerboeck observation model. *IEEE communications letters*, 9(8):720–722, 2005.

[28] S. Coleri, M. Ergen, A. Puri, and A. Bahai. Channel estimation techniques based on pilot arrangement in OFDM systems. *IEEE Transactions on broadcasting*, 48(3):223–229, 2002.

[29] I. . L. S. Committee et al. IEEE Standard for Information technology-Telecommunication and information exchange between systems-Local and metropolitan area networks-Specific requirements Part11: Wireless LAN Medium Access Control (MAC) and Physical Layer (PHY) Specifications Amendmentl: Radio Resource Measurement of Wireless LANs. *http://standards. ieee. org/getieee802/download/802.11 n-2009*, 2009.

[30] S. F. Cotter and B. D. Rao. Sparse channel estimation via matching pursuit with application to equalization. *IEEE Transactions on Communications*, 50(3):374–377, Mar 2002.

[31] C. Douillard, M. Jézéquel, C. Berrou, D. Electronique, A. Picart, P. Didier, and A. Glavieux. Iterative correction of intersymbol interference: Turbo-equalization. *Transactions on Emerging Telecommunications Technologies*, 6(5):507–511, 1995.

[32] A. Duel-Hallen and C. Heegard. Delayed decision-feedback sequence estimation. *IEEE Transactions on Communications*, 37(5):428–436, 1989.

[33] A. Duel-Hallen and C. Heegard. Delayed decision-feedback sequence estimation. *IEEE Transactions on Communications*, 37(5):428–436, May 1989.

[34] G. D. Durgin and T. S. Rappaport. Effects of multipath angular spread on the spatial cross-correlation of received voltage envelopes. In *1999 IEEE 49th Vehicular Technology Conference (Cat. No.99CH36363)*, volume 2, pages 996–1000 vol.2, Jul 1999.

[35] F. R. EASA. *Preliminary impact assessment on the safety of communications for UAS.* EASA.2008.OP.08, Issue 1.0, December 2009.

[36] S. M. Elnoubi. A simplified stochastic model for the aeronautical mobile radio channel. In *Vehicular Technology Conference, 1992, IEEE 42nd*, pages 960–963. IEEE, 1992.

[37] E. ETSI. Digital Video Broadcasting (DVB); Second Generation DVB Interactive Satellite System (DVB-RCS2);Part 4: Guidelines for Implementation and Use of EN 301 545-2. Technical report, Technical report, Tech. rep., ETSI.

[38] E. ETSI. Digital Video Broadcasting (DVB); Interaction channel for satellite distribution systems. *ETSI EN*, 301:790, 2005.

[39] E. ETSI. Digital video broadcasting (DVB); second generation framing structure, channel coding and modulation systems for broadcasting, interactive services, news gathering and other broadband satellite applications. Technical report, Technical report, Tech. rep., ETSI, 2005.

[40] E. ETSI. Digital Video Broadcasting (DVB); Second generation framing structure, channel coding and modulation systems for Broadcasting, Interactive Services, News Gathering and other broadband satellite applications. Part II: S2-Extensions (DVB-S2X) - (Optional). DVB Document A83-2. Technical report, Technical report, Tech. rep., ETSI, 2005.

[41] J. Everaerts. The use of Unmanned Aerial Vehicles (UAVS) for remote sensing and mapping. *The International Archives of the Photogrammetry, Remote Sensing and Spatial Information Sciences*, 37:1187–1192, 2008.

[42] M. V. Eyuboglu and S. U. Qureshi. Reduced-state sequence estimation with set partitioning and decision feedback. *IEEE Transactions on Communications*, 36(1):13–20, 1988.

[43] I. Fijalkow, A. Roumy, S. Ronger, D. Pirez, and P. Vila. Improved interference cancellation for turbo-equalization. In *Acoustics, Speech, and Signal Processing, 2000. ICASSP'00. Proceedings. 2000 IEEE International Conference on*, volume 1, pages 416–419. IEEE, 2000.

[44] E. Final Draft. EN 301 790 v 1.5. 1. *Digital Video Broadcasting (DVB): Interaction channel for satellite distribution systems*, 1, 2009.

[45] G. Forney. Maximum-likelihood sequence estimation of digital sequences in the presence of intersymbol interference. *IEEE Transactions on Information theory*, 18(3):363–378, 1972.

[46] M. J. Gans. A power-spectral theory of propagation in the mobile-radio environment. *IEEE Transactions on Vehicular Technology*, 21(1):27–38, 1972.

[47] K. Giridhar, J. J. Shynk, and R. A. Iltis. Reduced complexity MAPSD algorithms with spatial diversity for TDMA mobile radio signal recovery. In *Communications, 1993. ICC '93 Geneva. Technical Program, Conference Record, IEEE International Conference on*, volume 2, pages 1134–1138 vol.2, May 1993.

[48] A. Goldsmith. *Wireless communications*. Cambridge university press, 2005.

[49] D. Gómez-Barquero, C. Douillard, P. Moss, and V. Mignone. Dvb-ngh: The next generation of digital broadcast services to handheld devices. *IEEE Transactions on Broadcasting*, 60(2):246–257, 2014.

[50] F. Gray. Pulse code communication, March 17 1953. US Patent 2,632,058.

[51] Y. Gu and T. Le-Ngoc. Adaptive combined DFE/MLSE techniques for ISI channels. *IEEE Transactions on communications*, 44(7):847–857, 1996.

[52] B. Guan, X. Wang, X. Zhang, et al. A new decision feedback detection algorithm of LTE uplink. *The Airforce Radars Journal*, 2010.

[53] E. Haas. Aeronautical channel modeling. *IEEE transactions on vehicular technology*, 51(2):254–264, 2002.

[54] P. Hoeher, S. Kaiser, and P. Robertson. Pilot-symbol-aided channel estimation in time and frequency. *Multi-carrier spread-spectrum*, pages 169–178, 1997.

[55] Y. Hua, M. Nikpour, and P. Stoica. Optimal reduced-rank estimation and filtering. *IEEE Transactions on Signal Processing*, 49(3):457–469, 2001.

[56] G. Huang, A. Nix, and S. Armour. Decision feedback equalization in SC-FDMA. In *Personal, Indoor and Mobile Radio Communications, 2008. PIMRC 2008. IEEE 19th International Symposium on*, pages 1–5. IEEE, 2008.

[57] S. U. Hwang, S. Jeon, S. Lee, and J. Seo. Soft-output ML detector for spatial modulation OFDM systems. *IEICE Electronics Express*, 6(19):1426–1431, 2009.

[58] M. Itagaki, K. Takeda, and F. Adachi. Frequency-domain QRM-MLD block signal detection for single-carrier multi-user MIMO uplink. In *Network Infrastructure and Digital Content, 2010 2nd IEEE International Conference on*, pages 687–691. IEEE, 2010.

[59] ITU. Characteristics of unmanned aircraft systems and spectrum requirements to support their safe operation in non-segregated airspace. *International Telecommunication Union (ITU)*, page Tech. Rep. M.2171, December 2009.

[60] ITU-R. Caractéristiques Electriques du Sol. pages 527–3. 1999.

[61] ITU-R. Données de propagation nécessaires pour la conception de systèmes de télécommunication mobiles maritimes terre-espace. pages 680–3. 1999.

[62] ITU-R. Données de propagation nécessaires pour la conception de systèmes de télécommunication mobiles maritimes terre-espace. pages 680–1. 1999.

[63] J. Jacob, C. M. Panazio, and T. Abrão. PAPR and saturation effects of power amplifiers in SM OFDM and V-BLAST OFDM systems. In *Telecommunications Symposium (ITS), 2014 International*, pages 1–5, Aug 2014.

[64] J. Jeganathan, A. Ghrayeb, and L. Szczecinski. Spatial modulation: Optimal detection and performance analysis. *IEEE Communications Letters*, 12(8), 2008.

[65] J. A. Kakar. *UAV communications: Spectral requirements, MAV and SUAV channel modeling, OFDM waveform parameters, performance and spectrum management.* PhD thesis, Virginia Tech, 2015.

[66] R. Kalbasi, D. D. Falconer, A. H. Banihashemi, and R. Dinis. A comparison of frequency-domain block MIMO transmission systems. *IEEE Transactions on Vehicular Technology*, 58(1):165–175, 2009.

[67] R. J. Kerczewski, J. D. Wilson, and W. D. Bishop. Frequency spectrum for integration of unmanned aircraft. In *Digital Avionics Systems Conference (DASC), 2013 IEEE/AIAA 32nd*, pages 6D5–1. IEEE, 2013.

[68] T. Kos, I. Markezic, and J. Pokrajcic. Effects of multipath reception on GPS positioning performance. In *Elmar, 2010 Proceedings*, pages 399–402. IEEE, 2010.

[69] J. Kunisch, I. De La Torre, A. Winkelmann, M. Eube, and T. Fuss. Wideband time-variant air-to-ground radio channel measurements at 5 GHz. In *Antennas and Propagation (EUCAP), Proceedings of the 5th European Conference on*, pages 1386–1390. IEEE, 2011.

[70] C. Laot, R. L. Bidan, and D. Leroux. Low-complexity MMSE turbo equalization: a possible solution for EDGE. *IEEE Transactions on Wireless Communications*, 4(3):965–974, May 2005.

[71] F. K. H. Lee and P. J. McLane. Iterative parallel-trellis MAP equalizers with nonuniformly-spaced prefilters for sparse multipath channels. In *Proceedings IEEE 56th Vehicular Technology Conference*, volume 4, pages 2201–2205 vol.4, 2002.

[72] F. K. H. Lee and P. J. Mclane. Parallel-Trellis Turbo Equalizers for Sparse-Coded Transmission over SISO and MIMO Sparse Multipath Channels. *IEEE Transactions on Wireless Communications*, 5(12):3568–3578, December 2006.

[73] W. Lee and F. Hill. A Maximum-Likelihood Sequence Estimator with Decision-Feedback Equalization. *IEEE Transactions on Communications*, 25(9):971–979, Sep 1977.

[74] Y. Li, B. Vucetic, and Y. Sato. Optimum soft-output detection for channels with intersymbol interference. *IEEE Transactions on Information Theory*, 41(3):704–713, May 1995.

[75] M. Maleki, H. R. Bahrami, and A. Alizadeh. On MRC-based detection of spatial modulation. *IEEE Transactions on Wireless Communications*, 15(4):3019–3029, 2016.

[76] D. Matolak. AG Channel Sounding for UAS in the NAS. *NASA, Project presentation, University of South California*, 2014.

[77] D. W. Matolak. Wireless Channel Characterization in the 5 GHz Microwave Landing System Extension Band for Airport Surface Areas. (May), 2007.

[78] D. W. Matolak. Air-ground channels & models: Comprehensive review and considerations for unmanned aircraft systems. In *Aerospace Conference, 2012 IEEE*, pages 1–17. IEEE, 2012.

[79] D. W. Matolak. Air-ground channels amp; models: Comprehensive review and considerations for unmanned aircraft systems. In *2012 IEEE Aerospace Conference*, pages 1–17, March 2012.

[80] D. W. Matolak. Unmanned aerial vehicles: Communications challenges and future aerial networking. In *Computing, Networking and Communications (ICNC), 2015 International Conference on*, pages 567–572. IEEE, 2015.

[81] J. Mazo. Faster-than-Nyquist signaling. *The Bell System Technical Journal*, 54(8):1451–1462, 1975.

[82] N. C. McGinty, R. A. Kennedy, and P. Hocher. Parallel trellis Viterbi algorithm for sparse channels. *IEEE Communications Letters*, 2(5):143–145, May 1998.

[83] N. C. McGinty, R. A. Kennedy, and P. Hocher. Parallel trellis Viterbi algorithm for sparse channels. *IEEE Communications Letters*, 2(5):143–145, 1998.

[84] Y. S. Meng and Y. H. Lee. Measurements and characterizations of air-to-ground channel over sea surface at C-band with low airborne altitudes. *IEEE Transactions on Vehicular Technology*, 60(4):1943–1948, 2011.

[85] R. Mesleh, H. Haas, C. W. Ahn, and S. Yun. Spatial Modulation - A New Low Complexity Spectral Efficiency Enhancing Technique. In *2006 First International Conference on Communications and Networking in China*, pages 1–5, Oct 2006.

[86] R. Y. Mesleh, H. Haas, S. Sinanovic, C. W. Ahn, and S. Yun. Spatial Modulation. *IEEE Transactions on Vehicular Technology*, 57(4):2228–2241, July 2008.

[87] J. Mietzner, S. Badri-Hoeher, I. Land, and P. A. Hoeher. Trellis-based equalization for sparse ISI channels revisited. In *Proceedings. International Symposium on Information Theory, 2005. ISIT 2005.*, pages 229–233, Sept 2005.

[88] J. Mietzner, S. Badri-Hoeher, I. Land, and P. A. Hoeher. Equalization of sparse intersymbol-interference channels revisited. *EURASIP Journal on Wireless Communications and Networking*, 2006(1):029075, 2006.

[89] A. Neul, J. Hagenauer, W. Papke, F. Dolainsky, and F. Edbauer. Propagation measurements for the aeronautical satellite channel. In *Vehicular Technology Conference, 1987. 37th IEEE*, volume 37, pages 90–97. IEEE, 1987.

[90] W. G. Newhall, R. Mostafa, C. Dietrich, C. R. Anderson, K. Dietze, G. Joshi, and J. H. Reed. Wideband air-to-ground radio channel measurements using an antenna array at 2 GHz for low-altitude operations. In *Military Communications Conference, 2003. MILCOM'03. 2003 IEEE*, volume 2, pages 1422–1427. IEEE, 2003.

[91] R. Niazadeh, S. H. Ghalehjegh, M. Babaie-Zadeh, and C. Jutten. ISI sparse channel estimation based on SL0 and its application in ML sequence-by-sequence equalization. *Signal Processing*, 92(8):1875–1885, 2012.

[92] M. Nicoli and U. Spagnolini. Reduced-rank channel estimation for time-slotted mobile communication systems. *IEEE transactions on signal processing*, 53(3):926–944, 2005.

[93] J. Park and S. B. Gelfand. Turbo equalizations for sparse channels. In *2004 IEEE Wireless Communications and Networking Conference (IEEE Cat. No.04TH8733)*, volume 4, pages 2301–2306 Vol.4, March 2004.

[94] J. Park and S. B. Gelfand. Sparse MAP equalizers for turbo equalizations. In *2005 IEEE 61st Vehicular Technology Conference*, volume 2, pages 762–766 Vol. 2, May 2005.

[95] B. Raddadi, B. Gadat, C. Poulliat, N. Thomas, and M.-L. Boucheret. Equalization method for a parsimonious communication channel and device implementing the method, Aug. 1 2017. US Patent 9,722,817.

[96] B. Raddadi, C. Poulliat, N. Thomas, M. L. Boucheret, and B. Gadat. Channel estimation with a priori position for aeronautical communications via a satellite link. In *Personal, Indoor, and Mobile Radio Communications (PIMRC), 2015 IEEE 26th Annual International Symposium on*, pages 532–537, Aug 2015.

[97] B. Raddadi, R. Tajan, N. Thomas, C. Poulliat, and M.-L. Boucheret. Nouvelle structure codée de modulation spatiale utilisant une signalisation plus rapide que Nyquist (regular paper). In *Colloque GRETSI sur le Traitement du Signal et des Images (GRETSI), Juan-les-Pins, 05/09/2017-08/09/2017*, page (support électronique), http://www.traitementdusignal.fr/, septembre 2017. GRETSI CNRS.

[98] B. Raddadi, N. Thomas, C. Poulliat, and M.-L. Boucheret. On the use of spatial modulation in aeronautical communications. In *Wireless and Mobile Computing, Networking and Communications (WiMob), 2016 IEEE 12th International Conference on*, pages 1–8. IEEE, 2016.

[99] B. Raddadi, N. Thomas, C. Poulliat, and M.-L. Boucheret. Code-aided Antenna Selection for Spectrally Shaped DFT-precoded OFDM Spatial Modulation (regular paper). In *IEEE International Conference on Personal, Indoor and Mobile Radio Communications (PIMRC), Montreal, Quebec, Canada, 08/10/2017-13/10/2017*, page (electronic medium), http://www.ieee.org/, 2017. IEEE.

[100] B. Raddadi, N. Thomas, C. Poulliat, M. L. Boucheret, and B. Gadat. On an efficient equalization structure for aeronautical communications via a satellite link. In *2014 IEEE 10th International Conference on Wireless and Mobile Computing, Networking and Communications (WiMob)*, pages 396–401, Oct 2014.

[101] B. Raddadi, N. Thomas, C. Poulliat, M.-L. Boucheret, and B. Gadat. Estimation de canal avec apriori de position pour les communications aeronautiques par satellite. In *25eme Colloque Groupe de Recherche et d'Etudes du Traitement du Signal et des Images (GRETSI 2015)*, pages pp–1, 2015.

[102] R. Rajashekar, K. Hari, and L. Hanzo. Spatial modulation aided zero-padded single carrier transmission for dispersive channels. *IEEE Transactions on Communications*, 61(6):2318–2329, 2013.

[103] R. Rajashekar, K. V. S. Hari, and L. Hanzo. Antenna Selection in Spatial Modulation Systems. *IEEE Communications Letters*, 17(3):521–524, March 2013.

[104] M. M. Rana. Channel estimation techniques and LTE Terminal implementation challenges. In *Computer and Information Technology (ICCIT), 2010 13th International Conference on*, pages 545–549. IEEE, 2010.

[105] T. S. Rappaport et al. *Wireless communications: principles and practice*, volume 2. prentice hall PTR New Jersey, 1996.

[106] M. D. Renzo, H. Haas, and P. M. Grant. Spatial modulation for multiple-antenna wireless systems: a survey. *IEEE Communications Magazine*, 49(12):182–191, December 2011.

[107] M. Rice, A. Davis, and C. Bettweiser. Wideband channel model for aeronautical telemetry. *IEEE Transactions on Aerospace and Electronic Systems*, 40(1):57–69, 2004.

[108] P. Robertson, P. Hoeher, and E. Villebrun. Optimal and sub-optimal maximum a posteriori algorithms suitable for turbo decoding. *Transactions on Emerging Telecommunications Technologies*, 8(2):119–125, 1997.

[109] P. E. Ross. When will we have unmanned commercial airliners. *IEEE Spectrum Magazine*, 2011.

[110] A. Roumy, I. Fijalkow, and D. Pirez. Joint equalization and decoding: why choose the iterative solution? In *Vehicular Technology Conference, 1999. VTC 1999-Fall. IEEE VTS 50th*, volume 5, pages 2989–2993. IEEE, 1999.

[111] S. R. Saunders and S. R. Simon. *Antennas and Propagation for Wireless Communication Systems*. John Wiley & Sons, Inc., New York, NY, USA, 1st edition, 1999.

[112] F. Schuh, A. Schenk, and J. B. Huber. Matched decoding for punctured convolutional encoded transmission over ISI-Channels. In *Systems, Communication and Coding (SCC), Proceedings of 2013 9th International ITG Conference on*, pages 1–5. VDE, 2013.

[113] M. Sharp and A. Scaglione. Estimation of sparse multipath channels. In *MILCOM 2008 - 2008 IEEE Military Communications Conference*, pages 1–7, Nov 2008.

[114] M. Siala. Maximum a posteriori fast fading channel estimation based exclusively on pilot symbols. *Annals of Telecommunications*, 56(9):569–586, 2001.

[115] T. Simonite. Air traffic control for drones, 2014.

[116] M. Simunek. Propagation channel modeling for low elevation links in urban areas. Master's thesis, Ph.D. dissertation, Dept. Elect. Eng., Czech Tech. Univ., Prague, 2013.

[117] D. Sinanovic, G. Sisul, and B. Modlic. Low-PAPR Spatial Modulation for SC-FDMA. *IEEE Transactions on Vehicular Technology*, 66(1):443–454, Jan 2017.

[118] P. Som and A. Chockalingam. Spatial modulation and space shift keying in single carrier communication. In *Personal Indoor and Mobile Radio Communications (PIMRC), 2012 IEEE 23rd International Symposium on*, pages 1962–1967. IEEE, 2012.

[119] J. Soubielle, I. Fijalkow, P. Duvaut, and A. Bibaut. GPS positioning in a multipath environment. *IEEE Transactions on Signal Processing*, 50(1):141–150, Jan 2002.

[120] A. Steingass, A. Lehner, F. Pérez-Fontán, E. Kubista, and B. Arbesser-Rastburg. Characterization of the aeronautical satellite navigation channel through high-resolution measurement and physical optics simulation. *International Journal of Satellite Communications and Networking*, 26(1):1–30, 2008.

[121] S. Sugiura and L. Hanzo. Single-RF spatial modulation requires single-carrier transmission: Frequency-domain turbo equalization for dispersive channels. *IEEE Transactions on Vehicular Technology*, 64(10):4870–4875, 2015.

[122] R. Tajan, C. Poulliat, and M.-L. Boucheret. Circular Faster Than Nyquist: Transmitter and iterative receiver design. In *Turbo Codes and Iterative Information Processing (ISTC), 2016 9th International Symposium on*, pages 241–245. IEEE, 2016.

[123] N. Tao, M. Bousquet, A. Pirovano, and J. Radzik. DVB-S2/DVB-RCS satellite system performance assessment for IFE and ATN aeronautical communications. In *Satellite and Space Communications, 2006 International Workshop on*, pages 170–175. IEEE, 2006.

[124] M. Tuchler, A. C. Singer, and R. Koetter. Minimum mean squared error equalization using a priori information. *IEEE Transactions on Signal processing*, 50(3):673–683, 2002.

[125] G. Ungerboeck. Adaptive maximum-likelihood receiver for carrier-modulated data-transmission systems. *IEEE Transactions on Communications*, 22(5):624–636, 1974.

[126] A. Van Zelst and J. Hammerschmidt. A single coefficient spatial correlation model for multiple-input multiple-output (MIMO) radio channels. *Proc. 27th General Assembly of the Int. Union of Radio Science (URSI)*, 2002.

[127] S. N. Venkatasubramanian. Propagation channel model between unmanned aerial vehicles for emergency communications. Master's thesis, School of Electrical Engineering, Aalto University, 2013.

[128] P. Yang, Y. Xiao, Y. L. Guan, K. V. S. Hari, A. Chockalingam, S. Sugiura, H. Haas, M. D. Renzo, C. Masouros, Z. Liu, L. Xiao, S. Li, and L. Hanzo. Single-Carrier SM-MIMO: A Promising Design for Broadband Large-Scale Antenna Systems. *IEEE Communications Surveys Tutorials*, 18(3):1687–1716, thirdquarter 2016.

[129] A. Younis, W. Thompson, M. D. Renzo, C. X. Wang, M. A. Beach, H. Haas, and P. M. Grant. Performance of Spatial Modulation Using Measured Real-World Channels. In *2013 IEEE 78th Vehicular Technology Conference (VTC Fall)*, pages 1–5, Sept 2013.

[130] C. Zhan. An OFDM Channel estimation Algorithm Based on Pilot Signals. *TV technology*, 34(11), 2010.

[131] B. Zhou, Y. Xiao, P. Yang, J. Wang, and S. Li. Spatial modulation for single carrier wireless transmission systems. In *Communications and Networking in China (CHINACOM), 2011 6th International ICST Conference on*, pages 11–15. IEEE, 2011.